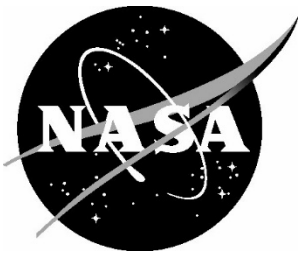
NASA/TP–20240004989



Scientific Ballooning Handbook
50th Anniversary Edition

Sarah A Roth
Erin M Reed
Christopher D Yoder
NASA Wallops Flight Facility, Wallops Island, VA
Ethan A Chaffee, World View Enterprises
Javier Romualdez, StarSpec Technologies

December 2025

NASA STI Program Report Series

Since its founding, NASA has been dedicated to the advancement of aeronautics and space science. The NASA scientific and technical information (STI) program plays a key part in helping NASA maintain this important role.

The NASA STI program operates under the auspices of the Agency Chief Information Officer. It collects, organizes, provides for archiving, and disseminates NASA's STI. The NASA STI program provides access to the NTRS Registered and its public interface, the NASA Technical Reports Server, thus providing one of the largest collections of aeronautical and space science STI in the world. Results are published in both non-NASA channels and by NASA in the NASA STI Report Series, which includes the following report types:

- TECHNICAL PUBLICATION. Reports of completed research or a major significant phase of research that present the results of NASA Programs and include extensive data or theoretical analysis. Includes compilations of significant scientific and technical data and information deemed to be of continuing reference value. NASA counterpart of peer-reviewed formal professional papers but has less stringent limitations on manuscript length and extent of graphic presentations.

- TECHNICAL MEMORANDUM. Scientific and technical findings that are preliminary or of specialized interest, e.g., quick release reports, working papers, and bibliographies that contain minimal annotation. Does not contain extensive analysis.

- CONTRACTOR REPORT. Scientific and technical findings by NASA-sponsored contractors and grantees.

- CONFERENCE PUBLICATION. Collected papers from scientific and technical conferences, symposia, seminars, or other meetings sponsored or co-sponsored by NASA.

- SPECIAL PUBLICATION. Scientific, technical, or historical information from NASA programs, projects, and missions, often concerned with subjects having substantial public interest.

- TECHNICAL TRANSLATION. English-language translations of foreign scientific and technical material pertinent to NASA's mission.

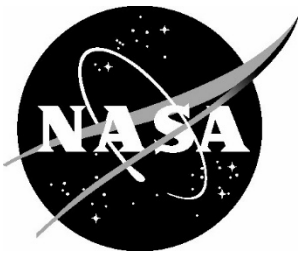
Specialized services also include organizing and publishing research results, distributing specialized research announcements and feeds, providing information desk and personal search support, and enabling data exchange services.

For more information about the NASA STI program, see the following:

- Access the NASA STI program home page at http://www.sti.nasa.gov

.

NASA/TP–20240004989



Scientific Ballooning Handbook
50th Anniversary Edition

Sarah A Roth
Erin M Reed
Christopher D Yoder
NASA Wallops Flight Facility, Wallops Island, VA
Ethan A Chaffee, World View Enterprises
Javier Romualdez, StarSpec Technologies

National Aeronautics and

Space Administration

Goddard Space Flight Center

Greenbelt, Maryland 20771

December 2025

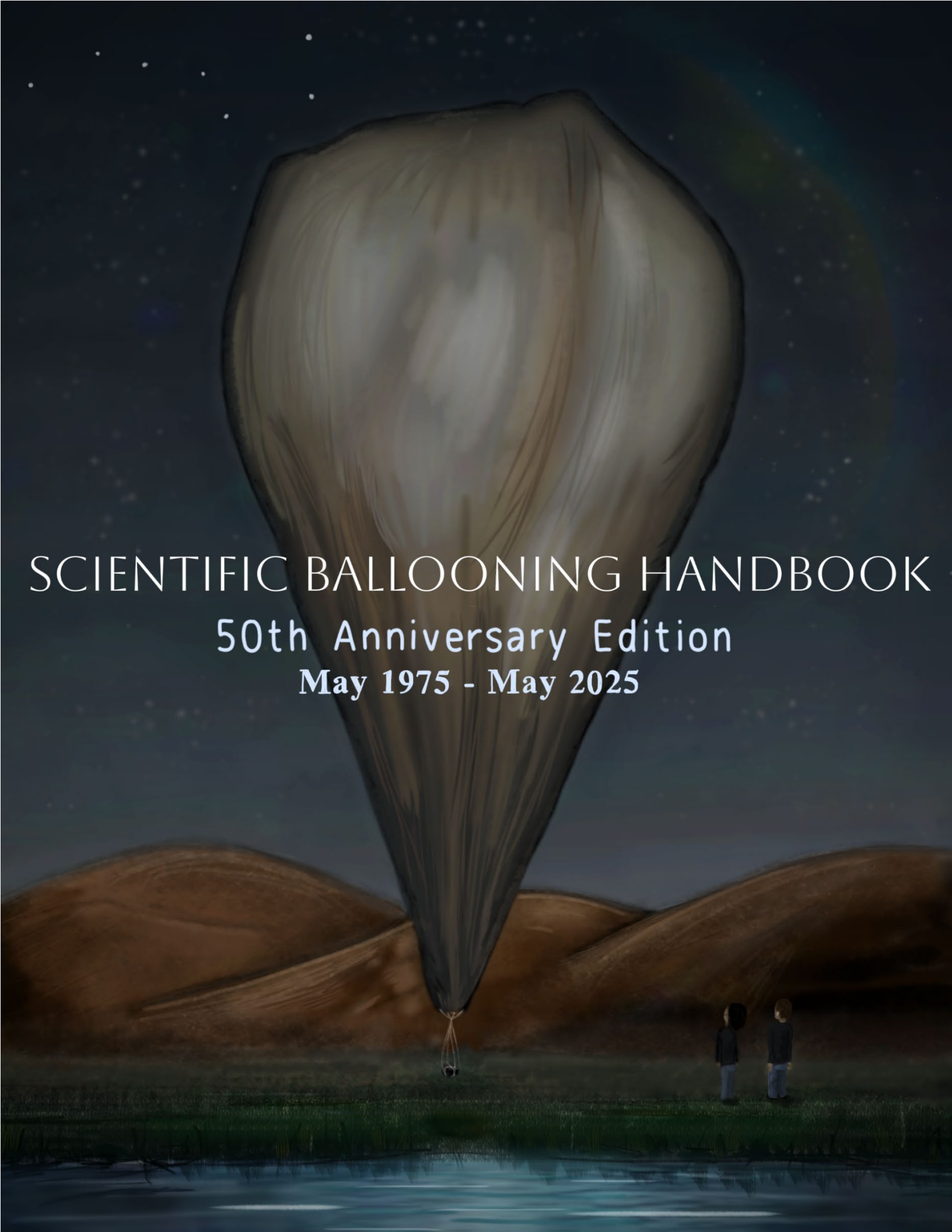
The use of trademarks or names of manufacturers in this report is for accurate reporting and does not constitute an official endorsement, either expressed or implied, of such products or manufacturers by the National Aeronautics and Space Administration.

Available from:

NASA STI Program / Mail Stop 050

NASA Langley Research Center

Hampton, VA 23681-2199


SCIENTIFIC BALLOONING HANDBOOK
50th Anniversary Edition
May 1975 - May 2025

Forward

I began my ballooning career in 1974 as an undergraduate at Texas A&M University, working in a materials testing lab contracted to the National Scientific Balloon Facility (NSBF). At that time, the NSBF was operated by the National Center for Atmospheric Research (NCAR). When I graduated in August 1974, I went to work directly for the NSBF, and it was there that I was first introduced to the *Scientific Ballooning Handbook* (NCAR-TN/IA-99). Later, in 1982, when NASA assumed funding and management of the NSBF, I took a position in the Balloon Program Office as part of the management team focused on balloon technology. In 2003, I left NASA for the Southwest Research Institute, where I continued to support scientific ballooning and stratospheric airships until my semi-retirement in August 2020. It is now 2025, and I still have my copy of the Handbook — its pages worn, but its insights timeless.

Throughout my career, I used the Handbook as the first training tool for every new engineer I worked with. It has been half a century since its publication. That first edition, compiled by Alvin L. Morris and his colleagues at NCAR, quickly became a cornerstone reference for engineers, scientists, and students entering the field. At a time when much of the pioneering work in high-altitude ballooning was dispersed across classified reports, obscure technical papers, and institutional archives, the Handbook offered the first unified picture of balloon flight theory, operations, instrumentation, and design. Its legacy endures not only because of the knowledge it preserved but because it inspired generations of engineers and researchers to view the near-space environment as a laboratory for exploration, discovery, and innovation.

The world of scientific ballooning has changed dramatically in the 50 years since that first volume appeared. We have learned much, and there is still more to discover. The intervening decades have brought increased payload masses and altitudes; long-duration flights spanning continents and oceans; the birth of super-pressure balloon technology; hybrid balloon designs; and planetary exploration concepts for Venus, Mars, and Titan. Balloons have enabled cutting-edge astrophysics missions such as BOOMERanG, SPIDER, and GUSTO. The ballooning community itself has grown more diverse and global, with NASA, CNES, JAXA, ISRO, and other agencies sharing technology, flight campaigns, and scientific ambitions. New commercial ventures have emerged to serve specialized applications. Advances in computing, telemetry, materials science, and thermal modeling have transformed both the scale and precision of balloon missions — unlocking capabilities unimagined in the 1970s.

This 50th Anniversary Edition honors and builds upon that legacy while embracing the future. Every chapter from the original Handbook has been revisited by subject-matter experts, with new sections added on educational development, solar and planetary balloons, modern communications systems, energy-balance modeling, and balloon

manufacturing and operations. The structure reflects both continuity and change: the core principles of flight theory and design remain, while entire new chapters address the transformative technologies and missions of the past half-century.

Above all, this edition remains true to the spirit of its predecessor. Neither the 1975 Handbook nor this update claims to be exhaustive — ballooning is too dynamic a field for any single volume to capture fully. Instead, its purpose is to provide a foundation: a comprehensive, technically rigorous, and historically grounded resource for today's scientists, engineers, students, and mission planners. Readers are invited to see this volume as both a record of achievements and a launchpad for the next fifty years of innovation in scientific ballooning.

May it serve as the resource for the next half-century, as its predecessor has been for me.

Ira Steve Smith, Jr.

Dedication

This 50th Anniversary Edition is dedicated to the memory of:

Loren G. Seely,	Rodger E. Farley,
Julian Nott,	James A. Winker,
Gregory T. Guzik,	Danny Ball,
James L. Rand,	W. Vernon Jones

whose vision, expertise, and leadership helped define the modern era of scientific ballooning. Their work spanned engineering innovation, program leadership, and the mentoring of new generations of scientists and engineers, ensuring that high-altitude research would remain a vital part of the scientific enterprise well into the 21st century.

Each of these individuals brought unique talents and perspectives to the field. Seely advanced the quality and reliability of balloon manufacturing; Nott's innovative designs and engineering excellence pushed the boundaries of altitude and endurance for manned flight; Guzik championed student Science, Technology, Engineering and Mathematics (STEM) development through the Louisiana Aerospace Catalyst Experience for Students (LaACES) and High Altitude Student Platform (HASP) projects; Rand introduced cutting-edge design and modeling techniques; Farley brought modern simulation and systems engineering to the development of super-pressure balloons; Winker preserved the technical history and operational lessons of decades of ballooning; Ball steered the development of novel launch operations techniques; and Jones, as NASA Program Scientist, championed long-duration missions and fostered collaborations across agencies and disciplines. Together, their contributions laid the groundwork for today's global scientific balloon program.

The authors recognize that the story of scientific ballooning has been shaped by many hands, from early pioneers to the countless technicians, engineers, scientists, and program leaders whose work has often gone unsung. Yet these individuals exemplified the spirit of dedication, curiosity, and technical excellence that elevated ballooning from its experimental roots to a mature scientific platform capable of addressing some of the most profound questions in astrophysics, atmospheric science, and engineering.

As this 50th edition reflects on half a century of innovation and discovery, it is fitting to pause and honor the memory of those who set the tone for the modern era. Their legacy continues to inspire current and future generations, reminding us that scientific progress rests not only on technical achievements but also on the passion, collaboration, and commitment of those who dare to lift humanity's gaze toward the edge of space.

Debora A. Fairbrother

Preface

In 1975, the National Center for Atmospheric Research (NCAR) published a Technical Note titled "Scientific Ballooning Handbook". Alvin L. Morris, editor of the Handbook and manager of the Scientific Balloon Facility, cited the necessity to consolidate decades of progress on the construction and operation of scientific balloons. The majority of the breakthroughs of the 1940s-1970s were classified, and even after declassification, the reports were difficult to locate.

Morris was certainly the ideal editor for a publication of this magnitude. As manager of the National Scientific Balloon Facility in Palestine, Texas, he saw the success rate of operations increase from 68% to 84% during his management from 1964 to 1971.

Morris pulled together many subject matter experts to compile the original Handbook, and it has been an invaluable resource to many who are starting their journey into scientific ballooning. The 50th Anniversary Edition employs a similar principle. Experts worked together to update the current Handbook to the state-of-the-art, and at least one editor reviewed each section. Ultimately, the content was determined by the author. The editors have also taken the liberty of rearranging the book's structure and adding information on significant achievements.

It should be noted that the contents of this edition are provided for educational purposes only. The authors and editors of this Handbook make no guarantee whatsoever for the efficacy or accuracy of the contents within. The reader is responsible and takes all risks for relying to any extent on the information provided throughout this chapter.

This Handbook is not comprehensive, and many other resources are available to aid scientists, engineers, and program managers in developing their own instruments, balloons, and flight programs. While regulatory programs such as the FAA and ITAR are mentioned, it is incumbent on the reader to fully read and understand the source material and not rely on this book for guidance in these matters.

Omissions

This edition of the Handbook is notably missing information about crewed balloons and the lighter-than-air aircraft known as aerostats. While there is great interest in both types of balloons, there is significant other literature related to gondolas for human flight, construction techniques, and aerostat applications.

Another notable omission is a thorough discussion of alternative balloon shapes such as the tetroon. This version of the handbook focuses on the ‘natural shape’ zero-pressure, spherical and pumpkin super-pressure, and

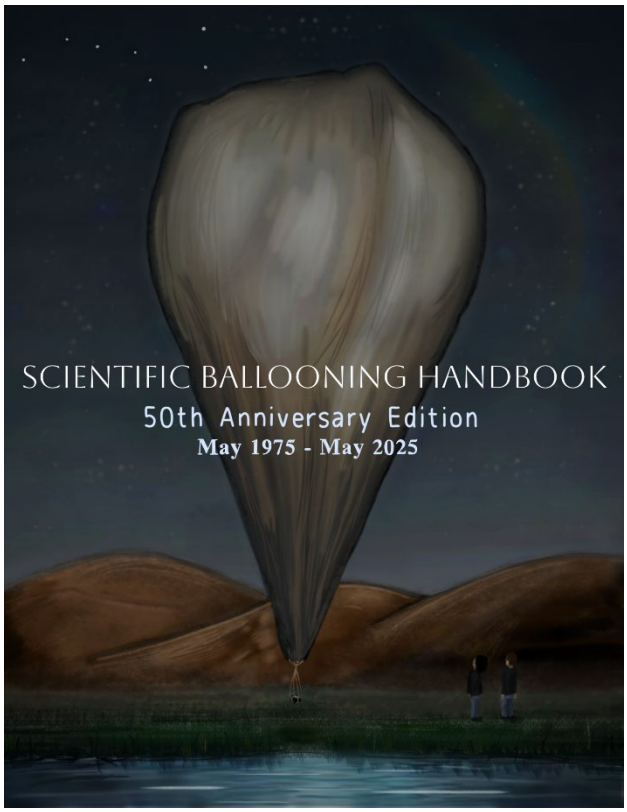
the standard solar balloon. In addition, small tethered or hybrid balloon systems are only noted briefly and not elaborated on.

This publication assumes the reader is familiar with certain acronyms related to the spaceflight industry, such as the European Space Agency (ESA) and the National Aeronautics and Space Industry (NASA). These and other similar acronyms may be encountered in each section without definition.

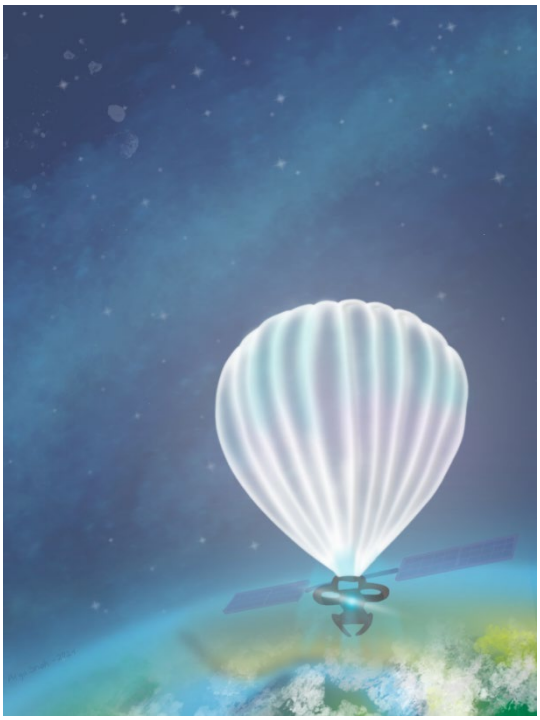
About the Art

The current editors desired to broaden participation across disciplines and created a contest for students to submit artwork to serve as the cover of this edition. 32 students between the ages of 13 and 18 participated from around the world. Three winners were selected, and the cover artist had her artwork printed and flown from an engineering test flight by NASA in the fall of 2025.

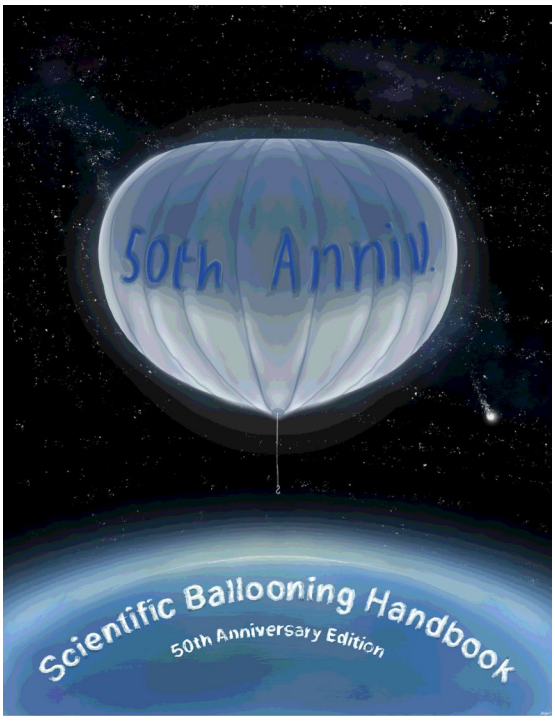
Details on each artist and their submissions:



- 1st place and cover
- Kaitlyn Geise
- Art Title: Scientific Ballooning
- Description: Digital art submission



- 2nd place
- Arya Shah
- Title: Leaving Earth: New Discoveries
- Description: My artwork represents leaving our home through the bravery of discovering new planets and new worlds. The balloon partially in the clouds and partially in space represent how we are making future goals for space discovery and possibly, inhabiting space ourselves. These balloons are the step forward in human discovery in space, a milestone that has led us to discovering new planets and possibly, life on other planets. I hope to honor this milestone, and to contribute to this historic moment.



- 3rd place
- Shriya Vasudevan
- Title: Scientific Balloon Handbook Cover
- Description: It is 8.5 — 11 inches, 300 dpi. I drew it on Adobe Express, then ran a posterize filter. Everything is original (no AI, pictures, etc.). My signature is on the bottom right. The piece reflects scientific discovery throughout. The multitude of stars and nebulae echo the vast unknown; the focal balloon shows human possibility and reach. While participating in this challenge, I learned about ANITA and detecting upward-going neutrinos--it's fascinating how scientific balloons are used even for particle physics!

Geographical Bias

Both the original Handbook and this update have been written primarily by balloon experts based in the United States; however, many organizations around the globe manufacture and launch balloons in pursuit of scientific research. Table 1 lists many organizations relevant to scientific ballooning that were active at the time of this publication. Any omission from this table is a genuine error, not a reflection of the organization's quality.

Table 1: Listing of balloon flight providers, manufacturers, and significant programs with contact information current at the time of publication.

Africa

Program Name	Type / Function	Headquarters Location	Link to Home Page
Digital Council Africa	Professional Network	Johannesburg, South Africa	https://www.digitalcouncil.africa/

Asia / Pacific

Program Name	Type / Function	Headquarters Location	Link to Home Page
Airservices Australia	Commercial	Canberra, Australia	https://www.airservicesaustralia.com/
Canberra Balloon Spectacular	Festival/Event	Canberra, Australia	https://www.canberraballoonspectacular.com
Northern Territory Government	National Agency	Darwin, Australia	https://nt.gov.au/
Chinese Academy of Sciences (CAS)	National Agency	Qinghai Province, China	http://english.aircas.ac.cn/Search/?keyword=balloon
Bharti Airtel Limited	Communications	New Delhi, India	https://www.airtel.in/
Lekha Wireless Solutions	Communications	Bangalore, India	https://www.lekhawireless.com/
NewSpace	Commercial	Bangalore, India	https://www.newspace.co.in/
Indian Institute of Astrophysics	Commercial	Bengaluru, India	https://www.iiap.res.in/
ISRO (Indian Space Research Organisation)	National Agency	Bengaluru, India	https://www.isro.gov.in/
Tata Institute of Fundamental Research	National Agency	Mumbai, India	https://www.tifr.res.in/~bf/

Program Name	Type / Function	Headquarters Location	Link to Home Page
Indonesia-ITU Concern Forum	Professional Network	Jakarta, Indonesia	https://www.iicf.or.id/tentang-kami.html
Orbit Communications	Communications	Netanya, Israel	http://www.orbit-cs.com/
Indian Institute of Astrophysics	Commercial	Bengaluru, India	https://www.iiap.res.in/
MEISEI ELECTRIC CO., LTD.	Commercial	Isesaki, Japan	https://www.meisei.co.jp/english/
Saga International Balloon Fiesta	Festival/Event	Saga, Japan	https://www.sibf.jp/
JAXA (Japan Aerospace Exploration Agency)	National Agency	Chōfu, Japan	https://global.jaxa.jp/projects/sas/balloon/
KDDI	Communications	Tokyo, Japan	https://www.kddi.com/english/
National Institute of Information and Communications Technology (NICT)	Commercial	Tokyo, Japan	https://www.nict.go.jp/en/
NTT Docomo	Communications	Tokyo, Japan	https://www.docomo.ne.jp/english/
Sky Perfect JSAT Corp.	Communications	Tokyo, Japan	https://www.skyperfectjsat.space/jsat/en/
SoftBank	Communications	Tokyo, Japan	https://www.softbank.jp/en/
Kea Aerospace	Commercial	Christchurch, New Zealand	https://www.keaaerospace.com/
Space & Upper Atmosphere Research Commission (SUPARCO)	National Agency	Karachi, Pakistan	https://www.suparco.gov.pk/
King Abdullah University of Science and Tech (KAUST)	Educational	Thuwal, Saudi Arabia	https://www.kaust.edu.sa/
picoNETS	Communications	Singapore, Singapore	https://piconets.com/

Program Name	Type / Function	Headquarters Location	Link to Home Page
Korea Aerospace Research Institute (KARI)	National Agency	Daejeon, South Korea	https://www.kari.re.kr/eng/
KT Corporation	Communications	Seoul, South Korea	https://corp.kt.com/eng/
Telecom Technology Center	Communications	Taipei, Taiwan	https://www.ttc.org.tw/eng/
Gilat	Communications	Bangkok, Thailand	https://www.gilat.com/
Hacettepe University	Educational	Ankara, Turkey	https://www.hacettepe.edu.tr/english
Ulak Haberleşme A.Ş	Communications	Ankara, Turkey	https://www.ulakhaberlesme.com.tr/en
Turkcell İletişim Hizmetleri A.Ş	Communications	Istanbul, Turkey	https://www.turkcell.com.tr/
Dong Nai International Hot Air Balloon Festival	Festival/ Event	Biên Hòa, Vietnam	https://khinhkhicaudongnai.com/en-us/

Europe

Program Name	Type / Function	Headquarters Location	Link to Home Page
NOKIA	Communications	Espoo, Finland	https://www.nokia.com/
Satrake Ltd.	Communications	Helsinki, Finland	https://www.satraka.com/
Centre National d'Études Spatiales (CNES)	National Agency	Paris, France	https://ballons.cnes.fr/en/balloons-0
European Space Agency (ESA)	International Agency	Paris, France	https://www.esa.int/
HEMERIA	Commercial	Toulouse, France	https://www.hemeria-group.com/en/

Program Name	Type / Function	Headquarters Location	Link to Home Page
Rocket and Balloon Experiments for University Students (REXUS/BEXUS) ESA	Educational	Paris, France	https://rexusbexus.net/
Stratolia	Commercial	Toulouse, France	https://www.stratolia.com/
TJ Innovation	Commercial	Toulouse, France	https://www.tj-innovation.com/
Max Planck Institute	Commercial	Munich, Germany	https://www.mpg.de/en
EANT	Communications	Potsdam, Germany	https://www.eant.de/
Deutsches Zentrum für Luft- und Raumfahrt (DLR)	National Agency	Cologne, Germany	https://www.dlr.de/en
Warsteiner Internationale Montgolfiade	Festival/Event	Warstein, Germany	https://warsteiner-welt.de/events/?lang=en
Agenzia Spaziale Italiana (ASI)	National Agency	Rome, Italy	https://www.asi.it/en/
Leonardo Electronics	Commercial	Rome, Italy	https://www.leonardo.com/en/home
Stratosyst	Commercial	Milan, Italy	https://www.stratosyst.com/
Roscosmos (Russian Space Agency)	National Agency	Moscow, Russia	https://www.roscosmos.ru/en/
RUNJOB (RUssia-Nippon JOint Balloon)	Commercial	Moscow, Russia	https://stratocat.com.ar/fichas-e/1997/KMC-19970709.htm
Parque Tecnológico de Fuerteventura	Commercial	Puerto del Rosario, Spain	https://www.ptfue.com/en/
Zero 2 Infinity	Commercial	Barcelona, Spain	https://www.zero2infinity.space/
GMV (Innovating Solutions)	Commercial	Tres Cantos, Spain	https://www.gmv.com/en
Embention Sistemas Inteligentes S.A	Commercial	Alicante, Spain	https://www.embention.com/en/

Program Name	Type / Function	Headquarters Location	Link to Home Page
Swedish National Space Agency (SNSA)	National Agency	Solna, Sweden	https://www.rymdstyrelsen.se/en/
Swedish Space Corporation	Commercial	Solna, Sweden	https://sscspace.com/esrange/rocket-ballon-activities/
University of Applied Sciences and Arts Northwestern Switzerland	Educational	Basel, Switzerland	https://www.fhnw.ch/en/
Armasuisse Science & Technology	Commercial	Thun, Switzerland	https://www.ar.admin.ch/en/armasuisse-wissenschaft-und-technologie-w-t/home.html
Comfone AG	Communications	Bern, Switzerland	https://www.comfone.com/
Meteomatics	Data Aggregate	St. Gallen, Switzerland	https://www.meteomatics.com/
HABHub	Commercial	Cambridge, UK	https://habhub.org/
Predict HAB Hub	Data Aggregate	Cambridge, UK	https://predict.habhub.org/
Raspberry Pi Forums – HAB	Educational	Cambridge, UK	https://forums.raspberrypi.com/viewforum.php?f=43
Stratospheric Platforms	Commercial	Cambridge, UK	https://www.stratosphericplatforms.com/
Filtronic	Communications	Sedgefield, UK	https://filtronic.com/
Bristol International Balloon Fiesta	Festival/Event	Bristol, UK	https://www.bristolballoonfiesta.co.uk/
World Mobile	Communications	London, UK	https://worldmobile.io/
Liverpool Hope University	Educational	Liverpool, UK	https://www.hope.ac.uk/
University of York	Educational	York, UK	https://www.york.ac.uk/
B2Space	Commercial	Newport, UK	https://b2-space.com/
Element14 Community – HAB Forum	Educational	Leeds, UK	https://www.element14.com/community/groups/high-altitude-ballooning
UK Space Agency (UKSA)	National Agency	Swindon, UK	https://www.gov.uk/government/organisations/uk-space-agency

North America

Program Name	Type / Function	Headquarters Location	Link to Home Page
Stratotegic	Commercial	Belleville, Canada	https://www.stratotegic.com/
Stratodynamics Aviation Inc.	Commercial	Kenilworth, Canada	https://www.stratodynamics.ca/
Carleton University	Educational	Ottawa, Canada	https://carleton.ca/
Stratospheric Balloons - Canadian Space Agency (CSA)	National Agency	Longueuil, Canada	https://www.asc-csa.gc.ca/eng/sciences/balloons/
ISTAR	Commercial	Montreal, Canada	http://www.istar.ca/
León International Balloon Festival	Festival/Event	León, Mexico	https://www.hotairballoon.com/International-Hot-Air-Balloon-Festival/
Space Data Corp.	Communications	Chandler, USA	https://spacedata.net/
Paragon Space Development Corp	Commercial	Tucson, USA	https://www.paragonsdc.com/
World View Enterprises	Commercial	Tucson, USA	https://www.worldview.space/
Kraus Hamdani Aerospace	Commercial	Brisbane, USA	https://www.khaero.com/
Amprius Technologies, Inc.	Commercial	Fremont, USA	https://www.amprius.com/
MSB Technologies	Commercial	Grass Valley, USA	https://msb-technologies.com/
HAPS Alliance	Professional Network	Menlo Park, USA	https://hapsalliance.org/
Google Loon (Shuttered)	Commercial	Mountain View, USA	https://x.company/projects/loon/
Swift Engineering	Commercial	San Clemente, USA	https://www.swiftengineering.com/
Kratos	Commercial	San Diego, USA	https://www.kratosdefense.com/
San Jose State University Research Foundation/NASA	Educational	San Jose, USA	https://www.sjsu.edu/research/
The WX Company	Commercial	Boulder, USA	https://www.thewxcompany.com/
Near Space Symposium	Conference	Colorado Springs, USA	https://www.spacesymposium.org/

Program Name	Type / Function	Headquarters Location	Link to Home Page
Urban Sky Theory Inc	Commercial	Denver, USA	https://www.urbansky.com/
Voyager Space/Pioneer Astronautics	Commercial	Denver, USA	https://voyagerspace.com/
Cubes in Space	Educational	Washington, USA	https://www.cubesinspace.com/
ILC Dover	Commercial	Frederica, USA	https://www.ilcdover.com/
Harbor Branch Florida Atlantic University	Educational	Boca Raton, USA	https://www.fau.edu/hboi/
Space Balloon Technologies Corp	Commercial	Daytona Beach, USA	https://spaceloon.com/
Space Perspective (Shuttered)	Commercial	Titusville, USA	https://spaceperspective.com/
SpaceHub Southeast – PongSat Program	Educational	Atlanta, USA	https://www.spacehubse.org/
Stratospheric Ballooning Association & Academic High Altitude Conference (AHAC)	Professional Network & Conference	Ames, USA	https://www.stratoballooning.org/
High Altitude Student Platform (HASP)	Educational	Baton Rouge, USA	https://laspace.lsu.edu/hasp/
UMaine High Altitude Ballooning Program	Educational	Orono, USA	https://umaine.edu/epscor/high-altitude-ballooning/
TCOM Aerostat	Commercial	Columbia, USA	https://tcomlp.com/
Johns Hopkins Balloon Program	Educational	Baltimore, USA	https://physics-astronomy.jhu.edu/research/particle-physics-and-high-energy-research/balloon-program/

Program Name	Type / Function	Headquarters Location	Link to Home Page
National Oceanic and Atmospheric Administration	National Agency	Silver Spring, USA	https://www.noaa.gov/
NWS (National Weather Service)	National Agency	Silver Spring, USA	https://www.weather.gov/
Altaeros	Commercial	Somerville, USA	https://www.altaeros.com/
Great Plains Super Launch (GPSL) & Symposium	Educational	Various, USA	https://www.superlaunch.org/
Minnesota Balloon Technologies Workshop	Conference	Minneapolis, USA	https://balloontech.umn.edu/
Stratos Solution Inc.	Commercial	Minneapolis, USA	https://stratos-solutions.com/
Eclipse Ballooning Project	Educational	Bozeman, USA	https://eclipse.montana.edu/
Nationwide Eclipse Ballooning Project	Educational	Bozeman, USA	https://eclipse.montana.edu/
Great Reno Balloon Race	Festival/Event	Reno, USA	https://renoballoon.com/
Albuquerque International Balloon Fiesta	Festival/Event	Albuquerque, USA	https://www.balloonfiesta.com/
Prismatic	Commercial	Albuquerque, USA	https://www.prismaticpowders.com/
Sandia Labs Student Solar Balloon Launch	Educational	Albuquerque, USA	https://www.sandia.gov/labnews/2025/06/12/soaring-into-stem/
New Mexico State Physical Science Laboratory	Commercial	Las Cruces, USA	https://psl.nmsu.edu/
Sceye	Commercial	Roswell, USA	https://www.sceye.com/
Near Space Labs	Commercial	Brooklyn, USA	https://nearspacelabs.com/
Windborne Systems Inc.	Commercial	New York City, USA	https://windbornesystems.com/
Radical	Commercial	Charlotte, USA	https://www.radicalaero.com/

Program Name	Type / Function	Headquarters Location	Link to Home Page
NC Space Grant – HAB Challenge	Educational	Raleigh, USA	https://ncspacegrant.ncsu.edu/opportunities/students/high-altitude-ballooning-challenge/
Edgecombe Community College – HAB STEM Day	Educational	Tarboro, USA	https://www.edgecombe.edu/hab-stem-day
Goodyear	Commercial	Akron, USA	https://www.goodyearblimp.com/
LTA Research	Commercial	Akron, USA	https://ltaresearch.com/
Near Space Corporation (AEROSTAR)	Commercial	Tillamook, USA	https://nsc.aero/
Aerostar	Commercial	Sioux Falls, USA	https://aerostar.com/
Overlook Horizon (OLHZN)	Educational	Nashville, USA	https://www.olhzn.com/
AT&T	Communications	Dallas, USA	https://www.att.com/
ERICSSON	Communications	Lewisville, USA	https://www.ericsson.com/
Columbia Scientific Balloon Facility (CSBF)	Services	Palestine, USA	https://www.csbf.nasa.gov/
Balloon Federation of America (BFA)	Professional Network & Conference	Various, USA	https://bfa.net/
Balloon Tracking Community (Tracker)	Data Aggregate	Various, USA	https://tracker.balloonfiesta.com/
Experimental Balloon & Airship Association (EBAA)	Conference	Post Mills, USA	https://www.brianbolandfoundation.org/
AeroVironment	Commercial	Arlington, USA	https://www.avinc.com/
Airbus US Space and Defense	Commercial	Arlington, USA	https://www.airbusus.com/
Aeroprobe Corporation	Data Aggregate	Christiansburg, USA	https://www.aeroprobe.com/

Program Name	Type / Function	Headquarters Location	Link to Home Page
Northrop Grumman	Commercial	Falls Church, USA	https://www.northropgrumman.com/
Aurora Flight Sciences	Commercial	Manassas, USA	https://www.aurora.aero/
NAL Research Corp	Data Aggregate	Manassas, USA	https://www.nalresearch.com/
The MITRE Corporation	Commercial	McLean, USA	https://www.mitre.org/
AIAA Balloon Technical Committee	Professional Network	Reston, USA	https://www.aiaa.org/committees/technical-committees
NASA Balloon Program Office	National Agency	Wallops Island, USA	https://www.nasa.gov/scientificballoons/
PowerLight Technologies	Commercial	Kent, USA	https://www.powerlighttech.com/
Sagetech Avionics, Inc.	Commercial	White Salmon, USA	https://www.sagetech.com/
Menet Aero	Commercial	Milwaukee, USA	https://menetaero.com/
Wyoming NASA Space Grant – High-Altitude Balloon Program	Educational	Laramie, USA	https://wyomingspacegrant.org/high-altitude-ballooning/
Central Wyoming College HAB Program	Educational	Riverton, USA	https://www.cwc.edu/academics/programs/stem/high-altitude-ballooning/

South America

Program Name	Type / Function	Headquarters Location	Link to Home Page
Comisión Nacional de Actividades Espaciales (CONAE)	National Agency	Buenos Aires, Argentina	https://www.argentina.gob.ar/ciencia/conae
StratoCat	Data Aggregate	Rio Cuarto, Argentina	https://stratocat.com.ar/index-e.html
Agência Espacial Brasileira (AEB)	National Agency	Brasília, Brazil	https://www.gov.br/aeb/pt-br
INPE (Instituto Nacional de Pesquisas Espaciais)	National Agency	Cachoeira Paulista, Brazil	http://www.inpe.br/

International

Program Name	Type / Function	Headquarters Location	Link to Home Page
ESA Symposium on European Rocket and Balloon Programmes and Related Research	Conference	Various, International	Google Search Result
Gordon Bennett Cup	Festival/Event	Various, International	https://www.fai.org/gordonbennett/
Pico Balloon Archive	Data Aggregate	Various, International	https://picoballoon.archive.com/
SondeHub	Data Aggregate	Various, International	https://predict.sondehub.org/
Tracker – HAB Tracker	Data Aggregate	Various, International	https://tracker.habhub.org/

Contents

This table provides a side-by-side comparison between the 1975 original Scientific Ballooning Handbook and the 50th Anniversary Edition. It highlights which chapters existed in 1975 and what has been updated, expanded, or newly introduced in the 2025 version.

1975 Handbook Chapter	2025 Edition Chapter(s) / Status
Preface & Introduction	**Preface, Foreword, Dedication**
I. Evolution of Ballooning	**1. Balloon History & Evolution**
(Not Present)	**2. Science from the Stratosphere**
(Not Present)	**3. Balloons for Education**
II. Theory of Balloon Flight	**4. Theory of Balloon Flight**
III. Energy Balance & Flight Model	**5. Energy Balance**
IV. Lift Gases	**6. Lift Gases**
X. The Atmosphere	**7. The Atmosphere**
(Not Present)	**8. Balloon Manufacturing and Materials**
V. Balloon Design Considerations	**9. Zero-Pressure Balloons** **10. Super-Pressure Balloons**
(Not Present)	**11. Flight Operations**
VI. Scientific Balloon Instrumentation	**12. Communications, Command & Control (C3)**
VII. Stabilization & Orientation	**13. Health, State, Pointing & Stabilization**
VIII. Hot-Air Ballooning	*(Cut to focus on science in the modern era)*

1975 Handbook Chapter	2025 Edition Chapter(s) / Status
IX. Parachutes	**14. Decelerators & Deployables**
(Not Present)	**15. Solar Balloons**
(Not Present)	**16. Planetary Balloons**
VI. Scientific Balloon Instrumentation	**17. Instrumentation**
XI. Tables, Graphs & Misc.	**Reference Material**

Chapter 1
The History and Evolution of Balloons for Scientific Exploration

Sarah A. Roth[1]

[1] National Aeronautics and Space Administration, Chief Technologist, Balloon Program Office

Acknowledgments

Alvin L. Morris published the original Scientific Ballooning Handbook in 1975. It has been helpful in providing general engineering details for the technical reader in the scientific balloon community.

This handbook's revision reflects the developments of the entire balloon community over the past fifty years. In addition, it celebrates the fiftieth anniversary of the original Scientific Ballooning Handbook's publication and its significance to the field of ballooning.

Numerous colleagues in the field of ballooning have contributed content to this revision, and their efforts are greatly appreciated.

Table of Contents

Acknowledgments 2

Table of Contents 3

Table of Figures 5

Table of Symbols 6

1. Introduction 7

2. Major Technological Breakthroughs 8

2.1. 240 CE Buoyancy 8

2.2. 1200 and 1600 Concepts of Lighter-Than-Air 8

2.3. 1780 Montgolfier Design and Hydrogen 8

2.4. 1780 - 1900 Military-Use and Airships 9

2.4.1. Military Ballooning 9

2.4.2. Airships 11

2.5. 1900 Helium, Rubber, and Sport Ballooning 11

2.5.1. Helium 11

2.5.2. Rubber 12

2.5.3. Sport Ballooning 15

2.6. 1930 Stratosphere, Plastic, and the Natural Shape 18

2.6.1. Stratosphere 18

2.6.2. Plastic 19

2.6.3. Natural Shape 21

2.7. 1950 Minnesota and Modern Scientific Balloons 21

2.7.1. Modern Scientific Ballooning 21

2.7.2. Women in the Stratosphere 23

2.8. 1960 Establishment of NSBF and Sport returns to Hot Air 27

2.8.1. NSBF 27

2.8.2. Hot-Air Sport Balloons 28

2.9. 1980 Material Selection, Development of Long-Duration Heavy-Lift Balloons and First Extraterrestrial Balloon 29

2.9.1. Material Selection 29

2.9.2. New Era Long-Duration Heavy-Lift 30

2.9.3. Extra-Terrestrial Balloons 31

2.10. 1990 Global Infrastructure for Scientific Ballooning..... 32

2.11. 2000 Computer-Aided Design and Pumpkin Super-Pressure Balloons 32

2.11.1. Computer-Aided Design 32

2.11.2. Pumpkin Super-Pressure 33

2.12. 2010 Gondola and Instrument Improvements..... 34

3. Conclusions..... 35

References..... 37

Appendix 1-A. Timeline of Balloon History..... 47

Table of Figures

Figure 1-1: 2024 Olympic cauldron at night, floating above the city by a hot-air balloon..... 7

Figure 1-2: Lowe's military balloon near Gaines Mill, Virginia, May 1862.Lowe stands to the right with his hand on the envelope. The portable hydrogen generators can be seen in to the left of the balloon..... 10

Figure 1-3: Goodyear III balloon at the 1925 Gordon Bennett Race, Brussels, Belgium..... 16

Figure 1-4: Ralph Upson after dirigible flight, 1917..... 17

Figure 1-5: Ward Van Orman [r] with C.K. Wollam, 1925..... 17

Figure 1-6: Launch day of the 50th Gordon Bennett Cup in Waasmunster, Oost-Vlaanderen..... 18

Figure 1-7: Evolution in balloon shape and design from Montgolfier at left, Piccard in the center, and Winzen at right.[44]..... 22

Figure 1-8: Jeannette Piccard after a balloon landing circa 1934.... 25

Figure 1-9: Vera Simons (Winzen/Habrecht) shown here as part of DaVinci II crew in 1976. Verea was founder and co-owner of Winzen Research, Inc. 26

Table of Symbols

Symbol	Definition	Dimension
Tm	Stress or tension	$M\ L^{-1}\ T^{-2}$
P	Pressure	$M\ L^{-1}\ T^{-2}$
G	Total weight at concentration point	$M\ L\ T^{-2}$
x	Horizontal coordinate	L
y	Vertical coordinate	L
Rm	Radius of material curvature (context: balloon film strength)	L
K	Constant (geometry or material property, context-dependent)	–
Θ_0	Initial angle or reference angle	–
V	Volume of gas / balloon envelope	L^3
b	Balloon shape parameter / gore width (context: geometry)	L
T	Absolute temperature (Charles's Law)	Θ
ρ	Fluid density (Archimedes' principle)	$M\ L^-$
m	Mass (payload, gas, or structure)	M
g	Gravitational acceleration	$L\ T^{-2}$
ΔP	Differential pressure	$M\ L^{-1}\ T^{-2}$
σ	Stress (tensile stress in film)	$M\ L^{-1}\ T^{-2}$
ε	Strain (engineering strain, dimensionless)	–
Θ	General angle (balloon natural-shape equations)	–
R	Radius of curvature (balloon gore or lobe)	L
n	Number of gores or panels	–
Δh	Change in altitude	L
q	Dynamic pressure (aerodynamic context)	$M\ L^{-1}\ T^{-2}$
E	Elastic modulus (material property)	$M\ L^{-1}\ T^{-2}$

1. Introduction

An undeniable trait of humankind is the desire to push the boundaries of "possible." Historically, flight has been an elusive capability, perennially driving youth to tape on cardboard wings and jump from heights (much to their parents' dismay). Today's technology enables society to reach the stars, yet a balloon flight's calm and peaceful nature still fills mankind with wonder. Since 1972, the Albuquerque International Balloon Fiesta has attracted over 800,000 visitors annually. The Gordon Bennett Cup has been in operation since 1906 (with a few breaks) and is known as the "Blue Ribbon" of aeronautics. Most recently, the 2024 Paris Olympics paid homage to the Montgolfier brothers, famed French balloon pioneers, by hoisting the Olympic caldron in a tethered hot-air balloon for the duration of the games, Figure 1-1.



Figure 1-1: 2024 Olympic cauldron at night, floating above the city by a hot-air balloon.

2. Major Technological Breakthroughs

It is likely that anyone reading this handbook already has a good idea of the history of balloon flight. The original handbook buoyed the reader along the timeline from Archimedes to the book's publication in 1975. There are a few points worth repeating here regarding the evolution of "scientific" balloon flight, and the best way to collect these thoughts is from the perspective of the technological breakthrough it involved. The dates used to group the topics are approximate, based on a significant discovery or flight. These can be referenced in Appendix 1-A. Timeline of Balloon History as well as throughout the chapter.

2.1. 240 CE Buoyancy

Balloons, like all floating bodies, demonstrate the Archimedes principle of buoyancy. He proved this principle experimentally and showed by sound reasoning that "a statically floating body must displace the weight of the fluid in which it floats." In its original form, this principle is as valid in the air as in water; yet, for 2000 years thereafter, humans watched smoke rising through the air without considering how it could be put to practical use.

2.2. 1200 and 1600 Concepts of Lighter-Than-Air

Two ideas of note through this long period: English philosopher, scientist, and theologian Roger Bacon's proposal in the middle of the 13th century of a (then hypothetical) lighter-than-air craft, and Italian priest and mathematics and physics professor, Francesco Lana Terzi's (Father Lana) proposal in 1670 of a vacuum balloon. The latter device, which is theoretically sound, is still frequently reinvented by people unfamiliar with shell structures, available materials, and the realities of atmospheric pressure [1].

2.3. 1780 Montgolfier Design and Hydrogen

In the late 1700s, the practical breakthrough was the French brothers Joseph-Michel and Jacques-Étienne Montgolfier's hot-air balloon, a tribute to the intelligent artisans' powers of observation and flair for feasible construction. The Montgolfier brothers originally believed that the lifting force came from a unique smoke gas generated by burning straw and wool. They did not understand that it was actually heated air creating the lift. Despite this misunderstanding, their technique gave rise to the development of the hot-air balloon. Shortly after, the noted scientist Jacques Charles, in collaboration with two artisans, Anne-Jean and Nicolas-Louis Robert, introduced the hydrogen-filled balloon, with methods of construction that remained standard for over 150 years.

Charles was so captivated by balloons that he performed hundreds of experiments. He is most well-known for his experiments and writings on the relationship of temperature to volume. He is immortalized by "Charles's Law," which states that under constant pressure, an ideal gas's volume is proportional to its absolute temperature. This is critical to the analysis of balloon performance, given the environment in which they fly.

The term "aeronaut" was popularized with these early balloon pioneers, and eventually, the early flying clubs would use it to denote whether someone was piloting a winged aircraft (aviator) or a balloon (aeronaut).

It is worth reiterating that balloons at this time were exclusively powered by hydrogen or hot air for lift, and the balloon shells were made from materials such as paper, linen, silk, or cotton canvas.

The 19th century saw increased use of balloons for scientific experiments. French scientists Jean-Baptiste Biot and Joseph Gay-Lussac launched from Paris in 1804 to study atmospheric composition and magnetic forces. Eugene Robertson, Lhoest (no first name found), and Gay-Lussac conducted 1803–1804 balloon ascents to test whether Earth's magnetic force decreased with altitude [2]. They disproved Robertson's earlier claim that magnetism diminished significantly with height.

Throughout the century, balloon ascents were used to measure temperature, pressure, and humidity at various altitudes. Instrumentation advanced from basic thermometers to more sophisticated meteorographs.

2.4. 1780 - 1900 Military-Use and Airships

2.4.1. Military Ballooning

It took very little time for the military to realize the potential applications of an aerial platform on the battlefield. In 1794, Jean-Marie-Joseph Coutelle became the first military officer of a balloon corps. As a friend of the Montgolfier brothers and Jacques Charles, he was well situated to build and operate balloons for the French Revolutionary armies. They were primarily used as an observation platform to gather intelligence on the enemy lines. The Battle of Fluerus in 1794 is credited as the first significant use of military balloons in history. The observation balloon was able to direct artillery fire more accurately and contributed to the French victory [3].

Early aeronauts were often a mixed bag of scientists, daredevils, and carnival performers. Two early Americans, Thaddeus Lowe and John La Mountain, combined all three in pursuit of long-distance balloon flight. Both aeronauts received military sponsorship in the early days of the American Civil War to provide the Union Army with intelligence and to

boost civilian morale. Although deployed in several battles, the Balloon Corps was abandoned shortly after the war in 1865, after the outcomes failed to outweigh expenses.

However, significant technological advancements were made to enable deployment on the battlefield. A hydrogen generator was designed to fit in a standard Army wagon and could be moved anywhere the Army was deployed, see Figure 1-2. The balloon envelopes were silk-coated on both sides with a mixture of raw linseed oil and benzene for leak prevention. The envelope was covered by a rope net that attached to the gondola. The balloon was tethered to the ground, and a telegraph line ran from the basket down to the local commander [3], [4].

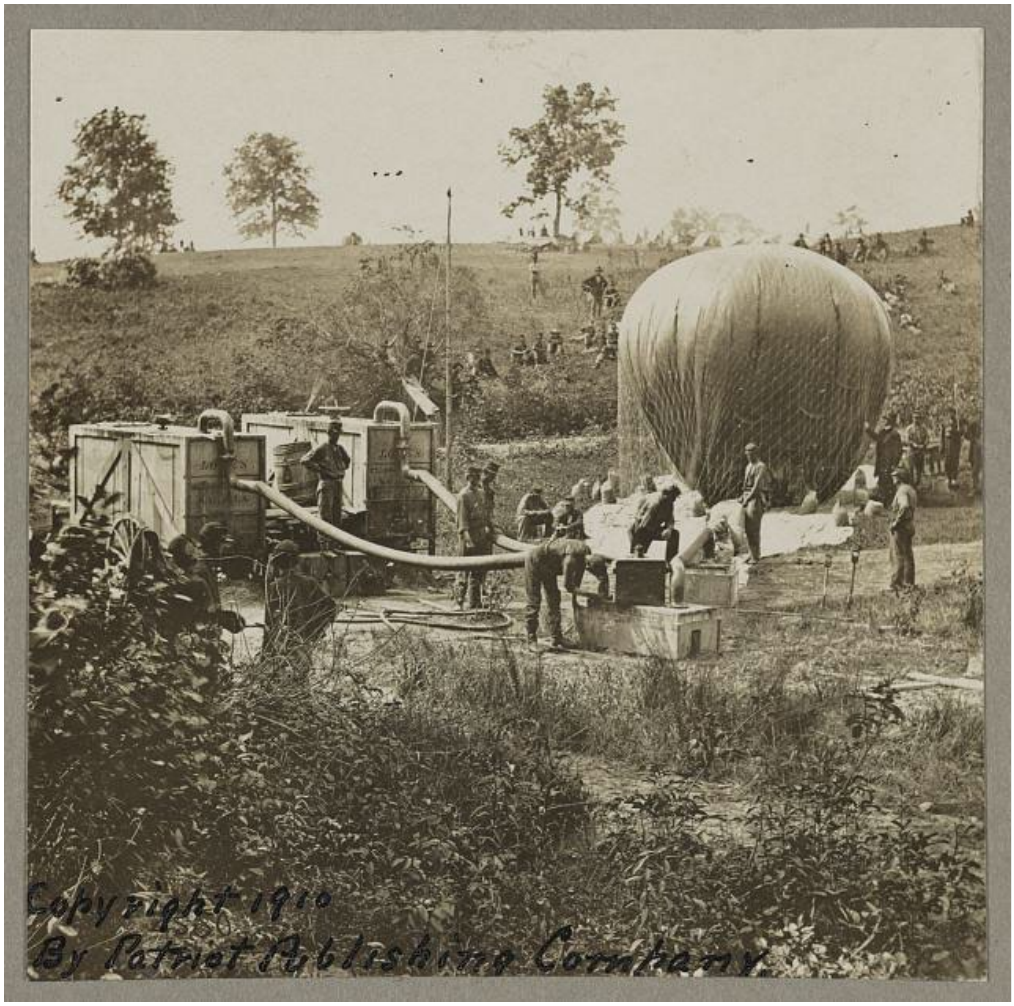


Figure 1-2: Lowe's military balloon near Gaines Mill, Virginia, May 1862.Lowe stands to the right with his hand on the envelope. The portable hydrogen generators can be seen in to the left of the balloon.

Source: Library of Congress Prints and Photographs Division, http://www.loc.gov/pictures/resource/ppmsca.33091.

Perhaps the most significant contribution of Civil War balloons was the inspiration provided by Count Ferdinand von Zeppelin. After he viewed one of Lowe's flights, he returned to Prussia inspired to develop his own airships. Military ballooning continues to evolve rapidly, and by World War I, both sides were deploying balloons for intelligence and to direct artillery fire [5], [6]. War is a unique motivator for technology development [7].

2.4.2. Airships

Henri Giffard successfully demonstrated a steam-powered airship in 1852, but it wasn't until July 1900, when the first Zeppelin model flew, that airships truly emerged on the scene. As briefly mentioned above, the use of airships in World War I is also when the balloon was first recognized as having a significant impact on warfare. Hence, the development of the airship and military ballooning is firmly entwined.

It is at this point that these topics begin to sharply diverge from the topic of scientific ballooning, and there are numerous resources on the topics of military ballooning and airships available for the reader to peruse [6], [8]-[11].

2.5. 1900 Helium, Rubber, and Sport Ballooning

2.5.1. Helium

Helium was discovered in 1868 as a bright yellow line in the Sun's spectrum during solar eclipse observations by Jules Janssen. This discovery has unusual ties to ballooning. At the time, the element was considered extraterrestrial and debated to possibly be a portion of another element rather than standing alone as something new. Janssen was rushing from Paris to Algeria to use an eclipse there to shore up his discovery just as Otto von Bismarck descended on Paris in what was termed the first blitzkrieg. To escape the siege, the French government began sending people up in hot-air balloons. Janssen himself used a balloon in an attempt to reach Algeria. He didn't make it via balloon and crashed near the Atlantic. He then boarded a train to Tours to arrange the remainder of his travel [12].

Jumping ahead to 1903, a natural gas well in Kansas failed to burn, disappointing the well owners and crowds of onlookers. It took 2 years before researchers at the University of Kansas were able to separate the various gases and identify that they contained helium. Contrary to contemporary scientific thought, this element was not just available from space. Many years would elapse before a representative from the US Bureau of Mines would suggest the military mine, extract, and store helium for use with lighter-than-air crafts for the Allies in World War I. Once again, war became a catalyst for technological advancements. The

benefits of helium as a lift gas were readily apparent: it has lift power similar to that of hydrogen without the risk of fire [13].

2.5.2. Rubber

The rubber industry had steadily grown since the discovery of vulcanization in 1839 made more practical uses for natural rubber feasible. Applications for this material expanded while, simultaneously, the aeronautical awakening occurred. Around 1910, the Goodyear Company conducted a brief, but unsuccessful trial of rubberized fabric for wing coverings. It was decided that balloons and airships were a much better market for such fabric. Additionally, since there was no fully established manufacturer of lighter-than-air (LTA) aircraft in the US, it appeared that there were no barriers to developing their own complete product in this field. Similar to free balloons (unguided and untethered), the components of the overall problem are as follows: material, general configuration, size, and panel geometry, assembly, flight testing, and operation. It would take some time before these craft begin to resemble the modern Goodyear blimp.

Using rubberized fabric they had already developed, Goodyear designed and built both balloons and airships. Material strength was not a critical factor since a net would take the majority of the load; hence, the spherical shape of a balloon was retained due to its maximum volume-to-weight ratio. This did not take into account the actual deformation of the shape in free flight with an open appendix (like a hot air balloon) of usual length and with a net proportioned to make its circumferential stress one-quarter of its meridional stress (width of each diamond mesh one-half of its height).

Two manufacturing strategies were considered to approximate a sphere from initially flat panels: 1) the commonly used meridional-gore system and 2) conical rings. The latter was chosen for the first balloon, primarily for its appearance and to facilitate arranging the panels in a brick fashion, thus avoiding four thicknesses of material at the corners. Each circumferential ring had the same number of identical panels except near the extreme top and bottom, which allowed for seam overlap. The number of panels per circumference was dictated by the need to economize labor and, at the same time, avoid excessive trim waste. Each pattern had typical dimensions tabulated as follows: chord length and offset for the convex and concave sides each, and width (end dimension). The chord length and offset, setting up the required arc length and radius, were determined by direct measurement on a simple double-bow device shaped to closely approximate a circular arc of any desired long radius which was set by a central screw. The bias ply was run in the same helical direction (not herringbone) around the balloon, since the resultant slight twist about the center axis would be of no conceivable harm in a free balloon.

Seam construction was a multi-step process in which seams were first cemented, then sewn, and then taped, following the same fabrication procedure as that for the Vaniman airship envelope. The sewing was always a major headache, however, as the cement kept fouling the machines. Later, a properly made and aged seam was found to be adequate without the sewing, reducing one step in the process. Some experimenting was done with small, varnished balloons. Varnishing reduced gas loss through diffusion and pin holes but it never became a widely accepted method because of the difficulty of tethering an essentially rigid, spherical balloon. Sticking, cracking, and spontaneous combustion were other difficulties that forced the abandonment of this technology.

A fabric testing program at Goodyear progressed in parallel with the development of the airship. This program produced results of interest in ballooning, such as the significant difference in yield between the warp and weft directions, and the extremely large local yield in the diagonal direction of a single ply. Early tests showed that the strength of a sample tested in a standard tensile machine was deceptively high compared to the strength of a sample under long, continuous loading. The reduction of strength that occurred under continuous load seemed to reach its minimum after one or two days. Accounting for random material variability, it was determined that none of the fabrics tested could be expected to hold more than about half of the machine-tested strength for any appreciable length of time.

Another important material test was resistance to exposure. In this program, hundreds of samples were labeled, dated, and exposed to the elements on the roof of the lab and then strength-tested at specified intervals. In general, the rubberized fabrics were much more affected by sunlight than by any other factor. Almost all samples proved capable of withstanding a winter of cold, wet, ice, and snow, but many were on the verge of falling apart after a month of hot summer sun. Samples kept in the shade fared better. A fabric found most resistant to such deterioration was one heavily compounded with carbon black and externally aluminized. In 1919, this fabric was used in the construction of a racing balloon, Goodyear II, that aeronauts and Goodyear scientists Ralph Upson and Ward Van Orman piloted to win the 1919 National Balloon Race (US).

A series of tests on internal heating due to radiation was also conducted. For this purpose, closed fabric envelopes containing thermometers were exposed to identical conditions of the sun. From its appearance, the aluminized fabric mentioned earlier seemed a likely candidate for minimal heating, but to save time, it was not actually tested prior to the construction of the balloon. Its flight performance was somewhat disappointing in this respect, and a subsequent comparative test showed it to heat more than the yellow fabric used in Goodyear I, possibly because of the carbon black under the thin aluminum surface, as a similar fabric without the aluminum heated the most. A chalky white

surface was the best, although not much better than yellow. No transparent material was tested, as none appeared suitable for balloon use at the time. The result of these considerable studies of fabric properties led to fabric improvements [15] that laid a foundation for modern airship design.

In 1923, a balloon designed by Upson but manufactured by Goodyear was tested with complete success. This balloon [17] is notable as a transitional design between early and modern styles. It had a single thickness of white, rubberized, woven fabric laid in a herringbone fashion, as in an old Upson parachute patent, and was strengthened with meridional load-carrying tapes. These tapes were fixed into a heavily reinforced conical cap at the top. The bias-laid fabric was self-adjusting to the effects of varying volumes and pressures. The conical top perfectly shed rain and was fitted with an offset valve and an equatorial rim, the latter serving also to dampen the vertical motion, a feature not recommended for use with helium, however. The single, precise offset valve served all gas discharge purposes except quick deflation, for which a conventional rip panel was provided.

The following year (1924), Van Orman continued Upson's innovative use of white, single-ply fabric in Goodyear III with an envelope weighing 315 lbs., compared with 720 lbs. for the similarly-sized Goodyear II. In this and subsequent balloons, up to Goodyear X in 1933, Van Orman set a phenomenal record, winning five national and three international distance races, beating Belgium's Ernest Demuyter, the previous three-peat winner of the Gordon Bennett cup. A similar single-ply fabric was used in the altitude record-breaking flight of Explorer II, piloted by Captain Albert Stevens and Captain Orvil Anderson, both of the U.S. Army Air Corps, in 1935. Other improvements by Van Orman included the use of a radio compass and celestial navigation, both of which were later adopted by air and ocean navigators alike.

In 1925, Goodyear introduced a major design change. This airship more closely resembled its Zeppelin cousin. It was non-rigid and helium-filled. Named "Pilgrim," this airship marked the start of Goodyear's Blimp program [17]-[18]. At this point, the evolutions of helium, airships, and materials briefly merge to bring about this resounding success. Due to these developments and successes, Akron can be referred to as the "Kitty Hawk of balloon flight".

Structural and aerodynamic experience with kite balloons and airships, particularly the metal-clad Zeppelin Metal Clad 2 (ZMC-2) [19], resulted in indirect benefits to all balloon development. In parallel, rubber and neoprene balloons had been improved to an extent permitting instrumented flights to altitudes previously unreached by the more conventional, vented type. However, the inevitable bursting of the balloon at altitude was a significant barrier to prolonged flight.

Vacuum balloons are still quite impractical, but the same type of equations, with modern materials, have parallels to the feasible application to super-pressure balloons. A generally sound example of such an application is in the mathematics of Albert Francis Zahm [20], an early aeronaut and professor of mathematics at the University of Notre Dame from 1885-1892. Zahm's work describes the relationship of stress and elastic yield required to maintain altitude in the event of gas leakage in a balloon envelope. As may be noted in the Appendix 1-A. Timeline of Balloon History, the super-pressure idea was also proposed by Melvin Vaniman in 1912. The first structure capable of acting in this manner, however, was the metal-clad ZMC-2 launched in 1929. Validated strength of the metal and seams, confirmed by water-model tests, showed that the hull could carry an ample reserve of pressure for altitude stabilization, although this was not an important feature in airship operation under power, where the propeller was also capable of altitude adjustment.

2.5.3. Sport Ballooning

As previously discussed, military conflict provides significant motivation for technological advancement. Motivation through sporting conflict can prove just as prolific without the devastating consequences. Contestants are motivated by the desire for money, fame, and recognition rather than money and conquest.

In 1898, the term "scientific ballooning" was applied to physical and atmospheric research. Later, it was applied to the use of scientific principles in balloon operation, replacing the largely rule-of-thumb techniques that were almost exclusively used up to 1913. These principles were first applied mainly to winning balloon races with the objective of spanning the greatest distance from the starting point. As outlined in Joseph Vaeth's *They Sailed the Skies: U.S. Navy Balloons and the Airship Program* [16], the operational improvements introduced after 1913 included better instruments, precise navigation, a means of sounding for air currents, and the establishment of quantitative balloon response to measured discharge of gas and ballast through the use of a stopwatch with a calibrated gas valve; all of these were coupled with the then-current best possible appraisal of the general weather conditions (literal appraisal or observation).

The Coupe Aéronautique Gordon Bennett (Gordon Bennett Cup) is the oldest and most well-known balloon race. The first was held in Paris in 1906 and, although interrupted by wars, it has been officially reinstated by the Fédération Aéronautique Internationale (FAI) since 1983 (see Figure 1-3 for an example of an early balloon). Several names previously mentioned have won or nearly won this race while making advancements in balloon technology. It is interesting to note that this race still utilizes hydrogen as the primary lift gas even in modern times.

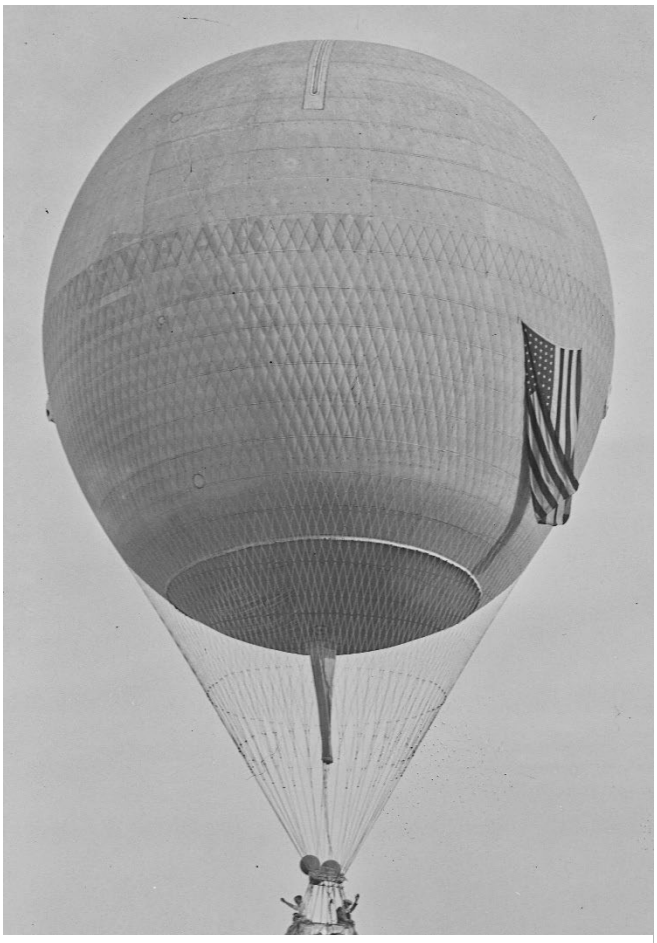


Figure 1-3: Goodyear III balloon at the 1925 Gordon Bennett Race, Brussels, Belgium

Source: gallica.bnf.fr / Bibliothèque nationale de France

A few sport balloonists of note who contributed to balloon design as well are Ralph Upson and Ward Van Orman.

Ralph Hazlett Upson (June 21, 1988 – August 13, 1968) won the Gordon-Bennett International Balloon Race in 1913 using the Goodyear I (then simply Goodyear) balloon. He began working for the Goodyear Tire & Rubber Company in 1910, straight after college graduation. He was essential to their manned balloon flight program and, during World War I, contributed to the development of the US Navy's and US Army's airships. He left Goodyear in 1920 and designed the world's only all-metal stressed-skin airship through his own company, the Aircraft Development Corporation. He went on to teach at the University of Michigan, New York University, and from 1946 to 1956 at the University of Minnesota.

Ward Van Orman (September 2, 1894 – March 11, 1978) was a lifelong employee of Goodyear Tire & Rubber Company. Orman was also employed by Goodyear directly out of college, where he notably graduated with a perfect 4.0 GPA. He produced many inventions for Goodyear, but, more notably, in the sport of ballooning, he won five annual US national balloon races and the first-ever Litchfield Trophy. He participated in ten and won three International Gordon Bennett Races, and during the 1925 race, he most spectacularly restrained a distraught and intoxicated partner and managed an emergency landing at sea onto a German freighter. Although he technically won the race, he was disqualified for not landing on 'land' [11].

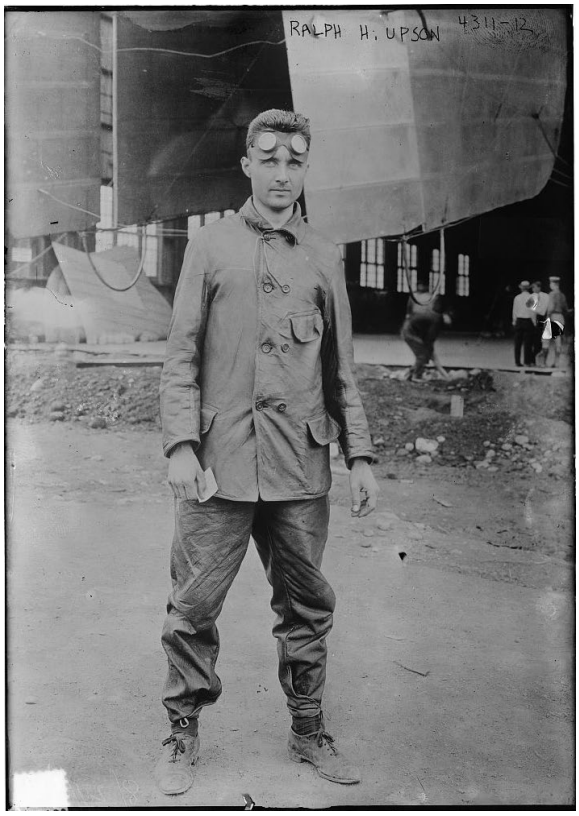


Figure 1-4: Ralph Upson after dirigible flight, 1917

Source: Library of Congress

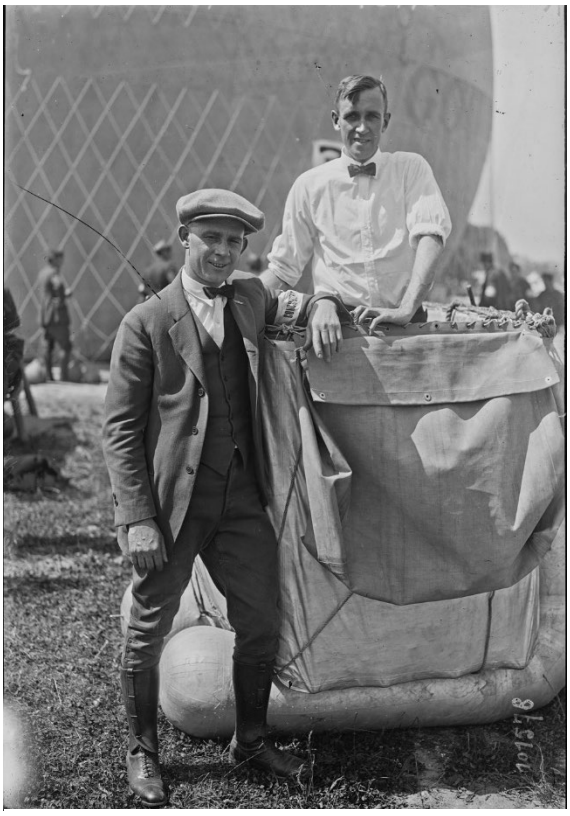


Figure 1-5: Ward Van Orman [r] with C.K. Wollam, 1925

Source: gallica.bnf.fr/BnF



Figure 1-6: Launch day of the 50th Gordon Bennett Cup in Waasmunster, Oost-Vlaanderen

By Larry and Linda Ellis - originally posted to Flickr as GordonBennett_0609_2_Launch_48, CC-BY, https://commons.wikimedia.org/w/index.php?curid=11641899

2.6. 1930 Stratosphere, Plastic, and the Natural Shape

2.6.1. Stratosphere

The next breakthrough in ballooning was in achieving higher altitudes. In 1901, Arthur Berson and Reinhard Süring reached 10,800 m (35,430 ft) in an open gondola launched from Berlin, Germany [21], [22]. They held that altitude record until 1927 when Captain Hawthorne Gray launched from Scott Field, Illinois, and reached 12.9 km (43,000 ft) [23]. Teisserenc de Bort coined the term "stratosphere" in 1902, when he presented data from approximately 200 balloon flights that showed the temperature remained constant at a certain altitude as one gained additional altitude. To that end, Auguste Piccard Paul Kipfer are recognized as the first people to reach the stratosphere using a

pressurize gondola launched from Augsburg, Germany that reached a height of 15.8 km (51,775 ft) [24]. Auguste Piccard and Max Cosyns set a new record in 1932 with a flight from Dübendorf Airfield in Zürich, Switzerland that reached 16,201 m (53,153 ft) [25], [26].

The US and the Soviet Union engaged in a little-known Space Race in the 1930s, competing for highest altitude achieved via balloons. On November 20, 1933. Lt. Cmdr. G. W. Settle (USN) and Maj. Chester Fordny (USMC) flew a 60,000-cubic-foot hydrogen-filled balloon (built by the Goodyear Company) to an altitude of 61,237 feet. In a quick follow-on, the Soviet Union launched a manned balloon on January 30, 1934, attaining an altitude of 72,200 feet, beating the American record, but its three-man crew was killed when the capsule crashed [27], [28].

A 3 million-cubic-foot helium balloon was next, named Explorer I. The flight launched from a box canyon, which would shield the balloon until it was fully inflated. The spot, located near Rapid City, South Dakota was named "The Strato Bowl" [29]. An issue with the canopy on Explorer I forced the flight to terminate early. Explorer II was quickly constructed by Goodyear, and another attempt was made. The inflation required 300+ personnel from nearby Fort Mead to handle the inflation and the crowds. The balloon launched on November 11, 1935, reached an altitude of 72,395 ft [30]. This effectively ended the balloon space race, as World War II would dominate the world for the next decade.

2.6.2. Plastic

Our current era of high-altitude scientific ballooning truly began when a new material was introduced to construct the balloon envelope: plastic. In general, a flexible, high-strength film permits making the balloon a self-contained unit without requiring a net to carry the load, resulting in weight savings that greatly extend the altitude capability.

The goal of cosmic ray research was to reach increasingly higher altitudes to understand the origin of atmospheric ionization radiation. In 1933, Arthur Compton, a physicist at the University of Chicago and 1927 Nobel laureate for his discovery of the particle nature of electromagnetic radiation, gave a lecture on the current state of cosmic ray research and prevailing theories about their origin and significance, including a "romantic" notion that proposed what is now known as the Big Bang Theory [31].

At the time of Compton's claims, the highest flight achieved for science purposes (an unmanned balloon carrying only instruments) was conducted by Erich Regener, reaching an altitude of 27 km (~90,000 ft) while working at the University of Stuttgart and, later to 28.1 km. Regarding ballooning, Regener innovated on previous experiments by encasing his gondola in cellophane plastic, turning the gondola into an effective

greenhouse that maintained the instruments at roughly room temperature [32].

Given Auguste Piccard's work and standing as a stratospheric aeronaut, tt should be no surprise his twin brother, Jean Piccard, also a physicist, got into ballooning. Jean made a splashy debut at the 1933 Chicago World's Fair with a sponsored and instrumented balloon named after the World's Fair, *Century of Progress,* piloted by sport balloonist Thomas "Tex" Settle. The flight itself was cut short due to a failed valve, but a second flight on the same balloon proved more successful, with a 2-hour flight to an altitude of 18,665 km (61,237 ft). After these two flights, the balloon was turned over to Jean, who conceived of a flight in which his wife, Jeannette, would pilot and he would operate the science instruments. They struggled to find sponsors due to the perceived risk to a wife and mother, but eventually found funds for a 1934 flight that lasted eight hours and reached an altitude of 17.55 km (57,579 ft), marking Jeannette as the first woman to reach the stratosphere.

Jean Piccard and Thomas H. Johnson of the Bartol Research Foundation began to experiment with new materials. They constructed a single-use cellophane balloon using 'orange peel'-type gores adhered with 1-inch 3M Scotch tape. This balloon was motivated by Johnson's drive to fly cosmic ray instruments, but before the balloon could be flown, Piccard moved to the University of Minnesota (UMinn), where he was offered a position as a Special Lecturer. Johnson and Piccard then worked in parallel on the cellophane balloons, and Piccard is credited with the first plastic balloon flight on June 24, 1936. Piccard continued the development of balloons with John D. Ackerman, a professor in the aeronautical engineering department at UMinn, using latex, [33] and additional uncrewed flights were conducted.

Polyethylene, another type of plastic of interest, was discovered by accident in 1933. It wasn't until 1933 that chemists at Imperial Chemical Industries (ICI) discovered practical uses. It was difficult to reproduce until another ICI chemist refined the process, and industrial production of low-density polyethylene began in 1939. This plastic gained popularity quickly and became the first to sell more than a billion pounds a year in the US [34]. Linear low-density polyethylene (LLDPE), which is used by NASA in modern times, wouldn't be introduced until 1978 [35].

Jean Piccard was reintroduced to Otto Winzen around 1945 when proposing a new balloon project to the U.S. Navy (Pleiades II). Pleiades II was proposed to be a spherical capsule with a cluster of cellophane balloons. Winzen, then chief engineer for the Minnesota Tool and Manufacturing Corporation, was interested in working with Piccard to find a material that was lightweight, inexpensive, and more flexible and radiation-tolerant than cellophane. Polyethylene was the ticket. The Navy approved

the project and renamed it to Project Helios and the cellophane was replaced with polyethylene. Piccard and Winzen approached a local manufacturing company, General Mills, to design the capsule. Winzen went to work for General Mills shortly after the capsule was built and designed the first polyethylene balloon that they manufactured. The Helios balloons and the succeeding ones of polyethylene built by the General Mills Company had a rough approach to a natural shape approximated by a cone-on-sphere [33], [36]. The cluster design was soon abandoned due to launch difficulties but the project paved the way for Project Skyhook.

2.6.3. Natural Shape

The evolution to a natural shape balloon, also called a tapered shape, was a significant improvement on the distribution of stress across the film. This design is derived mathematically and increases predictability for the internal gas pressure at the apex, volume of the balloon, and buoyant lift. These changes to the shape of the balloon reduced pendulum motion, altitude fluctuations, and stress concentrations. It played hand in hand with the development of polyethylene films to enable larger payloads at higher altitudes. The full mathematical evolution and derivation can be explored in Chapter 9.

2.7. 1950 Minnesota and Modern Scientific Balloons

2.7.1. Modern Scientific Ballooning

Minnesota and more specifically, Minneapolis, became a hub for balloon development in the 1940s due to a convergence of several factors. First, Minneapolis was the location of General Mills. Although known more commonly then and today as a flour and cereal company, the mill did have an engineering division. Focused on improving cereal production and bag sealing, this engineering group pivoted during World War II to support the war effort and General Mills began supplying the military with precision equipment. This division was maintained throughout the war and after [40]. Second, Minneapolis was the location of the University of Minnesota, which hired Jean Piccard as a lecturer from 1936-1952. During his tenure, Jean Piccard would teach and inspire others who would later become influential in ballooning, such as Edward Ney who was taught by Piccard as an undergraduate and returned to the university to teach and research cosmic rays. Third, it was the location of the Minnesota Tool and Manufacturing Corporation, which hired Otto Winzen after World War II as chief engineer. Otto Winzen had previously met Jean Piccard while studying aeronautical engineering at the University of Detroit Mercy, who, incidentally, introduced him to his wife, Vera Habrecht. Sources vary on the exact details, but sometime during his time there, Otto reconnected with Jean Piccard and moved to the aerospace and electrical division in General Mills to work on balloon contracts in collaboration

with the Piccards. Otto and Vera eventually established Winzen Research Inc. in which Vera and her "balloon girls" took an active role in balloon manufacture and quality assurance. James Winker is another early foundational member of this Minnesota group, although he was about eight years behind Winzen and J. Piccard. His early work with General Mills and, later, as chief engineer at Raven Industries, laid the foundations for the current static and dynamic launch techniques employed by NASA and others for very large stratospheric balloons.

Thanks to Piccard and Winzen, The University of Minnesota and General Mills (and later Winzen Research, Inc) played a significant role in executing several military contracts (Helios, Manhigh, Mogul, Moby Dick, and others) from the 1940s to the 1960s. The companies and military branches are so intertwined that it is not always apparent where the credit for developments should be placed [43]. These contracts and the combination of helium, polyethylene, and the natural shape design effectively bring us up to present-day ballooning, Figure 1-7. Piccard and Winzen would settle on their ideal design, which they coined Skyhook. The addition of load-bearing tapes at each gore's seams dramatically improved the flight vehicle's reliability. Over 1,500 Skyhook balloons flew to support scientific investigations in the 1940s and 50s. In 1956, the University of Minnesota launched a Mylar balloon, courtesy of the Schjeldahl Corporation, to set a new altitude record for uncrewed balloons at 145,000 feet. Winzen astutely filed various patents for balloon design, construction, and launching methods still used today [41]-[43].

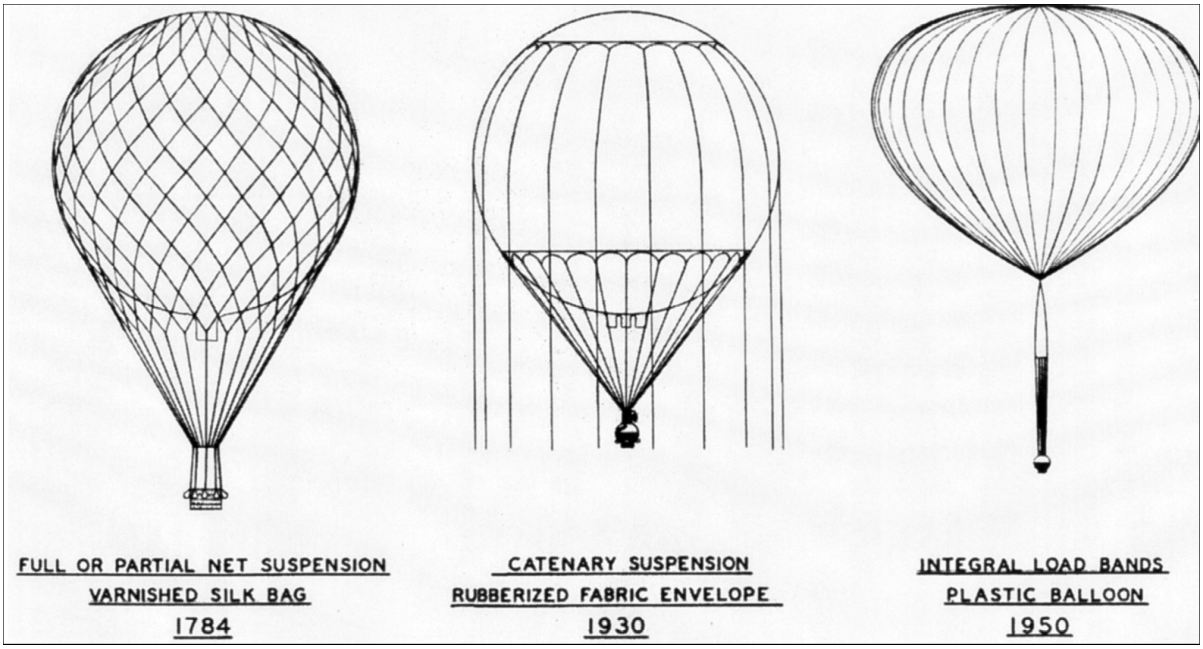


Figure 1-7: Evolution in balloon shape and design from Montgolfier at left, Piccard in the center, and Winzen at right.[44]

The goals of many of these balloon projects were to study astronomy and atmospheric physics while collecting data on human physiology at high altitudes. As part of this effort, several space suits were tested for eventual use on Project Mercury. Manhigh studied the effects of cosmic rays on humans, and followed on Excelsior, which tested parachutes from high altitude. It is noted in the Project Manhigh documentation that the Winzen manufacturing process changed the game in terms of quality control of the film and shape [45]. Schjeldahl's most significant contribution was the process of sealing and trimming the material with a hot knife that was initially used to make bread bags [46]. Also not explicitly stated was the decision by all US programs to adopt the use helium instead of hydrogen, given the increased safety, reliability, and availability of the gas in the US. Project Strato-Lab solidified the natural shape balloon and introduced a launch stress index to mitigate uneven stresses in the canopy during inflation and ascent (refer to the zero-pressure balloon chapter, Chapter 9 for more information) [43], [47]. Project Strato-Lab also utilized a valve at the apex of the balloon to control altitude. The method of clamping the film in the top plate, the valve (dubbed "EV-13"), and encasing the valve wiring in a polyethylene sleeve down a side seam of the balloon is still used today [41].

Project Moby Dick was a particularly controversial use of balloons to spy on the Soviet Union during the Cold War; remnants of a camera and balloon were discovered by the Soviets in 1956. It was followed by several other reconnaissance balloon projects (Mogul, Skyhook, Grandson, and Genetrix). Several also flew nuclear detection technology using infrasound, which is still used today.

Although helium would become the standard, throughout much of these programs, both hydrogen and helium gas were used as the lift gas. The long and successful record in using flammable gas for free balloons seems to justify re-evaluating hydrogen for the more demanding of these conditions, considering the skin material's electrostatic properties, avoidance of flame in operation, and suitable precautions generally. Experience shows that Mylar is much more prone to static sparks than polyethylene.

2.7.2. Women in the Stratosphere

The brief mention of Jeanette Piccard and Vera Winzen above is endemic in recorded history. The role of women and their achievements throughout time have been regularly glossed over. Élisabeth Thible was the first recorded woman to fly in a hot air balloon. Thible made her ascent in Lyon, France, on June 4, 1784, in a Montgolfier balloon. Her flight, lasting 45 minutes to a height of 1500 m, was only a year after the Montgolfier brothers' first crewed flight. She sang two arias while in flight, and some speculate that the reason she got the position was due

to the original passenger's fear because a previous Montgolfier balloon had caught fire earlier that year [51], [52].

The first professional female balloonist was likely Sophie Blanchard. After the death of her aeronaut husband, Jean-Pierre Blanchard, Sophie continued their work and became famous for her solo flights across Europe. Napoleon Bonaparte appointed her as the "Aeronaut of the Official Festivals." Although she started her career because she thought the novelty of a woman flying would draw crowds and money, she took the role seriously and performed over 60 recorded ascents. Unfortunately, she was also the first woman killed in an aviation accident when she launched fireworks from her balloon in Paris in 1819. The fireworks ignited her balloon, which then crashed onto a roof [53].

Aida de Acosta Root Breckinridge was 19 in 1903 and captivated by a dirigible flight she witnessed in Paris. A Brazilian aviator, Alberto Santos-Dumont, gave her three lessons before she flew solo. As an up-and-coming socialite, her parents were scandalized. But it was also said that Santos-Dumont never let anyone fly his airship except for Aida. She was the first woman to solo a powered dirigible (a full six months before the Wright brothers flew in Kitty Hawk) [54], [55].

In 1906, Marie Surcouf started a women's ballooning club in which men could be members but only ride as passengers and had no decision-making rights. The club was called La Stella. She is quoted as stating that (translated from French)

> "The sportswoman does not, believe it or not, erase the feelings of the woman. The empire of the air belongs to everyone, and who would dare to dispute that women do not have the right to conquer the stars. What men achieve through their muscular strength and physical endurance, women also achieve through their will, tenacity, and courage" [63].

Jeannette Piccard (Figure 1-8) was the first woman to fly to the stratosphere, reaching an altitude of 57,579 feet on October 23, 1934, in the balloon, Century of Progress, with her husband, Jean Piccard, in an eight-hour flight over Lake Erie. She later became the first licensed female balloon pilot in the United States. Jeanette earned a Bachelor of Arts from Bryn Mawr and a Master of Science in Organic Chemistry from the University of Chicago. She was a mother in a house full of boys and taught at the University of Lausanne and the Massachusetts Institute of Technology. After moving to Minnesota, she earned a Ph.D. in Education from the University of Minnesota in 1942 and a certificate in theology from the General Theological Seminary in 1973.

More than three decades after her stratospheric flight, while working as a NASA consultant, Piccard narrated a film about the expedition. After

her voiceover, an interviewer read from her preflight checklist, which included the task "wipe windows." He smiled at her and said, "Everything changes but the eternally feminine."

"Oh, there was nothing feminine about that," Piccard replied. "That's a safety engineer. You don't take off with dirty windows or windows that will frost up. Her work helped pave the way for future research into high-altitude and space flight [56], [57].

Vera Simons (previously Winzen née Habrecht) (Figure 1-9), wife of Otto, helped to found Winzen Research Inc. in 1949. She held over two-thirds ownership and eventually became vice president. She supervised and trained her "balloon girls" to handle the polyethylene and build the massive balloons with extreme precision and tight quality control, Figure 1-8. She held four patents for balloon construction techniques and envelope redesign. She earned a gas balloon pilot license in 1957 and represented the U.S. in the 30th Annual Gordon Bennett Race in Holland [58], [59].

As briefly mentioned in our section on Sport, the Gordon Bennett Cup is the oldest and most prestigious event in aviation. It is a long-distance gas balloon race where the goal is to fly the furthest non-stop distance from the launch site. The race was initiated by James Gordon Bennett, Jr. in 1906, and has continued throughout the 20th century. The competition is judged solely on distance traveled, with teams strategizing to maximize their flight path. Many women have participated over the years. A prominent modern female balloonist, Lindsay Muir, has won numerous international ballooning competitions and is known for her



Figure 1-8: Jeannette Piccard after a balloon landing circa 1934.

contributions to promoting women in the sport [60]. Carol Rymer-Davis was the first woman to win the Gordon Bennett Cup in 2004. She tragically died in 2010 during another race when their balloon went missing [61]. Marie Goldschmidt of France was the first woman to compete in the Gordon Bennett race, as pilot 2, finishing 6th in the 1913 race [62].



Figure 1-9: Vera Simons shown here as part of DaVinci II crew in 1976. Verea was founder and co-owner of Winzen Research, Inc.

Source: National Air and Space Museum Collection

2.8. 1960 Establishment of NSBF and Sport returns to Hot Air

2.8.1. NSBF

By the mid-1950s, responsibility for balloon-based science shifted from the military to civilian agencies. In 1961, the National Center for Atmospheric Research (NCAR) began coordinating stratospheric balloon efforts with NSF funding, paving the way for more structured scientific campaigns. In 1962, NCAR, with approval from the Federal Aviation Administration (FAA), requested that the National Science Foundation (NSF) establish a permanent scientific balloon launch facility in Palestine, Texas. The resulting National Scientific Balloon Facility (NSBF) was intended to provide year-round launch services for the research community. An important side benefit was the consolidation of launch expertise and the development of standardized support systems, which NCAR readily shared with the broader ballooning community.

During this period, the U.S. Navy, U.S. Air Force, Winzen Research, Inc., Raven Industries, Inc., Sheldahl Flexible Technologies, Inc., and General Mills, Inc. all operated active balloon programs. Advances in launch procedures and ground support equipment had improved reliability, enabling the use of larger balloons and heavier payloads. In the 1960s, a 0.085 million cubic meter (3 MCF) balloon was considered large; yet by 1968, NSBF successfully launched a 0.57 million cubic meter (20 MCF) balloon with a 3,052 kg gross load and a 42-hour flight duration. In 1975, the facility flew its first 1.5 mcm (50 MCF) balloon, meeting the science community's calls for higher float altitudes, greater lift capability, and longer flight durations [64].

By the late 1960s, computational analysis was emerging as a valuable design tool. Between 1963 and 1966, Justin Smalley published a series of ten reports titled *"The Determination of the Shape of a Free Balloon," building on research conducted at the University of Minnesota*. His work introduced normalized design parameters, expanded design tables, and provided a Fortran program for calculating balloon shapes—laying the groundwork for the computational methods that would later be integrated into modern design and finite element modeling.

On October 1, 1982, NSBF separated from NCAR as sponsorship of CSBF transferred from NSF to NASA. NASA established the Balloon Program Office (BPO) and the Balloon Working Group to advise the program on technical performance and management needs [65], [66]. In 2006, the NSBF was renamed the Columbia Scientific Balloon Facility (CSBF) to honor the astronauts who lost their lives on the Space Shuttle Columbia. As a nearby federal facility to the debris field, the NSBF served as the focal point for debris recovery [66].

During this time, high-altitude flights became more international. Japan developed its own stratospheric program, and Sweden's Esrange center began flying microgravity drop experiments using high-altitude balloon platforms. Brazil and India, by contrast, emphasized the continued use of hydrogen due to established infrastructure and cost advantages — a contrast to the U.S.'s helium-dominated approach. Canada's private firm, Scientific Instrumentation Limited, even maintained a small-scale scientific balloon effort after federal support declined. These examples reflect a global diversification of ballooning goals and infrastructure [67].

2.8.2. Hot-Air Sport Balloons

Since the mid-20th century, hot-air ballooning has undergone significant transformations driven by innovations in materials, burners, envelope control, and operational practices. The modern era begins with Ed Yost and colleagues at Raven Industries (later Aerostar), who developed propane-fired burner systems and heat-resistant synthetic-fabric envelopes; Yost's first untethered free flight on October 22, 1960 (Bruning, Nebraska) demonstrated practical, reusable hot-air flight and launched a commercial/sport market [68]-[70]. Jim Winker, a longtime Raven engineer and historian, contributed to the design of balloons across gas and hot-air systems and helped systematize sport balloon engineering during the industry's formative decades [71], [72]. Through the 1960s–70s, the sport matured: FAA recognition and handbooks codified training and airworthiness; manufacturers such as Cameron and Lindstrand professionalized design/production; and operational equipment evolved toward dual-redundant burners, improved fuel systems, and standardized maintenance [73]-[75]. A pivotal control innovation — the parachute valve ("parachute top") — is credited to Tracy Barnes/The Balloon Works and enabled repeatable venting/deflation rather than single-use rip panels; turning vents/rotation vents became common for in-flight yaw alignment [73], [75], [76]. From the late 1970s onward, record-setting projects showcased long-duration and global capability using hybrid Rozière balloons (hot-air + helium), culminating in Breitling Orbiter 3's first nonstop circumnavigation in 1999 and subsequent solo round-the-world flights—high-visibility milestones that leveraged modern envelopes, high-output/quiet burners, pressurized gondolas, and satellite navigation/communications [23], [77], [78]. Today's sport systems carry forward these advances — ripstop nylon or polyester with load tapes, multi-burner redundancy, parachute/turning vents, and standardized maintenance — within an updated regulatory environment (e.g., ADS-B LOA policies for Class C airspace), reflecting a continuous lineage from Yost's and Winker's Raven era to contemporary competitive and recreational ballooning.

2.9. 1980 Material Selection, Development of Long-Duration Heavy-Lift Balloons and First Extraterrestrial Balloon

2.9.1. Material Selection

By the mid-1960s, the rapid growth in balloon size and payload mass was accompanied by an alarming rate of burst failures, particularly between 10 and 18 km during ascent. These failures affected a range of operators, including Winzen Research, General Mills, Raven Industries, and the U.S. Air Force. Initial investigations showed that larger balloons were more susceptible to imperfections in the film, and that Cold Brittle Transition Temperature (CBTT) effects exacerbated by warm ground launches and extreme cold at the tropopause were a primary factor in material embrittlement and rupture. Professor Arnold Kerr (New York University) confirmed the link between film strength, stress levels, and tropopause temperature ranges, highlighting that differential pressure at the crown immediately after inflation was particularly critical [79]-[81].

Surprisingly, thinner polyethylene films (0.014 mm / 0.55 mil) often outperformed thicker variants (up to 0.051 mm / 2.0 mil) in consistency and tensile strength. Throughout this period, operational data including payload weight, balloon volume, film thickness, ascent rate, and atmospheric dynamics was collected to guide design refinements. The U.S. ballooning community also began using emerging computational analysis tools to correlate these variables with performance outcomes, setting the stage for later modeling work [82], [83].

By the late 1970s, an unusually high failure rate of heavy-lift systems (>1500 kg) led to a two-year moratorium on many high-altitude operations while a formal investigation was conducted. The review concluded that variability in film properties could lead to off-nominal balloon behavior, which is compounded by fabrication inconsistencies, launch dynamics, and weather conditions. In response, NASA's Balloon Program Office (BPO) launched a comprehensive R&D plan focused on structures, performance, materials science, chemistry/processing, and quality control [84].

The early 1980s again saw a spike in catastrophic failures during ascent, prompting a 1983 NASA study that identified film as the primary cause of the failures. In January 1986, NASA initiated the 18-month program Recovery Plan to:

- Standardize on 0.020 mm (0.8 mil) film.
- Implement stricter quality control in extrusion and sealing.

- Develop a dedicated flight-test program for qualifying improved films and designs.
- Cap flight configurations using a defined stress index.

The Recovery Plan also added permanent CSBF auditors in manufacturing plants, with NASA directing Winzen and Raven to search for alternative materials in cooperation with the Centre National d'Etudes Spatiales [CNES] (France). These efforts led to the long-term adoption of Stratofilm and later improved formulations. The U.S. National Bureau of Standards[2] performed microstructural analyses of films from different production periods, verifying that low-temperature elongation performance was key to preventing tropopause failures.

Innovations in film testing included biaxial tensile tests on capped cylinders and uniaxial tests that correlated mechanical properties with extrusion variables. Southwest Research, Inc. (SwRI) developed an in-flight film strain gauge that revealed significant stress in both meridional and circumferential directions—contradicting earlier assumptions that only one axis carried load in natural-shape balloons [85], [86].

Seal investigations by Winzen and Raven showed that weak heat seals were often due to boundary layer formation at the seal interface, aggravated by contamination or subtle changes in material composition [86], [87]. Adoption of new sealing specifications in 1986, along with optimized equipment and procedures, became a cornerstone of NASA's quality assurance process.

By the 1990s, these material, process, and QA improvements allowed for the design of larger, more reliable heavy-lift balloons, and the resulting NASA Standard Balloon Designs became the basis for qualification flights and modern performance modeling.

2.9.2. New Era Long-Duration Heavy-Lift

By the late 1970s, increasing demands for higher float altitudes and heavier payloads led to major structural refinements in balloon design. A key challenge was the extreme stress experienced in the apex region during inflation, launch, and ascent, as the upward force of the lifting gas concentrated on the crown of the envelope. To manage these loads, designers employed load tapes to distribute stress along the seams and adjusted gore patterns and widths to control whether the film acted as a load-bearing member or merely contained the lifting gas.

[2] The NBS later became the National Institute of Standards and Technology (NIST).

One of the most significant innovations was the use of caps — additional layers of material in the upper third of the balloon — to reinforce the crown. The first external-cap balloon flew in 1980, and in 1994, NASA conducted a direct comparison of internal vs. external caps. The results showed that internal caps became structurally ineffective during ascent as helium could migrate between film layers, while external caps remained effective throughout the flight [88]. External caps were therefore adopted as the preferred solution for sustaining structural reinforcement under dynamic flight conditions [85], [86].

Design refinements also addressed the need to model off-design shapes—balloons that temporarily depart from their fully inflated form during ascent or operational maneuvers. This required moving beyond the assumption of purely axial symmetry and adopting shape-finding methods that minimized system energy while satisfying material property constraints. Such modeling produced yield shapes that closely matched the observed in-flight behavior [86].

Structural studies further examined the placement of caps and the relationship between cap geometry and stress reduction. External caps were shown to mitigate concentrated loads at the crown, especially for heavy-lift systems exceeding 1500 kg, which are more susceptible to localized film overstress [85], [86].

The resulting best practices were incorporated into the NASA Standard Balloon Designs, which combine structural and material lessons into a consistent set of engineering specifications [87]. These designs—validated through dedicated qualification flights—set the template for modern heavy-lift, long-duration zero-pressure balloon configurations and continue to inform super-pressure balloon development.

2.9.3. Extra-Terrestrial Balloons

In 1984, the USSR launched the first VEGA Venus balloon. The program launched a total of five balloons by 1991 with the goal of gathering data on the Venus atmosphere and testing technologies critical to exploring new planets. The program was extremely successful, and the data is still being analyzed. To date, no other balloons have been deployed on another planet. Balloon technology is increasingly being adapted for planetary exploration. NASA has tested Mars balloon analogs in Earth’s upper atmosphere and explored Venus aerial platforms using phase-change lift systems. Balloon-based systems could float at 50–60 km above Venus, where temperatures and pressures are more Earth-like, offering a stable vantage point for atmospheric and geological research. These efforts illustrate ballooning’s potential beyond Earth — offering low-cost, high-altitude platforms for both exploration and technology demonstration. Further exploration of extra-terrestrial balloons is found in Chapter 16.

2.10. 1990 Global Infrastructure for Scientific Ballooning

As of the early 1990s, balloon operations had become a globally distributed activity. Bawcom (2012) identified 13 active programs at that time across Australia, Brazil, Canada, China, France, India, Italy, Japan, Sweden, the USSR, and the U.S. (via NASA and the Air Force), plus university-led efforts like Wyoming's [67]. Many of these programs were government-funded and supported both domestic and international users.

Launch sites built during this time and still in operation today include Alice Springs in Australia, the Sanriku Balloon Center in Japan, and Esrange in Sweden, each having distinct logistical and technical capabilities. For example, Alice Springs offers a 1,400 sq. ft. staging floor, while Sanriku employs a rotating launch clamp system for directional control. Esrange, located above the Arctic Circle, allows nearly continuous daylight tracking during summer launches.

NASA's Columbia Scientific Balloon Facility (CSBF) in Palestine, Texas, serves as the central operations hub for NASA-supported flights, conducting both domestic and international campaigns yearly.

2.11. 2000 Computer-Aided Design and Pumpkin Super-Pressure Balloons

2.11.1. Computer-Aided Design

Entering the 21st century, high-altitude balloon design has benefited from powerful computer-aided design (CAD) tools, finite element analysis (FEA), and advanced numerical modeling techniques capable of solving complex differential equations in minutes. These tools have enabled more precise prediction of balloon performance, stress distribution, and shape optimization across a wide range of flight conditions.

One prominent contributor to modern balloon design methodology is Rodger Farley, whose work expanded and updated the analytical framework established in the post-catastrophic failure era. Farley's refinements outline a systematic process for generating the shapes and configurations of natural-shape, zero-pressure balloons while integrating both historical analytical models and modern computational capabilities. His approach includes methods for calculating preliminary design parameters and for conducting more detailed analyses to account for structural, material, and operational constraints.

These updated analytical methods have allowed designers to more accurately model off-design configurations, incorporate material property characterization into simulations, and optimize gore and load tape layouts to better manage flight stresses. The improvements in

modeling fidelity have enhanced both the reliability and efficiency of balloon systems, extending operational envelopes for heavier payloads and higher float altitudes.

The integration of CAD and FEA into the design cycle has also shortened development timelines, reduced the reliance on large-scale physical prototypes, and provided engineers with rapid iteration capabilities. This shift has strengthened the connection between theoretical modeling, material testing, and full-scale flight validation—ensuring that modern balloon designs meet both performance goals and safety requirements.

2.11.2. Pumpkin Super-Pressure

Although super-pressure balloons (SPB) have been existed in a variety of forms for many years [119], many still believe the future of scientific stratospheric ballooning lies here. This design maintains positive differential pressure in the envelope throughout the flight and has the potential to provide ultra-long duration flight at a more stable altitude. When the balloon is fully inflated, the super-pressure style balloon has a positive differential pressure, internal to the ambient pressure. The pressurization allows the balloon to maintain a steady pressure altitude during the transitions between solar noon and midnight. The SPB is considered a game-changer for mid-latitude flights that experience extreme diurnal cycles [89]. However, there are various challenges related to the geometry of the balloon and the cutting patterns of the individual lobes. The modeling efforts are incredibly complex, and some, like the stress on the envelope throughout the entire launch process, have not been completed to date. Nonlinear creep and failure criteria based on strain instead of stress are still being investigated [90]. Chapter 10 dives into the specific changes in design and modeling that have occurred since 1975.

Prior to World War II, Japan had been researching applications for a hydrogen filled SPB that could be used to deliver explosives with a timed fuse up to 70 miles from the launch site. The project was initially pushed aside for more direct methods. Named Fu-Go, the balloons were constructed of five thin layers of washi (type-A) or rubberized silk (type-B). All in all, 285 balloon incidents were recorded by the U.S. Army as having reached North America. Many small fires were generated but only one lethal attack occurred when a group out for a picnic in Oregon came across an undetonated bomb suspended by balloon remnants. The bomb exploded and all six were killed. This prompted the U.S. press blackout to be lifted so the public could be warned of the danger of unexploded ordnance [117], [118].

SPBs for scientific endeavors were adopted soon after the end of the war. The U.S. Air Force used small mylar balloons to achieve stable, semi-permanent meteorological platforms. This program, titled Global

Horizontal Sounding Technique (GHOST), launched 88 balloons starting in March of 1966. The program lasted approximately 10 years with counterparts in NASA and the French government. These balloons mapped air circulation patterns and even transmitted data to a NASA meteorological satellite in 1970. This idea of transmitting data using a balloon in space was not new. The NASA Echo balloon was launched in 1960 by a rocket. It reached 1,000 miles above the earth, inflated, and orbited for 8 years. The balloon was effectively the first communications satellite as it reflected voice, music, and teletype signals from ground station sin the U.S. to receivers in Europe. The Echo I and Echo II balloons were both manufactured by G. T. Schjeldahl Co [119], [120].

Another exciting use of smaller SPBs will be to bridge the telecom gap. One notable company, Loon LLC (formerly Google Loon under the GoogleX program and later under parent company Alphabet, Inc.), had great success between 2011 and 2021 in flying small constellations of SPBs. Their goal was to bring mobile internet services to remote areas or during disaster recovery, such as after Hurricane Maria in Puerto Rico [91], [92]. This project was discontinued by Alphabet, Inc. in 2021.

2.12. 2010 Gondola and Instrument Improvements

Since 2010, scientific balloon gondolas and instruments have undergone substantial advancements in pointing stability, structural efficiency, avionics, communications, and payload integration. Precision pointing systems have seen some of the most dramatic improvements. NASA's Wallops Arc-Second Pointer (WASP) established a facility-class capability, using a rotator for coarse azimuth positioning and a two-axis gimbal for fine control to achieve arcsecond-class stability in engineering flights [93]-[95]. The Super Pressure Balloon-borne Imaging Telescope (SuperBIT) expanded this capability with a nested three-axis stabilized telescope, optical fine guidance, and a tip-tilt fast-steering mirror, delivering telescope pointing stability of ~0.34 ± 0.10″ and focal-plane stability of ~0.055 ± 0.027″ over five-minute exposures during a 45-night super-pressure balloon flight. Lessons from SuperBIT are informing the larger GigaBIT platform, which aims to scale these optical and control capabilities [96], [97].

These pointing achievements are enabled by sophisticated actuator and sensor suites. Systems such as SuperBIT utilize a high-torque reaction wheel for coarse yaw control, paired with a pivot stepper motor at the flight train to dissipate excess momentum and prevent wheel saturation. Roll and pitch are stabilized with frameless direct-drive motors and high-resolution encoders, minimizing static friction and improving precision [46]. Nested control architectures, as exemplified by the High Altitude Lensing Observatory (HALO) concept, combine coarse gondola slewing, fine gimbal positioning, telescope de-rotation, and fine-guidance optics to achieve sub-arcsecond stability [98]. Multi-sensor

fusion is standard, integrating star cameras, gyroscopes, GPS, sun sensors, magnetometers, and tilt meters, with in-flight data refined post-flight using extended Kalman filters—achieving post-reconstruction accuracies of <5″ RMS in platforms such as BLASTPol and SPIDER [99]. Experimental approaches, such as pyramid-configured single-gimbal control moment gyroscopes (CMGs), have been explored for damping pendulum-like modes in balloon suspensions [100].

Structural innovations, particularly the use of carbon-fiber-reinforced polymer (CFRP) components, have played a crucial role in enhancing pointing stability and payload capacity. SPIDER's gondola uses CFRP tube trusses with aluminum joints to reduce mass while maintaining stiffness, decreasing disturbance torques, and controlling inertia [101], [102]. BLAST-TNG employs a 2.5 m carbon-fiber composite primary mirror that reduces weight and thermal distortion, thereby easing momentum control requirements and improving image stability [102]. These structural choices, combined with advanced control systems, allow for higher control bandwidths and sustained sub-arcsecond performance.

Beyond pointing, other gondola and instrumentation improvements have included avionics and power system upgrades, such as the Columbia Scientific Balloon Facility's modernized Support Instrumentation Package (SIP), providing modular command, telemetry, and independent power systems, coupled with enhanced Iridium communication links for near-continuous data return [103]-[105]. Science payloads have advanced in parallel: the Taurus CMB polarimeter integrates modern cryogenics and detectors into a thermally optimized gondola [105], the ComPair gamma-ray telescope validated its medium-energy detector systems in 2023 flights [103], and PMC-Turbo's autonomous imaging systems have captured unprecedented mesospheric gravity wave dynamics.

Collectively, these advances—from lightweight CFRP gondola frames and precision actuators to sensor fusion algorithms and upgraded communication systems—have transformed balloon-borne platforms into stable, high-performance observatories, solidifying their role in technology maturation for future space-based missions.

3. Conclusions

It is essential to acknowledge the tireless efforts of all the launch and flight crews and engineers. These crews had to accommodate all of these developments in materials and designs for successful launch and operations. There have been huge developments in the launch methods and equipment to accommodate these changes and support continued successful launches.

From the smoky linen of the Montgolfier brothers to the sleek solar-lifted films of modern SPBs, ballooning has undergone centuries of

innovation. Scientific ballooning continues to push boundaries in astrophysics, atmospheric science, and planetary exploration.

The journey has been punctuated by both international cooperation and national ingenuity — from Sivel's spectroscopes to Kolhörster's confirmation of cosmic rays, from cellophane experiments to the revolution in polyethylene. Despite shifts in technology and funding, balloons remain uniquely capable of accessing near-space at low cost and high reliability.

The future likely includes even longer flights, hybrid aerial vehicles, and robotic balloon swarms — proof that the legacy of human curiosity, first aloft in 1783, is far from grounded.

References

[1] A. L. Morris, *Scientific Ballooning Handbook*. 1975.

[2] "Early Scientific Balloons," Centennialofflight.net, 2025. [Online]. https://www.centennialofflight.net/essay/Lighter_than_air/early_scientific_balloons/LTA7.htm

[3] K. S. Gould and D. J. Ulbrich, "Seizing The Highest Ground: The Union Army Balloon Corps."

[4] J. C. Scott, "The Infernal Balloon: Union Aeronautics During the American Civil War Union Aeronautics During the American Civil War on JSTOR," Army Hist., vol. No. 93, pp. 6–27, Fall 2014.

[5] T. D. Crouch, Lighter Than Air: An Illustrated History of Balloons and Airships. Johns Hopkins University Press, 2009. Accessed: Jan. 10, 2025. [Online]. Available: https://airandspace.si.edu/research/publications/lighter-air-illustrated-history-balloons-and-airships

[6] G. de Syon, Zeppelin!: Germany and the Airship, 1900–1939. JHU Press, 2002.

[7] P. Nowak, Sex, Bombs, and Burgers. Viking Canada, 2011.

[8] S. L. Kotar and J. E. Gessler, Ballooning: A History, 1782-1900. McFarland, 2011.

[9] V. Eaton and E. H, "Airships and the Modern Military," Mar. 1991, Accessed: July 28, 2025. [Online]. Available: https://apps.dtic.mil/sti/html/tr/ADA233610/

[10] "Military, Naval and Civil Airships - Google Books." Accessed: July 28, 2025. [Online]. Available: https://www.google.com/books/edition/Military_Naval_and_Civil_Airships/hfASDQAAQBAJ?hl=en&gbpv=1&dq=military+airships&pg=PT7&printsec=frontcover

[11] J. G. Vaeth, They Sailed the Skies: U.S. Navy Balloons and the Airship Program. Naval Institute Press, 2005.

[12] "The High-Flying, Death-Defying Discovery of Helium," Science History Institute. Accessed: Jan. 10, 2025. [Online]. Available: https://www.sciencehistory.org/stories/magazine/the-high-flying-death-defying-discovery-of-helium/

[13] "Discovery of Helium in Natural Gas - National Historic Chemical Landmark," American Chemical Society. Accessed: Jan. 10, 2025. [Online]. Available:

https://www.acs.org/education/whatischemistry/landmarks/heliumnaturalgas.html

[14] "The Airship 'America' of 1910: The First Attempt to Fly the Atlantic," Airships.net. Accessed: Aug. 01, 2025. [Online]. Available: https://www.airships.net/first-attempt-fly-atlantic-wellman-vaniman-airship-america/

[15] R. H. Upson, "1915: Relative Worth of Improvements in Fabrics," Goodyear Tire & Rubber Co., NACA Report #5, 1915.

[16] R. H. Upson, Free and Captive Balloons. Ronald Press Company, 1926.

[17] "Goodyear History." Accessed: Jan. 11, 2025. [Online]. Available: https://www.goodyear.com/en_US/blimp/history/the-first-goodyear-blimp.html

[18] "Goodyear 'Pilgrim' Gondola | National Air and Space Museum." Accessed: Jan. 11, 2025. [Online]. Available: https://airandspace.si.edu/collection-objects/goodyear-pilgrim-gondola/nasm_A19330024000

[19] R. H. Upson, "Metal-clad Rigid Airship Development," SEA J., Feb. 1926.

[20] A. F. Zahm, "Some Theorems in the Mechanics of High-Speed Balloons," presented at the International Aeronautic Congress, Zahm's Collected Papers University of Notre Dame Press., 1900.

[21] "Léon Teisserenc de Bort | Atmospheric Research, Stratosphere, Ozone Layer | Britannica." Accessed: Aug. 08, 2025. [Online]. Available: https://www.britannica.com/biography/Leon-Philippe-Teisserenc-de-Bort

[22] "Süring and Berson's Balloon Ascenton 31st July 1901," Potsdam Institute for Climate Impact Research. Accessed: Aug. 18, 2025. [Online]. Available: https://www.pik-potsdam.de/en/output/infodesk/telegraphenberg/suering-haus/reinhard-suring/hochfahrt

[23] "Captain H.C. Gray Balloon Basket | National Air and Space Museum." Accessed: Aug. 18, 2025. [Online]. Available: https://airandspace.si.edu/collection-objects/captain-hc-gray-balloon-basket/nasm_A19280013000

[24] "FAI celebrates 90th anniversary of Auguste Piccard breaking the stratospheric barrier | World Air Sports Federation." Accessed: Aug. 18, 2025. [Online]. Available: https://www.fai.org/news/fai-celebrates-90th-anniversary-auguste-piccard-breaking-stratospheric-barrier

[25] P. Murdin, Ed., Encyclopedia of Astronomy & Astrophysics. Boca Raton: CRC Press, 2000. doi: 10.1201/9781003220435.

[26] “18 August 1932 | This Day in Aviation.” Accessed: Aug. 18, 2025. [Online]. Available: https://www.thisdayinaviation.com/18-august-1932/

[27] “Osoaviakhim 1 | This Day in Aviation.” Accessed: Aug. 18, 2025. [Online]. Available: https://www.thisdayinaviation.com/tag/osoaviakhim-1/

[28] “USN 1147064.” Accessed: Aug. 18, 2025. [Online]. Available: http://public1.nhhcaws.local/our-collections/photography/numerical-list-of-images/nhhc-series/nh-series/usn-1147000/usn-1147064--century-of-progress--balloon.html

[29] “The Beauty and History of South Dakota’s Stratobowl,” Travel South Dakota. Accessed: Aug. 18, 2025. [Online]. Available: https://api.travelsouthdakota.com/trip-ideas/beauty-and-history-south-dakotas-stratobowl

[30] G. A. Larson, “The First Space Race? The Explorer Balloon Flight of 1935,” Air Power Hist., vol. 53, no. 3, pp. 40–50, 2006.

[31] “The Significance of Recent Measurements of Cosmic Rays | Science.” Accessed: Aug. 18, 2025. [Online]. Available: https://www.science.org/doi/10.1126/science.77.2003.480

[32] P. Carlson and A. A. Watson, “Erich Regener and the ionisation maximum of the atmosphere,” Hist. Geo- Space Sci., vol. 5, no. 2, pp. 175–182, Dec. 2014, doi: 10.5194/hgss-5-175-2014.

[33] J. D. Ackerman and J. Piccard, “Upper Air Study by Means of Balloons,” J. Aeronaut. Sci., June 1937.

[34] Jemully, “Plastic: It’s Not All the Same The History of Polyethylene,” Lone Star Chemical. Accessed: Jan. 12, 2025. [Online]. Available: https://lonestarchemical.com/plastic-its-not-all-the-same-the-history-of-polyethylene/

[35] “Linear Low Density Polyethylenes - an overview | ScienceDirect Topics.” Accessed: Jan. 09, 2025. [Online]. Available: https://www.sciencedirect.com/topics/chemical-engineering/linear-low-density-polyethylenes

[36] “Manned Space,” US Navy Hist., vol. space-and-the-united-states-navy, pp. 60–66.

[37] “Stresses in a Partially Inflated Free Balloon - with Notes on Optimum Design and Performance for Stratosphere Exploration |

Journal of the Aeronautical Sciences." Accessed: Jan. 08, 2025. [Online]. Available: https://arc.aiaa.org/doi/10.2514/8.800

[38] R. H. Upson and J. S. Holdbusen, "1952: Balloon Shapes or Stress Analysis and Design of Thin, Axially Symmetric Fluid Containers," General Mills Report #1143, Sept. 1952.

[39] K. W. Arnstein and F. G. Swan, "1935-36: Stratosphere Series Nos 1 & 2, Explorer I & II Balloons," Natl. Geogr. Soc. Contrib. Tech. Pap..

[40] "Our History - General Mills." Accessed: Aug. 18, 2025. [Online]. Available: https://www.generalmills.com/about-us/our-history

[41] R. L. Schwoebel, "Strato-Lab Development," Minneapolis, 1956.

[42] O. C. Winzen and D. P. Parks, "Operation Manhigh II," J. Jet Propuls., vol. 28.8, pp. 523–532, 1958.

[43] O. C. Winzen, "Ten Years of Plastic Balloons," in VIIIth International Astronautical Congress Barcelona 1957 / VIII. Internationaler Astronautischer Kongress / VIIIe Congrès International D'Astronautique, vol. 1, Berlin, Heidelberg: Springer Berlin Heidelberg, 1958, pp. 436–459. doi: 10.1007/978-3-662-39990-3_35.

[44] W. V. Jones, "Evolution of scientific ballooning and its impact on astrophysics research," Adv. Space Res., vol. 53, no. 10, pp. 1405–1414, May 2014, doi: 10.1016/j.asr.2013.12.028.

[45] "Space Men | American Experience | PBS." Accessed: Jan. 12, 2025. [Online]. Available: https://www.pbs.org/wgbh/americanexperience/films/spacemen/

[46] M. S. Smith and E. L. Rainwater, "Optimum designs for superpressure balloons," Adv. Space Res., vol. 33, no. 10, pp. 1688–1693, Jan. 2004, doi: 10.1016/j.asr.2003.07.042.

[47] O. C. Winzen and D. P. Parks, "Operation Manhigh II," J. Jet Propuls., vol. 28, no. 8, pp. 523–532, Aug. 1958, doi: 10.2514/8.7375.

[48] J. H. Smalley, "Determination of the shape of a free balloon (Report No. 2421)," 1963.

[49] J. H. Smalley, "Determination of the shape of a free balloon (Report No. 2500)," 1963.

[50] J. H. Smalley, "Determination of the Shape of a Free Balloon (Report No. 2560)," 1964.

[51] Gazette d'Amsterdam, June 25, 1784.

[52] "Journal des savants," J. Savants, vol. November, pp. 760–762, 1794.

[53] What'sHerName, "THE AERONAUT Sophie Blanchard," What'shername. Accessed: Aug. 18, 2025. [Online]. Available: https://whatshernamepodcast.com/sophie-blanchard/

[54] V. L. Ruiz and V. S. Korrol, Latinas in the United States, set: A Historical Encyclopedia. Indiana University Press, 2006.

[55] "Women Who Paved the Way: Mercedes De Acosta." Accessed: Aug. 18, 2025. [Online]. Available: https://www.advocate.com/women/2017/3/17/women-who-paved-way-mercedes-de-acosta

[56] "The University of Chicago Magazine: Features." Accessed: Aug. 18, 2025. [Online]. Available: https://magazine.uchicago.edu/1106/features/legacy.shtml

[57] "Family tree of Jeannette RIDLON," Geneanet. Accessed: Aug. 18, 2025. [Online]. Available: https://gw.geneanet.org/titeufs6?lang=en&n=ridlon&p=jeannette

[58] "High-Altitude Balloon Innovation | American Experience | PBS." Accessed: Aug. 18, 2025. [Online]. Available: https://www.pbs.org/wgbh/americanexperience/features/spacemen-balloon-innovation/

[59] "Vera Simons Papers | National Air and Space Museum." Accessed: Aug. 18, 2025. [Online]. Available: https://airandspace.si.edu/collection-archive/vera-simons-papers/sova-nasm-2016-0013

[60] "21 May 2000: The Story of Lindsay Muir's Hot Air Balloon World Record | World Air Sports Federation." Accessed: Aug. 18, 2025. [Online]. Available: https://www.fai.org/news/21-may-2000-story-lindsay-muirs-hot-air-balloon-world-record

[61] "Carol Rymer Davis: US Balloonist (Photo, Video) » RightFielders Women in Sports." Accessed: Aug. 18, 2025. [Online]. Available: https://web.archive.org/web/20101009122146/http:/sports.rightpundits.com/?p=5243

[62] "G - Who's Who of Ballooning." Accessed: Aug. 18, 2025. [Online]. Available: http://www.ballooninghistory.com/whoswho/who%27swho-g.html

[63] P. Arnaud, Histoire du sport féminin. Paris: L'Harmattan, 1996.

[64] R. S. Kubara, “The National Scientific Balloon Facility,” in NASA. Ames Res. Center Telescope Systems for Balloon-Borne Res., 1974, pp. 156–159.

[65] M. Pavey, “Long duration scientific ballooning platform development,” in 5th Aerodynamic Deceleration Systems Conference, Albuquerque,NM,U.S.A.: American Institute of Aeronautics and Astronautics, Nov. 1975. doi: 10.2514/6.1975-1391.

[66] D. Gregory, “NSBF A Quarter Century,” 2019.

[67] D. BAWCOM, “International survey of scientific ballooning support organizations,” in International Balloon Technology Conference, American Institute of Aeronautics and Astronautics. doi: 10.2514/6.1991-3677.

[68] June 30 and 2025, “Ed Yost,” The Linda Hall Library. Accessed: Aug. 18, 2025. [Online]. Available: https://www.lindahall.org/about/news/scientist-of-the-day/ed-yost/

[69] “Paul E. ‘Ed’ Yost (biographical PDF).” National Balloon Museum. [Online]. Available: https://www.nationalballoonmuseum.com/wp-content/uploads/2017/06/Paul-E.-Ed-Yost.pdf

[70] Aerostar, “History,” Aerostar. Accessed: Aug. 18, 2025. [Online]. Available: https://aerostar.com/about/history

[71] “Jim Winker (biographical PDF).” National Balloon Museum. [Online]. Available: https://www.nationalballoonmuseum.com/wp-content/uploads/2017/06/Jim-Winker.pdf

[72] “WINKER, James A. (1928 - 2017) - The balloon encyclopedia.” Accessed: Aug. 18, 2025. [Online]. Available: https://stratocat.com.ar/stratopedia/25.htm

[73] “Hot-Air Balloon Maintenance Manual.” Cameron Balloons, Dec. 21, 2011.

[74] “Ride Balloons - Lindstrand Balloons - Hot Air Balloon Manufacturer.” Accessed: Aug. 18, 2025. [Online]. Available: https://lindstrand.com/products/ride-balloons

[75] “Piloted Balloons | Federal Aviation Administration.” Accessed: Aug. 18, 2025. [Online]. Available: https://www.faa.gov/aircraft/air_cert/design_approvals/balloons

[76] “Hot Air Balloon History - Evolution of Ballooning at Balloon Fiesta,” Balloon Fiesta. Accessed: Aug. 18, 2025. [Online]. Available: https://www.balloonfiesta.com/about-us/history/hot-air-history/

[77] "Resources :: Gondola, Raven | Smithsonian Learning Lab." Accessed: Aug. 18, 2025. [Online]. Available: https://learninglab.si.edu/resources/view/4739

[78] "10 year anniversary of Breitling Orbiter 3 | World Air Sports Federation." Accessed: Aug. 18, 2025. [Online]. Available: https://www.fai.org/news/10-year-anniversary-breitling-orbiter-3

[79] J. F. Dwyer, "Zero Pressure Balloon Shapes, Past, Present, and Future," in Scientific Ballooning (COSPAR), 1978, pp. 9–19.

[80] T. W. Bilhorn, "Balloon Performance Analysis - NCAR Scientific Balloon Facility," in AFCRL Scientific Balloon Workshop, A. O. Korn, Ed., Bedford, Massachusetts: Air Force Cambridge Research Laboratories, 1965, pp. 59–64.

[81] J. F. Dwyer, "Some Polyethylene Balloon Statistics," in AFCRL Scientific Balloon Workshop, 1965.

[82] J. F. Dwyer, "Polyethylene Free Balloon Design from the Perspectives of User and Designer," 1982.

[83] A. D. Kerr and H. Alexander, "ON A CAUSE OF FAILURE OF HIGH ALTITUDE PLASTIC BALLOONS," 1968.

[84] I. S. Smith, "1983 Catastrophic Balloon Failure Investigation," 1985.

[85] I. S. Smith, "Recent Material Problems Relating to Catastrophic Balloon Failures," Adv. Space Res., vol. 5, no. l, pp. 9–11, 1985.

[86] H. C. Needleman, "Status of the NASA continuing investigation of catastrophic balloon failures," Adv. Space Res., vol. 7, no. 7, pp. 5–9, 1987, doi: 10.1016/0273-1177(87)90002-0.

[87] R. Ashley, "Industrial Adhesion Problems," 1985, Orbital Press, Oxford.

[88] D. P. Bell, "A comparative study of internally and externally capped balloons using small scale test balloons," 1994. doi: 10.1016/0273-1177(94)90068-X.

[89] H. M. Cathey, D. A. Fairbrother, and M. A. Said, "Performance Highlights of NASA Super Pressure Balloon Mid-Latitude Flights," in AIAA Balloon Systems Conference, American Institute of Aeronautics and Astronautics. doi: 10.2514/6.2017-3091.

[90] "The future of scientific ballooning | Philosophical Transactions of the Royal Society A: Mathematical, Physical and Engineering Sciences." Accessed: Feb. 17, 2025. [Online]. Available:

https://royalsocietypublishing.org/doi/full/10.1098/rsta.2007.0002?casa_token=k0pGaXMgiFEAAAAA%3AzFYe8uu7Ns61PjWTreGKohZ5oq_X5kpL_qGjx5UG0XmQqsYe3xFc-S8Eh8Bsh3BhO-VgRu6WyPIo9g

[91] D. K. K, A. J. Ponseelan, D. D. P. D, D. M. V. B, and S. S, "A Study on Google Project Loon- Opportunities and Challenges," Mar. 30, 2020, Social Science Research Network, Rochester, NY: 3565713. Accessed: Feb. 17, 2025. [Online]. Available: https://papers.ssrn.com/abstract=3565713

[92] P. Serrano, M. Gramaglia, F. Mancini, L. Chiaraviglio, and G. Bianchi, "Balloons in the Sky: Unveiling the Characteristics and Trade-Offs of the Google Loon Service," IEEE Trans. Mob. Comput., vol. 22, no. 6, pp. 3165–3178, June 2023, doi: 10.1109/TMC.2021.3135976.

[93] J. H. Adams et al., "A Review of the EUSO-Balloon Pathfinder for the JEM-EUSO Program," Space Sci. Rev., vol. 218, no. 1, p. 3, 2022, doi: 10.1007/s11214-022-00870-x.

[94] E. Udinski and A. Hamilton, "NASA Balloon Program Office Suborbital and Special Orbital Projects Directorate Wallops Flight Facility".

[95] D. Stuchlik, "The NASA Wallops Arc-Second Pointer (WASP) System for Precision Pointing of Scientific Balloon Instruments and Telescopes," in AIAA Balloon Systems Conference, in AIAA AVIATION Forum. , American Institute of Aeronautics and Astronautics, 2017. doi: 10.2514/6.2017-3609.

[96] A. S. Gill et al., "SuperBIT Superpressure Flight Instrument Overview and Performance: Near diffraction-limited Astronomical Imaging from the Stratosphere," Astron. J., vol. 168, no. 2, p. 85, Aug. 2024, doi: 10.3847/1538-3881/ad5840.

[97] P. Voyer et al., "From SuperBIT to GigaBIT: Informing next-generation balloon-borne telescope design with Fine Guidance System flight data," July 14, 2024, arXiv: arXiv:2407.10103. doi: 10.48550/arXiv.2407.10103.

[98] J. Rhodes et al., "Space-quality data from balloon-borne telescopes: The High Altitude Lensing Observatory (HALO)," Astropart. Phys., vol. 38, pp. 31–40, Oct. 2012, doi: 10.1016/j.astropartphys.2012.05.015.

[99] N. N. Gandilo et al., "Attitude determination for balloon-borne experiments," July 2014, p. 91452U. doi: 10.1117/12.2055156.

[100] A. D. Miller, I. Beveridge, A. Antonio, and T. Pirrone, "World View Enterprises altitude controlled balloons: a new stratospheric platform for persistent Earth and space imaging

campaigns," in Ground-based and Airborne Telescopes VII, SPIE, July 2018, pp. 1427–1435. doi: 10.1117/12.2313446.

[101] J. M. Nagy et al., "A New Limit on CMB Circular Polarization from SPIDER," Astrophys. J., vol. 844, no. 2, p. 151, Aug. 2017, doi: 10.3847/1538-4357/aa7cfd.

[102] N. P. Lourie et al., "Design and Characterization of a Balloon-Borne Diffraction-Limited Submillimeter Telescope Platform for BLAST-TNG," in Ground-based and Airborne Telescopes VII, July 2018, p. 69. doi: 10.1117/12.2314380.

[103] "PMC Turbo: Studying Gravity Wave and Instability Dynamics in the Summer Mesosphere Using Polar Mesospheric Cloud Imaging and Profiling From a Stratospheric Balloon - Fritts - 2019 - Journal of Geophysical Research: Atmospheres - Wiley Online Library." Accessed: Aug. 18, 2025. [Online]. Available: https://agupubs.onlinelibrary.wiley.com/doi/full/10.1029/2019JD030298

[104] "Sunrise iii: Overview of Observatory and Instruments." Accessed: Aug. 18, 2025. [Online]. Available: https://arxiv.org/html/2502.06483v1

[105] J. L. May et al., "Instrument overview of Taurus: a balloon-borne CMB and dust polarization experiment," in Ground-based and Airborne Telescopes X, SPIE, Sept. 2024, pp. 1319–1333. doi: 10.1117/12.3019051.

[106] J. Rotter, "Review & Disposition of Old Suspect Balloons," Palestine, 2013.

[107] A. S. Redner, "Nondestructive evaluation using polarized light," 1995.

[108] F. F. Alavi, "In-Line Extrusion Monitoring and Product Quality," University of Toronto, 2010.

[109] R. S. Kody and D. C. Martin, "Quantitative characterization of surface deformation in polymer composites using digital image analysis," Polym. Eng. Sci., vol. 36, no. 2, pp. 298–304, 1996, doi: 10.1002/pen.10416.

[110] L. Bassell, "How To Solve Blown Film Problems," LyondellBasell Ind., p. 31, 2009.

[111] ASTM International, "ASTM D746-20 Standard Test Method for Brittleness Temperature of Plastics and Elastomers by Impact," 2020, West Conshohocken, PA. doi: 10.1520/D0746-20.

[112] J. A. Brydson, Plastics Materials, Seventh Ed. Butterworth-Heinemann, 1999. doi: doi.org/10.1016/B978-075064132-6/50047.

[113] P. J. Hendra, H. P. Jobic, and K. Holland-Moritz, “Low temperature crystallization in polyethylene and the value of Tg,” J. Polym. Sci. Polym. Lett. Ed., vol. 13, no. 6, pp. 365–368, 1975, doi: 10.1002/pol.1975.130130610.

[114] I. S. Smith, “Advancements in NASA balloon research and development,” Adv. Space Res., vol. 17, no. 9, pp. 37–44, Jan. 1996, doi: 10.1016/0273-1177(95)00674-4.

[115] V. Thomas, “A Comparative J-Integral Fracture Toughness Study of Six Polyethylene Balloon Films,” 1994, Wallops Island.

[116] L. Mielke, “Balloon Material Development,” in Fifth AFCRL Scientific Balloon Symposium, L. A. Grass, Ed., Bedford, Massachusetts, 1968, pp. 131–147.

[117] R. Coen, “Fu-go : The curious history of japan’s balloon bomb attack on america : Coen, Ross Allen : Free Download, borrow, and streaming,” Internet Archive, https://archive.org/details/fugocurioushisto0000coen (accessed Sep. 4, 2025).

[118] R. C. Mikesh, “Japan’s World War II balloon bomb attacks on North America,” DSpace Home, https://repository.si.edu/items/dfd386e2-418f-4346-833f-dc5a577cfac2 (accessed Sep. 4, 2025).

[119] E. D. Angulo, J. G. Guidotti, and C. E. Vest, “Status of superpressure balloon technology in the United States,” NASA Technical Reports Server (NTRS), https://ntrs.nasa.gov/citations/19670009435 (accessed Sep. 4, 2025).

[120] “Echo 1 communications satellite,” Echo 1 Communications Satellite | National Air and Space Museum, https://airandspace.si.edu/collection-objects/communications-satellite-echo-1/nasm_A20030090000 (accessed Sep. 4, 2025).

Appendix 1-A. Timeline of Balloon History

1709 – Bartolomeu de Gusmão, born Bartolomeu Lourenço de Gusmão (1685-1724, Toledo, Spain), a priest and naturalist, demonstrated the world's first model hot air balloon before King John V of Portugal and his court. The model balloon rose to a height of about 11 feet.

1766 – Henry Cavendish discovered hydrogen and showed it to be at least seven times lighter than air.

1783 – First crewed flight. Joseph-Michel and Jacques-Étienne Montgolfier demonstrated the first manned hot air balloon flight in France. This marked humanity's initial exploration into the atmosphere. Pilatre de Rozier and the Marquis d'Arlandes flew in a Montgolfier in which the heat was replenished in flight by a straw fire. The balloon, 15 min diameter, ascended about 100 m and traveled 8 km in 20 min, during which time the balloon caught fire but was extinguished with water carried for that purpose.

1785 – Jean-Pierre Blanchard and John Jeffries were the first to cross the English Channel by air. Pilatre de Rozier and P.A. Romain attempted a Channel crossing (France to England) the same year. A chance was taken on the flammability of hydrogen in apparent confidence that its lightness would carry it up and away and that sparks could be contained. But less than a half-hour after the start, at about 1000 m, the craft burst into flame, with fatal results.

1793 – Jean-Pierre Blanchard made the first free flight in America (at least in a single balloon) under full control. He continued exhibitions over Europe but died from an unrecorded illness, impoverished by political complications. His widow, Marie Blanchard, continued successful exhibitions.

1794 – The first significant use of military balloons. a French balloon, the "L'Entreprenant", was used for reconnaissance over enemy positions. The aerial observer was able to direct artillery fire more accurately, contributing to the French victory.

1804 – The French Academy of Sciences, questioning the accuracy of previous upper-air data, commissioned physicists J. B. Biot and J. L. Gay-Lussac to make scientific observations.

1804 – First professional female balloonist Marie Blanchard made her first solo flight and later performed for Napoleon Bonaparte.

1810 – Marie Blanchard's fame grew across Europe due to her public ballooning demonstrations across Europe.

1819 – Marie Blanchard, after about 60 other flights, died in attempting a fireworks display from a gas balloon. It seems such displays were fairly common at the time, continuing even after her death.

1821 – First balloon use of coal gas by the leading British balloonist Charles Green, at the coronation of George IV. Green is also credited with first use of the drag rope (then termed 'guide rope').

1837 – Dr. John Rae, a trader and surgeon for the Hudson's Bay Co., tried unsuccessfully to raise a balloon by sun heat alone. He attributed his failure to the weakness of sunlight in northern latitudes, but this could have been only a minor factor.

1859 – John Wise, leading American balloonist, made the first airmail flight and, incidentally, set a new world distance record of about 1300 km from St. Louis to Henderson, N.Y. The first flight carrying official U.S. mail started from Lafayette, Ind., July 17, 1859, descending only a short distance away. To Wise is attributed the first use of the rip panel.

1862 – Under auspices of the British Association for the Advancement of Science, Henry Coxwell and James Glaisher, meteorologist, made an apparent new altitude record (without oxygen) with various physical and physiological observations. The highest altitude reading--from a non-recording barometer--claimed to be 8800 m while still rising, but this observation is questionable due to the physical condition of the men. Both became unconscious as the altitude increased. Tragedy was averted by Coxwell, who, with his hands already paralyzed, pulled the valve rope with his teeth. Consciousness was regained and readings resumed about 13 min later with barometer at 293 mm of mercury or 7300 m altitude. Of two pigeons carried, one died.

1875 – One of the first female aeronauts participated in long-distance balloon flights for exploration and adventure.

1875 – First use of oxygen, and also first anoxia victims, in a flight from Paris. H. T. Sivel, Croce-Spinnelli, and G. Tissandier reached 8500 m, but only Tissandier survived. They didn't start using oxygen soon enough, not realizing the insidious approach of paralysis.

1885 – Renard and Krebs in France made first fully successful application of power (electric motor) to an elongated balloon with a ballonet and steering organs. It was steered in a figure-eight at a speed of about 23 km/hr.

1897 – S.A. Andrée and crew started from Spitsbergen on a projected balloon trip to the North Pole. Their remains were found at an island in the Svalbard archipelago in 1930.

1898 – The Aero Club de France founded, primarily to promote ballooning. This is the parent organization of F.A.I. which sponsors international contests and controls official records.

1902 – Teisserenc de Bort sent instruments up in balloons that recorded temperature and air pressure. He was puzzled when he looked at the data from about 200 balloons and found that at a certain height in the atmosphere, temperature no longer dropped. He announced to the French Academy of Science of his discovery and called this layer of the atmosphere the stratosphere.

1905 – A total of 66 balloons, carrying 164 people and miscellaneous cargo, left Paris during its siege by the Germans in the Franco-Prussian War; for 4 months balloons provided the only contact between the city and the outside world.

1906 – The inaugural Gordon Bennett Cup (Coupe Aéronautique Gordon Bennett) balloon race took off from Paris, France featuring sixteen balloons from eight countries. An American team – Frank Lahm and Henry Hersey – were the first to win.

1910 – Based on previous European development, Goodyear Tire and Rubber Co. started making and improving single and multi-ply rubberized fabric suitable for lighter-than-air use. Previous American balloons were exclusively of varnished single-ply fabric.

1912 – Melvin Vaniman proposed wire-bound balloon to be stabilized by super-pressure. Apparently while experimenting with such pressure in his airship off Atlantic City, the fabric hull burst, causing death to himself and four crew members, a disaster erroneously attributed to fire in newspaper reports.

1920 – Post-war international balloon racing resumed. E. Demuyter of Belgium winner of the Gordon-Bennett race from Birmingham, Alabama.

1925 – In the mid-1920s the Goodyear Tire and Rubber Company of Akron, Ohio, built a fleet of small civil airships that were used to demonstrate the value of lighter-than-air flight and to train future airship pilots. One of those airships - the Pilgrim -- was the first ever designed for inflation with helium. It first flew at Akron, Ohio, on June 3, 1925 with pilot Jack Yolton at the controls. It flew with helium for the first time on July 17, and was christened on July 18 by Mrs. P. W. Litchfield, wife of the president of Goodyear. By the time the Pilgrim was retired on December 30, 1931, it had made 4,765 flights, carried 5,355 passengers, flown a total of 2,880 hours, and covered 153,000 kilometers (95,000 miles).

1927 – Capt. H. C. Gray of U.S. Army Air Corps died in altitude attempt; 12,950 m attained while still conscious, but record disallowed because

pilot not in control throughout, His clock stopped on ascent and oxygen apparently ran out at about 9000 m on descent. Official inquiry made particular note of unprecedentedly slow ascent and descent, but said nothing about kind of gas used. Gray definitely used hydrogen in previous altitude flights.

1931 – Swiss physicist Auguste Piccard and his twin brother, Jean Piccard, inverted a 1905 conception for a diving ship. The 1931 invention consisted of a spherical aluminum pressure cabin and a 14,000-cubic-metre lightweight rubberized-cotton netless hydrogen balloon. This would make possible the first successful stratosphere flight. It carried Auguste and his assistant, Paul Kipfer, to 15,781 metres (51,775 feet) on May 27, 1931.

1931 – A. Piccard and P. Kipfer used sealed, pressurized gondola for first time in setting altitude record of 15,781 m (cabin pressure equivalent to 3000 m). Max. cabin temperature 41° c with top of gondola black and bottom white.

1934 – Jeannette Piccard is the first woman to reach the stratosphere in a balloon, achieving an altitude of 57,579 feet, helping to advance high-altitude research.

1935 – Explorer II, 113,000 m^3 rubberized balloon (helium) made official record of 22,066 m in collecting atmospheric, cosmic-ray, and other data (crew, Anderson and Stevens).

1936 – First successful plastic balloon flights. J. F. Piccard in collaboration with T. H. Johnson and J. D. Akerman launched a series of four cellophane balloons, 65 m^3 each. A similar flight traveled 990 km in 10 hr. In cold weather, however, the material proved impractical due to cracking in the folds. The aerodynamic vertical stabilizer, working well with hydrogen, would be almost worthless with helium.

1943 – Several hundred Japanese paper balloons carried bombs across the Pacific Ocean but did little damage. These balloons were spherical of about 540 m^3 volume (hydrogen); ballast release was pressure-controlled. One balloon from a total of more than 9000 reached Kingston, Ontario; perhaps as many as 900, or 10%, reached North America.

1946 – Development of large polyethylene balloons undertaken by General Mills. Subsequent study of plastic balloon operation, stresses, and shape sponsored by U.S. Navy at University of Minnesota.

1955 – U.S. Air Force projects explored the upper atmosphere, studying human endurance and environmental conditions in preparation for spaceflight.

1959 – Water vapor first observed on Venus by C. M. Moore, Ross pilot, at 25,000 m with 406-mm telescope.

1960 – In 1960, Air Force Captain Joe Kittinger jumped from a balloon at 102,800 feet, setting a world record for highest parachute jump

1960 – Flight of the Stratoscope II mission, a 36" reflecting telescope in the visible/IR that was a precursor to Hubble, showing that telescopes could be operated remotely above the atmosphere.

1961 – World altitude record for manned aircraft of 34,700 m set by G. Mossolov, USSR, in E-66 jet airplane; first such record made by aircraft other than a balloon.

1961 – Manned balloon altitude record set by M. D. Ross, USNR, at 34,668 m over Gulf of Mexico, 28,300 m^3 balloon•, made by Winzen Research, Inc. Copilot V. A. Prather drowned in an accident after landing.

1968 – Polyethylene balloon of 812,693 m^3 launched at White Sands Missile Range, N.M., reached 48.5 km altitude with a scientific payload of 26.8 kg. This was the largest balloon flown to that date and set an altitude record for balloons.

1970 – Zero-pressure balloons were refined to allow controlled long-duration flights in the stratosphere, crucial for high-altitude atmospheric and space research.

1972 – The 511 keV line was discovered by a balloon-borne experiment in 1972. The 511 keV line in the Galactic center is a signature of positrons annihilating with electrons, and the source of the positrons is still not well understood (and is actively being studied by current instruments including COSI.

1980 – Enhanced telemetry enabled real-time data transfer from balloon-borne experiments. Payload capacities increased, allowing diverse instruments to study astrophysics, atmospheric science, and cosmic rays.

1985 – Vega 1 arrived at Venus on 11 June 1985 and Vega 2 on 15 June 1985, and each delivered a 1,500 kg (3,300 lb), 240 cm (94 in) diameter spherical descent unit. The units were released some days before each arrived at Venus and entered the atmosphere without active inclination changes.

1995 – Balloon missions using superconducting magnetic rigidity spectrometers first demonstrated the existence of cosmic baryonic antimatter through direct detection of cosmic antiprotons. Those measurements and balloon borne direct positron measurements (as opposed to 511keV line observations) underpin many indirect dark matter detection schemes. The antiproton and positron measurements led to the $1b+ AMS

spectrometer on the ISS. The balloon measurements are still superior at low energies. Bob Streitmatter (deceased 2017) and John Mitchell were both awarded NASA Exceptional Scientific Achievement medals for the Antiproton discovery.

1997 – BOOMERanG's measurement of the geometry of the Universe: It was the first experiment to make large, high-fidelity images of the CMB temperature anisotropies, and is best known for the discovery in 2000 that the geometry of the universe is close to flat.

2000 – Pumpkin-shaped balloon designs, with unique structural integrity, were introduced for long-duration planetary studies, including potential missions to Titan.

2009 – A NASA super-pressure balloon achieved a flight record of over 54 days.

2012 – The highest altitude achieved in a manned balloon was completed when Felix Baumgartner's Red Bull Stratos balloon reached an altitude of 39 km (127,852 ft) before he jumped from the stratosphere and performed a record-breaking freefall, providing data on human endurance and supersonic speeds.

2014 – The first official world championship take place for female balloon pilots, fostering greater participation by women in competitive ballooning.

2015 – The longest manned balloon flight record is set at 161 hours (6 days, 17 hours) by pilots Tony Bradley and Leonid Tiukhtvaey during their trans-Pacific flight in the "Two Eagles" helium balloon.

2018 – James Webb Space Telescope level pointing was achieved from a balloon during a balloon flight demonstration of coronagraph focal plane wavefront correction with PICTURE-C.
https://doi.org/10.1117/1.JATIS.9.2.025005

2020 – NASA's SuperBIT Telescope flight used balloon technology for high-resolution astrophysical observations, competing with space telescopes for cost efficiency.

2024 – Balloon-borne telescopes have been pivotal in probing ultraviolet (UV) emissions from high-redshift galaxies. These studies help understand star formation and the intergalactic medium.

Chapter 2
Academic Ballooning as an Educational Tool

Michael Walach[1], T. Gregory Guzik[2], Douglas Granger[2], Aaron Ryan[2], Mary Bowden[3]

[1] College of Agriculture, Montana State University, Bozeman, MT 59717
[2] Department of Physics and Astronomy, Louisiana State University, Baton Rouge, LA 70803
[3] Aerospace Engineering, University of Maryland College Park, College Park, MD 20742

Acknowledgments

Much of Sections 1 and 2 of this chapter have been adapted and updated from Chapter 4 of "*A Roadmap for Scientific Ballooning 2020-2030*", written by the NASA Balloon Program Analysis Group. (https://arxiv.org/abs/2210.01198) [1]. Additionally, Section 3 of this chapter includes significant contributions from Chris Koehler of the University of Colorado Boulder (BalloonSat Workshops), and Angela Des Jardins from Montana State University, Beth Covitt from University of Montana, and Ginny Smith of Virginia Tech (National Eclipse Ballooning Project).

Table of Contents

1. Introduction 5

1.1. Motivation 5

1.2. Academic Ballooning 7

1.3. Space Grant 8

2. Big (NASA) Balloons 9

2.1. Cubes in Space 9

2.2. High Altitude Student Platform (HASP) 10

2.3. Ride Share 12

3. Small (Weather) Balloons 13

3.1. BalloonSat Workshops 14

3.2. Louisiana Aerospace Catalyst Experiences for Students (LaACES) 15

3.3. Balloon Outreach Research Exploration And Landscape Imaging System (BOREALIS) 17

3.4. Nationwide Eclipse Ballooning Project (NEBP) 19

3.5. Supporting Organizations 22

4. Outcomes and Impact 23

4.1. Lessons Learned from BOREALIS 23

4.1.1. Team Formation and Dynamics 23

4.1.2. Good Practices and Procedures 24

4.2. Lessons Learned and The Public 25

4.2.1. Lessons Learned from NEBP 26

4.2.2. Outcomes from NEBP 28

4.3. Impact from Elementary School to Graduate School 30

References 32

Table of Figures

Figure 2-1: The High Altitude Student Platform (HASP) which carries multiple student development payloads to the edge of space was highlighted in the 2018 CoSTEM report as an exemplary example of transdisciplinary learning. 6

Figure 2-2: The Cubes in Space™ carrier during integration and on a NASA scientific balloon at float including about 100 individual experiments from grade 6 to 12 student teams. 10

Figure 2-3: The High Altitude Student Platform (HASP) can carry up to 12 advanced student payloads. 11

Figure 2-4: States that have utilized HASP as a student workforce development project are indicated by the blue shading. In addition, the number of institutions within the state that have contributed student teams is indicated by the bold number in or near the state. 12

Figure 2-5: Latex sounding balloon launch with multiple student payloads 14

Figure 2-6: The LaACES MegaSat student balloon payload including an Arduino Mega (bottom), the MegaSat shield (middle), and the Adafruit Ultimate GPS Logger shield. 16

Figure 2-7: BOREALIS Team readying a balloon for launch 18

Figure 2-8: Path of the Solar Eclipse in 2017, 2023, and 2024 20

Figure 2-9: The University of Alabama NEBP team obtained this picture at 100,000 ft, looking up along the flight line towards the balloon. The image clearly shows the moon's shadow on the Earth during the solar eclipse of 4/8/25. 21

Figure 2-10: Two balloons being inflated near an open PVC and plastic sheet enclosure during a University of Maryland practice eclipse launch 27

Figure 2-11: Payloads often land on the tops of tall trees 28

Figure 2-12: Bar graphs showing the change in student perceptions from the beginning of their NEBP involvement (Pre%) to the end of their involvement (Post%, after both eclipses) 29

Figure 2-13: University students watching the launch of their experiments carried by the High Altitude Student Platform (HASP) in September 2018 30

1. Introduction

1.1. Motivation

"Tell me and I will forget, show me and I may remember; involve me and I will understand." – Confucius

This old proverb describes the process of academic ballooning as a teaching tool very accurately. Students who enter the world of academic ballooning are thrust into an interdisciplinary team of students from multiple majors and backgrounds. Students are challenged with problems more extensive than their current skill sets and asked to make devices perform jobs they were never designed to perform. Experiments are sent to the edge of space, where they encounter a cold, space-like environment, yet electronics overheat with the lack of atmosphere, and payloads are pelted with the radiation of space. Students launch and recover payloads, and track and communicate with payloads during flight, just like launching and tracking a satellite or spacecraft in Earth orbit. Academic high-altitude ballooning truly offers students the closest analog to spaceflight that can be accomplished with a small budget. This chapter will explore how high-altitude ballooning inspires, challenges, and fosters student growth technically and socially. Ballooning is genuinely a life-changing experience for those few students brave enough to enter this weird and wild world.

During the first decade of this century, numerous studies [2-4] raised great concern that the declining number of students entering the workforce as engineers and scientists was a major U.S. national security and economic issue. In 2019, US Senate Commerce, Science, and Transportation Committee hearings emphasized STEM literacy and experiential activities to engage and prepare "a diverse workforce needed for the United States to lead and prosper in an increasingly competitive world driven by advanced technology [5]." Additionally, the 2018 report by the Committee on STEM Education (CoSTEM) of the National Science & Technology Council, "Charting A Course for Success: America's Strategy for STEM Education," [6] identified three primary objectives for NASA:

1) foster STEM ecosystems that unite communities
2) increase work-based learning and training through educator-employer partnerships, and
3) encourage transdisciplinary learning.

While ballooning contributes to all three objectives, it is the last one where ballooning has the most impact on STEM education. The CoSTEM report highlighted the NASA Balloon Program Office (BPO) / Louisiana Space Grant Consortium (LaSPACE) High Altitude Student Platform (HASP) balloon program as an excellent example of transdisciplinary learning

(see Figure 2-1). Further, both the NASA Strategic Plan 2022 [7] and the NASA Science Mission Directorate (SMD) Explore Science 2020-2024 Vision (Science Plan) [8] have multiple objectives to which ballooning can contribute. In particular, as stated in the SMD Science Plan:

> "SMD is also investing in students and early career faculty to help them grow into future leaders. SMD has been particularly focused on developing a new cadre of mission Principal Investigators through workshops and hands-on training as part of existing mission teams."



Figure 2-1: The High Altitude Student Platform (HASP) which carries multiple student development payloads to the edge of space was highlighted in the 2018 CoSTEM report as an exemplary example of transdisciplinary learning.

Thus, in addition to supporting multiple significant scientific objectives, ballooning contributes to the aerospace workforce development pipeline, enhancing public awareness of NASA programs and training the next generation of scientists and engineers. Because of these goals, and capabilities, a number of experiential projects, tools, and platforms have been developed that use ballooning to enhance the NASA workforce development pipeline. Some of these are discussed in the following sections.

1.2. Academic Ballooning

Ballooning is a unique capability with characteristics that enable and support STEM education and workforce development from middle school through early career faculty, training scientists and engineers to serve the NASA mission at the Agency and in the space science and space technology industry. A key feature of ballooning that aligns very well with NASA itself is that it encompasses both aeronautics and astronautics: aeronautics, because balloons ascend through the atmosphere allowing observations and measurements at all altitudes that are of interest to atmospheric scientists; and astronautics, because at the height of the balloon's trajectory, the conditions are very space-like in terms of temperature, pressure, and radiation, and because the blackness of space and the deep recesses of space can be observed.

Another essential characteristic of this flight platform is that many balloon payloads are recovered, enabling payload development to be iterated over multiple flights. Recovery is important for student programs where the failure of a balloon payload is used as a "teaching moment," and the recovered payload is then improved prior to the next flight. Another important characteristic is the short development cycle for balloon payloads. Typically, a professional-level scientific payload will need at least 5 or 6 years to go from concept to first flight, while smaller, lighter, limited student payloads are generally developed in less than one year. Such time scales are consistent with the times that academic students, from middle to graduate school, can participate and gain from the entire development cycle experience.

Finally, balloon systems provide low-cost access to the near-space environment. Balloon systems that cost less than a few thousand dollars can carry light payloads to an altitude in excess of 100,000 feet, above 99% of the Earth's atmosphere, and where the blackness of space and curvature of the Earth can be observed. Such systems are affordable for high schools, colleges, and universities, enabling teams of students across the country access to a space flight experience. The relatively low cost and limited project life cycle timeframe, coupled with the high likelihood of recovering the physical payloads, makes ballooning a remarkable testbed for payloads in development to fly on much more expensive platforms eventually. This combination of characteristics is

unique among NASA flight vehicle capabilities, and, as a result, multiple balloon flight programs have been developed to encourage and excite student involvement in NASA missions at all grade levels, ultimately feeding the workforce development pipeline.

Middle and high school programs that encompass a full balloon flight capability are relatively few in number because even a minimal program requires infrastructure, funding, and knowledgeable personnel for launch operations, tracking, and recovery. Payload development, on the other hand, can be accomplished by students of any age with progressively more sophisticated experiments becoming accessible to older students especially if they have the supplies and mentoring to allow for some basic electronics. Flight opportunities for payloads thus developed can be in the form of a nearby college ballooning team, or an established balloon flight opportunity (for example Edge of Space Sciences in Colorado), or a government sponsored piggyback ride.

College ballooning teams have become more numerous over the last 20 years, with many teams getting their start by attending a 'BalloonSat' Workshop, or more recently with NASA sponsored programs such as the Nationwide Eclipse Ballooning Project (NEBP). These teams may be hosted in a university department such as Physics, Atmospheric Sciences, or Mechanical, Electrical, or Aerospace Engineering, or in some cases, the ballooning team may be a student-run club. Long-term continuity of programs like these is a challenge, but given sufficient institutional or sponsorship support, these programs can develop fairly sophisticated payloads, test them on small balloons, and ultimately produce payloads for flight on big balloons such as HASP or other NASA balloons. There are also instances where balloon flights have been used to help develop and test concepts for sounding rocket experiments or even orbital CubeSats.

1.3. Space Grant

One of the enabling organizations that has played a key role in the development and continued support of authentic student balloon flight experiences across the United States is the National Space Grant College and Fellowship Program (Space Grant). Every state, plus Puerto Rico, Washington DC, Guam, and the Virgin Islands, has a Space Grant program that, among other associated activities, provides unique opportunities to support STEM workforce development in their jurisdictions. Over the years, Space Grant consortia in different states have supported the development of college-based ballooning programs, as well as participation in student ballooning projects such as "Cubes in Space™," the Aerospace Catalyst Experiences for Students (ACES), the Nationwide Eclipse Ballooning Project (NEBP), the Undergraduate Student Instrument Project (USIP), and the High Altitude Student Platform (HASP). Thus, taking advantage of the Space Grant network is an effective way to

augment available resources for the development of the workforce pipeline from middle and high school students through university undergraduate and graduate students. Further information about the Space Grant program, as well as links to all jurisdiction offices, can be found at: https://www.nasa.gov/learning-resources/national-space-grant-college-and-fellowship-project/

2. Big (NASA) Balloons

2.1. Cubes in Space

The Cubes in Space™ program promotes and enables the development and application of scientific research, critical thinking, problem-solving and technology development skills in high school and middle school students. Cubes in Space, an iEDU program, is offered in collaboration with NASA's Goddard Space Flight Center – Wallops Flight Facility and provides students 11-18 years of age access to NASA suborbital flights for scientific research, experiment design, and technology development and testing.

Cubes in Space is an experiential and inquiry-based STEM program with the goal of enabling young students, ages 11-18 years of age, to develop critical knowledge and skills that are sustainable and transferable across disciplines, future academic pursuits and careers. After acquiring and applying inquiry and research skills, along with knowledge about suborbital science and spaceflight, students identify a real-world Earth or space-based problem, need, or scenario for which an experiment hypothesis is designed. Students develop an experiment concept where suborbital flight or environmental conditions act on the chosen experiment subject, object, or material that is integrated into a small, plastic payload cube. Experiment concepts are proposed through the Application for Spaceflight system. If selected, experiments are launched on a sounding rocket or zero-pressure scientific balloon from a NASA facility in the summer and returned to students. Pre- and post-flight-testing methods and procedures are entirely designed by the students. The culminating deliverable, the Post-Flight Analysis Report, is submitted to iEDU and their Cubes in Space program office.

Since 2015, the Cubes in Space program has participated as piggyback payloads on 10 zero-pressure, conventional balloon missions. On a typical Cubes in Space mission, up to 100 powered and non-powered student experiments are flown. With the fall 2025 Balloon Program Office campaign in Fort Sumner, New Mexico, over 1150 student experiments representing at least 12,000 students in 15 countries, experienced near space, suborbital flight, see Figure 2-2.

Further information on Cubes in Space Program is available at https://www.cubesinspace.com/.



Figure 2-2: The Cubes in Space™ carrier during integration and on a NASA scientific balloon at float including about 100 individual experiments from grade 6 to 12 student teams.

2.2. High Altitude Student Platform (HASP)

In 2005/2006, the NASA Balloon Program Office (BPO) and the Louisiana Space Grant Consortium (LaSPACE) developed the High Altitude Student Platform (HASP). HASP is designed to provide students with an authentic experience, with associated skill development, that models a spaceflight

mission from from concept to flight result, analysis, and reporting [9]. HASP, shown in Figure 2-3, supports up to 12 student payloads.

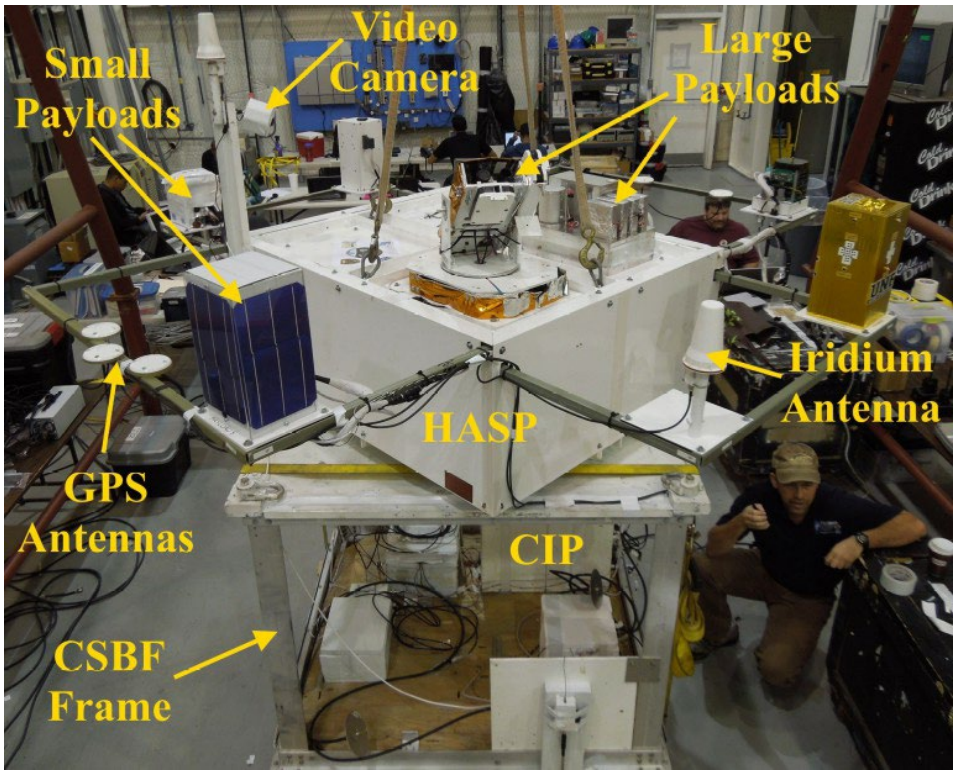


Figure 2-3: The High Altitude Student Platform (HASP) can carry up to 12 advanced student payloads.

In addition to the flight seat, the HASP platform provides teams with power (up to 75W), live downlink telemetry, uplinked commanding, and a live video stream of the payload in flight. The HASP program typically releases a call for payload proposals in August of a given year, and student teams must submit a flight application detailing their mission goals and preliminary design by early November. BPO, LaSPACE, and CSBF review all applications to determine selections for flight slots, which are announced in December. During payload development, student teams submit monthly reports, participate in monthly telecons and produce a series of design documents to track their progress. The completed student payloads are integrated with HASP and thermal/vacuum tested during July in preparation for flight at the beginning of September. Teams on HASP typically receive 10-20 hours at float altitudes greater than 110,000ft. A final project report is due within three months following the flight. Since 2006, HASP has had 18 flights for an accumulated time at float of over 240 hours, accepted more than 200 student teams into the program, involved more than 1,800 student participants, and successfully flown more than 76% of the accepted payloads [10]. Teams are from 50 institutions across 24 states, Puerto

Rico, the US Virgin Islands, Canada, Europe, and South America. Figure 2-4 shows a map of locations of institutions that have supported a HASP team.

Further information about HASP can be found at https://laspace.lsu.edu/hasp/ or by contacting HASP at hasp@lsu.edu.

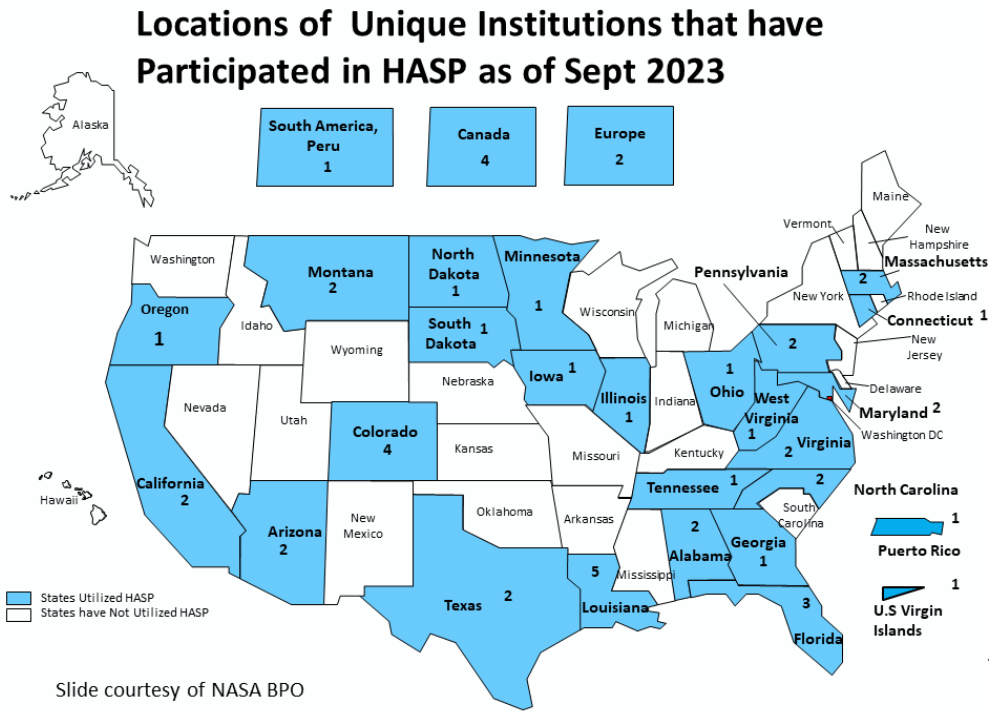


Figure 2-4: States that have utilized HASP as a student workforce development project are indicated by the blue shading. In addition, the number of institutions within the state that have contributed student teams is indicated by the bold number in or near the state.

2.3. Ride Share

In addition to HASP, the NASA ballooning program offers several other ride-share options, including the NASA Undergraduate Student Instrument Project (USIP) and possible piggyback payloads on large science balloons. The USIP program, which has its mission managed and conducted by Wallops Flight Facility, is limited to undergraduate students and is intended to "provide a hands-on flight project experience to enhance the science, technical, leadership, and project skills" and "to fly a science and/or technology investigation relevant to NASA strategic goals and objectives on a suborbital-class platform" [11].

Cubes in Space (see Section 2.1) and some USIP payloads fly as "piggybacks" on regular and experimental scientific balloon flights. Rides for such payloads are negotiated with the primary payload principal investigators and might or might not be supplied with payload power, telemetry bandwidth, or other resources. These kinds of payloads are also referred to as "Mission of Opportunity" payloads, and a Balloon Flight Support Application needs to be submitted to NASA at least six months prior to integration with the primary payload. [12]

Flight application and instructions:
https://www.nasa.gov/scientificballoons/fly-with-us/

3. Small (Weather) Balloons

Many high school and university groups use a standard method to reach high altitudes: the lightweight 1,500 to 3,000-gram latex sounding or "weather" balloon. These balloons generally ascend above 25 km, and a typical flight lasts around 2 hours. They are relatively easy to configure to conform to FAA regulations, so no NOTAM or flight waiver is required, though it is important to respect airspace restrictions and communicate with local FAA authorities as needed. In such a configuration, the vehicle can carry up to 12 pounds of total suspended weight to an altitude in excess of 100,000 feet before the flight is terminated, and the suspended payloads are parachuted back to the surface of Earth for recovery. Such flights typically require ~200-300 cubic feet of helium, which can reasonably be transported in a truck or SUV. Figure 2-5 shows an example of such a vehicle shortly after launch. These hand-launched balloons carry compact GPS trackers which use amateur radio or public radio frequency bands (for example, APRS protocol [14] or 900MHz LoRa band) to provide real-time latitude, longitude, and altitude information directly to chase vehicles on the ground or to the APRS network ground stations that repeat location infor mation to mapping websites such as https://aprs.fi/.

Another reason for the popularity of this kind of high-altitude ballooning configuration is the relatively low cost. Typically, only a few thousand dollars of investment is needed to support all the equipment and materials needed for ground and flight operations. This low cost is within reach of many high schools, colleges, and universities, enabling realistic flight payload development experiences for students in this age group. Many such programs, some with the support of the jurisdiction Space Grant, have been developed across the country and implemented as part of a STEM curriculum or extracurricular activity. In several cases, these programs are associated with course materials such as lectures and activities building basic skills in electronics, programming, atmospheric science, and project management.

Some programs have been adapted to support K-12 teacher in-service workshops.



Figure 2-5: Latex sounding balloon launch with multiple student payloads

3.1. BalloonSat Workshops

One of the first academic ballooning classes was taught at the University of Colorado Boulder (CUB) in 2000, by Chris Koehler who became Director of the Colorado Space Grant Consortium (COSGC) in 2004. This was a one-semester course providing students with hands-on experience in designing and launching flight hardware, but without all the cost (especially launch costs) associated with a CubeSat program. In the summer of 2002, the first BalloonSat Workshop was held at CUB, bringing in educators and interested participants from across the country and providing them with sufficient instruction and resources that they could go back to their home institutions and start a ballooning

class or club of their choosing. These workshops continued every summer until 2007 when it was felt that the supply of interested educators was tapped out.

The early BalloonSat Workshops were taught with input from others, such as Bill Hiscock, the Montana Space Grant Director at the time, and James Flaten from the University of Minnesota, and the launches were aided by EOSS (Edge of Space Sciences), a team of volunteers who provided ham radio expertise for tracking balloons in flight and recovering payloads. The payloads assembled in the workshop were a very straightforward set of atmospheric sensors, a data logger, and a camera, all of which could be put together, tested, and enclosed in a payload box in just a couple days.

Occasional smaller-scale ballooning workshops have occurred since 2007, and the ballooning courses and payload development programs have continued at many institutions across the country thanks to a never-ending supply of enthusiastic students.

3.2. Louisiana Aerospace Catalyst Experiences for Students (LaACES)

The Louisiana Aerospace Catalyst Experiences for Students (LaACES) (https://laspace.lsu.edu/laaces/) was initially developed in 2003 to provide university-level students with an authentic flight project experience not normally available through the classroom. LaACES includes the Student Ballooning Course (SBC), which consists of lectures, hands-on activities, videos, and materials to help entry-level students develop skills in basic electronics, real-time programming, mechanical development, and project management, and is available at this link: https://laspace.lsu.edu/laaces/student-balloon-course/. The SBC is generally organized as a two-semester extracurricular activity (although some institutions implement the SBC as a for-credit addition to their typical curriculum) with two 2-hour sessions per week, and students are expected to devote 10—15 hours per week for hands-on lab work. The first semester is devoted to skill building, while the second semester is focused on project management, payload development, testing, and flight operations.

Students new to LaACES develop the MegaSat balloon payload as their vehicle for conducting investigations during the balloon flight. The primary components of the MegaSat payload, as shown in Figure 2-6, consists of an Arduino Mega controller, an Adafruit Ultimate GPS Logger shield, and the MegaSat shield. While the Arduino Mega and Adafruit GPS shield are commercial units, the MegaSat must be assembled by the students during the course. The MegaSat board includes temperature, humidity, pressure sensors, and a 3-axis accelerometer and gyroscope. The students learn how to write code that can read the sensor data and

GPS information and write a data record onto an SD card file. Once the payload is recovered following the flight, the data on the SD card can be downloaded and analyzed. For more advanced payloads, there is a prototype area on the GPS Logger shield where the student can interface with other sensors (e.g., UV, radiation, Ozone) and record their data during the flight.

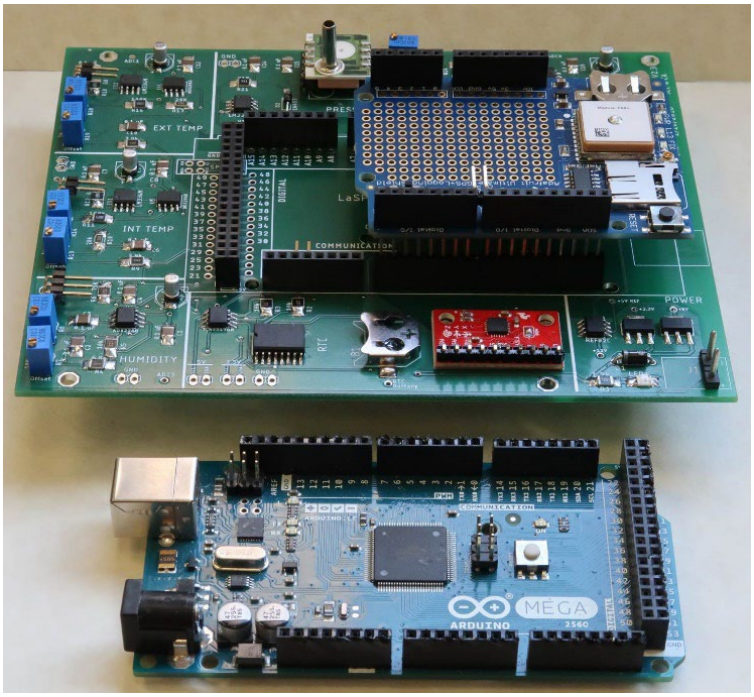


Figure 2-6: The LaACES MegaSat student balloon payload including an Arduino Mega (bottom), the MegaSat shield (middle), and the Adafruit Ultimate GPS Logger shield

As students proceed through the payload development semester, they are required to produce Preliminary Design Review (PDR), Critical Design Review (CDR), and Flight Readiness Review (FRR) documents and presentations. Templates are provided that help guide the students in organizing and composing the detailed documents. For many students, the PDR, CDR, and FRR are the most complicated writing and presentation exercises they encounter during their college career. For this reason, the Scientific Balloon Course also includes training on oral presentations, figure generation, flowcharts, and technical writing.

The lectures, activities, and auxiliary support materials (i.e., the document templates) are available for anyone to download from the LaACES website (https://laspace.lsu.edu/laaces/). In addition, a materials list, circuit board files, and suggested laboratory equipment are also available for institutions that wish to implement their version of LaACES. Institutions interested in developing their student ballooning

program can contact Louisiana Space Grant at laspace@lsu.edu for further information.

3.3. Balloon Outreach Research Exploration And Landscape Imaging System (BOREALIS)

At Montana State University in Bozeman, Montana, there is a high-altitude ballooning program called BOREALIS (Balloon Outreach Research Exploration And Landscape Imaging System). BOREALIS comprises a rotating group of approximately 10 students from a wide range of academic disciplines. While mechanical, electrical, and computer engineering are the most common majors among the students, BOREALIS has seen students from elementary education, technology education, mathematics, physics, astrophysics, and various other disciplines over the years. Students do not have to have specific skills to engage in ballooning; they simply need to have a passion for aerospace and exploration. Students are recruited through presentations by students and faculty, through ballooning workshops held on campus, and open-house nights held weekly at the BOREALIS lab on campus. When students come to the lab for the first time, they are given a tour and introduced to current and past interns (the title given to students who work for BOREALIS in the summer) and current apprentices (students working on research during the academic year). New students are connected with a project, problem, or current task that needs to be solved. New skills are learned "on the job" as needed as they work through a problem. The mentors present problems and provide resources, knowledge, and skills but do not generally know a solution to the problems presented. The student will be the one to generate novel answers to problems and invent new systems and processes. Student solutions will eventually be tested in flight.

Balloon flights dictate the problems that need to be solved. Flights often do not happen during the academic year, except for one fall and one spring flight due to weather and wind patterns in Montana. The summer months often see 7-10 flights, with flights once a week during a 10-week summer internship program (see Figure 2-7). The time in between flights is when all of the work happens. The flight systems include a balloon (latex or zero-pressure), a tracking system with GPS, a flight termination system (called cutdown), a recovery system (parachute or other devices), and a payload string with experiments. There is a ground control team with computers, antennas, and other electronics used to track the balloon and payloads and communicate with the balloon in flight. All this hardware, software, and the procedures to use them are student-developed. Flight days allow for the testing of hardware and systems and provide much-needed real-world data. Students are encouraged to explore areas that they are not familiar with, to challenge themselves, and to learn new skills. With such a wide range of systems, there are opportunities for software development, CAD design, 3D printing, CNC manufacturing, electronics design, printed

circuit board design and fabrication, sewing, assembling, and significant troubleshooting. With each flight, students experience successes and failures. While successes are wonderful and build confidence, it is through failure that most learning takes place.



Figure 2-7: BOREALIS Team readying a balloon for launch

Failure is difficult. Failure results in terse language, stomping feet, and a deflation of ego. Students get angry, lose faith in their abilities, and often need time to stew in their failure. However, a good mentor encourages the students to embrace failure as an opportunity to learn. At this point, they collect the broken pieces of hardware, the corrupted data, and the photos and video from the flight and begin the forensic analysis process. Students learn to seek proof of why something failed and not rely on guesses and conjectures. While an educated guess might provide a starting point, students are often surprised when they learn that a failure had nothing to do with the cause they were "sure" started the fault. Sometimes, the answers are found not in a video clip but in a set of data. Pulling altitude, pressure, temperature, and time stamps into an Excel spreadsheet can

often uncover answers just as well as a good photograph. Failures also encourage more interdisciplinary work. A software issue may have caused a hardware failure or vice versa. A good detective will often have to learn the basic workings of unfamiliar systems to understand how two or more components work in unison in one cohesive system. The difference between components and systems can only be understood when large complex systems are built and tested with a collection of smaller independent subsystems.

3.4. Nationwide Eclipse Ballooning Project (NEBP)

For most balloon flights, the timing and location of the launch is not generally a critical aspect of the flight, so if a subsystem is not working or if the weather is not favorable, most academic balloon launches can be delayed by minutes, hours, or even days. This is not the case for ballooning during a solar eclipse, however, because the goal is to be at altitude and near the center of the path of totality when maximum occultation happens. The Nationwide Eclipse Ballooning Project (NEBP) was conceived not just to challenge ballooning teams to achieve this goal, but more broadly to create, equip, and train a nationwide network of teams capable of performing high-precision balloon launches carrying complex payloads. Payloads and launches were configured to gather a substantial body of atmospheric data with the goal of posting it for scientists worldwide or any member of the public to use. Additionally, the project was configured to maximize student participation, perform STEM outreach, and engage the public with NASA missions, space exploration, and science in general. The NEBP was organized and proposed by the Montana Space Grant Consortium at Montana State University and became one of many large-scale projects funded through the Science Activation Program, which is part of the Astrophysics Division of the NASA Science Mission Directorate. During the last 10 years, three major solar eclipses have traversed the United States: in August 2017, the path of the Moon’s shadow crossed from Oregon to South Carolina [15]; in October 2023, an annular eclipse was visible from Oregon to Texas; and in April 2024, the path of totality stretched from Mexico up through Maine. All three of these tracks are shown in Figure 2-8.

The timing of these 3 eclipses lent itself nicely to the development of interest in eclipse ballooning and the creation and organizing of ballooning teams across the country. NEBP efforts during the 2017 eclipse were a tremendous success with many teams live-streaming over the internet and contributing to NASA’s eclipse day coverage. Some issues were identified with internet accessibility in remote sites and distributing live video real-time. Payloads and procedures were subsequently improved, and in 2022, interested schools and groups proposed to be part of the next phase of the NEBP project. Over 50 teams were equipped and trained by 2023, so they could use the annular eclipse

as a practice run for the total eclipse in 2024. This network of teams is still going strong even though no more eclipses are predicted for North America until 2044 and 2045.

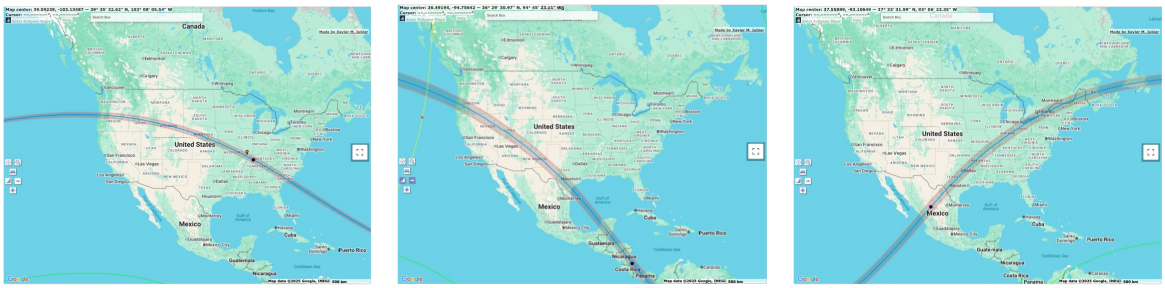


Figure 2-8: Path of the Solar Eclipse in 2017, 2023, and 2024

Credit: Xavier M. Jubier, http://xjubier.free.fr/

For the 2023 and 2024 eclipses, the NEBP ballooning teams were split into two types: atmospheric-science teams launching radiosondes every hour from 24 hours before the eclipse to 6 hours afterwards; and engineering teams launching only 1 or 2 large weather balloons carrying a set of payloads, some common to all teams and others unique. The main goal of the atmospheric science teams was to obtain a substantial body of data on the changing characteristics of the atmosphere as the eclipse moved through, with the hope of identifying atmospheric gravity waves in the data post-flight. The primary goal of the engineering teams was to capture and stream real-time video of the Moon's shadow coming across the Earth as seen from the edge of space (see Figure 2-9), and also to gather other imagery and a substantial set of atmospheric data from the various other payloads. Approaching 2023, there were 53 ballooning teams, 19 focused on atmospheric science and 34 focused on engineering, from 75 institutions, spread over 32 states. All of the NEBP teams were organized into regional pods, which allowed the pod leaders to run workshops, distribute equipment, and provide training on the basics of launch procedures and payload assembly and operations.

All atmospheric science teams flew standard radiosondes and operated Graw ground systems to collect the telemetry data from each balloon in flight, in addition to having a weather station for recording ground measurements throughout the entire 30 hours of observation. The engineering teams benefitted from being given all the components necessary to assemble 3 common payloads: a location and atmospheric data payload called PTERODACTYL designed at the University of Minnesota; a video-streaming and telemetry downlink payload called RFD900, designed by Montana State University; and an Iridium unit with associated electronics to track the balloon in flight. In addition, all engineering teams were given the parts and instructions for putting together two

ground station assemblies, one to track the balloon and the other to receive the telemetry stream real-time. Balloons were distributed to all the participating teams as well, and Montana also provided

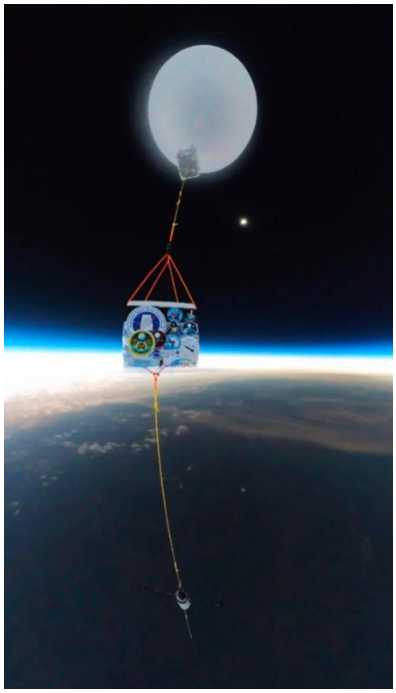


Figure 2-9: The University of Alabama NEBP team obtained this picture at 100,000 ft, looking up along the flight line towards the balloon. The image clearly shows the moon's shadow on the Earth during the solar eclipse of 4/8/25.

Photo Credit: Alabama Space Grant Consortium.

sufficient Helium on eclipse days to all the teams launching along the path of totality.

As part of the preparatory and training effort prior to the eclipses, the NEBP created two ballooning courses: a science-track course focused on studying atmospheric science using radiosondes, and an engineering-track course focused on developing, operating, and launching balloon payloads. Both courses are still available and can be found on the NEBP website (https://eclipse.montana.edu/), and both include lessons on mission planning and launch logistics for inexperienced teams. Links to these courses are at:

https://eclipse.montana.edu/education/sciencecourse.html
https://eclipse.montana.edu/education/engineeringcourse.html

On the day of the total eclipse (April 8th, 2024), all NEBP teams across the country launched balloons and participated in outreach events in or

near the path of totality. Over 650 students were actively involved on the ballooning teams, and between April 7th and April 9th, 2024, NEBP engaged over 22,000 members of the American public in eclipse learning. Some of the atmospheric science teams joined forces and set up 'super sites' where they could coordinate balloon launches and get even finer resolution in their data set with balloons released as often as every 15 or 30 minutes. NASA set up public viewing sites and featured some of the live video from NEBP in their eclipse coverage, which had over a million simultaneous viewers. These kinds of projects are uniquely positioned to engage the public while also teaching students, exciting their imaginations, and encouraging them to learn more about NASA ballooning in particular and NASA missions in general.

After the eclipses of 2023 and 2024, all NEBP teams were asked to upload their data files to the Montana server so they could be quality-controlled and documented, and then this entire set of data was uploaded to the Dryad Repository at the following links:

NEBP Atmospheric Data:
https://datadryad.org/dataset/doi:10.5061/dryad.v15dv426j

NEBP Engineering Data:
https://datadryad.org/dataset/doi:10.5061/dryad.rv15dv4jh

Following the conclusion of the eclipse campaigns, some of the NEBP atmospheric science teams followed up with a campaign to the East Coast in January 2025 to measure the divergence of winds over the Gulf Stream ocean current. Additionally, twenty of the engineering teams built radiation-sensing payloads and launched balloon flights all across the country to measure variations in the radiation environment at high altitudes during the second half of the 2024-2025 Solar Maximum Year. All of this data is currently being collected and will be uploaded to Dryad as soon as it is compiled and checked. These latest campaigns are examples of the kind of challenge that the NEBP ballooning network can take on with ease and enthusiasm going forward. The hope is that, once established, these teams can continue to thrive providing hands-on experience and a microcosm of a NASA-like launch experience for many students for many years to come.

3.5. Supporting Organizations

Edge of Space Sciences (EOSS) is a non-profit organization based in Denver, Colorado, that promotes science and education using amateur radio and high-altitude ballooning. As mentioned in Section 3.1 above, they have supported local groups with ballooning by coordinating with the FAA and providing volunteer ham radio operators to help with tracking of balloons and recovery of payloads. They are also recognized world-wide for their ballooning expertise. (https://www.eoss.org/)

The Stratospheric Ballooning Association (SBA) is an organization devoted to STEM education, research, and safety in high altitude ballooning and other stratospheric and space related activities. They organize a yearly conference, the Academic High-Altitude Conference (AHAC) which generally takes place in Iowa, Minnesota, or more recently (June 2025) in Alabama. This conference is focused primarily on undergraduates participating in sounding balloon programs, but the SBA also runs occasional workshops at AHAC teaching ballooning skills or demonstrating new ballooning technologies. Additionally, the SBA maintains the Journal of High Altitude Ballooning (JHAB), which is a peer-reviewed journal dedicated to high-altitude ballooning and related activities, including an archive of AHAC presentations and manuscripts. (https://www.stratoballooning.org/ahac)

It is also worth mentioning the Scientific Ballooning Technologies Workshop, which is hosted every other year by NASA and the University of Minnesota in Minneapolis. This conference focuses mostly on hardware, technologies, and topics relevant to the operation and research conducted on the large high-altitude long-duration NASA Balloons.

4. Outcomes and Impact

4.1. Lessons Learned from BOREALIS

Systems design is difficult and complex. Experience has shown many high-altitude ballooning students that just because all the individual pieces work, that does not mean the collection of those systems will work together as a whole. One lesson that BOREALIS students have learned many times over is the need to test their hardware in flight configuration under as close to flight-like conditions as possible. In other words, "Practice how you perform, so that you will perform as you practiced." End-to-end tests are critical in large system design. Only when everything is connected can one learn what problems, unthinkable as they may seem, might appear. Just as systems need to be tested together, end to end, people also need to work together as a team.

4.1.1. Team Formation and Dynamics

Teamwork is often recognized as a necessary skill in the workplace. Students on a ballooning team are forced to work together, and the better they perform as part of a team, the more successful the team becomes. A strong team is often the result of good leadership and mentoring, which includes leaders who work alongside their team members, keeping them all engaged and inspired, and mentors who listen and discuss problems without offering immediate answers to all challenges. The BOREALIS mentors select students to lead various subgroups, such as inflation, launch, recovery, ground station, payloads, etc. Generally, student leads will tend to step up and embrace their roles while also

feeling a sense of responsibility to be better in all ways. There is a danger that some students may become overconfident, and those in leadership positions may sometimes become bigheaded. This may negatively affect team dynamics and should therefore be recognized and dealt with as early as possible by having a frank and respectful conversation with the student in question and using humor, if possible, to keep things upbeat.

Teamwork and good leadership are important foundations on which the learning in a ballooning program will occur. To maximize learning and confidence building, giving students small tasks to achieve small successes is a good start. Then, building on those small successes and offering harder, more challenging tasks to individuals or to the team as a whole, will continue to build capability. Interestingly, failures often create even better learning environments, and surprisingly also tend to build confidence going forward. Learning to function as a team, deal with individual differences, and support one another is the greatest skill a student can take away from an academic ballooning program.

4.1.2. Good Practices and Procedures

With a new team, demonstrate what a launch day will look like ahead of time, by taking all the equipment outside and setting it up just as if you were going to do a launch. It's also a good idea to keep all the flight day equipment and tools together. Organize and store equipment in labeled containers. Keep a flight day inventory sheet and make checklists – ideally every procedure and every payload should have a checklist. It is also important that every person have a job even if that job may just be observing and looking out for safety hazards. It generally does not matter if students have backgrounds or experience in a particular area; it only matters that they are interested and enthusiastic. The role of the adult mentor is to provide resources for the students, tools, materials, a place to work, and a community of other students for support and instruction. They must also make sure safety procedures are followed.

Picking a launch site: Some teams are lucky enough to be able to launch from their campus, but more often, either because of restricted airspace or wanting to target a more favorable landing site, a team will have to pick a launch location and travel there on the morning of the launch. Community centers, libraries, and other places that hold public outreach events may be good launch sites. Airports may also be great places so long as they are small general aviation airports without a high volume of air traffic. The smaller the airport, the more likely you will be welcomed. Public land may be the next best thing if an airport is not an option. A park, a parking lot, or other public space will often work

if it has a large, clear area (clear of trees, lampposts, and power-lines) from which to launch.

Launch procedures: On launch day or during a pre-launch simulation, practice a NASA mission control preflight go/no-go roll call. Call out each of the critical roles: inflation, flight termination, tracking, payload 1, payload 2…, payload n, range safety, etc. Each team lead should respond with either a "go" or a "no-go." If they are "no-go," they must provide a short (only a few words) description of the issue. "Faulty switch," "dead battery," and "leaky valve" are all examples of "no-go" descriptors. It is also helpful to have the student give a time estimate. When done correctly, this "go/no go" routine looks and sounds very professional, and also adds a layer of error checking to the launch procedure. Typically, once all systems are "go", a short countdown followed by balloon release is typical.

Dealing with landowner on landing: Once the payloads and parachute have landed, landowner permission needs to be granted before venturing on their property to retrieve anything. This is a situation where the flight director needs to take the lead. It is best to go to the door of a landowner's house with only two people, explain briefly what the situation is, show the landowner where on their property the payloads are likely to be, and ask permission for a few students to go find them. No crops should be trampled and no damage should be done to the property during the retrieval process. Leave things as you found them.

Conclusion: Above all else, one of the great features of academic ballooning is that learning is actually more important than success. Even if a flight results in total failure of all systems, the team will learn and grow and will do better next time. Negativity is contagious, but so is positivity. As a leader, be as positive a force as possible and avoid negativity. Be the role model that the team wants to follow and emulate.

4.2. Lessons Learned and The Public

It is incumbent on the balloon operator to develop a good working relationship with the local FAA representative to ensure that all notifications have been properly filed and the public is aware of the event. FAA part 101 is the guiding documentation for unmanned balloons and states, *"No person may operate an unmanned free balloon- During the first 1,000 feet of ascent, over a congested area of a city, town, or settlement or an open-air assembly of persons not associated with the operation"* (FAR Part 101.33-d).

Public perception of what a ballooning team does will vary. It is important to reach out and educate the public on what your team is doing. If someone shows interest, share with them. Explain why you are

doing what you are doing. Sing the praises of your team and highlight the great things they are doing. Be positive and excited, and more often than not, the public will share your excitement. When searching for launch and ground station sites, search for people and places that might share in the love of aviation and space exploration. Airports are great places so long as they are small general aviation airports without a high volume of air traffic. Reach out to the airport far in advance (at least a week) of the planned balloon launch. Most small airports will have an FBO (Fixed Base Operator) that will make a good first point of contact. The FBO is the business entity on the airfield. There will also likely be a separate person who is the airport manager. It is important to speak to the FBO and the airport manager to get permission to launch from their airfield. Pilots love pilots and all things aviation. They will likely love what you are doing, but they will want to ensure that you are doing it safely and not posing a risk to the flight operations in the field.

4.2.1. Lessons Learned from NEBP

Lessons Learned from the Nationwide Eclipse Ballooning Project were very similar overall to those learned by the Borealis team over many years of mentoring ballooning activities. A significant number of the NEBP teams were new to ballooning so they no doubt had a steeper learning curve than those teams that were more experienced. One thing that all teams had in common, though, was the possibility of having to launch in unfavorable weather conditions because eclipse launches don’t have the luxury of waiting for better weather. Fortunately, weather along most of the path of totality for both eclipses in 2023 and 2024 was generally okay for launching balloons, other than areas of fog and overcast where teams may have had difficulty viewing the eclipse itself; some teams did have to deal with high winds, however, and there was snow in Maine for the total eclipse.

Because of the possibility of high winds, quite a few NEBP teams chose launch locations where they had the option of inflating the balloon inside an enclosure if necessary. Another option was to build a structure of PVC pipes covered with plastic sheet, that could then be used either as an enclosure or as a wind break for the balloons, as shown in Figure 2-10. In any case, when dealing with high winds, the goal is to have the partially inflated or fully inflated balloon exposed to the wind for as little time as possible before releasing it. This requires making sure all the payloads are ready to fly before bringing the balloon out of the enclosure, and then performing a safe release as quickly as possible. It is good practice to always release the balloon upwind of the payload string, especially for a flight line of any length (12 ft or more), so that the balloon will ideally ascend faster than it travels downwind once released, picking up payloads instead of dragging them.



Figure 2-10: Two balloons being inflated near an open PVC and plastic sheet enclosure during a University of Maryland practice eclipse launch

Another challenge that a lot of teams ran into with the eclipse launches was that payload recovery had to be done in unfamiliar territory. Usually teams develop a good sense of acceptable landing zones around their home institution, but when you have to travel to launch in a far off location, as many teams did for the eclipses, recovery operations can present new challenges: for example, difficulty finding information about property owners, lack of familiarity with restricted areas (like deer leases in Texas), and identifying a local tree climber willing to retrieve payloads from the top of trees (see Figure 2-11), to name just a few.

4.2.2. Outcomes from NEBP

There are two clearly distinguishable types of outcomes from the NEBP: first, science and engineering data and reports; and second, significant learning outcomes. The first type of outcome is most easily described and quantified:

- After the first eclipse but well before the end of the program, in February 2025, a preliminary publication tally was done with

the following results: 28 conference presentations, 6 poster presentations, and 5 journal publications. There are no doubt many more publications in the works, with peer-reviewed journal papers in atmospheric science, for example, being some of the expected outcomes that will understandably take the longest.

- Both atmospheric science and engineering teams recorded huge quantities of data during all their eclipse flights. All of this data for both eclipses was quality controlled and uploaded to the Dryad Archive Repository, one set for atmospheric data and one set for engineering data. All of this and more to come is open for public use by anyone who may be interested.

One of the publications that most succinctly summarizes useful information applicable to other similar programs is the paper entitled "Nationwide Eclipse Ballooning Project: A Toolkit for Broadening STEM Participation, Building Networks, and Bridging Education and Research." [16]. This paper was published between the two eclipses but still contains relevant information pertinent to running a nationwide outreach and education effort centered on academic ballooning.



Figure 2-11: Payloads often land on the tops of tall trees

The second type of outcome from the NEBP is more difficult to measure but since the NEBP is a NASA Science Activation project, it benefits from having a professional evaluator assess the program throughout. As a result, a couple of reports have been written that draw from surveys of all the students and mentors involved [17] and from focus groups that discussed the overall program in some detail after its conclusion [18].

Some of the highlights of the student surveys are shown in Figure 2-12. NEBP students indicated that the project had positive impacts on their self-confidence and their STEM identities. The rightmost bars are particularly striking: the number of students who have high confidence in their ability to get a good job after graduating almost doubled; and the percentage of students who see themselves as STEM professionals went from 33% to almost 70%. Overall, their interests and sense of competence in pursuing STEM studies and careers increased very noticeably, and the

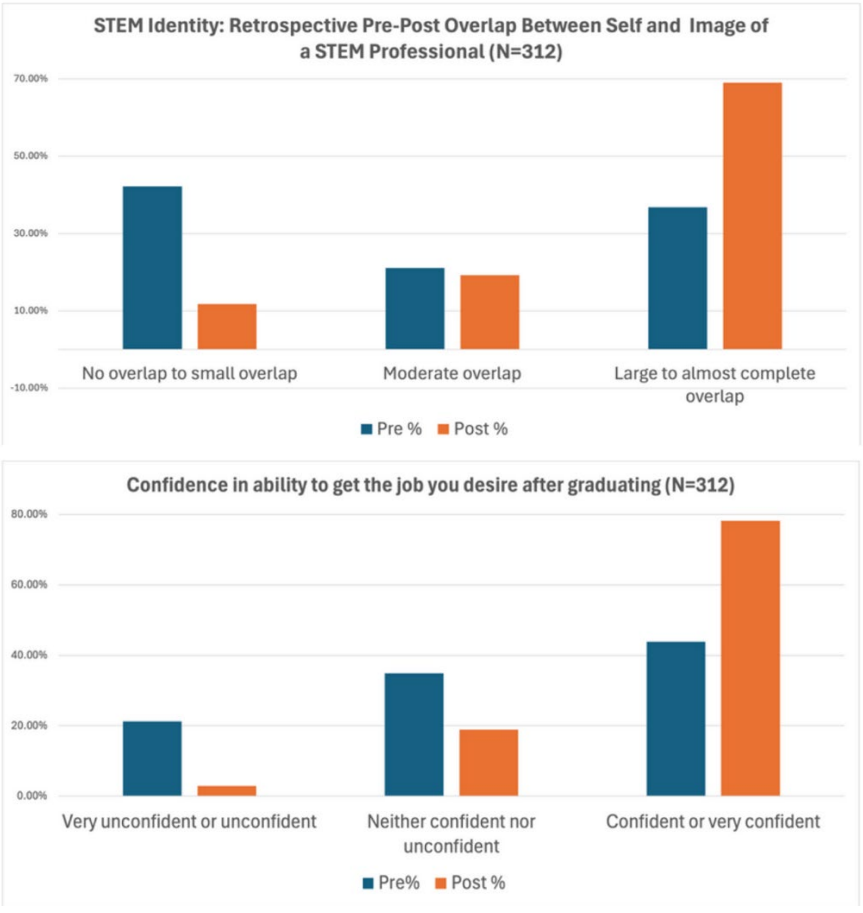


Figure 2-12: Bar graphs showing the change in student perceptions from the beginning of their NEBP involvement (Pre%) to the end of their involvement (Post%, after both eclipses)

NEBP also achieved significant goals around broadening participation and creating welcoming team environments.

4.3. Impact from Elementary School to Graduate School

In summary, balloon platforms are a critical vehicle for supporting Principal Investigator-class academic research due to the short time scale between conception and flight results, B) relatively low cost,



Figure 2-13: University students watching the launch of their experiments carried by the High Altitude Student Platform (HASP) in September 2018

and C) recoverability. This combination of characteristics enables universities to support research programs that develop near-space flight hardware while engaging future scientists and engineers. As most balloon experiments are recovered and re-flown, the acceptable risk on individual balloon payloads should be high relative to spacecraft. By accepting risk on balloon payloads, quality assurance requirements are reduced, which, in turn, will decrease development time and overall cost. As spacecraft instrumentation is unrecoverable, has high launch costs, and is generally managed for low-risk, student access to the development of actual spacecraft systems is generally highly restricted, resulting in limited training opportunities. However, the high acceptable risk aspect of balloon payloads allows post-docs, graduate students, and undergraduate students to directly interact with payload hardware and software and develop skills that will be applicable throughout their careers.

Workforce development platforms such as piggyback payloads and systems like HASP provide advanced degree students and early career scientists and engineers with the training and experience necessary for them to take their next step. The world of academic ballooning is facing some new challenges relating p rimarily to cost. Most small latex balloons are manufactured outside the US, primarily in China and Japan, so costs are increasing in part because of tariffs. Helium, also, is getting more expensive and is, in fact, quite difficult to procure in some parts of the country. As a result, some teams are switching to hydrogen as

their lifting gas, but this is difficult to do especially with younger or less experienced teams due to the additional safety precautions and training necessary. Another additional challenge on the horizon is the recognition that the FAA may want to regulate, or at least track, small balloon flights more than they have in the past and they may require transponders of some sort on all scientific balloons. This would incur a significant cost and weight penalty until reliable and light-weight beacons can be made available at low cost to ballooning teams.

Despite these concerns, however, ballooning remains an excellent platform for scientists and engineers of all ages to experience the joy of launching their unique experiments into the stratosphere. Whether small balloon payloads, piggyback payloads, or programs like HASP, they provide opportunities for students through early career scientists to obtain the training and experience necessary to take their next step (Figure 2-13). Prototype test flights on balloon platforms provide the data necessary to improve the Technical Readiness Level (TRL) of the device or experiment methodology. At the same time, early career scientists and engineers gain a unique hands-on training opportunity with all the excitement of NASA "space flight missions."

References

[1] NASA Balloon Program Analysis Group Executive Committee, "A Roadmap for Scientific Ballooning 2020-2030," P. Gorham, Chair, 2022. [Online]. Available: https://arxiv.org/abs/2210.01198

[2] R. S. Walker, F. W. Peters, and B. Aldrin, "Final Report of the Commission on the Future of the United States Aerospace Industry," 2002. [Online]. Available: http://ita.doc.gov/td/aerospace/aerospacecommission/aerospacecommission.htm

[3] E. Aldridge Jr., C. Fiorina, et al., "Report of the President's Commission on Implementation of United States Space Exploration Policy," 2004. [Online]. Available: https://www.nasa.gov/pdf/60736main_M2M_report_small.pdf

[4] National Academy of Sciences, National Academy of Engineering and Institute of Medicine, Rising Above the Gathering Storm, Revisited: Rapidly Approaching Category 5. Washington, DC: The National Academies Press, 2010. [Online]. Available: https://www.nap.edu/catalog/12999/rising-above-the-gathering-storm-revisited-rapidly-approaching-category-5

[5] "Building the Space Workforce of the Future: STEM Engagement for a 21st Century Education," Hearing before the US Senate Committee on Commerce, Science, and Transportation, Nov. 5, 2019. [Online]. Available: https://www.commerce.senate.gov/2019/11/building-nasa-s-workforce-of-the-future-stem-engagement-for-a-21st-century-education

[6] "Charting a Course for Success: America's Strategy for STEM Education," A Report by the Committee on STEM Education of the National Science & Technology Council, The White House, Dec. 2018. [Online]. Available: https://www.whitehouse.gov/wp-content/uploads/2018/12/STEM-Education-Strategic-Plan-2018.pdf

[7] "NASA Strategic Plan 2022," 2022. [Online]. Available: nasa.gov/ocfo/strategic-plan/

[8] "SCIENCE 2020-2024: A Vision for Scientific Excellence," 2020. [Online]. Available: https://science.nasa.gov/about-us/science-strategy

[9] T. G. Guzik, "The High Altitude Student Platform (HASP) as a model multi-payload balloon platform," in *2015 IEEE Aerospace Conference*, 2015, pp. 1–10.

[10] D. J. Granger, "The High Altitude Platform (HASP) for Training the Next Generation of SMD Scientists and Engineers – Fourth Annual Progress Report (Dec 2023 – Nov 2024)," 2024.

[11] NSPIRES, "Undergraduate Student Instrument Project (USIP) Student Flight Research Opportunity (SFRO), NASA solicitation," NNH15ZDA010C, 2015.

[12] NASA Balloon Program Office Piggyback Handbook, 820-HDBK-Piggyback-01, May 2024.

[13] "Cubes in Space: Ingenuity taking flight," 2019. [Online]. Available: https://www.cubesinspace.com/

[14] B. Bruninga, "Automatic Packet Reporting System." [Online]. Available: http://www.aprs.org/

[15] A. C. Des Jardins, S. Mayer-Gawlik, R. Larimer, et al., "Eclipse Ballooning Project Live Streaming Activity: Overview, Outcomes, and Lessons Learned," in *Celebrating the 2017 Great American Eclipse: Lessons Learned from the Path of Totality*, ser. Astronomical Society of the Pacific Conference Series, vol. 516, Jun. 2019, p. 353.

[16] M. E. Saad, B. Covitt, S. Taylor, A. Des Jardins, and N. Frank, "Nationwide Eclipse Ballooning Project: A Toolkit for Broadening STEM Participation, Building Networks, and Bridging Education and Research," *Bulletin of the American Astronomical Society (BAAS)*, Mar. 2024. [Online]. Available: https://doi.org/10.3847/25c2cfeb.a8f47e95

[17] B. A. Covitt, M. E. Saad, N. Frank, S. Taylor, and A. Des Jardins, "Leveraging Eclipses to Build a Network for Broadening STEM Participation: An Evaluation of the Nationwide Eclipse Ballooning Project," *Bulletin of the American Astronomical Society*, vol. 56, no. 9, Oct. 2024. [Online]. Available: https://doi.org/10.3847/25c2cfeb.7012f88b

[18] B. A. Covitt, A. C. Des Jardins, et al., "Insights From and Future Directions for a Nationwide Science and Engineering Education Collaboration in Stratospheric Ballooning," submitted to a special issue of *Frontiers in Astronomy and Space Science* highlighting education and public outreach efforts of the Heliophysics Big Year, July 2025.

Chapter 3
Science from the Stratosphere

Sarah A. Roth[1], Nicolas Zoghb[2], and Emily A. Kirchner[3]

[1] National Aeronautics and Space Administration, Chief Technologist, Balloon Program Office
[2] Professor, University of Bridgeport
[3] Student, Department of Physics, Salisbury University

Acknowledgments

This chapter was made possible by the contributions of many scientists and engineers who have made significant contributions to science using balloon-borne experiments. These contributions were compiled through email, academic papers, and verbal interviews. A complete list of those participants and their affiliations can be found below.

Contributors:

- Benton, Steve – Princeton University
- Besson, David – University of Kansas
- Boggs, Steven – University of California, San Diego
- Boering, Kristie – University of California, Berkeley
- Chakrabarti, Supriya – University of Massachusetts Lowell
- Filippini, Jeff – University of Illinois at Urbana-Champaign
- Hall, Jeffery – NASA Jet Propulsion Laboratory, California Institute of Technology
- Hamden, Erika – University of Arizona
- Hewawasam, Kuravi – University of Massachusetts Lowell
- Jones, William C. – Princeton University
- Kleinböhl, Armin – NASA Jet Propulsion Laboratory, California Institute of Technology
- Kogut, Alan – NASA Goddard Space Flight Center
- Krawczynski, Henric – Washington University in St. Louis
- Millan, Robyn – Dartmouth College
- Nagy, Johanna – Case Western Reserve University
- Nowicki, Suzanne – Los Alamos National Laboratory
- Pearce, Mark – KTH Royal Institute of Technology, Sweden
- Rahlin, Sasha – University of Chicago
- Roesler, Erika – Sandia National Laboratories
- Sample, John – Montana State University
- Seo, Eun-Suk – University of Maryland, College Park
- Siles, Jose – NASA Jet Propulsion Laboratory, California Institute of Technology
- Tang, Adrian – NASA Jet Propulsion Laboratory, California Institute of Technology
- Toon, Geoff – NASA Jet Propulsion Laboratory, California Institute of Technology
- Wender, Stephen – Los Alamos National Laboratory
- Wu, Qian – University Corporation for Atmospheric Research

Table of Contents

1. Introduction 6

2. Astrophysics 7

2.1 Microwave 8

2.2 Infrared 9

2.3 Visible 11

2.4 Ultraviolet 13

2.5 X-ray 13

2.6 Gamma Ray 14

2.7 Cosmic Rays 15

3. Heliophysics 17

4. Earth Science 18

4.1 Ozone 19

4.2 Thermospheric Winds 19

5. Planetary Science 20

5.1 The PICTURE balloon program 20

5.2 Extra Planetary Missions 23

6. Astrobiology 24

7. Conclusions 25

References 27

Table of Figures

Figure 3-1: This landscape of “mountains” and “valleys” speckled with glittering stars is actually the edge of a nearby, young, star-forming region called NGC 3324 in the Carina Nebula. Captured in infrared light by NASA’s new James Webb Space Telescope, this image reveals previously invisible areas of star birth for the first time. However, this is a static image. ASTHROS will complement these observations by providing key information about the dynamics of these regions and how stellar feedback affects star formation..... 10

Figure 3-2: NASA Jet Propulsion Laboratory (JPL)’s ASTHROS radio telescope being prepared for launch..... 11

Figure 3-3: Skyhook balloon launched as part of the Stratoscope project. 12

Figure 3-4: CREAM hardware used on balloon flights during integration activities at NASA Wallops Flight Facility..... 16

Figure 3-5: Distribution of positional centroids achieved by PICTURE-C shows that it achieved 1.7 mas RMS pointing stability, which is comparable to that of JWST..... 21

Figure 3-6: To image an exoplanet, one needs a contrast level of approximately 10^{-6}. PICTURE-C demonstrated a raw contrast level of 5×10^{-6}, which with post-processing, sufficient to image debris disks – exoplanet analogs of asteroid belts..... 21

Table of Tables

Table 3-1: Summary of CREAM flights..... 17

Table 3-2: Technology developed and matured by the PICTURE family of suborbital missions..... 22

Table of Symbols

Symbol	Meaning	Dimension
A	Area	L^2
c	Speed of light	$L\ T^{-1}$
d	Distance	L
E	Energy	$M\ L^2\ T^{-2}$
h	Planck's constant	$M\ L^2\ T^{-1}$
I	Intensity (radiant or signal)	$M\ T^{-3}$
N	Number of events, counts, particles	–
P	Pressure	$M\ L^{-1}\ T^{-2}$
R	Resistance (electrical)	$M\ L^2\ T^{-3}\ I^{-2}$
r	Radius	L
T	Temperature	Θ
t	Time	T
Δ	Change in (Δt, ΔE, etc.)	-
λ	Wavelength	L
ν	Frequency	T^{-1}
σ	Standard deviation / uncertainty	-
Φ	Flux (particle or energy)	$L^{-2}\ T^{-1}$
Ω	Solid angle	–

1. Introduction

Since their invention, balloons have extended scientific understanding beyond Earth-bound instruments and observations. Scientific research has motivated decades-long balloon programs from space agencies around the world. The last handbook did not touch on the subject of research, perhaps, because of the hand-in-hand nature of balloon programs with science. However, with this edition, it can be valuable to explore the breadth of science that balloons can support, as well as highlight some of their missions and discoveries. In recent years, access to space has eased significantly with the introduction of "CubeSats" and new commercial launch providers. However, for science researchers, balloons remain an integral part of the scientific landscape, and there is no desire to see their use wane. The US National Academies publish decadal reports on the state of science and supporting technologies. Three recent publications, *Solar and Space Physics: A Science for a Technological Society* (2013), *Pathways to Discovery in Astronomy and Astrophysics for the 2020s*, and *Origins, Worlds, and Life: A Decadal Strategy for Planetary Science and Astrobiology 2023-2032* cite the balloon platform as critical for continued science discovery [2]. Some reasons for their continued endorsement include shorter development timelines, flexibility in cost, weight, and schedule, and the availability of comparable low-cost orbiting satellites [2].

Additional reasons cited by scientists for balloon use include:

1. **Balloons operate at altitudes that overcome many of the restrictions of ground-based or even aircraft-borne instruments.** Across the electromagnetic spectrum, the atmosphere is reasonably transparent for the optical, radio, and some near-to-mid infrared frequencies. However, for astrophysics and other science fields requiring observations at other frequencies, such as the ultraviolet (UV), X-rays, gamma rays, or in most of the infrared, or at very long radio wavelengths, then the only way this can be achieved is to perform the data collection above the atmosphere [1]." Additionally, for other science research, key tracers can be blocked by water vapor, motivating missions like ASTHROS which specifically investigate stellar feedback [6].
2. **Long-duration missions of slow-moving balloons allow for continuous observation** of dynamic and complex processes and temporal changes in the stratosphere [46], and a chance to capture unpredictable, fast-moving phenomena such as solar flares, magnetic disturbances, and microbursts [65]. Additionally, hovering at specific altitudes allows for targeted observations and experiments, which are essential for understanding localized atmospheric phenomena [47] and directly measuring atmospheric conditions and chemical compositions [45].

3. **Balloons offer a test-bed platform for new technologies and science instruments before moving to orbiting platforms.** Without a dedicated balloon program, researchers would likely have to transition directly from laboratory instruments to satellites in space. Such a leap poses significant challenges in testing technologies and developing the necessary workforce to execute a satellite mission successfully [28, 30]. Balloons also have the potential to generate significant interest from theorists and scientists regarding the results of these observations, which may lead to the development of future satellite observatories. The foundational science can not only be conducted on balloons but must also be validated on these platforms before progressing to satellite missions [28, 30].
4. **Balloon platforms bridge the gap between ground-based experiments and orbital missions** [2]. Science observations within infrared research in astrophysics, for instance, will complement datasets from other NASA missions that have observed in the infrared wavelength range, including the Stratospheric Observatory for Infrared Astronomy (SOFIA), the Wide-Field Infrared Survey Explorer (WISE), the Herschel Space Telescope, the Spitzer Space Telescope, and the Hubble Space Telescope [3]. Potential future balloon missions, flying for longer at sustained altitudes, could make joint observations with upcoming satellites [38].
5. **Balloons contribute to the development of science researchers and engineers**, offering them hands-on experience that might otherwise be less accessible through satellite projects or solely through data analysis. Balloon missions provide a cradle-to-grave experience within a few short years, from designing and building instruments, collecting and analyzing data, and understanding the science [2].

With these advantages for a wide variety of fields and subjects, a small summary of the breadth of topics studied on balloons follows. To state all of the discoveries and contributions provided by balloons would require a significant body of work not undertaken here. Instead, this is meant to highlight some missions and some discoveries to provide the reader with an appreciation of the scientific work completed on balloons.

2. Astrophysics

Balloon flight has been critical to several major achievements in astrophysics, both directly and indirectly, as a springboard for the development of technology and the researchers who utilize it. The review of astrophysics research is divided by regions of the electromagnetic spectrum to categorize the various topics and types of research in this field.

2.1 Microwave

The most notable research in the microwave field involves studying the cosmic microwave background (CMB), which provides insights into the Universe's composition, geometry, and evolution. Light, emitted approximately 380,000 years after the Big Bang (which was ~13.8 billion years ago), provides a unique view of conditions in the hot early Universe. It is further shaped by the evolving cosmic structures that it travels past to arrive at/near Earth. Current and future measurements probe various topics in cosmology, ranging from the origin of the seeds that have grown into galaxies to the characteristics of fundamental particles [11, 12].

In the 1990s, NASA's scientific balloon program played a critical role in establishing observational CMB cosmology and developing critical technologies and techniques that have enabled multiple groundbreaking orbital missions [92, 93]. Dr. John C. Mather received the Nobel Prize in Physics for his research on the CMB. He began his research using small latex hand-launched balloons and credits that early research and engineering work to develop the balloon-borne instruments with the skills that aided him in a successful application for a satellite mission named "Cosmic Background Explorer" (COBE) that ultimately led to his Nobel Prize [9, 10]

Earth's atmosphere emits brightly at CMB frequencies, but from a balloon, the sky is a thousand times darker than even the best ground observation sites. Balloon missions can, therefore, deploy extremely sensitive detectors. Two pathfinding balloon missions — Balloon Observations of Millimetric Extragalactic Radiation and Geophysics (BOOMERanG) and Millimeter Anisotropy eXperiment IMaging Array (MAXIMA) — which detected the CMB's temperature fluctuations on small angular scales, conclusively showed that the Universe is spatially flat, supporting evidence of dark matter and dark energy [13], [14].

A more recent example, the Suborbital Polarimeter for Inflation Dust and the Epoch of Reionization (SPIDER), seeks evidence of primordial gravitational waves in the CMB [90, 91]. Just after the Big Bang, in the rapid expansion of several orders of magnitude in just a fraction of a second, it is likely that gravitational waves would have filled the universe with a background "hum". Though far too faint to detect today, this would have imprinted a unique "twist" pattern on the polarization of the CMB, known as B-mode polarization, varying across the sky on scales near one degree. SPIDER takes advantage of modern developments in large-format superconducting detector arrays and the long flight durations enabled by NASA's long-duration balloon (LDB) program. In its first Antarctic flight in 2015, SPIDER spent 16 days mapping approximately 5% of the sky at 95 and 150 GHz. The main results of this flight include a constraint on primordial B-mode polarization [16],

characterization of Galactic foreground emission [17], and a new limit on CMB circular polarization [18]. SPIDER's second flight in 2022-23 observed a similar region of the sky with the addition of a new 280 GHz channel. The SPIDER-2 data, currently under analysis, will provide deep measurements of polarized Galactic dust emission at a frequency complementary to the observations from the Planck satellite [19], providing dust maps of lasting value to the field.

Building on the heritage of SPIDER, the Taurus experiment [20] (planned for launch in 2027) will take advantage of super-pressure ballooning to measure CMB polarization across 70% of the sky at mid-latitudes. With its improved sky coverage, Taurus will be able to learn about the epoch of reionization, during which the bright first generation of stars ionized the gas between galaxies. Taurus will also characterize the polarized Galactic foregrounds across most of the sky at frequencies inaccessible from the ground.

2.2 Infrared

Infrared research primarily focuses on thermal blackbody emission, which allows scientists to study stellar dust and matter.

The GUSTO mission is one such mission. Launched in December 2024, it flew for 57 days above the Antarctic continent. GUSTO, which stands for Galactic/Extragalactic ULDB Spectroscopic Terahertz Observatory, aimed to look at the space between stars called the interstellar medium. Although the instrument measured in the far-infrared, the aim was to create a 3D map of a large part of the Milky Way in extremely high-frequency radio waves [6], [7], [8].

Astrophysics Stratospheric Telescope for High Spectral Resolution Observations at Submillimeter wavelengths (ASTHROS) is a high-altitude balloon mission to provide new information about stellar feedback, a process in which stars trigger or disrupt the formation of other stars in their galaxy. Stellar feedback has played a critical role in the evolution of galaxies throughout the universe's history. Without it, the available gas and dust in galaxies like ours would have coalesced into stars long ago, and no new star formation would have occurred.

To investigate stellar feedback, ASTHROS will use a technique called high-spectral resolution spectrometry, which allows scientists to identify specific chemical elements in gas and dust clouds and to measure precisely the density and dynamics of those elements. ASTHROS will conduct high spectral resolution spectrometry in a few specific wavelengths of light in the 1.4 to 2.7 THz range and identify two specific nitrogen ions formed by the processes that drive stellar feedback. This technology will enable astronomers to create 3D maps of star-forming

regions, as well as the density and movement of the gas, to learn about the influence of stellar feedback.

Set to launch from Antarctica, ASTHROS will aim to fly for 21 to 28 days at an altitude of about 130,000 feet (24.6 miles or 40 kilometers) - high enough to observe these wavelengths of light blocked by Earth's atmosphere.



Figure 3-1: This landscape of "mountains" and "valleys" speckled with glittering stars is actually the edge of a nearby, young, star-forming region called NGC 3324 in the Carina Nebula. Captured in infrared light by NASA's new James Webb Space Telescope, this image reveals previously invisible areas of star birth for the first time. However, this is a static image. ASTHROS will complement these observations by providing key information about the dynamics of these regions and how stellar feedback affects star formation

Credit: NASA, ESA, CSA, and STScI.



Figure 3-2: NASA Jet Propulsion Laboratory (JPL)'s ASTHROS radio telescope being prepared for launch.

ASTHROS is a collaborative science mission involving NASA's Jet Propulsion Laboratory (a division of Caltech), Media Lario S.r.l., Lockheed Martin Space Advanced Technology Center, as well as the Applied Physics Laboratory at Johns Hopkins University, for the design, build, and operation of the gondola, hardware, and science instruments.

2.3 Visible

Optical astronomy is the oldest genre of astronomy because it involves collecting data in the visible wavelengths detectable by the human eye. From the 1950s through the 1970s, the Stratoscope missions flew optical and IR telescopes [94, 95]. These flights were funded initially by the Office of Naval Research and later by NASA. The NASA program, led by Nancy Grace Roman, is credited with marking the beginning of NASA's scientific balloon program. The use of early iterations of the zero-pressure balloon design by General Mills and of the launch facility in Palestine, Texas, is of great significance to ballooning [21, 22, 23].

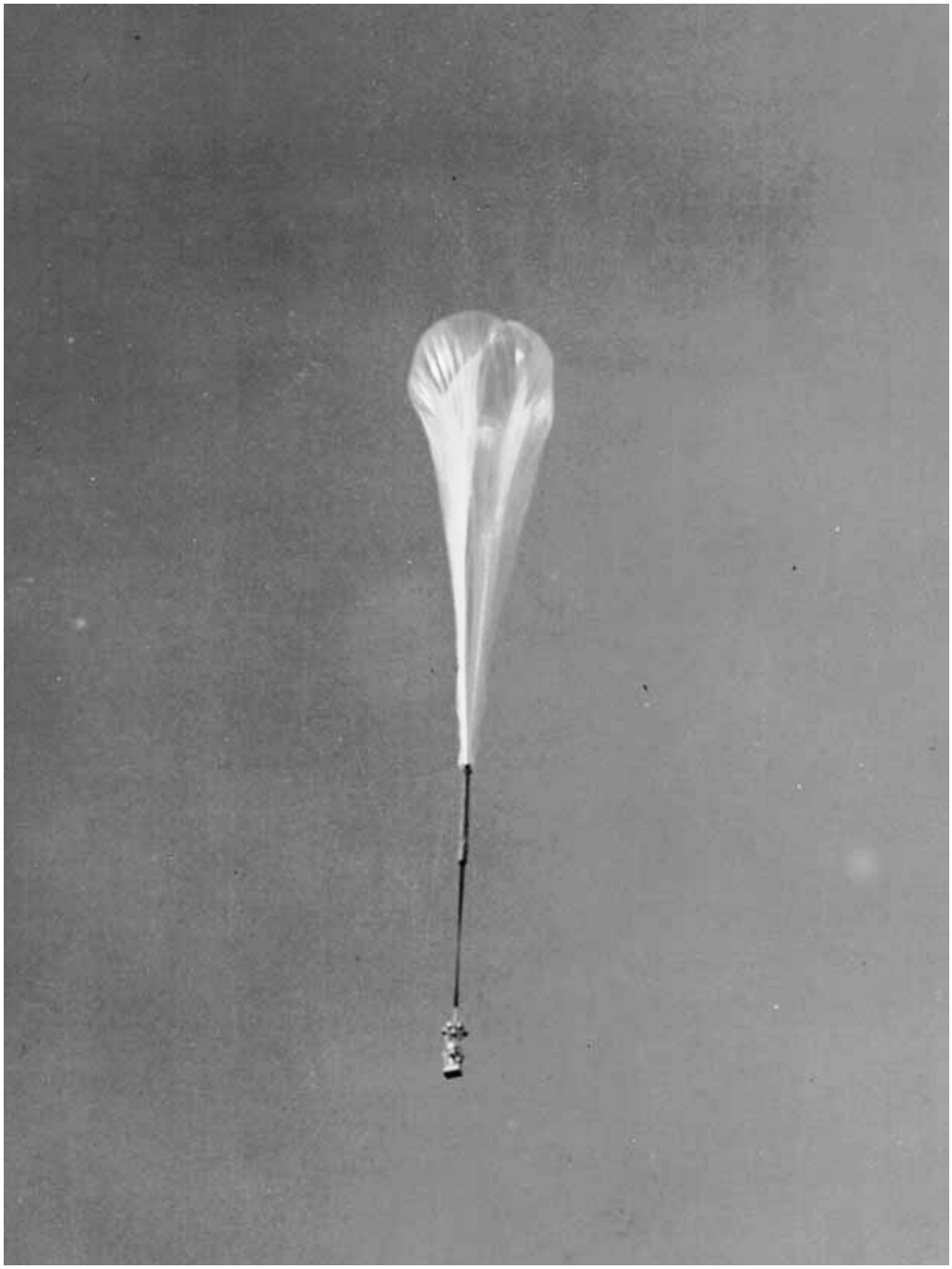


Figure 3-3: Skyhook balloon launched as part of the Stratoscope project.

By US Navy - US Navy, Public Domain,
https://commons.wikimedia.org/w/index.php?curid=7551141

2.4 Ultraviolet

Ultraviolet (UV) astronomy has historically been used as a probe of the interstellar medium's chemical compositions, densities, and temperatures. UV measurements can also help determine the evolution of galaxies and serve as a signature of the hottest objects in the initial or final stages of existence. Successful UV measurements are taken at night, eliminating launch locations with full sunlight, such as polar flights during austral and boreal summers. For this reason, such probes require batteries, which constitute the heavier portion of the payload for powering instruments.

One such successful mission that utilized UV measurements includes the Joint Exploratory Missions for the Extreme Universe Space Observatory (JEM-EUSO) and the EUSO-Balloon, a pathfinder for a space-borne observatory. This mission was the first to record laser tracks from Ultra-High Energy Cosmic Ray (UHECR)-induced Extensive Air Showers(EAS) using a fluorescence detector looking down on the atmosphere [26, 27].

Another is the Faint Intergalactic-medium Redshifted Emission Balloon (FIREBall) telescope, which is equipped with a fiber-fed UV integral field spectrograph, FIREBall-1, a fiber IFU flown in 2006 and 2009, and a UV Multi-object spectrograph (MOS, FIREBall-2, flown in 2018 and 2023). FIREBall was designed to detect low-redshift galaxies in the circumgalactic medium [24, 25].

2.5 X-ray

Compact remnants of massive stars, i.e., stellar mass black holes and neutron stars, continue to be fascinating and studied objects in the universe. The gas close to these objects is so hot that it is best studied in the X-ray band. A typical mission measures the X-ray energy, arrival time, and point of origin in the sky. Measurements of X-ray polarization provide information about the physical conditions that prevail at the X-ray emission site, e.g., magnetic field geometry or matter distribution. The number of X-rays depends on the altitude of the balloon (high altitudes minimize the atmospheric attenuation of the X-rays) and the duration of the flight (the longer the flight, the more X-ray photons that are collected).

In recent years, the first observations using instruments capable of celestial X-ray polarimetry have been made from stratospheric balloon platforms in the hard X-ray energy band (~10-100’s keV) [3,4,5]. The PoGO+ mission presented results on the Crab pulsar and wind nebula [4, 87] and black-hole binary Cyg X-1 [5], which were observed (~15-~200 keV) in the summer of 2016 during a week-long balloon flight from Esrange, Sweden, to Victoria Island, Canada.

Through a series of balloon flights from both northern and southern high latitude launch sites, XL-Calibur [28] aims to reveal the geometry and location of the X-ray bright corona of mass accreting stellar mass black holes, such as Cyg X-1 and Cyg X-3; identify the origin of the pulsed X-rays from accreting pulsars, such as GX 301-2, Her X-1 and Vela X-1; and probe the high-energy emission locale in rotation-powered pulsars, such as the Crab. Results from PoGO+ confirmed polarization in the Crab pulsar [4], and XL-Calibur has published first results on accretion geometry in Cyg X-1 [30].

This second-generation balloon-borne X-ray polarimeter mission follows the X-Calibur mission that flew from McMurdo in 2018 [2,3]. XL-Calibur flew from Esrange to the Kugluktuk region, Nunavut, Canada, in the summer of 2024. The flight was successful, and at the time of writing, results on observations of the Crab and Cyg X-1 are being prepared for publication. In the future, XL-Calibur will also measure southern sky sources during circumpolar flights from McMurdo, Antarctica. Measurements are made in the 15-80 keV energy band, where the low energy cut-off is due to atmospheric absorption, and the high energy cut-off is due to the focusing range of the X-ray mirror. The polarimetric sensitivity is an order of magnitude better than PoGO+, and the pixelated room temperature semiconductor detectors used in the polarimeter will allow spectropolarimetry in this energy band, with an X-ray energy resolution of ~6 keV.

2.6 Gamma Ray

Within gamma ray research, all of the initial discoveries and observations related to galactic antimatter positrons were pioneered on balloon platforms. In 1972, a balloon-borne experiment was responsible for discovering the 511 keV line in the galactic center [4]. This discovery was followed in 1995 by the confirmation of cosmic baryonic antimatter through the direct detection of cosmic antiprotons. Those measurements and balloon-borne direct positron measurements underpin many indirect dark matter detection schemes [5]. They also showed by about nine sigma that dark matter is not due to primordial black holes [5]. Balloon measurements have also shown that upper limits to the abundances of cosmic antihelium and antideuterons heavily disfavor primordial antimatter domains in the local Universe. Additionally, observed radioactive decays from aluminum-26, which serves as a tracer for massive star populations and supernovae, along with solar flare observations [32, 36], support this conclusion. These areas remain very interesting, and researchers continue conducting science on balloon platforms today.

The 2016 COSI flight was conducted on the super-pressure balloon platform, launched from New Zealand. During this flight, COSI achieved real-time detection of gamma-ray bursts and promptly notified the gamma-ray community [89]. From the data gathered during the flight, the team

has successfully mapped galactic positron annihilation, leading to the drafting or publication of numerous scientific papers around the time of this book's release.

One of the interesting initiatives that COSI is set to pursue is the measurement of polarization from gamma rays, which they initially began as part of their balloon instrument project. This effort represents a priority for the satellite and aims to contribute to developing the next generation of instruments capable of performing these measurements effectively. Much like light, gamma rays can be polarized depending on the processes that generate them. This polarization can provide insights into phenomena such as the geometry of material expelled from black holes and the magnetic structure surrounding neutron stars.

2.7 Cosmic Rays

Cosmic rays were an early discovery enabled by a balloon platform. Victor Hess measured high-energy radiation throughout multiple balloon flights from 1911 to 1913, but on April 17, 1912, he discovered that the radiation did not diminish during a solar eclipse. These measurements were confirmed in 1925 by Robert Millikan, who coined the term “cosmic rays.” Hess shared the Nobel Prize in Physics in 1936 for this discovery [37].

More recently, the ANITA (ANtarctic Impulsive Transient Antenna) instrument has been studying cosmic rays through various evolutions of its payload from 2006 to a new generation payload, PUEO (Payload for Ultrahigh Energy Observations), scheduled to launch from Antarctica in late 2025. The ANITA (now PUEO) & HICal (High-Altitude Calibration) experiments, a companion instrument to ANITA/PUEO, aim to search for neutrino interactions within cold polar ice, which produce radio-frequency signals that travel upwards to the surface and into the air. Placing radio-frequency receivers on an elevated balloon allows us to scan a massive amount of ice (imagine a circle with a diameter of 1200 km under the location of the balloon) for the scarce neutrino interactions. The HiCal experiment trails ANITA/PUEO to measure the fraction of radio signal that should emerge from the ice. ANITA observed a new class of signals (perhaps neutrinos) that, if correct, do not fit into current astrophysics models; many theories have been proposed to explain those signals.

CREAM (Cosmic Ray Energetics And Mass) is another such experiment designed to measure cosmic ray elemental spectra. CREAM’s balloon flights set a record with 191 days of total exposure time, see Figure 3-4, leading to the discovery of spectral hardening, which challenged previous assumptions that the cosmic ray spectrum followed a simple power law. CREAM revealed that different elements exhibited distinct spectral features, suggesting that cosmic ray acceleration may not be as uniform as previously thought.



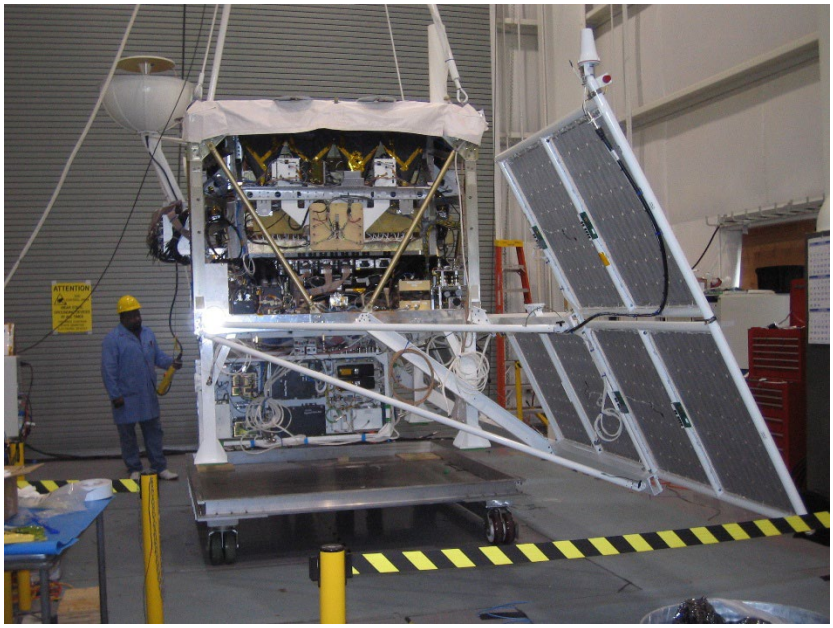


Figure 3-4: CREAM hardware used on balloon flights during integration activities at NASA Wallops Flight Facility.

Table 3-1: Summary of CREAM flights.

	Launch	Termination	Duration
CREAM-I	12/16/2004	1/27/2005	41 days, 22 hours
CREAM_II	12/15/2005	1/13/2006	28 days, 10 hours
CREAM-III	12/19/2007	1/17/2008	28 days, 22 hours
CREAM-IV	12/18/2008	1/17/2009	19 days, 13 hours
CREAM-V	12/1/2009	1/8/2010	37 days, 10 hours
CREAM-VI	12/21/2010	12/26/2010	5 days, 16 hours
BACCUS	11/28/2016	12/28/2016	30 days, 2 hours

3. Heliophysics

The balloon platform is just as useful and critical to heliophysical research as it is to astrophysics. In fact, gamma rays from a solar flare were detected during a balloon flight in 1957 [38] and balloon observations of X-rays from energetic electrons precipitating into the top of the atmosphere were first made in 1957 [88].

SUNRISE (Stratospheric Ultraviolet and Near-Infrared Interferometer for the Sun) is a high-resolution solar observatory that aims to observe the structure and dynamics of the sun’s magnetic field down to a resolution of about 60 miles across. This mission has flown with NASA three times and is the largest solar telescope to fly above the atmosphere. SUNRISE has multiple science goals, including looking at various magnetic field strengths in the photosphere and answering basic questions about the chromosphere's structure, dynamics, energy transport, and heating. The next iteration of SUNRISE will continue to study these questions. It will be the first observatory to examine the spectral region between 300 and 410 nm with high resolution to map the Sun’s magnetic field.

Hyperspectral Imager for Climate Science (HySICS) was an experiment to measure (a) the solar radiation received by the Earth and (b) the radiation emitted by the Earth. HySICS had two successful flights (2013 and 2014) aimed at scanning the 350-2300 nm wavelengths to determine whether the Earth emits more radiation than it receives and to watch for changes over time that could illuminate the causes of environmental change. HySICS is a prime example of a crossover between heliophysics and earth science in the classification of balloon-borne science.

The Balloon Observations Of Microburst Scales (BOOMS) is a NASA heliospheric mission designed to take the first-ever high-resolution spatial-temporal images of an X-ray version of the Earth’s aurora. The

X-ray aurora is dynamic and exhibits a wide range of scales, from phenomena that stretch across planetwide longitudes and last for hours to bursts that last under 100 ms and may be as small as a few km across. Still, at that time, no one had taken an image of the small-scale (~10km) short-duration (100ms) phenomenon called microbursts. The balloon platform is stationary below the X-ray generation region from 70–100km and can thus take multiple measurements of a bursty region over time, image the spatial scale in both longitude and latitude over a few hundred km field of view, and, by looking at the spectrum of the X-rays, determine the energy of the parent electrons.

At the other end of the scale, projects like BARREL (Balloon Array for Radiation-belt Relativistic Electron Losses), which flew a distributed network of balloons carrying non-imaging X-ray spectrometers, were able to show the large-scale structure of different types of X-ray aurora. BARREL balloons allowed for a multipoint, big-picture perspective on electron precipitation. The large-scale phenomena observed by BARREL could be monitored continuously for several hours.

4. Earth Science

Using balloons to probe the atmosphere is probably one of the first scientific investigations undertaken in this way. In the late 1890s and early 1900s, Teisserenc de Bort sent balloon instruments that recorded temperature and air pressure. He was puzzled when he looked at the data from about 200 balloons and found that the temperature no longer dropped at a certain height in the atmosphere. He had discovered a new layer of the atmosphere. On April 28, 1902, he coined the term stratosphere. Much of the scientific understanding of the atmosphere has come from balloon-borne observations. Balloons remain popular for continued atmospheric understanding.

The Orion Eagle mission aimed to study proton interactions at the top of the atmosphere using pixelated CZT (Cadmium Zinc Telluride) detectors. These detectors measured the position, energy, and direction of gamma-ray interactions while distinguishing charged particles without needing an anticoincidence shield. This mission marked the first demonstration of pixelated CZT detectors rejecting galactic cosmic rays in a space-like environment [43].

The TinMan instrument focused on measuring atmospheric thermal neutrons, critical for understanding neutron-induced single-event upsets in semiconductor devices, especially in commercial aircraft. To measure thermal neutron counts, TinMan employed two He-3 ionizing chambers, one bare and one Cd-shielded. By comparing measurements from aircraft and high-altitude balloons, TinMan highlighted the contribution of aircraft materials to thermal neutron production [44].

Another significant accomplishment is the measurement of stratospheric aerosols. Balloons have been used to collect data on the size, composition, and distribution of aerosol particles, which are important for understanding their impact on climate and atmospheric chemistry [49]. These measurements have been instrumental in assessing the effects of volcanic eruptions and human activities on the stratosphere [50].

The measurement of infrasound in the middle stratosphere using a free-flying acoustic array provides valuable insights into the capabilities and applications of infrasound monitoring from stratospheric balloons, which is a critical remote sensing tool for applications where we cannot get an instrument straight at the source [58].

The JPL Remote experiment focuses on understanding Earth's upper atmosphere, particularly stratospheric chemistry and ozone layer stability.

4.1 Ozone

One notable achievement is the detailed study of ozone depletion. The ozone layer in the lower stratosphere protects from UV radiation, absorbing most of the Sun's harmful ultraviolet (UV) radiation (e.g., UV-B and UV-C rays). Ozone loss in the lower stratosphere increases the risk of skin cancer and cataracts, affects flight crews and passengers, and harms wildlife and ecosystems [51, 52]. As a greenhouse gas, ozone influences Earth’s climate in the stratosphere, which impacts weather and climate in the troposphere [53]. Balloons equipped with ozone sensors have provided critical data on the concentration and distribution of ozone, helping to elucidate the mechanisms behind the ozone hole over Antarctica [48].

4.2 Thermospheric Winds

Thermospheric winds at altitudes of approximately 250 km are crucial for understanding the Earth's ionosphere. These winds are commonly measured using Doppler remote sensing with a Fabry-Perot Interferometer (FPI). Due to their role in space weather, thermospheric winds are key to understanding and forecasting instabilities in the ionosphere at low latitudes that can disrupt communication and navigation systems.

To enable daytime observations, the High-Altitude Interferometer WIND Experiment (HIWIND) was developed and flown on high-altitude balloons (~40 km), where atmospheric scattering is reduced by three orders of magnitude. HIWIND flew from Kiruna, Sweden, in 2011 and 2018, collecting high-quality daytime thermospheric wind data for the first time. These observations revealed unexpected patterns, such as equatorward winds at high latitudes, contradicting existing ionosphere and thermosphere models. The data from HIWIND has been instrumental in validating and

improving ionosphere and thermosphere models, filling a critical gap in daytime wind observations. The HIWIND flight from New Zealand, utilizing a super pressure balloon, was completed within the first half of 2025 [65].

5. Planetary Science

Within planetary science, balloons can serve as a platform test bed for science instruments that will later be sent to explore other planets or as a platform to remotely sense and observe phenomena related to planets and the discovery of exoplanets.

The Water Hunting Advanced Terahertz Spectrometer on an Ultra-Small Platform (WHATSUP), flown in 2021 and 2023, is one such mission. Using Terahertz spectrometers, the WHATSUP technology is designed to detect gases in planetary atmospheres with unprecedented sensitivity (up to single parts per billion) from compact and low-cost SmallSat and CubeSat platforms. THz spectrometers provide the ability to analyze the composition of planetary atmospheres in detail, specifically enabling the detection of trace gases that could indicate biological activity (biosignatures). They can also provide measurements of the isotopic ratios of water. This isotopic analysis is instrumental in reconstructing the history of water in our solar system, shedding light on planetary formation and its overall evolution.

5.1 The PICTURE balloon program

The Planetary Imaging Concept Testbed Using a Recoverable Experiment (PICTURE) is a series of experiments designed to directly examine exozodiacal dust disks and exoplanets around nearby stars. The original PICTURE and PICTURE-B experiments were flown on sounding rockets in 2011 and 2015, concluding with varying degrees of success [66, 67]. PICTURE-C (coronagraph) and the upcoming PICTURE-D (debris disk) experiments are high-altitude balloon-borne missions that leverage the pointing capability of the Wallops Arc Second Pointer (WASP) [68].

As shown in Table 3-2, several key technologies have been systematically matured aboard sounding rocket and balloon flights. PICTURE-C showed that it would be possible to image debris disks on several nearby planets. Continued efforts by the PICTURE team may make such a result possible with a PICTURE-D flight in 2025. Another key achievement of PICTURE-C was that it obtained the first space-based, on-sky high-contrast dark hole, a region around the image of a star where the starlight is suppressed to approximately 5×10^{-6} level (Figure 3-6), proving that pointing stability equivalent to the James Webb Space Telescope (JWST) is possible from a high-altitude balloon [70].

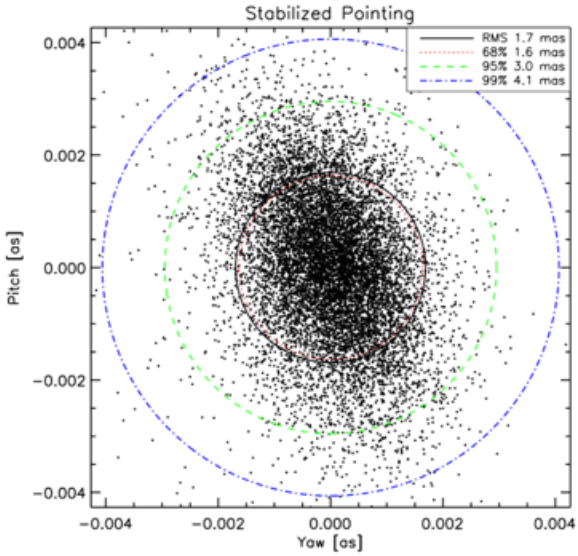


Figure 3-5: Distribution of positional centroids achieved by PICTURE-C shows that it achieved 1.7 mas RMS pointing stability, which is comparable to that of JWST

(adapted from https://doi.org/10.1016/j.actaastro.2023.09.009)

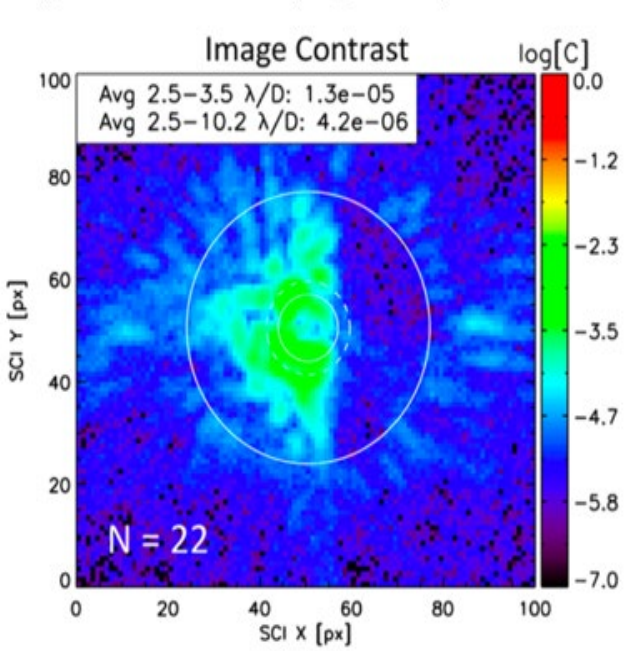


Figure 3-6: To image an exoplanet, one needs a contrast level of approximately 10^{-6}. PICTURE-C demonstrated a raw contrast level of 5 × 10^{-6}, which with post-processing, sufficient to image debris disks – exoplanet analogs of asteroid belts.

Table 3-2: Technology developed and matured by the PICTURE family of suborbital missions

(The Table is adapted from https://doi.org/10.1016/j.actaastro.2023.09.009).

Flight year and vehicle	**2011**	**2015**	**2019**	**2022**
	Sounding Rockets		High-altitude balloons	
Flight ID	PICTURE	PICTURE-B	PICTURE-C	
			Engineering flight	Science flight
Mission Goals	Technology validation for direct imaging of exoplanets		Debris disk imaging in reflected visible light	
Instrument/ technology highlights	0.5 m ULE telescope[4] [5]VNC 10^{-4} 32×32 MEMS DM[6] 600 – 750 nm CCD detector[7] Fine-pointing camera Fast steering mirror	0.5 m SiC telescope VNC 10^{-4} 32×32 MEMS DM 600 – 750 nm CCD detector Fine-pointing camera Fast steering mirror	0.6 m ULE telescope VVC[8] (Channel 4) 32×32 MEMS DM 540 – 660 nm CCD detector SH LOWFS + LLOWFS[9] 97 channel LODM[10] M2 on Hexapod Miniature DM ctrl.	0.6 m ULE telescope VVC (Channel 6) 32×32 MEMS DM 540 – 660 nm CCD detector SH LOWFS + LLOWFS 97 ch LODM M2 on Hexapod Miniature DM ctrl. EFC[11] dark zone: 10^{-7}

[4] ULE (ultra-low expansion) glass
[5] VNC is virtual network computing
[6] MEMS (micro-electro-mechanical systems) DM (decimeter) deformable mirror.
[7] CCD (charge coupled device) detector is a highly sensitive photon detector.
[8] VVC is versatile video coding
[9] Shack-Hartmann Low-Order Wavefront Sensor (SH LOWFS) and Lyot-based Low-Order Wavefront Sensor (LLOWFS)
[10] LODM is large-scale online dense mapping commonly used with UAVs
[11] Electric field conjugation (EFC)

5.2 Extra Planetary Missions

Relative to an orbital platform, an aerobot, or robotic aerial vehicle, has the advantage of being in intimate contact with the atmospheric environment, for analysis and direct measurement of properties such as temperature, pressure, atmospheric chemistry, particulate matter, and acoustic phenomena. Relative to an orbital platform, aerobots also provide greater proximity to the surface, which may permit higher-resolution imaging of the surface. In the case of Venus, where high surface temperatures make it impossible for scientific instrumentation to operate for more than a few hours, aerobots can function at an altitude with more favorable temperatures. Since an aerobot moves with the wind, external tracking of an emitted radio frequency signal (e.g., Doppler tracking) and/or onboard inertial guidance measurements can be used to measure the magnitude and direction of the wind vector relative to the planetary surface.

Measurements made as the aerobot moves with the prevailing wind around the planet provide widespread spatial and temporal coverage limited only by the duration of the flight. Multiple aerobots deployed from one or more entry vehicles to observe the same event from different locations provide additional coverage. In-situ aerobot measurements can also be combined with simultaneous observations from nearby orbiting spacecraft. Altitude-controlled aerobots can enable access to other parts of the atmosphere. Accordingly, deploying small, short-lived payloads that both fall below and rise above the aerobot, relaying data through it, can enhance the scientific capabilities of the aerobot itself.

Aerobots can also play a critical role in performing surface sample return. This is in contrast to the Mars Sample Return program, which was designed to feasibly launch surface samples from the Martian surface to space with limited impediment through the low-density atmosphere. That is also not the case for Venus or Titan, and the use of a buoyant lifting vehicle to transfer samples to an altitude where rocket ascent is feasible was identified as a possibility as early as the 1970s [83] [84]. More recently, the use of inflatable metal balloons to raise samples from the surface of Venus to an altitude where the temperature is suitable for sophisticated scientific instruments to analyze surface materials has been explored in greater depth [85]. Prospects for applying these technologies are yet to be realized and are beyond the scope of this book.

The National Academies of Sciences, Engineering, and Medicine (NASEM) produces decadal surveys that identify the critical questions in planetary science and mission concepts that address them, which NASA uses to align its own space science priorities. The 2023 survey, titled *Origins, Worlds, and Life: A Decadal Strategy for Planetary Science and Astrobiology 2023-2033* [86], contains an extensive discussion of the

science priorities for Mars, Venus, and Titan, where balloon technology can play a vital exploration role. The report particularly recognizes the unique role that aerobots can play at Venus, noting the need to complete the technological development of Venus balloons to make them ready for use. (Ref. [33], page 549)

The science questions to be addressed by the mission will determine the fundamental design constraints on the aerobot, including its size, payload, operating altitude or altitude range, mission duration, and the power, command, data handling, and telecommunications systems required to return the scientific data to Earth.

6. Astrobiology

Astrobiology is an interdisciplinary field exploring life in the universe and the impacts of space travel on Earth's life. Biological Samples Exposure Payload (BIOSEP) is one of the latter. The mission, sponsored by the Chinese Academy of Science, flew four times from 2019 to 2021 with a Chinese flight program to expose samples to stratospheric conditions analogous to those in the Martian atmosphere and protect the samples during their return to be able to analyze the stratospheric effects without additional contamination [73]. A similar payload, Exposing Microorganisms in the Stratosphere (E-MIST), has determined that bacteria that can survive radiation-rich environments like interplanetary space could indeed be introduced to Mars during the landing of a spacecraft from Earth [74, 75].

The recent 2017 and 2024 total solar eclipses across North America brought balloon research into the public eye. In 2017, students from the University of Bridgeport and the University of Hartford teamed up with the principal investigator of E-MIST to expose samples using small latex balloons in conjunction with the NASA Eclipse Ballooning Program [76]. These small hand-launched balloons and piggyback opportunities with large balloons provide an extremely low-cost method to research the effects of the stratospheric environment on living organisms [77].

In 2023, a student group from the middle-school and high-school student research program, “Cubes in Space”, reported that EpiPens can become poisonous when exposed to radiation above the ozone layer. These scientists, all 9-12 years old, designed an experiment to expose the medication through a flight on a NASA balloon in New Mexico. The samples were then analyzed at the University of Ottawa, where they discovered that no epinephrine was found and that a portion had been turned into “poisonous benzoic acid derivatives” [78].

7. Conclusions

Stratospheric balloons have become an indispensable asset for the scientific community, offering unique capabilities not fully replicated by other platforms such as satellites or ground-based observatories. They serve as a complementary observational platform to satellites. They provide in-situ and remote sensing measurements crucial for understanding various atmospheric phenomena. Unlike satellites that orbit at much higher altitudes, stratospheric balloons can operate at around 18 to 40 kilometers, offering "ground truth" data vital for validating satellite observations. This proximity to the Earth's surface allows for higher resolution measurements and improved signal-to-noise ratios, thereby refining the accuracy of scientific models and predictions [79].

The scientific community has recognized the potential of stratospheric balloons to address significant questions outlined in the Planetary Science Decadal Survey. Approximately 45 topics from the survey are potentially suitable for exploration using stratospheric balloon platforms. BOPPS, a mission flown in the fall of 2014, exemplifies the practical application of these platforms in contributing to planetary science [80]. The ability to answer over 20 percent of the key questions in the survey underscores the strategic role of stratospheric balloons in advancing scientific knowledge [80].

Stratospheric balloons are also instrumental as test beds for new technologies for long-duration space missions. The Canadian Space Agency, for instance, utilizes these platforms to validate technologies in conditions that closely mimic the space environment. This is facilitated by the unique characteristics of the stratosphere, such as low temperatures and reduced atmospheric pressure, which simulate the harshness of outer space [81].

A proposed global constellation of stratospheric super-pressure balloons by Global Aerospace Corporation could provide comprehensive diurnal coverage of the entire globe. This network would enable continuous or frequent observations, significantly enhancing the temporal resolution of data collection. Such a system could address major scientific questions related to Earth science by offering persistent monitoring capabilities that are not feasible with other platforms [82].

Despite their numerous benefits, stratospheric balloons are not without limitations. Their operational duration is typically shorter than that of satellites, and they are subject to atmospheric conditions that can affect their stability and trajectory. Moreover, the need for recovery can limit their use in remote or harsh regions of the Earth.

With almost all scientists, there is a desire for longer-duration missions and higher altitude flights. Super-pressure balloons aim to meet the need for longer flights that can also provide access at mid-latitudes. For a discussion of super-pressure balloons, please see Chapter 10. Additionally, in 2023, NASA certified a 60 million cubic foot volume balloon (called the “Big 60”), which enables flights as high as 160,000 ft (48.7 km).

Other improvements that could contribute to balloon science research include high bandwidth datalinks to mitigate the risk of data storage units being damaged/lost during mission termination/landing and provide real-time access to monitor and configure the payload/instruments to maximize measurement efficiency [45]. The development of smaller, lighter, and more sensitive sensors will enable more comprehensive and accurate measurements without significantly increasing the payload weight [50]. Another important technological advancement is the improvement of balloon navigation and control systems. Enhanced GPS and telemetry systems will allow for more precise positioning and tracking of balloons, facilitating targeted observations and reducing the risk of data loss [47]. In the past decade from the time of this publication, the expansion of altitude-controlled systems, which can be steered to specific locations, adjusted for altitude, and moved using prevailing wind patterns. This capability is most effective at relatively low altitudes where wind variability is more prevalent.

In conclusion, balloon platforms offer a versatile and effective means of conducting research in the lower stratosphere. They have contributed significantly to our understanding of atmospheric processes and have great potential for future discoveries. With continued technological advancements, balloons will remain vital for exploring and understanding this critical region of the Earth's atmosphere.

References

[1] S. Serjeant, M. Elvis, and G. Tinetti, "The future of astronomy with small satellites," *Nat. Astron.*, vol. 4, no. 11, pp. 1031–1038, Nov. 2020, doi: 10.1038/s41550-020-1201-5.

[2] P. Maier *et al.*, "Stratospheric Balloons as a Complement to the Next Generation of Astronomy Missions," Feb. 09, 2022, *arXiv*: arXiv:2202.04651. doi: 10.48550/arXiv.2202.04651.

[3] A. Bryant, A. Krabbe, B. Schulz, P. Maier, and H. Zinnecker, "The legacy of SOFIA and perspectives on the far-infrared," in *Space Telescopes and Instrumentation 2024: Optical, Infrared, and Millimeter Wave*, SPIE, Aug. 2024, pp. 108–124. doi: 10.1117/12.3019708.

[4] "Balloon Observations of the Galactic Center 511 keV Line and their Relationship to Satellite Results | SpringerLink." Accessed: Dec. 20, 2024. [Online]. Available: https://link.springer.com/chapter/10.1007/978-94-011-0067-0_21

[5] K. Yoshimura *et al.*, "Observation of cosmic-ray antiprotons at energies below 500 MeV," *Phys. Rev. Lett.*, vol. 75, no. 21, pp. 3792–3795, 1995, doi: 10.1103/PhysRevLett.75.3792.

[6] "GUSTO - NASA Science." Accessed: Dec. 26, 2024. [Online]. Available: https://science.nasa.gov/mission/gusto

[7] P. Bernasconi, C. Walker, and C. Kulesa, "The GUSTO balloon mission," *42nd COSPAR Sci. Assem.*, vol. 42, p. PSB.1-31, Jul. 2018.

[8] richardmitnick, "Galactic/Extragalactic ULDB Spectroscopic Terahertz Observatory," sciencesprings. Accessed: Dec. 26, 2024. [Online]. Available: https://sciencesprings.wordpress.com/tag/galacticextragalactic-uldb-spectroscopic-terahertz-observatory/

[9] "This Month in NASA History: COBE Scientists Were Celebrated for the CMB | APPEL Knowledge Services." Accessed: Dec. 20, 2024. [Online]. Available: https://appel.nasa.gov/2016/10/20/this-month-in-nasa-history-cobe-scientists-were-celebrated-for-the-cmb/

[10] "My Best Mistake: John Mather's 'Recognizing My Limits' | APPEL Knowledge Services." Accessed: Dec. 20, 2024. [Online]. Available: https://appel.nasa.gov/2015/03/02/my-best-mistake-john-mathers-recognizing-my-limits/

[11] S. Staggs, J. Dunkley, and L. Page, "Recent discoveries from the cosmic microwave background: a review of recent progress," *Rep.*

Prog. Phys., vol. 81, no. 4, p. 044901, Feb. 2018, doi: 10.1088/1361-6633/aa94d5.

[12] C. L. Chang *et al.*, "Snowmass2021 Cosmic Frontier: Cosmic Microwave Background Measurements White Paper," Mar. 15, 2022, *arXiv*: arXiv:2203.07638. doi: 10.48550/arXiv.2203.07638.

[13] A. Balbi *et al.*, "Constraints on Cosmological Parameters from MAXIMA-1," *Astrophys. J.*, vol. 558, no. 2, pp. L145–L145, Sep. 2001, doi: 10.1086/323608.

[14] P. de Bernardis *et al.*, "A flat Universe from high-resolution maps of the cosmic microwave background radiation," *Nature*, vol. 404, no. 6781, pp. 955–959, Apr. 2000, doi: 10.1038/35010035.

[15] W. C. Jones, R. Bhatia, J. J. Bock, and A. E. Lange, "Polarization-sensitive bolometric receiver for observations of the cosmic microwave background," in *Millimeter and Submillimeter Detectors for Astronomy*, SPIE, Feb. 2003, pp. 227–238. doi: 10.1117/12.459194.

[16] P. A. R. Ade *et al.*, "A Constraint on Primordial B-modes from the First Flight of the Spider Balloon-borne Telescope," *Astrophys. J.*, vol. 927, no. 2, p. 174, Mar. 2022, doi: 10.3847/1538-4357/ac20df.

[17] SPIDER Collaboration *et al.*, "Analysis of Polarized Dust Emission from the First Flight of the SPIDER Balloon-Borne Telescope," Jul. 30, 2024, *arXiv*: arXiv:2407.20982. doi: 10.48550/arXiv.2407.20982.

[18] J. M. Nagy *et al.*, "A New Limit on CMB Circular Polarization from SPIDER," *Astrophys. J.*, vol. 844, no. 2, p. 151, Aug. 2017, doi: 10.3847/1538-4357/aa7cfd.

[19] Y. Akrami *et al.*, "Planck 2018 results - XI. Polarized dust foregrounds," *Astron. Astrophys.*, vol. 641, p. A11, Sep. 2020, doi: 10.1051/0004-6361/201832618.

[20] J. L. May *et al.*, "Instrument overview of Taurus: a balloon-borne CMB and dust polarization experiment," in *Ground-based and Airborne Telescopes X*, SPIE, Sep. 2024, pp. 1319–1333. doi: 10.1117/12.3019051.

[21] "Balloon Astronomy on JSTOR." Accessed: Dec. 27, 2024. [Online]. Available: https://www.jstor.org/stable/24940300

[22] G. C. Ellerton, "Vitro Operation Plan 1-64 for Stratoscope II Evaluation Flight No. 6." Vitro Labs, CA, 1964.

[23] General Mills, "Stratoscope Operation." General Mills, Department of Public Relations, ca 1958.

[24] "NASA TechPort - Project." Accessed: Dec. 26, 2024. [Online]. Available: https://techport.nasa.gov/project

[25] "Suborbital." Accessed: Dec. 26, 2024. [Online]. Available: https://microdevices.jpl.nasa.gov/capabilities/advanced-detectors/suborbital/

[26] J. H. Adams *et al.*, "A Review of the EUSO-Balloon Pathfinder for the JEM-EUSO Program," *Space Sci. Rev.*, vol. 218, no. 1, p. 3, 2022, doi: 10.1007/s11214-022-00870-x.

[27] "Highlighted Articles - Astroparticle Physics | ScienceDirect.com by Elsevier." Accessed: Dec. 26, 2024. [Online]. Available: https://www.sciencedirect.com/journal/astroparticle-physics/about/highlighted-articles/euso-balloon-mission-leads-the-way-for-uv-investigations-of-the-atmosphere-at-night

[28] Q. Abarr *et al.*, "*XL-Calibur* – a second-generation balloon-borne hard X-ray polarimetry mission," *Astropart. Phys.*, vol. 126, p. 102529, Mar. 2021, doi: 10.1016/j.astropartphys.2020.102529.

[29] "Performance of the X-Calibur hard X-ray polarimetry mission during its 2018/19 long-duration balloon flight - ScienceDirect." Accessed: Dec. 19, 2024. [Online]. Available: https://www.sciencedirect.com/science/article/pii/S0927650522000536

[30] M. Chauvin *et al.*, "Accretion geometry of the black-hole binary Cygnus X-1 from X-ray polarimetry," *Nat. Astron.*, vol. 2, no. 8, pp. 652–655, Aug. 2018, doi: 10.1038/s41550-018-0489-x.

[31] M. Chauvin *et al.*, "Accretion geometry of the black-hole binary Cygnus X-1 from X-ray polarimetry," *Nat. Astron.*, vol. 2, no. 8, pp. 652–655, Aug. 2018, doi: 10.1038/s41550-018-0489-x.

[32] "Temporal properties of the terrestrial gamma-ray flashes from the Gamma-Ray Burst Monitor on the Fermi Observatory - Fishman - 2011 - Journal of Geophysical Research: Space Physics - Wiley Online Library." Accessed: Sep. 27, 2024. [Online]. Available: https://agupubs.onlinelibrary.wiley.com/doi/full/10.1029/2010JA016084

[33] T. Gjesteland, N. Østgaard, P. H. Connell, J. Stadsnes, and G. J. Fishman, "Effects of dead time losses on terrestrial gamma ray flash measurements with the Burst and Transient Source Experiment," *J. Geophys. Res. Space Phys.*, vol.. 115, no. A5, 2010, doi: 10.1029/2009JA014578.

[34] D. M. Smith, L. I. Lopez, R. P. Lin, and C. P. Barrington-Leigh, "Terrestrial Gamma-Ray Flashes Observed up to 20 MeV," *Science*, vol. 307, no. 5712, pp. 1085–1088, Feb. 2005, doi: 10.1126/science. 1107466.

[35] J. E. Grove *et al.*, "An Intense Terrestrial Gamma-ray Flash Observed at Ground Level," vol. 2015, pp. AE21A-04, Dec. 2015.

[36] "The spectroscopy of individual terrestrial gamma-ray flashes: Constraining the source properties - Mailyan - 2016 - Journal of Geophysical Research: Space Physics - Wiley Online Library." Accessed: Sep. 27, 2024. [Online]. Available: https://agupubs.onlinelibrary.wiley.com/doi/full/10.1002/2016JA022702

[37] "This Month in Physics History." Accessed: Dec. 20, 2024. [Online]. Available: https://www.aps.org/archives/publications/apsnews/201004/physicshistory.cfm

[38] A. Fludra, "The Sun from space: Discoveries from space missions over the past fifty years," *J. Phys. Conf. Ser.*, vol. 2877, no. 1, p. 012041, oct. 2024, doi: 10.1088/1742-6596/2877/1/012041.

[39] T. Berkefeld *et al.*, "The Wave-Front Correction System for the Sunrise Balloon-Borne Solar Observatory," *Sol. Phys.*, vol. 268, no. 1, pp. 103–123, Jan. 2011, doi: 10.1007/s11207-010-9676-3.

[40] "Sunrise: Ein ballongetragenes Sonnenobservatorium." Accessed: Dec. 26, 2024. [Online]. Available: https://www.mps.mpg.de/solar-physics/sunrise

[41] "Science Overview – CLARREO Pathfinder." Accessed: Dec. 26, 2024. [Online]. Available: https://clarreo-pathfinder.larc.nasa.gov/science-overview/

[42] "HySICS," Laboratory for Atmospheric and Space Physics. Accessed: Dec. 26, 2024. [Online]. Available: https://lasp.colorado.edu/missions/hysics/

[43] S. I. Lanctot and B. F. Sandoval, "The Analysis and Support for LANL Technology Testbed: High Altitude Balloon Gondola and Orion Eagle Gamma Ray Detection Instrument," Los Alamos National Laboratory (LANL), Los Alamos, NM (United States), LA-UR-22-21342, Feb. 2022. doi: 10.2172/1846108.

[44] S. Nowicki *et al.*, "Thermal neutron flux characterization at aircraft altitudes with the TinMan detector," in *2017 IEEE Aerospace Conference*, Big Sky, MT, USA: IEEE, Mar. 2017, pp. 1–9. doi: 10.1109/AERO.2017.7943669.

[45] "Assessing the climate impact of trends in stratospheric water vapor - Forster - 2002 - Geophysical Research Letters - Wiley Online Library." Accessed: Sep. 27, 2024. [Online]. Available: https://agupubs.onlinelibrary.wiley.com/doi/full/10.1029/2001GL013909

[46] A. R. Ravishankara, S. Solomon, A. A. Turnipseed, and R. F. Warren, "Atmospheric Lifetimes of Long-Lived Halogenated Species," *Science*, vol. 259, no. 5092, pp. 194–199, Jan. 1993, doi: 10.1126/science. 259.5092.194.

[47] O. B. Toon, R. P. Turco, P. Hamill, C. S. Kiang, and R. C. Whitten, "A One-Dimensional Model Describing Aerosol Formation and Evolution in the Stratosphere: II. Sensitivity Studies and Comparison with Observations," Apr. 1979, Accessed: Sep. 27, 2024. [Online]. Available: https://journals.ametsoc.org/view/journals/atsc/36/4/1520-0469_1979_036_0718_aodmda_2_0_co_2.xml

[48] S. Solomon, "Stratospheric ozone depletion: A review of concepts and history," *Rev. Geophys.*, vol. 37, no. 3, pp. 275–316, 1999, doi: 10.1029/1999RG900008.

[49] "Increase in background stratospheric aerosol observed with lidar at Mauna Loa Observatory and Boulder, Colorado - Hofmann - 2009 - Geophysical Research Letters - Wiley Online Library." Accessed: Sep. 27, 2024. [Online]. Available: https://agupubs.onlinelibrary.wiley.com/doi/full/10.1029/2009GL039008

[50] "Trends in the nonvolcanic component of stratospheric aerosol over the period 1971–2004 - Deshler - 2006 - Journal of Geophysical Research: Atmospheres - Wiley Online Library." Accessed: Sep. 27, 2024. [Online]. Available: https://agupubs.onlinelibrary.wiley.com/doi/full/10.1029/2005JD006089

[51] "European scientific assessment of the atmospheric effects of aircraft emissions - ScienceDirect." Accessed: Sep. 27, 2024. [Online]. Available: https://www.sciencedirect.com/science/article/pii/S135223109700486X

[52] World Health Organization. Regional Office for Europe, *Health risks of ozone from long-range transboundary air pollution*. 2008.

[53] Intergovernmental Panel on Climate Change (IPCC), *Climate Change 2013 – The Physical Science Basis: Working Group I Contribution to the Fifth Assessment Report of the Intergovernmental Panel on Climate Change*. Cambridge: Cambridge University Press, 2014. doi: 10.1017/CBO9781107415324.

[54] D. F. Heath, A. J. Krueger, H. A. Roeder, and B. D. Henderson, "The Solar Backscatter Ultraviolet and Total Ozone Mapping Spectrometer (SBUV/TOMS) for NIMBUS G," *Opt. Eng.*, vol. 14, no. 4, pp. 323–331, Aug. 1975, doi: 10.1117/12.7971839.

[55] A. Molod, L. Takacs, M. Suarez, and J. Bacmeister, "Development of the GEOS-5 atmospheric general circulation model: evolution from MERRA to MERRA2," *Geosci. Model Dev.*, vol. 8, no. 5, pp. 1339–1356, May 2015, doi: 10.5194/gmd-8-1339-2015.

[56] S. Pawson *et al.*, "Goddard Earth Observing System chemistry-climate model simulations of stratospheric ozone-temperature coupling between 1950 and 2005," *J. Geophys. Res. Atmospheres*, vol. 113, no. D12, 2008, doi: 10.1029/2007JD009511.

[57] "Summary report 4–8 November 2019," IISD Earth Negotiations Bulletin. Accessed: Sep. 27, 2024. [Online]. Available: http://enb.iisd.org/events/31st-meeting-parties-montreal-protocol-substances-deplete-ozone-layer-mop-31/summary-report

[58] D. C. Bowman and J. M. Lees, "Infrasound in the middle stratosphere measured with a free-flying acoustic array," *Geophys. Res. Lett.*, vol. 42, no. 22, p. 10,010-10,017, 2015, doi: 10.1002/2015GL066570.

[59] J. R. Holton, P. H. Haynes, M. E. McIntyre, A. R. Douglass, R. B. Rood, and L. Pfister, "Stratosphere-troposphere exchange," *Rev. Geophys.*, vol. 33, no. 4, pp. 403–439, 1995, doi: 10.1029/95RG02097.

[60] "Interannual Changes of Stratospheric Water Vapor and Correlations with Tropical Tropopause Temperatures in: Journal of the Atmospheric Sciences Volume 61 Issue 17 (2004)." Accessed: Sep. 27, 2024. [Online]. Available: https://journals.ametsoc.org/view/journals/atsc/61/17/1520-0469_2004_061_2133_icoswv_2.0.co_2.xml?tab_body=abstract-display

[61] "Albedo Enhancement by Stratospheric Sulfur Injections: A Contribution to Resolve a Policy Dilemma? - ProQuest." Accessed: Sep. 27, 2024. [Online]. Available: https://www.proquest.com/openview/9f0a629d28adfa02e164457e63fb7e6b/1?pq-origsite=gscholar&cbl=36297

[62] A. Robock, A. Marquardt, B. Kravitz, and G. Stenchikov, "Benefits, risks, and costs of stratospheric geoengineering," *Geophys. Res. Lett.*, vol. 36, no. 19, 2009, doi: 10.1029/2009GL039209.

[63] D. M. Murphy *et al.*, "Metals from spacecraft reentry in stratospheric aerosol particles," *Proc. Natl. Acad. Sci.*, vol. 120, no. 43, p. e2313374120, Oct. 2023, doi: 10.1073/pnas.2313374120.

[64] "Potential Ozone Depletion From Satellite Demise During Atmospheric Reentry in the Era of Mega-Constellations - Ferreira - 2024 - Geophysical Research Letters - Wiley Online Library." Accessed: Sep. 27, 2024. [Online]. Available:

https://agupubs.onlinelibrary.wiley.com/doi/full/10.1029/2024GL109280

[65] Q. Wu *et al.*, "HIWIND Balloon and Antarctica Jang Bogo FPI High Latitude Conjugate Thermospheric Wind Observations and Simulations," *J. Geophys. Res. Space Phys.*, vol. 129, no. 6, p. e2023JA032400, 2024, doi: 10.1029/2023JA032400.

[66] C. B. Mendillo *et al.*, "PICTURE: a sounding rocket experiment for direct imaging of an extrasolar planetary environment," in *Space Telescopes and Instrumentation 2012: Optical, Infrared, and Millimeter Wave*, SPIE, Sep. 2012, pp. 179–193. doi: 10.1117/12.926408.

[67] E. S. Douglas, C. B. Mendillo, T. A. Cook, and S. Chakrabarti, "Wavefront sensing in space from the PICTURE-B sounding rocket," in *Space Telescopes and Instrumentation 2016: Optical, Infrared, and Millimeter Wave*, SPIE, Jul. 2016, pp. 1933–1946. doi: 10.1117/12.2235631.

[68] T. Cook *et al.*, "Planetary Imaging Concept Testbed Using a Recoverable Experiment–Coronagraph (PICTURE C)," *J. Astron. Telesc. Instrum. Syst.*, vol. 1, no. 4, p. 044001, Sep. 2015, doi: 10.1117/1.JATIS.1.4.044001.

[69] C. B. Mendillo, K. Hewawasam, J. Martel, T. Potter, T. A. Cook, and S. Chakrabarti, "Balloon flight demonstration of coronagraph focal plane wavefront correction with PICTURE-C," *J. Astron. Telesc. Instrum. Syst.*, vol. 9, no. 2, p. 025005, May 2023, doi: 10.1117/1.JATIS.9.2.025005.

[70] J. Rigby *et al.*, "The Science Performance of JWST as Characterized in Commissioning," *Publ. Astron. Soc. Pac.*, vol. 135, no. 1046, p. 048001, Apr. 2023, doi: 10.1088/1538-3873/acb293.

[71] "Neural Network Attitude Control System Design for the Wallops Arc-Second Pointer | Journal of Guidance, Control, and Dynamics." Accessed: Dec. 19, 2024. [Online]. Available: https://arc.aiaa.org/doi/10.2514/1.G006465

[72] "Minimizing the Polarization Leakage of Geometric-phase Coronagraphs with Multiple Grating Pattern Combinations - IOPscience." Accessed: Dec. 19, 2024. [Online]. Available: https://iopscience.iop.org/article/10.1088/1538-3873/ab755f

[73] "Balloon-based exposed payload designed for astrobiological research in Earth's near space." Accessed: Dec. 27, 2024. [Online]. Available: https://www.eppcgs.org/article/doi/10.26464/epp2024070

[74] C. L. Khodadad *et al.*, “Stratosphere Conditions Inactivate Bacterial Endospores from a Mars Spacecraft Assembly Facility,” *Astrobiology*, vol. 17, no. 4, pp. 337–350, Apr. 2017, doi: 10.1089/ast.2016.1549.

[75] “| NASA Astrobiology Institute.” Accessed: Dec. 27, 2024. [Online]. Available: https://astrobiology.nasa.gov/nai/seminars/featured-seminar-channels/university-of-washington-seminars/2015/10/13/exposing-microorganisms-in-the-stratosphere-e-mist-preliminary-results-from-a-nasa-balloon-program-flight-experiment/index.html

[76] “CTSGC High-Altitude Balloon to Carry NASA Experiment During Solar Eclipse | Connecticut Space Grant Consortium.” Accessed: Dec. 27, 2024. [Online]. Available: https://ctspacegrant.org/4872/ctsgc-high-altitude-balloon-to-carry-nasa-experiment-during-solar-eclipse

[77] D. J. Smith and M. B. Sowa, “Ballooning for Biologists: Mission Essentials for Flying Life Science Experiments to Near Space on NASA Large Scientific Balloons,” *Gravitational Space Res. Publ. Am. Soc. Gravitational Space Res.*, vol. 5, no. 1, pp. 52–73, Jul. 2017.

[78] J. N. published, “Elementary schoolers prove EpiPens become toxic in space — something NASA never knew,” livescience.com. Accessed: Dec. 27, 2024. [Online]. Available: https://www.livescience.com/elementary-schoolers-prove-epipens-become-fatally-toxic-in-space-something-nasa-never-knew

[79] K. Nock, “Global Constellation of Stratospheric Scientific Platforms.” Global Aerospace Corporation, Feb. 08, 2001.

[80] T. Kremic *et al.*, “Stratospheric balloons for planetary science and the Balloon Observation Platform for Planetary Science (BOPPS) mission summary,” in *2015 IEEE Aerospace Conference*, Mar. 2015, pp. 1–10. doi: 10.1109/AERO.2015.7119008.

[81] C. S. Agency, “About stratospheric balloons,” Canadian Space Agency. Accessed: Dec. 28, 2024. [Online]. Available: https://www.asc-csa.gc.ca/eng/sciences/balloons/about-stratospheric-balloons.asp

[82] “Global stratospheric balloon constellations - ScienceDirect.” Accessed: Dec. 28, 2024. [Online]. Available: https://www.sciencedirect.com/science/article/pii/S0273117702005288

[83] A. L. Friedlander and H. Feingold, "Balloon-Assisted Ascent to Venus Orbit," in *AIAA/AAS Astrodynamics Conference paper 78-1438*, Palo Alto, 1978.

[84] V. Kerzhanovich, J. Hall, A. Yavrouian, and J. Cutts, "Two Balloon System to Lift Payloads for the Surface of Venus," in *AIAA Paper 2005-7322*, Arlington, 2005.

[85] V. Scott, "Venus In Situ Transfer and Analysis (VISTA) Mission," DOI: 10.26206/78tbr-5ta74, 2023.

[86] National Academies of Science, Engineering and Medicine, "Origins, Worlds, and Life: A Decadal Strategy for Planetary Science and Astrobiology 2023-2032," The National Academies Press, 2023.

[87] M. Chauvin et al., "Calibration and performance studies of the balloon-borne hard X-ray polarimeter PoGO+," Nuclear Instruments and Methods in Physics Research Section A: Accelerators, Spectrometers, Detectors and Associated Equipment, vol. 859, pp. 125–133, 2017.

[88] J. R. Winckler, "X-rays from energetic electrons precipitating into the atmosphere," Journal of Geophysical Research, vol. 62, no. 3, pp. 465–472, Sep. 1957.

[89] A. W. Lowell, S. E. Boggs, C. A. Kierans, A. Zoglauer, and J. A. Tomsick, "The 2016 Super Pressure Balloon flight of the Compton Spectrometer and Imager," 2017 IEEE Nuclear Science Symposium and Medical Imaging Conference (NSS/MIC), Atlanta, GA, USA, 2017, pp. 1–3, doi: 10.1109/NSSMIC.2017.8532985.

[90] P. A. R. Ade et al. (SPIDER Collaboration), "Constraints on cosmic birefringence from the SPIDER 2015 long-duration balloon flight," Physical Review Letters, vol. 122, no. 4, p. 041301, Jan. 2019, doi: 10.1103/PhysRevLett.122.041301.

[91] J. P. Filippini et al., "SPIDER: A balloon-borne CMB polarimeter for large angular scales," Astrophysical Journal Supplement Series, vol. 210, no. 2, p. 19, Feb. 2014, doi: 10.1088/0067-0049/210/2/19.

[92] P. de Bernardis *et al.*, "A flat Universe from high-resolution maps of the cosmic microwave background radiation," *Nature*, vol. 404, pp. 955–959, Apr. 2000, doi: 10.1038/35010035.

[93] S. Hanany *et al.*, "MAXIMA-1: A measurement of the cosmic microwave background anisotropy on angular scales of 10 arcminutes to 5 degrees," *Astrophysical Journal Letters*, vol. 545, no. 1, pp. L5–L9, Dec. 2000, doi: 10.1086/317322.

[94] M. Schwarzschild, R. H. Schwarzschild, and R. Danielson, "Stratoscope: A balloon-borne telescope," *Scientific American*,

vol. 200, no. 5, pp. 54–64, May 1959, doi: 10.1038/scientificamerican0559-54.

[95] R. Giacconi, R. N. Wilson, and M. Schwarzschild, “Performance of the 36-inch balloon-borne Stratoscope II telescope,” *Astrophysical Journal*, vol. 148, p. L129, Apr. 1967, doi: 10.1086/180030.

Chapter 4
Theory of Balloon Flight

Christopher D. Yoder[1]

[1] NASA Wallops Flight Facility, Aerospace Engineer, Balloon Program Office

Acknowledgements

To the giants of yesterday on whose shoulders we stand today.

Table of Contents

1. Introduction 7

2. Coordinate and Units Systems 7

2.1. Units 7

2.2. Coordinate Frames 7

2.3. Kinematics 8

2.4. Relationship between frames 9

3. Balloon System and Masses 10

3.1. Center of Mass of the System 10

3.2. Weight 12

4. Environmental Forces 13

4.1. Archimedes principle 13

4.2. Center of Buoyancy 14

4.3. Distribution of Pressure 15

5. Lift and Drag 16

6. Virtual Mass 19

7. Equations of Motion 19

8. A Balloon System in Equilibrium 20

9. Trajectory Control Methods 22

9.1. Uncontrolled balloon trajectories 22

9.2. Altitude control 23

9.3. Propelled flight 24

9.4. Alternate strategies 25

References 26

Table of Figures

Figure 4-1: Coordinate frame of reference..... 8

Figure 4-2: A balloon beginning the ascent phase of flight as viewed from the ground..... 11

Figure 4-3: Ratio of gravitational acceleration over the Earth's planetary atmosphere..... 13

Figure 4-4: Approximate shape of a zero-pressure balloon for a payload of 1800 kg and a float altitude of 40km using Smalley notation [5,6] 14

Figure 4-5: Illustration of the pressure distribution on a spherical zero-pressure balloon..... 16

Figure 4-6: Drag coefficient as a function of Reynolds number for a sphere..... 18

Figure 4-7: (left) the geometry of the test article used by Peters et al. to measure lift, drag, and pitching moment on a natural shaped balloon. (right) the aerodynamic data for a Reynolds number of 1.59x10^6. 18

Figure 4-8: Sketch of a nominal ZPB and the bobbing frequency as illustrated by Morris [1]..... 21

Figure 4-9: Plot of wind speed and direction for the continental US for the month of September in 2024 at 10 hPa. Arrow denotes direction of wind (an arrow with a tail left and head right denotes wind from West to East)..... 22

Figure 4-10: Example sounding files for ABQ during the North American fall..... 24

Table of Symbols

Symbol	Definition	Dimension
$\vec{a}_{CM}$	Acceleration of the center of mass	LT^{-2}
$\vec{B}$	Force of buoyancy	MLT^{-2}
C_B	$= v_{vb0}\rho_{air}$, bobbing coefficient	$ML^{-2}T^{-1}$
C_D	Coefficient of drag	
$\vec{D}$	Drag force	MLT^{-2}
g	Acceleration due to gravity	LT^{-2}
G	Newton's gravitational constant	$M^{-1}L^{3}T^{-2}$
h	Height	L
i,j,k	Axes of a rectilinear coordinate frame	
k	Effective spring constant of bobbing	MT^{-2}
$\vec{L}$	Lift force	MLT^{-2}
m	Effective mass for bobbing	M
m_a	Mass of the displaced air by the balloon	M
m_A	Mass of the air inside the ballonet	M
m_B	Mass of the balloon, including fittings and items mounted on the balloon	M
m_{FT}	Mass of the flight train, including the parachute, cable ladder, rotator, etc.	M
m_G	Mass of the lift gas inside the balloon	M
m_i	Mass of the i^{th} component in the system	M
m_P	Mass of the payload, including the scientific gondola and equipment, but excluding ballast mass	M
m_S	Mass of the ballast carried on the payload	M
m_{SYS}	Mass of the entire system	M
m_V	Virtual mass	M
P	Pressure	$ML^{-1}T^{-2}$
R_P	Radius of the planet	L
R_B	Magnitude of the vector from the planetary center to the balloon	L
R_{gas}	Specific gas constant	$L^{2}T^{-2}\theta^{-1}$
s_{CM}	Coordinate of the center of mass of the system	L
s_i	Center of mass of the i^{th} component in the system	L
S_{ref}	Reference area for aerodynamic forces	L^2
u,v,w	Time rate of change of position along the i,j,k axes of a coordinate frame	LT^{-1}

Symbol	Definition	Dimension
V	Volume	L^3
$\vec{W}$	Force of gravity	MLT^{-2}
x, y, z	Position of a point on the i,j,k axes of a coordinate frame	L
κ	Mathematical constant	M
λ	Longitude	deg
μ	$\sim Gm$, gravitational parameter of the planet	L^3T^{-2}
v_{vb0}	Velocity of vertical winds for bobbing	$L\ T^{-1}$
ρ	Density	ML^{-3}
ϕ	Latitude	deg
$\vec{\Omega}$	Rotation of the Earth about the North pole	T^{-1}
$\vec{\omega}$	Angular velocity	T^{-1}

1. Introduction

This chapter is meant to provide an outline for the physics of a balloon, from launch to float altitude. Concepts are generalized where applicable, with the focus being on a zero-pressure balloon (defined within) around the planet Earth. The material here is founded in material from the initial handbook, with updates provided in areas of significant change since the initial publication (e.g. trajectory control). Extra-terrestrial applications are found in Chapter 15: Planetary Balloons.

2. Coordinate and Units Systems

2.1. Units

For this section, the International System of Units (SI units) will be used. Where applicable, conversions to a feet-pound-second unit systems will be given for context.

2.2. Coordinate Frames

To begin, consider the inertial reference frame denoted by the unit vectors $\{\hat{\imath}_O, \hat{\jmath}_O, \hat{k}_O\}$. The inertial frame is centered at the center of the planet and the planet is assumed fixed with respect to the stars (i.e. the motion of the planet about the Sun is neglected). $\hat{k}_O$ is defined as the vector from the center of the planet through the North pole, while $\hat{\imath}_O$ is defined as the vector from the center of the planet through the equatorial plane and normal to $\hat{k}_O$. $\hat{\jmath}_O$ is defined by the Right Hand Rule.

Next, the planet frame of reference is fixed within the planet and is denoted with unit vectors $\{\hat{\imath}_E, \hat{\jmath}_E, \hat{k}_E\}$. The planet frame is centered at the geometric center of the planet and rotates with the Earth. The unit vector $\hat{k}_E$ is defined as normal to the equatorial plane and extends through the North Pole (parallel to $\hat{k}_O$). The unit vector $\hat{\imath}_E$ is defined as the vector from the center of the planet through the intersection of the equatorial plane and the prime meridian. The unit vector $\hat{\jmath}_E$ is defined by the Right Hand Rule.

Third, the local frame of reference (hereby termed the balloon frame) is embedded within the balloon with unit vectors $\{\hat{\imath}_B, \hat{\jmath}_B, \hat{k}_B\}$. This local frame is used to define quantities of interest for operations. The $\hat{k}_B$ axis is aligned with the local vertical (i.e. pointing radially from the center of the planet to the surface). The $\hat{\imath}_B$ axis points from the balloon towards the South pole. Finally, the $\hat{\jmath}_B$ is defined by the Right Hand Rule (resulting to the East), as shown in Figure 4-1.

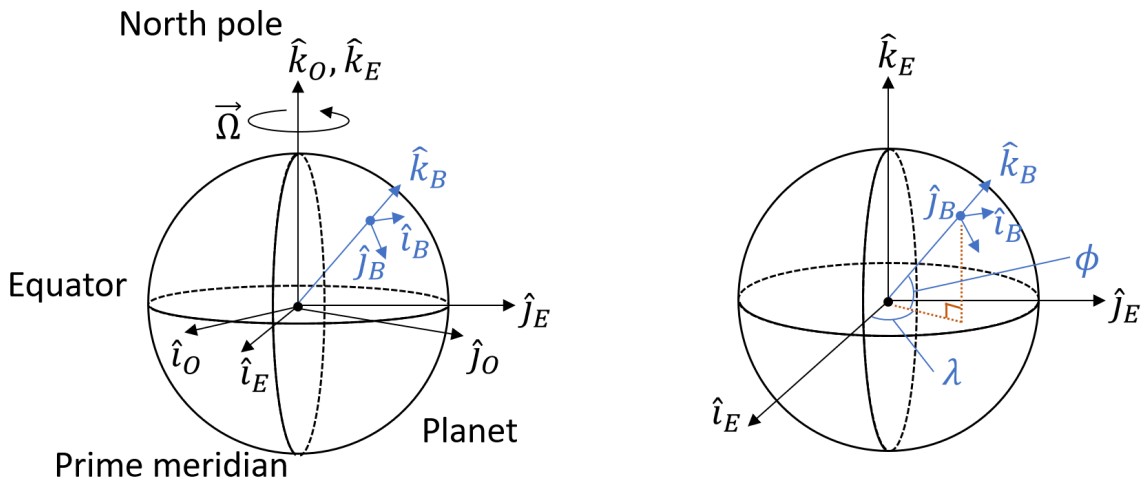


Figure 4-1: Coordinate frame of reference.

One consequence of the balloon frame definition is that there will be a rotation of the balloon frame during flight about $\hat{k}_B$. However, for most flights, an azimuth rotation is acceptable, and this rotation does not have a significant bearing on the dynamics of the balloon due to the axisymmetric nature of the system. Thus, the rotation is ignored here. For missions in which attitude is of concern (e.g. pointed telescopes), a coarse azimuth pointing system is used to orient the payload beneath the balloon (termed a rotator, see Section 8).

2.3. Kinematics

The position of the balloon in the planet frame is expressed as:

$$\vec{r}_B = x_B\hat{\imath}_E + y_B\hat{\jmath}_E + z_B\hat{k}_E \tag{4-1}$$

Here, the coordinates of the balloon (x_B, y_B, z_B) are measured from the center of the planet. Using the Transport Theorem [1], the derivative with respect to time of each quantity yields the inertial velocity of the balloon system:

$$\vec{v}_B = (\dot{x}_B - y_B\Omega_E)\hat{\imath}_E + (\dot{y}_B + x_B\Omega_E)\hat{\jmath}_E + \dot{z}_B\hat{k}_E \tag{4-2}$$

Likewise, the inertial acceleration of the system can be found by differentiating the velocity with respect to time using the Transport Theorem again [1]:

$$\vec{a}_B = (\ddot{x}_B - 2\dot{y}_B\Omega_E - x_B\Omega_E^2)\hat{\imath}_E + (\ddot{y}_B + 2\dot{x}_B\Omega_E - y_B\Omega_E^2)\hat{\jmath}_E + \ddot{z}_B\hat{k}_E \tag{4-3}$$

Note that velocity and acceleration are both expressed in the planet frame and that derivatives are left in dot notation (e.g. dx/dt is denoted $\dot{x}$).

2.4. Relationship between frames

For operational purposes, it is often convenient to express the position of the balloon in a polar coordinate notation (latitude, longitude, altitude) and relative to objects on the planet (e.g., cities, airports, mountains, etc.). To express the position in terms of polar coordinates, the following convention is employed:

$$R_B = |\vec{r}_B|_2 = \sqrt{x_B^2 + y_B^2 + z_B^2} \tag{4-4}$$

$$\phi = \text{atan}\left(\frac{z_B}{\sqrt{x_B^2 + y_B^2}}\right) \tag{4-5}$$

$$\lambda = \text{atan}\left(\frac{y_B}{x_B}\right) \tag{4-6}$$

Note in Equation (4-4), the notation $|\cdot|_2$ denotes the norm of the vector. Conveniently, λ and ϕ are the longitude and latitude coordinates, respectively. The altitude of the balloon can be found by subtracting the planetary radius from the magnitude of the radius vector, namely:

$$h_B = R_B - R_P = \sqrt{x_B^2 + y_B^2 + z_B^2} - R_P \tag{4-7}$$

The inverse relationship (converting from polar to rectilinear coordinates) is a straightforward one, given by:

$$R_B = R_P + h_B \tag{4-8}$$

$$x_B = R_B \cos(\phi)\cos(\lambda) \tag{4-9}$$

$$y_B = R_B \cos(\phi)\sin(\lambda) \tag{4-10}$$

$$z_B = R_B \sin(\phi) \tag{4-11}$$

Practically, the velocity of the balloon will be expressed in a similar frame to the balloon frame (for example, GPS units may express velocity in a North-East-Down frame). A set of rotations about the balloon frame axes can be used for the instantaneous rotation, if desired.

3. Balloon System and Masses

Consider a generic balloon system (see Figure 4-2) composed of the following: a thin-film envelope, a flight train consisting of the parachute and a cable ladder, and finally the scientific gondola, or payload. For the remainder of this chapter, the following definitions are used:

- Balloon mass, m_B, comprised of the mass of the balloon vehicle above the base fitting including the film/fabric envelope, tendons, load tapes, fittings, valves, balloon-mounted electronics, sensors, ballonets, etc.
- Payload mass, m_P, comprised of the mass of the scientific gondola and all equipment attached to the payload.
- Ballast mass, m_S, which is the amount of mass able to be dropped during flight.
- Gas mass, m_G, is the mass of the lift gas inside the balloon.
- Air mass, m_A, is the mass of air contained within a ballonet within the balloon system.
- Flight train mass, m_{FT}, which is the mass of the parachute, cable ladder, termination boxes contained within the flight train, and any sensors included in the train.

The gross mass of the system, m_{SYS}, is defined as:

$$m_{SYS} = m_B + m_P + m_S + m_A + m_{FT} \tag{4-12}$$

Note that Equation (4-12) does not include the mass of lifting gas, m_G. This convention was adopted by the initial handbook [2], which will be continued here. Additionally, the discussion of virtual mass (sometimes called added mass), m_V, will occur in Section 6 of this chapter.

3.1. Center of Mass of the System

The center of mass location for the balloon system can be found in a similar method for finding the center of mass for a system of rigid bodies. Assume the center of mass of all components lie on the axis of symmetry of the balloon. Then, the position of the center of mass of the system is:

$$s_{CM} = \frac{\sum_i s_i m_i}{\sum_i m_i} \tag{4-13}$$

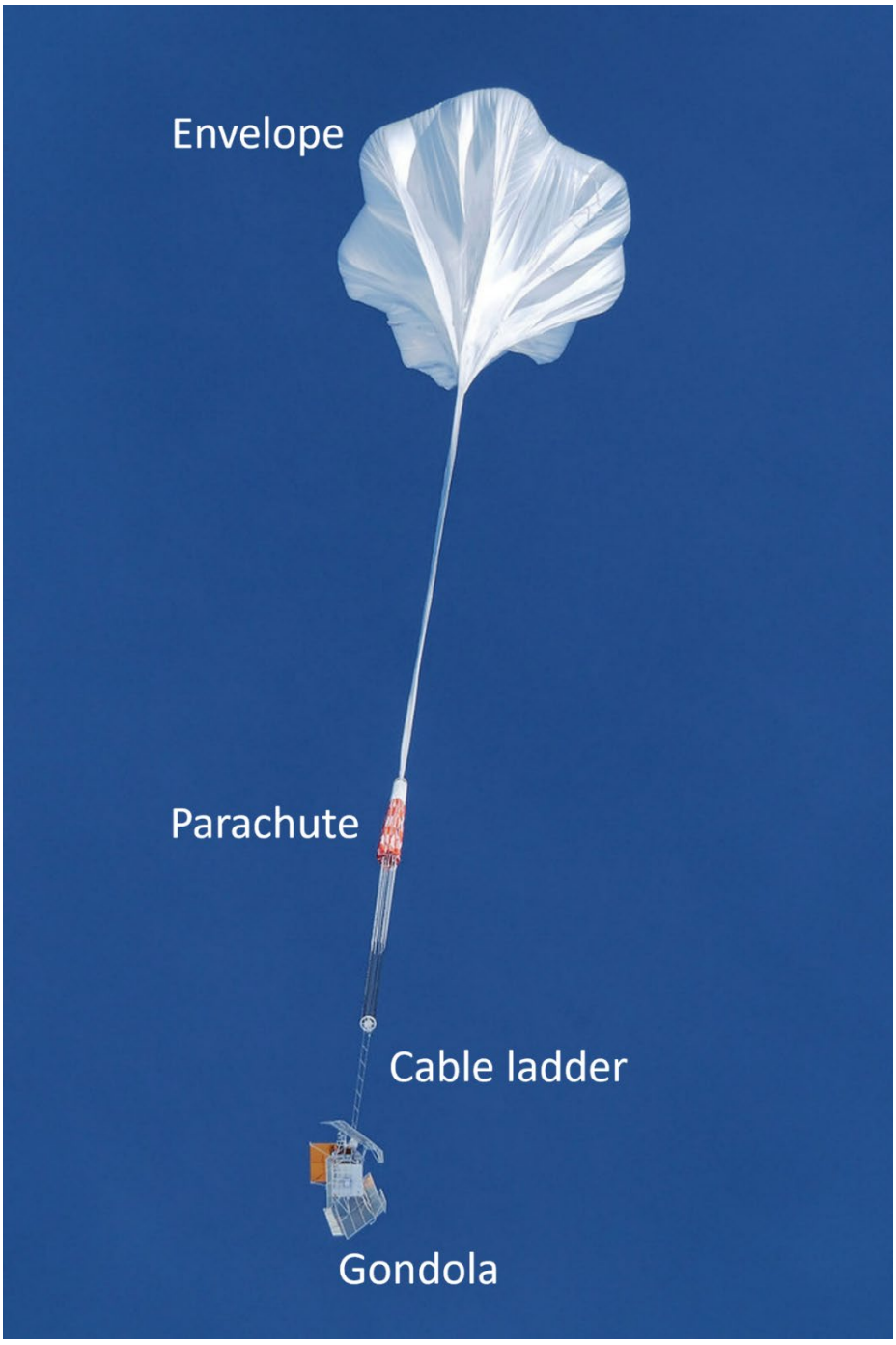


Figure 4-2: A balloon beginning the ascent phase of flight as viewed from the ground

Source: NASA/ Scott Battaion

In Equation (4-13), s_i denotes the distance along the line of symmetry of the balloon as measured from the apex fitting of the balloon to the center of mass of the i^{th} component. The value of mass of the i^{th} component is denoted by m_i. Since the balloon will change height over the course of the flight, the position of the center of mass of the system will vary over ascent and then minimally once at float. For larger balloons, the movement of the center of mass can be shown to be approximately 10% of the total length of the system and concentrated around the base fitting. Thus, the motion of the center of mass of the system is often neglected.

3.2. Weight

The gravitational force between two objects is proportional to the product of the masses of the two objects. From Newton's law of gravity:

$$\vec{F}_g = \frac{-Gm_1m_2}{r^2}\vec{k}_B \tag{4-14}$$

When one object is much larger than another, such as the case with a balloon aloft in a planetary atmosphere, then the gravitational force can be written as:

$$\vec{W} = \frac{-\mu}{(R_P + h)^2} m_{SYS}\vec{k}_B \tag{4-15}$$

Where $\vec{W}$ is the force due to gravity, $\mu = Gm_1$ is the gravitational parameter of the planet, R_P is the radius of the planet, and h is the altitude of the balloon above the planet's surface. Thus, the force due to gravity has a dependency on $1/h^2$ of the balloon. For terrestrial ballooning applications, the ratio of the gravity force at the top of the atmosphere to sea level is:

$$\frac{\left|\vec{W}|_{h=h_{TOA}}\right|}{\left|\vec{W}|_{h=0}\right|} = \frac{\frac{-\mu}{(R_P + h_{TOA})^2} m_B}{\frac{-\mu}{(R_P + 0)^2} m_B} = \frac{r_P^2}{(R_P + h_{TOA})^2} \tag{4-16}$$

Plotting Equation (16) with R_P as 6378 km, it is seen that at Earth's Kármán line (100 km), there is only a ~3% reduction in gravitational acceleration. Therefore, for most applications in ballooning, the weight of the balloon system is approximated as:

$$\vec{W} = \frac{-\mu}{(r_P)^2} m_B\vec{k}_B \tag{4-17}$$

Where the term $g = \mu/r_p^2 \approx$ 9.81 m/s^2 is the gravitational acceleration of the Earth at sea level.

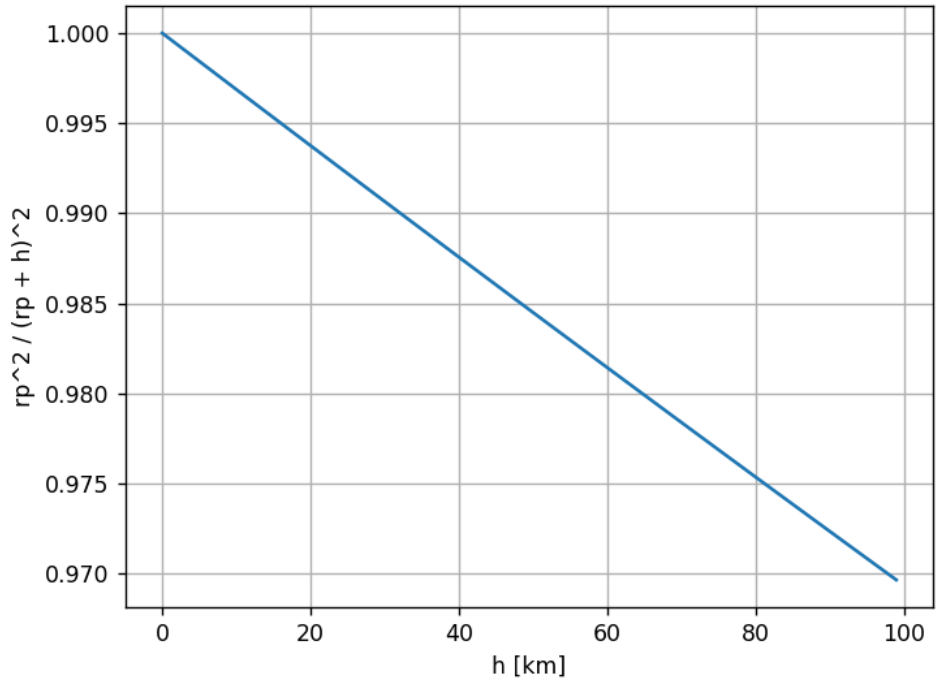


Figure 4-3: Ratio of gravitational acceleration over the Earth's planetary atmosphere.

4. Environmental Forces

4.1. Archimedes principle

Archimedes' principle states that a body inside a fluid will experience a buoyant force equal to the weight of the displaced fluid opposite to the local acceleration vector. For a balloon at a stable float altitude in Earth's atmosphere at perfect equilibrium (i.e. no bobbing motion), this is written:

$$\vec{B} = \rho_{air} V_B g \vec{k}_B \tag{4-18}$$

Where $\vec{B}$ is the buoyant force on the balloon, ρ_{air} is the density of the displaced air, V_B is the volume of the balloon, and g is the magnitude of the acceleration due to gravity. Note that the product $\rho_{air} V_B$ is the mass of the displaced air of the balloon. In practice, the total buoyant volume includes the volume of air displaced by the entire flight train and gondola, but this volume is assumed negligible when compared to the volume of the balloon.

It is convention in the ballooning community to subtract out the mass of the lift gas when calculating the buoyancy on the structure [3,4].

The justification behind this convention being that sizing a balloon (during the mission design phase) is easier if buoyancy per unit volume of lift gas (termed specific buoyancy) is used (see Chapter 9 on Zero-Pressure Balloons for more detail and a worked example). Thus, Equation (4-18) is commonly expressed as:

$$\overrightarrow{B'} = g(m_a - m_G)\vec{k}_B \tag{4-19}$$

Where $m_a = \rho_{air} V_B$ is the mass of the displaced air, and not to be confused with m_A from Section 3, which denotes the control air ballast mass in a ballonet (see Section 9 for more detail). The assumption with this simplification is that the center of buoyancy and center of mass are co-located at all points during flight.

4.2. Center of Buoyancy

The buoyant force on an object (balloon) fully submerged in a fluid (the atmosphere) can be shown to act through the center of buoyancy [9]. The center of buoyancy is found by calculating the centroid of the displaced volume of fluid. For ballooning, this is practically the volume of the balloon during flight. For the axisymmetric shape of revolution of a fully inflated balloon, the centroid can be found by integrating the

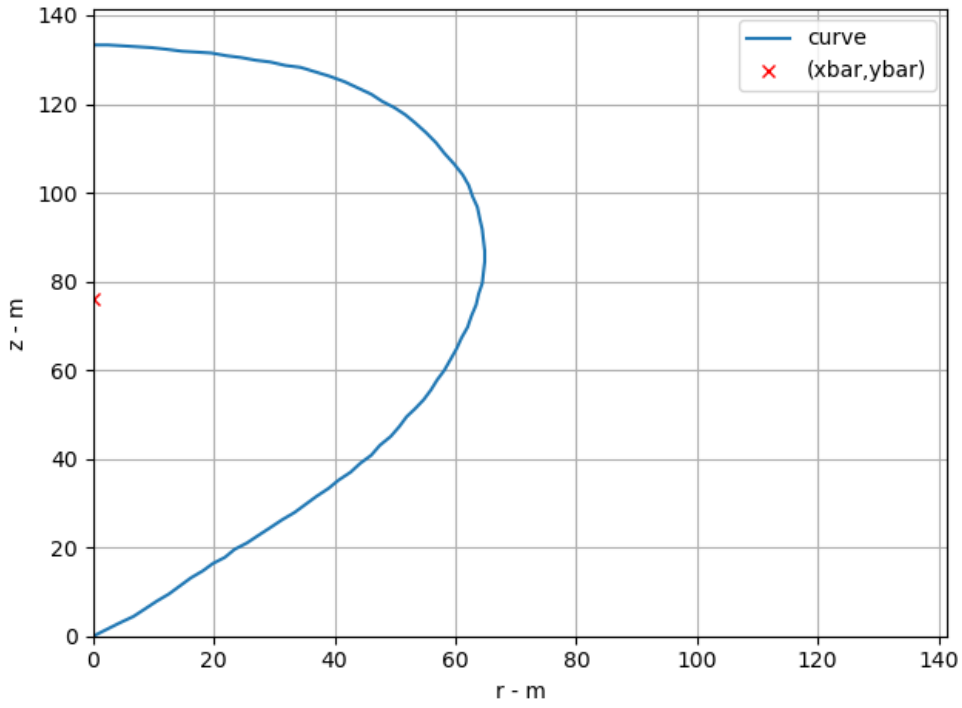


Figure 4-4: Approximate shape of a zero-pressure balloon for a payload of 1800 kg and a float altitude of 40km using Smalley notation [5,6]

Taken from the SINBAD shape tables [5]

area between the curve and the z axis (normalized to Smalley length factor), see Figure 4-4 for an example).

4.3. Distribution of Pressure

The buoyant force described in Equation (4-19) gives a simplification of the physics acting on the structure. In general, there is a pressure difference across the envelope of the balloon which exerts the force on the balloon. This overall pressure distribution is the mechanism that gives rise to the buoyant force.

Consider first the hydrostatic pressure on a small parcel of gas:

$$dP = -g\rho\, dz \tag{4-20}$$

In Equation (4-20), P is the fluid pressure and the notation $d(\cdot)$ denotes an infinitesimal segment. Integrating yields:

$$\int dP = -g\rho \int dz$$

$$P|_z = P|_{z_0} - g\rho(z - z_0) \tag{4-21}$$

Where the quantities g and ρ are constant (i.e. constant mass) over the interval $dz = z - z_0$, which holds only for small distances (e.g. the height of a balloon). The term $P|_z$ is shorthand notation for the pressure, P, evaluated at the altitude z. Consider now the pressure difference across the balloon envelope to be $P_{gas} - P_{air}$:

$$\begin{aligned} P_{gas} - P_{air} &= P_{gas}(z) - P_{air}(z) \\ &= \left[P_{gas}|_{z_0} - g\rho_{gas}(z - z_0)\right] \\ &\quad - \left[P_{air}|_{z_0} - g\rho_{air}(z - z_0)\right] \\ &= \left[P_{gas}|_{z_0} - P_{air}|_{z_0}\right] - g(z - z_0)\left[\rho_{gas} - \rho_{air}\right] \end{aligned} \tag{4-22}$$

For the case of a zero-pressure balloon, the term $\left[P_{gas}|_{z_0} - P_{air}|_{z_0}\right] = 0$ because the vents are open at the base of the balloon (or slightly below). Then, $P_{gas} - P_{air} > 0$ for any gas which is lighter than air. Farley represented this graphically for the case of a zero-pressure spherical balloon [5], reproduced here in Figure 4-5.

For a fully inflated zero-pressure balloon shape, the apex differential pressure (maximum differential pressure) can be estimated by substituting $h = z - z_0$ and $\rho_{gas} = m_{gas}/V_B$:

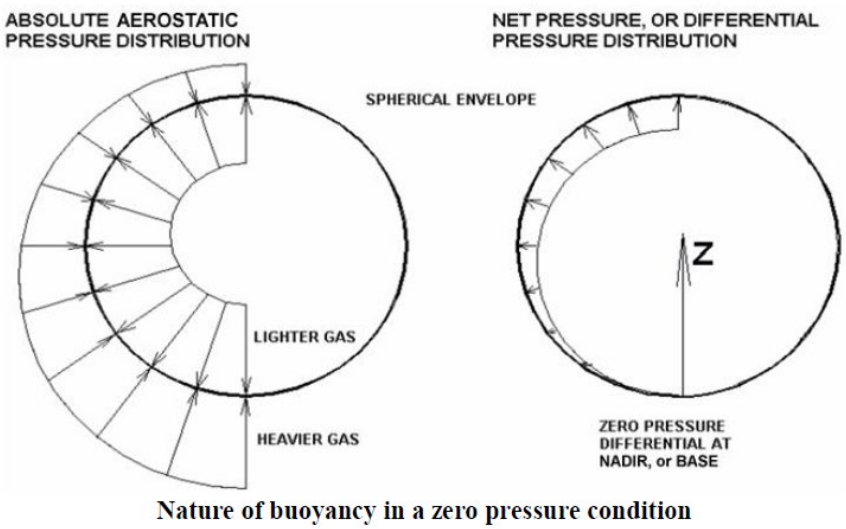


Figure 4-5: Illustration of the pressure distribution on a spherical zero-pressure balloon

Taken from [4] with permission.

$$P_{gas} - P_{air} = -gh\left[\frac{m_{gas}}{V_B} - \rho_{air}\right] \tag{4-23}$$

Smalley's sigma tables [4,6] generalized the zero-pressure design and listed zero-pressure heights for under- and fully-inflated balloon designs. An example of such a shape is shown in Figure 4-4.

5. Lift and Drag

Both in the spool and during flight, the balloon will experience a resultant aerodynamic force due to the wind flowing around the balloon. This resultant force can be resolved into a force component parallel to the direction of flow (drag) and a force component perpendicular to the flow (lift) [10]. A third force (drag) will be present if the balloon is ascending or descending in the atmosphere. Each will be taken, in turn.

First, consider the relative wind, or the wind that is "seen" by the balloon. From Equation (4-2), the balloon has a velocity expressed in the balloon frame of $\vec{v}_B = u_B\,\hat{\imath} + v_B\,\hat{\jmath} + w_B\,\hat{k}$. Likewise, assume that the winds in the atmosphere have components $\vec{v}_{wind} = u_w\,\hat{\imath} + v_w\,\hat{\jmath} + w_w\,\hat{k}$. Thus, the relative wind is expressed as:

$$\begin{aligned}\vec{v}_{rel} &= \vec{v}_{wind} - \vec{v}_B \\ &= (u_w - u_B)\,\hat{\imath} + (v_w - v_B)\,\hat{\jmath} + (w_w - w_B)\,\hat{k}\end{aligned} \tag{4-24}$$

Alternatively, the relative wind can be expressed in the planet frame of reference using the rotation matrix between the two frames of reference. The drag on a balloon shape is given in the general form:

$$\vec{D} = \frac{1}{2}\rho\vec{v}_{rel}|\vec{v}_{rel}|C_D S_{ref} \tag{4-25}$$

Note that in Equation (4-25), C_D represents the drag coefficient of the balloon and S_{ref} is the reference area of the balloon itself, often taken as the cross-sectional area seen by the wind. The direction of the drag force is the same as the relative wind, aligning with the flow. For an axisymmetric shape, such as a balloon about the center axis (from apex to base), the azimuth direction has no bearing on the drag coefficient or reference area. However, estimating frontal area is a challenge, especially during ascent when the balloon is partially inflated. Smalley provided a technique for calculating the volume of a balloon (and via some manipulation, the cross-sectional area) in several reports [4,6], and the same has been completed by others since [11]. For the case of ascent, Smith et al. took one step further and completed CFD analyses on an ascending balloon to better understand the flow field around the structure [12].

Lift on a balloon follows the same form as drag:

$$\vec{L} = \frac{1}{2}\rho\vec{v}_{rel}|\vec{v}_{rel}|C_L S_{ref} \tag{4-26}$$

Where C_L is the lift coefficient. For lateral winds, the lift coefficient was shown to be dependent on the inclination of the wind relative to the balloon by an angle alpha [13], termed the angle of attack.

A common approximation for balloon shape is that of a sphere, which simplifies the aerodynamics significantly. For a sphere, Hoerner has shown that the drag coefficient is only a function of Reynolds number, and lift coefficient is zero [14], see Figure 4-6. Since a sphere is symmetric about all axes, the total aerodynamic force can be reduced to a single force (drag) and the direction can be resolved by the unit vectors of the relative wind (as written in Equation (4-25)).

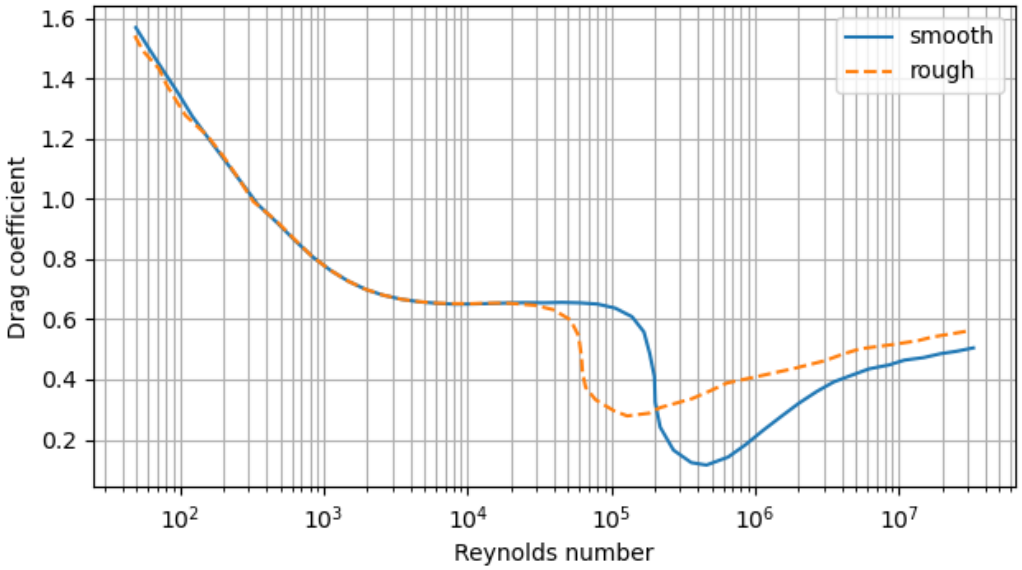


Figure 4-6: Drag coefficient as a function of Reynolds number for a sphere

Data reproduced from [32]. Additional data available from [6]

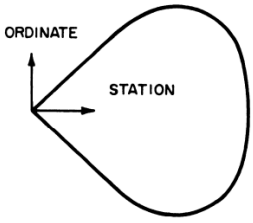


Table 2-1. Ordinates of Natural Shape Balloon

Station (percent length from tether point)	Ordinate (inches)	Station (percent length from tether point)	Ordinate (inches)
0	0	74.8	12.17
14.6	3.42	80.3	11.70
29.2	6.85	85.4	10.95
41.9	9.83	87.7	10.49
46.9	10.70	91.7	9.39
52.0	11.40	94.8	8.12
57.5	11.94	97.1	6.73
63.2	12.27	98.6	5.27
69.0	12.35	99.5	3.78
		100.0 = 25.87"	0

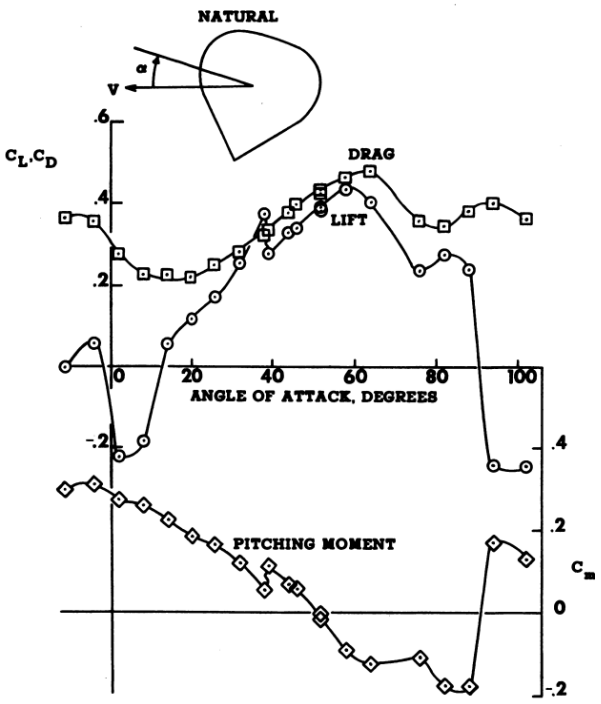


Figure 4-7: (left) the geometry of the test article used by Peters et al. to measure lift, drag, and pitching moment on a natural shaped balloon. (right) the aerodynamic data for a Reynolds number of 1.59x10^6.

Published by Peters et al. [6].

6. Virtual Mass

The concept of virtual mass originated as a method to handle fluid motion around a body [15]. Specifically, when a body accelerates through a fluid, the fluid must accelerate around the body to allow the prescribed body motion. This force (the product of fluid mass and fluid acceleration) differs from the lift and drag forces described above because the force is proportional to the acceleration of the body, not the steady-state velocity.

For a general force proportional to an acceleration term, $\vec{F}(\vec{a}_{sys})$, it can be shown that the force can be modeled as an "added mass" term, m_V:

$$m_{sys}\vec{a}_{sys} = \Sigma\,\vec{F} = -m_V\vec{a}_{sys} + \vec{F}_a + \cdots$$

$$(m_{sys} + m_V)\vec{a}_{sys} = \vec{F}_a + \cdots \qquad (4\text{-}27)$$

For a single Degree of Freedom (DOF), or for symmetric bodies in flow, m_V reduces to a constant. Approximating a balloon as a sphere accelerating in a flow with equivalent radius r, it can be shown:

$$m_V = \frac{2}{3}\pi\rho_{fluid}r^3 \qquad (4\text{-}28)$$

For bodies which are not symmetric, m_V can be shown to take on different values in each axis, as well as include components for rotation about said axis. Various simplifications can be made for each axis of symmetry (e.g. ellipsoidal shapes), but for complex shapes such as blimps, the complex geometry requires significant effort to estimate added mass terms [15].

7. Equations of Motion

Newton's second law of motion states that the acceleration of the center of mass of a body is equal to the product of the mass of the body and the summation of all external forces [1]. Neglecting the change in mass center of the balloon system with shape change yields:

$$m_{SYS}\vec{a}_{CM} = \Sigma\vec{F}_{external}$$

$$(m_{sys} + m_G + m_V)\vec{a}_{CM} = \vec{B} + \vec{D} + \vec{L} + \vec{W} \qquad (4\text{-}29)$$

In addition, the rate of change of system mass is:

$$\dot{m}_{SYS} = \dot{m}_S + \dot{m}_A \qquad (4\text{-}30)$$

Note that in Equation (4-30), $\dot{m}_S$ denotes the rate of ballast mass being dropped, and $\dot{m}_A$ denotes the rate of accumulation of air ballast mass. Under conditions of venting and/or significant leaks, the rate of change of lift gas $\dot{m}_G$ needs to be included to track losses for a full accounting of mass change.

The set of equations given by Equation (4-29)-(4-30) constitute the accelerations of the system and can be integrated numerically in time to produce a solution of the balloon's motion in an atmosphere. Each term in Equation (4-29) are discussed above, as well as in prior literature. Additionally, since balloons are thermal vehicles, the buoyancy term is the most technically challenging quantity to model due to the complex heat transfer between the lift gas, balloon structure, and the atmosphere. If a complete model of the balloon is desired, then the equations found in Chapter 5: Energy Balance must be implemented to refine the volume of the balloon appropriately. The avid reader is hereby warned.

8. A Balloon System in Equilibrium

At float, the balloon flight is one of calm and quiescence. During ascent, significant rotation is observed on payloads which can be viewed from the ground. At float, rotations have been observed at nominal rates of approximately 90 deg/min in prior flights. There is sufficient rotation to require the use of an azimuth pointing joint (commonly termed a "rotator") if coarse azimuth stability is desired. Relative wind velocities are believed to be small (<1 m/s) at float conditions.

The main disrupter of quiescent flight at balloon altitudes is believed to be upward turbulence due to weather patterns and geology on the ground. Gravity waves originating at mountain ranges, for example, are known to excite the atmosphere and can be felt at balloon float altitudes. These waves manifest by exciting the pendulum modes of the gondola.

Many balloons commonly undergo vertical oscillations in altitude. This motion, commonly termed "bobbing", is present due to slight changes in the buoyancy of the system, which behaves as a lightly damped oscillator. Morris discussed the bobbing about the nominal float altitude of a balloon in the first edition of the handbook [2]. For the case of reaching float, Morris notes that not all balloons bob. Some approach float in an asymptotic manner, gently easing into a more stable altitude.

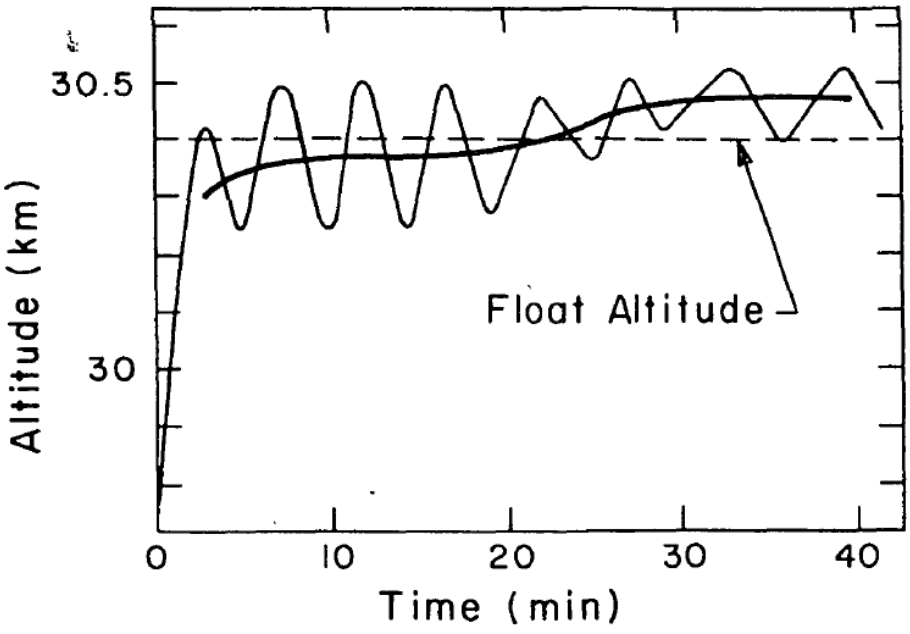


Figure 4-8: Sketch of a nominal ZPB and the bobbing frequency as illustrated by Morris [1].

Farley formulated the bobbing stiffness and period for both zero-pressure and super-pressure balloons as [5] functions of the gravity wave displacing the balloon:

$$\left.\frac{k}{m}\right|_{zpb} = \frac{g}{\rho_{air}(1+C_B)}\left[\frac{\frac{d}{dz}P_{air}}{R_{gas}T_{air}\gamma_g}\frac{\rho_{air}}{\rho_{gas}} - \frac{d}{dz}\rho_{air}\right] \tag{4-31}$$

$$T|_{zpb} = \frac{2\pi}{\sqrt{\left.\frac{k}{m}\right|_{zpb}}} \tag{4-32}$$

$$\left.\frac{k}{m}\right|_{spb} = -\frac{d}{dz}(\rho_{air})\frac{g}{\rho_{air}(1+C_B)} \tag{4-33}$$

$$T|_{spb} = \frac{2\pi}{\sqrt{\left.\frac{k}{m}\right|_{spb}}} \tag{4-34}$$

In Equations (4-31)-(4-34), C_B denotes a coefficient defined as $C_B = v_{vb0}\rho_{air}$ where v_{vb0} is the velocity magnitude of the gravity wave at a given spot in the atmosphere.

9. Trajectory Control Methods

Lateral trajectory control for balloons (and other lighter-than-air vehicles) has been a long-standing goal of several groups. The past several decades has seen a boom in controllability of balloon vehicles, from passive altitude control to active lateral control. Control of balloons can be generalized into several groups, which are reviewed in turn below.

9.1. Uncontrolled balloon trajectories

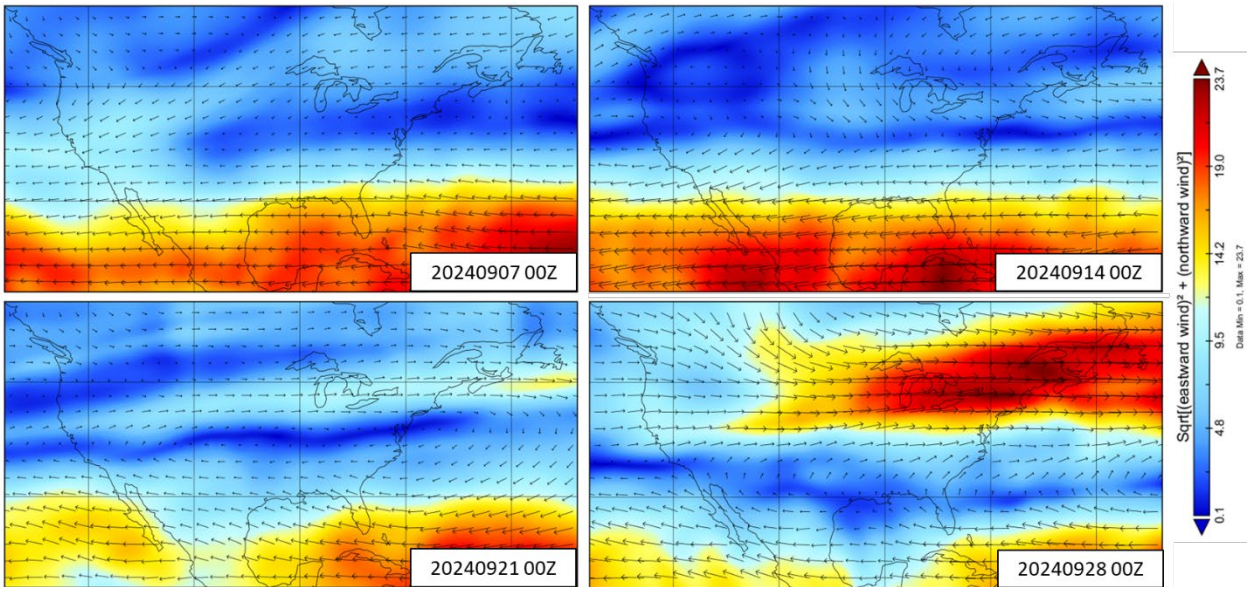


Figure 4-9: Plot of wind speed and direction for the continental US for the month of September in 2024 at 10 hPa. Arrow denotes direction of wind (an arrow with a tail left and head right denotes wind from West to East).

Generated from available data and plotted using Panoply.

Wind patterns in the atmosphere are key to understanding the trajectory of a balloon system. Zonal winds (blowing East-West) are the primary driver of trajectories, with meridional winds (blowing North-South) being the secondary driver. Weather patterns are the primary reason for flights in certain regions of the world. For example, "turnaround" is a phenomenon that occurs in North America where the winds transition from flowing to the West to instead flowing to the East, as shown with GFS data [16,17] in Figure 4-9 (generated using Panoply [18]). Balloons launched in North American have long taken advantage of this pattern to conduct long duration flights. Other common patterns, such as Artic/Antarctic cyclones, are reviewed in Chapter 7: The Atmosphere of this book.

One major characteristic of the atmosphere is the vertical gradient of wind speed and direction that occurs at almost every latitude and season. For example, see data of wind speed magnitude versus altitude in Figure 4-10 taken from vertical soundings [19]. There is a region of low-speed flow with high variability in direction that can be exploited for navigation. By allowing the wind direction to alter the path of the balloon, control can be achieved with significantly less power and thrust compared to flying against or into the winds [20].

9.2. Altitude control

Rough altitude control is typically implemented by carrying ballast mass that can be jettisoned on command. This loss of mass allows buoyancy to overcome the system weight and drives the balloon upward towards a new equilibrium. Currently, most balloon systems utilize a hopper and fine ballast (either sand or steel shot) with a timer and known flow rate to control the dispense rate.

Where ballast is used to increase the altitude of a balloon system, venting gas is the most comment method for decreasing the altitude of a balloon system. Vent valves at the apex allow gas to escape, causing the internal pressure at the apex of the balloon to drop and thus reduce the volume of the balloon. Once the balloon descends (from a reduction in buoyancy from the shape reduction), the structure gains pressure and inflates, allowing the balloon to equilibrize. Typically, apex vents are controlled to allow a controlled amount of gas to escape every maneuver, or to command descent at a nominal rate.

In the mid-1900s, various groups began experimenting with the idea of air ballast to provide fine control of altitude. By the early 2010s, several groups had demonstrated this concept repeatedly in an operational setting [21–23]. The implementation by each group differs, but the main components include an air tank (termed an air ballonet [24]) or anchor balloon (if the tank is external to the main balloon [25]) and an air compressor.

The principle behind the system is to pump external atmospheric air into the air ballonet to increase the system mass. With an increase in mass, the balloon system descends in the atmosphere until the new system mass equals the buoyancy of the lower atmosphere. If air is pumped out of the ballonet, the system mass reduces and allows the balloon to ascend to a higher altitude. By using air, the supply of ballast mass is essentially unlimited unlike the limit with conventional ballast. The trade off comes as a mass penalty (for the ballonet film weight and compressor hardware) and a power penalty (required pump power scales linearly with flowrate).

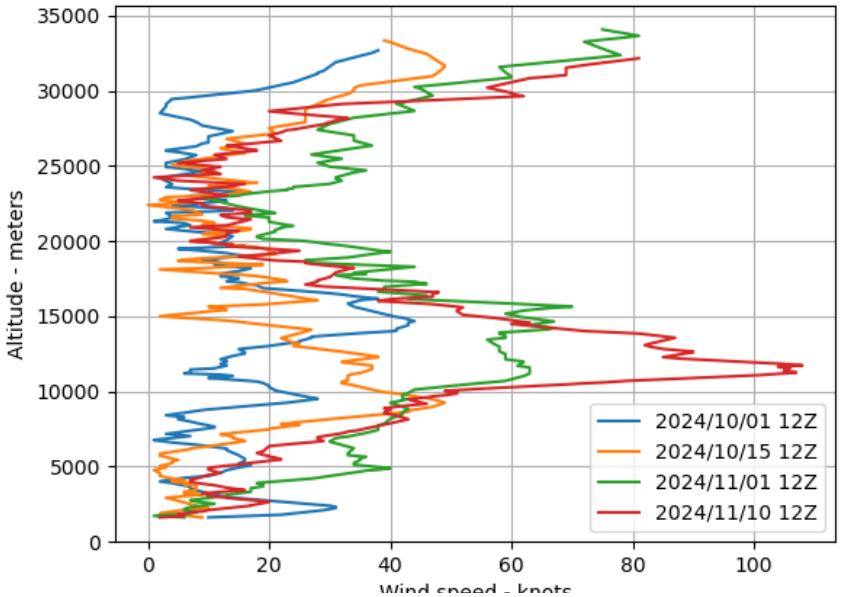


Figure 4-10: Example sounding files for ABQ during the North American fall.

Data taken from Wyoming Weather Web soundings.

9.3. Propelled flight

Propellers have been around since the dawn of powered aviation in the early 1900s. The premise is to generate thrust by spinning the propeller in the direction of the desired motion. Several airships and lighter-than-air vehicles have implemented propellers for lateral control with success [26]. Despite their presence on high-altitude airships, propellers have a limited history for ballooning due to the difficulties with flight in the stratosphere.

The primary concern with high-altitude propellers is the extremely low Reynolds number, specifically below 50,000. For NASA's high-altitude balloons, Eppler and Somers designed three airfoils and several blades, but admitted the lack of experimental validation of low Reynolds numbers regimes could hinder performance [27]. Since then, Project Loon was successful in demonstrating lateral control for several balloon flights using a 2-meter propeller up to 90,000 ft [24]. Additionally, propeller power scales as the cube of lateral guidance speed (the speed imparted by the propeller on the balloon), leading to high power penalties on the design.

9.4. Alternate strategies

In addition to the two main groups of trajectory control, there are other proposed concepts for trajectory control. One proposed method is a shape control of the balloon, termed mechanical compression. In this method, the shape of the system is modulated to control the buoyant force (and in turn, the float altitude) [23,28]. Shape change requires strong materials, an actuation method to change the shape, and a stability analysis to ensure the balloon is structurally stable at all possible shapes.

Another proposed method for altitude control is to vary the temperature of the lift gas. Like the mechanics of a hot air balloon, heating the lift gas allows for the gas to expand, becoming lighter and more buoyant. For balloons without a vent, or at a fixed volume, the additional temperature change can lead to higher pressures and thus stresses in the envelope. Additionally, heaters require fuel which is expendable.

Finally, other thrusters have been proposed instead of propellers. Electric thrusters were proposed for a station-keeping concept [29], albeit with a mass and power penalty. Another concept that was proposed was termed a “Tether and Sail” system [30,31]. This system hung a sail beneath the balloon to act as a rudder and provide a lateral guidance force. While being low power (once deployed), the mass penalty is considerable, and the challenges associated with deployment must be overcome.

References

[1] L. Meirovitch, *Methods of Analytical Dynamics*. Mineola, NY: Dover, 2003.

[2] A. L. Morris, "Scientific Ballooning Handbook."

[3] J. Warren, J. Smalley, and A. Morris, "Aerostatic Lift of Helium and Hydrogen in the Atmosphere," UCAR/NCAR, 1971, p. 4088 KB, doi: 10.5065/D6057CWH.

[4] J. Smalley, "Determination of the Shape of a Free Balloon: Report 1," Air Force Cambridge Research Laboratories, 1963.

[5] R. Farley, "BalloonAscent Theory Manual," NASA GSFC, July 2020, p. 145.

[6] J. H. Smalley, "Balloon Shapes and Stresses Below the Design Altitude," 1966.

[7] H. M. Cathey, D. A. Fairbrother, and M. A. Said, "Performance Highlights of NASA Super Pressure Balloon Mid-Latitude Flights," in *AIAA Balloon Systems Conference*, American Institute of Aeronautics and Astronautics, doi: 10.2514/6.2017-3091.

[8] "Qualification of the NASA Super Pressure Balloon | AIAA AVIATION Forum." [Online]. Available: https://arc.aiaa.org/doi/abs/10.2514/6.2015-2909. [Accessed: Jan. 9, 2025].

[9] B. R. Munson, T. H. Okiishi, W. W. Huebsch, and A. P. Rothmayer, *Fundamentals of Fluid Mechanics*. Hoboken, NJ: John Wiley & Sons, Inc., 2013.

[10] "Fundamentals Of Aerodynamics 5th Edition : John D. Anderson, Jr." [Online]. Available: https://archive.org/details/FundamentalsOfAerodynamics5thEdition/page/n15/mode/2up. [Accessed: Jan. 9, 2025].

[11] F. Baginski, T. Williams, and W. Collier, "A Parallel Shooting Method for Determining the Natural Shape of a Large Scientific Balloon," *SIAM Journal on Applied Mathematics*, vol. 58, no. 3, pp. 961–974, 1998, doi: 10.1137/S0036139995292355.

[12] M. Smith, R. Scott, and J. Marsh, "Refinements to the Aerodynamic Modeling of an Ascending Balloon," presented at the AIAA Balloon Systems Conference, Seattle, Washington, 2009, doi: 10.2514/6.2009-2804.

[13] P. Peters, H. Lysons, and S. Shindo, "Aerodynamic Coefficients of Four Balloon Shapes at High Attack Angles."

[14] S. F. Hoerner, *Fluid-Dynamic Drag: Practical Information on Aerodynamic Drag and Hydrodynamic Resistance*. Bakersfield: Hoerner Fluid Dynamics, 1992.

[15] I. Imlay, "The Complete Expressions for 'Added Mass' of a Rigid Body Moving in an Ideal Fluid."

[16] D. P. Dee et al., "The ERA-Interim Reanalysis: Configuration and Performance of the Data Assimilation System," *Quarterly Journal of the Royal Meteorological Society*, vol. 137, no. 656, pp. 553–597, 2011, doi: 10.1002/qj.828.

[17] NOAA National Centers for Environmental Information, "Global Forecast System (GFS) 1.0 Degree," NCEI 6174, 2004.

[18] "NASA GISS: Panoply 5 netCDF, HDF and GRIB Data Viewer." [Online]. Available: https://www.giss.nasa.gov/tools/panoply/. [Accessed: Aug. 24, 2025].

[19] "University of Wyoming Atmospheric Science Radiosonde Archive." [Online]. Available: https://weather.uwyo.edu/upperair/sounding.shtml. [Accessed: Aug. 24, 2025].

[20] M. Young, S. Keith, and A. Pancotti, "An Overview of Advanced Concepts for Near Space Systems," presented at the 45th AIAA/ASME/SAE/ASEE Joint Propulsion Conference & Exhibit, Denver, Colorado, 2009, doi: 10.2514/6.2009-4805.

[21] A. Alexander, "Loon Library: Lessons from Building Loon's Stratospheric Communications Service," 2021, p. 431.

[22] A. D. Miller, I. Beveridge, A. Antonio, and T. Pirrone, "World View Enterprises Altitude Controlled Balloons: A New Stratospheric Platform for Persistent Earth and Space Imaging Campaigns," in *Ground-based and Airborne Telescopes VII*, vol. 10700, 2018, pp. 1427–1435, doi: 10.1117/12.2313446.

[23] P. B. Voss, E. E. Riddle, and M. S. Smith, "Altitude Control of Long-Duration Balloons," *Journal of Aircraft*, vol. 42, no. 2, pp. 478–482, 2005, doi: 10.2514/1.7481.

[24] A. Alexander, "Loon Library: Lessons from Building Loon's Stratospheric Communications Service."

[25] T. Lachenmeier, "Design of a Trans-Global Manned Balloon System with Relevance to Scientific Ballooning," presented at the International Balloon Technology Conference, Albuquerque, NM, U.S.A., 1991, doi: 10.2514/6.1991-3687.

[26] J. Morgado, M. Abdollahzadeh, M. A. R. Silvestre, and J. C. Páscoa, "High Altitude Propeller Design and Analysis," *Aerospace Science and Technology*, vol. 45, pp. 398–407, 2015, doi: 10.1016/j.ast.2015.06.011.

[27] R. Eppler and D. Somers, "Aerodynamic Design of a Propeller for High-Altitude Balloon Trajectory Control," NASA/CR-2012-215893, Airfoils, Incorporated, 2012.

[28] N. Yajima, N. Izutsu, and H. Honda, "Structure Variations of Pumpkin Balloon," *Advances in Space Research*, vol. 33, no. 10, pp. 1694–1699, 2004, doi: 10.1016/j.asr.2003.09.048.

[29] E. Van Wynsberghe and A. Turak, "Station-Keeping of a High-Altitude Balloon with Electric Propulsion and Wireless Power Transmission: A Concept Study," *Acta Astronautica*, vol. 128, pp. 616–627, 2016, doi: 10.1016/j.actaastro.2016.08.017.

[30] K. T. Nock, K. M. Aaron, M. K. Heun, and A. A. Pankine, "Aerodynamic and Mission Performance of a Winged Balloon Guidance System," *Journal of Aircraft*, vol. 44, no. 6, pp. 1923–1938, 2007, doi: 10.2514/1.31922.

[31] R. Waghela, C. D. Yoder, A. Gopalarathnam, and A. P. Mazzoleni, "Aerodynamic Sails for Passive Guidance of High-Altitude Balloons: Static-Stability and Equilibrium Performance," *Journal of Aircraft*, vol. 56, no. 5, pp. 1849–1857, 2019, doi: 10.2514/1.C035353.

[32] M. V. Krumins, "A review of sphere drag coefficients applicable to atmospheric density sensing," NOLTR 72-34, Naval Ordinance Laboratory, 1972.

Chapter 5
Energy Balance

Ethan A. Chaffee[1]

[1] World View Enterprises, Inc., Program Manager, Programs Department

Table of Contents

1. Introduction 6

2. Energy Balance of High-Altitude Balloon Systems 6

2.1. Atmospheric Parameters..... 8

2.2. Balloon Envelope Parameters..... 9

3. Radiative Heat Loads on the Film 12

3.1. Absorbed Direct Sunlight Heating (***Qsun***) 12

3.2. Absorbed Albedo Heating (***Qalb***)..... 14

3.3. Absorbed Planetary IR Heating (***QIRplanet***) 15

3.4. Absorbed Sky IR Heating (***QIRsky***)..... 17

3.5. Absorbed Film IR Heating (***QIRfilm***)..... 17

3.6. Emitted IR Heating (***QIRout***)..... 18

4. Convective Heat Loads on the Film 18

4.1. Air and Lift Gas Properties..... 18

4.2. Free Convection..... 19

4.3. Forced Convection..... 20

4.4. External Convection Heat Load (***QConvExt***) 20

4.5. Internal Convection Heat Load (***QConvInt***)..... 21

5. Temperature Rate of Change Equations 21

5.1. Lift Gas Temperature Differential Equation..... 21

5.2. Film Temperature Differential Equation..... 22

6. Gondola Considerations 22

6.1. Coating Properties for Radiation..... 22

6.2. Thermal Design Considerations..... 23

7. Conclusion 24

References..... 25

Table of Figures

Figure 5-1. Energy transfer environment of balloon systems in the stratosphere [1]..... 7

Figure 5-2. Position of the sun relative to the balloon..... 8

Figure 5-3. Sketch of reflection of energy within a balloon. Taken with permission from R. Farley's BalloonAscent theory manual [7]..... 10

Table of Tables

Table 5-1: Common variables and their descriptions..... 7

Table 5-2. Example material properties for Zero-Pressure Balloon (ZPB) Material SF372, 0.8 mil thick [7]..... 9

Table 5-3. Orbital parameters for some planets in the solar system [1] 13

Table 5-4. Example generalized albedo data at the top of the atmosphere [7]..... 14

Table 5-5. Ground emissivity for common terrains [1]..... 16

Table 5-6. Downwelling sky IR heat flux at different altitudes [7].. 17

Table 5-7: Common materials and their thermal coefficients [8]..... 23

Table of Symbols

Symbol	Definition	Dimension
A	Area	L^2
$AirMass$	Mass of air in the atmosphere	M
Alb	Albedo	-
c	Specific heat	-
CF	Cloud Fraction	-
D	Diameter	L
Day	Day of the year	-
Dip	Angle below the true horizon	deg
e	Eccentricity	-
Elv	Solar elevation angle	deg
Gr	Grashof number	-
HC	Heat transfer coefficient	$P\ L^{-2}\ °^{-1}$
I	Solar irradiance	$P\ L^{-2}$
k	Thermal conductivity	$P\ L^{-1}\ °^{-1}$
m	Mass	M
Nu	Nusselt number	-
P	Pressure	$F\ L^{-2}$
Pr	Prandtl number	-
q	Flux	$P\ L^{-2}$
Q	Energy	E
r	Reflectivity	-
R	Radius (of a planet, for example)	L
Re	Reynolds number	-
t	Time	T
T	Temperature	°
TA	True anomaly	rad
VF	View factor	-
X_{AM}	Air Mass Correction Factor	-
z	Altitude	L
α	Absorptivity	-
ϵ	Emissivity	-
θ	Half cone angle	deg
μ	Dynamic viscosity	$F\ L^{-2}\ T$

Symbol	Definition	Dimension
ρ	Density	$M\ L^{-3}$
σ	Stefan-Boltzmann constant	$P\ L^{-2}\ T^{-4}$
τ	Transmissivity	-

Subscript	Definition
0	Pertaining to an initial value
alb	Pertaining to albedo
air	Pertaining to air
atm	Pertaining to the atmosphere
AU	Astronomical Unit
$Conv$	Pertaining to convection
E	Pertaining to the Earth
eff	Effective
ext	External
$film$	Pertaining to the film
in	Inward
int	Internal
IR	Pertaining to IR radiation
out	Outward
$planet$	Pertaining to the planet
$proj$	Projected
sky	Pertaining to the sky
Sun	Pertaining to the Sun
$Surf$	Surface
top	Top

1. Introduction

Energy is a critical component to the understanding of the performance of scientific balloon systems. In the guide "BalloonAscent: 3-D Simulation Tool for the Ascent and Float of High-Altitude Balloons", Rodger Farley commented that "the high-altitude scientific balloon is a thermal vehicle" [1]. The gas inside the envelope of a scientific balloon expands and contracts based on the inputs of the surrounding thermal environment. Therefore, the performance of scientific balloons, including much of the analysis outlined within this handbook, is dictated by the operational environment. High-altitude vehicles exist in a primarily radiative environment which fluctuates throughout a standard diurnal cycle and with changing weather conditions. The work outlined within this chapter has been extracted from the work of Rodger Farley with his permission from various materials he provided.

While the effects of the energy environment impacting vehicle performance is critical to understanding scientific ballooning in general, the author felt it was also important to provide context for thermal design of vehicle systems in the stratosphere. Additional content has been provided within this chapter to extend the analysis of thermal environments and design for gondola structures to expand upon the works previously provided related to high-altitude balloon systems.

2. Energy Balance of High-Altitude Balloon Systems

The equations outlined in this section define the energy interactions between a high-altitude balloon system and the surrounding environment [1]. The energy balance analysis is governed by the conservation of energy as defined by the 1st law of thermodynamics [2]. Energy from the surrounding environment goes into or out of the balloon envelope based on the relative thermal conditions of the vehicle. Assuming the balloon does not generate or lose internal energy (e.g. by venting gas, gas burner, etc.), the sum of energies reduces to:

$$Q_{in} = Q_{out} \tag{5-1}$$

The energy balance for high-altitude balloon systems is highly dominated by radiative and convective energy transfer. Figure 5-1 illustrates the basic energy transfer methods of heat transfer for standard balloon systems. Radiative heat transfer dominates the thermal environment in the stratosphere, with convection becoming less of an influence as the balloon ascends in altitude. Inside the balloon, convection dominates as the primary method of heat transfer between the film and lifting gas [3]. Conduction only occurs on the vehicle itself, since the system is free-floating through the atmosphere, and will not be discussed here.

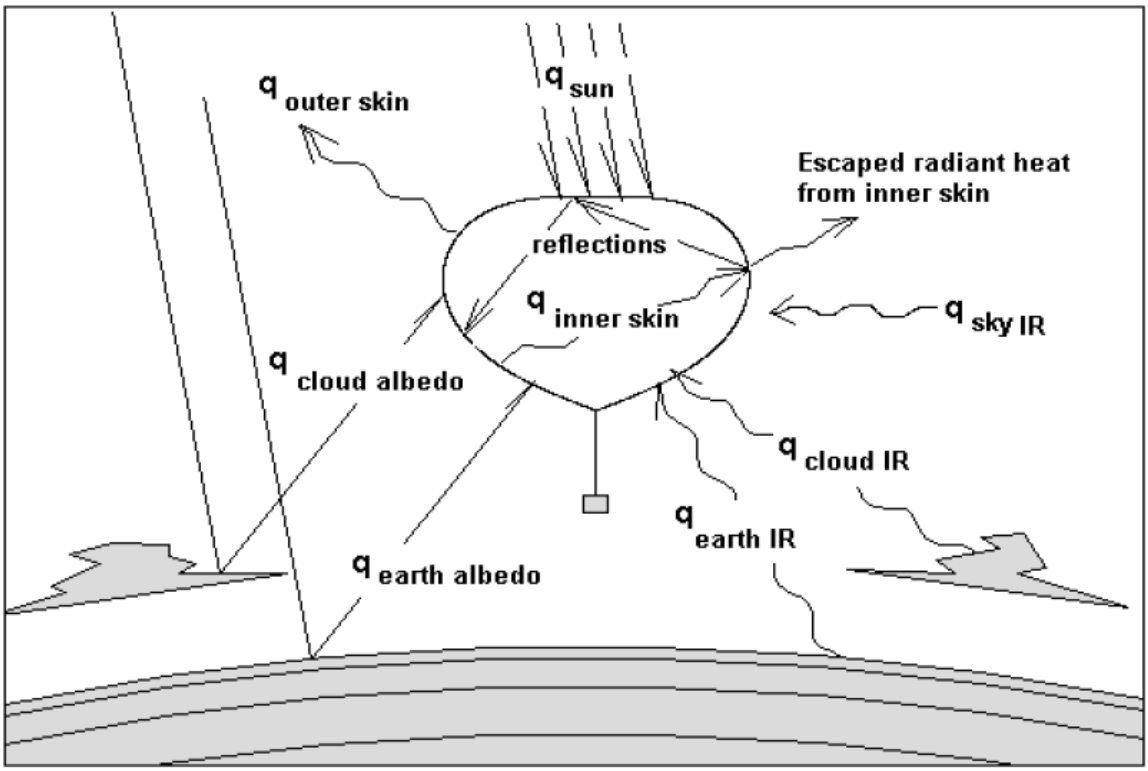


Figure 5-1. Energy transfer environment of balloon systems in the stratosphere [1].

The different thermal parameters are defined by two distinct groups below: radiative heat loads and convective heat loads. The variables for the heat transfer parameters are defined as:

Table 5-1: Common variables and their descriptions.

Variable	Description	Method of transfer
Q_{sun}	Absorbed direct sunlight heating	Radiation
Q_{alb}	Absorbed albedo heating	Radiation
$Q_{IR_{planet}}$	Absorbed planetary IR heating	Radiation
$Q_{IR_{sky}}$	Absorbed sky IR heating	Radiation
$Q_{IR_{film}}$	Absorbed film IR heating	Radiation
$Q_{IR_{Out}}$	IR heating loss	Radiation
$Q_{ConvExt}$	External convective heating	Convection
$Q_{ConvInt}$	Internal convective heating	Convection

2.1. Atmospheric Parameters

The position of the sun at a given time and the interactions with the atmosphere drive the temperature profile for the balloon envelope. As an example, there is a significant change in performance of the vehicle throughout a diurnal cycle which is observed during operations [4], [5], [6]. Therefore, understanding the position of the sun is important for modeling and understanding the performance of a balloon.

First, the solar positioning must be estimated. There are many tools and descriptions for the process of calculating solar position as a function of time. These calculations will not be replicated here but can be found in literature [7], [8]. The solar elevation parameter (ELV) should be defined at this time as an input for the thermal calculations.

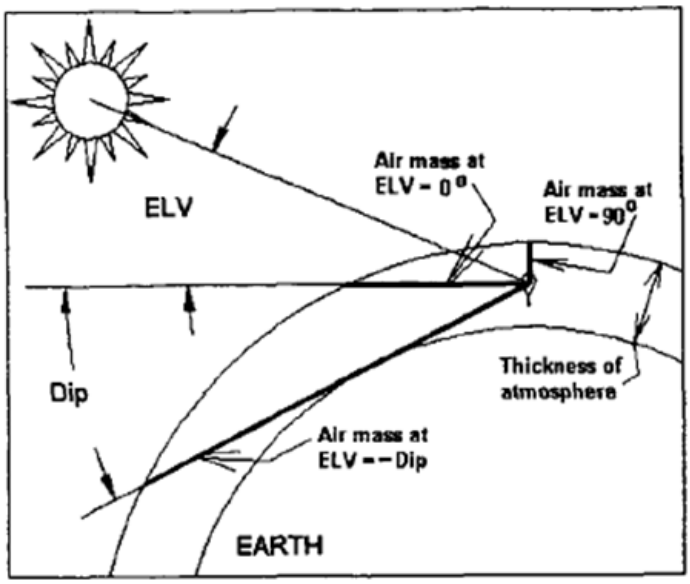


Figure 5-2. Position of the sun relative to the balloon

The sun can still affect the balloon even when it is below the "true horizon" but still above the "apparent horizon", known as the (Dip), as demonstrated in Figure 5-2. Dip can be approximated as:

$$DIP = \cos^{-1}\left(\frac{R_E}{R_E + z}\right) \tag{5-2}$$

Where R_E is the radius of the Earth and z is the altitude of the balloon.

Next, the attenuation of the atmosphere must be considered to determine how much of the energy is diffused before it reaches the balloon at altitude. The transmissivity of the atmosphere is determined by the air mass ratio ($AirMass$) based on the surface pressure (P_0) and pressure at altitude (P_{air}) [9]. A correction factor (X_{AM}) is used to account for fog

and smoke that attenuates the energy transmission further. For cases where $ELV > 0$:

$$AirMass = X_{AM} * \left(\frac{P_{air}}{P_0}\right) * \left[\sqrt{1229 + (614 * \sin(ELV))^2} - (614 * \sin(ELV))\right] \quad (5\text{-}3)$$

If the sun elevation angle is below the true horizon but above the apparent horizon, i.e. $0 > ELV > Dip$, then the following equation is used instead to approximate the air mass ratio.

$$AirMass = \frac{P_{air}}{P_0} * \left[1 + \frac{ELV}{Dip}\right] - \left(70 * \frac{ELV}{Dip}\right) \quad (5\text{-}4)$$

Now, the air mass ratio is applied to the transmissivity of the atmosphere [9].

$$\tau_{atm} = 0.5 * \left[e^{-0.65 * AirMass} + e^{-0.95 * AirMass}\right] \quad (5\text{-}5)$$

Transmissivity in the IR spectrum must also be calculated. The equation for IR atmospheric transmissivity is structured similarly to the above equation. However, the equation is dependent on the pressure ratio between the surface and the operational altitude rather than the air mass.

$$\tau_{atmIR} = 1.716 - \left(0.5 * \left[e^{-0.65 * \frac{P_{air}}{P_0}} + e^{-0.95 * \frac{P_{air}}{P_0}}\right]\right) \quad (5\text{-}6)$$

2.2. Balloon Envelope Parameters

Balloon envelope parameters include material properties, which are defined as inputs for the energy balance calculations, and derived parameters related to the geometry of the envelope. Material properties, such as absorptivity (α), emissivity (ε), and transmissivity (τ), are area-averaged values across the various components of the balloon envelope. Note that $\alpha + \epsilon + \tau = 1$ for a given material.

Table 5-2. Example material properties for Zero-Pressure Balloon (ZPB) Material SF372, 0.8 mil thick [7]

	1 layer	2 layers	3 layers	4 layers
$\boldsymbol{\alpha}$	0.024	0.042	0.057	0.087
$\boldsymbol{\varepsilon}$	0.134	0.234	0.314	0.475
$\boldsymbol{\tau}$	0.916	0.847	0.788	0.667
$\boldsymbol{\tau_{IR}}$	0.866	0.766	0.686	0.525
$\boldsymbol{\alpha/\varepsilon}$	0.176	0.180	0.182	0.184

As is evident in the diagram in Figure 5-3, the balloon system is also affected by reflections of energy within the system. The multiple reflections increase the effective interior absorption. Therefore, the effective reflectivity (r_{eff}) is captured by the geometric series below.

$$r_{eff} = r + r^2 + r^3 + r^4 + r^5 \ldots \quad (5\text{-}7)$$

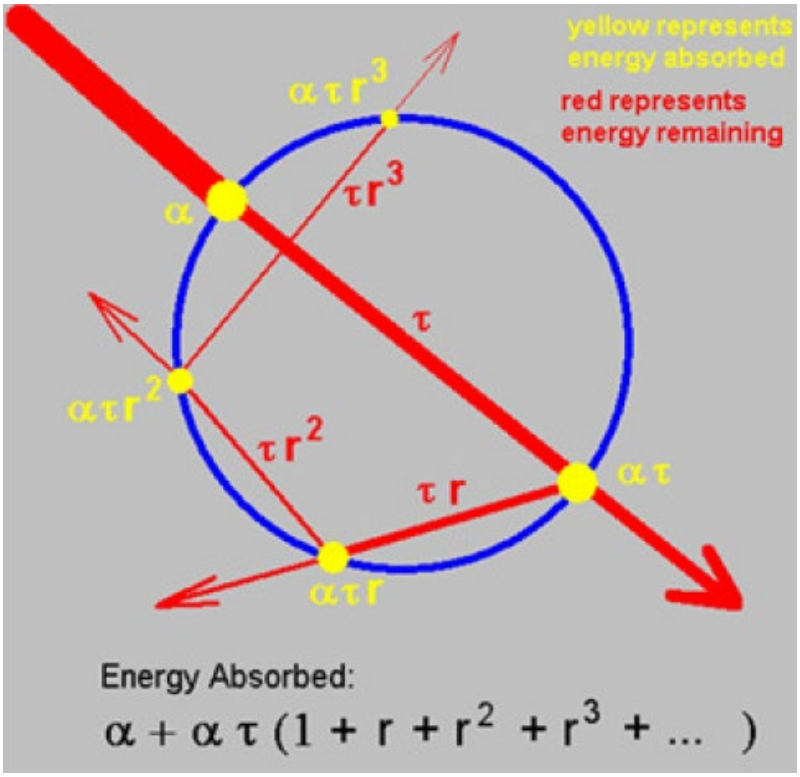


Figure 5-3. Sketch of reflection of energy within a balloon.

Taken with permission from R. Farley's BalloonAscent theory manual [7].

The geometry of the vehicle envelope must also be considered. Shape parameters should be defined from the design of the envelope. The relevant envelope shape parameters to consider for the energy balance calculations include the diameter of the envelope and the surface area. These parameters should be calculated for the specific time and conditions in flight. Additional characterization of balloon envelope geometry is provided in Chapter 9 for zero-pressure balloons and Chapter 10 for super-pressure balloons as well.

One derived parameter for the envelope geometry is the projected area, or the region of the envelope that is normal to the incoming energy. The projected area is derived from the top projected area (or the area visible when viewing the envelope from above) and varies with the solar elevation. The top projected area is defined from the diameter of the envelope in Equation (5-8).

$$A_{top} = \frac{\pi}{4} * D^2 \tag{5-8}$$

The following equations calculate the projected area of the vehicle envelope for zero-pressure (ZP), super-pressure (SP) and spherical envelope shapes. The projected area calculations modify the top projected area based on the elevation of the sun and the particular geometry of the vehicle envelope.

- Zero-Pressure Shape:

$$A_{proj} = A_{top} * \left[0.9125 + \left(0.0875 * \cos\left(\pi - (2 * ELV)\right)\right)\right] \tag{5-9}$$

- Super-Pressure Shape:

$$A_{proj} = A_{top} * \left[0.8219 + \left(0.1781 * \cos\left(\pi - (2 * ELV)\right)\right)\right] \tag{5-10}$$

- Sphere:

$$A_{proj} = A_{top} \tag{5-11}$$

Next, the surface area (A_{surf}) of the envelope is considered. The surface area can be determined from the design of the envelope. However, if the vehicle is not fully inflated, then the shape parameters need to be adjusted for the variation in the geometry of an underinflated envelope. The diameter for an underinflated envelope can be determined from the size of the lift gas bubble. When the envelope is partially inflated, sections of the envelope surface area are reduced. To capture this surface area region in the uninflated portion of the envelope, a calculation for the crenellated region should be applied as outlined in Equation (5-12).

$$A_{surf1} = 4.94 * V^{2/3} * \left(1 - \cos\left(\pi \frac{L_b}{L_g}\right)\right) \tag{5-12}$$

The modified surface area calculation takes the volume of the envelope and is scaled based on the ratio of the gore length for the lift gas bubble region (L_b) over the total gore length of the envelope (L_g). The combination of the surface area for the inflated section of the envelope and the crenellated section produces an "effective" surface area (A_{eff}):

$$A_{eff} = \left(0.65 * A_{surf}\right) * \left(0.35 * A_{surf1}\right) \tag{5-13}$$

The last characterization impacting the energy balance is the view factor (VF). The amount of energy that reaches the balloon depends on how much of the source is seen by the balloon at its current position. This is known as the view factor.

The relative geometry between the balloon and the planet is characterized by the half cone angle (θ_{HC}). This angle is a function of the radius of the planet and the altitude of the vehicle (Z).

$$\theta_{HC} = \sin^{-1}\left[\frac{R_{planet}}{R_{planet} + Z}\right] \tag{5-14}$$

The view factor (VF) is then calculated from the half cone angle to determine the view of the planet below.

$$VF = \frac{1 - \cos(\theta_{HC})}{2} \tag{5-15}$$

3. Radiative Heat Loads on the Film

Thermal radiation is the transfer of energy through electromagnetic waves. The intensity of the thermal radiation is dependent on the wavelength of the energy. In the equations below, various spectrum-dependent parameters are called out as the interaction of the various materials can be dependent on the type of energy transferred. The radiative heating sources visualized in Figure 5-1 are broken out into individual components in the following sections.

3.1. Absorbed Direct Sunlight Heating (Q_{sun})

Direct solar heating is the result of the energy from the sun heating the envelope in a manner dictated by the material properties of the specific film. Because solar heating depends on the presence of the sun shining on the vehicle, there is a distinct thermal variation between day and night which is observed in the performance of the vehicle.

The solar position was defined previously in Section 2.1 in terms of the diurnal cycle. The relative position of the sun and the planet must also be defined to determine the overall intensity of the sun.

The solar irradiance at the top of the atmosphere (I_{sun}) must be determined. This depends on the orbital eccentricity (e), mean orbital radius (R_{AU}) and true anomaly (TA). The true anomaly defines the relative position between the sun and the planets. For small orbital eccentricities, the true anomaly (TA) can be approximated by the equation for the mean anomaly (MA) which is easier to determine, see Equation (5-16). In the mean anomaly equation, the day number begins at the

perihelion, the point in the orbit where the planet is closest to the sun.

$$TA \cong MA = 2\pi * \frac{Day_{num}}{DaysPerYear} \tag{5-16}$$

Equation (5-17) describes the solar irradiance at the top of the atmosphere as a function of the True Anomaly and orbital eccentricity. Values of the eccentricity and orbital radius are provided in Table 5-3 for different planets within the solar system.

$$I_{sun} = \frac{1358}{{R_{AU}}^2} * \left[1 + \left(\frac{1}{2} * \left[\left\{\frac{1+e}{1-e}\right\}^2 - 1\right] * \cos(TA)\right)\right] \tag{5-17}$$

Table 5-3. Orbital parameters for some planets in the solar system [1]

	Orbital Radius (R_{AU})	**Orbital eccentricity (e)**
Earth	1	0.016708
Mars	1.52368	0.093400
Venus	0.72300	0.006800

The solar irradiance at the balloon altitude (Z) can be determined by factoring in the atmospheric transmittance:

$$I_{sunZ} = I_{sun} * \tau_{atm} \tag{5-18}$$

Solar heating must also account for cloud coverage, as seen in Equation (5-19). If the vehicle is below a cloud layer (where clouds exist between the vehicle and the sun), the clouds will dissipate the total solar energy input. The Cloud Factor (CF) is defined as the percentage of the sky obscured by the clouds, with $CF = 0$ implying the balloon is above the cloud layer, or no clouds are present.

$$q_{sun} = I_{sunZ} * (1 - CF) \tag{5-19}$$

Finally, from the inputs defined above, the heat load from the solar radiative source is defined as:

$$Q_{sun} = \alpha * A_{proj} * q_{sun} * \left[1 + \tau * \left(1 + r_{eff}\right)\right] \tag{5-20}$$

The parameters of the solar heating equation are defined as:

- α = Absorptivity of the balloon envelope material, the ratio of the amount of energy that is absorbed by a material over the total energy input
- A_{proj} = The projected area of the balloon envelope normal to the solar radiation

- q_{sun} = Solar radiation heat flux
- τ = Transmissivity of the balloon envelope material, the ratio of the amount of energy that passes through a material over the total energy input

3.2. Absorbed Albedo Heating (Q_{alb})

Albedo is a measure of reflected incident sunlight from a given surface measured on a scale of 0 to 1. Different parts of the environment, from the ground to the clouds, all reflect part of the solar energy that they interact with. Albedo data for ground emissions and cloud emissions is available from various sources online (e.g. [10]) to calculate the albedo heat loading. Albedo data should be sourced for the ground (Alb_{ground}) and clouds (Alb_{cloud}) to proceed with the calculation of the total albedo input (Alb) to the vehicle. As a reference for general albedo values, the data in Table 5-4 provides various ground and cloud conditions as a guide.

Table 5-4. Example generalized albedo data at the top of the atmosphere [7].

Ground		**Clouds**	
Surface Type	**Albedo**	**Surface Type**	**Albedo**
Black soil or evergreen trees	0.10	High clouds, cirrus	0.20-0.25
Grass or deciduous trees	0.15	Mid clouds	0.35-0.50
Dry soil or crops	0.20	Low clouds	0.6
Desert	0.25-0.30	Nimbostratus	0.60-0.75
Fresh snow	0.67-0.85	Cumulonimbus	0.70-0.80
Snow and ice	0.95	Stratocumulus	0.45-0.60
Arctic regions, summer	0.48-0.60		
Alaska, summer	0.36-0.48		
Canada, summer	0.24-0.48		
Greenland, summer	0.60-0.72		
North Atlantic, summer	0.36-0.60		
Southern Ocean, summer	0.12-0.36		
Antarctic regions, summer	0.60-0.72		

Cloud coverage affects the amount of albedo energy which impacts the balloon system. Albedo is attenuated differently based on the number of times the solar energy passes through the clouds. There are two different cases to consider when calculating the total albedo effect.

- If the balloon is below the cloud level, then the following equation defines the albedo value:

$$Alb = Alb_{ground} * (1 - CF) \tag{5-21}$$

- If the balloon is above the cloud level, the equation changes to the following:

$$Alb = \left(Alb_{ground} * (1 - CF)^2\right) + (Alb_{cloud} * CF) \quad (5\text{-}22)$$

The incident reflected energy depends on the angle of the sun. The equation for the albedo heat flux takes the solar irradiance at the top of the atmosphere, calculated above, and corrects for the solar elevation angle. The total albedo of the view below the balloon is applied as well.

$$q_{alb} = Alb * I_{sun} * \sin(ELV) \quad (5\text{-}23)$$

From the albedo heat flux and the view factor of the planet below, the equation for the albedo heat load is calculated.

$$Q_{alb} = \alpha * A_{surf} * q_{alb} * VF * \left[1 + \tau * \left(1 + r_{eff}\right)\right] \quad (5\text{-}24)$$

The parameters of the albedo heating equation are defined as:

- α = Absorptivity of the balloon envelope material, the ratio of the amount of energy that is absorbed by a material over the total energy input
- A_{surf} = The total surface area of the balloon envelope geometry
- q_{alb} = Albedo heat flux
- VF = View factor, the portion of the energy that leaves one body and impacts another, dependent on geometric positioning, obscurity, and other factors
- τ = Transmissivity of the balloon envelope material, the ratio of the amount of energy that passes through a material over the total energy input
- r_{eff} = Effective reflectivity of the balloon envelope material, the ratio of the amount of energy reflected by a material over the total energy input, effective reflectivity accounts for self-reflection

3.3. Absorbed Planetary IR Heating ($Q_{IR_{planet}}$)

The planetary elements below the balloon emit thermal energy which impacts the vehicle as a function of their temperature. Equations for the IR heat flux of the ground ($q_{IR_{ground}}$) and clouds ($q_{IR_{cloud}}$) surrounding the vehicle are provided as follows.

$$q_{IR_{ground}} = \varepsilon_{ground} * \sigma * {T_{ground}}^4 \quad (5\text{-}25)$$

$$q_{IR_{cloud}} = \varepsilon_{cloud} * \sigma * {T_{cloud}}^4 \quad (5\text{-}26)$$

The specific terrain of the ground beneath the balloon dictates the energy emitted. Deserts have the greatest difference in temperature between day and night due to little water acting as heat storage, sometimes varying up to 20°C. Conversely, oceans are the most stable in

terms of surface temperature. The surface coverage also has varying emissivity values. It is fortuitous that the hottest regions have the lowest emissivity while the coldest regions have the highest emissivity values. Cloud emissivity varies more specifically depending on the type of cloud, cloud altitude, etc. and requires more context to define [11].

Table 5-5. Ground emissivity for common terrains [1]

	Ground Emissivity (ε_{ground})
Desert	0.85
Avg. Ground	0.95
Snow	0.98

To calculate the thermal energy reaching the balloon at the given altitude, the emitted IR energy from the ground and clouds is modified by the IR atmospheric transmissivity:

$$q_{IR_{groundZ}} = q_{IR_{ground}} * \tau_{atmIR} \quad (5\text{-}27)$$

$$q_{IR_{cloudZ}} = q_{IR_{cloud}} * \tau_{atmIR} \quad (5\text{-}28)$$

To combine the planetary diffuse IR into a single parameter for the view of the planet below, the ground emittance must be modified to account for clouds. If the vehicle is operating below the cloud layer, then the definition for the planetary IR is:

$$q_{IR_{planet}} = q_{IR_{groundZ}} + \left(CF * q_{IR_{cloudZ}}\right) \quad (5\text{-}29)$$

If the balloon is operating above the cloud layer, then the above equation is modified to the following definition to include the cloud factor covering part of the ground.

$$q_{IR_{planet}} = \left(q_{IR_{groundZ}} * (1 - CF)\right) + \left(CF * q_{IR_{cloudZ}}\right) \quad (5\text{-}30)$$

The total heat load for the planetary emissions is then calculated as shown below.

$$Q_{IR_{planet}} = \alpha_{IR} * A_{surf} * q_{IR_{planet}} * VF * \left[1 + \tau_{IR} * \left(1 + r_{eff}\right)\right] \quad (5\text{-}31)$$

The parameters of the planetary IR heating equation are defined as:

- α_{IR} = Absorptivity of the balloon envelope material specific to the IR spectrum, the ratio of the amount of energy that is absorbed by a material over the total energy input
- A_{surf} = The total surface area of the balloon envelope geometry
- $q_{IR_{planet}}$ = Planetary IR heat flux
- VF = View factor, the portion of the energy that leaves one body and impacts another, dependent on geometric positioning, obscurity, and other factors

- τ_{IR} = Transmissivity of the balloon envelope material specific to the IR spectrum, the ratio of the amount of energy that passes through a material over the total energy input

3.4. Absorbed Sky IR Heating ($Q_{IR_{sky}}$)

The downwelling sky IR environment is typically almost non-existent at high altitudes. Therefore, when the vehicle is at high altitudes, the sky IR heat flux term ($q_{IR_{sky}}$) goes to zero. When the vehicle is close to the surface however, the heat flux value is typically within a range of 250-300 W/m^2. The values in Table 5-6 should be applied to the heat load calculation in Equation (5-32).

Table 5-6. Downwelling sky IR heat flux at different altitudes [7]

	Downwelling Sky IR ($q_{IR_{sky}}$)
High Altitude	0
Avg. Surface	250-300 W/m^2

From the sky IR heat flux, the total sky heat load is calculated. Because the view factor is defined as the view looking at the ground, the remaining view can be assumed to be all sky.

$$Q_{IR_{sky}} = \alpha_{IR} * A_{surf} * q_{IR_{sky}} * (1 - VF) * \left[1 + \tau_{IR} * \left(1 + r_{eff}\right)\right] \quad (5\text{-}32)$$

The parameters of the sky IR heating equation are defined as:

- α_{IR} = Absorptivity of the balloon envelope material specific to the IR spectrum, the ratio of the amount of energy that is absorbed by a material over the total energy input
- A_{surf} = The total surface area of the balloon envelope geometry
- $q_{IR_{sky}}$ = Downwelling sky IR heat flux

3.5. Absorbed Film IR Heating ($Q_{IR_{film}}$)

The film will absorb radiation from itself, called "self-glow" as energy is emitted. To capture this effect, Equation (5-33) below describes the film heating from IR emittance.

$$Q_{IR_{film}} = \sigma * \varepsilon * \alpha_{IR} * A_{surf} * {T_f}^4 * \left(1 - r_{eff}\right) \quad (5\text{-}33)$$

The parameters of the film IR heating equation are defined as:

- σ = Stefan-Boltzmann constant, defining the relationship between radiation emitted from a body and that body's temperature, defined as $5.67x10^{-8}\ \frac{W}{m^2K^4}$

- ε = Emissivity of the balloon envelope material, the ratio of the energy emitted by a material over the total energy

3.6. Emitted IR Heating ($Q_{IR_{out}}$)

To conclude the radiative heat loads, the thermal mass of the balloon and its radiation must also be considered. This is defined based on the standard blackbody radiative heat transfer equation shown below for a body that emits thermal radiation proportional to its temperature.

$$Q_{IR_{out}} = \sigma * \varepsilon * 2 * A_{surf} * {T_f}^4 \quad (5\text{-}34)$$

The parameters of the IR output heating loss equation are defined as:

- σ = Stefan–Boltzmann constant, defining the relationship between radiation emitted from a body and that body's temperature, defined as $5.67x10^{-8}\ \frac{W}{m^2K^4}$
- ε = Emissivity of the balloon envelope material, the ratio of the energy emitted by a material over the total energy
- A_{surf} = The total surface area of the balloon envelope geometry
- T_f = Temperature of the balloon envelope film

4. Convective Heat Loads on the Film

Convective interactions are defined by various dimensionless values. The equations for these values simplify the complex interactions between fluids in the heat transfer process, making it easier to compare and scale different systems. The equations below are defined assuming helium is the lift gas chosen for operations [8]. The equations could be modified to account for hydrogen with proper research regarding the associated gas properties.

4.1. Air and Lift Gas Properties

The following equations outline the properties of the air and lift gas to generate the values needed to define the convective heat transfer processes. These parameters are tabulated in more detail in the Appendix of this work. However, the following relationships work well for quick approximations for ballooning applications.

Dynamic viscosity is a measure of a fluid's resistance to flow due to its own internal friction [12]. The following equations define the dynamic viscosity for both air (Equation (5-35)) and helium (Equation (5-36)) lift gas as a function of temperature.

$$\mu_{air} = \frac{1.458x10^{-6} * {T_{air}}^{1.5}}{T_{air} + 110.4} \quad (5\text{-}35)$$

$$\mu_{gas} = 1.895x10^{-5} * \left(\frac{T_{gas}}{273.15}\right)^{0.647} \quad (5\text{-}36)$$

Gases conduct heat just like solids and liquids do, but usually not as well, due to large spacing between molecules [13]. The conductivity values defined below the ability to conduct heat for both air (Equation (5-37)) and helium (Equation (5-39)) lift gas as a function of temperature.

$$k_{air} = 0.0241 * \left(\frac{T_{air}}{273.15}\right)^{0.9} \quad (5\text{-}37)$$

$$k_{gas} = 0.144 * \left(\frac{T_{gas}}{273.15}\right)^{0.7} \quad (5\text{-}38)$$

The Prandtl number is a dimensionless value that defines the ratio of momentum diffusivity (or a fluid's ability to transport momentum) to thermal diffusivity (a fluid's ability to transport heat) [14]. This value is important in characterizing a fluid's capacity be a good conductor or heat transfer agent. The Prandtl number for air (Equation (5-39)) and helium (Equation (5-40)) are defined below as functions of temperature.

$$Pr_{air} = 0.804 - (3.25x10^{-4} * T_{air}) \quad (5\text{-}39)$$

$$Pr_{gas} = 0.729 - \left(1.6x10^{-4} * T_{gas}\right) \quad (5\text{-}40)$$

4.2. Free Convection

For external convection, the process for determining the heat transfer diverges into two paths. The first is for free, or natural, convection where no external forces are acting on the system. The following dimensionless values contribute to the calculation of the free convection heat transfer coefficient. This heat transfer is appropriate where vertical speeds, or relative wind speeds, are small over the balloon.

The Grashof number is a dimensionless value that defines the ratio of buoyant forces to viscous forces acting on a fluid [15]. This value is important in determining the flow regime of fluid boundary layers in laminar systems which impacts a fluid's ability to transfer heat. The Grashof number for air is:

$$Gr_{air} = \frac{{\rho_{air}}^2 * g * \left|T_f - T_{air}\right| * D^3}{T_{air} * {\mu_{air}}^2} \quad (5\text{-}41)$$

The Nusselt number is a dimensionless value that defines the ratio of convective heat transfer to conductive heat transfer [16]. This value indicates the efficiency of heat exchange between a solid surface and a surrounding fluid. For the Nusselt equation below, the geometry of the fluid is approximated as a sphere in free convective fluid.

$$Nu_{air} = 2 + (0.45 * (Gr_{air} * Pr_{air})^{0.25}) \quad (5\text{-}42)$$

Now, combining the Nusselt number with the conductivity of the air and the diameter of the balloon produces the free convection heat transfer coefficient. The parameter for the heat transfer coefficient is the sum of thermal resistance per unit area for a given interaction [17].

$$HC_{free} = \frac{Nu_{air} * k_{air}}{D} \quad (5\text{-}43)$$

4.3. Forced Convection

In cases where the balloon is ascending, then the velocity of the system creates relative movement of air which requires a calculation of forced convection [18]. The heat transfer coefficient for forced convection is dependent upon the Reynold's number, which is a dimensionless value that defines the ratio between internal and viscous forces [19]. The Reynold's number is often used to characterize general flow profiles of fluids moving over a body in aerodynamics. Below, both the Reynold's number for the balloon envelope (Equation (5-44)) and the forced convection heat transfer coefficient (Equation (5-45)) are calculated.

$$Re = \frac{v * D * \rho_{air}}{\mu_{air}} \quad (5\text{-}44)$$

$$HC_{forced} = \frac{k_{air}}{D} * \left(2 + (0.41 * Re^{0.55})\right) \quad (5\text{-}45)$$

Finally, the heat transfer coefficient for the internal interaction between the balloon envelope and the lift gas is defined in Equation (5-46).

$$HC_{int} = 0.13 * k_{gas} * \left(\frac{{\rho_{gas}}^2 * g * |T_f - T_{gas}| * Pr_{gas}}{T_g * {\mu_{air}}^2}\right)^{1/3} \quad (5\text{-}46)$$

Now, having defined the fluid properties characterizing the interactions between the different systems, the heat loads for the external and internal convective transfers can be defined.

4.4. External Convection Heat Load ($Q_{ConvExt}$)

The external convection, outlined in Equation (5-47), is dictated by the flow of air around the envelope from the fluid parameters calculated above.

$$Q_{ConvExt} = HC_{ext} * A_{eff} * (T_{air} - T_f) \quad (5\text{-}47)$$

The parameters of the external convection heating equation are defined as:

- HC_{ext} = External heat transfer coefficient, defined as the greater of the two values between the free and forced convective heat transfer coefficient
- T_{air} = Temperature of the air

4.5. Internal Convection Heat Load ($Q_{ConvInt}$)

The internal convective heat transfer between the balloon film and the lift gas is defined in Equation (5-48). Utilizing the internal heat transfer coefficient, the internal convective heat loads describe the transfer of energy driving the temperature of the lift gas.

$$Q_{ConvInt} = HC_{int} * A_{eff} * (T_f - T_{gas}) \quad (5\text{-}48)$$

The parameters of the planetary IR heating equation are defined as:

- HC_{int} = Internal heat transfer coefficient
- A_{eff} = Effective area, the area where the fluid is interfacing with the convective surface to experience heat transfer
- T_f = Temperature of the lift gas
- T_{gas} = Temperature of the lift gas

5. Temperature Rate of Change Equations

5.1. Lift Gas Temperature Differential Equation

The differential equation in Equation (5-49) defines the change in the temperature of the balloon film over a change in time ($\Delta T_g / \Delta t$). The rate of temperature change is governed by the specific heat formula as a function of heat transfer, specific heat capacity, and mass [20]. The temperature profile relies on the internal convective exchange where one system is losing heat and the other is gaining heat. The lift gas energy balance also depends on the adiabatic expansion of the gas inside the envelope. Adiabatic expansion is the thermodynamic process by which gas can either expand or contract without any heat exchange with its surroundings. Therefore, the gas's own internal energy is used to do the work which results in a temperature change [20]. Therefore, even without the internal convective interactions, the gas could change temperature as a result of mass loss or volume change, represented in the calculation below by the density terms (ρ_g).

$$\frac{dT_{gas}}{dt} = \frac{Q_{ConvInt}}{c_v * m_{gas}} + \left[(\gamma - 1) * \frac{T_{gas}}{\rho_{gas}} * \frac{d\rho_{gas}}{dt}\right] \quad (5\text{-}49)$$

In the above equation, the gamma term (γ) represents the ratio of the heat capacity at a constant pressure (c_p) and heat capacity at a constant volume (c_v), known as Laplace's coefficient [20].

$$\gamma = \frac{c_p}{c_v} \tag{5-50}$$

5.2. Film Temperature Differential Equation

The differential equation in Equation (5-51) defines the change in the temperature of the balloon film over a change in time ($\Delta T_f / \Delta t$). The differential equation below has the same structure for the specific heat formula as previously described, but with more terms representing the extensive interactions that the balloon film encounters. The radiative heat loads and convective heat loads are totaled as outlined by the 1st law of thermodynamics to define the heat transfer. The heat capacity of the film (c_f) and the mass of the film (m_f) then are used to define the temperature change rate.

$$\frac{dT_f}{dt} = \frac{(Q_{sun} + Q_{alb} + Q_{IR_{planet}} + Q_{IR_{sky}} + Q_{IR_{film}} + Q_{ConvExt} - Q_{ConvInt} - Q_{IR_{Out}})}{c_f * m_f} \tag{5-51}$$

6. Gondola Considerations

While heat transfer to the balloon is critical for modeling the performance of the vehicle, of equal importance is the thermal management of the gondola structure. The principles governing heat transfer and thermal design related to gondola structures share similarities with that of common aerospace and spacecraft systems [21, 22], given the unique position high-altitude balloons operate within. The information provided here outlines common best practices for thermal management related to gondola structures for reference.

6.1. Coating Properties for Radiation

Table 5-7 presents a table of materials and some nominal radiation values from the initial handbook. There are many such references for heat transfer values in literature, and the user is encouraged to utilize these texts.

Table 5-7: Common materials and their thermal coefficients [8].

Material	IR Emissivity	Solar Absorption	Ratio
Silver (polished)	0.02	0.07	3.50
Platinum	0.05	0.10	2.00
Aluminum	0.08	0.15	1.88
Nickel	0.12	0.15	1.25
Stellite	0.18	0.30	1.67
Aluminum paint	0.55	0.55	1.00
White lead paint	0.95	0.25	0.26
Zinc oxide paint	0.95	0.30	0.32
Gray paint	0.95	0.75	0.79
Black paint	0.95	0.95	1.00
Lamp black	0.95	0.97	1.02
Silver sulfide[1]	0.03	0.60	20.00
Nickel black[1,2]	0.10	0.90	9.00
Cupric oxide[1,2]	0.15	0.90	6.00

[1] These are special surfaces where a metal is covered with a very thin layer of absorbing material. The layer is so thin that it is a fraction of a wavelength thick in the infrared and is, therefore, almost transparent to IR. The result is that the IR emissivity is nearly that of the underlying metal. However, the thickness is large compared to the wavelength of the maximum solar spectrum, so the absorptivity is large for solar radiation.
[2] H. Tabor, 1961: Solar Energy.

6.2. Thermal Design Considerations

The primary concerns on scientific gondola reside in two groups: ground operations and operations at float. Ground operations are somewhat more manageable, given the ability to plug in chillers or heaters to auxiliary power on the launch vehicle or in the hanger up until minutes before launch. For piggyback missions without thermal heating or cooling, overheating is often a primary concern for flight computers or sensors. Copper thermal straps connecting critical components to a chassis, gondola frame, or large heat sink can passively control temperature. Care should be taken to position hotter components (i.e. components that generate a lot of heat during operation) next to cooler components, or near a heat sink.

For operations at float, passive thermostats are a common way to control heaters above a given temperature while minimizing power consumption. When wired in-line with a heater and power source, the thermostat closes the circuit below a fixed temperature and opens the circuit above a relief temperature. Active control of heaters by a flight computer can be used where items are more critical, albeit with more complexity and risk.

For payloads which require cryogenic conditions (e.g. the GUSTO mission from 2024 [21]), a common practice is to use a radiator plate [22]. Pointed away from the Sun, a radiator plate takes warmer liquid (or other working fluid) and exposes it to the void of space. Heat is thus radiated out of the fluid, cooling the fluid before being pumped back into a chiller or the instrument. The advantage is increased rejection of heat (produced by the gondola instrumentation for example) at the added complexity and cost of maintaining azimuthal pointing. Regardless of payload or mission, there are several common practices for gondola design:

1. *Surfaces:*
   Gondolas are generally painted white on exposed surfaces to reject heat. Reflective surfaces, such as aluminized-mylar are used to reject heat (more-so than white paint) on critical components. To hold the mylar in place, foam boxes are formed around the component, which also provides a light-weight passive insulation layer. For payloads sensitive to mass, space-grade insulation blankets can be used at increased cost.
2. *Shielding:*
   Structures that are expecting to see large heat sources or sinks are often enclosed in thin sheet metal panels on the sides of the gondola which provide a break in the radiation view factor. Solar panels can be positioned to provide shade for large faces on the gondolas.
3. *Component selection:*
   Electrical components are ensured to have industrial thermal ratings (e.g. -40C to +85C) to minimize the heating required from heaters. For places where temperatures need to be measured, thermal paste is used to bond thermistors/thermocouples to parts to ensure a good measurement.
4. *Insulation:*
   Conduction paths are broken by making standoffs of insulating materials, such as G10 fiberglass.

7. Conclusion

Energy plays a significant role in the design and evaluation of high-altitude balloon systems. Whether regarding the balloon envelope or gondola, the environment in which the system is operating will have an outsized effect on the performance of the vehicle during flight. It is important to contextualize this environment using the parameters and equations outlined in the preceding chapter. The environment in the stratosphere is a complex system with a lot of interconnected features. Chapter 7 provides additional guidance and references regarding atmospheric parameters that can help guide in the calculations of energy balance parameters.

References

[1] R. Farley, "BalloonAscent: 3-D Simulation Tool for the Ascent and Float of High-Altitude Balloons," in *AIAA 5th ATIO and16th Lighter-Than-Air Sys Tech. and Balloon Systems Conferences*, Arlington, Virginia, 2005.

[2] M. Moran, H. Shapiro, D. Boettner and M. Bailey, Fundamentals of Engineering Thermodynamics, Wiley, 2010.

[3] G. E. Carichner and L. M. Nicolai, Fundamentals of Aircraft and Airship Design: Volume 2 - Airship Design and Case Studies, AIAA, 2013.

[4] E. Udinski and A. Hamilton, "2024 NASA Balloon Program," in *JAXA and Hiroshima University Collaboration Meetings*, 2024.

[5] P. Gorham, "Particle astrophysics in NASA's long duration balloon program," *Nuclear Physics B-Proceedings Supplements,* vol. 243, pp. 231-238, 2013.

[6] E. L. Rainwater and M. S. Smith, "Ultra high altitude balloons for medium-to-large payloads," *Advances in Space Research,* vol. 33, no. 10, pp. 1648-1652, 2004.

[7] R. Farley, BalloonAscent Theory Manual, Greenbelt: Farley Flight Aerospace, 2020.

[8] A. L. Morris, Scientific Ballooning Handbook, 1975.

[9] F. Kreith and J. F. Kreider, Principles of Solar Engineering, McGraw-Hill, 1978.

[10] Y. Yu, "STAR JPSS - Environmental Data Record Teams - Surface Albedo," US Department of Commerce NOAA NESDIS, 23 11 2024. [Online]. Available: https://www.star.nesdis.noaa.gov/jpss/albedo.php.

[11] S. K. Cox, "Observations of cloud infrared effective emissivity," *Journal of Atmospheric Sciences,* vol. 33, no. 2, pp. 287-289, 1976.

[12] M. J. Neale, The tribology handbook, Elsiver, 1995.

[13] A. K. Coker, Fortran programs for chemical process design, analysis, and simulation, Elsiver, 1995.

[14] B. Sunden, Hydrogen, batteries and fuel cells, Academic Press, 2019.

[15] R. Smith, H. Inomata and C. Peters, "Chapter 8 - Heat Transfer and Finite-Difference Methods," in *Supercritical Fluid Science and Technology*, Elsiver, 2013, pp. 557-615.

[16] A. G. Caket, C. Wang, M. A. Nugroho, H. Celik and M. Mobedi, "Recent studies on 3D lattice metal frame technique for enhancement of heat transfer: Discovering trends and reasons," *Renewable and Sustainable Energy Reviews,* vol. 167, p. 112697, 2022.

[17] M. Stewart and O. Lewis, Heat Exchanger Equipment Field Manual, Science Direct, 2013.

[18] F. T. Gallyer, Plant Engineer's Handbook, Science Direct, 2001.

[19] P. J. LaNasa and E. L. Upp, "2 - Basic Flow Measurement Laws," in *Fluid Flow Measurement (Third edition)*, Science Direct, 2014, pp. 19-29.

[20] F. P. Incropera, D. P. Dewitt, T. L. Bergman and A. S. Lavine, Fundamentals of Heat and Mass Transfer, John Wiley & Sons, 2007.

[21] R. Coker, "Thermal Design, Analysis, and Testing of GUSTO," in *2020 International Conference on Environmental Systems*, 2020.

[22] N. Marcelli, "The GAPS experiment: Low-energy antinuclei measurements for dark matter searches," in *EPJ Web of Conferences*, Rome, 2023.

Chapter 6
Lift Gases

Alvin L. Morris, Erin M. Reed[1]

[1] National Aeronautics and Space Administration, Technology Manager, Balloon Program Office

Table of Contents

1. Introduction 5

2. Lift Gas Selection 5

3. Lift Gas Characteristics and Considerations 8

3.1. Air 8

3.2. Ammonia 9

3.3. Helium and Hydrogen 11

4. Lift Determination 13

4.1. Gas Pressure 15

4.2. Gas Temperature 15

4.3. Gas Volume 15

4.4. Compressibility Factor 16

4.5. Helium Measurement during Balloon Inflation 17

5. Gas Handling Considerations during Inflation Operations 18

5.1. High-Pressure Hazards 18

5.2. Cryogenic Hazards 19

5.3. Flammable Gas Hazards 19

5.4. General Filling Hazards 20

6. Conclusions 21

References 22

Table of Tables

Table 6-1: Common Gases Considered for Lift in Ballooning..... 7

Table 6-2: Gases for Consideration in Planetary Ballooning..... 8

Table 6-3: Values for Factors in Stretched Volume Equation..... 16

Table 6-4: Values for Constants in Compressibility Factor Equation.. 17

Table of Symbols

Symbol	Definition	Dimension
B	Buoyancy force, exerted on a volume of gas	$M\ L\ T^{-2}$
f_s	Stretch factor, pressure effects on volume of steel cylinder	-
f_t	Thermal factor, temperature effects on volume of steel cylinder	-
g	gravitational acceleration	$L\ T^{-2}$
$\vec{k}$	Notation vector	-
M_a	Molar mass of air	$M\ N^{-1}$
M_g	Molar mass of lift gas	$M\ N^{-1}$
m_g	Mass of lift gas	M
M_m	Molar mass of a mixture of gases	$M\ N^{-1}$
P_b	Standard pressure of the International Standard Atmosphere	$M\ L^{-1}\ T^{-2}$
P_g	Pressure of lift gas	$M\ L^{-1}\ T^{-2}$
R	Universal gas constant	$M\ L^2\ T^{-2}\ K^{-1}$
T_a	Temperature of air	K
T_b	Standard temperature of the International Standard Atmosphere	K
T_g	Temperature of lift gas	K
V_a	Volume of air	L^3
V_0	Nominal volume of steel cylinder, which holds lift gas	L^3
V_g	Volume of lift gas	L^3
$V_{g,s}$	Volume of gas within a stretched cylinder	L^3
Z_g	Compressibility Factor for lift gas (real gas constant for use with ideal gas equation)	-
ρ_0	Nominal density of hydrogen gas, as used in calculation of compressibility	$M\ L^{-3}$
ρ_a	Density of air	$M\ L^{-3}$
ρ_g	Density of lift gas	$M\ L^{-3}$
σ	Ratio of molar masses, air to lift gas	-

1. Introduction

The physics of lift gases and lift determination has not changed since the first edition of this handbook in 1975. However, the types of gases that are considered for use has been expanded to include applications that extend beyond large-scale scientific Earth-bound balloons. Additionally, lift determination equations have been revisited and examined with respect to more recent virial equation formulations for helium and hydrogen. Due to the fact that this text intends to be a tool for performing simple calculations without requiring complex computations or significant computing resources, these virial equations remain in their unchanged form. Additionally, since the first edition, helium inflation determination has expanded beyond the use of tables and calculations to include the use of Coriolis flowmeters, which has become a standard mass flowmeter within the fluid community due to recent advancements in electronic sensitivity. It is expected that flowmeters will continue to expand in use, but inflation tables will remain a valuable resource.

2. Lift Gas Selection

The buoyant force, $\vec{B}$, exerted on a volume of gas V_g, displacing a volume of air V_a is

$$\vec{B} = \vec{k}(\rho_a V_a - \rho_g V_g)g \tag{6-1}$$

Where ρ_a and ρ_g are the density of air and lift gas, respectively, g is the acceleration due to gravity, and $\vec{k}$ is a unit vector directed upward. Only the buoyant force will be considered in this section; therefore, the vector notation will be dropped. If B>0, it is a force directed upward. If B<0, it is directed downward. Also, except for the small volume occupied by the balloon film, the rigging, and the payload, $V_a = V_g$. With these simplifications, the equation may now be written

$$B = \rho_a V_a g\left(1 - \frac{\rho_g}{\rho_a}\right) \tag{6-2}$$

Although some potentially useful lift gases, such as ammonia, may be readily liquified, most gases will be used in balloons only under conditions of pressure and temperature that are above critical to be considered ideal gases. Thus,

$$\rho_a = \frac{p_a M_a}{RT_a} \text{ and } \rho_g = \frac{p_g M_g}{RT_g}$$

And

$$\frac{\rho_g}{\rho_a} = \frac{p_g M_g T_a}{p_a M_a T_g} \tag{6-3}$$

Where p, M, and T are pressure, molecular weight, and temperature, respectively; the subscripts a and g identify their symbols with air and gas, and R is the universal gas constant.

Equation 6-3 then becomes the governing equation for choosing and utilizing an appropriate lift gas for ballooning. That is, an upward buoyant force is generated when $\frac{\rho_g}{\rho_a} < 1$. Generally, $\rho_g > \rho_a$, which works against buoyancy. In a zero-pressure balloon, this difference is only slight and is often assumed to be negligible. In a super-pressure balloon, it may be more appreciable. While theoretically possible, a balloon to hold a slight vacuum has proven impractical for a pressure differential across any balloon material that would deform under the force, and any balloon material structurally strong enough to withstand deformation is often too heavy to take advantage of the buoyant force generated. Often $T_g \approx T_a$, although the difference can be quite significant. Utilizing this difference is the principle behind a hot-air balloon or a solar balloon, which both utilize means to heat the gas (air) within the balloon to generate lift [1].

This leaves the relationship of M_g and M_a to identify appropriate gases that may be used as lift gases. Any gas having a molecular weight less than the molecular weight of air is a potentially useful gas for ballooning. If we assume $p_g T_g \approx p_a T_a$ as a first approximation so that

$$\frac{\rho_g}{\rho_a} = \frac{M_g}{M_a} \tag{6-4}$$

Then from Equation (6-2)

$$\frac{B}{\rho_a V_a g} = \left(1 - \frac{M_g}{M_a}\right) = (1 - \sigma^{-1}) \tag{6-5}$$

Where σ is substituted for the ratio Ma/Mg for convenience. This new equation and the term $(1 - \sigma^{-1})$ may be interpreted as the lift of the gas per unit weight of displaced air. Thus, it serves as a helpful index for selecting lift gases, although other characteristics, such as inflammability and toxicity, must also be considered.

Table 6-1 (modified from [2]) provides a table of some common gases with molecular weights that make them attractive options for use as, making them attractive options for lift gases in ballooning. It should be noted

that this table applies for to terrestrial scientific ballooning missions. The ambient gases of other planet atmospheres may limit or open other lifting gases as effective alternates for use. The comparison to the molecular weight of the ambient gas is the applicable process for identifying appropriate lifting gases.

Table 6-1: Common Gases Considered for Lift in Ballooning

GAS	**CHEMICAL FORMULA**	**MOLECULAR WEIGHT**	**LIFT INDEX** $(1-\sigma^{-1})$	**COMMENT**
AIR		28.97	0	Provides lift only if the density inside the balloon is less than that outside
AMMONIA	NH_3	17.03	0.412	Readily liquifies, toxic, and inflammable at concentrations in air of 15-28%
HELIUM	He	4.00	0.862	Inert, increasingly expensive
HYDROGEN	H_2	2.02	0.930	Inflammable at concentrations in air of 4-75%, relatively inexpensive
HYDROGEN FLUORIDE	HF	20.01	0.309	Toxic, flammable
METHANE	CH_4	16.04	0.446	Inflammable at concentrations in air of 5.3-14%
NEON	Ne	20.19	0.303	Inert
WATER VAPOR	H_2O	18.02	0.378	Readily liquifies

Table 6-2: Gases for Consideration in Planetary Ballooning

BODY	ATMOSPHERE	MOL. WEIGHT	COMMON GASES (IN ORDER OF MOLECULAR WEIGHT)								
			H_2	He	CH_4	NH_3	H_20	Ne	N_2	CO	O_2
JUPITER	H_2/He	2.22	✓								
MARS	CO_2/N_2	43.34	✓	✓	✓	✓	✓	✓	✓	✓	✓
NEPTUNE	H_2/He	2.53	✓								
SATURN	H_2/He	2.07	✓								
TITAN	N_2/CH_4	28	✓	✓	✓	✓	✓	✓			
URANUS	H_2/He	2.64	✓								
VENUS	CO_2/N_2	43.45	✓	✓	✓	✓	✓	✓	✓	✓	✓

Due to their properties, hazards, and/or cost, methane, hydrogen fluoride, water vapor, and neon are not viable options for lifting gases for terrestrial scientific balloons. However, water vapor has been considered for balloons in the Venus atmosphere ([3-5]). Each of the rest of the lift gases provided in Table 6-1 will be examined for their uses, limitations, and considerations.

3. Lift Gas Characteristics and Considerations

3.1. Air

Considerations/Attributes: Air only becomes practical as a lifting gas when the gas within the balloon is heated to a temperature difference of tens of degrees Celsius (scores of degrees Fahrenheit) [6].

Applications: First recommended in 1968 at a balloon scientific conference [7], the solar-powered balloon, or solar balloon, has since become a popular use case for air as a lifting gas [8-10]. Utilizing materials that absorb solar energy through radiative means, a solar balloon can ascend to altitudes ranging from 15 to 23 km (50 to 75 kft) [8-10]. Solar balloons are usually simple to construct and are cheaper to manufacture and operate than other scientific balloons [7]. Several solar ballooning groups utilize a high-density polyethylene construction and a pyrotechnic-grade air-float charcoal powder to coat the inside of

the balloon to provide advantageous solar absorption properties to generate lift [8]. Additionally, leaks in the balloon are negligible to performance (unless they affect heating). Solar balloons are limited to flights that occur only during daylight due to cooling that occurs once the sun sets and the resulting descent of the balloons.

Solar balloons have generated significant interest in the planetary exploration of Venus, Mars, Jupiter, and Saturn [11-16] as a cost-effective way of performing science in the atmospheric of a planet without requiring a lift gas to be transported to the planet. To date, no such balloon has been deployed on a planet, but JPL has performed several successful proof-of-concept prototypes [17]. (Note: The only planetary balloon flight to date utilized two helium balloons in twin 1985 explorations to Venus, Vega 1 and Vega 2, by the Soviet Union. See Chapter 16 for more information.)

Since the 1970s, the Centre National d'Etudes Spatiales (CNES) has developed an Infrared Montgolfiere balloon that utilizes a low emissivity material for the upper of the balloon (for surfaces facing the sky), such as an aluminized mylar and a low emissivity material for the lower part of the balloon (for surfaces facing the earth), thus creating a non-homogeneous balloon, which results in diurnal cycling with a difference in altitude from night and day of about 5 km but does allow for long-duration balloon flights [6], [18]. CNES successfully flew infrared balloons for an average of 3 weeks (and a maximum of 69 days) from the tropical, arctic, and equatorial regions [6], [18].

3.2. Ammonia

Considerations/Attributes: Ammonia is an interesting gas. Its critical temperature is 132.9°C and may readily be liquified at normal atmospheric temperatures. In fact, it is usually stored and transported as a liquid under its own vapor pressure, which equals 294.8 psia at a temperature of 50°C (122°F). The liquid boils readily under normal atmospheric conditions, providing a gas. Ammonia can be decomposed into nitrogen and hydrogen according to the following formula:

$$2NH_3 + heat \rightleftharpoons N_2 + 3H_2 \qquad (6\text{-}6)$$

The decomposition is endothermic, i.e., it requires heat. The reaction can proceed in either direction, but if nitrogen and hydrogen are mixed at normal atmospheric temperatures, the combination reaction is extremely slow. Further, the amount of ammonia in an equilibrium mixture of ammonia, nitrogen, and hydrogen is very low at atmospheric pressures. Therefore, if decomposition of ammonia can be accomplished, the hydrogen and nitrogen mixture can be used as a ballooning lift gas. Interestingly, when completely decomposed, two volumes of ammonia produce one volume of nitrogen and three volumes of hydrogen, so the decomposed gas provides

greater than the original ammonia. This relationship can be demonstrated quantitatively by comparing molecular weights. The molecular weight of this mixture of gases, M_m, may be calculated as follows:

$$M_m = \frac{N_{N_2} M_{N_2} + N_{H_2} M_{H_2}}{N_{N_2} + N_{H_2}} \tag{6-7}$$

$$M_m = \frac{1 \times 28.013 + 3 \times 2.016}{4}$$

$$M_m = 8.515$$

Where N_x and M_x refer to the number of molecules and the molar mass of X. This then provides a lift index of 0.706. A given volume of decomposed mixture then provides 1.7 times the lift of a like volume of ammonia and 0.82 times the lift of a like volume of helium.

Application: At least one lift gas generator makes use of this property of ammonia, using a catalyst to aid in the decomposition. Unfortunately, the decomposition is incomplete, and the mixture contains a small amount of ammonia, which somewhat decreases the effectiveness. Using this method and present equipment, the rate at which lift gas can be generated at the launch site is great enough to provide gas for small meteorological sounding balloons but not for large scientific balloons.

Although ammonia has not been used as a lift gas for balloons, it has been recommended as an alternate for helium and hydrogen, particularly taking advantage of the decomposition of ammonia into hydrogen [19]. It takes a significant amount of energy to generate a spark (8 mJ compared to <0.2 for hydrogen); thus, ammonia is safer for handling and requires fewer regulatory restrictions, making it an attractive alternative lift gas [19]. Some suggestions have also been put forth to utilize a two-phase ballonet that takes advantage of the ready liquidation of ammonia to alternate its use as ballast or lift gas, depending on the thermal qualities of the ammonia and the needs of the balloon for altitude [20-21]. Additionally, ammonia has been cited as a possible lift gas for the carbon dioxide atmosphere in planetary exploration balloons, particularly in the Venus atmosphere [12-13, 22].

Handling Considerations: Ammonia is a highly toxic gas, and exposure to gaseous anhydrous ammonia can result in corneal injury and burns on the skin [23]. However, ammonia has such a pungent smell (detectable at concentrations as low as 5 ppm) that it is rare for a person to be exposed to dangerous levels without their knowledge. Thus, more commonly, people escape the harmful environment before the onset of symptoms [23].

"There is minimal absorption of ammonia…if there is short-term (under 120 sec) inhalational exposure" [24].

3.3. Helium and Hydrogen

Considerations/Attributes: For terrestrial scientific ballooning, helium, and hydrogen have historically persisted as the two most prevalent lifting gases for serious use. Thus, it is appropriate to discuss them in tandem. Hydrogen has the highest fraction of maximum possible lift of any of the gases and is also non-toxic and a renewable lift gas source. It can be obtained at a relatively cheap cost and wide availability. Helium produces a large fraction of the maximum possible lift, just behind hydrogen. Helium is non-toxic but unfortunately, a non-renewable entity. However, helium has one exceptional advantage that prioritizes its use: it is inert, unlike hydrogen, which is highly inflammable. A lesser advantage of helium is that it has more adiabatic stability in the atmosphere than hydrogen. The use of hydrogen versus helium as a primary lifting gas has thus been largely a matter of economic factors. When helium is available in large quantities for a reasonable cost, it is the primary lifting gas with almost no use of hydrogen. However, hydrogen use has become more widespread when helium has become harder to obtain and has higher costs. This was the case historically up to and through World War II. At that time, the United States started to prioritize the storage of helium, providing sources for helium use and reducing its cost. In recent years, after the United States has sold off its helium stores and helium demand in other fields (such as medical diagnostic equipment) has resulted in helium shortages and significant price increases, hydrogen is once more a viable lifting gas for scientific ballooning.

Applications: Scientific ballooning is synonymous with the use of helium or hydrogen as a lifting gas. Only the use of a lifting gas other than helium or hydrogen bears comment. As mentioned above, hydrogen was the primary lifting gas for lighter-than-air vehicles. However, in the 1950s and 1960s, balloon launch methods and hardware, including telemetry, hydrogen, and helium, were used regularly with the development of balloon films. In 1967, the National Center for Atmospheric Research, NASA's predecessor of the United States public civil scientific balloon program, published a set of tables for balloonists that included both the consideration of helium and hydrogen properties for lift [25]. When NASA adopted the Balloon Program, they continued using hydrogen ballooning for international campaigns at locations such as India, Japan, and Brazil as late as 1982. Outside of the United States, CNES used hydrogen in about 2000 zero-pressure balloons from 1963 to 1999, ISAS flew hydrogen balloons from Japan until 1971 [26], and TIFR continues to maintain a hydrogen capability for scientific ballooning today [27-28]. However, due to flammability hazards, many organizations switched to helium exclusively. In recent years, with significant demand and increased cost

of helium, scientific balloon programs are again examining the use of hydrogen as a potential lift gas [29]. To date, several commercial entities in the United States, including Aerostar and Space Perspective, have successfully launched balloons high-altitude balloons using hydrogen as a lifting gas [30-31].

Helium and hydrogen scientific balloons are capable of reaching the stratosphere, with the record altitude being 53.7 km (176 kft) in 2002 [32].

Handling Considerations: Hydrogen is a colorless, odorless gas that, when ignited, is either invisible or barely visible with a blue flame. Most of the electromagnetic emission occurs in the ultra-violet and the infrared. Hydrogen is highly inflammable in the air within the range of 4 – 74% hydrogen by volume, with a minimum ignition energy (MIE) of 0.02 mJ at 30% hydrogen by volume [33]. Sparks, even those small enough to not be seen, can be sufficient to ignite hydrogen in air at this stoichiometric concentration. There are three significant considerations for handling hydrogen for its safe use: preventing hydrogen concentrations in air or oxygen, preventing ignition sources, and detecting hydrogen gas and fire. It should be noted that this is a very brief treatment of the considerations for hydrogen use in scientific ballooning. Please refer to the AIAA Guide to Safety of Hydrogen and Hydrogen Systems as well as the Center for Hydrogen Safety [34-35] for more information.

1. **Prevention of Hydrogen Concentrations**: Fortunately, most scientific balloon inflations occur in the open air, which helps provide sufficient ventilation for hydrogen leaks and hydrogen/air mixtures to dissipate [59]. However, care should be taken for hardware in which hydrogen may mix with air or oxygen in enclosed structures, such as pressure lines, storage tanks, and hydrogen supply trucks. Ignition in these cases can result in detonation, producing shock waves that can result in significant damage from energy build-up and release [36]. Even in cases where deflagration and not detonation occurs, nearby structures can be subject to overpressure, in case of ignition, and incur damage from energy build-up and release in the form of a pressure wave and loud noise [36]. Leak prevention and purging all hardware before use with an inert gas are also critical in reducing the risk of hydrogen concentration build-up.

2. **Prevention of Ignition Sources**: Due to the low minimum ignition energy of hydrogen, all possible sources of sparks should be removed from the area during inflation. Thus, the appropriate selection of anti-static clothing for personnel, use of proper electrical grounding, and use of non-sparking tools, as well as best practices in drop-protection and removing all welding,

cutting, smoking, and open flame operations from the inflation site, are encouraged [34-36], [59]. Current balloon construction consists of a plastic film, in which friction between its fold, as well as handling can be sources of static. Operations involving personnel around the balloon envelope during hydrogen filling/use should be scrutinized for appropriate mitigations.

3. **Detection of Hydrogen Gas and Fire:** Thanks to hydrogen being used in other applications, a number of hydrogen detectors have been developed. Types of hydrogen detector technologies include catalytic, electro-chemical, semiconducting oxides, thermal conductivity, mass spectrometer, sonic, acoustic, optical, glow plug, and chemo-chromic devices. These types of devices can be used in personnel monitors, stationary monitors, and tapes. Types of hydrogen fire detectors: temperature sensor, heat-sensitive cable, optical (in UV, in mid/near-infrared or infrared), broadband imaging, narrowband imaging, and also a corn straw broom have all provided reliable detection of hydrogen fires [34].

Additional considerations for hydrogen ballooning include the appropriate use of materials that resist hydrogen embrittlement, which can cause materials to fail over repeated use. The use of austenitic stainless steels, aluminum alloys, copper, and copper alloys is considered appropriate for hydrogen service [33 – 37, 59].

4. Lift Determination

By following a series of steps like that used in deriving Equation (6-5), the following equivalent form can be derived:

$$\frac{B}{g} = \rho_g V_g(\sigma - 1) \qquad (6\text{-}8)$$

This form is more convenient as a starting point for measuring the buoyant gas lift in a balloon. The product $\rho_g V_g$ is the mass for the gas required to provide a lift of magnitude B when the local acceleration due to gravity is g, and the conditions assumed in Equation (6-3) are fulfilled, that is, $p_g T_g \approx p_a T_a$. Thus, under these conditions, the mass that can be lifted is a function *only* of the mass of gas placed in the balloon and the ratio of the molecular weight of that gas to the molecular weight of air. Normally, at the time of either zero-pressure or super-pressure balloon inflation, conditions approximate the assumed conditions well enough that Equation (6-8) may be used to determine the mass of gas required to lift the mass B/g.

The challenge, then is to accurately determine the mass of gas placed in the balloon. The mass of the gas may be measured directly or indirectly by measuring the volume and density and taking the product. It can be,

and sometimes is, measured by measuring the balloon's lift, but measuring the lift of very large balloon systems in the turbulent atmosphere is complicated enough that it does not often serve as the primary means of determining how much gas to put into a balloon.

For conditions of temperature and pressure for which the ideal gas law serves as an acceptable equation of state, the product $\rho_g V_g$ is easily expressed in terms of the measurable quantities p_g, T_g, and V_g. For gases stored under high pressure, any of several equations of state might serve to measure the amount of gas. Equations of state take many forms, including forms of van der Waals, which are based on attractive and repulsive interactions, virial equations based on statistical mechanics, or molecular-based semi-empirical equations [38-39]. For this discussion, which intends to provide some understanding of the important parameters related to understanding gases and the lift they provide, we will cite the same virial equations used in the first edition of this handbook, those developed in references [40] and [41] for helium and hydrogen, respectively. The reasons are three-fold: One, these equations are derived from experimental data in the pressure and temperature-range lift-gases experienced for inflation operations [42-43]; two, these equations are still utilized in the field both in the form of tables and in equations used for calculating and determining lift during ballooning operations [44]; and three, these equations are straightforward to calculate and use compared to other more recently developed equations of state, which require many more parameters, series of equations, or determining roots before use [38-39], [45-47]. It should be noted that all equations have strengths and weaknesses, and these equations, while useful for lift gases in a gaseous state, may not represent the substance in other forms, at critical states, supercritical states, or vapor-liquid equilibrium. For properties of a substance in other forms and uses, please refer to highly cited equations, such as the Peng-Robinson two-term cubic equation used widely in academia and industry [45-50].

The form most commonly used for engineering purposes is to include a compressibility factor Z to account for deviations of the real gas from an ideal gas.

This equation of state for mass can thus be expressed as

$$m_g = \frac{P_g M_g V_g}{Z_g R T_g} \tag{6-9}$$

The quantities that make up this equation of state, P_g, T_g, V_g, and Z_g, to be discussed in turn.

4.1. Gas Pressure

Pressure gauges, which are carefully handled and checked, with an accuracy of ±0.5% that measures when no gas is flowing form the container, is representative. In scientific ballooning a single tube rarely contains enough gas to inflate a balloon. Therefore, computations must be made of the total gas in a number of individual tubes or several must be joined by a manifold. The pressure of all tube is then equal and may be read by a single gauge. For trailers that deliver gas to the launch site, which are used during inflation, are interconnected at the rear by a manifold, but each is usually sealed separately to minimize leakage.

4.2. Gas Temperature

Obtaining a temperature representative of the gas in a container is more difficult than measuring pressure. In practice, a temperature sensor is placed on the container, but the temperature obtained is the container's temperature, not the gas's. Precautions must be taken to ensure that the temperature is representative of the gas inside the container. The best measurements are probably made at night when the ambient air temperature is at a minimum. Then, air temperature does not change rapidly, and if air circulation is maintained in the container, the container and the gas in it are likely to be in thermal equilibrium with the air. The temperature shown by the thermometer will be representative of the gas temperature. A temperature taken during the day when the ambient air temperature changes rapidly or when the sun is shining on the container is not likely accurate.

4.3. Gas Volume

A container's nominal volume (also called the water volume) is usually determined by weighing the container empty and then weighing it when filled with water with a known temperature. The difference in weight divided by the known specific weight of the water yields the water volume of the container. The actual (stretched) volume of a container is a function of the temperature of the container and the pressure exerted against its walls by the fluid it contains. Kalman expresses the stretched volume of a cylindrical steel tube as a function of its nominal volume, known hereafter as V_0, its temperature, and the pressure of the gas it contains [51]:

$$V_{g,s} = V_0\left[1 + f_t\left(T_{g,s} - T_b\right)\right]\left[1 + f_s\left(P_{g,s} - P_b\right)\right] \quad (6\text{-}10)$$

Where the subscript, "g,s" refers to the gas property and "b" refers to the base conditions (often at International Standard Atmosphere, or ISA, conditions), f_t or thermal factor refers to the temperature effects and

f_s or stretch factor refers to the pressure effects on the steel container, respectively. For the two types of unit systems, these values are provided in below.

Table 6-3: Values for Factors in Stretched Volume Equation

Units	Thermal factor, f_t	Stretch factor, f_s	ISA T_b	ISA P_b
English Engineering	1.89×10^{-5}	7.4×10^{-7}	529.67 R	14.7 psia
Système International	3.40×10^{-5}	10.7×10^{-10}	288.15 K	101,325 Pa

There are three assumptions within the derivation of this equation. First, quantities beyond the first order have been neglected for thermal expansion because the thermal factor is three times the thermal expansion of steel. Second, that the stretch factor is an average of two values obtained through different means – one through hydrostatic testing of tank-car cylinders with Amagat's water compressibility factors and one through physical dimensions of the cylinders – weighted equally due to equal soundness in the method [51]. Third, all steel cylinders have essentially the same characteristics as the helium tank-car cylinders used in the U.S. during and prior to the Kalman derivation in 1968. In the event that helium tank-car cylinders are significantly different from those the experimenter currently uses, Kalman may be referred to for a detailed explanation to derive new factors.

In theory, this equation should work for both hydrogen and helium. However, since steel is subject to hydrogen embrittlement, other materials may be used instead, such as special hydrogen-resistant steels or the use of liners, aluminum, or even composites [52]. Any of these options calls into question the assumption that these cylinders would behave like those for storing hydrogen.

4.4. Compressibility Factor

The compressibility, Z_g, is a function of pressure and temperature. For computing the volume of helium in cylindrical steel containers, Miller et al. [40] developed the following empirical expression (used by Kalman [51]):

$$Z_{g,s} = 1 + \left(b_1 + b_2 T_{g,s} + b_3 T_{g,s}^2\right) p_{g,s} + c_1 p_{g,s}^2 \qquad (6\text{-}11)$$

In which the constants b and c are provided in the table below, $T_{g,s}$ is provided in Kelvin and Rankine, and $p_{g,s}$ is provided in Pa and psia, respectively.

Table 6-4: Values for Constants in Compressibility Factor Equation

Units	b_1	b_2	b_3	c_1
English Engineering	1.48369×10^{-8}	-5.03856×10^{-11}	5.5620×10^{-14}	-4.664×10^{-18}
Système International	10.2297×10^{-5}	-19.2998×10^{-8}	1.1836×10^{-10}	-2.217×10^{-10}

For hydrogen, the compressibility factor can be calculated using a modified form of an equation by Wooley et al. [41]. Only the equation in SI units, without a counterpart in English units:

$$Z_{g,s} = exp\left[\frac{1}{T_{g,s}^{1.25}}\left(b_1 T_{g,s} - b_2 T_{g,s}^{\frac{1}{2}} - b_3\right)\frac{\rho_{g,s}}{\rho_0} + \frac{1}{T_{g,s}^2}\left(c_1 T_{g,s}^{\frac{1}{2}} - c_2\right)\left(\frac{\rho_{g,s}}{\rho_0}\right)^2\right] \qquad (6\text{-}12)$$

Where $b_1 = 5.5478 \times 10^{-3}$, $b_2 = 3.6877 \times 10^{-2}$, $b_3 = 2.2004 \times 10^{-1}$, $c_1 = 4.788 \times 10^{-3}$, $c_2 = 4.053 \times 10^{-2}$, and $\rho_0 = 8.9886 \times 10^{-2}$ kg/m^3.

4.5. Helium Measurement during Balloon Inflation

The determination of the amount of helium used is not trivial within scientific ballooning. Even if the gas in cylinders can be determined, several cylinders are simultaneously opened to withdraw helium to limit inflation times, resulting in residual gas in multiple containers after inflation. Neither gas pressure nor temperature can be measured accurately while gas is being withdrawn. The pressure of the flowing gas will be lower than the static pressure of the gas in the container due to the Bernoulli effect, and the temperature of the gas is likely to be less than the temperature of the container because of the cooling of the expanding gas. In practice, the method to determine the amount of helium withdrawn is to calculate lift before and after inflation, with the after-inflation measurements of temperature and pressure occurring long enough after for the gas temperature and pressure to return to steady-state conditions. That difference in lift accounts for the amount of lift provided by the gas. This measurement can take place as much as 24

hours (or more) after inflation. Thus, two methods have been generally adopted for more immediate determination of helium used.

1. Using lift tables, as well as pre-inflation measurements of pressure and temperature, accounting for size and number of cylinders utilized, as well as considering cooling effects of partially filled cylinders (as found at the end of inflation), a cutoff pressure can be calculated and helium flow to the balloon appropriately shut off. This method has widespread use, general acceptance, and proven flight history [53-54].

2. Using a mass flowmeter, helium flows through the meter into the balloon until the total mass matches what gas is required to provide the necessary lift and then shut off. Of the many types of flowmeters, coriolis flowmeters have the highest reported accuracy. [55]. Coriolis flowmeters, which measure the angular momentum of mass moving through a pipe to calculate mass flow, have become found increased use within multiple industries with the advancement of electronics that have improved their sensitivity and responsiveness to minor variations, and thus accuracy [56-58].

5. Gas Handling Considerations during Inflation Operations

5.1. High-Pressure Hazards

Any container filled with gas under high pressure constitutes a potential hazard; care should be taken to protect the container. It should not be struck violently or dropped. It should be stored in a dry area where the temperatures are not excessively high; 50°C (125°F) is usually stated as the maximum for compressed gas cylinders in the U.S. Flame should never be allowed to touch a cylinder, and a cylinder should never be allowed to become part of an electrical circuit. In particular, an electrical welding arc should never be struck against a cylinder containing pressurized gas. Cylinders should never be dragged or rolled. Small cylinders should be moved short distances on a hand cart, and when moved in a truck, care should be taken to ensure they do not strike each other violently. Safety devices in valves or cylinders should never be tampered with, and the cap should be left in place until a cylinder has been securely fixed in place and is ready to be used.

Gas is frequently carried through high-pressure hoses from the container to the balloon inflation tubes. Care should be taken to avoid kinking these hoses because kinks may cause invisible weakness in them. All hoses, valves, gages, and other equipment used with the inflation system should be inspected regularly, and high-pressure hoses should be replaced periodically, depending on the use and handling they receive, whether or not they show evidence of damage.

5.2. Cryogenic Hazards

Gas is being transported increasingly as a cryogen because of the lower transport cost, and cryogenic hydrogen has been used to inflate balloons. The large Dewars used to transport cryogenic gases must receive special care to avoid damage that will break the vacuum. Even the best Dewars leak heat to the cryogen, and eventually, some gas will have to be removed to prevent excessive pressure build-up. Periodic use may take care of this build-up, but a safety valve will release gas if necessary. The gas may be released at any hour of the day or night, and precautions must be adequate to ensure it does not create a hazard. Placing the Dewar in an open field where it will not be molested is desirable. Lift gases, if expelled into the atmosphere, rise and do not create a hazard at the surface for long unless trapped. The very cold gases coming from a Dewar may not rise immediately, however, so it is possible for them to flow along the surface and become trapped at some distance from the Dewar.

Another danger associated with cryogens occurs when they are used in large quantities, as in scientific ballooning. As the cryogen is removed from the dewar, air condenses on the outside of the pipes and tubes carrying the cryogen. This liquid air drips off and may collect in sizeable quantities. The boiling point of nitrogen is lower than oxygen, and as the nitrogen boils off, the liquid that remains becomes increasingly rich in oxygen. Then, any material which will oxidize constitutes a danger if it comes into contact with this liquid. The usual precautions include catching the liquid air in an aluminum trough and being very careful to keep other materials away from it. The problem is associated with extreme cold, so any cryogenic gas, including inert ones, will create it.

5.3. Flammable Gas Hazards

Flammable gases should not be stored with oxygen or other oxidizing materials, and special care should be taken to avoid open flames or sparks in an area where flammable gases are being stored or used. Only explosion-proof equipment and spark-proof tools should be used where gases are being stored or used. All equipment should be grounded. People working with flammable gases should also keep themselves electrically grounded.

When a balloon is being inflated with a flammable gas, great care should be exercised by everyone in the vicinity. All possible preparations incident to the flight should be made away from the site of inflation or before inflation begins. In particular, no electrical testing should be done in the vicinity of the balloon or gas source during inflation. Also, all equipment should be grounded before any gas is released from its container. If it should be necessary to connect two pieces of equipment where there may be gas, they should first be connected by a

wire either prior to the presence of the gas or outside of the area where gas may exist. No car or truck engine should be started or left running anywhere where gas may reach it or where sparks from it may reach the gas. Even the handling of the balloon or work at the base of the bubble should be kept to an absolute minimum.

All who are handling inflation hoses or who must go near the sources of the gas should wear heavy flame-proof clothing and a conducting strip that makes contact with the leg and extends under the shoe. Anyone who must work under or near the gas bubble of the inflating balloon should also wear a hood – one with a small hole in the top to allow gas to escape. Each such person should also be in constant communication with someone well outside the area of danger and watching for fire. Because hydrogen burns with an invisible flame, the first warning anyone has of fire may be the heat radiating from it or the start of the collapse of the balloon. The two events will occur nearly simultaneously, and a person working near the balloon will be in far more danger from the molten plastic of the balloon, which may rain down under and downwind of the bubble, than from the burning gas that will rise. Therefore, upon receiving a warning, anyone working near the balloon should retreat along the shortest path to a safe area. It is a good idea to have the danger area marked before the start of inflation and to have each person constantly aware of the optimum retreat route. In general, the area of danger may be visualized as an oval area oriented with its long dimension (major axis) parallel to the wind and with the balloon bubble near the upwind end. Anyone upwind of the balloon should move into the wind if they receive a warning; from all other locations, it is usually best to move crosswind away from the major axis of the oval. Except in very unusual circumstances, one should never move toward or across the major axis if one perceives danger.

Any balloon which has contained a flammable gas and is lying on the ground constitutes a hazard. It may contain small pockets of gas that are large enough to inflict serious burns if ignited. Consequently, it should not be left unattended until all pockets can be opened and the gas allowed to escape, and it should be handled with care by everyone working with it.

Anyone using flammable gases should study carefully the safety standards for handling hazardous gases, including local standards.

5.4. General Filling Hazards

Other general hazards to be mindful of during the inflation of balloons include noise, heavy equipment, overhead loads, as well as environmental conditions the operators are exposed to at the launch site. Anyone who participates in filling exercises should utilize appropriate personal protective equipment, which may include ear plugs or ear muffs, oxygen

monitors, hard hats, reflective vests, composite or steel-toed footwear, as well as gloves.

6. Conclusions

In the past 50 years, helium has remained the dominant lift gas for scientific ballooning. However, in light of other developed technologies, other lift gases both for Earth-bound and extraterrestrial mission may become viable considerations in the next 50 years. It will be exciting to see where and how lift gases utilized will continue to grow the scope and application of scientific ballooning.

References

[1] K. Stefan, "Performance Theory for Hot Air Balloons," *Journal of Aircraft*, vol. 16, no. 8, pp. 539-542, August 1979.

[2] A. L. Morris, "Buoyancy of Gases in Air," in *Helium Symposia Proceedings in 1968 – A Hundred Years of Helium*, U.S. Department of Interior, Bureau of Mines Information Circular 8417, 1968, pp. 9-16.

[3] N. Izutzu, N. Yajima, H. Honda, and T. Imamura, "Venus Balloons using water vapor," *Advances in Space Research*, vol. 33, no. 10, pp. 1831-1835, 2004.

[4] J. A. Jones, "Innovative Balloon Buoyancy Techniques for Atmospheric Exploration," in *2000 IEEE Aerospace Conference Proceedings*, Big Sky, MT, 2000, pp. 397-402.

[5] G. A. Landis, "Low-Altitude Exploration of the Venus Atmosphere by Balloon," in *AIAA Paper 2010-628*, 2010, doi: 10.2514/6.2010-628.

[6] P. Malaterre, "Long Duration Balloon Flights in the Middle Stratosphere," *Advanced Space Research*, vol. 13, no. 2, pp. 107-114, 1993.

[7] L. Ashman and R. Jolkovski, "The Solar-Powered Balloon," in *Proceedings, Fifth AFCRL Scientific Balloon Symposium*, U.S. Air Force Cambridge Research Laboratories.

[8] T. K. Schuler et al., "Solar High-Altitude Balloons (SHAB) as a Long Duration Controllable Aerial Platform," in *AIAA Paper 2022-0282*, December 2021, doi: 10.2514/6.2022-0282.

[9] E. Hough et al., "Solar Balloon Development for High Altitude Observations," in *AIAA Paper 2022-4113*, June 2022, doi: 10.2514/6.2022-4113.

[10] T. K. Schuler, M. Debbins, M. Cobar, J. Thangavelautham, and D. Sofge, "Altitude control with Vented Solar High Altitude Balloons (SHAB-Vs)," in *2023 IEEE Aerospace Conference*, Big Sky, MT, 2023, pp. 1-11.

[11] R. Manoj Kumar, S. Abinash Nataraj, S. Haribalan, and S. Adithya, "Design and analysis of Solar heated hot air balloon for Mars exploration," in *AIAA Paper 2022-2579*, December 2021, doi: 10.2514/6.2022-2579.

[12] J. A. Jones and J. J. Wu, "Solar Montgolfiere Balloons for Mars," in *AIAA Paper 1999-3852*, 1999, doi: 10.2514/6.1999-3852.

[13] J. A. Jones, D. Fairbrother, A. Lemieux, T. Lachenmeier, and R. Zubrin, "Wind-Driven Montgolfiere Balloons for Mars," in *AIAA Paper 2005-844*, 2005, doi: 10.2514/6.2005-844.

[14] E. J. Gaido and J. D. Burke, "To Sail the Skies of Mars Scientific Ballooning on the Red Planet," in *AIAA 1983-3483*, 1983, doi: 10.2514/6.1988-3483.

[15] B. M. Malaya Kumar and A. Ramesh Naidu, "Design of Mars Sample Return Mission Using Solar Montgolfier and In-Situ Propellant Plant," in *AIAA Paper 2021-2699*, 2021, doi: 10.2514/6.2021-2699.

[16] T. K. Schuler, D. C. Bowman, J. S. Izraelevitz, D. Sofge, and J. Thangavelautham, "Long duration in flights in Venus' atmosphere using passive solar hot air balloons," *Acta Astronautica*, vol. 191, pp. 160-168, February 2022.

[17] "JPL's Venus Aerial Robotic Balloon Prototype Aces Test Flights." [Online]. Available: https://www.jpl.nasa.gov/news/jpls-venus-aerial-robotic-balloon-prototype-aces-test-flights/. [Accessed: Apr. 10, 2025].

[18] G. Letrenne, G. Nouel, and V. Dubourg, "French Long Duration Balloon Activity: - The Infrared Montgolfiere (MIR) – The Superpressure Balloon (BPS)," in *AIAA Paper 1999-3888*, 1999, doi: 10.2514/6.1999-3888.

[19] D. P. Horkheimer, "Ammonia – A Solution for Airships Demanding Rapid Changes in Net Buoyancy," in *AIAA Paper 2005-7393*, 2005, doi: 10.2514/6.2005-7393.

[20] S. Niu, Z. Zhou, D. He, and Z. Li, "Analysis of the Combined Control Ability of Stratospheric Balloon Phase Change Gasbag and Auxiliary Gasbag," in *38th Youth Academic Annual Conference of Chinese Association of Automation*, 2023, pp. 427-432.

[21] W. Zheng, Q. Zhou, Z. Li, X. Zhang, Y. Liu, and M. Li, "Performance analysis of a novel stratospheric airship concept based on gas-liquid phase change," *Applied Thermal Engineering*, vol. 159, 113748, August 2019.

[22] M. K. Heun, J. A. Jones, and J. L. Hall, "Gondola Design for Venus Deep-Atmosphere Aerobot Operations," in *AIAA Paper 1998-897*, 2007, doi: 10.2514/6.1998-897.

[23] R. P. Padappayil and J. Borger, "Ammonia Toxicity." [Online]. Available: https://www.ncbi.nlm.nih.gov/books/NBK546677/. [Accessed: Apr. 10, 2025].

[24] H. D. Landahl and R. G. Herrmann, "Retention of Vapors and Gases in the human nose and lung," *Archives of Industrial Hygiene and Occupational Medicine*, vol. 1, no. 1, pp. 36-45, Jan. 1950.

[25] "Table of Atmospheric Properties and Lifts of Helium and Hydrogen," Scientific Balloon Facility, National Center for Atmospheric Research, December 1967.

[26] J. Nishimura, "Ten Years of Scientific Ballooning Activities in Japan (1966-1975)," *Tokyo University, Institute of Space and Aeronautical Science Bulletin (Tokyo Daigaku Uchu Koku Kenkyujo Hokoku)*, vol. 12, no. 2B, pp. 517-555, 1976.

[27] D. Anand, B. S. Kumar, and D. Ojha, "TIFR zero-pressure balloon programme crosses a milestone," *Current Science*, vol. 120, no. 11, pp. 1672-1678, June 2021.

[28] S. V. Damle and M. N. Joshi, "Developments and advances in scientific balloon capability of the TIFR National Balloon Facility, Hyderabad," *Advances in Space Research*, vol. 21, no. 7, pp. 941-948, 1998.

[29] J. Gary, B. Dellery, G. Letrenne, S. Venel, and S. Vargas, "Returning to Hydrogen Gas: a Strategic Decision to Continue Achievement of Stratospheric Balloon Flights," in *AIAA Paper 2015-2911*, June 2025, doi: 10.2514/6.2015-2911.

[30] "Space Perspective Successfully Completes Development Flight 2." [Online]. Available: https://spaceperspective.com/journal/space-perspective-successfully-completes-development-flight-2. [Accessed: Apr. 11, 2025].

[31] "Aerostar Harnessing Hydrogen for Near-Space Flight." [Online]. Available: https://aerostar.com/news/aerostar-harnessing-hydrogen-for-near-space-flight. [Accessed: Apr. 11, 2025].

[32] "Ultra-thin high-altitude balloon (BS13-08) breaks the world record for the altitude reached by an unmanned balloon." [Online]. Available: https://www.isas.jaxa.jp/j/topics/topics/2013/0920.shtml. [Accessed: Apr. 11, 2025].

[33] R. Kubara, "Safe Handling Procedures for Gaseous Hydrogen," Operations Policy Memo, March 1976.

[34] "Guide to Safety of Hydrogen and Hydrogen Systems," ANSI/AIAA G-095A-2017, December 2017.

[35] "Hydrogen Tools Portal," U.S. Department of Energy Office of Energy Efficiency and Renewable Energy's Hydrogen and Fuel Cell Technologies Office. [Online]. Available: https://h2tools.org. [Accessed: Apr. 11, 2025].

[36] "Hydrogen Safety Manual," NASA Technical Memorandum X-52454, 1968.

[37] "Safety Standard for Hydrogen and Hydrogen Systems," NASA Technical Memorandum 112540, 1997.

[38] D. O. Ortiz Vega, "A New Wide Range Equation of State for Helium-4", Ph.D. dissertation, Texas A&M University, College Station, Texas, 2013.

[39] D. O. Ortiz Vega, K. R. Hall, J. C. Holste, A. H. Harvey, and E. W. Lemmon, "An Equation of State for the Thermodynamic Properties of Helium," NIST Internal Report 8474, August 2023, doi: 10.6028/NIST.IR.8474.

[40] J. E. Miller, L. W. Brandt, and L. Stroud, "Compressibility Factors for Helium and Helium-Nitrogen Mixtures," Bureau of Mines Report of Investigation 5845, 1961, p. 3.

[41] H. W. Wooley, R. B. Scott, and F. G. Brickwedde, "Compilation of Thermal Properties of Hydrogen in its Various Isotopic and Ortho-Para Modifications," U.S. Department of Commerce, NBS Research Paper R P 1932, vol. 41, pp. 426-427, 1948.

[42] J. H. Dymond, K. N. Marsh, R. C. Wilhoit, K. C. Wong, and M. D. Frenkel, *Virial Coefficients of Pure Gases*, Berlin: Springer, 2002.

[43] J. H. Dymond and E. B. Smith, *Virial Coefficients of Pure Gases and Mixtures: A Critical Compilation*, Oxford: Clarendon Press, January 1980.

[44] *Helium Inflation Tables*, General Mills, Incorporated, Mechanical Division, Minneapolis, MN.

[45] D. Y. Peng and D. B. Robinson, "A New Two-Constant Equation of State," *Industrial and Engineering Chemistry Fundamentals*, vol. 15, no. 1, pp. 59-64, 1976.

[46] G. Soave, "Equilibrium constants from a modified Redlich-Kwong equation of state," *Chemical Engineering Science*, vol. 27, no. 6, pp. 1197-1203, June 1972.

[47] R. D. McCarty and V. D. Arp, "A New Wide Range Equation of State for Helium," in *Advances in Cryogenic Engineering*, vol. 35, Boston, MA: Springer, 1990, pp. 1465-1475.

[48] J. S. Lopez-Echeverry, S. Reif-Acherman, and E. Araujo-Lopez, "Peng-Robinson equation of state: 40 years through cubics," *Fluid Phase Equilibria*, vol. 447, pp. 39-71, September 2017.

[49] G. Soave, "20 years of Redlich-Kwong equation of state," *Fluid Phase Equilibria*, vol. 82, pp. 345-359, February 1993.

[50] A. Bertucco and M. Fermeglia, "50 years of Soave Equation of State (SRK): A source of inspiration for chemical engineers," *Fluid Phase Equilibria*, vol. 566, 113678, March 2023.

[51] H. S. Kalman, "Computing Volume of Helium in Cylindrical Steel Containers at 10 to 10,000 PSIA," U.S. Department of Interior, Bureau of Mines Information Circular 8367, 1968.

[52] A. Zuettel, "Hydrogen storage methods," *Naturwissenschaften*, vol. 91, pp. 157-172, 2004.

[53] B. D. Gildenberg, "Investigation of Inflation Technologies for Nonextensible Balloons," Holloman Air Force Base, New Mexico, 1954.

[54] M. S. Smith, "Review and Assessment of Helium Inflation Calculation Methods," in *AIAA Paper 2013-1271*, March 2013, doi: 10.2514/6.2013-1271.

[55] "Standard Methods for Gas Flow Measurement," ASHRAE Standard 41.7-2021, American National Standard Institute, March 2021.

[56] "Measurement of fluid flow in closed conduits – Guidance to the selection, installation and use of Coriolis flowmeters (mass flow, density and volume flow measurements)," ISO 10790, International Organization for Standardization, 2015.

[57] D. Waugman, "Support of Gas Flowmeter Upgrade Final Summer Faculty Fellowship Report," NASA's White Sands Test Facility Internal Report, 1995.

[58] T. Wang and R. Baker, "Coriolis flowmeters: a review of developments over the past 20 years, and an assessment of the state of the art and likely future directions," *Flow Measurement and Instrumentation*, vol. 40, pp. 99-123, September 2014.

[59] K. Stefan, "Plan for Liquid Hydrogen Exercise," Technical Report, National Center for Atmospheric Research, 1970.

Chapter 7
The Atmosphere

Matthew K. Laffin[1]

[1] World View Enterprises, Inc., Meteorologist, Mission Operations Department

Table of Contents

1. Introduction 6

2. Thermal Structure of the Atmosphere 7

2.1. Temperature and Density..... 7

2.1.1. The Hydrostatic Relationship 7

2.1.2. The U.S. Standard Atmosphere (1976) 7

2.1.3. Mean Thermal Structure 7

2.2. Thermal Radiation..... 9

3. Atmospheric Circulation 9

3.1. Mean Zonal Structure..... 9

3.2. Polar Wind Structure..... 10

3.3. Equatorial Zonal Wind Structure..... 11

3.4. Middle Latitude Vertical Structure in the Free Atmosphere.. 11

3.5. Boundary Layer..... 12

3.6. Low-Level Jet..... 12

4. Climatological and Meteorological Data Sources 13

5. Forecasts 15

6. Operational Planning 17

7. Summary 18

References..... 20

Table of Figures

Figure 7-1. Temperature as a function of geopotential height in the U.S. Standard Atmosphere 1962 [10]..... 8

Figure 7-2. Example of mean zonal winds in the summer and winter across altitudes..... 10

Figure 7-3. Example of polar vortex structures [16]..... 11

Figure 7-4. Equatorial zonal wind structures across time. The black dashed line indicates the height of the Tropopause [18]..... 12

Figure 7-5. Example radiosonde sounding operation at the Long-Duration-Balloon Facility in Antarctica. Cr: Scott Battaion..... 14

Table of Symbols

Symbol	Definition	Dimension
C_p	Specific heat at constant pressure	$L^2\ T^{-2}\ deg^{-1}$
C_v	Specific heat at constant volume	$L^2\ T^{-2}\ deg^{-1}$
g	Gravitational acceleration	$L\ T^{-2}$
h	Height or altitude	L
Nu	Nusselt number (convection efficiency parameter)	-
P	Pressure	$M\ L^{-1}\ T^{-2}$
Pr	Prandtl number (momentum vs thermal diffusivity)	-
Q_{solar}	Absorbed direct solar radiation	$M\ T^{-3}$
Q_{albedo}	Reflected solar radiation (albedo heating)	$M\ T^{-3}$
QIR	Incoming longwave (infrared) radiation	$M\ T^{-3}$
R	Specific gas constant	$L^2\ T^{-2}\ deg^{-1}$
Re	Reynolds number (flow regime indicator)	-
T	Temperature	deg
α	Absorptivity (fraction of radiation absorbed)	-
ε	Emissivity of a surface or atmospheric layer	-
k	Thermal conductivity	$M\ L\ T^{-3}\ deg^{-1}$
ρ	Density	$M\ L^{-3}$
σ	Stefan-Boltzmann constant	$M\ T^{-3}\ deg^{-4}$
τ	Transmissivity (fraction transmitted)	-
ω	Angular velocity (e.g., Earth's rotation)	T^{-1}

Editor's Note on Chapter Update

This chapter has been substantially updated from the original version in the Stratospheric Ballooning Handbook to reflect advances in atmospheric science, forecasting techniques, and operational practices. While foundational concepts from the original handbook remain, new research, modern data sources, and contemporary modeling approaches have been integrated throughout. Readers familiar with earlier editions will notice expanded discussions on wind regimes, thermal radiation, and forecasting tools, as well as references to satellite reanalysis products and numerical weather prediction models. Where applicable, content has been supplemented or edited from the original handbook to ensure it remains relevant to current ballooning operations.

1. Introduction

Balloon flights are possible because the density of the ambient atmosphere is equal to or greater than the density of the balloon system, regardless of the planet on which the flight takes place. Atmospheric density is, therefore, critically important to the success of ballooning. Engineers and scientists who calculate lift tables and analyze heat exchange between the balloon and its environment must carefully consider atmospheric density and, to a lesser extent, atmospheric composition. For many terrestrial scientific ballooning applications, "standard atmosphere" models provide sufficient data on these properties.

The U.S. Standard Atmosphere[2] (1976) [1], is a widely accepted model that defines temperature, density, and composition as functions of altitude. From these fundamental properties, numerous other useful atmospheric parameters can be derived. While the Standard Atmosphere provides a general representation of these features, supplementary models are available to account for variations in atmospheric conditions at different latitudes and seasons.

For those involved in balloon operations, wind is the most crucial atmospheric variable for launching and trajectories. Although other factors, such as cloud cover (and associated regulations), can affect operations, wind predictions remain a primary and ongoing concern. Accurate wind data, especially at the high altitudes where modern scientific balloons operate, can be sparse and highly variable. Consequently, idealized circulation models are often employed, despite their inherent limitations.

Forecasting atmospheric conditions for balloon flights requires a thorough understanding of atmospheric behavior and access to current atmospheric data. Modern weather forecasting relies heavily on numerical weather prediction models, satellite data, and advanced data assimilation techniques. Experienced forecasters can provide valuable 24-hour wind forecasts and longer-term planning information.

This chapter discusses the most important atmospheric properties relevant to scientific ballooning, including challenges in forecasting and planning. The explanations and descriptions in this chapter are simplified for clarity. For more detailed information, readers are encouraged to consult prior versions of this handbook and specialized literature [2–4].

[2] The 1976 publication will be referred to throughout this chapter as simply "Standard Atmosphere".

2. Thermal Structure of the Atmosphere

2.1. Temperature and Density

The Standard Atmosphere along with supplementary models [6], provides a comprehensive description of the atmosphere, including how temperature and density vary with altitude, latitude, and season. These models are generally sufficient for most stratospheric ballooning needs.

2.1.1. The Hydrostatic Relationship

The hydrostatic relationship, $dP = -g * \rho * dz$, describes the balance between gravity and the vertical pressure gradient in the atmosphere. In simpler terms, it explains why atmospheric pressure decreases with increasing altitude. This occurs because the air above any given point weighs less as height increases. While the atmosphere is always in motion, this relationship holds true in most large-scale situations. Additional information can be found in the previous balloon handbook, including driving equations for this relationship.

2.1.2. The U.S. Standard Atmosphere (1976)

The U.S. Standard Atmosphere (1976) defines the average state of the atmosphere from the Earth's surface up to 1,000 kilometers. It is based on a wealth of observational data and fundamental physical principles. For ease of calculation, the atmosphere is often divided into layers, and within each layer, the temperature is assumed to change linearly with height.

The Standard Atmosphere provides reference values for key parameters at sea level, including temperature, pressure, and density. It is important to note that while the Standard Atmosphere is a useful model, the actual atmosphere can vary significantly from this idealization. The 1976 version of the Standard Atmosphere has been the go-to reference for operations for over 50 years now. Additional models, such as the ICAO Standard Atmosphere (1993) [7], the NRLMSISE-00 (2000) [8], and the COSPAR International Reference Atmosphere (2012) [9] provide alternative examples of data sets for atmospheric characterization.

2.1.3. Mean Thermal Structure

Atmospheric temperature varies significantly with both latitude and season. For instance, temperatures tend to be warmer near the equator and colder near the poles. Similarly, temperatures vary between summer and winter due to changes in solar radiation. To account for these variations, scientists use supplementary atmospheric models that provide a more accurate representation of the atmosphere under different conditions than the Standard Atmosphere provides alone. Figure 7-1 below

provides a temperature profile as a function of geopotential height from the U.S. Standard Atmosphere (1962) [10]. Having been published prior to the updated U.S. Standard Atmosphere (1976) [1], the original handbook relied upon the 1962 version. Updated information is provided within this revised chapter to provide the information that has been published in the intervening years.

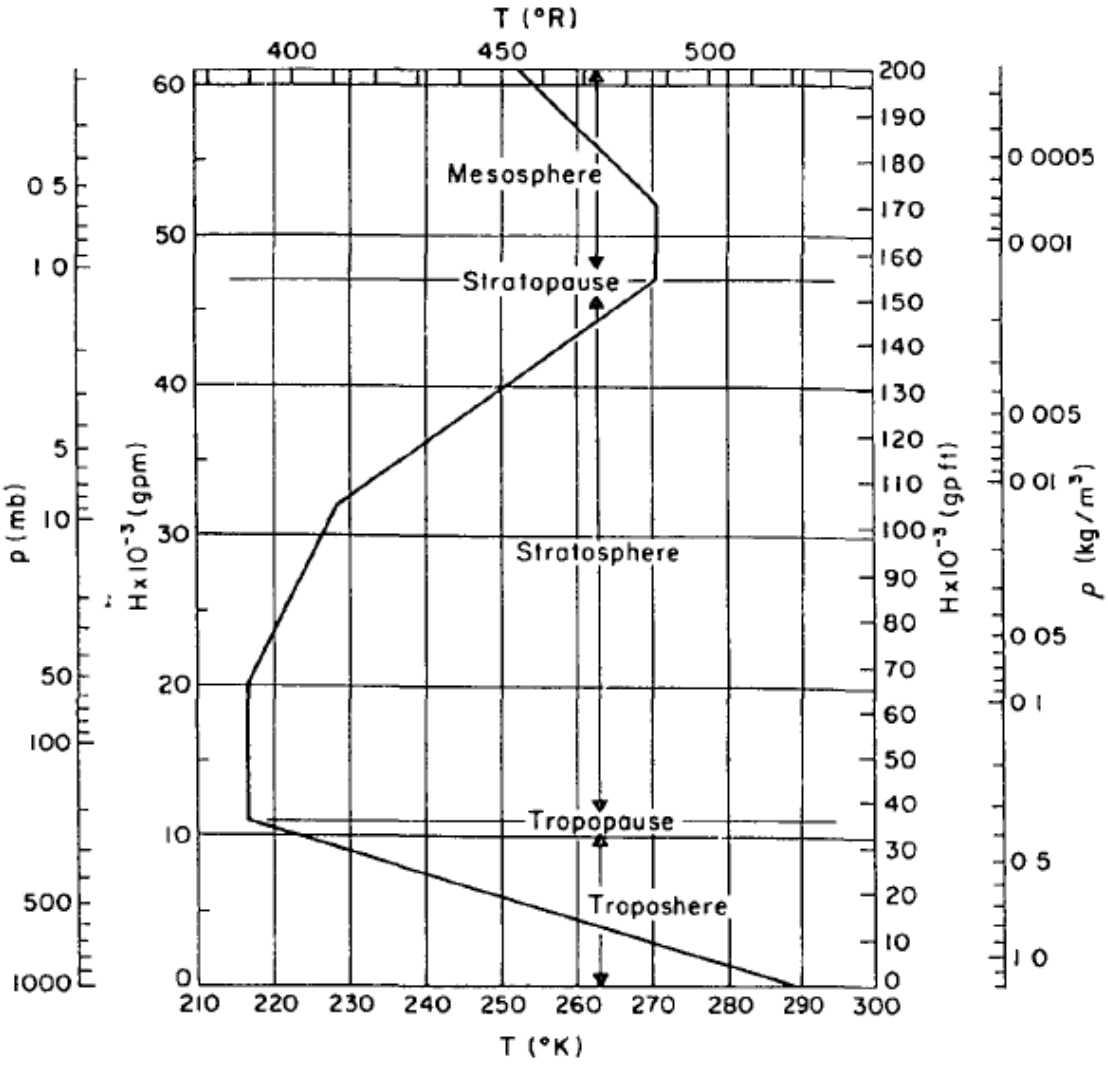


Figure 7-1. Temperature as a function of geopotential height in the U.S. Standard Atmosphere 1962 [10].

2.2. Thermal Radiation

Thermal radiation, which is energy transferred in the form of electromagnetic waves, plays a crucial role in determining atmospheric temperature. The primary sources of this radiation are:

- The Sun: Solar radiation is the main source of energy for the Earth's atmosphere.
- The Earth's surface: The Earth absorbs solar radiation and re-emits it as infrared radiation.

The amount of solar radiation received at any point on Earth varies with factors such as:

- Latitude
- Time of year
- Time of day

Gases in the atmosphere, such as water vapor and carbon dioxide, absorb and emit infrared radiation. This process, known as the greenhouse effect, helps keep Earth's atmosphere warm enough to support life. The balance between incoming solar radiation and outgoing infrared radiation determines the Earth's overall temperature and climate.

3. Atmospheric Circulation

Atmospheric circulation is the large-scale movement of air that redistributes heat and momentum globally, driven by uneven heating and influenced by the Earth's rotation. The zonal mean circulation refers to the average east-west component of the wind, shaped by the Coriolis effect into distinct wind belts, such as the trade winds, westerlies, and polar easterlies. These wind belts vary with height, featuring jet streams near the tropopause. Large-scale waves, such as Rossby waves [11], play a key role in global atmospheric circulation. The polar regions are characterized by the polar vortex, which can influence mid-latitude weather. The equatorial region features the Hadley cells [12], the quasi-biennial oscillation (QBO), a periodic reversal of zonal winds in the stratosphere, and the semiannual oscillation (SAO).

3.1. Mean Zonal Structure

The zonal mean circulation describes the average east-west component of atmospheric motion, illustrating how wind patterns vary with latitude and altitude, and is a fundamental aspect of the Earth's climate system, driven by the uneven distribution of solar energy and the planet's rotation. Modern understanding has been refined by satellite observations and sophisticated climate models, revealing complex

interactions between atmospheric layers and forcing mechanisms [13]. Key features include Hadley Cells, Ferrel Cells, Polar Cells, and Jet Streams. The zonal mean circulation varies seasonally and over longer time scales, influenced by factors such as seasonal changes in solar radiation, land-sea distribution, and phenomena such as the El Niño-Southern Oscillation (ENSO). Recent research has also highlighted the role of high-frequency atmospheric waves, such as Rossby waves and Kelvin waves, in modulating the zonal mean circulation and driving regional climate variability [14].

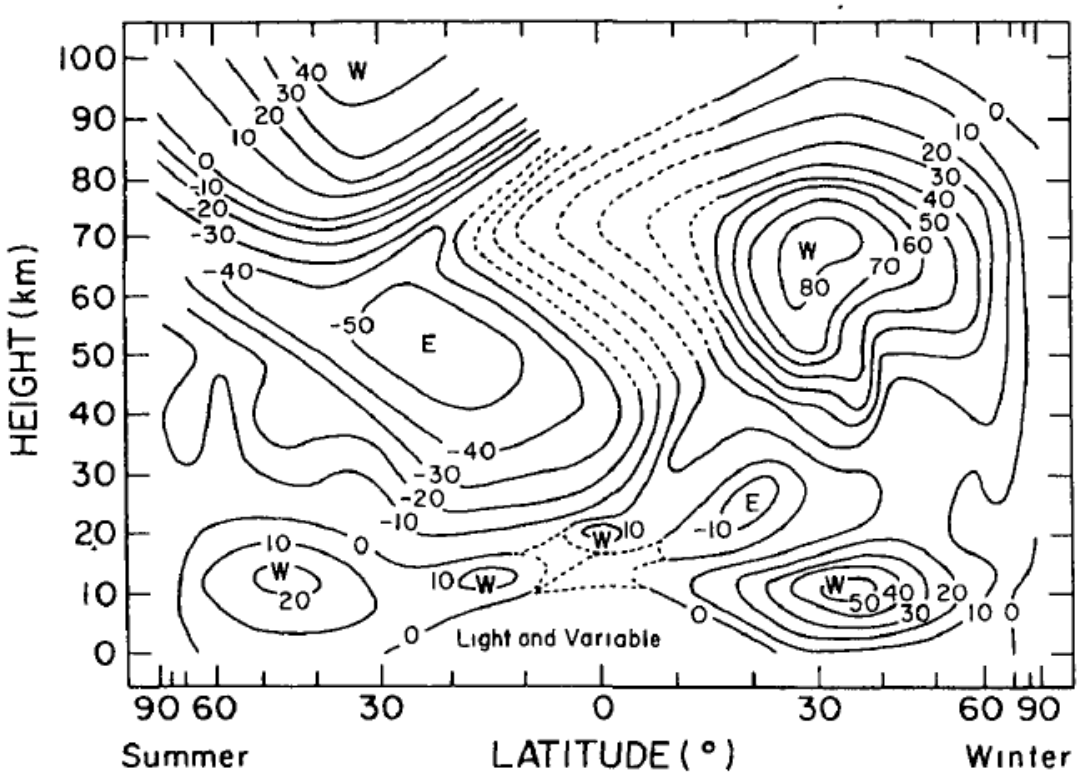


Figure 7-2. Example of mean zonal winds in the summer and winter across altitudes

3.2. Polar Wind Structure

The polar regions exhibit distinct wind patterns: a large-scale, high-altitude circulation that forms in the stratosphere above the Arctic (and Antarctic) during winter, characterized by strong westerly winds that circle the pole. The polar vortex is influenced by radiative cooling, ozone depletion, and planetary waves. It can weaken or break down, leading to disruptions such as sudden stratospheric warmings (SSWs), which can trigger cold air outbreaks in the mid-latitudes (such as polar vortices). Emerging evidence suggests that changes in Arctic

sea ice and increased greenhouse gas concentrations may influence the polar vortex, potentially leading to more frequent disruptions and associated extreme weather events [15].

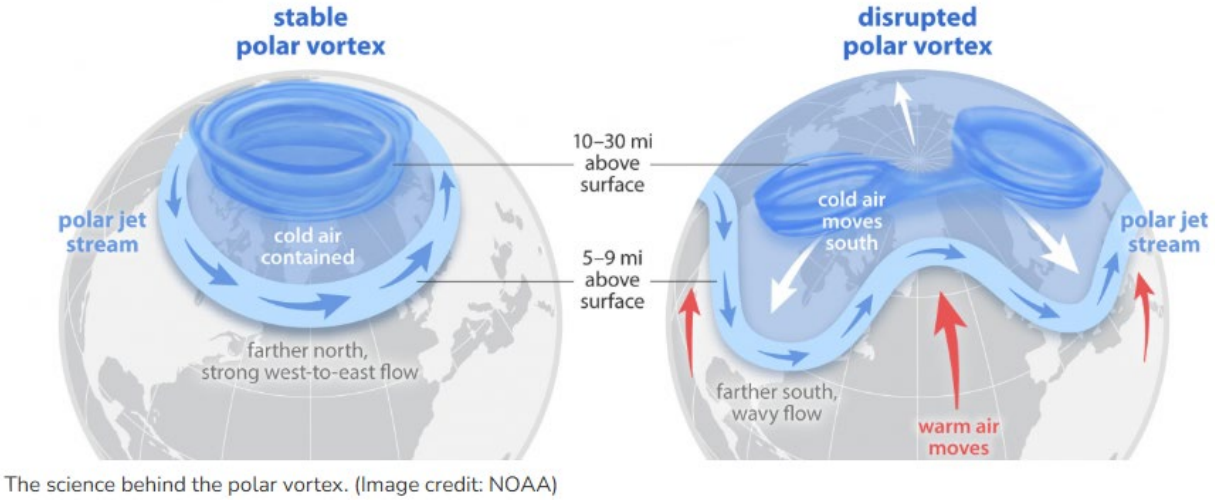


Figure 7-3. Example of polar vortex structures [16].

3.3. Equatorial Zonal Wind Structure

The equatorial region, characterized by strong solar heating and weak Coriolis force, exhibits unique zonal wind patterns, notably the quasi-biennial oscillation (QBO) and the semiannual oscillation (SAO). The QBO is a periodic oscillation in the zonal winds of the equatorial stratosphere, with a period of about 28 months, characterized by alternating bands of easterly and westerly winds that propagate slowly downward. Recent studies suggest the QBO may be changing due to climate change [17]. The SAO is another periodic oscillation in the zonal winds of the equatorial stratosphere and mesosphere, with a period of about 6 months, driven by seasonal variations in solar heating.

3.4. Middle Latitude Vertical Structure in the Free Atmosphere

The mid-latitudes are characterized by significant temperature and wind variations, with jet streams being a key feature. Strong horizontal temperature gradients drive these fast-flowing air currents near the tropopause. Their position and strength vary seasonally, influenced by factors such as seasonal temperature contrasts, land-sea distributions, and topography. Climate change is projected to significantly impact jet streams, increasing the wind speeds within this regime and creating more destabilized flow, potentially altering regional weather patterns [19].

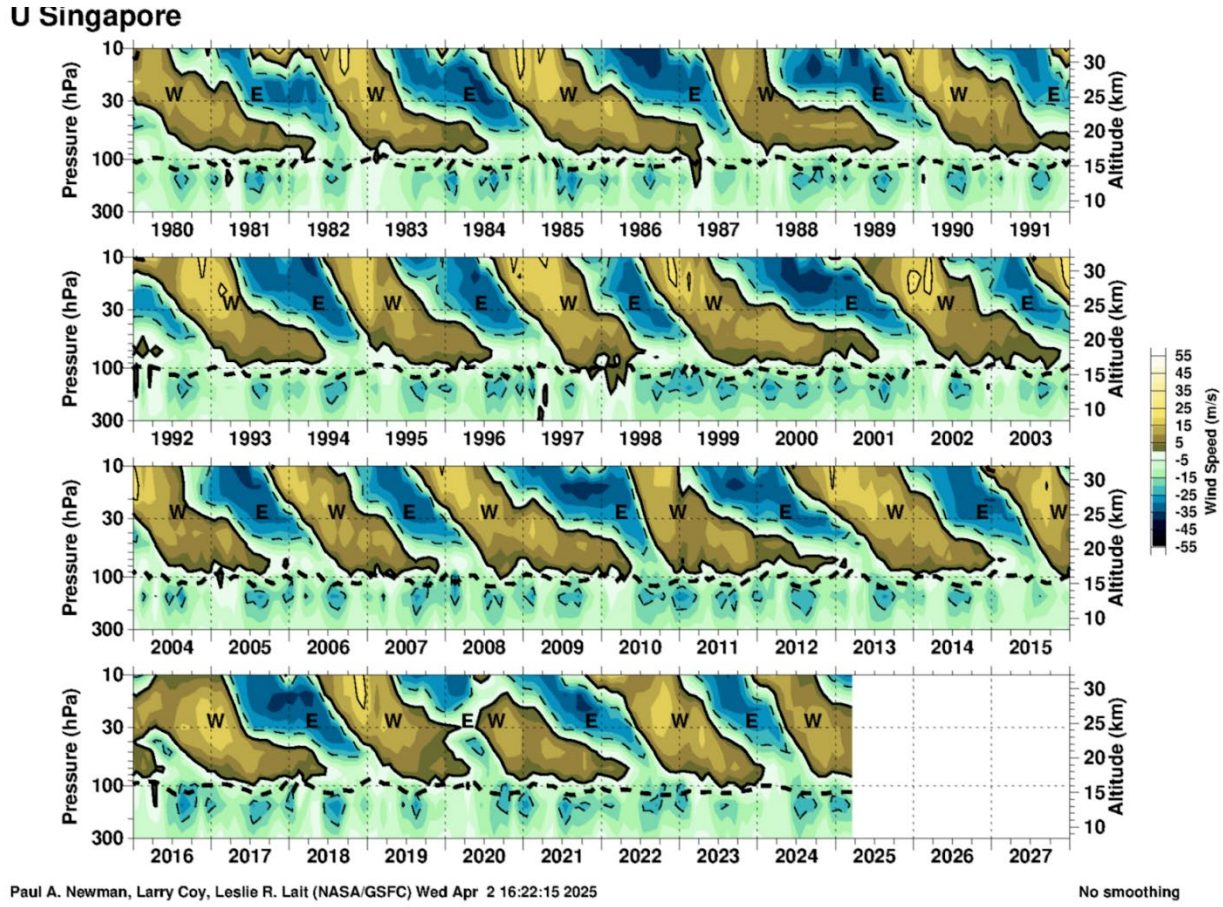


Figure 7-4. Equatorial zonal wind structures across time. The black dashed line indicates the height of the Tropopause [18]

3.5. Boundary Layer

The boundary layer, the lowest part of the atmosphere, is directly influenced by the Earth's surface and characterized by turbulent flow and significant vertical variations in wind speed and direction. Its structure is influenced by surface friction, diurnal heating and cooling, and surface roughness.

3.6. Low-Level Jet

The low-level jet (LLJ) is a phenomenon characterized by a maximum wind speed at low altitude - typically below 2 km - often occurring at night and frequently observed in the U.S. Great Plains. LLJs are influenced by factors like nocturnal temperature inversions, inertial oscillations, and synoptic-scale weather patterns. The interplay of these factors yields LLJs with varying characteristics and accurately predicting them remains challenging. LLJs have significant implications for severe weather forecasting, wind energy, and agriculture [20].

4. Climatological and Meteorological Data Sources

The thermal structure and general circulation of the atmosphere have been briefly reviewed in sections 2 and 3. However, comprehensive descriptions of global cloudiness, visibility, and other fine-scale atmospheric properties affecting balloon operations are beyond the scope of this guide. These variables are often too dynamic or localized to generalize meaningfully without specific geographic and seasonal context.

Once the proposed balloon launch site has been narrowed down to a few candidate regions, a qualified meteorologist can provide more detailed climatological context and operational forecasts. With the broad availability of online weather and climate resources, it is now easier than ever to integrate historical data, reanalysis products, and real-time observations to inform mission planning and identify reliable launch windows.

Below is a curated list of modern and authoritative data sources — most of which are publicly available — that can support forecasting and planning for scientific ballooning operations:

Reanalysis and Climate Data

- **ERA5 Reanalysis (ECMWF Copernicus Climate Data Store)**
  High-resolution global atmospheric reanalysis covering 1940 to present, including 3D fields of temperature, wind, humidity, and more.
  https://cds.climate.copernicus.eu

- **MERRA-2 (NASA GES DISC)**
  NASA's Modern-Era Retrospective Analysis for Research and Applications, Version 2, provides gridded atmospheric variables from 1980 onward.
  https://gmao.gsfc.nasa.gov/reanalysis/MERRA-2/

- **NOAA NCEI Climate Data Online (CDO)**
  Access to U.S. and global surface and upper-air observations, station summaries, and long-term climatology.
  https://www.ncei.noaa.gov/cdo-web/

Upper-Air Soundings and Profiles

- **University of Wyoming Atmospheric Soundings Archive**
  Worldwide radiosonde data with vertical profiles of temperature, humidity, and wind. Essential for pre-launch condition assessment.
  http://weather.uwyo.edu/upperair/sounding.html

- **NOAA Integrated Global Radiosonde Archive (IGRA v2)**
  Quality-controlled long-term radiosonde dataset for climatological analysis of upper-air trends and conditions.
  https://www.ncei.noaa.gov/products/weather-balloon/integrated-global-radiosonde-archive



Figure 7-5. Example radiosonde sounding operation at the Long-Duration-Balloon Facility in Antarctica. Cr: Scott Battaion

Forecast Models and Tools

- **Global Forecast System (GFS) via NOAA NOMADS**
  Operational forecast model output available for wind, temperature, pressure, and moisture at multiple levels, useful for ascent trajectory modeling.
  https://nomads.ncep.noaa.gov/

- **ECMWF Open Data Portal**
  Medium-range forecasts and deterministic model output from the ECMWF with global coverage and high resolution.
  https://www.ecmwf.int/en/forecasts/datasets/open-data

- **Skew-T and Atmospheric Profile Tools (e.g., Pivotal Weather, TropicalTidbits)**
  Useful for visualizing model forecast soundings and identifying critical layers for balloon ascent and float.

https://www.pivotalweather.com
https://www.tropicaltidbits.com

Satellite and Remote Sensing Products

- **NOAA CLASS Archive**
  Repository for satellite imagery and products, including temperature profiles, cloud top heights, and atmospheric motion vectors.
  https://www.class.noaa.gov

- **NASA Earthdata Portal**
  Access to satellite datasets such as AIRS, MODIS, and CALIPSO, which can provide vertical structure and cloud characteristics for launch site evaluation.
  https://earthdata.nasa.gov

Specialized Balloon Forecasting Tools

- **NOAA Balloon Trajectory Modeling (HYSPLIT)**
  Tools for modeling balloon trajectories based on forecast winds and ascent profiles.
  https://www.ready.noaa.gov/HYSPLIT.php

- **Cambridge University Spaceflight Balloon Predictor**
  A simple web-based tool using GFS forecast data to simulate balloon paths.
  https://predict.cusf.io/

Launch Site Climatology

- **WMO World Weather Records**
  Long-term station-based climate summaries for global cities and regions.
  https://library.wmo.int

- **NASA Global Modeling and Assimilation Office (GMAO) Climatology**
  Regionally averaged upper-air and surface climatology used in mission support.
  https://gmao.gsfc.nasa.gov

5. Forecasts

A meteorologist can produce a truly effective forecast for a balloon operation only if three conditions are met: they must (1) fully understand the mission objectives and how they are affected by atmospheric conditions; (2) have access to current, high-quality meteorological data; and (3) possess a deep understanding of atmospheric

structure, dynamics, and variability across multiple layers—from the surface to the upper stratosphere.

As discussed in Chapter 11, balloon operations are highly sensitive to weather, and even minor variations in wind structure or thermal conditions can substantially alter a mission's trajectory, duration, or recovery feasibility. The examples provided serve as a starting point for operational planning, but as balloon technology and scientific objectives evolve, so too must the forecasting and support requirements. Each flight should be approached as a unique event, with updated reviews of mission sensitivity to atmospheric conditions and a tailored forecasting strategy. To ensure this alignment, the meteorologist should be integrated as a core member of the operations team from the earliest planning stages through flight execution and post-flight analysis.

For launch and recovery operations, both of which typically occur in the lower troposphere, most experienced airways forecasters, once properly briefed on balloon-specific requirements, can provide useful and often reliable forecasts. These forecasts may also include conditions relevant to aircraft involved in tracking or support roles. Because the lower atmosphere is well observed, with frequent radiosonde launches and dense model initialization data, operational forecasts at these levels benefit from both high temporal and spatial resolution.

In contrast, forecasting conditions in the middle and upper stratosphere present far greater challenges. Observations at altitudes above 20 km are sparse, often limited to satellite retrievals, reanalysis products, or occasional special soundings. The dynamics at these altitudes—including wave activity, jets, and circulation reversals—are complex and not always well resolved in operational models. As such, meaningful analysis and forecasting at these levels can only be performed by specialists who have devoted substantial time to understanding stratospheric behavior.

Routine forecast offices may provide limited high-level data, but specialized requests often require advance coordination and are outside the scope of standard forecasting services. Moreover, the computation of ascent and descent vectors — although straightforward in theory — requires precise input and a nuanced understanding of balloon physics and vertical wind structure. These calculations must be performed in conjunction with accurate high-altitude wind forecasts to produce reliable trajectory and timing estimates. For this reason, ascent and descent forecasting should be handled by a balloon meteorologist or a dedicated atmospheric scientist with relevant experience, rather than delegated to general forecasting personnel.

The success of a balloon mission increasingly hinges on a collaborative, data-informed approach in which meteorology is not simply an external

input, but a continuously engaged function of the operations team. When forecasting expertise is applied holistically—from site selection to post-flight assessment—balloon programs can minimize risk, improve mission efficiency, and maximize scientific return.

6. Operational Planning

It is essential to consult an experienced balloon meteorologist before finalizing an operational plan for routine balloon flights. A skilled meteorologist working closely with a knowledgeable operations analyst can evaluate the atmospheric environment to determine the mission's feasibility, reduce the risk of failure, and enhance mission success. By fitting operational requirements into favorable meteorological conditions, they can also suggest minor modifications that improve efficiency, cost-effectiveness, and flight safety.

Because most scientific balloon flights are conducted in the middle latitudes—and because a successful flight depends so heavily on winds aloft—the following considerations are offered.

The stratospheric easterlies in summer are the scientific balloonist’s best friend. These are the steadiest winds known, and during the season in which they prevail, a balloon can be launched a considerable distance (~120 km) upwind from a target area with reasonable confidence that it will cross the target meridian in a known time and practically over the desired location. The optimum months for such flights are July and August at latitude 35°N—somewhat earlier farther north and later farther south—at any altitude above 25 km. Long-range flights, including potential around-the-world missions, can be planned using these winds with excellent prospects for controlled flight and recovery.

In contrast, the stratospheric westerlies in winter offer opportunities for transcontinental flights, with durations of up to three days from West Coast U.S. sites, and one- to two-day flights from more easterly launch locations. However, winter ballooning is more severely constrained by adverse surface weather. Furthermore, West Coast U.S. sites may become inoperative for several weeks during periods of circulation reversal, when zonal wind directions temporarily change. Unlike the steady easterlies, the westerlies often contain large-amplitude planetary waves, which introduce significant variability in wind direction and speed. These conditions require flexible tracking systems and adaptable recovery logistics.

A stratum of minimum winds exists near 20 km altitude and may be exploited, particularly in spring and fall, for long-duration flights with limited horizontal drift. Although the vector mean wind at these levels may approach zero, the scalar wind speeds are typically nonzero, with meandering winds of at least ~6 m/s. Such conditions can be

favorable for observational missions that require minimal displacement from a particular area of interest.

Hovering or station-keeping flights are also feasible in early summer. These involve taking advantage of diurnal variations in balloon altitude, rising during the daytime due to solar heating and descending at night as the balloon cools. By carefully timing and planning these altitude changes, the balloon can shift between wind layers with differing directions and speeds, allowing for limited horizontal displacement or near-stationary positioning over a region. Because wind direction and magnitude can vary significantly with altitude, such flights require high-resolution forecasts, detailed wind profile analysis, and continuous meteorological support throughout the mission.

7. Summary

This chapter provides a comprehensive overview of the atmospheric conditions essential to scientific ballooning, integrating modern meteorological science with mission-planning requirements. It begins by emphasizing the importance of accurate atmospheric modeling for every stage of balloon flight—from launch site selection and forecasting through ascent, float, descent, and recovery. Building upon the U.S. Standard Atmosphere (1976), the chapter now incorporates real-time data sources, numerical weather prediction (NWP) models, and satellite reanalysis products to provide a significantly more accurate representation of atmospheric structure, winds, and thermal properties than was possible in the 1975 Handbook.

A major expansion in this version is the discussion of thermal radiation and its effects on balloon systems. The chapter details how solar radiation, terrestrial longwave radiation, and atmospheric absorption interact with balloon envelopes, influencing temperature profiles and flight performance. Equations for radiative and convective heat transfer, along with standard atmospheric parameters like pressure, density, and temperature, are summarized with definitions and units for easy application in energy balance modeling. These sections bridge the gap between atmospheric physics and practical balloon engineering, enabling more accurate simulations of lift-gas behavior, material thermal stress, and diurnal altitude variations.

The chapter also offers a thorough treatment of atmospheric dynamics, including the structure and behavior of zonal winds, jet streams, polar vortices, and equatorial oscillations such as the quasi-biennial oscillation (QBO) and the semi-annual oscillation (SAO). Seasonal wind regimes—stratospheric easterlies in summer and westerlies in winter—are connected directly to flight planning, enabling mission designers to exploit periods of stable circulation for long-duration or station-keeping flights. Modern climate considerations, including the impacts

of greenhouse gas forcing and changing Arctic conditions on polar vortices and jet stream variability, are introduced for the first time, highlighting emerging challenges for stratospheric missions.

Operational forecasting receives significant attention, with balloon meteorologists described as integral members of mission teams rather than external consultants. The chapter explains how high-resolution wind profiles, ensemble forecasts, and real-time tracking tools inform launch decisions, flight path optimization, and recovery planning. Specific guidance is provided on minimum wind speeds for inflation, launch timing relative to synoptic-scale weather systems, and recovery site selection under variable wind conditions. By combining climatological analysis with real-time operational forecasting, the chapter sets a new standard for integrating atmospheric science into balloon mission planning.

Finally, the updated chapter concludes with curated references to modern atmospheric data sources, reanalysis products (e.g., ERA5, MERRA-2), and balloon-specific forecasting tools such as HYSPLIT and the Cambridge University Spaceflight Predictor. This ensures readers have direct access to the same state-of-the-art resources used in operational decision-making today. Overall, this update transforms the chapter from a static descriptive summary into a dynamic, operations-focused resource that unites atmospheric science, forecasting, and mission execution for modern scientific ballooning.

References

[1] "U.S. Standard Atmosphere, 1976," NOAA-S/T-76-1562, October 1976.

[2] J. R. Holton and G. J. Hakim, *Introduction to Dynamic Meteorology*. 2012. [Online]. Available: https://www.abebooks.com/9780123848666/Introduction-Dynamic-Meteorology-Volume-International-0123848660/plp. [Accessed: Nov. 3, 2025].

[3] J. Coiffier, C. Sutcliffe, O. Talagrand, and A. Staniforth, *Fundamentals of Numerical Weather Prediction*. 2012. [Online]. Available: https://www.abebooks.com/9781107001039/Fundamentals-Numerical-Weather-Prediction-Coiffier-110700103X/plp. [Accessed: Nov. 3, 2025].

[4] D. S. Wilks, *Statistical Methods in the Atmospheric Sciences*, 4th ed. 2019. [Online]. Available: https://www.abebooks.com/9780128158234/Statistical-Methods-Atmospheric-Sciences-Wilks-0128158239/plp. [Accessed: Nov. 3, 2025].

[5] "Tropopause | SKYbrary Aviation Safety." [Online]. Available: https://skybrary.aero/articles/tropopause. [Accessed: Nov. 3, 2025].

[6] "U. S. Standard Atmosphere Supplements, 1966." 1966. [Online]. Available: https://apps.dtic.mil/sti/html/tr/AD0659543/index.html. [Accessed: Nov. 3, 2025].

[7] M. De, "Manual of the ICAO Standard Atmosphere."

[8] "NRLMSIS 00." [Online]. Available: https://ccmc.gsfc.nasa.gov/models/NRLMSIS~00/. [Accessed: Nov. 3, 2025].

[9] "Project Record: COSPAR International Reference Atmosphere (CIRA)." [Online]. Available: https://catalogue.ceda.ac.uk/uuid/0c778590394ea5d9d5c175a7e4be772d/. [Accessed: Nov. 3, 2025].

[10] N. Sissenwine, M. Dubin, and H. Wexler, "The U.S. Standard Atmosphere, 1962," *Journal of Geophysical Research*, vol. 67, no. 9, pp. 3627–3630, 1962, doi: 10.1029/JZ067i009p03627.

[11] US Department of Commerce, NOAA, "What Is a Rossby Wave?" [Online]. Available: https://oceanservice.noaa.gov/facts/rossby-wave.html. [Accessed: Nov. 3, 2025].

[12] "Hadley Cells." [Online]. Available: https://groups.seas.harvard.edu/climate/eli/research/equable/hadley.html. [Accessed: Nov. 3, 2025].

[13] D. Dee and National Center for Atmospheric Research Staff (Eds), "The Climate Data Guide: ERA-Interim." [Online]. Available: https://climatedataguide.ucar.edu/climate-data/era-interim.

[14] *Middle Atmosphere Dynamics*, 1987.

[15] J. A. Screen, C. Deser, D. M. Smith, X. Zhang, R. Blackport, P. J. Kushner, et al., "Consistency and Discrepancy in the Atmospheric Response to Arctic Sea-Ice Loss across Climate Models," *Nature Geoscience*, vol. 11, pp. 155–163, 2018, doi: 10.1038/s41561-018-0059-y.

[16] "The Science behind the Polar Vortex: You Might Want to Put on a Sweater | National Oceanic and Atmospheric Administration," Jan. 29, 2019. [Online]. Available: https://www.noaa.gov/multimedia/infographic/science-behind-polar-vortex-you-might-want-to-put-on-sweater. [Accessed: Nov. 3, 2025].

[17] J. A. Anstey, T. P. Banyard, N. Butchart, L. Coy, P. A. Newman, S. Osprey, et al., "Prospect of Increased Disruption to the QBO in a Changing Climate," June 26, 2021.

[18] J. M. Wallace, "General Circulation of the Tropical Lower Stratosphere," *Reviews of Geophysics*, vol. 11, no. 2, pp. 191–222, 1973, doi: 10.1029/RG011i002p00191.

[19] T. G. Shepherd, "Atmospheric Circulation as a Source of Uncertainty in Climate Change Projections," *Nature Geoscience*, vol. 7, no. 10, pp. 703–708, 2014, doi: 10.1038/ngeo2253.

[20] W. D. Bonner, "Climatology of the Low Level Jet," 1968. [Online]. Available: https://journals.ametsoc.org/view/journals/mwre/96/12/1520-0493_1968_096_0833_cotllj_2_0_co_2.xml. [Accessed: Nov. 3, 2025].

Chapter 8
Balloon Manufacturing and Materials

Mitzi A. Giles[1], Sarah Roth[2], Ethan A. Chaffee[3]

[1]Balloon Manufacturing and Development Lead, Space Perspective
[2]National Aeronautics and Space Administration, Chief Technologist, Balloon Program Office
[3]World View Enterprises, Inc., Program Manager, Programs Department

Acknowledgements

Thanks to Loren Seely, Kurt Sehnert, Taber MacCallum for imparting their technical knowledge and leadership in high-altitude balloon manufacturing.

Table of Contents

1. Introduction 5

2. Historical Lessons & Design Evolution 5

3. Balloon Manufacturer Business Intelligence and Strategy 6

3.1. Market Demand 6

3.2. Typical High-Altitude Balloon Program Types 6

3.2.1. National Defense 7

3.2.2. Science and Education 7

3.2.3. Commercial 9

4. Manufacturing Considerations 10

4.1. Manufacturing Facilities 10

4.2. The Human Element: People and Culture 10

4.3. Engineering Functions 11

4.4. Production Functions and Roles 14

4.5. Production Materials 14

4.5.1. Supply Chain Management 14

4.5.2. Extruded Materials 15

4.5.3. Textiles 15

4.5.4. Other Components 16

4.5.5. Equipment 16

4.6. Fabrication 17

4.6.1. Process 17

4.6.2. Envelope 17

4.6.3. Balloon 18

4.6.4. In-Process Verification and Controls 18

4.6.5. Product Performance Feedback 19
4.7. Quality Control During Manufacturing 19
5. Materials & Testing 20
5.1. Extruded Materials 20
5.2. Polarized Light Inspection (PLI) 20
5.3. Thickness Testing 21
5.4. Uniaxial and Biaxial Tensile Strength 22
5.5. Glass Crystallization Testing 22
5.6. Fracture Toughness Testing 22
5.7. Additives Effects Testing 23
5.8. Textiles 23
6. Flight and Mission Closeout Considerations 24
7. Conclusions 24
References 26

Table of Figures

Figure 8-1. LLDPE film with finger-pull defects (left side) and without defects (right side) illuminated under a polarized light inspection tool. 21
Figure 8-2: Examples of ductile (left) and brittle (right) break of LLDPE material 23

1. Introduction

While this Handbook has covered significant portions of theory and historical practice to this point, it is also critical to address the practicalities of manufacturing balloons. This chapter aims to cover some of that in detail, outlining the business strategies of balloon manufacturers to meet the various high-altitude ballooning needs, as well as the manufacturing roles, considerations, and material testing approaches.

2. Historical Lessons & Design Evolution

A series of balloon failures in the 1960s spurred investigations to determine root causes [1]. The failures were attributed to warm launch temperatures and cold tropopause temperatures. This created a concern for examining plastic balloon film's performance over a variety of temperatures [1, 2]. Testing for temperatures at which plastic would fracture in a brittle, rather than ductile, manner would become a critical property for plastic materials testing.

As mentioned in Chapter 1, a series of failures in the late 1970s of heavy-lift balloon systems caused a 2-year stand-down from these types of missions while NASA convened a failure investigation which concluded that the likely culprit of the failures was due to variability in balloon envelope material properties. This variability had a knock-on effect in off-nominal balloon designs that could be aggravated further by fabrication, among other conditions [3, 4].

In the 1980s when failures continued despite previous efforts, a comprehensive balloon research and development program plan was developed by NASA's Balloon Program Office (BPO) to address the failures. The objectives of this program were to develop the "understanding of balloon system performance, limitations and failure mechanisms" [5]. This work made several major contributions, but a few that pertain specifically to manufacturing are summarized below.

- **Development of stronger and lighter balloon films** was pursued through experiments with fiber- and scrim-reinforced materials, which produced mixed results in achieving desired strength-to-weight improvements [5].

- **Improved material characterization and standardization** had the greatest impact on balloon modeling accuracy and manufacturing consistency. NASA refined the definition of material properties and aligned batch characteristics across production runs to ensure predictable performance [5].

- **Optimal cap placement emerged as a key design factor** in enabling heavy-lift systems to withstand higher stress loads. Tests comparing configurations found that external caps remained effective throughout flight, whereas internal caps became "structurally ineffective during ascent," likely because external caps stay supported against the balloon wall [6, 7].

- **Gore seam strength was found to be highly variable**, contradicting earlier assumptions of uniformity from end to end. This discovery led to improvements in seal machine setup and the introduction of verification testing to ensure consistent seam integrity [8, 9].

All of the efforts to characterize and understand the intricacies of balloon performance were combined into the "NASA Standard Balloon Designs[4]." Qualification flights were conducted to validate the new design process and the resulting products [10, 11]. Since the 1980s, improvements have continued by manufacturers as new balloon designs and the use of new materials and polyethylene formulations have been introduced.

3. Balloon Manufacturer Business Intelligence and Strategy

3.1. Market Demand

Understanding the needs of the high-altitude balloon market is critical to developing a successful balloon manufacturing organization and business strategy. There are markets with both unmet and fully satisfied demand, along with a large untapped market of latent demand. Current fulfillment ranges indicate that existing balloon manufacturers have room to grow and that new manufacturers can tap into an untapped customer base. For each market type in this industry, the manufacturer should consider specific factors to deliver high-quality products and services.

3.2. Typical High-Altitude Balloon Program Types

There are two main categories of high-altitude programs: long-lasting/repetitive and non-recurring. Long-lasting/repetitive programs or a series of similar programs can typically last over ten years. In contrast, non-recurring programs are short-term endeavors involving unique custom balloons that serve a specific purpose or mission without an expectation of long-term continuity. Occasionally, a non-recurring program may uncover a new market need or balloon capability, potentially leading to the development of a long-lasting/repetitive program. It is

[4] The most recent iteration of this Standard Array was published in 2014 and cited here.

crucial for a balloon manufacturing facility to understand these program types and their respective customer bases to serve each one.

3.2.1. National Defense

Long-standing national defense programs include balloon-based payload delivery, communications, and surveillance. Due to their secretive nature, the exact number of flights and demand is not publicly verifiable, but historical programs are explored in Chapter 1. Working on these programs may require security clearances, which some foreign nationals are not eligible for. Products involve custom balloons with special capabilities, requiring strong contracting, engineering, and launch, flight, and recovery skills. These programs expand capabilities, starting with development and moving to standardization. Robust products and procedures ensure operational readiness, enabling the production of standard offerings or new capabilities. Sometimes opportunities arise to collaborate with the defense industry on tailored balloon solutions with quick turnaround, which often increase during international conflicts. Close coordination between the engineering team and the contracts office is essential to bid successfully; poor coordination can lead to unprofitable programs. Development costs and timelines should be evaluated, with contingency plans included, especially if technology is not pre-existing. When bidding on existing tech, manufacturers must validate that products meet new requirements. A balloon manufacturer with strong contracting, engineering, launch, flight, and recovery skills is advantageous for serving this client base. The goal is to propose solutions for long-term initiatives that add value and ensure program longevity, often providing turnkey systems for customer operation.

3.2.2. Science and Education

The NASA’s Balloon Program Office (BPO), Swedish Space Corporation (SSC), Japan Aerospace Exploration Agency (JAXA), National Center for Space Studies (CNES), and Tata Institute of Fundamental Research (TIFR) are a few of the long-lasting nationally supported balloon programs supporting large heavy payload university and research flights. The BPO, for example, flies an average of 14 flights a year, with balloon volumes ranging from 1.1 to 60 million cubic feet (0.03 to 1.7 million cubic meters) [13]. Long-term steady use of large zero-pressure balloons by these organizations has allowed the balloon industry to boast very high success rates by learning from each launch and developing a highly skilled workforce. These organizations typically have well-established in-house launch capabilities or partnerships with established launch service contractors. Furthermore, they collaborate on programs, creating symbiotic relationships. This collaboration is beneficial for the balloon manufacturer, as the product's success depends on proper operations and collaboration.

As science payload weights vary from flight to flight, standard balloon product lines are often developed to deliver consistent products that achieve optimal performance. This standardization benefits the manufacturer by enabling repeat builds of the same products, reducing design and setup time, and improving employee retention of product/process information. Typical payload weight ranges and float altitudes should be considered when setting up the product line design requirements. Additionally, this customer base is typically not risk-tolerant and requires the balloon manufacturer to limit design changes once a successful design is qualified. To successfully implement changes, the balloon manufacturer must have a robust design, development, and validation process that withstands rigorous scrutiny. These customers often have an on-site auditor to monitor the manufacturing process. It is recommended that the balloon manufacturer assign a relationship manager to these auditors to ensure effective communication of continuous improvement efforts and the resolution of issues as they arise.

At times, these organizations fund development programs to further develop the balloon platform capabilities offered to science groups beyond the standard balloon product lines. These development programs may focus on material development or balloon design. To accommodate these needs, a balloon manufacturer will have a strong engineering team and a test lab to enable consistent collaboration with the science organization's development team. This collaboration can involve data sharing and confirmation between respected test labs, which benefits the manufacturer by improving the products offered across all markets.

3.2.2.1. Smaller Balloons

These organizations use smaller balloons, like NASA-funded university programs such as LaSPACE's HASP [14], based at Louisiana State University, which offers flight courses and payloads. Weather agencies and universities mainly use latex balloons for sounding data. To compete, polyethylene balloon makers might design lightweight, affordable products for various altitudes, with sensitivity to high-quality standards and failure reduction, which are advantages over latex, along with longer flights. Providing easy-to-use solutions, including manuals and accessories such as valves, parachutes, and gondolas, can help. Volume manufacturing ensures supply and quick support. Education programs often reuse products but occasionally pursue new projects, such as JPL's Venus balloon, which require specific materials and testing beyond in-house capabilities [15]. Collaboration with vendors and labs is key, and contracting specialized design or testing supports program success. These projects expand knowledge and open new markets. Vast details on educational and science programs are available in Chapters 2 and 3.

3.2.3. Commercial

In recent history, there have been no long-lasting commercial programs. However, new markets and companies worldwide continue to explore repeatable human commercial flights that could qualify as a long-lasting commercial program. Balloon manufacturers should consider the liabilities associated with producing a manned-rated balloon and determine what protections are necessary if pursuing such a program. A cautious approach to design margins, material selection, and quality standards will be prioritized because of the crewed nature of these flights. Close collaboration or ownership of flight operations allows input and influence over the quality and simplicity of the operations. This is key to reducing liabilities and risks linked to product use. If this market proves viable in the coming years, demand for reliable large-class balloons will increase significantly. Addressing this expected demand successfully will require substantial automation, cost-reduction efforts, and improvements in overall quality and robustness. Additionally, it is worthwhile for providers to investigate materials and packaging strategies for a reusable balloon structure. Reusable balloons are generally uncommon in high-altitude balloon programs because of the challenging environment the structure faces during ascent, descent, and retrieval. Significant challenges exist for recertification, and the associated costs and risks often outweigh the benefits of a reusable structure. Customers frequently request reusability in this market, and a manufacturer capable of achieving it will hold a competitive advantage. If a balloon manufacturer chooses to explore reusable balloons, considerations should include operational modifications to minimize damage risk and material degradation, component lifespan and performance over time across various environments, requalification, packaging practices, and durability studies to determine an appropriate number of uses with sufficient margins. Warranty discussions are also common with these customers, who are accustomed to non-developmental products.

Commercial programs will also be launched that have specific missions. Often, these have marketing and advertising benefits for the customer and are one-time endeavors. This customer base typically lacks the resources and preparation to conduct a high-altitude balloon flight. For this kind of customer, the opportunity cost is high for a likely short-term program. The balloon provider may need to decide whether pursuing this type of business is worthwhile, considering these variables. An experienced launch operations team must support these programs. If this is not an in-house capability to offer the customer, then partnering with an experienced launch services provider is beneficial to ensure proper operations. Other types of commercial programs have provided services to the public, such as LOON, a Google X Project [12]. This program nearly qualified for the long-lasting program category but concluded after nine years. The Loon program advanced understanding of

low-altitude, high-altitude, super-pressure balloons and was a positive technological disruption for the balloon industry. The Google LOON program was generously funded, enabling rapid flight testing and development cycles that advanced the technology quickly. For these programs, the balloon provider should have robust engineering and service capabilities and be able to respond swiftly to high-volume orders. Configuration management is also critical for high-volume, fast-paced development since design changes are often made and must be quickly reconciled with performance outcomes. If successful, this kind of program benefits everyone and can often lead to new opportunities.

4. Manufacturing Considerations

4.1. Manufacturing Facilities

Due to the linear fashion of the polyethylene balloon manufacturing process, most balloon manufacturing facilities are long. The desire for heavier payloads at higher float altitudes leads to an increase in the size of the balloon needed. However, a large facility is not always required for small balloon volumes to be profitable.

The layout of each facility is unique to the product and/or service being offered. If a facility with long manufacturing tables and segregated work areas is required, then restrooms and breakrooms could be strategically placed such that the distance travelled for the employee is minimalized. Technicians working on the same product may use breakrooms on opposite sides of the building, for example. Small "pop up" break-out areas can also be beneficial to minimize technician fatigue. Product life cycle flow should be considered when laying out workstations and material storage areas. It is good practice for all tools and materials to be staged in the area where they will be used. Mobile workstations are also beneficial for accessories installations or equipment maintenance efforts. Having a clean organized work area allows the employees to be in a safer, ordered work environment which can improve work output volume and quality. Intentional facility design, such as introducing color and music to the workplace, can increase employee satisfaction, lending to an environment that is pleasant at which to spend 8-10 hours a day.

4.2. The Human Element: People and Culture

People are the most powerful resource in an organization and often prove to have the greatest impact on product quality. Manufacturing managers and support personnel significantly affect if the work environment is one of integrity and growth. Honesty and integrity of the employees is paramount due to the integrated nature of the product. The way in which the management team reacts to issues and problems sets the cultural tone of the organization. Employees need to be empowered to bring up an issue

or a professional shortcoming. Managers need to provide the means for the employee to look at these occurrences as opportunities to improve while remaining focused on successfully meeting the project goals. Providing opportunities for group activities promotes technical and social growth within the team. Mutual respect to all individuals regardless of position or department is critical to allow innovative growth and collaboration.

One of the major tools to ensure a culture of growth, quality, and efficiency is a robust training program. Manufacturing training programs are co-developed with the quality and engineering departments, then executed by the manufacturing department and/or support teams. Balloon manufacturing technicians have diverse skill sets due to the various functions they perform in the manufacturing process. Training programs can be presented to new employees in an order that considers the technical skill and difficulty required for each function. Once trained for a particular function, employees may be periodically audited to validate their knowledge and performance of the function. Training certifications are given upon completion, and it is a good practice to incentivize employees to obtain training on many functions of the manufacturing process. Each certification needs to have an expiration date to ensure every employee is current on the most up-to-date information and operations. Quality teams may actively participate in developing training programs and measuring their effectiveness through audits. Up-to-date training materials and employee certifications are required and verified before process performance. When an employee is properly trained and confident in their ability to perform their function, the quality and consistency of the product will improve.

4.3. Engineering Functions

The engineering discipline is responsible for the design, development, and operational support of the balloon system and, potentially, subsystems of the flight train or payload. Engineers are involved through the entire life cycle of the system from the development of requirements through manufacturing and mission operations. The size and capabilities within an engineering group depend on the needs of the business. For instance, if the balloon provider only sells the balloon product without services or associated flight train accessories, the engineering team may be smaller and focused on design. For turnkey offerings, other engineering disciplines will be required such as avionics, power and controls, structures, decelerator systems, fluids and thermal systems, etc. In either case, support roles such as manufacturing engineering, systems engineering, and program management help balloon designs come to fruition.

Within engineering, emphasis should be placed on configuration management and change management. With a wide variety of balloon sizes,

materials, accessories, and mission profiles, the ability to accurately track and document the design evolution and current configurations of the product is critical to customer satisfaction and product development. Digital assets and applications such as design software and performance analysis tools, too, need to continually evolve and be refined over time to incorporate the latest advancements. As these tools and software are updated and improved, they must be diligently managed through robust configuration management practices. Standard engineering design and reporting processes are beneficial so that information over time is easily referenced and design progression understood.

The balloon engineering team plays a crucial role in selecting material and vendors to ensure that the required technical and fabrication expertise is present. Materials used in the construction of high-altitude balloons often are not commonly available. Construction techniques and joining mechanisms need to be evaluated along with the raw material characteristics to fully develop a material with the necessary properties for use in high-altitude balloon construction. Further, vendor selection can be a challenge due to the nature of the business being relatively low volume. Thus, material development and procurement can be costly and must be completed with proper forethought. Fortunately, documentation about appropriate balloon film is readily available in technical papers to aid in the development and characterization of known resins and film types [35]. Material characterization and properties must be confirmed and incorporated into the design parameters.

As new designs are developed, in addition to materials, the engineering team needs to consider manufacturing techniques, safety, equipment parameters, ergonomics, quality requirements related to critical design points, and cost factors regarding materials and labor to facilitate the smooth transfer of knowledge to administrative, production, and quality teams. Maintaining a consistent engineering presence in the manufacturing spaces is crucial to supporting these efforts effectively. The high-level requirements of a product are typically developed with the customer and the program management/sales team or the product development team. For high-altitude balloons the high-level requirements are defined by the desired altitude, suspended mass, and anticipated flight duration and location. Then any special requirements such as altitude control/change sequences or launch variables that could affect the balloon configuration or packaging are factored in. Engineers will also use appropriate design principles to validate the quality of the balloon design such as using a lower launch stress index limit for high gross inflation balloons, requiring a minimum amount of design margin, and requiring a prescribed number of iterations to ensure pattern convergence. In addition to the design-derived requirements, dissimilar materials and how they behave relative to each other in the operational environment once assembled must be considered. This includes analysis

of the structural design requirements and material mechanical properties over the anticipated operational environments.

It is best if ease of fabrication and operation are considered when defining product design requirements. For instance, if the standard human reach for laying out a balloon gore is 36 inches it may be advantageous to limit the gore maximum material width to 72 inches; in this way, the material is accessible from both sides. This consideration will, in turn, drive the number of resulting gores needed for a given balloon volume. Best practice is to develop some standard design requirements derived from the manufacturing capabilities of people and equipment that are applied consistently from product to product. The operational and service lifecycle of the product will need to be considered as well. For instance, placement of accessories such as inflation tubes on certain gores or how the balloon is stacked/folded may better facilitate more proficient flight line choreography. Packaging schemes that allow for quick payload integration and balloon layout may also be considered. In addition, one should not exclude requirements for aesthetics of the final product and its packaging.

The engineering team contributes greatly to the day-to-day manufacturing and operational goals. Manufacturing review boards typically contain an engineering representative to help resolve issues as they arise on the manufacturing floor with documentation, materials, process, product or equipment. In addition, the release of controlled documentation such as product specifications and blueprints per project are typically released and controlled by the engineering team. The need is exacerbated by not having standard product lines as each project is then unique and demands more engineering presence to execute. Manufacturing Engineering support roles also include industrial engineering efforts and working with administrative teams regarding procurement and general program/project management activities. Manufacturing support engineers should be constantly looking for improvements in the equipment, process, and product design.

If mission services are provided by the manufacturer, the balloon engineering team plays a crucial role in supporting the customer throughout the various phases of the balloon mission. The engineering team's involvement ensures the seamless execution of the mission by addressing any technical challenges or issues that may arise, and by collaborating closely with the customer to predict the performance and success of the mission. The volume of missions will indicate the level of staff needed exclusively for mission support or if design staff undertake the responsibilities as opportunities arise. The engineering department should be the driving force behind continuous product improvement, even though solutions may come from sources outside the department. Improvements in processes ultimately result in enhanced consistency or reduced cost. The engineering team should leverage

feedback from the customer engagement, manufacturing, and mission support processes to identify opportunities for product improvement.

4.4. Production Functions and Roles

Production functions are typically grouped by skill set and comprise load member technicians, table technicians, accessories technicians, finishing technicians, and other support personnel.

The **load member technicians** fabricate and prepare the load-bearing components for installation in the balloon envelope. This function is primarily a machine operator but may also conduct other pre-processing activities for the load members.

The **table technician's** primary responsibility is to cut and assemble the gores and load members into the primary envelope. Table technicians must be well-versed in material handling and methods for repairing and reinforcing materials. Table technicians typically use production equipment for dispensing, cutting, and sealing/seaming materials.

Accessories technicians preassemble inflation tubes, ducts, fittings, valves, and other balloon accessories so that finishing and table teams can have the most efficient installation of the balloon envelope.

Finishing team members install fittings to close out the top and bottom portions of the balloon envelope and final packaging arrangements.

If parachute or other soft goods manufacturing is supported, there will also be **sewing technicians** to support those subsystem builds.

Support personnel, such as inventory specialists and pickers, manufacturing engineers, planners and schedulers, and supervisors, primarily focus on enabling production technicians on the manufacturing floor to produce the best possible product. Technicians should be included on the manufacturing review board for the respective issue's correction and resolution. The technicians know the product and process more than anyone else and should be included in issue resolution. Additionally, this inclusion empowers the employee and fosters a sense of ownership [16].

4.5. Production Materials

4.5.1. Supply Chain Management

Effective supply chain management is crucial in balloon manufacturing, as the materials required are typically custom-ordered long-lead critical items. Forecasting material needs a year or even several years in advance may be necessary. However, careful consideration must also be given to buying material in bulk, as that could cause issues with

obsolescent overstock. Supply chain management teams need to collaborate closely with engineering and quality teams to understand specifications and source control requirements for product components. Additional requirements, such as configuration traceability, first-in first-out, just-in-time materials, and material handling, should also be considered. Balloon films are particularly noteworthy, as their lead times encompass internal qualification efforts. The occasional occurrence of defective films can impact production schedules. Maintaining strong relationships with film suppliers is of utmost importance, as open information-sharing collaboration is necessary to obtain the highest quality film.

4.5.2. Extruded Materials

Variables in film extrusion parameters have been shown to directly affect the mechanical properties of the materials [36-37]. Often balloon manufacturers specify what resins, process aids, layer configurations, and extrusion line configurations and setups are to be used to facilitate desirable mechanical properties. Balloon QA departments work in close collaboration with the vendor to ensure that the extrusion variables are clearly defined, performed, and audited consistently. Audit variables should be defined beforehand and verified periodically during extrusion runs. Due to normal material variability that can often occur from run to run, all materials should be tested and qualified before use in balloon construction. Over time, degradation of extrusion equipment will have a negative impact on film performance and increase defect count. Film run test results over time should be reviewed to correct any downward trends.

4.5.3. Textiles

Textiles are also often used in balloon construction. Regarding the load members for the balloon structure, these textiles are often made of straight fibers or braided/woven materials. As with extruded materials, vendor process controls may be necessary if a specification doesn't control the vendor's process or if the specification doesn't meet the application's requirements. For instance, braiders often use process aids such as lubricants and sizing agents, which can affect the material's behavioral characteristics in the desired operational environment [33-34]. Thus, elimination or control of the amount and type of aid used may be needed. Mechanical properties are often confirmed with in-house testing. Some textiles have specific environmental requirements for storage that should also be considered. The Parachute Industry Association (PIA) has made material specifications available to characterize and standardize parachute materials, which are good baselines for QC/QA test requirements and validation efforts. The parachute industry's knowledge base is continually growing, as is the balloon industry's. Stratospheric parachute dynamics are not as well-

defined as those of low-altitude parachutes; therefore, further characterization and validation testing may be necessary to qualify a material for the specific use case. Assembled textiles, storage and handling, seaming and joining methods, and resulting strength will need to be validated to ensure the assembly process does not compromise design intent.

4.5.4. Other Components

Metallic and electrical components should be functionally tested and physically inspected for conformity prior to use in any assembly. Requirements are defined by industry standards and pre-established engineering specifications. Adhesives, grease, gasketing and other materials should undergo environmental and mechanical testing for their respective applications.

4.5.5. Equipment

The manufacturing equipment used in the construction of high-altitude balloons is often designed in-house or highly customized by the balloon engineering team for specific materials and processes. Thus, expertise is critical to ensure that equipment designs are effective, safe, and robust. Due to the need for customization and variations in materials used, verification that the equipment can operate as intended and produce high-quality balloons without damaging or compromising the materials is needed. Quality teams can develop a pre-process verification test plan hand-in-hand with engineering teams to qualify a piece of equipment prior to use. This can be routine start-up tests, parameter limit verifications, mechanical evaluations, etc. For newly procured equipment, the initial pre-process equipment verification plan may require additional verifications. Equipment verification studies allow the engineering team to certify that their designs are effective and create the basis for the knowledge transfer to production and operations via specifications and manuals. Documentation demonstrating compliance with pre-process verification tests and the organization's preventative maintenance programs is captured and approved before any aerospace product is built.

The characteristics that should be reviewed when evaluating a good fin heat seal produced in typical polyethylene balloon materials include melt flow evaluation and the effects of seaming temperature pressure and dwell, seam opacity, tensile modulus of the seam and any cold brittleness effects, tensile strength in the heat-affected area, seam thickness, and seam edge geometry among others. For other types of seam configurations such as butt seams joined with adhesive tapes, there are other characteristics to verify that the seam doesn’t compromise the parent material strength. Characterizing the adhesive properties during the

lifecycle of the product may be needed as operational environments can have drastic effects on the behavior of the adhesives.

To verify the suitability of this equipment for balloon manufacture, it is recommended that the equipment be evaluated for its ability to work with the materials without introducing damage to the materials or creating foreign object debris that can degrade the product. It is recommended that safety and ergonomic features are implemented and routinely evaluated for effectiveness and to ensure safe operation. It is critical to reduce repetitive operator movements, when possible, to prevent worker fatigue and injury.

4.6. Fabrication

4.6.1. Process

Manufacturing process ownership is shared between the core disciplines and is typically co-developed by the teams. In the phase of initial process development, the engineering team often leads the effort. Small teams are most effective in drafting the initial process, usually consisting of 1-2 engineers, 1 quality person, and 1-2 production/mission operations persons. Using small teams initially can allow inclusiveness of ideas as everyone brings a different expertise. Diversity in disciplines permits the team to produce an effective process that satisfies all parties. At this stage, critical inspection points, material traceability documentation, test locations/sample configurations and processes are identified and documented so that effective work practice is defined.

During development, the quality team ensures the process and manufacturing techniques do not compromise the product efficacy. The complete product life cycle should be reviewed with engineering and manufacturing teams for processes that could potentially cause a defect. Any potential issues identified can then be mitigated or eliminated. Critical inspection points can be identified and captured in manufacturing and quality inspection procedures and inspection records.

4.6.2. Envelope

In its simplest form, a scientific balloon is composed of shaped gores. The gore pattern is based on design principles covered in Chapter 9 for Zero-Pressure and Chapter 10 for Super-pressure. Please refer to those chapters for detailed discussion on the design of these balloons and their various configurations and shapes. Gores are matched along their seams in the transverse direction, with as many gores as necessary to create the full shape and volume of the balloon. When gores are made from materials like fabric, they can be connected by stitching, as with parachutes. With the adoption of plastic as a balloon envelope material,

the use of a plastic sealer has dominated the method for connecting gores along their seams. Impulse heat sealing, invented in the 1940s, which allowed for greater quality control of the plastic seal and its resulting seal strength, proved a valuable invention for plastic balloons [12,29]. The use of heat-sealing machines for balloon manufacture with polyethylene film has become the industry standard, enabling the production of balloons with reliable performance characteristics.

Although the envelope provides structure and shape to the balloon, the load-carrying members of the balloon construction are often load tape or tendons incorporated along the gore seams through a combination of sealing and tacking. However, perhaps more complicated are the addition of inflation tubes, venting ducts, and destruct line and destruct panels that must be built into the balloon's walls and reinforced along seams. The addition of these critical elements requires careful team construction and diligent accounting of gore number and balloon location to ensure proper use during operations.

4.6.3. Balloon

Of course, balloons are not simply composed of the plastic envelope material but also include interfaces for connecting telemetry instrumentation, as well as destruct devices and valves used during termination operations. As a result, balloon fabrication will also involve certain finishing work, including incorporating metal components (apex and base fittings or connections) into the polyethylene film and load members. Each manufacturer has its own design for how these components are integrated, but it may include the use of bolts and gaskets to account for the gaps introduced by the gathering of plastic film at the top or bottom of the balloon. Criticality for leak paths is determined by the location of potential leaks (apex vs base) and the balloon type (zero-pressure vs super-pressure).

4.6.4. In-Process Verification and Controls

Balloons are typically single-use and therefore cannot be functionally tested post-assembly via an inflation test. Effective in-process controls ensure that the design intent and product functionality requirements are met. Every time balloon materials are handled there is potential to induce damage. Due to the quantity of materials used and inherent handling in the process, defects do happen and therefore inspection is required (as well as repair and reinforcement). Defect types and repair reinforcement methods need to be well defined and repair techniques verified for effectiveness. As some general repetitive material defects are known and the impacts on performance are well-defined, the repair/reinforcement method can be standardized and implemented in real-time without external support for the operator.

Representative assembled samples are tested throughout the manufacturing cycles to ensure the process parameters are producing a reliable product. Typically at the beginning and end of a shift or activity, equipment tests are conducted to validate the operational performance of the equipment and materials used to construct the balloons and accessories. Equipment visual inspection and maintenance logs may also be verified that all critical maintenance has been performed per the maintenance schedule. In addition, the quality department also ensures that all have been addressed, and documentation is complete and correct before product release for shipment. The quality teams should be as efficient as possible to avoid delays within the process.

4.6.5. Product Performance Feedback

Indications of product performance can be real-time if the mission is supported or after the fact if the products are used in a mission that the balloon manufacturer does not support. Regardless of when the feedback is received, it is crucial to receive and respond to it. It is a best practice to log all feedback from customers, users, or flight performance for future statistical reference.

4.7. Quality Control During Manufacturing

A balloon quality team is of the utmost importance due to the nature and volume of the materials used. For balloons using extruded films, there is an array of mechanical properties that must be within specification. Many organizations look at industry standards and technical publications regarding the study and characterization of thin film material properties and their use in balloon construction. Quality and engineering teams should collaborate closely to define the type and frequency of test or inspection that is to occur for a product to ensure functionality and statistical success. Additionally, it can benefit high-altitude balloon quality departments to contain an in-house metrology lab to characterize and validate materials. In addition to the mechanical properties of the assembled balloon and raw materials, there can be many acres of balloon film in one balloon that require inspection and repair/reinforcement throughout the assembly process. Given the critical nature of the extruded materials, a robust quality management system must be in place to identify defects early on and drive continuous improvements to minimize them through enhanced process controls, inspection regimes, and proactive mitigation strategies. Adequate defect tracking and reporting should also occur and have traceability back to the product produced. For structural components, the engineering team has likely performed sufficient analysis and testing that emerges as robust receiving inspection criteria and material certificate requirements which are then communicated to and performed by the balloon QA team. Quality teams can work with management and administrative teams to ensure business

processes and internal services are conducted in the highest quality manner.

5. Materials & Testing

As a result of the investigations of the 1980s in response to catastrophic balloon failures, not only were material specifications established but seal strength requirements were established. To ensure material and manufacturing quality, manufacturers adopted quality control programs that focused specifically on these two aspects of balloon builds. These quality control programs necessarily included significant testing, reporting, and data retention [6, 12, 29].

5.1. Extruded Materials

The NASA specification for film identifies several types of tests that are critical for scientific balloons:

- Film Screening to identify film defects during the extrusion process using a process known as Polarized Light Inspection (PLI).
- Uniaxial tensile testing to ensure inherent film strength prior to manufacturing.
- Glass Crystallization testing to ensure film will survive cold temperatures while passing through the tropopause and other cold regions within the atmosphere.
- Fracture toughness testing to determine flaw and tear propagation throughout the material

Other testing that is not enumerated in the NASA material specification includes testing for UV degradation, electrostatic resistance additive studies, as well as DSC crystallinity measurements for polymer chain orientation [31].

5.2. Polarized Light Inspection (PLI)

One unique feature of LLDPE is the capability to screen the film for defects using polarized light imaging (PLI). The material passes between two polarizing filters with perpendicular axes when a light source is behind the filters. An observer can monitor the film as it passes through the filters, and any anomaly that deforms the film surface can be detected and marked [17], see Figure 8-1.

This process is typically performed between film extrusion and the beginning of balloon construction. The primary defects identified by this process are gels, holes, white streaks, and abrasions. Of these defects, gels have received the most attention from researchers. Most PLI inspections are qualitative and rely on the user to identify the

defects. However, recent advancements in image processing are allowing the quality assessment of film defects to become semi-automated, enabling more successful identification and determination of which defects are likely to be a problem. Defects are avoided by the thoughtful placement of the film sheet during gore cutting during balloon construction. If they appear in the balloon itself, they are reinforced as any manufacturing-induced defect with a specialized tape patch.



Figure 8-1. LLDPE film with finger-pull defects (left side) and without defects (right side) illuminated under a polarized light inspection tool.

5.3. Thickness Testing

A critical component of characterizing thin films is an accurate measurement of the material's thickness. This is the driving factor in determining stress during tensile testing and can drastically influence the test results. Certain testing methods can also damage the film and skew the tensile results. Care should be taken to use minimally invasive techniques that are extremely accurate and precise.

Another method to consider is a profile thickness measurement that provides a relative analysis based on the material's theoretical thickness. This method scans a larger sample and can provide a snapshot of the consistency of the raw film from the extrusion facility.

5.4. Uniaxial and Biaxial Tensile Strength

Both biaxial and uniaxial tensile testing have historically been employed to determine the yield and breaking point of various materials. Polyethylene tensile testing can follow the American Society for Testing and Materials methods, with an alteration to better resemble flight conditions. These tests are useful for tracking film extrusion consistency, but, historically, have not provided significant insight into potential flight performance.

Biaxial testing using an inflated balloon film cylinder can be more useful for emulating the balloon's stress state in flight. In this case, a combination of axial force and internal pressure can be combined with a thermal chamber to mimic the reality of common flight environments [18-21].

5.5. Glass Crystallization Testing

A difference in crystallinity impacts the brittleness, toughness, stiffness or modulus, optical clarity, creep or cold flow, (vapor) barrier resistance, and long-term stability [22–24]. There are two methods for testing the transition to crystallinity in a film. One is the Cold Brittleness Transition Temperature (CBTT) test for LLDPE, which is completed by dropping a metal ball of prescribed weight from a designated height at various temperatures [23, 24, 25]. The films are then examined for fracture type: brittle or ductile. An example of the resulting samples from a CBTT test is presented in Figure 8-2, where the ductile break (left) shows more significant stretching before failure than the brittle break (right). The differences in the CBTT can be used to evaluate changes in mechanical properties resulting from crystallization at various temperatures. The second method is the determination of the glass transition temperature (T_g) found by differential scanning calorimetry (DSC), which is similar to CBTT testing. DSC is a more quantitative tool and can better describe the material’s crystallinity.

5.6. Fracture Toughness Testing

Another standard performance test is fracture toughness, which is the material's ability to resist the propagation of a flaw. CBTT testing focuses on the initiation of the flaw and, over time, is considered the more critical property. The fracture toughness of the films has been studied at various temperatures, and it has been determined that it is

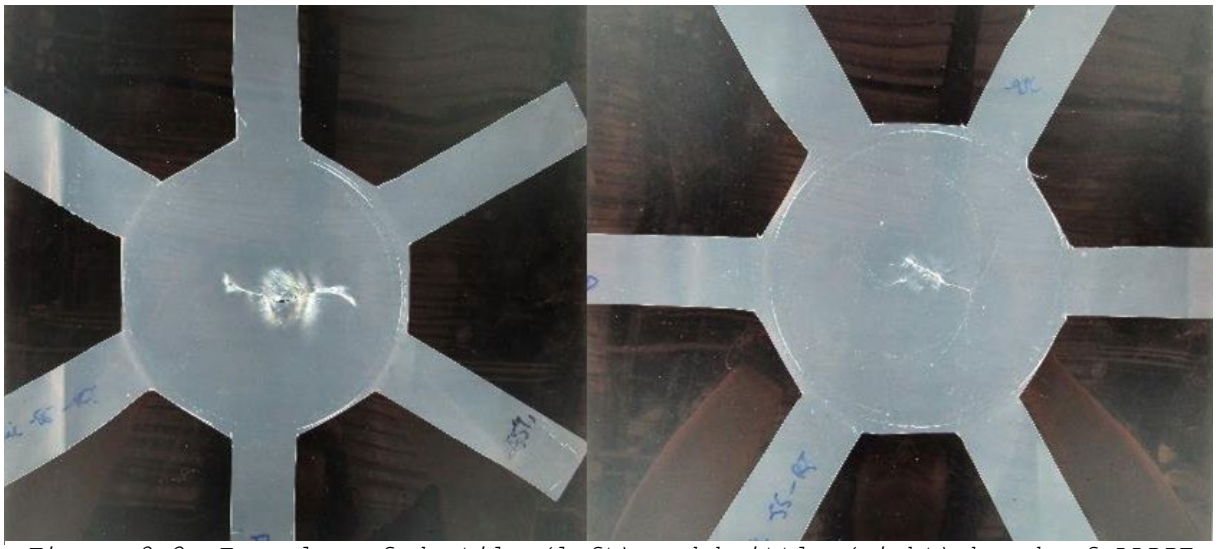


Figure 8-2: Examples of ductile (left) and brittle (right) break of LLDPE material

Courtesy: World View

not entirely independent of geometry. Six films were studied in-depth in the early ’90s. Astrofilm E2, Astrofilm C, StratoFilm 85, StratoFilm 372, X-124, and ‘French film’. Laboratory and flight testing had already confirmed that Astrofilm C and StratoFilm 85 were less robust films; the fracture toughness testing confirmed that the lowest temperature they could achieve was considerably warmer than the other four films [26–28].

5.7. Additives Effects Testing

There have been investigations into additives in balloon film to achieve specific properties, such as UV resistance or electrostatic discharge resistance. It appears that StratoFilm blends favorably with these additives within acceptable limits of performance [29]. This property is critical when considering hydrogen as a lift gas, and these studies should be reinvestigated [30-32]. However, additives can have negative impacts on sealability and other surface properties due to “blooming” or “bleeding” [38-40]. Testing parameters should also consider these effects on manufacturing, shelf life, and product performance.

5.8. Textiles

Several items in ballooning are constructed from textile material, such as rip-stitch (energy absorbers), load straps, and parachutes. Parachutes, for example, fly exposed to the radiation environment, which has been shown to degrade the ultimate strength of the base fabric material [41]. Further, repeated loading of textiles (specifically troop and cargo parachutes, which are deployed multiple times) has been shown to reduce nominal tensile strength [42]. Quantifying the decrease in strength is critical for future design and operations. Uniaxial pull-

to-failure tests on specimens after exposure at various levels of solar radiation are one method to assess strength loss. Often, flights can carry specimens in the flight train to expose new materials in flight-like environments. Finally, after parachutes are retired, pull-to-failure testing on large sample sizes can be completed to establish lifetime strength losses as a function of exposure and location on the parachute.

6. Flight and Mission Closeout Considerations

If the flight or mission involves a mishap, anomaly, or failure, an investigation panel comprising representatives from Quality, Engineering, and Production/Mission services can be established to determine the causes and make improvements to the process for future flights. Every detail about the materials, production assembly, launch execution, flight performance, recovery, and flight articles must be reviewed and analyzed for any off-nominal occurrences that could have led to the issue. Quality teams should work closely with flight performance engineers to determine if any flight data can identify the type of failure. Obvious signs such as failure through the tropopause, or a burst at float, or a large leak can be seen in the flight data. This investigation of documents and articles typically rules out potential contributors and leads the team to focus on the areas of interest suspected to be the root cause.

Interviewing personnel involved in the build and launch of the defective product or process will also provide clues to any process failure or critical observation that may have occurred. It is essential to approach performers positively to foster honesty and a culture free of fear. If flight articles are recovered, a physical inspection and reconciliation against records should be conducted, if possible. Inspection of balloon critical areas, such as gore-to-seam interfaces, installed accessories, and metallic interfaces to soft goods, should be conducted, as these items have been assembled beyond the parent material. All findings should be compiled and then reviewed to identify corrective and preventive actions. Customer disclosure of findings and resulting actions should occur to foster collaborative, continuous improvement. Defects, failures, and mishaps, although unfortunate, provide the balloon manufacturer with an opportunity to learn and improve. Maintaining this state of mind keeps the investigation and revelation of root causes manageable for all stakeholders.

7. Conclusions

The high-altitude ballooning industry plays a vital role by providing unique solutions across sectors such as science, government, and commercial applications. Balloons will continue to serve as workhorse vehicles for high-altitude operations, offering versatile and cost-

effective platforms. This chapter outlined the diverse markets and the high-level approaches to serving them, with special consideration given to philosophy and the specialized technical and professional aptitudes required. Regardless of the specific business objectives or program needs, the industry must be prepared to address a range of technical challenges. Having a strong baseline of capability provides the pathway to effectively solve these challenges and deliver innovative solutions to meet the industry's evolving needs.

References

[1] A. D. Kerr and H. Alexander, "On a Cause of Failure of High Altitude Plastic Balloons," New York University; Dept. of Aeronautics and Astronautics, 1968, pp. 1–28.

[2] J. F. Dwyer, "Polyethylene Free Balloon Design from the Perspectives of User and Designer," Air Force Systems Command, 1982, pp. 1–119.

[3] R. A. Andrews, P. J. Cannon, T. W. Markhardt, M. West, and J. A. Winker, "Analysis of Ascent Failures and Recommendations for Heavy Lift Scientific Balloons," Raven Industries, 1985.

[4] "1985 Proposed Heavy Payload Standard Balloon Designs," 1985.

[5] I. S. Smith, "Advancements in NASA Balloon Research and Development," *Advances in Space Research*, vol. 17, no. 9, pp. 37–44, 1996, doi: 10.1016/0273-1177(95)00674-4.

[6] I. S. Smith, "A Stress Index Model for Ascending Balloons," Ocean City, MD, U.S.A., 1986, doi: 10.2514/6.1986-2566.

[7] I. S. Smith, "A Stress Index Model for Balloon Design," *Advances in Space Research*, vol. 7, no. 7, pp. 19–24, 1987, doi: 10.1016/0273-1177(87)90004-4.

[8] CSBF, "Specifications for Band Sealing of Polyethylene Zero-Pressure Balloons," NASA Balloon Program Office, 2014.

[9] J. A. Winker, "Progress in Scientific Balloon Materials and Manufacturing Technology," *Advances in Space Research*, vol. 7, no. 7, pp. 25–32, 1987, doi: 10.1016/0273-1177(87)90005-6.

[10] I. S. Smith, "NASA Balloon Design and Flight - Philosophy and Criteria," *Advances in Space Research*, vol. 13, no. 2, 1993, doi: 10.1016/0273-1177(93)90276-H.

[11] CSBF, "Standard Technical Specifications for Polyethylene Zero-Pressure Balloons," NASA Balloon Program Office, 2014.

[12] A. Alexander, M. Alvidrez, W. Beg, Z. Benezet-Parsons, L. Bouygues, S. Coriell et al., "Loon Library: Lessons from Building Loon's Stratospheric Communications Service," Loon LLC, August 2021, https://storage.googleapis.com/x-prod.appspot.com/files/The%20Loon%20Library.pdf

[13] "Scientific Balloons - NASA." [Online]. Available: https://www.nasa.gov/scientificballoons/. [Accessed: Oct. 26, 2025].

[14] "High Altitude Student Platform (HASP)." [Online]. Available: https://sg-webserver.phys.lsu.edu/. [Accessed: Oct. 26, 2025].

[15] *JPL's Venus Aerial Robotic Balloon Prototype Aces Test Flights*. Retrieved from JPL: https://www.jpl.nasa.gov/news/jpls-venus-aerial-robotic-balloon-prototype-aces-test-flights

[16] C. Duhigg, *The Power of Habit: Why We Do What We Do in Life and Business*. New York: Random House Trade Paperbacks, 2014.

[17] A. S. Redner, "Nondestructive Evaluation Using Polarized Light," *Materials Evaluation*, vol. 53, no. 6, pp. 642–644, 1995.

[18] E. Lamkanfi, W. Van Paepegem, J. Degrieck, C. Ramault, A. Makris, and D. Van Hemelrijck, "Strain Distribution in Cruciform Specimens Subjected to Biaxial Loading Conditions. Part 1: Two-Dimensional versus Three-Dimensional Finite Element Model," *Polymer Testing*, vol. 29, no. 1, pp. 7–13, 2010, doi: 10.1016/j.polymertesting.2009.08.009.

[19] E. Lamkanfi, W. Van Paepegem, J. Degrieck, C. Ramault, A. Makris, and D. Van Hemelrijck, "Strain Distribution in Cruciform Specimens Subjected to Biaxial Loading Conditions. Part 2: Influence of Geometrical Discontinuities," *Polymer Testing*, vol. 29, no. 1, pp. 132–138, 2010, doi: 10.1016/j.polymertesting.2009.10.002.

[20] J. L. Rand, "The Biaxal Behavior of the ULDB Balloon Film," Winzen Engineering Inc, 2004.

[21] J. Rand and D. Grant, "Optical Measurement of Biaxial Strain in Thin Film Polymers," *Nontraditional Methods of Sensing Stress, Strain, and Damage in Materials and Structures*, pp. 123–137, 2009, doi: 10.1520/stp11896s.

[22] H. Brice, J. Ketcham, and M. Short, "Effects of Radiation on Mechanical Behavior of Crystalline Materials," 2008.

[23] P. J. Hendra, H. P. Jobic, and K. Holland-Moritz, "Low Temperature Crystallization in Polyethylene and the Value of Tg," *Journal of Polymer Science: Polymer Letters Edition*, vol. 13, no. 6, pp. 365–368, 1975, doi: 10.1002/pol.1975.130130610.

[24] J. A. Brydson, *Plastics Materials*. Butterworth-Heinemann, 1999, doi: 10.1016/B978-075064132-6/50047.

[25] ASTM International, "ASTM D746-20 Standard Test Method for Brittleness Temperature of Plastics and Elastomers by Impact," West Conshohocken, PA, 2020, doi: 10.1520/D0746-20.

[26] V. Thomas, "A Comparative J-Integral Fracture Toughness Study of Six Polyethylene Balloon Films," NASA Balloon Program Office, Wallops Island, 1994.

[27] J. T. Tielking, "A Fracture Toughness Test for Polymer Film," *Polymer Testing*, vol. 12, no. 3, pp. 207–220, 1993, doi: 10.1016/0142-9418(93)90003-8.

[28] M. I. T. Opencourseware, "Plasticity and Fracture of Microelectronic Thin Films (SOI - Silicon on Insulator)," 2008.

[29] "Material Strength Properties of Winzen Stratofilm," Winzen Engineering Inc, 1971.

[30] Y. Nakamura, "Antistatic Agents for Polyethylene Film and Sheets."

[31] K. B. Walters, D. W. Schwark, and D. E. Hirt, "Surface Characterization of Linear Low-Density Polyethylene Films Modified with Fluorinated Additives," *Langmuir*, vol. 19, no. 14, pp. 5851–5860, 2003, doi: 10.1021/la026293m.

[32] F. Khoury, J. M. Crissman, B. M. Fanconi, H. L. Wagner, and L. H. Botz, "Structure and Properties of Polyethylene Films Used in Heavy Lift Balloons," NAS 1.26:176227, March 1985.

[33] M. J. Fedro and K. Willden, "Characterization and Manufacture of Braided Composites for Large Commercial Aircraft Structures," June 01, 1992.

[34] D. G. Baird, *Polymer Processing: Principles and Design, 2nd Edition*. Wiley.

[35] B. S. Kumar, S. Sreenivasan, J. V. S. Rao and R. K. Manchanda, "Mechanical properties of ANTRIX balloon film and fabrication of single cap large volume balloons," *Advances in Space Research*, vol. 42, no. 10, pp. 1691-1697, 2008.

[36] B. Krisnamurti, H. Irawati, M. A. E. Hafizah and A. Manaf, "Blow-up ratio's effect on LLDPE film's properties with different material types," in *THE 18TH JOINT CONFERENCE ON CHEMISTRY 2023 (18th JCC - 2023): Chemistry for Sustainable Development*, Semarang, Indonesia, 2025.

[37] F. Cuesta, A. M. Camacho and E. M. Rubio, "Influence of the Main Blown Film Extrusion Process Parameters on the Mechanical Properties of a High-Density Polyethylene Hexene Copolymer and Linear Low-Density Polyethylene Butene Copolymer Blend Used for Plastic Bags," *Applied Sciences,* vol. 13, no. 22, p. 12164, 2023.

[38] M. Nouman, J. Saunier, E. Jubeli and N. Yagoubi, "Additive blooming in polymer materials: Consequences in the pharmaceutical and medical field," *Polymer Degradation and Stability,* vol. 143, pp. 239-252, 2017.

[39] Brighton Science, "How to Control Additive Blooming in Polymer Films," Brighton Science, June 2020. [Online]. Available: https://www.brighton-science.com/blog/how-to-control-additive-blooming-in-polymer-films.

[40] SpecialChem, "Troubleshooting Antioxidant Blooming and Migration in Polymers," SpecialChem, 28 December 2023. [Online]. Available: https://www.specialchem.com/polymer-additives/guide/antioxidant-blooming.

[41] S. R. Fischer, "Service life of stratospheric balloon gondola recovery parachutes - Part 1," in AIAA AVIATION Forum, Denver, CO, 2017.

[42] R. A. Segars, "The degradation of parachutes: age and mechancial wear," NATICK, Natick, MA, 1992.

Chapter 9
Zero-Pressure Balloon Design

Ethan A. Chaffee[1]

[1] World View Enterprises, Inc., Program Manager, Programs Department

Table of Contents

1. Introduction 6

2. Theory of Natural Shape for Zero-Pressure Balloons 6

3. Zero-Pressure Balloon Design Equations 11

4. Balloon Performance Metrics 16

5. Balloons at Off-Design Conditions 22

5.1. Balloon Shapes and Stresses Below the Design Altitude..... 22

5.2. Cutting the Duct to Change the Float Altitude..... 25

6. Considerations of Other Balloon Designs 26

7. Conclusions 27

Appendix 9-A..... 28

References..... 28

Table of Figures

Figure 9-1. Representative drawing of a natural-shape, zero-pressure balloon configuration with the associated components identified [2].. 7

Figure 9-2: Example zero-pressure apex fitting (left) and base fitting (right) 8

Figure 9-3. Example of horse-tail ducts on a NASA zero-pressure balloon 8

Figure 9-4. Comparison of a partially inflated (left) and fully inflated (right) profile for a natural-shape, zero-pressure balloon envelope [1]. 10

Figure 9-5. Illustration to describe the forces on the inside of a pressurized sphere..... 17

Figure 9-6. The shape profile at various buoyancy ratios below the design altitude for a $\Sigma = 0.2$ natural-shape balloon [5]. 24

Figure 9-7. Zero-pressure level in balloons below their design altitude as a basis for cutting the vent ducts [1]..... 26

Table of Tables

Table 9-1. Balloon shape parameters below its design altitude for a $\Sigma = 0.2$ natural-shape balloon [4]. 23

Table of Symbols

Symbol	Definition	Dimension
A	Surface area of the balloon envelope	L^2
$\bar{A}$	Non-dimensional surface area parameter	-
b	Specific buoyancy of a lifting gas, the potential lifting force of gas per unit volume	$M*L^{-2}*T^{-2}$
b_d	Specific buoyancy at the design altitude	$M*L^{-2}*T^{-2}$
D	Diameter of the balloon envelope	L
$\bar{D}$	Non-dimensional diameter parameter	-
GI	Gross inflation force, total potential lifting force	$M*L*T^{-2}$
GW	Gross weight, total weight of a balloon system exclusive of the lift gas	$M*L*T^{-2}$
H	Height of the balloon envelope	L
$\bar{H}$	Non-dimensional height parameter	-
L	Suspended load, load carried at the bottom of the balloon	$M*L*T^{-2}$
$\bar{L}$	Load ratio, the ratio of the suspended load to the gross weight of the system	-
m_{sus}	Suspended mass, total mass carried at the bottom of the balloon	M
N_g	Number of Gores	-
P	Pressure, the force exerted by a fluid dependent on density and height	$M*L^{-1}*T^{-2}$
S	Gore length, distance measured along the gore	L
$\bar{S}$	Non-dimensional gore length	-
SF	Shape factor, defines the relationship between the load ratio and the Σ_F parameter	-
T	Total meridional tension, the combined forces along the meridional direction of the envelope	$M*L*T^{-2}$
$\bar{T}$	Non-dimensional meridional tension	-
T_{LT}	Tension per load tape	$M*L*T^{-2}$
V	Volume, the amount of space that is occupied by the envelope of the balloon	L3
w	Average areal weight, total weight of a unit area of balloon film	$M*L^{-1}*T^{-2}$
W_{max}	Maximum gore width	L
Z	Altitude, height above mean sea level	L

Symbol	Definition	Dimension
κ	Dimensionless constant; $\kappa = (2\pi)^{-1/3}$	-
λ	Natural length, a length unit defined so that λ^3 is the volume of gas required to lift the payload alone	-
λ_F	Characteristic length, a length unit defined so that ${\lambda_F}^3$ is the volume of gas required to lift the gross weight	-
Σ	Non-dimensional film weight parameter, ratio of skin weight to buoyancy and suspended load	-
Σ_F	Non-dimensional film weight parameter, ratio of skin weight to buoyancy and gross weight	-

1. Introduction

From the original "Scientific Ballooning Handbook" chapter regarding "Balloon Design Considerations" [1], the authors provide the derivation for a set of differential equations to determine the characteristics of various balloon shapes. The information provided in the source material defines key processes for understanding the design of balloon envelopes and the theory behind the parameters affecting balloon envelopes in flight. As the successor to the original handbook, the intention of this updated chapter is to provide the reader with a concise and summarized process for calculating a preliminary balloon design along with its associated geometric features. The contents of this chapter provide a guide to the calculations that define the shapes and stresses of natural-shape, free balloon systems, relying on the extensive research and development that has been conducted on the subject. The contents dive into the theory of balloon design and establish practices that have since been expanded to define current standard procedures. To expand upon the theory of balloon design calculations, readers should refer to the original handbook content in addition to the subsequent analysis published on these topics for supplemental background as desired.

The contents of this chapter focus on natural-shape, zero-pressure balloons, which have become standard among the high-altitude scientific community. Brief considerations and references for further research regarding alternative configurations of free balloons are provided in section 6. First, some initial theory on the forces and functions of high-altitude balloons are provided for context before introducing an abbreviated process for determining the size and shape of a natural-shape, zero-pressure balloon envelope. For additional context, the reader should also refer to Chapter 1 regarding the history of balloon development and the highlights of the significant changes and contributions that have been made since the publication of the original handbook.

2. Theory of Natural Shape for Zero-Pressure Balloons

It is important to first define the key theories behind the design of zero-pressure balloons. In Figure 9-1, the components of a typical envelope for a zero-pressure balloon are identified to provide the context for the design equations which will be presented throughout this chapter. The elements shown in the graphic below are not all necessary for the construction of a fully functional balloon envelope. However, each element serves an important purpose to the performance of a high-altitude system. A brief description of each component is provided below.

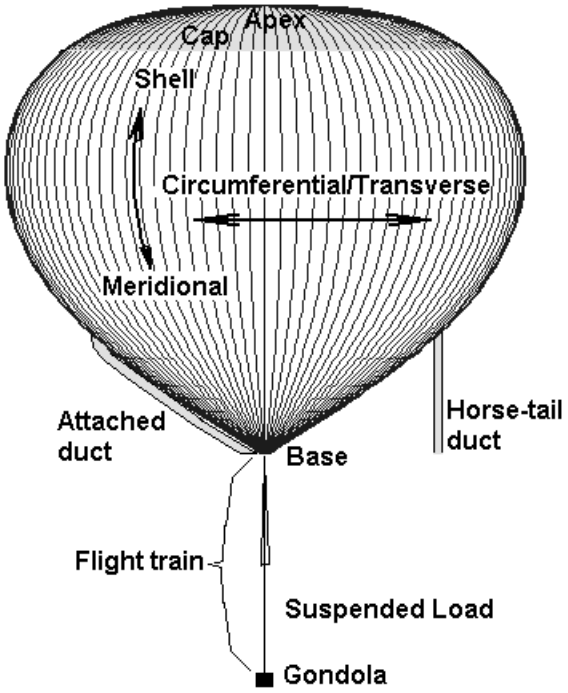


Figure 9-1. Representative drawing of a natural-shape, zero-pressure balloon configuration with the associated components identified [2].

- Shell – The shell is the gas barrier that holds the lift gas inside the envelope.
- Gore – A gore is an individual panel that is used to construct the shell. Gores are sealed together in a rotationally axisymmetric pattern to create the shape of the envelope. The gore pattern is tailored to provide the natural shape and is terminated in a rigid fitting at both the apex and base of the balloon, see Figure 9-2.
- Load Tape – Load tape is the primary structural element integrated with each seal of the gore. The load tape is fiber-reinforced to provide strength to support the system.
- Caps – Caps are an optional, additional layer of material built into the top of the balloon to manage stress on the envelope. Caps allow designers to build lighter balloons using thinner material towards the base while reinforcing the areas where stresses are concentrated at the apex.
- Exhaust Duct – An exhaust is a vent connected to the envelope and open to the atmosphere that allows excess lift gas to escape the envelope if it becomes over-pressurized. A duct can either be "attached", meaning directly connected to the envelope over the length of the duct, or "hanging" as shown in Figure 9-3, hanging from the pass-through point on the envelope.
- Inflation Tube: polyethylene tube inserted into the sidewall of the balloon to facilitate filling the balloon with lift gas.



Figure 9-2: Example zero-pressure apex fitting (left) and base fitting (right)

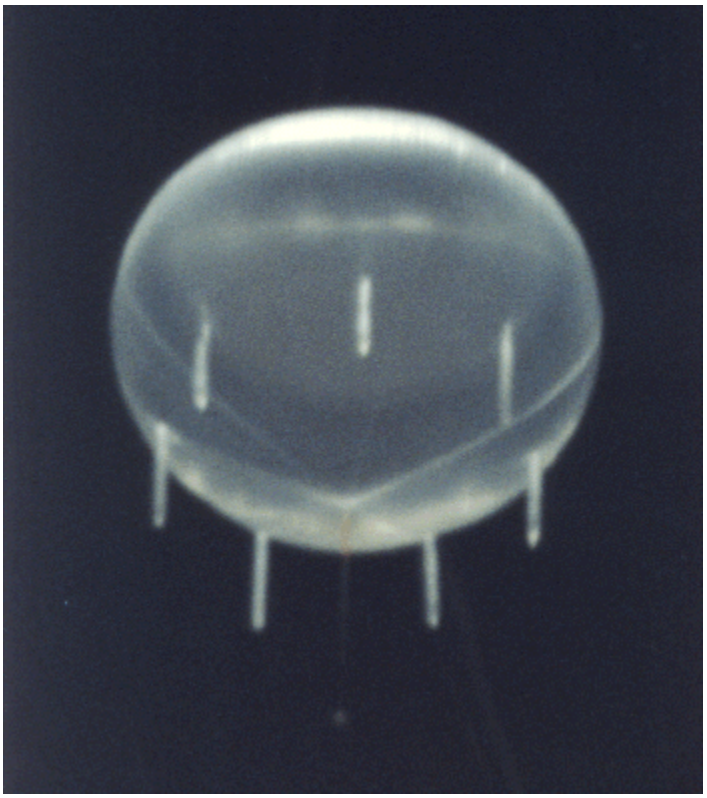


Figure 9-3. Example of horse-tail ducts on a NASA zero-pressure balloon

Courtesy: NASA Balloon Program

A modern plastic balloon is essentially a shell structure of material that is incapable of carrying compression and has a small but appreciable weight. Each element of the skin is in static balance due to its tangential tension and the normal pressure difference between the inside

and outside. This pressure difference can also be negative in gas below the level of zero-pressure difference.

A balloon's profile or axial section was formerly arbitrarily assumed and commonly designed to be a circle. A free balloon was referred to as a spherical balloon to distinguish it from an elongated kite balloon or a dirigible balloon (also known as an airship). Even the early netless balloons were close to spherical, with long footropes attached to loading points near the equator [3]. Although the spherical design has the greatest stress to volume shape with a fairly simple pattern and design, in practice balloons never inhabited the full spherical shape during flight. As a result, over time the spherical concept was slowly replaced in favor of the sphere-on-cone shape of the early plastic designs that more effectively mimicked balloon shape in flight. Still, its structural limitations for high-altitude use have already been recognized.

The so-called natural shape of the freely vented balloon dates back to 1934, after the failure of the Explorer I balloon. This failure was the stimulus for a shape-and-stress analysis of a partially inflated balloon [4]. This study at General Mills [5] resulted in a mathematically derived curve that was applied to the designed profile of the entire balloon. In the meantime, engineers Arnstein and Swan at Goodyear simulated a form of the same curve by a system of weights and pulleys acting on a chain [6]. Further development of this type of profile resulted in the natural shape becoming the standard for vented plastic balloons with only minor variations in the design geometry due to skin weight, vent location, and load attachment.

Experience shows that it is not the full balloon envisioned by the design geometry that usually poses the most critical problem. The critical condition in any high-altitude operations almost invariably occurs, as it did with the old Explorer I, when the balloon is inflated to a small fraction of its design volume. Under these conditions, the netless balloon of the type here considered takes a natural shape over a substantial portion of its surface, but this is a natural shape only in the mathematical sense, as defined by Equation (9-2). It has little apparent resemblance to the full profile of Figure 9-4 and is highly variable, as changes in altitude alter the volume ratio.

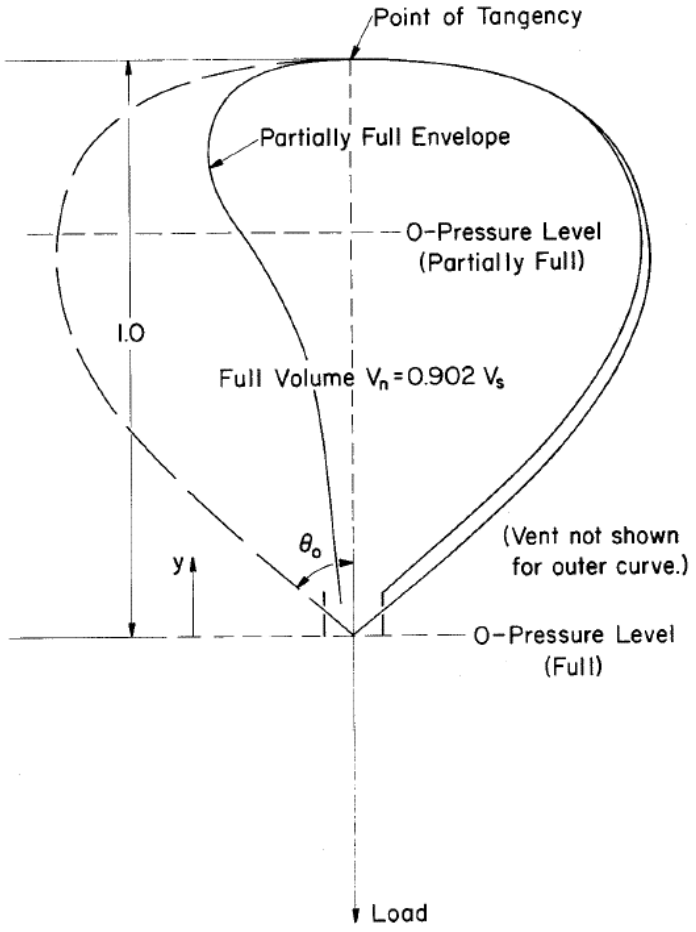


Figure 9-4. Comparison of a partially inflated (left) and fully inflated (right) profile for a natural-shape, zero-pressure balloon envelope [1].

In a balloon carrying the usually concentrated payload, this gravity load must, of course, reappear in the axial component of circumferentially integrated (total) meridional tension adjacent to the load attachment level, where such stress must also be in normal balance with the local gas pressure. Since there must always be stress in the meridional direction, it is clear that any slack to accommodate a less-than-full condition must be in the circumferential direction. It is also clear that with gas pressure normal to the surface, only the skin weight or other applied load can change the total tension within a slack portion of the balloon at a given altitude. Thus, in such a portion of the balloon, aside from skin weight, the stress or tension, t_m, per unit of horizontal circumference, varies inversely with the circumference.

$$t_m = \frac{G}{2\pi \cos\theta_0} = \frac{bV}{2\pi \cos\theta_0} = pR_m \qquad (9\text{-}1)$$

where G is the total weight carried at the concentration point, also the same stress is all that carries the pressure, which in this simplified

case varies as the gas head measured from the level of zero-gauge pressure, or $p = by$. Then $t_m \propto \frac{1}{x}$ and $p \propto y$ or

$$\frac{p}{t_m} = \frac{1}{R_m} = Kxy = \frac{2\pi xy}{V}\cos\theta_0 \qquad (9\text{-}2)$$

where x and y are the coordinates of the profile curve, $1/R_m$ is the meridional curvature at the same point, and K is a constant applied to a particular slack portion of a balloon, which is quantitatively determined by the design and operational conditions. For finite skin weight, the effective pressure, p, must include the normal weight component of unit skin weight and the integrated meridional component of skin weight t_m.

This is the basic equation of what has come to be known as the natural shape. Even in its elementary form for weightless skin carrying zero circumferential stress, the integrated curve of the profile can take an infinite variety of shapes depending on the starting coordinates and slope, and on the value of K. Several examples shown in literature, but a particular shape of interest studied by Smalley [24] was approximately the profile of a gas bubble in a partially-filled balloon designed as a sphere. Here, on the left, the circumferential elements of the skin are slack below a certain critical level where the designed circle and the natural shape come tangent to each other. Above this level, the envelope is free to fill out to its full designed shape in what has been called the taut cap, and the maximum stress is determined by the meridional stress at its edge.

The next step in design development came with the thought that the natural shape, prevailing over most of the surface during most of an ascent to high altitude, might logically be made the designed shape of the full balloon. In other words, for a balloon vented to the atmosphere, the circumferential stress is of so little use that it may as well be assumed of no use, and the balloon is designed accordingly. This assumption also fitted well the commonly prevailing condition of meridional gores joined by relatively low-strength, unreliable seams carrying meridional reinforcing tapes.

3. Zero-Pressure Balloon Design Equations

The equations highlighted in this section provide a characterization of the high-level parameters for a zero-pressure balloon design. Rodger Farley provides the process for calculating the preliminary design to determine an initial estimate of the geometry of a zero-pressure envelope, provided operational requirements [2]. The resulting calculation yields parameters only for the envelope geometry. Calculations to determine the design of the other associated components (e.g. tendons, fittings, caps) are omitted.

To begin the design process, one starts with the most essential parameters: the suspended load the balloon will carry (not including the weight of the balloon itself), defined as L, and the desired altitude, Z, that the balloon can achieve. Specific buoyancy (the amount of lift provided by a unit volume of lift gas), is required to be known. To provide a generalized method for determining the specific buoyancy (b) for the operational parameters, Equation (9-3) is provided below. The equation is derived using the 1962 Standard Atmosphere [7] and assumes that the balloon conditions (pressure and temperature) equal those of the atmosphere. Although in reality, there may be a slight gradation throughout the balloon, this will not affect the calculation significantly, so the assumption holds for a zero-pressure balloon. This equation also only applies to the use of helium as a lift gas, where the altitude, Z, is in meters.

$$\begin{aligned} b(Alt) &= -1.2 + 19 * e^{-0.9*10^{-4}*(Z+5500)}\ [N/m^3] && 0 < Z < 11000 \\ b(Alt) &= 0.003 + 28 * e^{-1.61*10^{-4}*(Z+2600)}\ [N/m^3] && 11000 < Z < 40000 \end{aligned} \tag{9-3}$$

Due to the principle of buoyancy, the volume of helium that must displace air per unit weight is a function of altitude given a standard atmosphere. Thus, although neither the volume of the balloon nor the weight of the system has been calculated, the film and load tape average areal density (w) can be determined using the altitude. The average areal density is a measure of the envelope weight per unit area. The equations below were defined from historical data for various operational conditions across standard NASA mission profiles. The distinction between "light" and "heavy" systems in the equations below is not clearly defined. Generally, if a system would require more than one cap, it could be classified as a "heavy" system.

$$\begin{aligned} w(Alt) &= 0.77 - (1.25 * 10^{-5} * Z)\ [N/m^2] \quad \text{"Light"} \\ w(Alt) &= 1.43 - (2.7 * 10^{-5} * Z)\ [N/m^2] \quad \text{"Heavy"} \end{aligned} \tag{9-4}$$

Equation (9-5) can be used to define the load ratio ($\bar{L}$). The load ratio defines the relationship between the total gross weight and the suspended load. The equation was derived through early research related to suspended loads and non-dimensionalized forces to provide a relationship between the shape and load parameters [2]. The equation for the load ratio requires some iterative calculations as it contains a circular reference to itself. It is typically recommended to start with a load ratio of 0.6 and iterate the calculation until the solution converges.

$$\bar{L} = 1 - \left(\frac{SF}{\kappa} * \frac{w}{b} * \left(\frac{\bar{L}}{L} * b \right)^{1/3} \right) \tag{9-5}$$

There are two constant parameters in the load ratio equation that have not yet been defined. First is the shape factor (SF), which defines the general relationship between the load ratio and the sigma value (see equation (9-9) for reference). The shape factor values are defined below for various typical envelope configurations defined from the equations outlined by Farley [2]. These values are derived from the relationship between shape and size characteristics using linear regression.

- Sphere: SF = 2.62074
- Zero-pressure Natural-Shape: SF = 2.682
- Super-pressure Pumpkin: SF = 2.738

The constant value (κ) in the equation for the load ratio is defined as follows:

$$\kappa = \left(\frac{1}{2\pi}\right)^{1/3} \tag{9-6}$$

Now, the estimated gross weight of the system can be defined from the load ratio and the suspended load value:

$$GW = \frac{L}{\bar{L}} \tag{9-7}$$

At equilibrium float conditions, the gross weight is equal to the gross inflation ($GI = GW$). Using the gross inflation, the envelope volume (V) is calculated based on the specific buoyancy at the operational conditions.

$$V = \frac{GI}{b} \tag{9-8}$$

Next, a series of non-dimensionalized parameters are defined that characterize the shape of the envelope given the load conditions calculated previously. This work by Farley builds upon the concept of the sigma tables previously outlined by Justin Smalley, which relates the load to the shape of the envelope [4]. Smalley had previously defined this relationship based solely on the suspended load. Farley, however, defines a new sigma value (Σ_F) as a function of the gross inflation. Use of Farley's sigma values and subsequent design equations will be utilized here. The reader is encouraged to refer to the previous handbook version for a discussion of the Smalley method [8] [4].

$$\Sigma_F = \frac{1 - \bar{L}}{SF} \tag{9-9}$$

Based on the same concept of using gross inflation (where volume is a function of gross inflation), Farley defined a "characteristic length" (λ_F) as:

$$\lambda_F = V^{1/3} \tag{9-10}$$

Now, using the sigma value, the following set of equations was defined for determining the geometric parameters of the envelope for gore length (S), diameter (D), height (H), surface area (A), and tension (T). The bar designation above the variable symbols indicates non-dimensionalized values.

- The calculation for the non-dimensional gore length parameter ($\bar{S}$) is defined as:

$$\bar{S} = 1.994 - (0.336 * \Sigma_F) - (0.049 * {\Sigma_F}^2) \tag{9-11}$$

- The calculation for the non-dimensional diameter parameter ($\bar{D}$) is defined as:

$$\bar{D} = 1.305 + (0.164 * \Sigma_F) + \left(0.479 * {\Sigma_F}^2\right) - \left(1.478 * {\Sigma_F}^3\right) + (3.667 * {\Sigma_F}^4) \tag{9-12}$$

- The calculation for the non-dimensional height parameter ($\bar{H}$) is defined as:

$$\bar{H} = 1.275 - (0.445 * \Sigma_F) - (1.496 * {\Sigma_F}^2) \tag{9-13}$$

- The calculation for the non-dimensional surface area parameter ($\bar{A}$) is defined as:

$$\bar{A} = 4.913 + (2.598 * (\Sigma_F - 0.05)^3) \tag{9-14}$$

- The calculation for the non-dimensional meridional tension parameter ($\bar{T}$) is defined as:

$$\bar{T} = 1.556 - (0.66 * \Sigma_F) - (1.59 * {\Sigma_F}^2) \tag{9-15}$$

The characteristic length parameter is then used to convert the non-dimensional geometric parameters to the dimensionalized values. The relationships between the non-dimensional shape parameters and the dimensionalized values are provided below. These calculations result in the geometric parameters that define the generalized shape of the balloon envelope.

$$S = \bar{S} * \lambda_F \tag{9-16}$$

$$D = \bar{D} * \lambda_F \tag{9-17}$$

$$H = \bar{H} * \lambda_F \tag{9-18}$$

$$A = \bar{A} * {\lambda_F}^2 \tag{9-19}$$

$$T = \bar{T} * b * {\lambda_F}^3 \tag{9-20}$$

Additional parameters defining the characteristics of the envelope can also be calculated from the values determined above. First, one can calculate the differential pressure at the apex of the envelope. This calculation assumes that the envelope is fully inflated. If the zero-pressure line is above the bottom of the balloon, then the height in Equation (9-21) is the distance from the zero-pressure line to the apex fitting.

$$\Delta P = H * b \tag{9-21}$$

The number of gores can also be determined. For a conventional zero-pressure design with flat-paneled gores connected to form its shape, the number of gores needed is based on the circumference of the envelope divided by the maximum width of each gore panel. The gore count should be rounded up to the nearest whole number, given that having a partial gore geometry in the envelope is impractical.

$$N_g = \frac{\pi * D}{W_{max}} \tag{9-22}$$

Finally, the tension per load tape is calculated by dividing the total tension by the number of load tapes. This value is important for analyzing the configuration of the load tape for the envelope design.

$$T_{LT} = \frac{T}{N_g} \tag{9-23}$$

These equations outline the preliminary design of a natural-shape, zero-pressure balloon envelope. There are additional parameters for components of the envelope, highlighted elsewhere, which are not captured here. The reader is encouraged to explore the available literature regarding a more detailed analysis of zero-pressure balloon design to provide a full encapsulation of the design process. An example problem

to demonstrate the application of the design process is provided in the appendix (Appendix 9-A).

4. Balloon Performance Metrics

During the catastrophic failures that plagued the ballooning community in the 1970s and 1980s (refer to Chapter 1 for background), it became necessary to evaluate the design and performance of high-altitude balloon systems analytically and better predict the success of flight operations before launch. To do so, the team that executed the investigation initiated at the time of the failures developed predictive metrics to assess the success and survivability of balloon designs.

Various metrics describe the balloon, flight configuration, and performance. Three specific parameters related to balloon design and performance are considered here: Launch Stress Index (LSI), Ascent Stress Index (ASI), and Dynamic Loading (F_d). All three parameters are defined to predict the performance of a balloon design in operation and provide guidelines for design criteria that have been determined through flight analysis. LSI was originally intended to determine the necessary cap thickness during the design stage of the balloon build. The ASI was intended to determine the cap length during the design phase. These two metrics looked at two different stress events. The LSI focused on the bubble while in the spool and the ASI on the bubble as it ascended and expanded into its full design shape [9]. Dynamic loading captures the stress state of the balloon envelope at launch which can provide significant loading to the balloon film. The background and equations for each parameter are explored further below.

The first published mention of Launch Stress Index to approximate film stresses during launch/ascent and particularly 'while the balloon is in the troposphere' appeared in the report *Strato-Lab Development* by R. L. Schwoebel in 1956 [10], but it wasn't until 1986 that this metric began to be used in both cap design and in discussions of potential flight reliability. It has since been determined that the LSI cannot accurately predict flight performance [11].

Schwoebel assumes that the gas bubble approximates a sphere (Figure 9-5) and that the "circumference of the sphere is equivalent to the amount of gas sustaining the gross lift [12]."

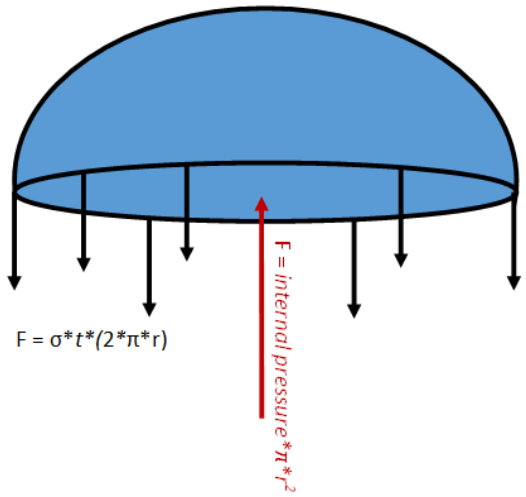


Figure 9-5. Illustration to describe the forces on the inside of a pressurized sphere.

The following equation represents the force on the balloon material and is presented in its original form using United States customary units:

$$f = \frac{2}{3}(b)^{1/3}\left(\frac{3G}{4\pi}\right)^{2/3} \qquad (9\text{-}24)$$

where:
f = load per unit length (lb/ft) of balloon material surrounding the bubble of gas
b = lift per unit volume of the inflation gas (lb/ft^3) at the altitude of the launch site, and
G = gross lift (or gross inflation) of gas within the balloon (lb)

Schwoebel then rearranges Equation (9-24) to solve for gross lift and substitutes $(\sigma = f/t)$ for film stress which results in the following:

$$G = \frac{4}{3}\pi\left(\frac{18\sigma t}{b^{1/3}}\right)^{3/2} \qquad (9\text{-}25)$$

Where:
σ is film stress (lb/in^2), and
t is film thickness (inches).

Schwoebel uses a buoyancy value for β equivalent to the lift of 1 ft^3 of He at an altitude of 1000 ft to distill Equation (9-25) to:

$$G = 1260(\sigma t)^{3/2} \qquad (9\text{-}26)$$

and rearranged to get the equation in terms of stress:

$$\sigma = \frac{(G)^{2/3}}{(0.1167)t} \tag{9-27}$$

Equation (9-27) is known as the Launch Stress Index and was originally designed to determine the ideal cap thickness.

The complete derivation of LSI is as follows (using SI units). First, the spherical bubble force is:

$$F_s = \sigma t(2\pi r) \tag{9-28}$$

Next, buoyant force is defined as:

$$F_B = g(\rho_{air} - \rho_{He})V \tag{9-29}$$

Third, gross inflation, G, is defined as:

$$G = bV \tag{9-30}$$

where:

$$b = g(\rho_{air} - \rho_{He}) \tag{9-31}$$

At launch, the spherical bubble force, F_S, equals the buoyant force, F_B, and the gross inflation, G. The final equation should be expressed in terms of G, b, and thickness t. Knowing that $F_S = F_B$ and gross inflation equals the buoyant force at launch:

$$G = \sigma t(2\pi r) \tag{9-32}$$

$$G = b * V = b\left(\frac{4}{3}\right)\pi r^3 \tag{9-33}$$

Set both Equations (9-32) and (9-33) equal for r:

$$G/_{(2\pi\sigma t)} = r \tag{9-34}$$

$$\left(\frac{3}{(4\pi)}\right)^{\frac{1}{3}}\left(\frac{G}{b}\right)^{\frac{1}{3}} = r \tag{9-35}$$

Set Equation (9-34) equal to Equation (9-35):

$$\left(\frac{3}{(4\pi)}\right)^{\frac{1}{3}}\left(\frac{G}{b}\right)^{\frac{1}{3}} = \frac{G}{(2\pi\sigma t)} \tag{9-36}$$

Rearrange Equation (9-36) to get an expression in terms of launch stress, σ:

$$\sigma = \left(\frac{\left(G^{2/3} * b^{1/3}\right)}{t}\right) * \left(\left(\frac{4\pi}{3}\right)^{\frac{1}{3}}\left(\frac{1}{2\pi}\right)\right) = \left(\frac{\left(G^{2/3} * b^{1/3}\right)}{t}\right) * 0.25656 \tag{9-37}$$

where G is gross inflation (N), $b = g(\rho_{air} - \rho_{He})$ with respect to launch location, and t is the total thickness of shell + caps (m).

A report by Douglas Bell in 1994 described the maximum allowable LSI as 11.0 mPa (1600 psi) for volumes less than 0.11 mcm (4 mcf) and 9.7 mPa (1400 psi) for those greater than or equal to 0.11 mcm (4 mcf). The test flights mentioned in the report suggest that the balloons could handle 12.4 mPa (1800 psi) LSI and 26.2 mPa (3800 psi) ASI [30]. The balloon design requirement documented in "Technical Specifications for Polyethylene Zero Pressure Balloons Revision C," published by CSBF in 2014, puts a limit on the LSI for qualified zero-pressure balloons at 12.4 mPa (1800 psi) (except the 34 Heavy at 10.0 mPa (1450 psi)).

Equation (9-37) solves the launch stress in Pascals (Pa) which can then be converted to psi for comparison to past values. A simplified version of LSI, represented by Equation (9-28), is used along with the nominal balloon weight and reported payload weight to verify the LSI remains under the 12.4 mPa (1800 psi) limit for launch. However, this implies that the science team is 100% accurate in their weight estimation before final compatibility is complete and that the mass of helium used for inflation is known at the time of launch and provides exactly 10% free lift.

Ascent Stress Index was developed to provide a model for assessing the relative stress magnitudes along the balloon's gore as a function of altitude. According to work summarized by Steve Smith, "A data base of over 550 balloon flights was used to determine if a correlation exists between a balloon's stress state and performance" [13]. The challenge at the time for such an analysis was the determination of the shape of an ascending balloon at a given altitude, which has since become much easier with modern analysis tools and calculations (see the sigma tables and calculations for details [3]). To simplify these calculations however, the team determined a process for comparing the design conditions to the discrete conditions at any given time. Equation (9-

38) determines the effective sigma shape (Σ_S) due to load and gross inflation. The balloon shape was calculated by iterating for the buoyancy ratio in 1000 ft intervals over the full altitude profile. This allowed the analysts to determine the approximate shape of the envelope to assess the stress index during ascent.

$$\Sigma_S = \Sigma_d * \left[\left(\frac{b}{b_d}\right)^2 * \left(\frac{m}{m_d}\right)\right]^{-1/3} \quad (9\text{-}38)$$

Where:
Σ_S = the effective sigma shape (non-dimensional) at a given flight condition,
Σ_d = the design sigma shape (non-dimensional),
b = buoyancy value () where the parameter with no subscript is calculated for the flight conditions and the subscript "d" defines the values at the design conditions, and
m = payload mass (mass units), where the parameter with no subscript is calculated for the actual payload mass flown on the system and the subscript "d" defines the designed nominal payload mass.

Calculation of the stress index is based on the simple expression approximated by Equation (9-39) for hoop stress in a thin-walled cylindrical pressure vessel [14].

$$\sigma = \frac{\Delta P * r}{t} \quad (9\text{-}39)$$

Where:
σ is film stress (Pa)
ΔP is differential pressure (Pa)
r is the radius of the balloon envelope at a given time (m)
t is the thickness of the balloon envelope material (m)

Differential pressure here is defined as the pressure acting on the crown of the balloon envelope due to the pressure head inside the balloon from the gas pushing upwards during ascent. Equation (9-40) calculates the differential pressure as a result of the

$$\Delta P = H_P * b \quad (9\text{-}40)$$

Where:
H_P is the height from the zero-pressure line to the apex of the balloon envelope (m)
b is the buoyancy calculated at the given altitude (N/m^3)

Substituting equation (9-40) for the differential pressure based on the shape of the envelope and buoyancy into the stress equation (9-39) provides the solution for the Ascent Stress Index as defined in equation (9-41).

$$ASI = \frac{P_h * b * r}{t} \qquad (9\text{-}41)$$

The assessment of the ASI equation for balloons during the ascent phase demonstrated significant results in the analysis of balloon design performance. The analysis revealed a number of interesting conclusions based on mapping the stress acting on the envelope against altitude:

- The stress magnitude immediately begins to decrease after launch due to the pressure head decreasing faster than the balloon radius is increasing.
- When the pressure head reaches the length of each cap, the stress magnitude spikes with the change in film thickness before continuing to decrease.
- The maximum magnitude for the stress index occurs when the last cap drops off for most designs. This typically occurs at the point in the altitude region where minimum temperature is experienced where the majority of catastrophic failures occur.
- Finally, when the balloon is nearing float, a sudden increase in stress magnitude occurs, caused by the gas no longer expanding in a spherical bubble, but in the section of the envelope more closely represented by a cone shape causing the pressure head to increase faster.

In January 1985, NASA BPO established a stress index specification to limit the design and flight stresses for improved reliability [15]. The limit was set at 19.0 mPa (2750 psi) Ascent Stress Index for the standard film thickness of 0.020 mm (0.8 mil) film. This limit resulted in some design and application inefficiencies but improved reliability significantly across all the payload ranges [16]. At that time, the reliability of balloons launched by NASA was approximately 85% [13]. It should be noted that in the literature, ascent stress index and flight stress index may be referenced but are equivalent and interchangeable [9].

In 1982, James Dwyer proposed another simplified equation that would capture the dynamic load on the film at launch. The force required to erect the balloon from the spool is represented by the gross inflation minus the balloon weight, and this multiplied by the gore length would approximate the energy absorbed by the balloon during this process. He assumes that the normal manufacturing variations in the gore widths would cause the loading to be taken up by the gore material and not the load

tapes. The second big assumption is that film quality is proportional to its thickness; therefore, the effective thickness is t^2. Given these assumptions, an index of dynamic loading or shock during spool release is approximated by F_d in Equation (42) below. Dwyer analyzed 93 flights and suggested that a limit of $F_d = 10$ be placed on all balloons to increase the probability of success [17].

$$F_d = (G - W_{balloon}) * \frac{l_{gore}}{{t_{shell}}^2} \tag{9-42}$$

Where:
G = gross lift (or gross inflation) of gas within the balloon ($kg \cdot m/s^2$)
$W_{balloon}$ = weight of the balloon ($kg \cdot m/s^2$)
l_{gore} = length of the balloon gore (m)
t_{shell} = thickness of the balloon shell (m)

5. Balloons at Off-Design Conditions

The design process outlined in Section 3 above is intended to generate specifications for a balloon envelope given a set of standard requirements. However, not all balloons are used under those exact conditions for every flight. It is more economical to design a set of standard balloon designs that can be used under various conditions rather than create a new design for each scenario. The following sections outline how to adapt the design of a given system for off-nominal conditions and account for the resulting changes in vehicle performance. Two cases are laid out below: 1) the changing shapes and stresses of the balloon when operating below the design altitude of the envelope, and 2) utilizing duct length to modify the float altitude of an envelope irrespective of the system mass.

5.1. Balloon Shapes and Stresses Below the Design Altitude

Studies regarding balloon reliability [18] have shown that most balloon failures tend to occur during the ascent phase of the mission, indicating that stresses on the balloon envelope are greater during this phase than when operating under float conditions. It is, therefore, crucial to accurately quantify the shape and stresses acting on a balloon envelope below the design altitude.

In the analysis "Balloon Shapes and Stresses Below the Design Altitude" [3], Smalley calculates the shapes and stresses of a "natural-shape balloon, in equilibrium, at altitudes below their design altitude." The balloon shape parameters, stresses, zero-pressure level, and top pressure are presented for three different sigma value shapes of a

natural-shape balloon ($\Sigma = 0.2, 0.4, 1.0$). Smalley defined the sigma value as:

$$\Sigma = w\left(\frac{2\pi}{b^2}L\right)^{1/3} \tag{9-43}$$

The resulting calculations have been normalized relative to the gore length to allow for analysis of any size balloon, independent of style or design. The altitude levels are normalized by finding the resultant data at altitudes where the unit lift is a certain magnitude of the unit lift at the design altitude, also known as the buoyancy ratio (b / b_d). An example data set is presented in Table 9-1 below for a $\Sigma = 0.2$ natural-shape balloon, which is the common shape for most zero-pressure scientific balloons. The shape data is normalized in terms of gore length values. To calculate the shape parameters of a specific balloon design, multiply the values in the table below by the gore length of the given design.

Table 9-1. Balloon shape parameters below its design altitude for a $\Sigma = 0.2$ natural-shape balloon [4].

	Bottom of Bubble		Zero-Pressure Level			Maximum Radius		
b / b_d	Gore Position	Initial Angle	Gore Position	Radius	Height	Radius	Height	Balloon Height
1.0	0	58.89	0	0	0	0.3460	0.371	0.5985
1.1	0	47.14	0.20	0.148	0.1368	0.3289	0.428	0.6428
1.2	0	39.13	0.27	0.179	0.2054	0.3158	0.461	0.6709
1.5	0	24.50	0.37	0.195	0.3093	0.2878	0.529	0.7191
2.5	0	7.16	0.48	0.169	0.4381	0.2384	0.615	0.7802
6	0	0.26	0.60	0.119	0.5796	0.1760	0.718	0.8411
15	0.26	0.37	0.71	0.090	0.6884	0.1289	0.794	0.8846
40	0.45	0.33	0.79	0.064	0.7743	0.0927	0.852	0.9174
100	0.57	0.16	0.84	0.045	0.8333	0.0680	0.892	0.9394
300	0.70	0.17	0.89	0.031	0.8842	0.0470	0.925	0.9581
1000	0.80	0.19	0.93	0.023	0.9224	0.0313	0.950	0.9720

The analysis of balloon shapes and stresses below the design altitude presents interesting findings regarding the dynamics under the off-nominal operating conditions.

- During ascent, at low altitudes, the section of the balloon envelope filling with gas can be approximated as spherical in shape and the uninflated balloon is approximated as hanging vertically down. At higher altitudes, the entire envelope begins to expand and the zero-pressure level (the height at which the external pressure equals the internal pressure, see Figure 9-4) moves towards the base fitting. When the ZP line passes the inflection

point in the natural shape curve, the envelope is more conical in shape, causing the pressure at the apex to increase.

- The data calculated for the zero-pressure level also provides a straightforward method for determining the pressure head within the balloon envelope. Prior methods included assuming a spherical shape to approximate the pressure head, which was less accurate. Smalley presents the comparison of these methods for the pressure head calculation to show the discrepancies between these two methods (spherical assumption vs Smalley's balloon shape solution) [3].
- An example of the profiles of balloon shapes below their design altitudes is presented in Figure 9-6. These figures represent the changes the balloon envelope experiences over a range of altitudes. The figure shows the envelope shape for various buoyancy ratios representing the changing altitude and is normalized for gore length in both the X and Y axes.

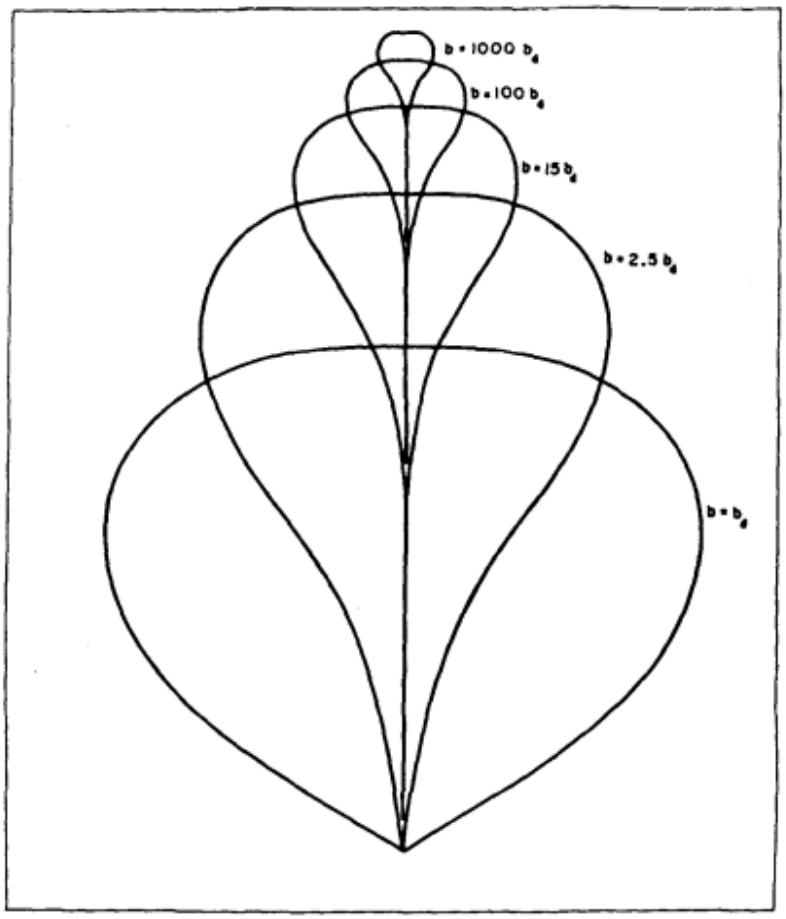


Figure 9-6. The shape profile at various buoyancy ratios below the design altitude for a $\Sigma = 0.2$ *natural-shape balloon [5].*

The evolution of the shape of the balloon envelope over time directly impacts the analysis and operations of balloons in flight. As discussed in Chapter 4, since buoyancy is a principle based on volume, the shape of the balloon is critical in modeling the flight dynamics of the vehicle. The analysis presented here provides a method for approximating the shape of the balloon envelope at or below the design altitude. This data can be used to calculate the volume of the lift gas (critical for calculating buoyancy) and surface area normal to each dimension (critical for drag calculations and thermal analysis). Using the tables and data presented [3] [4], the dynamic modeling of a high-altitude balloon systems can be refined with greater accuracy in shape prediction and resulting aerodynamic forces.

5.2. Cutting the Duct to Change the Float Altitude

Sometimes changes to the mission profile may require alteration to adjust for a different float altitude. One clever way to address this issue is to tailor the length of the escape ducts on the balloon, to optimize the float altitude of the resulting envelope.

The same processes and information [3] also apply to determining where to cut the vent ducts to cause a balloon to float below its design altitude. Figure 9-7 can be used to find the position of the zero-pressure level in gore length units. First, one must define the ratio of the new gross weight to the design payload weight, represented by G/P_d below. Then one must define the buoyancy ratio relative to the design buoyancy, represented as b/b_d. The convergence of these two parameters in the figure below defines the ratio of the gore position at the cut location to the overall gore length, S_c/S.

Cutting the ducts to create a new zero-pressure level position will cause the balloon to level off at a lower altitude when carrying the design payload. It should be noted, however, that new load-altitude curves should be plotted to determine the zero-pressure profiles of off-design systems.

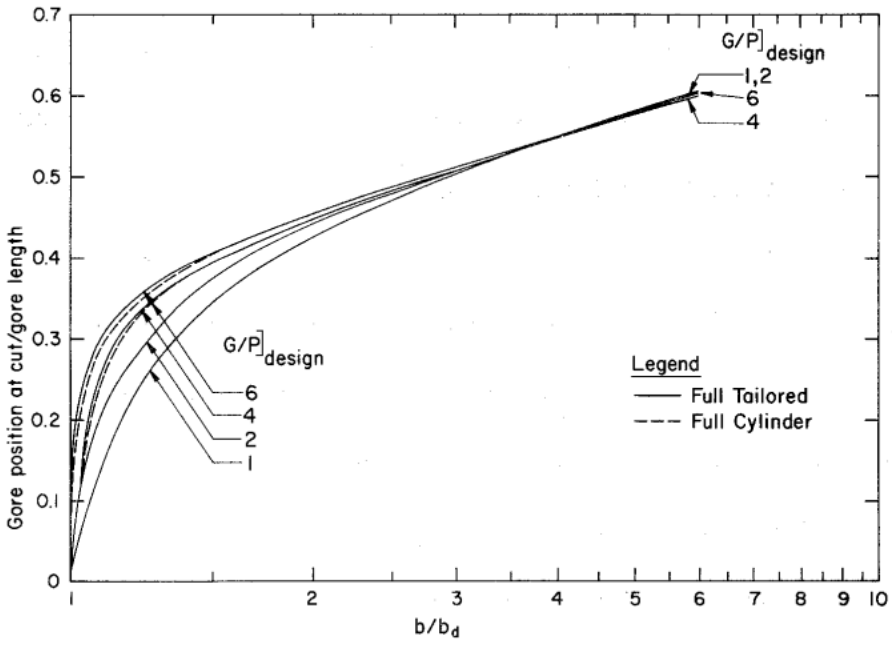


Figure 9-7. Zero-pressure level in balloons below their design altitude as a basis for cutting the vent ducts [1].

6. Considerations of Other Balloon Designs

This chapter has thus far focused on natural-shape, zero-pressure balloon designs as the primary vehicle for scientific applications. However, these are not the only zero-pressure balloon shapes that are used within the community, and it is worth touching on a few other classifications of balloon envelopes. The second most common envelope configuration is the cylinder balloon, highlighted below. Other balloon types, such as sphere-in-cone, taper tangent, and "tetroon" balloons, have fallen out of favor as being less practical [19].

The appeal of the cylinder balloon is in the ease of manufacturing. However, the shape of these systems is not optimized for the ideal volume-to-mass ratio, limiting their applications in the scientific community. They are preferential for smaller systems, which can be made cheaply and quickly. Cylinder balloons were also some of the first designs produced where the circumferential stress was intentionally zero, simplifying the stress analysis of the envelope. Smalley has outlined the shape of cylinder balloons [19] in various configurations, with the primary focus on zero-pressure systems. As with the natural-shape balloons, Smalley has outlined the shape of the cylinder balloons in the form of Sigma tables for $\Sigma = 0 \; to \; 0.4$ in the associated shape analysis reports. Refer to the reports generated by Smalley regarding cylinder balloon design considerations.

7. Conclusions

The contents of this chapter provide a summary of the basic process for determining and calculating the basic shape and configuration of natural-shape zero-pressure balloon systems for high-altitude, scientific applications. The reader is encouraged to explore the considerable research that has been published throughout the past 50 years related to the development and analysis of ZP balloon envelopes to dive deeper into how these systems work. Zero-pressure balloons are being used in new and interesting ways all the time which will challenge the previous conceptions for high-altitude ballooning. Work related to advanced materials development and computational algorithms for more complicated designs look to optimize balloon envelopes to fly higher and lift heavier payloads. It is the hope that over the next 50 years, further advancement across the scientific ballooning community will provide new information in the next update of this handbook.

References

[1] A. L. Morris, Scientific Ballooning Handbook, 1975.

[2] G. E. Carichner and L. M. Nicolai, Fundamentals of Aircraft and Airship Design: Volume 2 - Airship Design and Case Studies, AIAA, 2013.

[3] Smalley and J. H, "Balloon Shapes and Stresses Below the Design Altitude," National Center for Atmospheric Research, Boulder, CO, 1966.

[4] J. H. Smalley, "Determination of the shape of a free balloon - Balloons with Zero Superpeessure and Zero Circumferential Stress," Air Force Cambridge National Laboratory, Medford, MA, 1965.

[5] J. H. Smalley, "Beginning studies of balloons at off-design conditions," NCAR Report, 1966.

[6] K. Arnstein and W. Swan, *1935-1936: Stratosphere Series Nos. 1 & 2, Explorer I and II Balloons,* National Geographic Society, 1936.

[7] J. C. Warren, J. H. Smalley and A. L. Morris, "Aerostatic Lift of Helium and Hydrogen in the Atmosphere," NCAR, Boulder, CO, 1971.

[8] J. H. Smalley, " Determination of the shape of a free balloon," NCAR, Boulder, CO, 1962.

[9] I. S. Smith, *Personal Correspondance,* 2021.

[10] R. L. Schwoebel, "Strato-Lab Development," General Mills Inc, Minneapolis, MN, 1956.

[11] S. A. Roth, "Launch Decision Tool for NASA High-Altitude Scientific Balloons," George Washington University, Washington DC, 2022.

[12] R. L. Schwoebel, "Strato-Lab Development," General Mills Inc, Minneapolis, MN, 1956.

[13] I. S. Smith, "A stress index model for balloon designs," *Advances in Space Research,* vol. 7, pp. 19-24, 1987.

[14] J. M. Gere and B. J. Goodno, Mechanics of Materials, Cengage Learning, 2012.

[15] I. S. Smith, "A stress index model for ascending balloons," in *7th Conference on Sounding Rockets, Balloons, and Related Space Systems*, Ocean CIty, MD, 1986.

[16] I. S. Smith, "NASA test flights with increased fight stress indices," in *International Balloon Technology Conference*, 1991.

[17] J. F. Dwyer, "Polyethylene free balloon design from the perspective of user and designer," Aerospace Instrumentation Division, Air Force Geophysics Laboratory, Medford, MA, 1982.

[18] M. Fortenberry, "Zero-pressure balloon reliability - contributing factors," in *AIAA International Balloon Technology Conference*, Norfolk, VA, 1999.

[19] J. H. Smalley, "Determination of the Shape of a Free Balloon: Cylinder, Cylinder-End, Taper-Tangent, and Tangent-Harness Balloons," Air Force Cambridge National Laboratory, Medford, MA, 1964.

[20] T. W. Bilhorn, "Balloon Performance Analysis - NCAR Scientific Balloon Facility," in *AFCRL Scientific Balloon Workshop*, Bedford, MA, 1965.

[21] J. F. Dwyer, "Some Polyethylene Balloon Statistics," in *AFCRL Scientific Balloon Workshop*, Bedford, MA, 1965.

[22] J. F. Dwyer, "Zero pressure balloon shapes, past, present, and future," in *Scientific Ballooning (COSPAR)*, Innsbruck, Austria, 1978.

[23] A. D. Kerr and H. Alexander, "On a cause of failure of high altitude plastic balloons," New York University, New York, New York, 1968.

[24] J. Rand, D. Grant and T. Strganac, "The nonlinear biaxial characterization of balloon film," in *34th Aerospace Sciences Meeting and Exhibit*, 1996.

[25] K. Yang, R. A. Natherson, C. D. Yoder and S. A. Roth, "A Comparison of Two Non-Contact Strain Measurement Techniques with Applications to Scientific Balloons," in *2021 AIAA Aviation Forum and Exposition*, 2021.

[26] J. Blandino, J. Sterling, F. Baginski, E. Steadman, J. Black and R. Pappa, "Optical strain measurement of an inflated cylinder using photogrammetry with application to scientific balloons," in *45th AIAA/ASME/ASCE/AHS/ASC Structures*, 2004.

[27] J. Sterling and J. Rand, "Biaxial stress limit for ULDB film," in *AIAA 5th ATIO and 16th Lighter-Than-Air Systems Tech and Balloon Systems Conferences*, 2005.

[28] A. S. Redner, "Nondestructive evaluation using polarized light," *Materials evaluation,* vol. 53, no. 6, pp. 642-644, 1995.

[29] J. A. Brydson, Plastic materials, Butterworth Heinemann, 1999.

[30] P. J. Hendra, H. P. Jobic and K. Holland-Moritz, "Low temperature crystallization in polyethylene and the value of Tg," *Journal of Polymer Science,* vol. 13, no. 6, pp. 365-368, 1975.

[31] ASTM International, *ASTM D746-20 Standard test method for brittleness temperature of plastics and elastomers by impact,* West Conshohocken, PA: ASTM International, 2020.

[32] I. S. Smith, "Advances in NASA balloon research and development," *Advances in Space Research,* vol. 17, no. 9, pp. 37-44, 1996.

[33] V. Thomas, "A J-integral fracture toughness study of polyethylene films.," Texas A&M University, College Station, TX, 1996.

[34] L. Mielke, "BT-1039.14 Balloon Material Development," Winzen Research Inc, 1968.

Appendix 9-A

To highlight the application of the contents of this chapter, the following example design scenario has been laid out to validate the design process and provide a reference for utilizing the above information. This process is heavily influenced by the work of Rodger Farley and the analysis he produced alongside others contributing to the understanding of high-altitude balloon design. The authors would like to thank Rodger for his immense contributions to both the work outlined within this chapter and the scientific ballooning industry.

Example Design Scenario

To demonstrate the process for zero-pressure balloon design calculations outlined in section 3 above, the following example design scenario has been provided. This scenario highlights a common design problem and walks through the calculations to determine the critical parameters for a high-altitude scientific balloon. The calculations which were presented within this chapter only provide a preliminary outline of a full envelope design. These calculations do not capture the full design process and some secondary design details are not included here. All calculations are performed in SI units as is standard under NASA guidelines except where identified.

Defining Design Input Parameters

The design team has identified a need for a new high-altitude balloon system to meet the needs of potential customers. After talking to potential end users, the team has communicated that the balloon needs to have the capacity to carry a nominal suspended load of 1000 kg at an altitude of 36.5 km

$$m_{sus} = 1000\,kg$$
$$Z = 36500\,m$$

From the suspended mass, the suspended load is calculated. Below, the gravitational force constant is defined as 9.807 m/s^2. The resulting mass requirement produces a load value of 9807 N.

$$L = m_{sus} * g$$
$$L = 1000 * 9.807$$
$$L = 9807\,N$$

Two other critical assumptions are needed at this time. First, it is assumed that the lift gas used during operations is helium. Second, assume standard atmospheric conditions apply. Based on this known information, the first step is to calculate the specific buoyancy. The

following equations define the specific buoyancy for a system as a function of altitude. The altitude ranges listed below are provided in meters.

$$b(Alt) = -1.2 + 19 * e^{-0.9*10^{-4}*(Alt+5500)} \qquad 0 < \text{Alt} < 11000$$
$$b(Alt) = 0.003 + 28 * e^{-1.61*10^{-4}*(Alt+2600)} \qquad 11000 < \text{Alt} < 40000$$

Since the prescribed altitude is 36500m, the equation below is applicable here to calculate the specific buoyancy as shown below.

$$b = 0.003 + 28 * e^{-1.61*10^{-4}*(36500+2600)}$$
$$b = 0.0547\ N/m^3$$

Next, one must also calculate the film + load tape average areal density. This value provides an approximate average weight parameter based on historical design data for standard balloon applications. The areal weight is proportional to the altitude of the system and is characterized by both "light" and "heavy" systems.

$$w(Alt) = 0.77 - (1.25 * 10^{-5} * Z) \quad \text{"Light"}$$
$$w(Alt) = 1.43 - (2.7 * 10^{-5} * Z) \quad \text{"Heavy"}$$

Here, the "light" system equation is applied based on the suspended mass specifications. The average areal weight parameter is calculated below from the provided altitude limit.

$$w = 0.77 - (1.25 * 10^{-5} * 36500)$$
$$w = 0.3138\ N/m^2$$

Calculating Geometric Parameters

Now that the basic mission parameters are defined, the geometric parameters of the resulting balloon envelope can be calculated. The first calculation in equation defines the load ratio. This equation requires iterating the calculation until the resulting value converges. It is suggested to start with a value where $\bar{L} = 0.6$ and update the value after each step. The constant values for the shape factor (SF) and κ are also defined below. The iterative calculation results in a load value of 0.58 as defined in.

$$\bar{L} = 1 - \left(\frac{SF}{\kappa} * \frac{w}{b} * \left(\frac{\bar{L}}{L} * b\right)^{1/3}\right)$$

$$SF = 2.682$$

$$\kappa = \left(\frac{1}{2\pi}\right)^{1/3} = 0.521926$$

$$\bar{L} = 1 - \left(\frac{2.682}{0.541926} * \frac{0.3138}{0.0547} * \left(\frac{0.6}{9807} * 0.0547\right)^{1/3}\right)$$

$$\bar{L} = 0.58$$

The load ratio is used to calculate the gross weight of the system, as shown in the equations below.

$$GW = \frac{L}{\bar{L}}$$

$$GW = \frac{9807}{0.58}$$

$$GW = 16908\,N$$

At equilibrium, gross weight is equal to gross inflation. Gross inflation can be used to define the volume of the system required to achieve the specified altitude with the specified mass.

$$GW = GI = 16908\,N$$

$$V = \frac{GI}{b}$$

$$V = \frac{16908}{0.0547}$$

$$V = 309286\,m^3$$

Additionally, the load ratio parameter is used to calculate the non-dimensional shape parameters that characterize the envelope geometry. The following parameters for Σ_F (Farley's shape parameter) and λ_F (Farley's characteristic length parameter) provide the relationship between the gross inflation and shape of the envelope.

- Farley's Shape Sigma Value (Σ_F)

$$\Sigma_F = \frac{1 - \bar{L}}{SF}$$
$$\Sigma_F = \frac{1 - (0.58)}{2.682}$$
$$\Sigma_F = 0.1566$$

- Farley's Characteristic Length Value (λ_F)

$$\lambda_F = V^{1/3}$$
$$\lambda_F = (309286)^{1/3}$$
$$\lambda_F = 67.63\ m$$

The non-parameters previously outlined in section 3 define the general shape of the ZP balloon envelope. The following parameters are calculated to determine the shape parameters of the envelope starting with the non-dimensionalized values using the XX before converting to the dimensional parameters.

- Gore Length (S)

$$\bar{S} = 1.994 - (0.336 * \Sigma_F) - (0.049 * {\Sigma_F}^2)$$
$$\bar{S} = 1.994 - (0.336 * 0.1566) - (0.049 * (0.1566)^2)$$
$$\bar{S} = 1.9402$$
$$S = \bar{S} * \lambda_F$$
$$S = 1.9402 * 67.63$$
$$S = 131.21\ m$$

- Diameter (D)

$$\bar{D} = 1.305 + (0.164 * \Sigma_F) + \left(0.479 * {\Sigma_F}^2\right) - \left(1.478 * {\Sigma_F}^3\right) + (3.667 * {\Sigma_F}^4)$$

$$\bar{D} = 1.305 + (0.164 * 0.1566) + (0.479 * (0.1566)^2) - (1.478 * (0.1566)^3) + (3.667 * (0.1566)^4)$$

$$\bar{D} = 1.3390$$

$$D = \bar{D} * \lambda_F$$

$$D = 1.3390 * 67.63$$

$$D = 90.55\ m$$

- Height (H)

$$\bar{H} = 1.275 - (0.445 * \Sigma_F) - (1.496 * {\Sigma_F}^2)$$

$$\bar{H} = 1.275 - (0.445 * 0.1566) - (1.496 * (0.1566)^2)$$

$$\bar{H} = 1.1686$$

$$H = \bar{H} * \lambda_F$$

$$H = 1.686 * 67.63$$

$$H = 79.03\ m$$

The differential pressure at the top of the envelope can be calculated from the height of the envelope and the specific buoyancy. The following equations define the pressure head present in the envelope for the fully inflated system.

$$\Delta P = H * b$$

$$\Delta P = 79.03 * 0.0547$$

$$\Delta P = 4.32\ Pa$$

- Surface Area (A)

$$\bar{A} = 4.913 + (2.598 * (\Sigma_F - 0.05)^3)$$

$$\bar{A} = 4.913 + (2.598 * (0.1566 - 0.05)^3)$$

$$\bar{A} = 4.916$$

$$A = \bar{A} * {\lambda_F}^2$$

$$A = 4.916 * (67.63)^2$$

$$A = 22484\ m^2$$

- Number of Gores (N_g)

$$N_g = \frac{\pi * D}{W_{max}}$$

$$N_g = \frac{\pi * 90.55}{2.54}$$

$$N_g = 112$$

- Meridional Tension (T)

$$\bar{T} = 1.556 - (0.66 * \Sigma_F) - (1.59 * {\Sigma_F}^2)$$
$$\bar{T} = 1.556 - (0.66 * 0.1566) - (1.59 * (0.1566)^2)$$
$$\bar{T} = 1.414$$
$$T = \bar{T} * b * {\lambda_F}^3$$
$$T = 1.414 * 0.0547 * (67.63)^3$$
$$T = 23903\ N$$

- Tension per Load Tape (T_{LT})

$$T_{LT} = \frac{T}{N_g}$$

$$T_{LT} = \frac{23903}{112}$$

$$T_{LT} = 213\ N$$

The summary of the parameters that were calculated is provided below to verify the results.

- Inputs

Suspended Mass: $m_{sus} = 1000\ kg$

Float Altitude: $Z = 36500\ m$

- Operational Parameters

Suspended Load: $L = 9807\ N$

Specific Buoyancy: $b = 0.0547\ N/m^3$

Average Areal Weight: $w = 0.3138\ N/m^2$

- Shape Characterization

Load Ratio: $\bar{L} = 0.58$

Gross Weight: $GW = 16908\,N$

Volume: $V = 309286\,m^3$

Sigma Value: $\Sigma_F = 0.0.1566$

Characteristic Length: $\lambda_F = 67.63\,m$

- Non-dimensional Parameters

Gore Length: $\bar{S} = 1.9402$

Diameter: $\bar{D} = 1.3390$

Height: $\bar{H} = 1.1686$

Surface Area: $\bar{A} = 4.916$

Meridional Tension: $\bar{T} = 1.414$

- Dimensional Geometric Parameters:

Gore Length: $S = 131.21\,m$

Diameter: $D = 90.55\,m$

Height: $H = 79.03\,m$

Surface Area: $A = 22484\,m^2$

Meridional Tension: $T = 23903\,N$

Number of Gores: $N_g = 112$

Differential Pressure: $\Delta P = 4.32\,Pa$

Tension per Load Tape: $T_{LT} = 213\,N$

To complete the design for a zero-pressure balloon envelope at this point, additional steps are required to calculate the gore shape and other parameters that are not captured within the scope of this chapter. One could calculate the gore width and use the sigma tables to determine the gore shape for manufacturing, define load tape material, and input component parameters such as fittings, vent ducts, cabling, etc. The design process is iterative and may require reevaluation throughout these steps to identify and verify the results of the ZP balloon design.

Chapter 10
Super-pressure Balloon

Leyland G. Young[1] and Christopher D. Yoder[2]

[1] NASA Wallops Flight Facility, Aerospace Engineer, Mechanical Engineering Group
[2] NASA Wallops Flight Facility, Aerospace Engineer, Balloon Program Office

Acknowledgments

The authors would like to thank Rodger Farley for his permission to use the bulk of his unpublished work, as well as materials from his balloon courses. Sections of this chapter pull from his content without citation as they were never published.

Table of Contents

1. Background 6
2. Theory 7
2.1 Smooth surface balloon shape determination 7
2.2 Simple shapes and stresses 10
2.2.1 Sphere 10
2.2.2 Cylinder 10
2.3 Pumpkin shape (meridionally reinforced balloon) 11
2.3.1 Pumpkin Bulge Design 11
2.3.2 Pumpkin Shape Profile 12
2.3.3 Pumpkin Stresses 13
3. Design 13
3.1 Components 13
3.2 Foreshortening 14
3.3 Manufacturing considerations 15
3.4 Stability 15
3.5 Materials 16
3.6 Validation 17
4. Performance 19
4.1 Altitude performance 19
4.2 Loss of gas mass 19
4.3 Natural Oscillations 21
References 24

Table of Figures

Figure 10-1: Float altitude variation for a ZPB (blue) and SPB (orange). 6

Figure 10-2: (left) balloon with a surface element;(right) forces acting on the surface element..... 7

Figure 10-3: (left) Scale model of a pumpkin SPB at Wallops;(right) Film bulge/lobe..... 11

Figure 10-4 (a) Smooth surface showing the shape profile and bulge between two tendons; (b)Planar relationship of bugle radius and angle to global radius and angle..... 12

Figure 10-5: Image of an S-Cleft at float for NASA Flight 555NT (left) and a scale model balloon in a hanger undergoing structural validation (right). Original images are provided by NASA BPO and reproduced elsewhere..... 16

Figure 10-6: 4-meter pumpkin balloon gore with photogrammetry targets. 17

Figure 10-7: Gore 11 meridional creep behavior..... 18

Figure 10-8: Gore 47 hoop stress as a function of time (log axis)... 19

Figure 10-9: Altitude and differential pressure time history for 662NT (SN05) [1]..... 20

Figure 10-10: NASA 18.8mcf SPB flight 669NT showing degraded performance due to a leak..... 20

Figure 10-11: An example contour plot of leak rate for various discharge coefficients and hole size for 160 Pa..... 22

Figure 10-12: (top) 616NT altitude time history around float, alongside a center point moving average. (bottom) Oscillations in float altitude (raw data less filtered data) compared with theoretical oscillations of +/-50m with a 278-second period..... 23

Table of Symbols

Symbol	Definition	Dimension
A	Surface area	L^{-2}
b	Specific buoyancy	$M\ L^{-3}$
g	Gravitational acceleration	$M\ T^{-2}$
F	Force	$M\ L\ T^{-2}$
p	Differential pressure	$M\ L^{-1}\ T^{-2}$
s	Arclength	L
T	Tension	$M\ L\ T^{-2}$
r	Horizontal coordinate	L
V	Volume	L^{3}
w	Weight of balloon film per unit area	$M\ L^{-2}$
z	Vertical coordinate	L
α	Bulge angle	rad
θ	Angle between vertical and balloon shape	rad
ρ	Density	$M\ L^{-3}$
σ	Stress	$M\ L^{-1}\ T^{-2}$
φ	Angle between vertical planes defining the surface element	rad

1. Background

The super-pressure balloon (SPB) is a non-extensible balloon that is sealed to prevent gas release. Once the balloon reaches the float altitude, extra gas (free lift) is converted into super-pressure (i.e. having a greater internal bulk pressure than the ambient atmospheric pressure). The variations in the radiation environment produce significant changes in the super-pressure but, generally, negligible changes in the balloon volume. As long as the balloon maintains a positive super-pressure, it will continue to float at a constant-density level in the atmosphere [1]. An example of the altitude stability is shown in Figure 10-1.

The use case for an SPB vehicle comes from the inherent altitude stability at night. Specifically, NASA's 18.8mcf SPB was initially designed to last 100 days anywhere in the world [2], [3]. Several groups have demonstrated the capability for long duration flights with SPB vehicles, especially in lower altitudes in the atmosphere with colder air temperatures [4], [5].

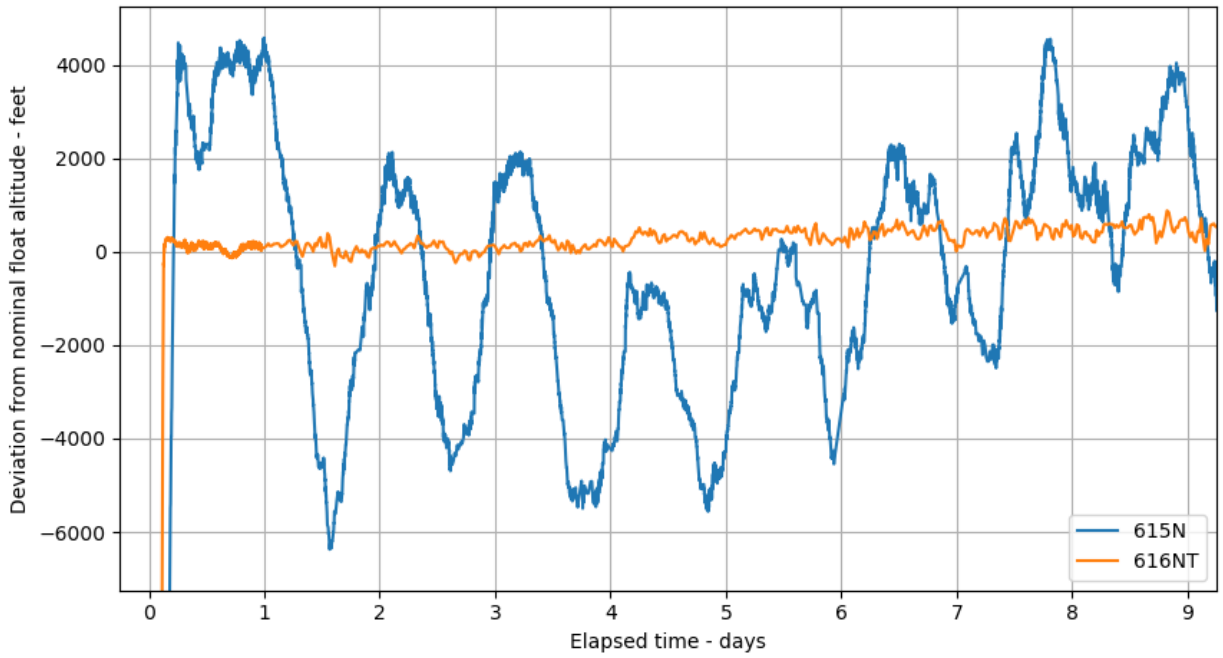


Figure 10-1: Float altitude variation for a ZPB (blue) and SPB (orange).

2. Theory

2.1 Smooth surface balloon shape determination

The following section is taken from the first version of the balloon handbook for the shape deformation of a "smooth surface" balloon. The simplest development of the equations considers the balance of forces on an elemental surface area of a balloon, as shown in Figure 10-2a. The element and the forces on it are shown in detail in Figure 10-2b. Z is the vertical coordinate and r is the horizontal coordinate to describe an axisymmetric balloon.

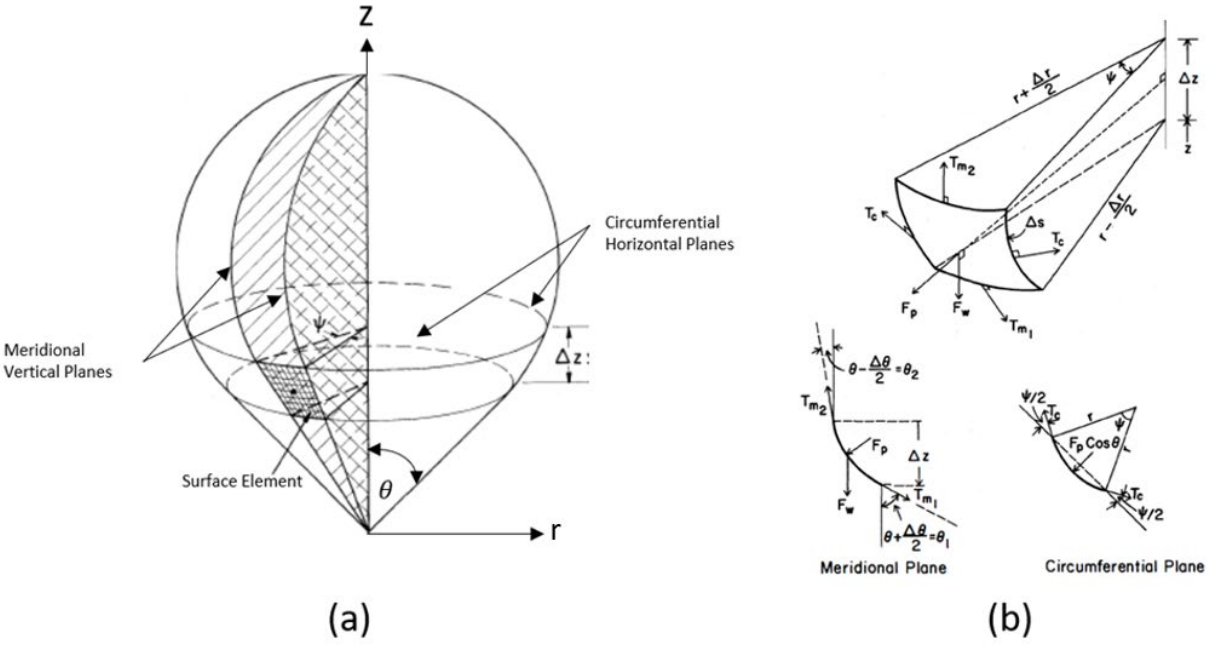


Figure 10-2: (left) balloon with a surface element;(right) forces acting on the surface element.

The top and bottom of this surface element are defined by two horizontal parallel planes normal to the axis of symmetry and located a distance Δz apart. The intersection of such planes with the balloon surface defines the circumferential direction. The sides of the element are defined by two vertical planes containing the axis of symmetry and separated by an angle $\varphi \cdot$ The intersection of such planes with the balloon surface defines the meridional direction. The tangents to the meridional and circumferential directions and the normal to the surface form an orthogonal set.

From in Figure 10-2b, F_p, the pressure force on the element; F_w, the weight of the element; T_c, the circumferential force, and T_m, the

meridional force. Using a tiny element (i.e., $\Delta z \ll 1$ and $\varphi \ll 1$), to first-order accuracy:

$$F_p = p(\varphi r \Delta s) \tag{10-1}$$

$$F_w = w(\varphi r \Delta s) \tag{10-2}$$

where p is the differential pressure across the balloon film, w is the weight of the balloon film per unit area, and $(\varphi r \Delta s)$ is the area of the element. Also,

$$T_c = \sigma_c \Delta s \tag{10-3}$$

$$T_{m_1} = \left(\sigma_m - \frac{\Delta\sigma_m}{2}\right)\varphi\left(r - \frac{\Delta r}{2}\right) \tag{10-4}$$

$$T_{m_2} = \left(\sigma_m + \frac{\Delta\sigma_m}{2}\right)\varphi\left(r + \frac{\Delta r}{2}\right) \tag{10-5}$$

where σ_c and σ_m are the circumferential and meridional stresses per unit length, respectively. From Figure 10-2b:

$$\theta_1 = \theta + \Delta\theta/2 \tag{10-6}$$

$$\theta_2 = \theta - \Delta\theta/2 \tag{10-7}$$

Summing forces vertically and horizontally, respectively, in the meridional plane:

$$T_{m_2}\cos(\theta_2) - T_{m_1}\cos(\theta_1) - F_p\sin(\theta) - F_w = 0 \tag{10-8}$$

$$T_{m_2}\,sin(\theta_2) - T_{m_1}\,sin(\theta_1) + F_p\,cos(\theta) - 2T_c\,sin(\varphi/2) = 0 \tag{10-9}$$

It can be shown that when higher-order infinitesimals are omitted,

$$T_{m_2}\cos(\theta_2) - T_{m_1}\cos(\theta_1) = \varphi\Delta(r\sigma_m\cos\theta) \tag{10-10}$$

$$T_{m_2}\,sin(\theta_2) - T_{m_1}\,sin(\theta_1) + F_p\,cos(\theta) = \varphi\Delta(r\sigma_m\,sin\,\theta) \tag{10-11}$$

And then substituting further, assuming $sin(\varphi/2) = \varphi/2$:

$$\Delta(r\sigma_m Cos(\theta)) - rw\Delta s - pr\sin(\theta)\,\Delta s = 0 \tag{10-12}$$

$$\Delta(r\sigma_m Sin(\theta)) - \sigma_c\Delta s - pr\,cos(\theta)\,\Delta s = 0 \tag{10-13}$$

Dividing by Δs and taking the limit as Δs approaches zero:

$$\frac{d(r\sigma_m\cos\theta)}{ds} - rw - pr\sin(\theta) = 0 \tag{10-14}$$

$$\frac{d(r\sigma_m\,sin\,\theta)}{ds} - \sigma_c + pr\,cos(\theta) = 0 \tag{10-15}$$

Another form of these equations is more convenient for integration. When the indicated differentiation is carried out:

$$\frac{d(r\sigma_m)}{ds}\cos(\theta) - (r\sigma_m)\sin(\theta)\frac{d\theta}{ds} - rw - pr\sin(\theta) = 0 \tag{10-16}$$

$$\frac{d(r\sigma_m)}{ds}sin(\theta) + (r\sigma_m)cos(\theta)\frac{d\theta}{ds} - \sigma_c + pr\ cos(\theta) = 0 \tag{10-17}$$

Eliminating $d(r\sigma_m)/ds$ and substituting $p = b(z + a)$ where a is the distance the zero-pressure level is below the bottom of the balloon, and b is the specific buoyancy of the lifting gas, gives

$$r\sigma_m d\theta ds = \sigma_c\cos(\theta) - rw\sin(\theta) - rbz + a \tag{10-18}$$

Then eliminating p gives

$$\frac{d}{ds}(r\sigma_m) = \sigma_c\ \sin(\theta) + rw\cos(\theta) \tag{10-19}$$

To complete the set of equations necessary to define a balloon, it is noted that

$$\frac{dr}{ds} = \sin(\theta) \tag{10-20}$$

$$\frac{dz}{ds} = \cos(\theta) \tag{10-21}$$

where A and V are the surface area and volume, respectively. By definition:

$$\frac{dA}{ds} = 2\pi r \tag{10-22}$$

$$\frac{dV}{ds} = \pi r^2\cos(\theta) \tag{10-23}$$

The total film load in the meridional direction is

$$T = 2\pi\ (r\sigma_m) \tag{10-24}$$

There are three variables in the above equations that may be directly specified. They are σ_c, w, and a. When σ_c (circumferential stress) is set equal to zero everywhere, the natural-shape balloon results. If a is zero, the balloon is known as the zero-pressure type. If w is held constant, the resulting balloon is fully tailored. If the term rw is constant, the balloon is a cylinder type.

Various boundary conditions are of interest. In the usual case, $0 < \theta < \pi/2$ at the bottom of the balloon and $\theta = -\pi/2$ at the top (i.e., flat-topped). If $\theta = \pi/2$ at the bottom, there is no payload, and it must be

carried elsewhere. If $\theta < -\pi/2$ at the balloon top, an additional lift force is being applied there.

If at either the top or the bottom of the balloon, rw is zero, and $\sigma_c \neq \sigma_m$, then σ_m becomes infinite. Although, σ_m may diverge, the total film load will not. If there is a load L at the bottom of the balloon, the initial value of the total film load is $T = L/\mathrm{Cos}(\theta)$.

2.2 Simple shapes and stresses

A balloon can be manufactured in almost any desired shape. When the balloon is pressurized, the stress distribution will vary over the surface, with the highest stresses in areas of maximum radii of curvature. Several common shapes and stresses are outlined below.

2.2.1 Sphere

Only a sphere provides uniform stress distribution over the entire surface. Intuitively, the sphere is the most efficient shape for providing the largest enclosed volume at a given maximum stress and a given mass of material. However, constructional difficulties arise, which can offset much of the geometric efficiency of the sphere. In addition, the application may be one where factors other than efficiency are of prime importance.

The stress on the envelope of a spherical balloon is:

$$\sigma = \frac{R\Delta P}{2t} \qquad (10\text{-}25)$$

Where R is the balloon radius, ΔP is the differential pressure, and t is film thickness.

2.2.2 Cylinder

The cylinder is an inefficient shape for a super-pressure balloon. Still, it is simple to manufacture, and a cylindrical balloon, which is long compared to its diameter, provides a low drag relative to an equivalent sphere for motion that is normal to its circular cross-section. It has application to low-altitude flight with light payloads. The circumferential stress (hoop stress) on a long cylinder is [6]:

$$\sigma_h = \frac{R\Delta P}{t} \qquad (10\text{-}26)$$

Where R is the balloon radius, ΔP is the differential pressure, and t is film thickness.

2.3 Pumpkin shape (meridionally reinforced balloon)

The pumpkin super-pressure balloon (SPB) is a meridionally reinforced design and is currently being adapted by NASA to perform at near constant float altitude for payloads less than 5,500 lbs. NASA's pumpkin balloons are fabricated from 1.5 mils polyethylene film panels called gores for the gas containment. Highly flexible stiff material called load tape tendons align in the meridional direction act as the structural components to take the differential pressure and distribute the payload weight within the balloon structure.

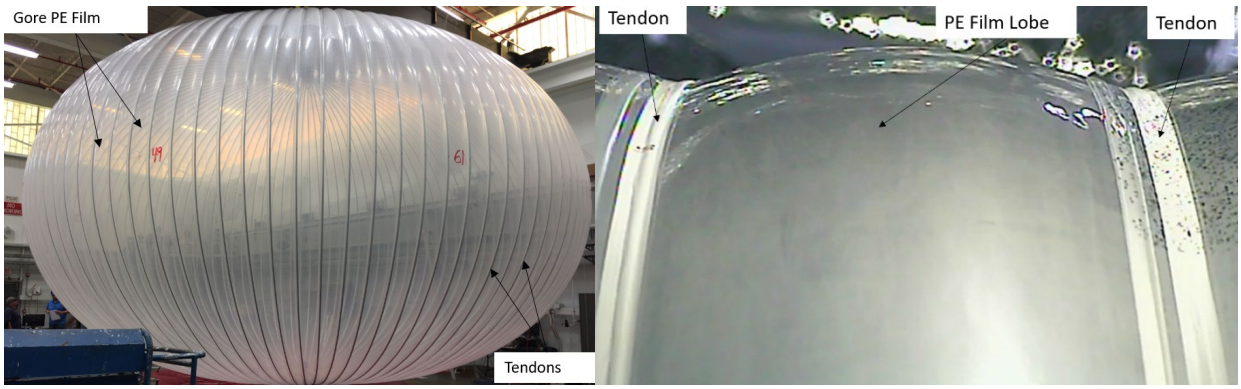


Figure 10-3: (left) Scale model of a pumpkin SPB at Wallops;(right) Film bulge/lobe.

Figure 10-3 (left) shows a pressurized scale model pumpkin SPB detailing the polyethylene gores between the meridional load tape tendons. Figure 10-3 (right) shows the formation of bulges from the differential pressure on the gores between the meridional load tape tendons.

2.3.1 Pumpkin Bulge Design

Referring to Figure 10-4, the bulge geometry is design using "bulge geometric parameters" which could be a constant radius R_B, a constant angle α_B , or a constant bulge hoop stress $hoop_{stress}$ concept along the length of the shape profile. In Figure 10-4, R_C is the smooth surface planar radius of curvature and α_C is the angle between adjacent LTT referenced to the axis of symmetry. Equations (10-27), (10-28), (10-29), (10-30), and (10-31) provide the geometric relationship of the bulge and the impact the bulge has on the circumferential stress.

$$Chord = 2\,R_B \sin\left(\frac{\alpha_B}{2}\right) = 2\,R_C \sin\left(\frac{\alpha_C}{2}\right) = 2\,r \sin\left(\frac{\pi}{N_{gores}}\right) \qquad (10\text{-}27)$$

$$R_B = r \sin\left({}^{\pi}/_{N_{gore}}\right) / \sin\left({}^{\alpha_B}/_{2}\right) \qquad (10\text{-}28)$$

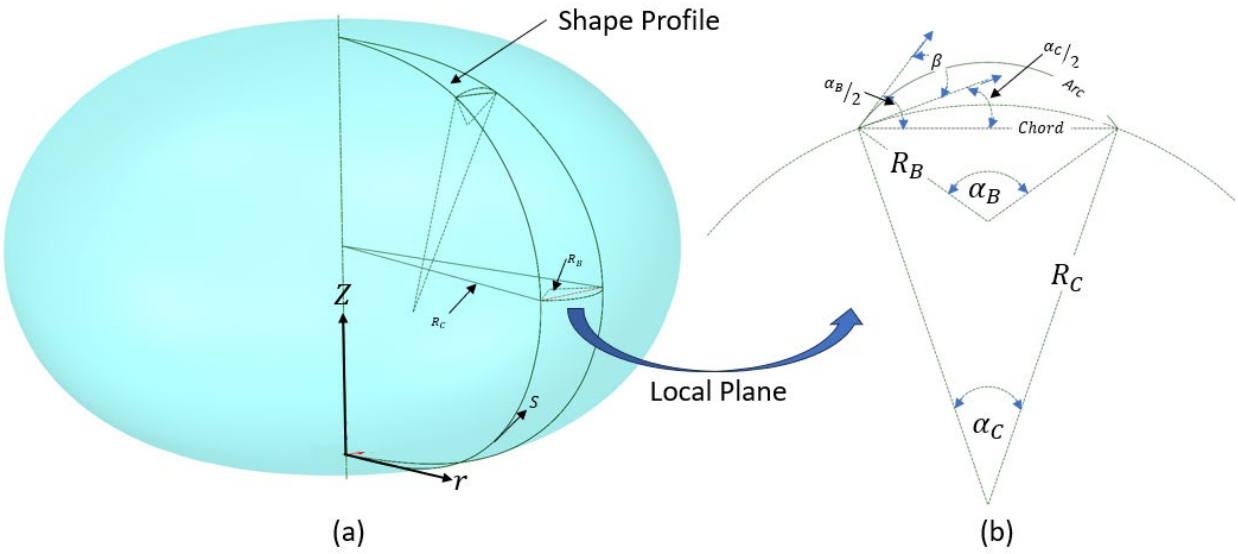


Figure 10-4 (a) Smooth surface showing the shape profile and bulge between two tendons; (b)Planar relationship of bugle radius and angle to global radius and angle.

The arc-length is the gore's width which equals to:

$$arc_{length} = Gore_{width} = R_B\alpha_B \tag{10-29}$$

$$\beta = \frac{\alpha_B - \alpha_C}{2} \tag{10-30}$$

$$\sigma_C = \sigma_{hoop}\, t \cos(\beta) \tag{10-31}$$

2.3.2 Pumpkin Shape Profile

The pumpkin shape profile is determined by solving Equations (10-18), (10-19), (10-20), and (10-21). However, Equations (10-18) and (10-19) are modified to incorporate weight from the load tapes (tendon and heat seal material) and extra film for bugle formation by making the film areal weight density W a geometric function. The following relationships are prescribed to modify Equations (10-18) and (10-19) to generate the pumpkin shape profile.

$$\mathrm{W} = (R_B\alpha_B w_{film} + W_{load-tape})N_{gores} \tag{10-32}$$

$$Q = 2\pi\sigma_c \tag{10-33}$$

$$P = 2\pi r \Delta P \tag{10-34}$$

$$\Delta P = \Delta P_{base} + bZ \tag{10-35}$$

Where N_{gore} is the number of gores/load-tapes, w_{film} is the film weight per unit length, $W_{load-tape}$ is the load-tape per unit length. Substituting Equation (10-24) into Equations (10-18) and (10-19) and adopting the relationship of equations (10-32), (10-33), (10-34), and (10-35), results in the differential equations for a meridionally-reinforced pumpkin structure.

$$\frac{d\theta}{ds} = \frac{Q\cos(\theta) - W\sin(\theta) - P}{T} \tag{10-36}$$

$$\frac{dT}{ds} = Q\sin(\theta) + W\cos(\theta) \tag{10-37}$$

Hence, Equations (10-36) and (10-37) can be used with Equations (10-20) and (10-21) to generate the shape profile. The boundary conditions include the differential pressure P_{base} at the base (coordinate origin), initial total tension T_b (base) and T_a (apex) and base angle θ_b and apex angle θ_a.

2.3.3 Pumpkin Stresses

The hoop and meridional stresses in a pumpkin balloon are given as:

$$\sigma_h = \frac{E_x}{(1 - \nu_{xy}\nu_{yx})}\left[\epsilon_x + \nu_{xy}\epsilon_x\right] \tag{10-38}$$

$$\sigma_m = \frac{E_y}{(1 - \nu_{xy}\nu_{yx})}\left[\epsilon_y + \nu_{yx}\epsilon_y\right] \tag{10-39}$$

where σ and ν represent stress and Poisson's ratio, and ϵ is the strain. If the Youngs modulus and Poisson's ratio are unknown, then a local approximation of a cylinder is often used for hoop stress given by Equation (10-26). If a viscoelastic material is used, then the static values of Youngs modulus and Poisson's ratio become time, temperature, and pressure dependent and there must be a model to account for time histories (see Section 3.5 and prior work on the topic [7, 8]).

3. Design

3.1 Components

All SPB vehicles are slightly different given the differences in size/volume, shape, and materials. However, some components are universal:

- Shell
  The shell is the main gas retention barrier. For SPB vehicles, this film is thicker than conventional ZPB films to account for the larger stresses in the structure at higher differential pressures.
- Tendons
  The tendons are present to take the load of the payload from the film. Tendons are either exposed to the atmosphere or encased in sleeves to protect them from strength degradation. Foreshortening can be specified by controlling the tendon length.
- Nets
  Nets have been studied as an alternate method for distributing meridional load like tendons [9], [10].
- End fittings
  At the top and bottom of an SPB, the fittings are a method to join the film of the shell together with the tendons. Fittings are also used as the mechanical interface for valves, payloads, and other sensors flown on the vehicle.
- Valves
  Valves can serve several key roles in a balloon structure. For large volume balloons, such as the NASA's 18.8mcf super-pressure balloon, they are used for gas inflation while the bubble is in the spool. Valves also serve as a secondary termination method, allowing gas to be vented to enable a descent at a desired rate.

3.2 Foreshortening

Foreshortening is defined as the difference between the tendon length and the gore length at room temperature. The no-foreshorten design intent addresses the fabrication complexity by ensuring the film and load tape tendon (LTT) length are the same during fabrication. However, the balloon shell carries the meridional load at low pressure and low temperature. That is, any thermal mismatch in length and LTT slack must be overcome for the LTT to become the meridional structural member.

The foreshortened design accounts for the thermal mismatch between the polyethylene (PE) film and the Zylon tendon, plus the effects of Poisson's ratio shrinkage and any slack in the braided tendon. Polyethylene film is more sensitive to temperature than the Zylon tendon. Thus, to compensate for the PE thermal contraction at float with tendon slack, the tendon is shortened between 3.5% to 5.5% when fabricated at room temperature. This tendon shortening requires management of the excess PE film length such that the thermal contraction reduces the excess film length to an equivalent length of the tendon after it undergoes elongation under the pressurization. The management involves gathering excess length and tacking it to the tendons. However, the "film tacking" add complexity to the fabrication and could results in undesirable consequences.

3.3 Manufacturing considerations

There are several considerations when manufacturing the SPB compared to a normal ZPB:

1. The manufacturing process induces a nominal strain due to handling of the material. Viscoelastic materials have a component of stress related to their strain history [1]. Minimizing the amount of stretching is critical.
2. Gore pattern is critical for SPB manufacturing as the shape of the gore fixes the stress state of the shell film. For higher differential pressures, film strength is a concern for nominal load cases but also fatigue loading [2].
3. Foreshortening is a large consideration for SPBs. If the goal of tendon is to strain-arrest the film (i.e. the tendons take the meridional loads instead of the film) [3], then the tendons must be loaded before the film. Prior work has identified a foreshortening range of 3-7% depending on the application [2], [3], with optimization within this range.

3.4 Stability

The stability of a super-pressure balloon is a key aspect of a super-pressure design. It is believed that Julian Knott was the first to encounter the S-Cleft, a form of instability, during his flights in the 1980s [11]. Instability has been observed in flight by several groups since then, including the Japanese program [12] and the NASA program [13], [14]. An example of an S-Cleft can be seen in Figure 10-5, both for a balloon in flight and a replica scale model in a hanger.

Many groups have studied instabilities to find the line between stable and unstable balloon designs. Calladine put forth one of the first stability relationships for lobed balloons for as a stability criteria [11] which was later shown to exclude certain stable balloon designs [13]. Baginski et al. presented a structural model for buckling and stability of super-pressure balloons based on the sign of all eigenvalues of the Hessian matrix of the potential energy of the deployed balloon [15]. Wakefield adapted the dynamic relaxation technique used for balloon structural analyses to show such geometric instabilities for a given gore pattern and balloon design [16]. Pellegrino et al. studied the effects of material properties and viscoelasticity on buckling around the same time [17].

Fundamentally, the tendency of a balloon to develop a cleft (and thus the stability of a balloon) are related to the geometry of the balloon lobe. Specifically, when lobes are designed with a bulge angle (or gore width) such that an excess of material in the hoop direction, the balloon

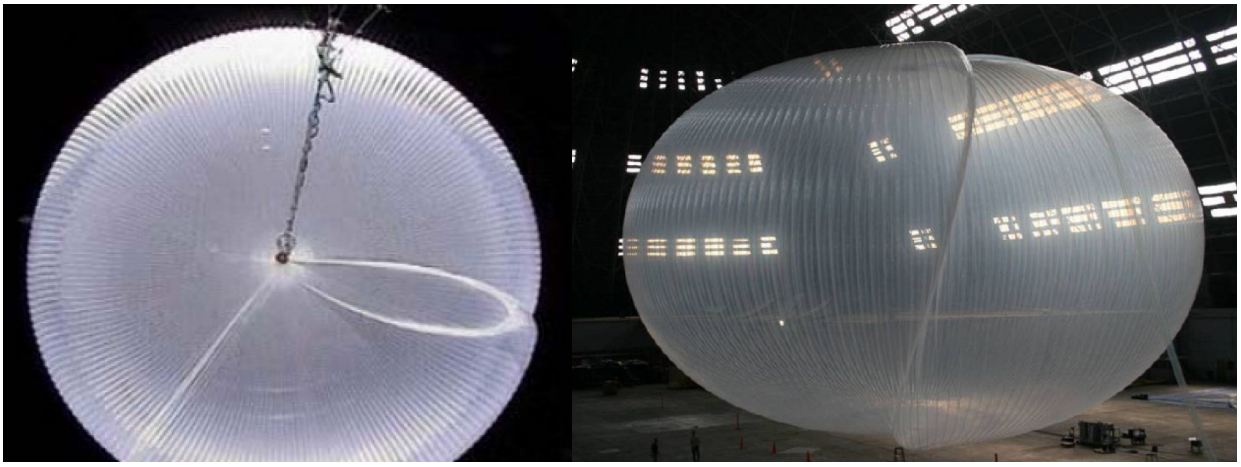


Figure 10-5: Image of an S-Cleft at float for NASA Flight 555NT (left) and a scale model balloon in a hanger undergoing structural validation (right). Original images are provided by NASA BPO and reproduced elsewhere.

surface area folds inward (i.e. clefts) to reduce the energy of the system. Farley, one of the last ones to approach the problem of lobed structure stability, proposed a simple method of cleft factors to determine stability of a design in a closed form approach. In short, the Cleft Factor, CF, of a balloon design must adhere to two criteria to be stable:

$$CF = 1000\frac{\sin(\pi/N_{gores})}{\sin(\alpha_B/2)}\cos\left(\frac{\alpha_B}{2} - \frac{\pi}{N_{gores}}\right) > 16 \tag{10-40}$$

$$\frac{CF}{\Sigma} > 120 \tag{10-41}$$

where Σ, the sigma number, is defined as:

$$\Sigma = \left(\frac{2\pi}{V}\right)^{1/3}\frac{\rho_A}{b} \tag{10-42}$$

and ρ_A is the average aerial density of the balloon (including film, tendons, etc).

3.5 Materials

NASA's pumpkin balloon is fabricated with primarily two materials: A three-layer co-extrusion of linear low-density polyethylene (LLDPE)SF-420 with a total thickness of 38 microns (1.5 mil) for gas containment and Zylon (PBO) tendon as the structural load carrying member. However, to integrate the Zylon tendon into the balloon structure, it is laminated between polyethylene sheets and becomes a composite "load tape tendon" (LTT). Additionally, the heat sealing of the polyethylene film with the LTT during fabrication creates a heat seal that has different properties from the LLDPE SF-420 PE film.

LLDPE SF-420 exhibits viscoelastic and creep behavior. Dr. James L. Rand [18], [19] employed the viscoelastic theory Dr. Richard A. Schapery [20] published to model the SPB LLDPE SF-420 film.

3.6 Validation

The fundamental principle of the pumpkin SPB is that the load tape tendon controls the polyethylene film meridional stress and the geometric change of radius of curvature from the bulge formation containing the hoop stress. Hence, several scale model balloons were tested to verify this principle, and photogrammetry measured strains (see Figure 10-6 for an example of photogrammetry targets on a scale model balloon). The expectation is that the polyethylene film between tendons deforms when pressurized. The polyethylene film bulges outward normal to the pressure, and the LTT would contain meridional stress (deformation). The bulge formation reduces the radius of curvature, which reduces the membrane hoop stress.

The example of a 4-meter scale model test and the results are outlined here to serve as a case study. For this test, the balloon was pressurized over several days to increasingly higher gauge pressure levels and allowed to settle. During the test, images of a grid of photogrammetry targets were taken and strains were calculated. Several instances of photogrammetry techniques can be found in the literature [21], [22].

Figure 10-7 is an example plot of meridional strains in the plastic as a function of time. As time progresses, pressure is increased in steps and held constant to allow the balloon to respond. As seen, increasing pressure corresponds to an increase in meridional strain in the film. After the high pressure is removed, the residual strain can be measured at a nominal pressure required to inflate the structure (e.g. 50 Pa). This plot is an example of a SPB design where the tendons do not strain arrest the film, leading to residual strain in the shell.

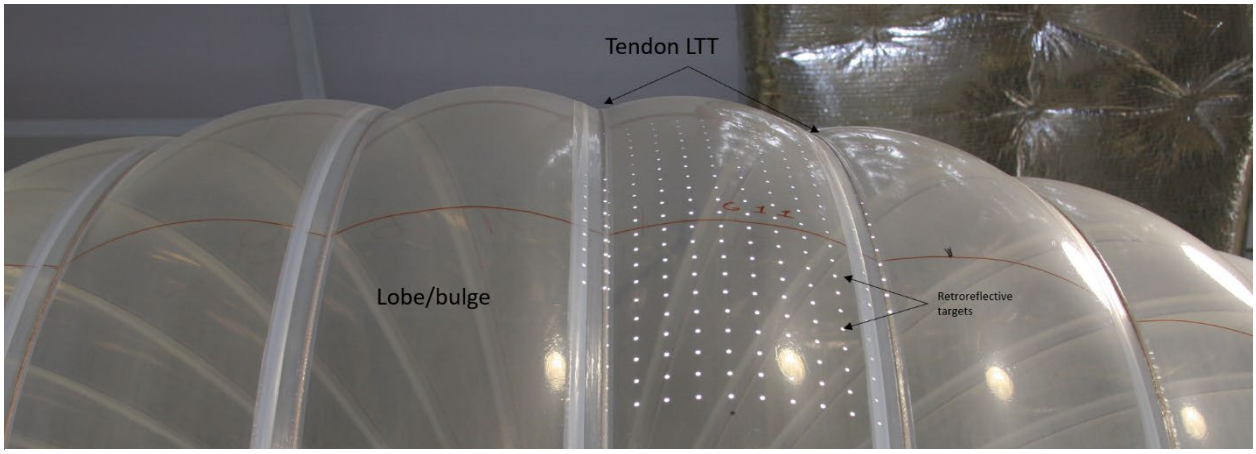


Figure 10-6: 4-meter pumpkin balloon gore with photogrammetry targets.

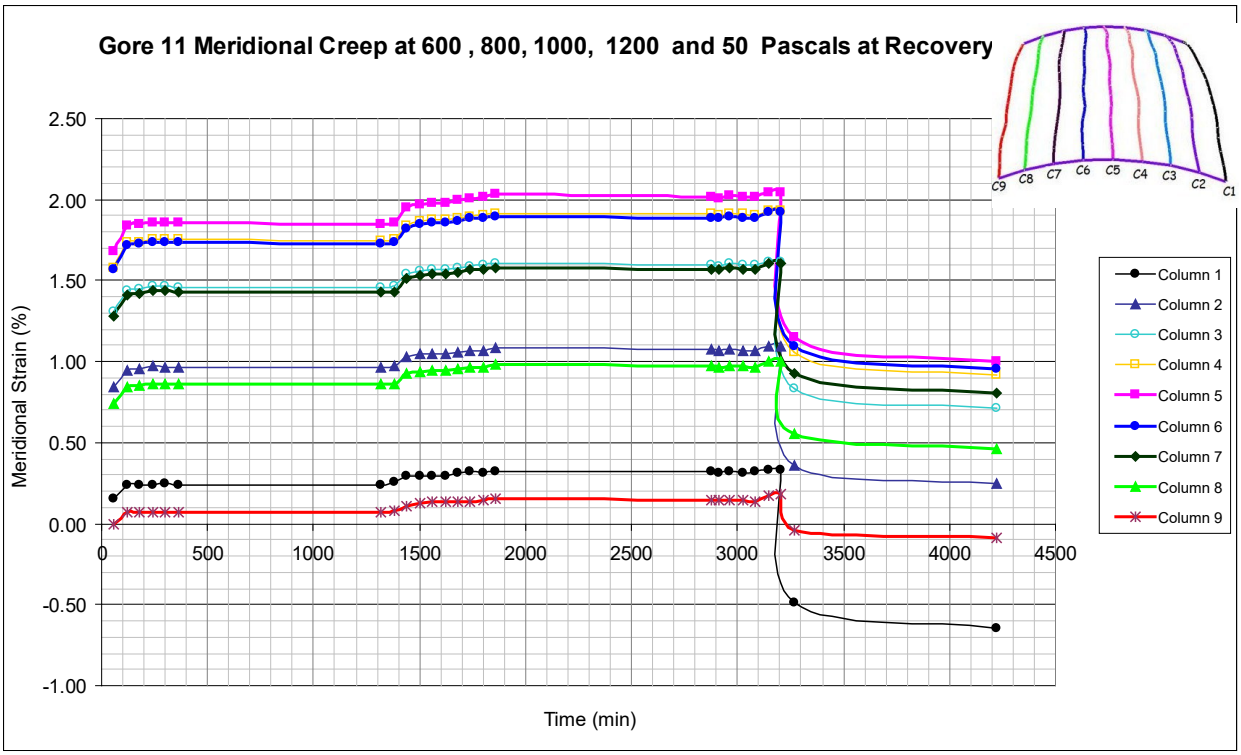


Figure 10-7: Gore 11 meridional creep behavior.

Figure 10-8 is a plot from the same test showing calculated hoop stress as a function of elapsed time. Each curve represents a different differential (gauge) pressure, with the longest dwell times at 800 and 1000 Pa of over 1000 minutes (16.7 hours). As seen, for each trend, there is a slight decrease due to the slow, creep behavior of the plastic in the shell. As the plastic creeps (increases in strain), the length of the circumference in the bulge increases, thus decreasing the bulge radius. Since hoop stress increases with increasing radius of curvature (see Equation (10-26)), the stress in the material decreases, which is validated by Figure 10-8.

While scale model tests are a good method to measure aspects of a balloon design in a controlled environment, scaling laws can be difficult to hold between the test unit and the full flight balloon. Often, a determination must be used to keep the values of interest measurable and compromise on other aspects of the design. For example, equatorial stress and strain in hoop and meridional directions are often a focus of scale model tests. To generate similar stresses on a smaller overall diameter, e.g. 4-meter scale model for an 18.8mcf (115-meter diameter) balloon, the gore number is reduced (e.g. from 280 to 48 gores) and the end fittings are buoyed with Helium. Further, as a balloon envelope strains, the pressure inside a scale model may be held constant, where as a flight balloon could reduce. Therefore, it is important to validate mathematical models which account for nuances between test articles and flight vehicles.

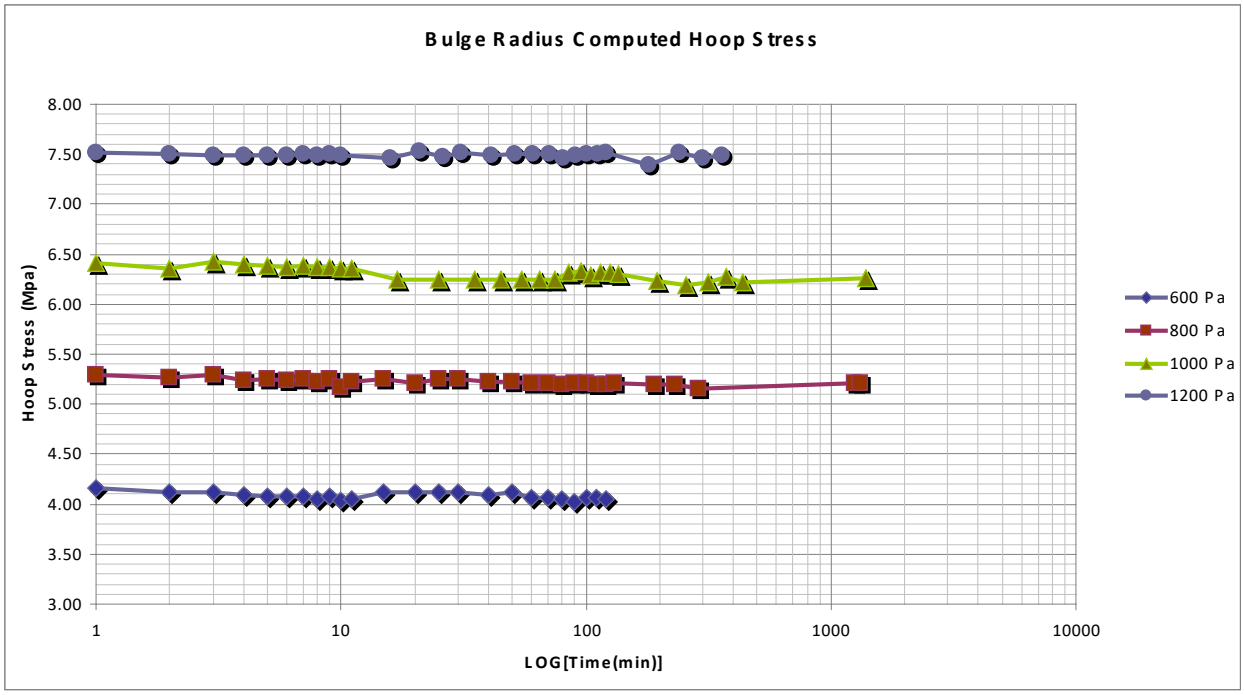


Figure 10-8: Gore 47 hoop stress as a function of time (log axis).

4. Performance

4.1 Altitude performance

The performance of the SPB is one markable different. Consider for example the case of NASA's 18.8mcf SN07 (662NT) balloon [4]. The altitude is stable around the 33.5km altitude with the differential pressure (internal minus external pressure at the apex) showing significant fluctuations. Only several times during the flight does the differential pressure flatten, correlating with a drop in altitude.

4.2 Loss of gas mass

The performance degradation of an SPB is particularly bad under the loss of gas. For example, consider the NASA Flight 669NT from the subsequent year [4].

The performance degradation seen in the first three-five days of flight are hypothesized to be the result of cold storms beneath the balloon, given the recovery of differential pressure and subsequent stability in altitude in the days immediately following the altitude excursions. However, the overall downward trend of peak differential pressure suggests a loss of gas mass. Further, the rise in differential pressure with significant altitude excursions around 6/19/2025 and onward suggest a volume change of the balloon (i.e. loss of full shape with pressurization).

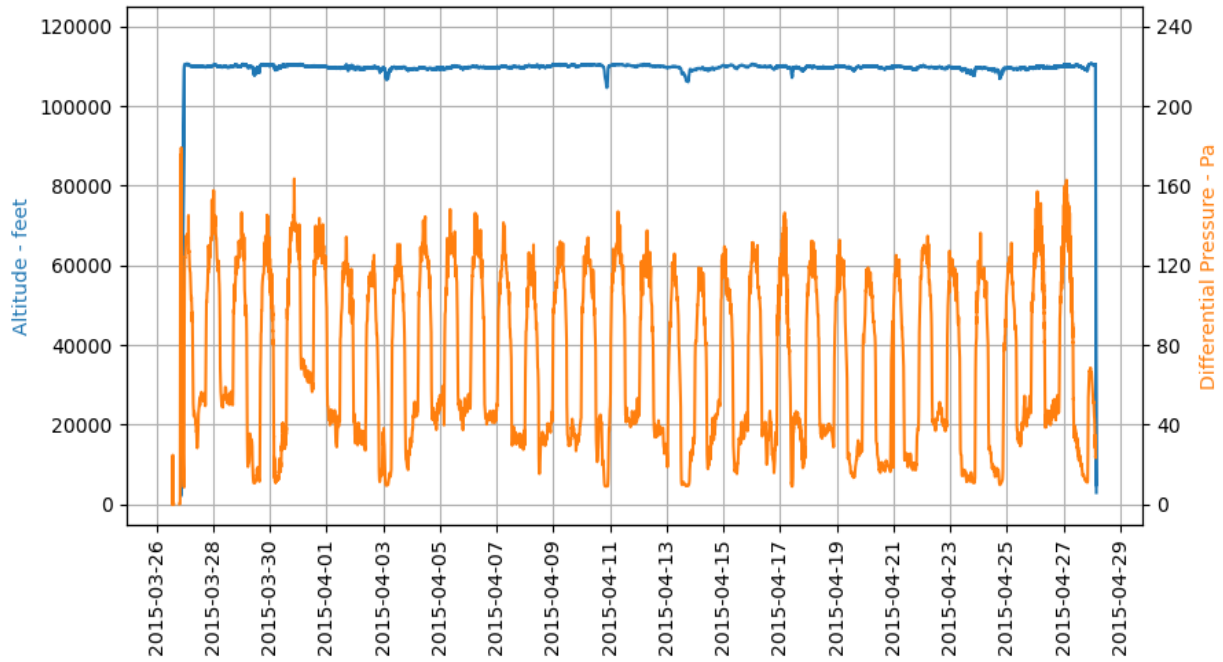


Figure 10-9: Altitude and differential pressure time history for 662NT (SN05) [1].

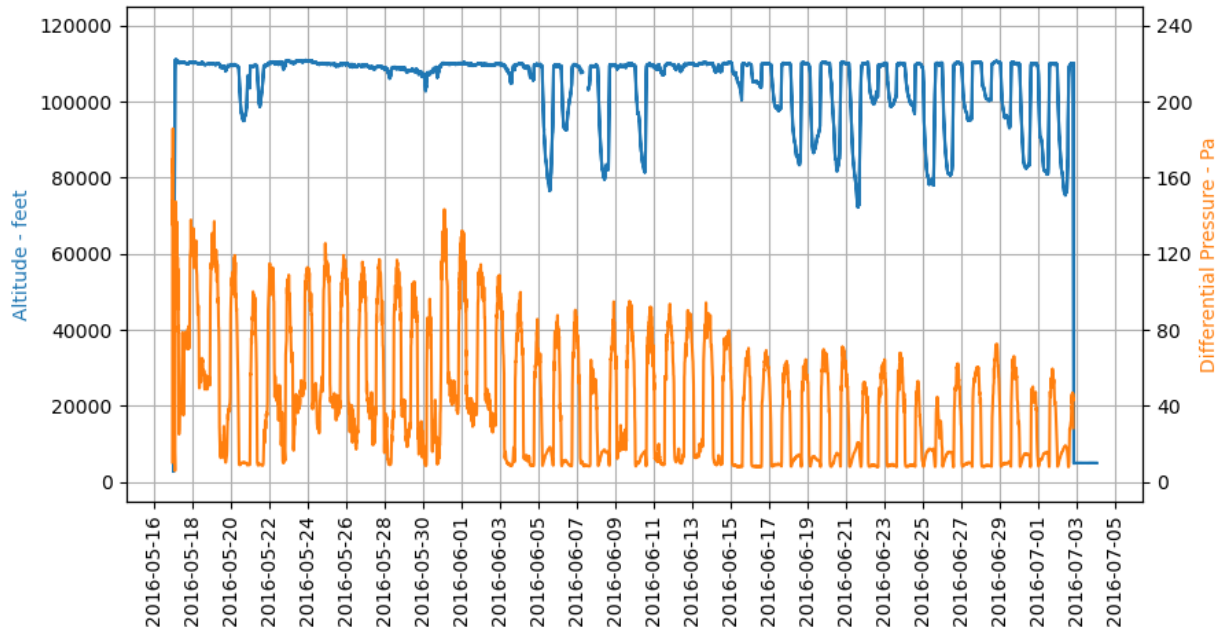


Figure 10-10: NASA 18.8mcf SPB flight 669NT showing degraded performance due to a leak.

At this point, the SPB will behave like a healthy ZPB, but will continue to lose gas through an effective duct area which is the size of the hole in the film or gas barrier. The hole in a SPB is generally modeled either as a duct or a hole, depending on the technique. For both ducts and holes, Farley has modeled the loss of gas mass:

$$\frac{dm}{dt} = -AC_{dis}\sqrt{2\Delta P\rho_{gas}} \tag{10-43}$$

$$u_{flow} = C_{dis}\sqrt{\frac{2\Delta P}{\rho_{gas}}} \tag{10-44}$$

Note that in Equation (10-43) (mass flow rate) and Equation (10-44) (flow velocity), A is the cross-sectional area of the orifice, C_{dis} is an effective discharge coefficient and ΔP is the differential pressure. While effective gas mass (and thus the overall overage loss of gas dm/dt) can be reasoned from long observations (on the order of days) of the balloon environment and the balloon itself, the location and size are coupled. For example, Equation (10-43) suggests that the flow rate is proportional to:

$$\frac{dm}{dt} \propto AC_{dis}\sqrt{\Delta P(h)} \tag{10-45}$$

Plotting contours of dm/dt for the NASA 18.8mcf SPB yield the trends seen in (a similar plot can be made for hole location along the gore). As seen, there is not a unique combination of area and discharge coefficient over either differential pressure or location. Thus, determining IF a leak is present is much easier than WHERE a leak is located. If the hole cannot be seen visually from a camera on the ground, estimation techniques (and simulations of various cases) must be used.

4.3 Natural Oscillations

The oscillations of a balloon are discussed in detail in Chapter 4 but are revisited here. The oscillations of a balloon are theorized to be due to momentum carrying an ascending balloon past the equilibrium altitude. The balloon system continues to oscillate like a lightly damped spring-mass-damper system until the effective momentum is dissipated [5].

Another source of motivation to study balloon oscillations are gravity waves, or Brunt-Vaisala waves. These are waves of air that propagate upward from the surface of the Earth towards the balloon and cause a

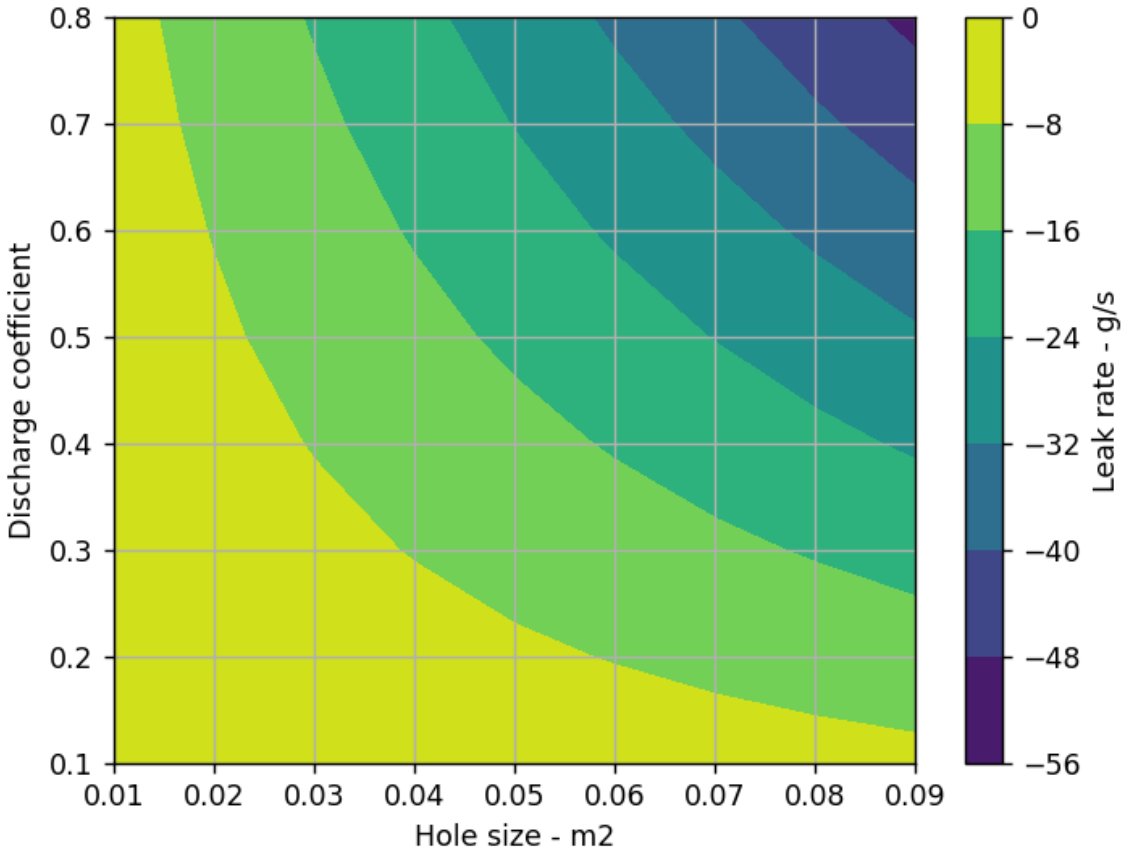


Figure 10-11: An example contour plot of leak rate for various discharge coefficients and hole size for 160 Pa.

displacement on the balloon. The restoring force on these waves is the action due to gravity, for which the name is derived.

For a given SPB at float that is perturbed (from any source), Farley derived the period of these oscillations to be [23]:

$$T_{spb} = \frac{2\pi}{\sqrt{-g\frac{d\rho/dz}{\rho_{air}} - \frac{g^2}{\gamma_{air}R_{air}T}}} \qquad (10\text{-}46)$$

where γ_{air} is the ratio of specific heats in air (1.4), $d\rho/dz$ is the rate of change of air density with altitude, R_{air} is the specific gas constant of air, and T is the absolute temperature. Note that Equation (10-46) is a more general form of the equations presented in Chapter 4. Taking the example of Flight 616NT (shown in Figure 10-12), the oscillations can be shown to roughly align for a period of ~250 seconds (when picking peaks from raw data), while estimates from Equation (10-46) are ~278 seconds.

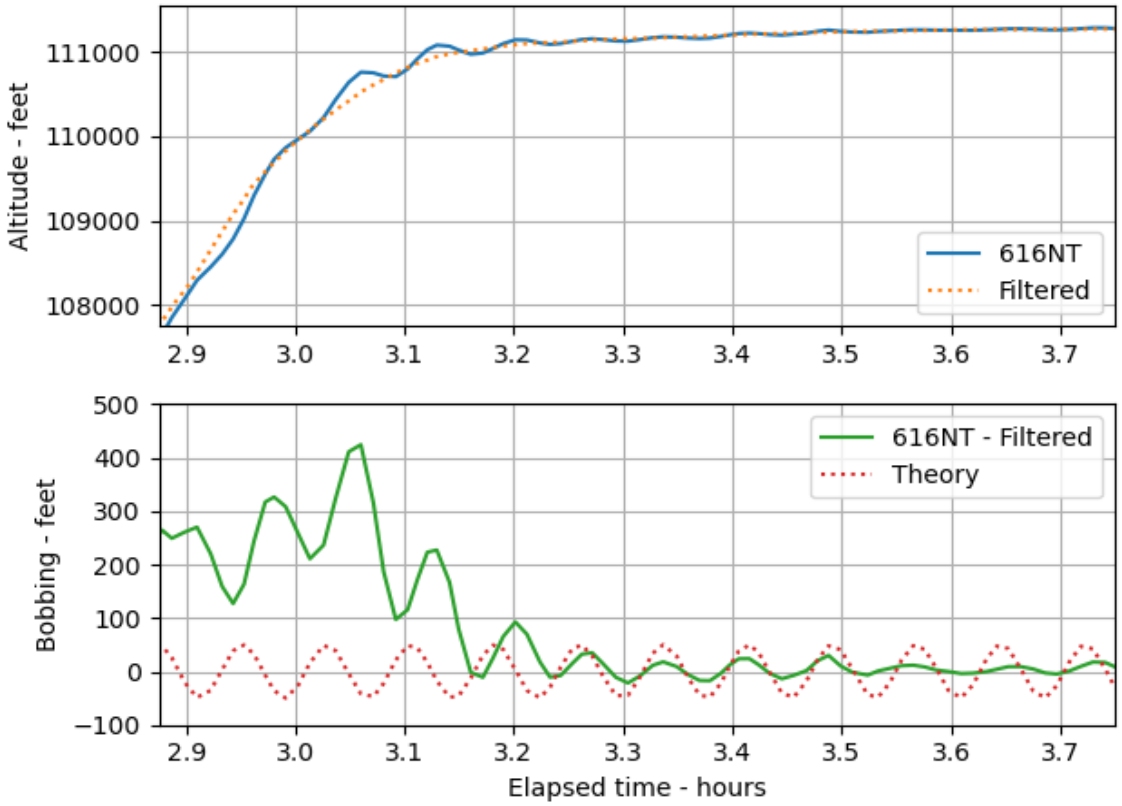


Figure 10-12: (top) 616NT altitude time history around float, alongside a center point moving average. (bottom) Oscillations in float altitude (raw data less filtered data) compared with theoretical oscillations of +/-50m with a 278-second period.

References

[1] D. B. A. Wakefield, "Non-Linear Analysis of the NASA Super Pressure Balloons: Whole Flight Simulations," in *AIAA Balloon Systems Conference*, 2017.

[2] A. Aswin, "Loon library: Lessons from building loon's stratospheric communications service," Project Loon, 2021.

[3] M. S. R. S. H.M. Cathey Jr, "Design and Testing of the ULDB Vehicle," in *Advances in Space Research*, 2002.

[4] D. A. F. M. A. S. H M Cathey, "Performance highlights of NASA super pressure balloon mid-latitude flights," in *AIAA Balloon Systems Conference*, 2017.

[5] A. L. Morris, Scientific Ballooning Handbook, 1975.

[6] K. Yang, R. A. Natherson, C. D. Yoder and S. A. Roth, "A Comparison of Two Non-Contact Strain Measurement Techniques with Applications to Scientific Balloons," in *2021 AIAA Aviation Forum and Exposition*, 2021.

[7] T. Gerngross, Y. Xu and S. Pellegrino, "Viscoelastic behavior of pumpkin balloons," *Advances in Space Research,* vol. 42, no. 10, pp. 1683-1690, 2008.

[8] K. Kawai and S. Pellegrino, "Large strain viscoelastic model for balloon film," in *11th AIAA Aviation Technology, Integration, and Operations (ATIO) Conference*, Virginia Beach, VA, 2011.

[9] Y. S. K. G. D. A. T. M. K. M. H. H. K Nakashino, "Super pressure balloon with diamond-shaped net: A numerical study of its structural characteristics," in *4th AIAA Spacecraft Structures Conference*, 2017.

[10] Y. Saito, N. Kyoichi, D. Akita and T. Matsuo, "Recent Developments on the Super-Pressure Balloon with a Diamond Shaped Net," *TRANSACTIONS OF THE JAPAN SOCIETY FOR AERONAUTICAL AND SPACE SCIENCES,* 2021.

[11] C. R. Calladine, "Stability of the 'Endeavour' Balloon," *Studies in Applied Mechanics,* pp. 133-149, 1988.

[12] H. Fuke, N. Izutsu, D. Akita, I. Iijima, Y. Kato, J. Kawada, K. Matsushima and Y. Matsuzaka, "Progress of super-pressure balloon development: A new "tawara" concept with improved stabilityH Fuke," *Advances in Space Research,* pp. 1136-1146, 2011.

[13] W. W. Schur and C. H. Jenkins, "Deployment destiny, stable equilibria, the implications for Gossamer design," in *43rd AIAA/ASME/ASCE/AHS/ASC Structures, Structural Dynamics, and Materials Con*, Denver, CO, 2002.

[14] M. S. Smith and E. L. Rainwater, "OPTIMUM DESIGNS FOR SUPERPRESSURE BALLOONS," *Advances in Space Research,* pp. 1688-1693, 2004.

[15] F. E. Baginski, K. A. Brakke and W. W. Schur, "Cleft formation in pumpkin balloons," *Advances in Space Research,* pp. 2070-2081, 2004.

[16] D. Wakefield, "Numerical Modeling of Pumpkin Balloon Instability," in *AIAA 5th Aviation, Technology, Integration, and Operations Conference (ATIO)*, Arlington, VA, 2005.

[17] M. Pagitz and S. Pellegrino, "Buckling pressure of "pumpkin" balloons," *International Journal of Solids and Structures,* pp. 6963-6986, 2007.

[18] J. Rand, "A constitutive equation for balloon film," in *AIAA Balloon Systems Conference*, Williamsburg, VA, 2007.

[19] R. L. Rand, "Mechanical Behavior of Superpressure Balloon Film," 2013.

[20] R. A. Schapery, "On the characterization of nonlinear viscoelastic materials," *Polymer Engineering & Science,* pp. 295-310, 1969.

[21] J. Rand, D. Grant and T. Strganac, "The nonlinear biaxial characterization of balloon film," in *34th Aerospace Sciences Meeting and Exhibit*, 1996.

[22] J. R. Blandino, H. M. Brown, S. K. Long and J. Sterling, "A Primer on Photogrammetry for Ground Testing Scientific Balloons Using a ULDB Model," in *AIAA Balloon Systems Conference*, Williamsburg, VA, 2007.

[23] R. Farley, BalloonAscent Theory Manual, Greenbelt: Farley Flight Aerospace, 2020.

Chapter 11
Flight Operations

Christy A Hales[1], Erin Reed[2], Matthew Laffin[3], Ethan A. Chaffee[4]

[1]National Aeronautics and Space Administration, Mission Operations Manager, Balloon Program Office
[2] National Aeronautics and Space Administration, Technology Manager, Balloon Program Office
[3] World View Enterprises, Inc., Meteorologist, Mission Operations Department
[4] World View Enterprises, Inc., Program Manager, Programs Department

Table of Contents

1. Introduction 4

2. Historical Lessons 4

3. Balloon Operations 5

3.1. Operations Roles 5

3.2. Launch Hardware Architecture 9

3.3. Pre-Flight Operations 11

3.3.1. Launch Site Requirements 11

3.3.2. International Cooperation & Regulatory Compliance 11

3.3.3. Pre-Mission Operations and Planning 12

3.3.4. Gondola Integration 13

3.3.5. Day-of-Launch Activities 14

3.4. Launch and Flight Operations 15

3.4.1. Launch Methods and Operations 15

3.4.2. Flight Stages 18

3.4.3. Final Reporting and Mission Close-out 20

4. Conclusions 20

References 21

Table of Figures

Figure 11-1: Super-pressure balloon launched by NASA with the common launch components annotated for reference..... 9

Figure 11-2: Static launch cartoon..... 15

Figure 11-3: Dynamic launch cartoon..... 16

Figure 11-4. Zero-Pressure Balloon Launch Configuration..... 17

1. Introduction

This chapter addresses basic balloon operations and the many roles that contribute to a successful balloon mission. To launch, fly, land, and recover a balloon and its payload requires significant coordination among balloon providers, launch providers, meteorologists, safety, scientist or the customers, and includes regulatory agencies that oversee airspace and, potentially, international cooperation. It should be noted that while this chapter aims to remain agnostic regarding operations and methods, it still maintains a heavily NASA- and US-based approach due to the limited experience of the contributing authors. However, the authors have made a conscious effort to remove organization-specific language for terms on the balloon launch flight line, adopting a broader approach to these practices. It is hoped that a future edition of this handbook will improve upon the treatment taken here.

2. Historical Lessons

Those well familiar with balloon launch operations may look at historic pictures of balloon use during the Civil War (Chapter 1) or videos from 1950s launches during such programs as Stratolab, or Manhigh, and marvel at the similarity in launch architecture that still exists today. Part of this is due to the unchanging requirements for a successful balloon launch: stored lift gas must be inserted into a relatively delicate balloon envelope under ideally low-wind conditions. Part of this is due to work in the 1950s by several early researchers, including General Mills, the U.S. Air Force, and the U.S. Navy [1-2], New York University, Tufts University, and Winzen Research [3-6]. Launch techniques considered include launching from inside a building [7], from a ship [8], from an aircraft, or from a wagon [9]. Inflation methods were either vertical (static) or dynamic with upwind and downwind launches [10]. Much of the launch hardware was also developed during this time, including the use of cranes, carts, and a spool to contain the balloon bubble. But other options, such as the use of a shroud to hold down the balloon [11], the use of a balloon within a balloon (Ferguson Launch Method) [12], as well as dual balloon or tandem balloon launches [3].

Since then, there have been improvements in the reliability of launch equipment, the size of the balloons, and technology that aids in operations. However, the underlying architecture remains largely comparable. There are exceptions, of course. In the past few years, though, as balloon sizes and uses continue to evolve with the development of lightweight, powerful telemetry and electronics, as well as continued investigation into different lift gases or smaller launch crews, new launch procedures and operations are once again emerging. Although this chapter will focus on methods that are largely well established in industry, it is anticipated that the handbook user may identify

significant variations from this as scientific ballooning continues to change to meet novel and growing demand.

3. Balloon Operations

Although each balloon and launch provider may differ in the details of their mission planning and execution, there are enough similarities to merit inclusion in this handbook, providing a more complete picture of the logistics and considerations required for a successful balloon mission. This discussion does not purport to cover all aspects of operations for all types of missions and does have a bias towards American-based scientific balloon operations. The interested reader is encouraged to research other organizations to gain a full appreciation of the variety of methods used in ballooning.

3.1. Operations Roles

Launching a large scientific balloon requires a team that has been trained over many years in highly specific roles to ensure the system is safely assembled and integrated between the balloon, flight train, and science payload. The launch itself is a complex and hazardous process that requires several years of training and a combination of uniquely acquired skills, including meteorology, ordnance, engineering, telemetry, mechanical integration, international diplomacy, and planning. The launch, monitoring, termination, and recovery processes require a highly integrated, synergistic team that understands the inherent hazards and dangers associated with a large-volume balloon with a payload. Personnel need to be experienced in operating specialized equipment, such as heavy-lift cranes, for launching a balloon. While each launch may have unique requirements and logistics, some general functions are common across many launch operations and are described here. Role titles are generic and not specific to titles from any given organization.

The **Launch Management Team (LMT)** can be composed of several individuals and even several organizations but is ultimately responsible for overseeing campaign operations and ensuring the safe implementation of all activities. The LMT serves as the interface among all parties, including on-site safety representatives, local authorities, air traffic control, the launch crew, and the launch customer. The LMT is also responsible for ensuring the safe performance of operations associated with the campaign and provides the clearance (go/no go) per the launch commit criteria to proceed for launch. The LMT typically has the authority to call for a launch abort in the event of a launch mishap or flight termination. To perform the LMT role, personnel must have detailed knowledge of all operations and hazards related to launching a scientific balloon, air traffic regulations, flight safety requirements, ground safety requirements, operational requirements, and hazards associated

with all science missions. In addition, LMT must be able to communicate effectively with government personnel, contractors, engineers, scientists, technicians, and laymen.

The **Launch Safety Representatives (LSR)** are responsible for ensuring public safety during launch, flight, and termination operations, and for supporting the launch clearance (go/no go) per the launch commit criteria to proceed to launch. The LSR implements the flight safety plan for the campaign, including the coordination and establishment of roadblock locations and other on-site safety implements, based on the winds on launch day; verification of proper implementation of hazard areas for the launch site; and typically has the authority to call for a launch abort or a flight termination in the event of a launch mishap, overflight risk issue, or other situation creating the need for a termination command decision for purposes of ensuring safety. To perform the LSR role, one must have detailed knowledge of all operations and hazards related to launching a scientific balloon, flight safety requirements, ground safety requirements, operational requirements, and hazards associated with the balloon mission and payload.

The mechanical lead, referred here to as a **Crew Chief** (CC), is responsible for the successful physical launch of the payload with the balloon system. The CC is responsible for overseeing the mechanical technicians and ensuring processes are followed. The CC also ensures the mechanical technicians support the assembly of the payload and integration into the gondola, as required. In addition, the CC determines the gross inflation mass for the launch, ensures gas inflation processes during launch opportunities are followed, and oversees the mechanical technicians' use of heavy equipment. The CC has the authority to call for a launch abort in the event of a launch mishap or when circumstances require an abort command decision to ensure safety. To perform the CC role, one must have detailed knowledge of all operations and hazards related to launching a scientific balloon, ground safety requirements, operational requirements, hazards associated with the balloon mission and payload, high pressure systems, cryogenic systems, ordnance systems, lifting device and equipment, gross inflation calculations, and the affects that winds have balloon during inflation and launch. Also, the CC requires expert knowledge of the mobile launch vehicle's payload dynamics and handling during the launch process.

The **Electrical Lead (EL)** is responsible for the successful execution of all electrical systems during pre-launch, launch, and flight activities. The EL is responsible for overseeing the electrical technicians and ensuring processes are followed. The EL also ensures that electrical technicians support the payload connections and integration with the gondola, as required. To perform the EL role, one must have detailed knowledge of all operations and hazards related to launching a scientific balloon, ground safety requirements, operational requirements, hazards

associated with all science missions, ordnance systems, radioactive frequency (RF) hazards, and electromagnetic compatibility and interference considerations.

The **Launch Customer (LC)** personnel are responsible for assembling, integrating, and testing their payload to ensure that it is flight-ready prior to launch opportunities. The LC team is responsible for adhering to the requirements outlined in the campaign's Ground Safety Plan and Radio Frequency Safety Plan for their scientific payload, as applicable. The LC team provides the technical knowledge uniquely required for their payload.

The **Telemetry Engineer (TE)** is responsible for verification, integration, and operation of line-of-sight/satellite communications systems, telemetry and command/control systems, and battery/solar power systems. These systems are functionally verified prior to integration with the gondola and balloon, during pre-flight compatibility testing, and during pre-launch testing. After launch, the TE team monitors the health and performance of the systems within line-of-sight range, including providing Global Positioning System tracking data for flight tracking and flight safety evaluation. The TE also assists the electrical technicians with pre-launch equipment connections and post-launch flight tracking. The TE is also responsible for interfacing with the launch customer to verify that communications interfaces —both uplink commanding and downlink telemetry —are functioning properly throughout the payload build-up, testing, launch, and flight stages. The TE coordinates with the Operations Control Center during instrument compatibility, pre-launch, and flight stages. The TE also verifies satellite availability and requests/coordinates satellite scheduling. To perform the TE role, one must have detailed knowledge of all operations and hazards related to launching a scientific balloon, satellite scheduling, telemetry systems, command and control systems, tracking systems, and solar power systems.

The **Mechanical Technicians**, or **Riggers**, are responsible for providing support during the integration of the balloon mechanical systems into the payload, which are required for the safe and successful flight of the mission. Riggers assist the science team with the fabrication and installation of structural items (such as antenna booms), the installation of flight support equipment (such as ballast hoppers and crush pads), and the installation of all rigging to the attachment point of the balloon system. In addition, riggers are responsible for inspecting, maintaining, and testing mechanical units, systems, and subsystems (such as ballast hoppers and parachutes). Riggers also inspect, maintain, and/or operate the mobile launch vehicle, spool trailer, balloon trailer, and helium trailers. Rigger's responsibilities during launch also include, but are not limited to, the layout of the ground cover and balloon, helium inflation operations, and

crane operations. To perform the mechanical technician role, one must have detailed knowledge of all operations and hazards related to launching a scientific balloon, ground safety requirements, operational requirements, hazards associated with all science missions, high-pressure systems, cryogenic systems, ordnance systems, lifting devices, and equipment.

The **Electrical Technicians** provide support to the TE during payload build-up, testing, pre-launch, and flight stages. They are responsible for assembling the telemetry and commanding equipment at the launch site and for operating that equipment during testing, pre-launch, and post-launch line-of-sight stages. In addition, they are responsible for the mapping computer and software that track and plot the balloon's location and trajectory during the line-of-sight phase of flight. Other electronics technician responsibilities include verifying battery functionality prior to installation, making connections to the flight termination and parachute separation systems, and performing any required cable fabrication or repair work, including to support the LC team. To perform the electrical technician role, one must have detailed knowledge of all operations and hazards related to launching a scientific balloon, ground safety requirements, operational requirements, hazards associated with all science missions, ordnance systems, communications systems, and battery systems.

The **Balloon Quality Engineer (BQE)** may participate in balloon operations in the field, depending on the mission's needs and the balloon's design. The BQE is responsible for overseeing the overall quality of the balloon and ensuring that all personnel are aware of and follow proper balloon handling and operational procedures related to the success of the mission. To perform in the balloon quality role, one must have detailed knowledge of balloon manufacturing, balloon handling procedures, balloon material defect types and repair methods, balloon inspection techniques, operations for loading and unloading a balloon, and balloon historical performance to inform and provide real-time mission operations assessment of balloon health during ascent and float.

The **Meteorologist** contributes directly to the determination of launch windows, flight altitudes, and trajectory forecasts. Their ability to analyze real-time and climatological data allows them to suggest modifications to flight timing or target coordinates, often improving cost-efficiency and reducing operational risk. In missions that require station-keeping or precise overflight of target areas, such as those exploiting the summer stratospheric easterlies, the meteorologist’s input is vital to ensuring the balloon takes full advantage of favorable wind regimes. Additionally, balloon meteorologists play a key role during flight operations, providing updates on atmospheric conditions, advising on ballast adjustments or altitude shifts, and supporting recovery teams with real-time tracking and trajectory predictions. Their involvement extends across all phases of the operation, from pre-flight planning to

post-flight analysis, making them an indispensable asset in any successful ballooning endeavor. The role of the meteorologist requires detailed knowledge of historical balloon ascent and descent performance, the ability to interpret current weather models for forecasting, and the ability to use simulation software for balloon trajectories (ascent, descent, float).

The **Videographer** or other documentation specialist may be on site to capture balloon launch operations using both photography and filmography. Those involved in operations may desire high-quality video, especially of the inflation and balloon launch, for investigative purposes, should an anomaly occur with the balloon. The videographer understands the scale and timing of operations and can fully capture the activities without being escorted by operations staff members or causing a hazard.

3.2. Launch Hardware Architecture



Figure 11-1: Super-pressure balloon launched by NASA with the common launch components annotated for reference.

Gondola: Used interchangeably with the payload, refers to the system carried to the stratosphere by the balloon for science and other purposes. The gondola itself can refer to just the frame to which the instrumentation package(s) are attached for launch. A simple, lightweight gondola structure that can accommodate multiple instruments

in diverse configurations provides the advantage of reusable gondola frames.

Launch vehicle: A vehicle, often with a boom attached, that has carrying capacity for the gondola or balloon during the launch process. Having a drivable vehicle allows in-situ adjustments to align the payload with the balloon and the winds, easing forces on the system during launch and payload release. This is particularly helpful for flight lines that take a long time to lay out or balloons that require long inflation times.

Spool/Roller/"Hutch clutch"/"peanut": Even if its names are varied, this hardware's use is singular – to hold the balloon down and prevent premature ascent during inflation and pre-launch operations. This piece of hardware can be on a cart, a truck, a trailer, or even a sled. Understandably, balloon film experiences significant stresses during inflation due to opposing forces from the helium and the spool. Thus, care must be taken in design, handling, and inspections. Parachute: Included in a packed or open configuration, a parachute is critical for those who wish to recover payloads after a balloon flight. Parachutes are sized according to the payload's size and weight.

Termination Package: Flight lines typically include a termination system that separates the parachute and balloon at the end of the float phase. A termination package may include a variety of methods to effect this separation, but the use of small firing "squibs" is a successful approach.

Lift Gas Vehicle: No matter the balloon's size, there is a means to transport the lift gas and align it with the rest of the flight line. The lift gas vehicle can be a truck or trailer that transports bottles, manifolded cylinders, or intermodal tanks ("iso-pak"). Inflation lines connect the lift gas source to the balloon.

Balloon: Although an obvious part of a balloon launch flight line, it bears repeating here. Balloons can be brought to the flight line on a trailer, truck, or sled. Dependent on the size, balloons can be laid out in full or in part before inflation or laid out as inflation continues. Due to the delicate nature of the thin films that balloons are composed of, they may be wrapped in protective layers and packaged to resist excessive handling. Additionally, laying ground cover and/or maintaining the launch area can help reduce wear and tear during launch activities.

3.3. Pre-Flight Operations

3.3.1. Launch Site Requirements

Site selection for launch is crucial to the success of any balloon launch. When selecting a suitable launch location, potential launch days with favorable weather conditions need to be identified. Considerations include typical surface-level and low-level wind magnitudes and directions, local population density, and accessibility of the launch site. Also critical are the seasonal stratospheric wind profiles, areas likely to be overflown, downrange telemetry options, and potential recovery locations. The ideal location depends on mission objectives, such as the Area of Interest (AOI), as well as meteorological and topographical considerations. To minimize the impact of high winds, sites in topographic depressions, such as river valleys or basins, are often preferred. For example, the lee of a mountain range can provide shelter from prevailing winds. Additionally, the interaction between expected wind direction and local topography requires careful consideration. Launch sites downwind of significant terrain features may experience increased turbulence and unpredictable wind gusts.

Most launch providers have several launch sites for customers to choose from. In these cases, considerations typically include factors such as latitude, potential flight duration, science goals, cost, and timeline.

Recovery location(s) can also be baselined at this point, and plans and personnel readied for that portion of the mission's services. When recovery operations are conducted in another country, special consideration will need to be given to how personnel and equipment can be brought in, and the recovered item can be taken out of that country. A common issue is that the balloon system may not have been adequately imported into said country, which causes problems when exporting. Preliminary and final flight plans are also communicated and approved by the safety group. An overflight risk analysis is conducted, and any concerns are addressed. This exercise can change the flight plan depending on the risk score and safety evaluations. Customer review and approval of the flight plans are recommended. Flight plans may undergo many iterations before being finalized as the baseline.

3.3.2. International Cooperation & Regulatory Compliance

For balloon operations in the United States of America, the regulations are codified in 14 CFR Part 101 – Moored Balloons, Kites, Amateur Rockets, and Unmanned Free Balloons. The regulatory agency for Part 101 is the Federal Aviation Administration (FAA), specifically within the air traffic control (ATC) function. The regulation provides guidance on the classification of balloon types and acceptable weights and flight altitudes that do not require permission, reporting, or Notice to Airmen

(NOTAM) submittal to FAA ATC. However, all balloon users are encouraged to contact the local ATC facility to ensure full compliance. It should also be noted that some airspaces are restricted from balloon operation and others may require additional limitations or requirements for flight by the controlling agency [13].

The use of radio frequency for telemetry and instrumentation purposes during a balloon flight is codified in 47 CFR Part 87. However, the United States is a member state and remains in compliance with the Radio Regulations (RR) established by the United Nations' International Telecommunications Union (ITU), which is the specialized agency for all communications technologies [14]. The balloon user is invited to utilize these regulations to appropriately choose and operate any on-board, air-to-ground, or (in some cases) air-to-air communications.

For flights that may traverse multiple countries and continents, international coordination will be required. Depending on the organizations involved, this could include communication through the Department of State or a Foreign Ministry, governmental and civil aviation authorities, international air traffic control, and any entities involved in recovery efforts. For launches outside the organization's native country, rules for coordination, importing, and exporting flight hardware may apply, as well as personnel visa regulations. The launch location may have some experience with launch coordination and meeting requirements for successful missions. For instance, the Swedish Space Corporation (Esrange) in Kiruna, Sweden, is a site for many scientific ballooning groups and has historically helped coordinate launch permissions and launch notifications with nearby countries. In New Zealand, high-altitude vehicle licenses are required. Some countries that a balloon may overfly may also require detailed information about the purpose, predicted flight path, flight durations, science instruments, and flight safety plans before approving a balloon to overfly their territory. Countries often require multiple months to review overflight requests, and any service provider has an obligation to become familiar with the applicable laws of any countries that may be overflown. As a result, communication and coordination with all stakeholders may start upwards of a year before the expected launch date.

Chapter 2 contains lessons learned from student-launched balloons that can be applied to larger missions and commercial operations. It is also incumbent upon the launch entity to research all rules and regulations pertaining to launch, flight through various airspaces, and recovery.

3.3.3. Pre-Mission Operations and Planning

Mission planning generally occurs several months or years before a desired launch. Launch customers likely have an area of interest they would like to fly over or under and have an ideal launch location and

duration already selected when they approach a balloon and launch provider. Additionally, they may identify instruments, technologies, and hardware that need to be developed before the mission. On a similar time scale, those involved in the launch will also have several activities underway to ensure the mission's success: baseline flight planning, generation of success criteria for both the balloon and the payload, and balloon selection based on preliminary theoretical flight altitude, duration, and payload size and weight. Preliminary theoretical system weights and standard atmosphere and temperatures are used at this early stage. Some considerations that may affect payload size and weight include proposed payload instrumentation, telemetry hardware including air traffic transponders, use of batteries and/or solar panels, and ballast, as well as the sizes and capabilities of launch support equipment such as launch vehicles, cranes, and hangar doors.

Once the balloon flight system is completed, actual masses and more accurate flight environmental data variables are incorporated to create the most accurate flight plan.

The roles described above all play a role in pre-flight coordination through numerous coordination events, including reviews, planning meetings, and resource assessment and allocation (such as schedules, personnel, and hardware). Prior to the flight, the balloon's predicted trajectory and expected altitudes are communicated to all stakeholders. It is recommended that this data be reviewed by multiple members of the mission control team and once finalized, used during flight to compare the actual value with the prediction and identify potential anomalies.

3.3.4. Gondola Integration

Typically, the balloon system must integrate with customer components and avionics, as well as power and control packages. This integration process is initiated during requirement generation for each subsystem, allowing them to connect and integrate to form the entire flight system. Personnel should be aware of the customer interface beforehand and be fully prepared to integrate customer payloads into the flight system. Tooling and assembly kits should be created in advance, along with all necessary procedures.

The integration event usually involves installing science/customer instrumentation and launch provider instrumentation on the gondola. Other components, such as parachute systems, flight ladders, and other gondola components, are typically installed during this time as well. In general, this is done near the launch site, in an integration hangar, where personnel and equipment are available to troubleshoot and correct any issues found. System-level performance checks for electromechanical assemblies and command/control systems can be performed without the pressures of the day-of-launch environment. Records for traceability and

process accountability should be kept for the integration process, with quality teams conducting their verifications in parallel. In addition, proper forethought should go into the arrangement of integrated subsystems in the hangar and the ease and efficacy of rollout to the flight line area and the respective launch equipment, so as not to cause any damage to the now-assembled flight system. During integration, final weights for the entire system may be completed to provide accurate assessments useful for launch prediction and forecasting of ascent to float, float duration, descent, and the altitude the balloon system can achieve. The ballast on board the system can be reduced or increased as needed to optimize flight performance.

3.3.5. Day-of-Launch Activities

Accurate launch weather forecasts are essential for identifying suitable launch conditions. Modern numerical weather prediction (NWP) models are the primary tools for predicting these conditions. Prior to launch, the meteorologist combines climatological data with real-time weather model outputs to estimate a launch window. The climatology of a launch site includes historical weather data and even previous launches and conditions to understand typical weather patterns and potential risks. Once the launch window is set, operations will often be timed appropriately, with personnel showing up on-site with enough time and buffer to account for instrumentation and telemetry checkouts, moving equipment out to the flight line, and laying out the flight line and balloon.

The day before a launch, the crew chief likely has directed checks on the lift gas containers, the launch vehicle, and the spool/roller cart to avoid delays on the day of launch due to mechanical issues. Additionally, riggers and/or balloon personnel often review the balloon documentation and inspect what parts of the balloon can be accessed without a full deployment to ensure no damage has occurred in transportation or handling. Likewise, the electrical lead has directed technicians and engineers to complete end-to-end checks of electrical components that often extend from the payload gondola to the top of the balloon, ensuring all is in working order. For flight coordination, a NOTAM or other notification to flight authorities is filed at least the day before a launch attempt. Additionally, the launch customer should be happy with the operational status of their instruments before a launch attempt is scheduled and made. On the day of a potential launch, systems that were previously in go status may encounter issues that require last-minute troubleshooting. If enough buffer is provided in the launch schedule, these issues can be addressed to avoid missing the launch window.

Once the gondola checkout is complete and the meteorologist continues to confirm that the weather conditions are conducive, the flight hardware

is taken out to the flight line. Despite the fact that there are multiple types of launches – hand, static, upwind dynamic, and downwind dynamic – these all have common elements on the flight line.

3.4. Launch and Flight Operations

3.4.1. Launch Methods and Operations

Different launch methods have been developed in scientific ballooning to address varied logistical and resource constraints, but three have remained dominant: static, upwind dynamic, and downwind dynamic. These methods are described here, but they do not include the range of ways in which even these may be implemented by various organizations throughout the world. The reader is invited to research the launch method of each scientific ballooning organization to get a full appreciation of the creativity and variety of launches within the community.

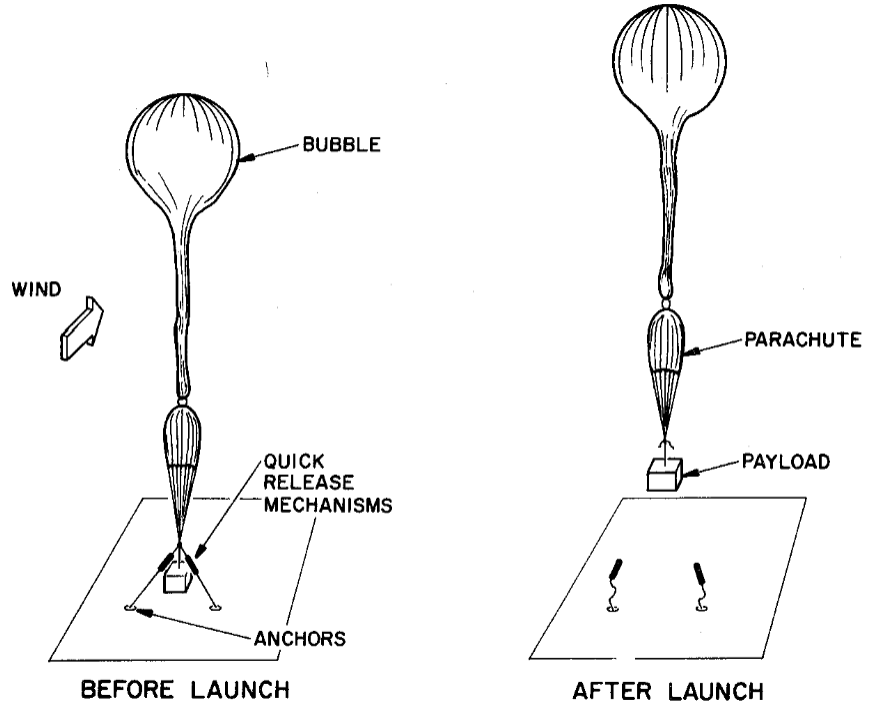


Figure 11-2: Static launch cartoon.

In a static launch, the balloon is held erect over the payload and released. This method has been used successfully by JAXA [15-17] as well as the Air Force during its experimental balloon work in the 1950s (see section 2). Wind conditions throughout the balloon's height are critical, as large balloons can act like sails, but the advantages of this method include a reduced footprint for the flight line. This method may also

be appropriate for the launch of quick-inflation, quick-release of smaller balloons.

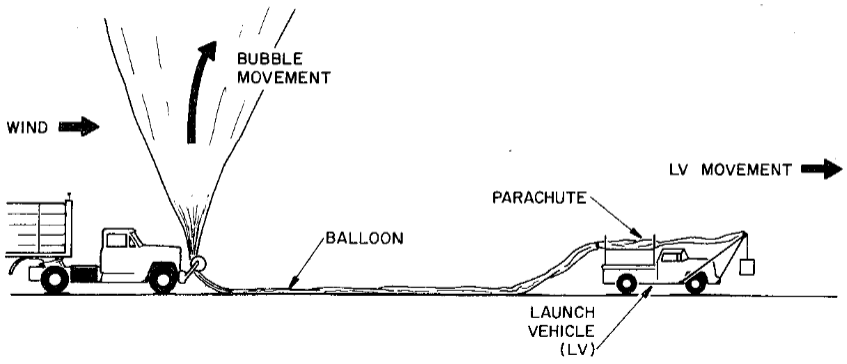


Figure 11-3: Dynamic launch cartoon.

In a dynamic launch, the balloon is launched while lying on the ground. This method exposes the balloon to less surface wind. Both upwind and downwind launch techniques are used, and wind speed is a critical factor in both. Modern dynamic launch systems and procedures have enabled launches in higher wind conditions.

For an upwind dynamic launch, the flight train should be laid out so the balloon is positioned upwind of the payload, ensuring the balloon ascends towards the payload once the bubble is released. Releasing the payload once the balloon is directly overhead will minimize loads on the balloon and flight and ground hardware but does require a flight area that can accommodate the entire length of the flight train, often increasing the difficulty of communication over a wide area and slowing the launch process to accommodate the deployment of all components. There are a variety of potential inflation and launch configurations, depending upon the size and type of balloon. A common one used for dynamic ZP balloon launches is shown in Figure 11-4.

Downwind dynamic launches lay out the flight line in the opposite direction; that is, the balloon is set up downwind of the payload. For this, once the balloon is released, the launch vehicle holding the gondola and flight line components is driven to catch up to the balloon as the balloon ascends. Using this method, the balloon can experience stresses if the winds are too high and pull it away from the payload at high speed, but it does take advantage of the launch vehicle to actively build the payload's momentum for a smooth release from the launch vehicle.

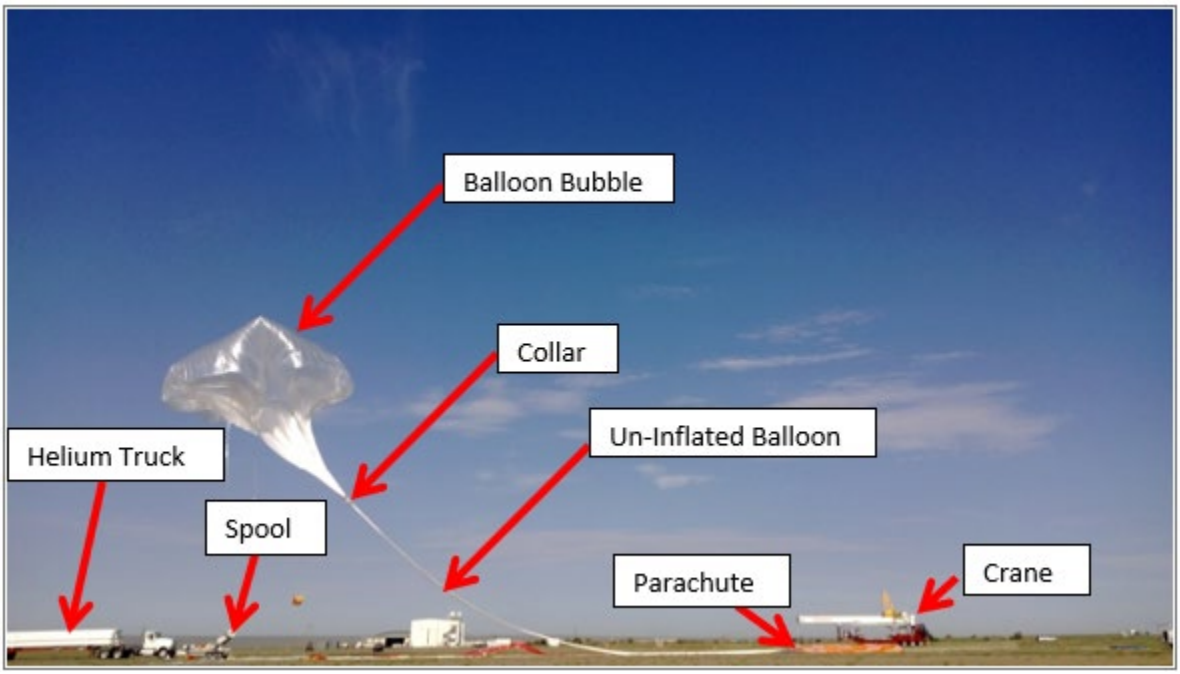


Figure 11-4. Zero-Pressure Balloon Launch Configuration

Wind remains the most restrictive meteorological factor during launch. Until sufficient gas is inside the balloon to provide it with shape and rigidity, the balloon fabric is susceptible to being moved by even light winds. Rapid inflation minimizes this risk. The acceptable wind speed during inflation depends on the strength of the balloon fabric and supporting launch equipment. For thin polyethylene balloons used in high-altitude flights, steady winds less than 5 m/s are generally acceptable. However, because winds are often gusty, even lighter and more consistent wind conditions are preferred. Precipitation and the risk of lightning are also important considerations due to potential risks to human safety and the functionality of electronics. Moisture accumulation on the balloon envelope, either from precipitation or humidity, can be highly detrimental to balloon operations. The added weight from moisture on the balloon envelope can either slow or arrest ascent, essentially killing the mission before it even begins.

In all of these launch methods, at some point before, during, or after inflation, a collar is installed at the bottom of the "bubble" or inflated portion of the balloon to prevent the entire length of the balloon from unfurling in the wind and experiencing stresses from the balloon effectively acting as a sail, like on a boat. This collar will be remotely released either just before or after the flight train is released, allowing the gas to extend into the balloon and deploy its full volume as the balloon ascends.

Chapter 6 provides detailed information on lift gases for various operations, along with the hazards associated with each. Thorough risk management is key to successful and repeatable flight.

3.4.2. Flight Stages

3.4.2.1. Ascent

The flight train, once released, is now free to ascend to the stratosphere. After launch, the balloon and flight train are now free of any earth-bound constraints and no longer "fight" the winds but move with the ambient air, thus reducing wind-driven stresses on the balloon. The balloon's thermal environment, ambient temperature, and free lift of lift gas in the balloon determine the ascent rate. In the past, too high an ascent rate was determined to have negative impacts on the balloon, (but since balloon redesign work in the 1980s, high ascent rates have not given cause for concern (per experience). As a balloon ascends, it encounters decreasing temperatures until it reaches the troposphere, where it reaches a minimum, and then temperatures increase in the stratosphere. As a balloon ascends, it encounters decreasing temperatures, particularly near the tropopause, where the lapse rate changes abruptly. For high-altitude flights reaching 160,000 ft (~48.8 km), the balloon may pass through multiple tropopause layers, including double tropopauses, which are common near the subtropical jet and can influence ascent dynamics and thermal stress on the payload. While crossing the tropopause, the lift gas may condense enough that the ascent rate drops or levels off. The careful use of ballast can help a balloon push through this temperature drop without risking flight performance or flight duration. Modern balloon materials can withstand very low temperatures, but extremely cold conditions can still present challenges. The meteorological tropopause, defined by lapse rate criteria, may differ from the thermal tropopause used in operational models, and understanding this distinction is important for predicting ascent behavior [19]. Clouds can also affect a balloon's ascent rate by altering its radiative environment. It is recommended to have a thorough understanding of the likely ascent profile prior to launch to identify any anomalous behavior and correctly predict float altitudes.

3.4.2.2. Float

Tracking the balloon is essential for scientific data acquisition and may be legally required. Modern tracking methods include GPS tracking, satellite communications (e.g., Iridium, Starlink), and radar. Cloudiness and low visibility can hinder visual tracking, but electronic tracking methods are generally unaffected by weather conditions. Tracking can be conducted from the launch site, remote ground stations, or aircraft. Aircraft tracking is often used for long-duration flights.

Typically, the parties involved in the flight planning phase are the primary performers of flight monitoring and control functions. Flight system health for each subsystem and trajectory against the plan is monitored and reported. This team adjusts and controls the flight system to meet the desired performance requirements. Customers are also typically monitoring and controlling their systems during this phase and are included in the flight monitoring and control activities. Depending on the flight duration, this effort can last from a few hours to several weeks or months. Once the mission objectives of the flight are achieved or the flight is deemed necessary to terminate, the flight monitoring and control team initiates payload and balloon descent. The descent and impact location, as well as any other imperative details, are communicated to the recovery teams that should be pre-staged in the anticipated recovery area.

3.4.2.3. Descent and Landing

Balloon-borne experiments are typically returned to Earth by parachute or parafoil. The meteorological considerations during descent are similar to those during ascent but occur at a different location and time, requiring longer-range forecasts. The descent rate of a parachute or parafoil can be accurately calculated using the Standard Atmosphere [18]. An accurate prediction of the descent trajectory is crucial for recovery operations. Daytime parachute descents can often be visually tracked.

Radio transmitters on the payload aid in tracking, especially at night or in poor visibility. Descents in the vicinity of thunderstorms or convective clouds should be avoided. Accurate predictions of surface winds are highly important, as high winds can damage payloads upon landing.

Immediately after touchdown, the parachute should be deflated or detached to prevent it from dragging the payload. The ideal landing site is a firm, accessible, dry, unoccupied area. Surface and low-level winds, recent and anticipated precipitation, and visibility are important meteorological factors. Modern recovery operations often use GPS and real-time weather data to optimize landing and recovery. The expected landing location should be identified prior to termination to target a good location and minimize risk to the public and property. Essential hardware for termination events is discussed in detail in Chapters 12 and 14.

3.4.2.4. Recovery

The Recovery team often consists of recovery crew members and technical representatives for the flight system or subsystems. Customer representatives may also be present during this operation to gather and

assess their respective components. Balloon recovery can often be performed in hazardous, remote locations and is hard, dirty work. The recovery team should have standard operating procedures and tooling for recovery, as well as off-nominal procedures and associated tooling. Off-nominal procedures should be used when the flight had an anomaly and physical flight articles are now needed for forensic analysis. This typically requires specific actions and documentation of the article prior to or during the recovery process. The team should be prepared to execute either process that the situation may demand or as directed. Once the recovery process is completed, items are packaged for return shipment or disposal.

3.4.3. Final Reporting and Mission Close-out

Once all mission activities are completed, the performers should produce a final report of all data and outcomes to properly close out the mission. In addition to general flight performance data, reports should include any investigative findings, lessons learned, and opportunities for improvement. Change implementation plans should then be documented and executed, thereby cultivating the healthiest designs and processes.

4. Conclusions

The high-altitude ballooning industry plays a vital role by providing unique solutions across sectors such as science, government, and commercial applications. Balloons will continue to serve as workhorse vehicles for high-altitude operations, offering versatile and cost-effective platforms. This chapter outlined the diverse markets and the high-level approaches to serving them, with special consideration given to philosophy and the specialized technical and professional aptitudes required. Regardless of the specific business objectives or program needs, the industry must be prepared to address a range of technical challenges. Having a strong baseline of capability provides the pathway to effectively solve these challenges and deliver innovative solutions to meet the industry's evolving needs.

References

[1] "Evolution of Constant Level Balloon Launch Techniques 1947 to 1975," Air Force Geophysics Laboratory, 1976.

[2] B. Gildenberg, "Techniques Developed for Heavy Load Non-Extensible Balloon Flights," TN 54-3, Holloman Air Development Center.

[3] J. C. Swisher, "Balloon Launchings," GMI Report No 2110, General Mills, Inc, September 1960.

[4] C. B. Moore, J. R. Smith, and S. Goldstein, "Constant Level Balloon," Technical Report No. 1, Balloon Group, Constant Level Balloon Project, New York University, April 1948.

[5] A. Howell, "New Balloon Launching Equipment and Techniques," Technical Report No. 39, Tufts University, Air Force Cambridge Research Laboratory, January 1956.

[6] O. C. Winzen, "Notes on Early Balloon Launch Methods," Early 1960s.

[7] "NCAR Inflation and Launch Shelter," Final Design, National Center for Atmospheric Research, 1964.

[8] N. Orsini, "Balloon Launching Operations from the USS Windham Bay During July 1958," Air Force Cambridge Research Laboratories, 1958.

[9] B. D. Gildenberg, "Covered Wagon Balloon Launcher: Development and Test Results," Summary Report HDT-21, Holloman Air Development Center, 1952.

[10] R. M. Enderson, J. Flocken, and J. A. Winker, "Dynamic Launch Study for National Center for Atmospheric Research," Report No. 1063, Raven Industries, Inc., August 1963.

[11] B. D. Gildenberg, "Development of Shroud Inflation Technique for Plastic Balloons," HADC TN 54-4, Holloman Air Development Center.

[12] D. M. Ferguson, "Ferguson Launching Method," Air Force Cambridge Research Laboratories, December 1953.

[13] "14 CFR Part 101 -- Moored Balloons, Kites, Amateur Rockets, and Unmanned Free Balloons." [Online]. Available: https://www.ecfr.gov/current/title-14/part-101. [Accessed: Nov. 2, 2025].

[14] "Radio Regulations 2020 - ITU." [Online]. Available: https://www.itu.int/hub/publication/r-reg-rr-2020/. [Accessed: Nov. 2, 2025].

[15] H. Akiyama, J. Nishimura, M. Namiki, Y. Okabe, Y. Matsuzaka, and H. Hirosawa, "A New Static-launch Method for Plastic Balloons," *Advances in Space Research*, vol. 3, no. 6, pp. 97-100, 1983, doi: 10.1016/0273-1177(83)90084-4.

[16] J. Nishimura, H. Hirosawa, N. Yajima, S. Ohta, H. Akiyama, M. Fujii, et al., "The Improvement of the Static Launch method in Japan," *Advances in Space Research*, vol. 13, no. 2, pp. 63-66, February 1993, doi: 10.1016/0273-1177(93)90277-I.

[17] J. Nishimura, C. Ishii, W. Seki, and M. Fujii, "A large B30-Type Balloon Launcher," *Tokyo University, ISAS Bulletin*, vol. 5, no. 1B, pp. 83-91, 1969.

[18] "U.S. Standard Atmosphere, 1976," NOAA-S/T-76-1562, October 1976.

[19] "Tropopause," SKYbrary Aviation Safety, Jun. 19, 2021. [Online]. Available: https://skybrary.aero/articles/tropopause.

Chapter 12
Communications, Command & Control

Javier Romualdez[1], Emaad Paracha[2]

[1] StarSpec Technologies Inc., Toronto, Canada
[2] University of Toronto, Toronto, Canada

Table of Contents

1. Introduction 5

2. Telemetry & Data Recovery 5

2.1. Downlink Throughput & Latency Considerations 5

2.2. Mission Planning Guidelines 7

2.2.1. Robustness 7

2.2.2. Adaptability 9

2.2.3. Integrated Development 10

2.3. Planning for Recovery 11

3. Command & Control 12

3.1. Uplink Throughput & Latency Considerations 12

3.2. Mission Planning Guidelines 13

3.2.1. Robustness 14

3.2.2. Command Diversification 15

3.2.3. Integrated Development 16

3.3. Remote Terminal Access 16

4. Flight Computers 17

4.1. Environmental Considerations 19

4.1.1. Ambient Pressure 19

4.1.2. Thermal Environment 20

4.1.3. Radiation Environment 21

4.2. Operation 23

5. Broadband Satellite Constellations 24

5.1. Early Adoption with Starlink 24

5.2. Operational Benefits 26

5.3. Challenges Observed 26

5.4. Beyond Starlink 27

5.5. Future Work and Collaboration 27

6. Conclusions 28

Table of Figures

Figure 12-1: Pictures of EXCITE Master Control Computer (MCC, the top photo shows the outside of the box mounted to the gondola. The bottom photo shows the inside of the MCC 18

Figure 12-2: Thermal profiles of reference components from the SuperBIT mid-latitude, super pressure balloon (SPB) mission at 32 km float altitude 20

Figure 12-3: In the presence of shielding > 5 mm of Aluminum, trapped protons dominate the radiation profile for space-based electronics; trapped proton power spectra are given for benchmarks at a 550 km orbit (left) versus a 100 km orbit (right); balloon-borne flux at 30 km orbit can be scaled appropriately; all data is obtained for a typical solar maximum period from the Space Environment, Effects, and Education System (SPENVIS) online tool 22

Table of Tables

Table 12-1: Empirically determined downlink throughput and latency figures for telemetry links typically employed and available for balloon-borne systems 6

Table 12-2: Empirically determined uplink throughput, latency figures, and typical contact cadency for commanding links typically employed and available for balloon-borne systems (refer to references provided in Table 12-1) 13

Table 12-3: Starlink Balloon Flight Results 25

Table of Symbols

Symbol	Definition	Dimension
B	Bandwidth	T^{-1}
C	Speed of light	$L\,T^{-1}$
f	Frequency	T^{-1}
G	Antenna gain	-
N	Noise power	$M\,L^2\,T^{-3}$
P	Power	ML^2T^{-3}
S	Signal strength	$M\,L^2\,T^{-3}$
S/N	Signal-to-noise ratio	-
λ	Wavelength	L

1. Introduction

This chapter examines the architecture, technologies, and operational considerations for Communication, Command, and Control (C3) systems in the context of planetary and space exploration. It emphasizes the interplay between communication infrastructure, signal integrity, and command hierarchies that enable mission success across Earth-based stations, orbital assets, and deep-space probes. The text examines frequency allocation, bandwidth optimization, and system redundancy strategies, underscoring the need for robust design against interference, latency, and hostile environmental conditions. Finally, it integrates emerging concepts such as autonomous UAV relays and AI-supported data routing, illustrating the convergence of traditional aerospace engineering with advanced computation and automation technologies [1], [2].

Portions of this chapter were drafted with the assistance of AI-based language tools to support clarity, consistency, and style; all technical content and interpretations remain the responsibility of the authors. There are also references at the ends of each section that offer the reader additional information regarding the topic at hand.

2. Telemetry & Data Recovery

This section discusses canonical telemetry and data recovery for balloon systems. This includes canonical approaches that may be provided by a balloon-borne Launch Provider, as well as typical capabilities from modern commercial offerings [3], [4], [5].

2.1. Downlink Throughput & Latency Considerations

When designing access to data from balloon-borne systems, there are typically two primary considerations in the regime where telemetry is made available in flight. First, downlink throughput is defined as the amount of uncorrupted data received from a balloon-borne system on the ground by flight operators per unit of time. Second, latency is defined as the time delay between when data is ready for downlink onboard the balloon-borne system and when that data is received on the ground by flight operators. A balloon-borne telemetry system with high downlink throughput is often referred to as a "high-bandwidth" system, whereas a system with low latency can be described as "real-time operated" [6].

From a system requirements perspective, the concepts of downlink throughput and latency are intrinsically linked to the Concept of Operations for the balloon-borne system, as with any remotely operated system. For example, a technology demonstration mission with operations that involve direct teleoperations may require low latency, while a long-duration imaging payload would require high downlink throughput. A given

mission may incorporate different operational modes or mission phases that pose different requirements concerning latency and downlink throughput, where early operations and commissioning may impose lower latency. In contrast, nominal post-commissioning operations may focus on downlink throughput to obtain usable data products in flight.

As one might expect, lower latency and higher downlink throughput positively correlate with technical complexity, requirements for existing infrastructure, and overall integrated cost. The following is a brief survey of agency-level and commercial capabilities currently available for balloon-borne telemetry purposes at the time of this writing [6].

Table 12-1: Empirically determined downlink throughput and latency figures for telemetry links typically employed and available for balloon-borne systems.

Telemetry Link	**Availability**	**Average Downlink Throughput**	**Latency**	**Notes**
Iridium Short Burst Data (SBD)[1], [7]	Commercial	340 Byte/packet	1–10+ minutes	SBD accommodates one packet every 2–3 minutes
Iridium Pilot / Open Port [8], [9] (discontinued)	Commercial / NASA (legacy)	70 kbit/s	< 2 seconds	Connection is described as "bursty," with inconsistent downlink throughput
Tracking and Data Relay Satellite System (TDRSS) (decommissioning in 2030) Omni [10], [12]	NASA	Single-digit kbit/s	10-30 seconds	TDRSS, in general, is only available through NASA-launched and operated systems
Tracking and Data Relay Satellite System (TDRSS) (decommissioning in 2030) High-Gain [13], [14], [15]	NASA	Tens of kbit/s	< 5 seconds	Access to high-gain telemetry involves initial scheduling overhead on the order of 30–60 minutes

Ethernet Via Telemetry (EVTM) [3], [16], [17], [18], [19]	Commercial / NASA	1–4 Mbit/s	< 1 seconds	Downlink is only line-of-sight to a compatible ground receiving station
PASTIS [18], [19]	CSA / CNES	1 Mbit/s	< 1 seconds	Downlink is only line-of-sight to a compatible ground receiving station
Other Custom Line-of-Sight (LOS)	Commercial	Variable	< 1 seconds	Downlink is only line-of-sight to compatible ground hardware
Starlink (maritime terminal) [45]	Commercial (SpaceX)	0.5–100+ Mbps (variable per location and latitude)	< 1 seconds	First flown atop SuperBIT in 2023, varying downlink speeds based on location of balloon, latitude, and temperature.

2.2. Mission Planning Guidelines

When designing a given balloon-borne system, it is often the case (and recurrently so) that the requirements for a given mission will tend strongly toward exceeding the capabilities of existing telemetry systems. One may remark that short of instantaneous data access (zero latency) to an unconstrained amount of data (near-infinite downlink throughput), there will always remain constraints and compromises to be made when designing effective telemetry for a remotely operated balloon-borne mission. The following presents some general yet empirically justified guidelines for telemetry design that one may consider in this respect.

2.2.1. Robustness

Over-the-air data access from any remote system is subject to various intermittent or systematic factors that directly impact link fidelity and reliability [20]. Such factors can include environmental variations, such as changes in cloud cover, barometric pressure, and general atmospheric conditions between the balloon-borne system and the operator's receipt, as well as electrical and mechanical effects, including pointing deviations, amplifier noise, and synchronization drifts. As such, an effective telemetry downlink must be robust to potential data corruption or dropouts regardless of their cause. This robustness is crucial for many telemetry links that are considered

unidirectional, which preclude data validation and feedback, or handshaking, that are typical of more localized communication.

At a conceptual level, the robustness of balloon-borne systems in telemetry downlink has been significantly improved by implementing error detection and correction at various levels. At the most basic level, error detection via the utilization of checksums provides a low overhead (often less than 5%) and a simple-to-implement method to flag data that has been corrupted. Additionally, forward error correction (FEC) enables the detection and correction of errors in a given segment of data, albeit at the expense of additional overhead (10–50%, depending on the implementation) [20], [21]. Lastly, robustness in telemetry downlink can be improved through redundancy in transmission, either via parallel links or repeated transmission on a given link (with an effective overhead of 100% or higher).

The tradeoff between data overhead and data integrity depends on the type of link and the characteristics of data corruption, often learned empirically. For example, a telemetry link that experiences long periods of data dropouts may tend to retransmit data as standard practice. In contrast, a consistent link with spurious corruption in data can often be addressed with basic error detection. For a large majority of modern balloon-borne missions, the current state of available telemetry downlinks is more consistent with the latter case, where checksums are often sufficient for most applications.

When paired with a mismatched uplink (ground-to-balloon system) at a significantly lower rate than the downlink, using checksums with uplink feedback in the form of “data retransmit” has thus far proven to be an effective balance of system complexity, overhead, and overall robustness. In this scheme, corrupted data segments/packets are identified as corrupted, and their unique data identifiers are sent back via uplink to effectively command the balloon-borne system to retransmit the corrupted or omitted data. As uplink throughput approaches downlink throughput (i.e., matched uplink/downlink) and bidirectional latency decreases, this data retransmit concept approaches canonical handshaking and closed-loop data validation typical of more localized systems (e.g., WiFi, Bluetooth).

Emerging broadband satellite constellations, such as Starlink (provided by SpaceX), provide TCP-based links that inherently include error detection, retransmission, and flow control. This architecture enables high-throughput file transfers with low latency and reliability approaching terrestrial WiFi, representing a significant step toward closed-loop telemetry for balloon-borne systems.

While most communication systems suitable for balloon-borne instrumentation remain limited to simpler schemes such as checksums or

FEC, broadband constellations and advanced line-of-sight implementations (e.g., EVTM) point toward the future of fully closed-loop data validation in flight.

It should be noted that, as of the time of this writing, the majority of communication systems that are suitable for remotely operated balloon-borne instrumentation are not capable of implementing this level of closed-loop data validation; however, promising candidates include the Starlink system (provided by SpaceX) [22] and some line-of-sight implementations, including developments in EVTM.

2.2.2. Adaptability

Although missions vary widely in capability, scope, and purpose, all balloon-borne systems, by their role as technology development platforms, involve components of demonstration or commissioning that pose different telemetry and downlink requirements compared to what might be considered nominal operations. As such, data access for balloon-borne systems is most effective when implemented in a manner that is adaptable to operator needs and modes of operation. This adaptability can be crucial during the early commissioning stages of a balloon-borne mission, when calibration, tuning, and debugging are performed to prepare for nominal operations, similar to the Launch and Early Operations Phase (LEOP) of a comparable satellite mission.

Given the constraints on telemetry regarding both downlink throughput and latency, one must often prioritize the type, resolution, and cadence of specific telemetry items in different operational or debugging scenarios. Even for a system that utilizes multiple telemetry links operating simultaneously, it is beneficial to be able to assign and prioritize data per link depending on the present operational needs. For example, power monitoring and sun-sensing data would have priority over some high-bandwidth line-of-sight link soon after the float condition is reached, to monitor or facilitate the first solar charging. In contrast, tuning of a pointing system would prioritize control inputs and sensing feedback, perhaps through a medium-bandwidth TDRSS link.

One way to achieve this level of flexibility is through a packet-based “data-on-demand” scheme, in which specific telemetry items are sent on schedule or command, based on the current operational needs. In this scheme, each type of telemetry is sent from the balloon-borne system on an as-needed basis, with some overhead per packet type to accommodate unique identifiers, timestamps, and checks. The benefit of this method is complete flexibility in obtaining any telemetry item only as needed, thereby maximizing the utilization of the downlink while minimizing the overhead per packet. An alternative approach to achieving this flexibility is a frame-based streaming scheme, in which predefined frames can be selected on schedule or command based on the current operational

needs. In this scheme, each predefined frame contains several prioritized telemetry items based on anticipated operational modes (e.g., nominal and debugging). The type of frame that is streamed over a given telemetry link can be selected by operators. The benefit of this method is minimal overhead per frame and increased contiguous data throughput, albeit at the expense of reduced flexibility in downlink selection.

In addition to flexibility in data types, balloon-borne telemetry is also subject to varying constraints in downlink throughput due to unpredictable conditions during float. For example, float winds may cause the line of sight to become unavailable sooner than anticipated, or balloon-borne orientation may affect transmission gain (i.e., an increased corruption rate) in a networked satellite system such as TDRSS. Regardless of the cause, successfully implemented balloon-borne telemetry often incorporates two key components. First, throttling allows for operator-controllable telemetry rates per link to prevent buffer overruns and not further exacerbate data corruption when a given link is sub-nominal. This is typical of satellite links, which depend on a good downlink margin (e.g., Eb/N0) to maintain high fidelity at a given demanded downlink rate. Second, dynamic error mitigation is a concept in which error detection or correction can be dynamically specified per data segment to ameliorate variations and characteristics of data corruption. This mitigation has been demonstrated to be effective for balloon-borne missions that implement features such as operator control over checksum cadence and the ability to control error correction in flight dynamically [23], [24], [25], [26].

2.2.3. Integrated Development

A key component of the development process for balloon-borne systems, often utilized as technology development platforms, is incorporating and iterating on the design of telemetry systems in the assembly, integration, and testing (AI&T) phases. Doing so in this phase ensures that the choice of telemetry architecture is validated through hands-on application and that various operational and debugging modes are thoroughly explored during a period of system development when systems are expected to be off nominal. The inclusion of “telemetry simulators” to emulate the specific framing, encodings, or even corruption characteristics of a given link provides the opportunity to design telemetry systems defensively while allowing prospective operators to learn how to mitigate balloon-borne operations amid potentially inconsistent telemetry links. Further to this point, simulated flight and hang tests of the balloon-borne system in the lab — a capability that is notably less involved than a satellite system — improve operator familiarity with the balloon-borne system while allowing for iteration on desired modes of operation and consequential prioritizations of telemetry. All in all, this level of telemetry integration in the

development process for a given balloon-borne system is instructive and effective in improving the chances of mission success.

2.3. Planning for Recovery

Despite careful design and rigorous optimization of telemetry for a given balloon-borne system, it is often the case, as previously noted, that data requirements surpass even the maximum capabilities of telemetry systems in providing data in flight. As such, many balloon-borne systems require post-flight recovery of data, a concept that is somewhat unique to remotely operated space-based systems, particularly compared to satellite systems. This is also a uniquely suited "capability" in general in that the short operational lifespan of a balloon-borne system per flight is consistent with data storage capacities that can be easily employed onboard. It should be noted that data recovery can in itself impose conditions for mission success, a consequence that must be given due consideration due to the high level of unpredictability and inherent risk post-flight. Nonetheless, for missions that require data recovery, specific considerations are pertinent in effectively designing data systems for recovery.

The physical considerations for effective data recovery involve ensuring that data is physically accessible from the balloon-borne system in a clearly identified manner. The design of physical data systems for recovery must consider that the balloon-borne system may land in extremely remote and harsh regions, which may also be inaccessible due to environmental or logistical constraints. As such, the design of physical data systems for recovery benefits significantly from the use of easily removable electrical and mechanical interfaces, as well as clearly marked and modular packaging. In this way, data is more likely to be recovered after the balloon-borne system lands, and data integrity is physically maintained between recovery and the eventual backup of data by operators.

Regarding architectural considerations for effective data recovery, the primary concern is redundancy; that is, when mission success depends on the successful physical retrieval of data, having multiple copies of that data is recommended. Data redundancy in this sense can take the form of primary data received via telemetry in-flight, with physical backups recovered, in the case where telemetry throughput is sufficient. Alternatively, it can involve multiple redundant copies of primary data stored in physically distinct locations onboard, both of which are to be recovered post-flight. When storing redundant data onboard, the most straightforward and foolproof method is often to make direct one-to-one copies of data stored during the flight, where two distinct copies are often sufficient for most balloon-borne systems. Regardless of architecture, in-lab dry runs for physically and digitally recovering data from a balloon-borne system have been proven to be the most

effective means of ensuring data recovery success, which aligns with the philosophy of integrated development for telemetry systems [27], [28].

3. Command & Control

This section discusses canonical commanding uplink and general control considerations for balloon systems. This discussion includes canonical approaches that may be provided by a balloon-borne Launch Provider, as well as typical capabilities from modern commercial offerings.

3.1. Uplink Throughput & Latency Considerations

As with telemetry downlink, requirements for commanding balloon-borne systems are centered on uplink throughput and latency, the former defined as the amount of uncorrupted data sent from ground operators to a given balloon-borne system per the time, and the latter defined as the time delay between when data is sent from the ground and received onboard. Though also intrinsically linked to the Concept of Operations for a given balloon system, commanding uplink often imposes notably different constraints and requirements than the telemetry downlink counterpart. Telemetry and commanding systems for remotely operated balloon-borne systems are often mismatched, in that throughput and latency differ significantly between the commanding and telemetry systems, with the latter typically having a higher bandwidth link from float to ground.

In addition to uplink throughput and latency considerations, the design of uplink systems for remotely operated systems more regularly considers the concept of contact cadence, compared to the design of the downlink counterpart. That is, whereas telemetry is thought of as continuous or regular for remotely operated systems, commanding is often considered on-demand or as-needed, the cadence of which is a factor in the design for different missions as well as distinct phases of a given mission. For example, a balloon-borne technology demonstrator might require a level of teleoperation that necessitates sending commands as frequently as every few seconds. In contrast, a fully commissioned balloon-borne observatory may only need a few contacts per day to update its scheduling. Currently, most readily available uplink and downlink capabilities are insufficient for achieving the required uplink cadence for closed-loop or real-time teleoperation of balloon-borne systems (i.e., remotely operated human-in-the-loop systems).

As one might expect, lower latency, higher uplink throughput, and higher contact cadence are positively correlated with technical complexity, requirements for existing infrastructure, and overall integrated cost. The following is a brief survey of agency-level and commercial capabilities currently available for balloon-borne commanding purposes at the time of this writing.

Table 12-2: Empirically determined uplink throughput, latency figures, and typical contact cadency for commanding links typically employed and available for balloon-borne systems (refer to references provided in Table 12-1).

Commanding Link	**Availability**	**Uplink Throughput / Cadence**	**Latency**	**Notes**
Iridium Short Burst Data (SBD)	Commercial	340 Byte/packet at 2–3 minute cadence	1–10+ minutes	SBD is a matched dual link for sending and receiving packets
Iridium Pilot / Open Port (discontinued)	Commercial / NASA (legacy)	70 kbit/s	< 2 seconds	Connection is described as "bursty," with inconsistent uplink throughput
Tracking and Data Relay Satellite System (TDRSS) omni (decommissioning in 2030)	NASA	8 kbit/s	10-30 seconds	Access to commanding is only available through NASA and involves initial scheduling overhead on the order of 30–60 minutes
PASTIS	CSA / CNES	1 Mbit/s	< 1 seconds	Uplink is only line-of-sight to a compatible ground receiving station
Other Custom Line-of-Sight (LOS)	Commercial	Variable	< 1 seconds	Uplink is only line-of-sight to compatible ground hardware
Starlink (maritime terminal)	Commercial (SpaceX)	~Mbps-class	< 1 seconds	TCP-based interactive uplink, with the ability to support near real-time operations

3.2. Mission Planning Guidelines

Although not to the same extent as telemetry, the commanding requirements for a given mission tend to exceed the capabilities of readily available systems. As previously noted, the concept of zero latency and high cadence uplink is currently beyond the capabilities of commanding systems for balloon-borne systems; as such, constraints and compromises will always remain when designing effective commanding systems. The following

presents some general yet empirically justified guidelines for commanding design that one may consider in this respect.

3.2.1. Robustness

As with designing a telemetry downlink, the fidelity of the commanding uplink is a primary concern when transmitting over potentially unreliable air links. One could argue that the robustness and end-to-end fidelity of commanding are a much stronger concern, given that data received on board a balloon-borne system often elicits a state change or active response onboard, whether intentional or unintentional. With factors affecting over-the-air communications similar to those affecting telemetry, an effective commanding system must be robust to potential data corruption and dropouts, regardless of their cause, and to erroneous action or potentially malicious intent.

At a conceptual level, implementing error detection can significantly enhance the robustness of the uplink command for balloon-borne systems. At the most basic level, given the on-demand nature, this often takes the form of simple checksums incorporated into the upload data, which provide a first-order vetting of the received data. Regardless of the specific checksum implementation, pairing received commanding uplink data with downlink feedback is recommended, not only to confirm that data is received, but also to indicate if uplink data has been rejected and potentially requires retransmission. The form of this feedback can be as simple as a command counter, a timestamp since the last received data, and/or a data identifier for the previous received uplink.

In addition to basic error detection, error correction or error handling plays a vital role in mitigating spuriously corrupt or unreliable commanding uplinks. Error handling, such as uplink data sanitization or state-based checks, has proven effective for remotely operated balloon-borne systems. This handling can take the form of programmable command timeouts to prevent, for example, severely delayed packet receipt over the Iridium network or command-driven state machines that expect operator-defined command sequences to ensure the validity of highly sensitive commands. In practice, it is often the case that forward error correction schemes are over-specified for commanding, and therefore, are not usually necessary for most uplink implementations. Exceptions may include the uplinking of larger quantities of data, such as files or software patches, that require extended uplink throughput.

Unlike telemetry, the inherent sensitivity of commanding to actions elicited, either unintentionally or, in the worst case, maliciously, may require additional uplink integrity and security in the form of encryption. This encryption applies not only to the over-the-air link from the ground to a given balloon-borne system but also between operator terminals and the point of transmission. In general, even basic

encryption can serve as a dual function, acting both as a form of data validation in the event of corrupted transmission and as a means to prevent external parties from undertaking malicious actions within the remotely operated system. Although this is unlikely for the majority of balloon-borne systems, ensuring the security of the command uplink in this manner remains an implementable and low-overhead best practice [27].

3.2.2. Command Diversification

Although missions vary in capability, scope, and purpose, all balloon-borne systems, by their role as technology development platforms, involve aspects of demonstration or commissioning that pose different commanding and uplink requirements compared to what might be considered nominal operations. Control of remotely operated balloon-borne systems is most effective when implemented in a way that provides a level of command diversity and breadth of scope to accommodate operator needs, as well as various modes and levels of operation. In addition to its essential utility in debugging, this is particularly important during the early commissioning stages of a balloon-borne mission, when calibration, tuning, and/or debugging are performed to prepare for nominal operations, similar to the so-called Launch and Early Operations Phase (LEOP) of a similar satellite mission.

Although uplinks for balloon-borne systems are typically too low throughput and high latency to accommodate real-time, human-in-the-loop command and Control (at the time of this writing), maintaining commands at the lowest level, remains a practical philosophy for off-nominal operations. This goes hand-in-hand with the philosophy of adaptable telemetry design, where specific feedback can be queued for downlink while probing low-level commands. For example, a balloon-borne rotator (or pivot) motor may, in nominal operations, servo to a given speed based on feedback from external sensors; however, the ability to disable that closed loop, command low-level speed or torque open-loop, and obtain direct feedback on motor feedback (e.g., power, thermal, etc.) would be invaluable when that servo motor requires debugging due to potentially faulty behavior.

Of course, with a large diversity of command uplinks comes the need to maintain effective organizational design strategies such that operators are clear on given tasks and modes of operation during a balloon flight. From an operator perspective, maintaining a record of command uplink use cases, intended modes of operation, and operational effects is essential for a balloon-borne system, as with any remotely operated system. In addition to this, an effective operational organization can be built from the ground up by structuring commands in a hierarchy that bases higher-level nominal operational commands on lower-level ones. For example, a single command for enabling a mode to point the solar arrays of a balloon-borne system towards the sun may be built on separate

commands for enabling sun position feedback and servo-ing azimuth motors to computed positions. At the same time, each of these may be based on low-level commands for tuning the estimation/filtering of sun sensor readouts, open-loop torque of motors, and manual power switching of these subsystems. In this way, nominal operations can be understood in terms of lower-level commands, such that diagnostics and debugging of a given operation are intrinsic to the structure of operations.

3.2.3. Integrated Development

As with developing telemetry uplink, it is often most effective to integrate the design and development of the command uplink system throughout the assembly, integration, and testing phases of the entire balloon-borne system. In testing, the development and iteration of low-level commands in developing and debugging subsystems become the same commands available in flight upon which higher-level operational commands may be based. In this way, balloon-borne operators establish the command uplink interface that will be used in flight, as validated through ground-based testing. Using "command simulators" to emulate flight-like timing, latency, and overall command availability effectively trains and enables prospective operators through simulated flights and debugging scenarios that inform nominal and off-nominal flight operations. All in all, this development-based integration of commanding during the ground-based development stage is an effective way to establish operational modes while enhancing mission assurance through operator involvement at every stage.

3.3. Remote Terminal Access

Increasingly seen in balloon-borne command and control is the idea of establishing a low enough latency and high enough throughput uplink and downlink system that the concept of remote terminal access becomes viable, compared to perhaps "traditionally constrained" systems. The concept of "logging in" to a balloon-borne system during the flight has the potential to greatly enhance mission assurance through direct operator remote control and configuration. Some demonstrated examples include Iridium Pilot and Starlink, while promising yet-to-be-demonstrated concepts involve two-way EVTM (line-of-sight) systems, all of which offer this kind of access to varying degrees of fidelity and reliability.

SuperBIT (2023)'s use of Starlink enabled and demonstrated SSH-like sessions, live configuration changes, and interactive file transfers during flight, helping reduce reliance on other links and capsule-based data recovery. Starlink's performance there strongly suggested the feasibility of commercial broadband constellations for direct balloon-borne operations.

At the time of this writing, given the current state of these remote access systems, it is recommended that these prospects be considered an effective redundant fallback for operational scenarios where traditionally constrained commanding and telemetry, implemented in parallel, prove inadequate. Furthermore, although these prospects are likely to become more available and reliable for use on balloon-borne systems in general, remote terminal access should, to no degree, stand in as a substitute or replacement for the judicious, well-thought-out, and diligent ground-based testing through which traditionally constrained commanding and telemetry have developed. That is to say, although remote terminal access as described here may at some point prove to be a de facto and generally available option, the tools, techniques, and philosophies asserted in developing effective commanding and telemetry remain a core aspect of the balloon-borne system design and development process, not only in enabling prospective operators directly but as a result, providing a robust standard against which to measure the likelihood for mission success. At the time of this writing, given the current state of these remote access systems, it is recommended that these prospects be considered an effective redundant fallback for operational scenarios where traditionally constrained commanding and telemetry, implemented in parallel, prove inadequate. Furthermore, although these prospects are likely to become more available and reliable for use on balloon-borne systems in general, remote terminal access should, to no degree, stand in as a substitute or replacement for the judicious, well-thought-out, and diligent ground-based testing through which traditionally constrained commanding and telemetry have developed. That is to say, although remote terminal access as described here may at some point prove to be a de facto and generally available option, the tools, techniques, and philosophies asserted in developing effective commanding and telemetry remain a core aspect of the balloon-borne system design and development process, not only in enabling prospective operators directly but as a result, providing a robust standard against which to measure the likelihood for mission success [29], [30], [31], [32].

4. Flight Computers

This section discusses modern design, development, implementation, and testing considerations for flight computers typically used on board balloon-borne systems. For the purposes presented here, flight computers are considered the heart of a balloon-borne system, mitigating aspects of low- to high-level operations by serving as a gateway for communication, control, feedback, archiving, monitoring, and overall mission health. As remotely operated systems that often include aspects of technology development and demonstration, balloon-borne flight computers share similar remotely operated constraints as satellite-based



Figure 12-1: Pictures of EXCITE Master Control Computer (MCC, the top photo shows the outside of the box mounted to the gondola. The bottom photo shows the inside of the MCC.

systems but are often less constrained in technical aspects, such as mass and power, as well as implementation aspects, such as the need for heritage (i.e., high Technology Readiness Level [TRL]) and mission longevity. This section attempts to provide guidelines within the context of modern balloon-borne systems.

4.1. Environmental Considerations

Environmental considerations for balloon-borne instrumentation, in particular for flight computers, can be broken down into three main categories: pressure, thermal, and radiation. This section discusses these three aspects concerning the selection and design of flight computers.

4.1.1. Ambient Pressure

The balloon-borne pressure environment trends directly with the altitude of the balloon-borne system, which can vary from 200 mbar (0.2 atm) at 10 km altitude (the cruising altitude of a jet) in the lower atmosphere to 3 mbar (0.003 atm) at 30 km altitude in the stratosphere. Though certainly not at the so-called ”hard vacuum” that one might expect for a satellite-based system, the effects of these low pressures on flight computer operation have historically been a topic of notable consideration. Much of this historical consideration has stemmed from the so-called “softening” of electrolytic capacitors, which are heavily utilized in industrial and commercial computing systems under prolonged exposure to low pressures.

Though this is a readily apparent effect seen in orbital satellite systems, there is an apparent mismatch in both the relative degree of pressure drop concerning the standard atmosphere (i.e., three mbar for balloons versus hard vacuum for satellites) and the duration of exposure to such an environment (i.e., order months for balloons versus order years for satellites). This is not to say that low ambient pressures do not affect sub-components of candidate commercial- or industrial-based flight computers. However, the degree to which these effects are relevant is substantially reduced for balloon-borne systems. Studies have shown, and in-flight demonstrations have validated, that the capacitive components (electrolytic or otherwise) used by the majority of modern commercial and industrial systems that could serve as flight computing systems do not experience significant changes in properties, robustness, or function over the duration and degree of exposure experienced by balloon-borne systems. That is to say that ambient pressure concerns for the majority of balloon-borne systems are no longer considered a relevant or driving factor in selecting a flight computer.

That said, there remain components adjacently related to flight computers that are indeed sensitive to ambient pressure at a level relevant for balloon-borne systems (e.g., hard disk drives). This requirement is further discussed in Chapter 13, Section 2.1.2, specifically concerning pressure vessels.

4.1.2. Thermal Environment

The balloon-borne thermal environment and subsequent implications for flight computer selection vary considerably depending on the altitude and phase of a mission. For a balloon-borne platform bound for the stratosphere at an altitude of 30 km, there are three altitude-dependent thermal regimes: launch/lower ascent, tropospheric ascent, and float altitude. In this case, the first two regimes are transitory, with the total time from launch to float lasting from 1 to 3 hours, during which ambient pressure remains high enough for convection to cool system components to −60°C or lower. The third operational regime exists at an ambient pressure low enough for heat transfer to be dominated by radiation and conduction through air. Extremes in this regime include temperatures upwards of 100°C for components in direct sunlight during the day and temperatures as low as −40°C for inert components (i.e., no power) during the night. Typical temperatures for component

ts well shielded and thermally coupled to the balloon-borne platform (e.g., flight computers) range from −25°C to 20°C over diurnal cycles. Temperature profiles for reference components are provided in Figure 12-2 for a representative stratospheric balloon mission [33].

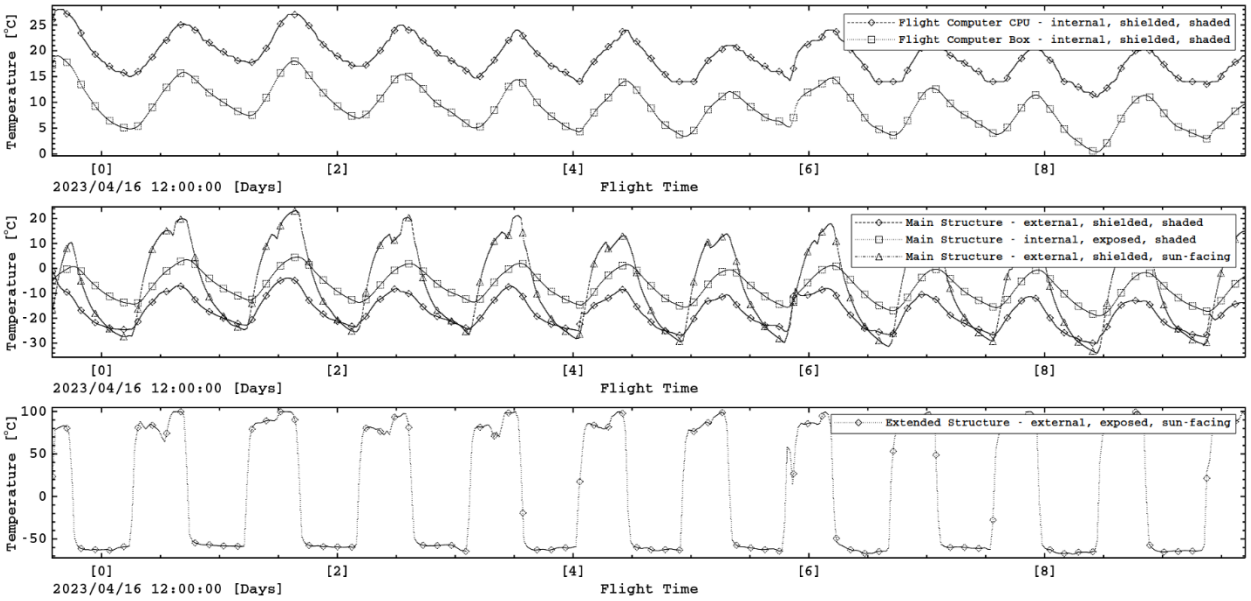


Figure 12-2: Thermal profiles of reference components from the SuperBIT mid-latitude, super pressure balloon (SPB) mission at 32 km float altitude.

Given this, flight computers must be capable of operating at a range of float temperatures in nominal operations while surviving some extreme temperatures experienced during ascent. Furthermore, the lack of effective convection in the stratosphere (i.e., above the troposphere) necessitates the implementation of direct conductive thermal sinking of high-density power components, such as CPUs or FPGAs, to prevent thermal

runaway at low ambient pressures. Empirically, industrial and commercial computing systems with extended operating temperature ranges (−40°C to 85°C) have been shown, with adequate heat sinking, to meet these requirements at a level sufficient for operations in a balloon-borne environment. Even computing components with narrower operating temperature ranges are thermally suitable for balloon systems if appropriate thermal treatment is applied. For example, this could include passive components, such as radiators and shielding, as well as active components, such as heaters and thermoelectric coolers. For the majority of flight computers used on balloon-borne instrumentation, the need for more robust cooling through cryogenics or fluid cooling loops has not typically been implemented; however, mission-specific needs for higher-performance computing resources could consider such approaches if deemed necessary.

For both the thermal and pressure environment, a given balloon-borne system must undergo rigorous thermal modeling as well as validation through thermal vacuum (TVAC) testing. Given the central importance of the flight computer component for any mission, pre-flight validation of performance and survivability is essential to mission success. It is, in fact, a large majority of balloon-borne failures that can be attributed to thermal effects due to improper modeling or insufficient ground-based testing. It is recommended that thermal simulations consider up to subsystem-level modeling and that all critical components, including flight computers, be thoroughly TVAC tested to mitigate this failure mode. The primary goal of this is to produce actionable results for thermal mitigation, be it the addition of radiator plates to dissipate excess heat during the day and/or heaters to provide further heating during the night or ascent. For the majority of flight computers, it is a good rule of thumb that sufficient cooling of components, rather than heating, is often the dominant consideration; however, this is not to be taken for granted without judicious modeling and testing for a given balloon-borne system.

4.1.3. Radiation Environment

Due to a significant decrease in atmospheric protection at higher altitudes, balloon-borne instrumentation undoubtedly experiences a more active cosmic ray and solar-induced radiation environment than typically observed on the ground. At the same time, a notable distinction remains, both in energy content and total flux, between the sub-orbital radiation environment and that of an orbital satellite in low-Earth orbit (LEO). Where highly shielded electronic components (> 5 mm Aluminum or equivalent) in LEO at 500 km orbit may experience a typical dosage of 1 krad over 5 years with a peak energy of 500 MeV, a similarly implemented and shielded balloon-borne system (at high latitudes, closer to the poles) may experience a worst-case dosage of closer 10–20 rad over a 1–3 month flight with a peak energy of 1 MeV. Variations in flux and

activity are seen to be correlated with geographic location (i.e., higher at the poles and near the South Atlantic Anomaly) as well as the present level of solar activity. Regardless, it is clear that there are notable differences in the radiation environment for balloon-borne systems, and therefore, they must be given separate consideration.

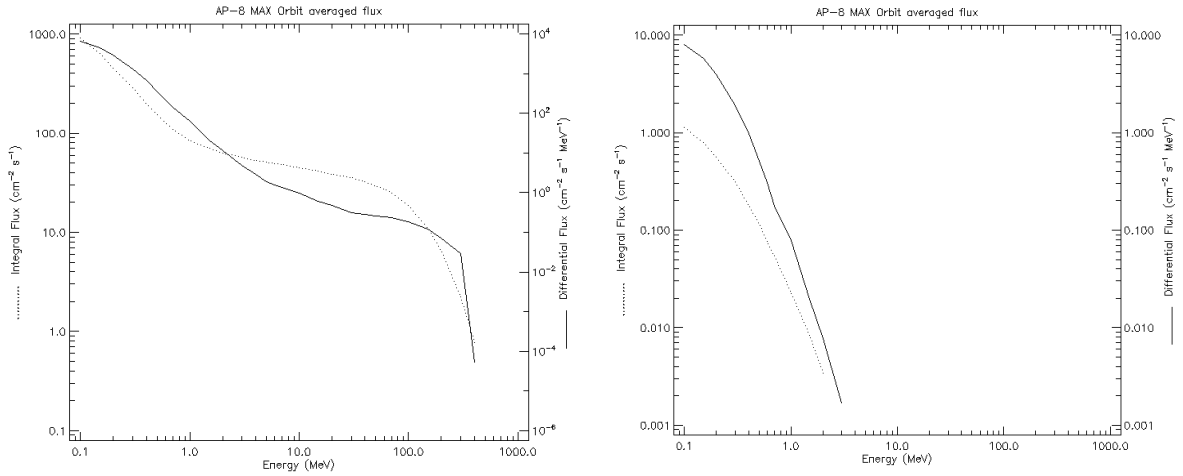


Figure 12-3: In the presence of shielding > 5 mm of Aluminum, trapped protons dominate the radiation profile for space-based electronics; trapped proton power spectra are given for benchmarks at a 550 km orbit (left) versus a 100 km orbit (right); balloon-borne flux at 30 km orbit can be scaled appropriately; all data is obtained for a typical solar maximum period from the Space Environment, Effects, and Education System (SPENVIS) online tool.

While the radiation environment at balloon altitudes is more benign than in orbit, there have been historically significant implications for flight computer selection and implementation. Earlier industrial or commercial components used for balloon-borne flight computers had experienced notable operational effects due to single-event upsets (SEU), the severity and pervasiveness of which could vary by manufacturer and even lot number. Although this had been a significant concern in past balloon-borne implementations, modern industrial and commercial computing has benefited significantly from improved robustness in firmware and increased tolerance for error. Improvements in hardware-level error correction driven by industrial electronics, as well as a reduction in cross-section due to continuing miniaturization, are likely leading factors contributing to this considerable increase in electronics reliability for balloon-borne systems. Regardless of the cause, these improvements have been seen to occur, at the time of this writing, on relatively short timescales, where a balloon-borne stratospheric mission flown 15 years ago would empirically suffer from upsets every 1–2 days while a similarly-scoped mission flown in the past 3–5 years exhibits virtually zero flight computer upsets due to radiation effects over a 1–2 month flight.

Ground-based beamline tests have demonstrated the resilience of commercial and industrial computing electronics to radiation, verifying these effects, where computing electronics have been shown to suffer upsets at the worst case every 2–4 weeks on average from LEO. Even "hobby-grade" electronics, such as Raspberry Pis and Arduinos, have demonstrated remarkable resilience to radiation effects at levels suitable for certain classes of orbital missions and a wider range of balloon-borne missions. All that said, this is not to say that radiation effects for flight computers are a so-called "solved problem," since beamline tests have also shown acute sensitivity of peripheral interfaces and supporting devices. These particular newer interfaces rely on high signal fidelity to achieve high data rates (e.g., USB 3). This implies that appropriate consideration should be given to the effects of radiation on flight computer hardware and that the inherent risk of new implementations should be mitigated both in the design and operation of a given balloon-borne system [34], [35], [36], [37], [38].

4.2. Operation

Although balloon-borne missions may vary in size, scope, implementation, and purpose, the concepts and principles of operation for the flight computer often share common elements in response to remote operational needs and the unique characteristics of the balloon-borne environment. While specific implementations may differ in detail, this section provides guidelines for flight computer operations that have empirically demonstrated success in modern balloon-borne systems.

First, the concept of operations stems from the reality that balloon-borne systems are remotely operated and are only directly accessible in flight via often highly constrained uplink and downlink channels. This is not to say that a balloon-borne flight computer should be implemented for fully autonomous operations, but rather that it be considered a standalone system that can otherwise perform all or a subset of nominal operations in isolation. In the absence of operator access, the flight computer can automatically mitigate mission operations, thereby increasing the chances of mission success. For example, a small hand-launched balloon-borne flight computer may operate exclusively in an operator-free mode wherein data is collected continuously and independently. In contrast, a large balloon-borne astronomical observatory may default to scheduled onboard data collection if not otherwise commanded by ground operators.

Hand-in-hand with independence is the concept of robustness, in the sense of flight computer tolerance and the mitigation of errors or faults that will inevitably occur during flight. While a flight computer is often tasked with monitoring and maintaining the nominal operations of subsystems, mechanisms for disciplining the flight computer itself in response to errors, such as single-event upsets, are essential to

maintaining the robustness of any remotely operated system. The canonical approach is to implement a so-called watchdog, which monitors the "aliveness" of a flight computer and issues restarts, reboots, or power cycles as deemed necessary to restore nominal independent operations. These watchdogs can range from simple software implementations that monitor the main flight computer control program to completely independent computing systems that provide external hardware monitoring of the flight computer based on digital feedback.

For balloon-borne systems that require completely uninterrupted operations at a level where restarts or reboots of the flight computer are deemed inadequate, implementing parallel flight computer systems with watchdog-monitored switching is an effective method of maintaining control and independent operational continuity. This also provides a level of redundancy and an effective operational fallback, which can de-risk the specific implementation of a flight computer, particularly for balloon-borne technology demonstrations intended for future use in satellite systems. That said, the additional complexity of implementing such an approach should be balanced with the tolerance of the balloon-borne system to upsets resulting in watchdog intervention. For many modern applications that utilize commercial hardware resilient to the balloon-borne environment, this balance increasingly tends towards a robust single-computer implementation.

5. Broadband Satellite Constellations

Broadband low-Earth orbit (LEO) constellations, such as Starlink, OneWeb, and the forthcoming Amazon Kuiper system, have emerged as a transformative development for balloon-borne science. Whereas traditional communications systems, like Iridium, TDRSS, and line-of-sight links, are constrained to kilobit-level throughput and carry high scheduling or geographic limitations, broadband constellations provide megabit-to-hundred-megabit data rates with latencies on the order of one second. These links make it possible to operate balloon payloads in ways much closer to terrestrial observatories, with near-real-time downlink of science data, interactive commanding, and reduced reliance on capsule recovery for mission success.

5.1. Early Adoption with Starlink

The first use of a broadband constellation for scientific ballooning occurred with the SuperBIT flight in 2023, which carried and used a Starlink maritime antenna. That mission demonstrated the immense potential of broadband links, with measured burst rates above 100 Mbps, while also highlighting operational caveats such as outages during high drift speeds and reduced performance over mid-ocean regions.

Since then, Starlink has remained the primary broadband system flown on balloon campaigns, with multiple missions using the maritime terminals. Other constellations are expected to be tested in the future.

Table 12-3 summarizes performance outcomes from these missions, reporting speeds and ranges where available, highlighting the performance to date.

Table 12-3: Starlink Balloon Flight Results

Mission (Antenna Type)	**Launch Date**	**Duration**	**Location**	**Data downlink speeds**	**Notes**
SuperBIT (Maritime)	April 2023	40 days	Southern mid-latitudes (New Zealand with global drift)	Speeds up to and greater than 100 Mbps [45]	Average file downlinks of 16Mbps. High variability with outages in mid-ocean locations, interactive SSH sessions enabled.
GUSTO (Maritime)	December 2023	57 days	Antarctica	Speeds up to 600 Kbps	Continuous coverage but limited throughput; polar geometry constraints.
HELIX (Maritime)	May 2024	6 days	North Sweden with Arctic drift	Speeds up to 13 Mbps	Stable link, no dropouts or latency issues reported.
SUNRISE III (Maritime)	July 2024	6 days	North Sweden with Arctic drift	No data available	Starlink flown but no performance data available.
HiWinds (Maritime)	April 2025	17 days	Southern mid-latitudes (New Zealand with global drift)	Speeds up to 1.3 Mbps	Unstable due to antenna placement obstructions.
SN12 (Maritime)	May 2025	9 days	Southern mid-latitudes, mostly South Pacific	Speeds up to 3.1 Mbps	Power anomaly ended operations after 7 days.
Salter Test Flight (Mini)	August 2025	2 hours	Fort Sumner, New Mexico	10.9 Mbps to 26.1 Mbps	Average speeds of 16.7 Mbps, short-duration test, best consistent performance to date.

The table illustrates a strong latitude dependence for performance. At mid-latitudes (SuperBIT, SN12), throughput routinely exceeded 3 Mbps, and in the case of SuperBIT, averaged near 16 Mbps. By contrast, Antarctic flights such as GUSTO achieved only a few hundred Kbps despite continuous coverage, reflecting constellation geometry and reduced

satellite density near the poles. Likewise, intermediate-latitude campaigns in Sweden produced stable, moderate uplink speeds (~10 Mbps).

5.2. Operational Benefits

Broadband constellations offer several clear operational advantages over legacy systems:

- **Near real-time science return:** Data downlink kept pace with acquisition during SuperBIT, reducing post-flight backlogs.
- **Interactive commanding:** SSH-like sessions enabled live adjustment of payload parameters and troubleshooting.
- **Risk reduction:** By transmitting bulk data in-flight, reliance on capsule recovery for science return is reduced.
- **Hybrid architectures:** Broadband serves as the primary science link, while Iridium/TDRSS remain essential for command and redundancy.

Beyond these immediate benefits, broadband systems also enable entirely new operational models. Teams can conduct remote collaborations with distributed science groups, downlink engineering video feeds for anomaly diagnosis, and adjust observing strategies dynamically in response to real-time conditions. These capabilities align balloon operations more closely with the responsiveness of ground-based observatories and significantly increase the scientific value of each mission.

5.3. Challenges Observed

Equally, these flights have revealed limitations that must be addressed:

- **Power demand:** Starlink terminals can have anomalous current draw with spikes at certain times, particularly when reacquiring or reconnecting to satellites. SN12's unrecoverable power anomaly underscores this risk.
- **Thermal cycling:** Links performed best at −40°C nighttime conditions, with throughput degraded at +20°C daytime heating. Day–night cycles have also been found to degrade antenna performance over time, as was exhibited during the SuperBIT mission.
- **Radiation exposure:** The long-term effects of cosmic rays on terminal reliability remain unquantified.
- **Placement constraints:** Antenna mounting strongly affects link stability. SN11's "obstruction" flags highlight the importance of gondola design.

Together, these challenges indicate that while broadband systems are promising, they cannot yet be assumed reliable for long-duration flights without careful engineering mitigation. Power, thermal, and structural

considerations must be central to mission planning when deploying broadband terminals.

5.4. Beyond Starlink

While Starlink has led early deployments, broader options are emerging:

- OneWeb, operating a constellation of over 600 satellites in polar and near-polar orbits, could provide coverage across high latitudes, making it well suited for Antarctic balloon campaigns where Starlink performance has been limited [39].
- Amazon's Project Kuiper, a fully licensed LEO broadband constellation planning over 3,200 satellites, began launching in 2025 and aims to deliver global high-speed, low-latency internet service within the decade [40], [41].
- Optical relay constellations, employing laser-based inter-satellite and ground links, could offer 10–20× higher throughput than traditional RF systems, drastically increasing burst rates. Though still in early development phases, this reflects the direction of next-generation space networking [42].

The emergence of multiple providers introduces opportunities for redundancy, competitive performance, and tailored mission planning. Rather than a single-vendor dependency, balloon operators could eventually select services based on latitude, payload volume, or regulatory environment.

Academic research further shows that both Starlink and OneWeb signals can also be exploited for navigation augmentation, providing meter-level positioning in GNSS-denied environments. This dual-purpose use case, for communications and navigation, could become central to next-generation balloon operations [43].

5.5. Future Work and Collaboration

Broadband constellations are not yet "plug-and-play" for balloon science. To become reliable mission components, they require deep collaboration with providers and rigorous in-flight testing:

- Electrical design must accommodate high current spikes and ensure power redundancy.
- Thermal management needs to counteract diurnal cycling and extend antenna lifespan.
- Radiation testing should assess long-term operational stability in the stratospheric environment.
- Integration protocols must ensure seamless interplay between broadband and traditional telemetry systems.

Operational and regulatory cooperation is also essential in covering spectrum usage, command access, satellite API interfaces, and co-operation models. Crucially, continued balloon campaigns across latitudes, seasons, and durations are needed to build a statistically rigorous performance dataset.

With sustained testing, logical co-design, and shared lessons, broadband constellations can graduate from experimental demonstrations to flight-qualified infrastructure, reshaping how science is conducted from balloon-borne platforms.

6. Conclusions

The development of robust Communication, Command, and Control (C3) systems has revolutionized planetary exploration, enabling precise coordination between Earth-based mission control, orbiting assets, and surface operations on the planet. Through advancements in signal processing, antenna technology, and data routing, modern C3 architectures provide reliable, high-bandwidth links despite the challenges of long distances, environmental interference, and limited power availability. These systems form the foundation upon which scientific, operational, and safety objectives are executed in real-time.

At the same time, innovations in automation and artificial intelligence have begun reshaping C3 capabilities. Autonomous relay satellites, UAV-based atmospheric communication nodes, and adaptive frequency allocation algorithms now allow networks to self-optimize, minimizing latency while increasing resilience to data loss and interference. Such capabilities are particularly critical in planetary environments where conditions can rapidly degrade signal quality or delay command execution, demanding systems that can operate with partial independence from Earth-based operators.

Recent demonstrations of commercial broadband constellations, such as Starlink, also highlight a major shift in capability. For the first time, balloon-borne observatories achieved megabit-to-hundred-megabit downlinks with sub-second latency, enabling interactive operations in flight. While challenges remain in terms of thermal management, antenna robustness, and long-duration reliability, this milestone points to a future where commercial networks augment traditional NASA links and capsule recovery, offering resilient hybrid architectures for science return.

Looking forward, the integration of optical communication technologies, interplanetary internet concepts, and intelligent network management promises to further expand mission capabilities. These advancements will not only support scientific exploration but also enable long-duration

human presence on the Moon, Mars, and beyond. As mission complexity grows, the importance of reliable, high-capacity C3 systems will remain central to achieving both operational success and the long-term goals of space exploration. Looking forward, the integration of optical communication technologies [44], interplanetary internet concepts, and intelligent network management promises to further expand mission capabilities. These advancements will not only support scientific exploration but also enable long-duration human presence on the Moon, Mars, and beyond. As mission complexity grows, the importance of reliable, high-capacity C3 systems will remain central to achieving both operational success and the long-term goals of space exploration.

References

[1] "Iridium short burst data (SBD)," Iridium Satellite Communications, https://www.iridium.com/services/iridium-sbd/ (accessed Sep. 9, 2025).

[2] C. Gomez, S. M. Darroudi, H. Naranjo, and J. Paradells, "On the energy performance of Iridium Satellite IOT Technology," *Sensors*, vol. 21, no. 21, p. 7235, Oct. 2021. doi:10.3390/s21217235

[3] S. Roth, "Balloon Capabilities at NASA," NASA, https://ntrs.nasa.gov/api/citations/20250001036/downloads/Balloon%20Cap%20at%20NASA%20-%20NASA%20-%20ROTH%20-%20SSC%202025.pdf (accessed Sep. 9, 2025).

[4] "Iridium Pilot," Iridium Satellite Communications, https://www.iridium.com/products/iridium-pilot/ (accessed Sep. 9, 2025).

[5] "Iridium OpenPort," Iridium Satellite Communications, https://www.iridium.com/services/iridium-openport-broadband-services/ (accessed Sep. 9, 2025).

[6] G. P. Calzolari, ECSS E-50 Space Data Link Communications, https://ecss.nl/wp-content/uploads/2023/05/ECSS_E-50.SDLCommunications.2023v1.0.pdf (accessed Sep. 9, 2025).

[7] S. Sevanto *et al.*, *Small burst data (SBD) Satellite Communications*, Aug. 2014. doi:10.2172/1149967

[8] Iridium Pilot / openport: High-speed satellite internet - american satellite, https://www.americansatellite.us/iridium-pilot-/-openport-128-kbps-200-kbps-data-plan.htm (accessed Sep. 9, 2025).

[9] A. Denney, "Iridium satellite based global communications for high altitude scientific ballooning," *AIAA Balloon Systems Conference*, May 2007. doi:10.2514/6.2007-2609

[10] L. Hilliard, "Performance characteristics of omnidirectional antennas for spacecraft using NASA networks - NASA technical reports server (NTRS)," NASA, https://ntrs.nasa.gov/citations/19870020151 (accessed Sep. 9, 2025).

[11] "Tracking and Data Relay Satellites (TDRS)," NASA, https://www.nasa.gov/missions/tdrs/tracking-and-data-relay-satellite-tdrs-generations-of-spacecraft (accessed Sep. 9, 2025).

[12] M. Toral, G. Heckler, P. Pogorelc, N. George, and K. S. Han, "Payload performance of third generation TDRS and future services - NASA technical reports server (NTRS)," NASA, https://ntrs.nasa.gov/citations/20170010176 (accessed Sep. 9, 2025).

[13] M. Bacon, "Paper Session III-C - Tracking and Data Acquisition (T&DA) support to launch vehicles by the Tracking and Data Relay Satellite System (TDRSS)," Scholarly Commons, https://commons.erau.edu/space-congress-proceedings/proceedings-1997-34th/may-1-1997/19/ (accessed Sep. 9, 2025).

[14] N. Gopalswamy *et al.*, "The balloon-borne investigation of temperature and speed of electrons in the Corona (BITSE): Mission description and preliminary results," *Solar Physics*, vol. 296, no. 1, Jan. 2021. doi:10.1007/s11207-020-01751-8

[15] T. Hams, Astrophysics Balloon Program Update, https://science.nasa.gov/wp-content/uploads/2023/04/Hams_APAC_NASA_Balloon_Program_Update_V2_TAGGED.pdf (accessed Sep. 9, 2025).

[16] EVTM Datasheet, https://www.quasonix.com/files/evtm-datasheet.pdf (accessed Sep. 9, 2025).

[17] M. Schultz, EVTM (Ethernet-via-Telemetry): Get Ethernet Packetized Data Directly from your test article, https://www.quasonix.com/files/ethernet-via-telemetry-itc-paper.pdf (accessed Sep. 9, 2025).

[18] F. Blon, PASTIS V2 Integration Guide, https://cnes.fr/sites/default/files/2024-07/9_cnes_ballons_-_pastis_telemetry_integration_guide_-_2019_en.pdf (accessed Sep. 9, 2025).

[19] Canadian Space Agency, "Flights and fieldwork for the Advancement of Science and Technology (FAST 2023)," Canadian Space Agency, https://www.asc-csa.gc.ca/eng/funding-programs/funding-opportunities/ao/2023-fast.asp (accessed Sep. 9, 2025).

[20] "Soho Commissioning Phase," NASA, https://soho.nascom.nasa.gov/operations/commissioning/ (accessed Sep. 9, 2025).

[21] AOS Space Data Link protocol, https://ccsds.org/Pubs/732x0b4.pdf (accessed Sep. 9, 2025).

[22] S. Miller, Starlink as an Interface on NASA CSBF Balloon Missions,

https://ntrs.nasa.gov/api/citations/20250004776/downloads/Starlink%20as%20an%20Interface2.pdf (accessed Sep. 9, 2025).

[23] TC Space Data Link protocol, https://ccsds.org/Pubs/232x0b4e1c1.pdf (accessed Sep. 12, 2025).

[24] Design Standard Communications, https://sma.jaxa.jp/TechDoc/Docs/E_JAXA-JERG-2-400A.pdf (accessed Sep. 9, 2025).

[25] Space engineering - Space data links – Telecommand protocols, synchronization and channel coding, https://ecss.nl/wp-content/uploads/standards/ecss-e/ECSS-E-50-04A14November2007.pdf (accessed Sep. 9, 2025).

[26] Communications Operation Procedure-1, https://ccsds.org/Pubs/232x1b2e2c1.pdf (accessed Sep. 9, 2025).

[27] J. W. Dankanich, *Planetary Balloon-Based Science Platform Evaluation and Program Implementation, Final Report*. Cleveland, OH: National Aeronautics and Space Administration, Glenn Research Center, 2016.

[28] C. Hales, Balloon Program Office - Piggyback Handbook, https://www.nasa.gov/wp-content/uploads/2024/10/820-hdbk-piggyback-01.pdf?emrc=673171221b726 (accessed Sep. 9, 2025).

[29] T. J. Conlon, P. J. Hart, and P. F. Wilbur, "Balloon one: Spontaneous long-range emergency infrastructure from space for telemetry and text," *2013 10th Annual Conference on Wireless On-demand Network Systems and Services (WONS)*, pp. 39–43, Mar. 2013. doi:10.1109/wons.2013.6578319

[30] J. Peterson, Investigating New Service System Solutions for high altitude balloons: Feasibility Study and Design Challenges, https://ltu.diva-portal.org/smash/record.jsf?pid=diva2%3A1048184&dswid=175 (accessed Sep. 9, 2025).

[31] P. Clark *et al.*, "An open source toolkit for the tracking, termination and recovery of high altitude balloon flights and payloads," *Journal of Instrumentation*, vol. 14, no. 04, Apr. 2019. doi:10.1088/1748-0221/14/04/p04003

[32] G. Clark, G. Landis, E. Barnes, B. LaFuente, and K. Collins, "Testing a neural network accelerator on a high-altitude balloon," *2019 IEEE Cognitive Communications for Aerospace Applications Workshop (CCAAW)*, pp. 1–8, Jun. 2019. doi:10.1109/ccaaw.2019.8904886

[33] A. S. Gill *et al.*, "Superbit superpressure flight instrument overview and performance: Near-diffraction-limited astronomical imaging from the stratosphere," *The Astronomical Journal*, vol. 168, no. 2, p. 85, Jul. 2024. doi:10.3847/1538-3881/ad5840

[34] J. Juneau, "A compact lightweight approach for telemetry systems in ballooning," *AIAA Balloon Systems Conference*, May 2007. doi:10.2514/6.2007-2611

[35] M. Cortesão *et al.*, "MARSBOx: Fungal and bacterial endurance from a balloon-flown analog mission in the stratosphere," *Frontiers in Microbiology*, vol. 12, Feb. 2021. doi:10.3389/fmicb.2021.601713

[36] A. W. Brewer and A. W. Wilson, "Measurements of solar ultraviolet radiation in the stratosphere," *Quarterly Journal of the Royal Meteorological Society*, vol. 91, no. 390, pp. 452–461, Oct. 1965. doi:10.1002/qj.49709139006

[37] The Radiation Dosimetry Experiment (RAD-X) Flight Mission, https://www.swpc.noaa.gov/sites/default/files/images/u33/Mertens_RaD-X_SpWxWk16_v1.pdf (accessed Sep. 9, 2025).

[38] B. Moision *et al.*, "Demonstration of free-space optical communication for long-range data links between balloons on Project Loon," *SPIE Proceedings*, vol. 10096, Feb. 2017. doi:10.1117/12.2253099

[39] Our network | oneweb, https://oneweb.net/our-network (accessed Sep. 9, 2025).

[40] J. Roulette, Amazon launches first Kuiper Internet satellites, taking on Starlink | Reuters, https://www.reuters.com/business/media-telecom/amazon-launches-first-kuiper-internet-satellites-taking-starlink-2025-04-28/ (accessed Sep. 9, 2025).

[41] "Project Kuiper," About Amazon, https://www.aboutamazon.com/what-we-do/devices-services/project-kuiper (accessed Sep. 9, 2025).

[42] P. Host, "Optical Data Relay: NASA's big bet on lasers for Space Communications," Potomac officers club, https://www.potomacofficersclub.com/articles/nasa-optical-data-relay-lasers-space-communications-navigation/ (accessed Sep. 9, 2025).

[43] W. Barrett, S. Kozhaya, J. Sanderson, and Z. M. Kassas, "Exploiting Starlink and OneWeb Leo satellite signals for high-altitude platform station opportunistic navigation," *2025*

IEEE/ION Position, Location and Navigation Symposium (PLANS), pp. 1388–1393, Apr. 2025. doi:10.1109/plans61210.2025.11028466

[44] F. Fidler, M. Knapek, J. Horwath, and W. R. Leeb, "Optical Communications for high-altitude platforms," *IEEE Journal of Selected Topics in Quantum Electronics*, vol. 16, no. 5, pp. 1058–1070, Sep. 2010. doi:10.1109/jstqe.2010.2047382

[45] E. Paracha *et al.*, "Overview of communications and Observation Strategies in the stratosphere for the super pressure balloon-borne imaging telescope (superbit)," *Ground-based and Airborne Telescopes X*, p. 95, Aug. 2024. doi:10.1117/12.3019360

Chapter 13
Gondola Health, State, Pointing, & Stabilization

Javier Romualdez[1]

[1] StarSpec Technologies Inc., Toronto, Canada

Table of Contents

1. Introduction 5

2. System Health & State Determination 5

2.1. Environmental Considerations & Mitigation 5

2.1.1. Thermal Housekeeping 5

2.1.2. Pressure Vessels 7

2.2. Gondola Geolocation & Orientation Determination 9

2.2.1. Global Navigation Satellite Systems (GNSS) 9

2.2.2. Inertial Sensors 10

2.2.3. Sun Sensors & Magnetometers 11

2.2.4. Star Cameras 12

2.2.4.1. Modes of Operation 13

2.2.4.2. Trade-offs 14

2.2.4.3. Operational Considerations 14

3. Gondola Pointing & Stabilization Control 16

3.1. Coarse Control & Pendulation Dampening 16

3.1.1. Rotators & Pivots 17

3.1.2. Reaction Wheels 18

3.1.3. Principle of Pendulation Dampening 20

3.2. Fine Control & Stabilization 22

3.2.1. Gimbal Systems 22

3.2.1.1. Wallops Arcsecond Pointer (WASP) 22

3.2.1.2. The FIREBall Pointing & Guidance System 24

3.2.1.3. The SuperBIT Pointing System 25

3.2.2. Image & Component Stabilization 26

3.2.2.1. Flight Demonstrations 27

3.2.2.2. Prospective Applications 28

4. Conclusions 28

References 30

Table of Figures

Figure 13-1: Picture of BLAST-TNG hard-drive pressure vessel, orange boxes at the very bottom of the image 7

Figure 13-2: Example pictures of SuperBIT star camera data (right top, displays centroid behavior, and right bottom, a histogram of the standard deviation of the multi-axis star camera centroids)and the physical device on the left [17] 12

Figure 13-3: Sky background relative intensity within the visible spectrum 15

Figure 13-4: Pictures of example rotators; NASA 5.5k bottom left[18], BLAST bottom right, EXCITE top left, TAURUS top right 17

Figure 13-5: SuperBIT as-flown reaction wheel 19

Figure 13-6: PICTURE-C (with the WASP system) pre-flight prior to the successful 2019 test flight out of Ft. Sumner, New Mexico 23

Figure 13-7: Typical in-flight performance from the WASP system showing (left) tracking error from rate gyroscopes and (right) star tracker residuals from on-sky pointing at a given target 23

Figure 13-8: Schematic of FIREBALL-2 24

Figure 13-9: In-flight performance from the FIREBall pointing and guidance system showing (left) the time history of fine guiding and (right) a summary of elevation and cross-elevation residual errors during a 1-hour observation 25

Figure 13-10: SuperBIT in Wanaka, New Zealand, in pre-flight prior to its highly successful 45-day science observational campaign; this flight was facilitated by NASA’s Columbia Scientific Balloon Facility (CSBF) utilizing the Super-Pressure Balloon (SPB) capabilities that enable mid-latitude flights 26

Figure 13-11: In-flight performance from the SuperBIT pointing system during the 45-day super pressure flight; (left) boresight star camera residual tracking errors and (right) roll star camera residual tracking errors over 30 minutes of tracking on a single target..... 27

Figure 13-12: In-flight performance from the SuperBIT FGS during the 45-day super pressure flight; image stabilization runs over nearly 500 hours of science observation time, and is collated to show performance throughout the flight..... 28

Table of Symbols

Symbol	Definition	Dimension
c_p	Specific heat at constant pressure	$L^2\ T^{-2}\ \Theta^{-1}$
g	Gravitational acceleration	$L\ T^{-2}$
h	Height / Altitude	L
k	Thermal conductivity	$M\ L\ T^{-3}\ \Theta^{-1}$
m	Mass	M
P	Pressure	$M\ L^{-1}\ T^{-2}$
Q	Heat	$M\ L^2\ T^{-2}$
R	Specific gas constant	$L^2\ T^{-2}\ \Theta^{-1}$
T	Temperature	Θ
V	Volume	L^3
μ	Dynamic viscosity	$M\ L^{-1}\ T^{-1}$
ρ	Density of air or gas	$M\ L^{-3}$

1. Introduction

This chapter presents a comprehensive overview of the methods and technologies used to monitor and maintain the health and operational state of high-altitude and planetary balloon systems. Covering environmental factors such as temperature, pressure, and radiation, as well as structural and power-system performance, it highlights both real-time diagnostic tools and predictive modeling approaches that safeguard mission integrity. Emphasis is placed on integrating sensor data, computational simulations, and automated decision-making to ensure reliability across increasingly complex and autonomous flight operations. By combining lessons from current missions with emerging capabilities in materials, instrumentation, and artificial intelligence, the chapter outlines a path toward longer, safer, and more scientifically productive balloon missions in Earth and planetary environments.

Portions of this chapter were drafted with the assistance of AI-based language tools to support clarity, consistency, and style; all technical content and interpretations remain the responsibility of the authors.

2. System Health & State Determination

This section discusses remotely operated balloon-borne systems in the context of overall health when exposed to the sub-orbital environment, as well as in determining states such as geo-positioning, altitude, and orientation. These guidelines are provided for the design, implementation, and operation of modern balloon-borne systems and should be considered within the context of specific implementations, scopes, and mission objectives.

2.1. Environmental Considerations & Mitigation

Expanding Chapter 12 beyond flight computers, all balloon-borne instrumentation is subject to an environment that is unique to both ground and space. As such, maintaining effective mitigation of potential environmental effects and exposure is essential for mission success. Some techniques and empirically determined best practices are provided here.

2.1.1. Thermal Housekeeping

As described in Chapter 12, balloon-borne instrumentation, in general, is subject to operational and survival requirements for a wide range of thermal profiles (see Chapter 12, Section 4.1) depending on mounting location, power state, and shielding. Following judicious subsystem-to-component-level thermal modeling and validation through thermal-vacuum (TVAC) tests, thermal mitigation may be required to be applied to meet these requirements.

Starting with passive treatment, a primary consideration for balloon-borne instrumentation is effective heat dissipation during the day and thermal insulation at night. For stratospheric flights where convection is subdominant, materials with improper heat dissipation or solar rejection can easily enter thermal runaway with temperatures above 100°C. In comparison, unpowered materials that are improperly insulated can experience temperatures as low as −60°C at night. Passive treatment, achieved by applying highly reflective materials (e.g., white paint, aluminized Mylar) on top of insulating materials (e.g., high-density foam, multi-layer insulation), can be a first step in mitigating these extreme temperatures. For large balloon-borne structures, an often effective method for maintaining acceptable thermal profiles is heat-sinking components directly to the structure itself, which can provide a thermal bath that moderates temperature extremes. For components with high power consumption and inadequate structural heat sinking, appropriately sized radiators with high thermal emissivity treatments (e.g., white paint) can effectively dissipate heat passively. Of course, the specific implementation and the degree to which passive treatment can be effective should be based on thermal modeling and TVAC test validation.

For components that are shown to require more active thermal control than passive methods can provide, feedback (e.g., via thermistors or thermocouples) becomes an important component of the balloon-borne flight system. With feedback, temperature-sensitive components can be actively heated (e.g., resistive heaters) or cooled (e.g., thermoelectric coolers) via a simple PID control loop, providing thermal control over long timescales. While tuning and calibration of this kind of active thermal mitigation can be baselined in TVAC and during ground testing, the ability to have operator control at a high level (i.e., temperature setpoints and control gains) as well as a low-level (i.e., manual heater outputs and temperature offsets) is highly recommended as part of the command and control philosophies outlined in Section 4. More autonomous closed-loop control of perhaps less critical components includes hardware-based thermostats, which self-regulate heating power through thermo-mechanical feedback. However, this should be considered at best a fallback for more robust, operator-configurable thermal control, given the propensity of these to underperform in a non-actionable way in-flight.

More involved methods for thermal management, particularly for heat dissipation and cooling, include active fluid cooling loops for balloon-borne heat transport. With this method, excess heat can be transferred from internal balloon-borne components to the outer structure, where larger radiating areas are available to dissipate heat into the environment. As a benchmark, this approach has been demonstrated to be successful for balloon-borne systems with internal components requiring heat dissipation on the order of 300–400 W, and endpoint radiating

surfaces on the order of 2–3 square meters. Although more extreme heat dissipation may be achieved for a limited time through the use of consumables, a discussion of cryogenic thermal control for scientific instrumentation or otherwise is beyond the scope of this work [1], [2], [3].

2.1.2. Pressure Vessels

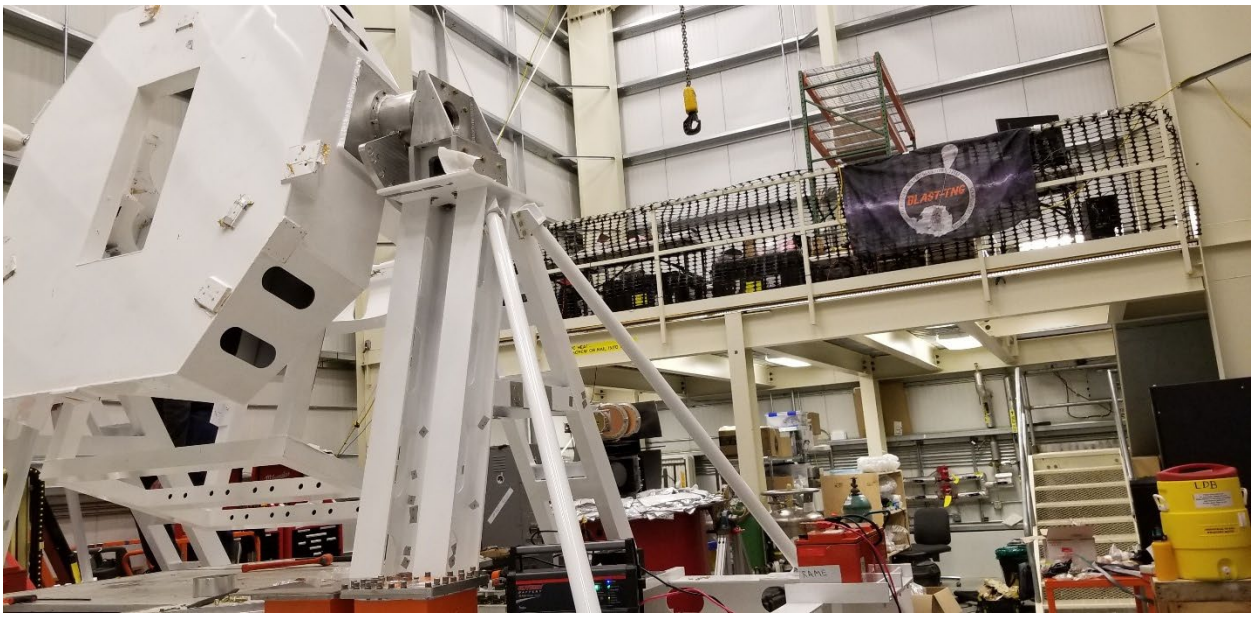


Figure 13-1: Picture of BLAST-TNG hard-drive pressure vessel, orange boxes at the very bottom of the image.

Outside the domain of cryogenics, the concept of pressure vessels for balloon-borne instrumentation stems not only from satellite-based design considerations, as discussed with regard to flight computers, but also from components that, to some degree, require atmospheric pressures to maintain the precision placement of mechanical components. Examples of these types of devices include enclosed optical assemblies, such as compound lenses, and high-speed disk-based mechanical hard drives. Both experience pressure-related performance degradation and, in some cases, failure when mechanical components lose alignment.

For the former, a traditional approach is to enclose an entire optical assembly, such as one used in a star tracking system, within a pressure vessel to maintain optical alignment and focus. While this approach has shown success in balloon-borne missions, pressure vessels are expensive in terms of mass contribution and the added system complexity of implementing a 1 atm hermetically sealed vessel with electronic pass-throughs. Alternatively, it has been demonstrated that star tracking assemblies, in particular, that utilize commercial lenses can be made to be tolerant to potential pressure gradients by implementing a) controllable focus to account for changes between ground and float, and

b) imposing additional mechanical margin within the controlled focus range to be able to fully correct for focus corrections. Using commercial lenses without a pressure vessel depends on the specific implementation, and the system must be designed for and validated in TVAC pre-flight.

Mechanical hard drives as onboard digital storage are another class of pressure-sensitive devices that have been shown to suffer performance hits and, in many cases, fail under pressure gradients, where the spacing between disk platters and read heads can be extremely sensitive to ambient pressure. In addition to implementing a pressure vessel solution with significant mass and complexity consequences, one alternative mitigation strategy comes from industrial computing, which provides hermetically sealed helium-filled drives that can be demonstrated to be tolerant to low pressure and even vacuum conditions. Furthermore, the advent of solid-state drives (SSDs) has provided options for balloon-borne data storage that are robust to pressure gradients. Although some early models of SSDs suffered from firmware-related issues unsuitable for effective balloon-borne operations, modern SSDs from the past decade, at the time of this writing, have demonstrated adequate robustness for both balloon-borne and satellite-based applications. At the time of this writing, all of the above approaches have been validated by recent modern stratospheric balloon missions and have been shown to be effective in mitigating the pressure sensitivity of balloon-borne digital storage devices.

In addition to electronic components that require maintaining a level of atmospheric pressure to operate, structural components with enclosed volumes capable of maintaining pressure to some degree have traditionally been considered problematic due to the possibility of unintentionally creating pressurized systems. This ranges from macroscopic structures, such as electronics enclosures or tube frame structures, to material substrates, including aluminum honeycomb or closed-cell insulating foam. For the former, it is generally best practice to ensure that these large-volume structures incorporate venting through pilot holes. This allows the release of the enclosed atmosphere during ascent and prevents, however unlikely, the possibility of structural failure due to pressure gradients across structural elements. For the latter, it is generally good practice to select substrates that are explicitly open-cell or perforated to prevent any potential for volume expansion or bloating at low pressures. However, barring the potential for outgassed elements to damage balloon-borne instrumentation, TVAC tests, and flight demonstrations have shown that the majority of passive substrates, including closed-cell foam and aluminum honeycomb, are largely unaffected by the potentially built-up pressure differentials induced at balloon-borne altitudes. That said, it is, of course, recommended that any new prospective closed structure or substrate with closed-cell properties be appropriately treated, tested, and validated at the

designed-for balloon-borne barometric pressure to ensure adequate performance prior to flight [4], [5], [6].

2.2. Gondola Geolocation & Orientation Determination

Beyond survivability and tolerance for the balloon-borne environment, balloon-borne systems are almost always responsible to some degree for maintaining accurate estimates of geolocation due to the inherent unpredictability in balloon trajectory compared to a more deterministic orbit. Furthermore, balloon-borne payloads, or colloquially referred to as "gondolas," are increasingly required to maintain and provide accurate estimates of orientation, whether in-flight for high-gain communications pointing feedback or post-flight for pointing reconstruction, as common examples. This section specifically discusses both geolocation and attitude determination in relation to the balloon-borne gondola.

2.2.1. Global Navigation Satellite Systems (GNSS)

Global Navigation Satellite Systems (GNSS), such as the widely used Global Positioning System (GPS) and others, have become the canonical approach for tracking and providing high-fidelity geo-positioning for balloon-borne payloads. The widespread use and miniaturization of GNSS for ground-based consumer applications have made it a cost-effective, easy-to-implement, and de facto solution for balloon-borne positioning, with commercial and industrial units capable of providing sub-meter accuracy or better. This provides a highly effective solution for not only tracking a balloon-borne payload in flight and recovery but also serving balloon-borne applications that require high-accuracy positioning, such as the sophisticated techniques involved in balloon trajectory control.

Commercial GNSS also provides dual or differential systems, enabling balloon-borne systems to obtain higher accuracy in positioning and gondola orientation information. This requires multiple antennas separated by a fixed distance or baseline, from which the differential signals of commercial differential GNSS (e.g., DGPS) can reconstruct pointing information. A technique commonly employed on modern balloon-borne systems is the so-called "GPS-compass," which, with a meter-scale baseline, can provide gondola azimuth estimates at a level sufficient for pointing feedback of high-gain communications antennas (typically better than 1 degree). In principle, these DGPS solutions can provide full orientation information (e.g., yaw, pitch, roll), but this often requires careful implementation in both mechanical mounting and signal mitigation. Empirically, moderate-cost DGPS solutions implemented on balloon-borne platforms have been shown to provide approximately 1-degree accuracy, but with solution dropouts during periods of high angular speed (e.g., gondola-commanded slews).

It is worth noting that the concept of DGPS may be extended to differential signals between well-located ground-based receivers and remote balloon-borne receivers to achieve higher accuracy in flight. This technique, known as Real-Time Kinematic (RTK) positioning, does offer promising performance for applications that require ultra-precision positioning beyond what is typically implemented for balloon-borne applications [7], [8], [9].

2.2.2. Inertial Sensors

In addition to global geolocation through GNSS, inertial sensors also play a vital role in the real-time onboard state estimation of position and orientation, providing higher bandwidth than GNSS. Typical components include magnetometers, accelerometers, and rate gyroscopes, which can be commercially packaged together as high-fidelity Inertial Measurement Units (IMUs) to provide high-fidelity position and orientation information. These IMU components, both packaged and as separate devices, have significantly benefited from miniaturization for on-chip (MEMS) applications, offering reasonably high performance with low mass and volume impact, as well as low cost. Typical IMUs have been shown to provide sub-meter position and arcminute-level orientation precision with accuracies at 1–10 meters (GPS corrected) and sub-arcminute, respectively [10].

Given that the orientation precision and accuracy specification are often much tighter than positioning, balloon-borne gondolas tend to place higher emphasis on orientation and attitude feedback. For gondola attitude applications with specifications beyond what can be afforded on-chip, fiber optic and ring laser rate gyroscopes have been shown to be well-suited for balloon-borne applications. They not only meet the pointing and stabilization requirements but also maintain a low impact on balloon-borne mass and volume. Though often more costly, these high-fidelity rate gyroscope devices have been shown to provide feedback sufficient for arcsecond-level accuracy and sub-arcsecond precision pointing applications. Several dual-use aerospace-grade rate gyroscopes have been demonstrated in balloon-borne flight to provide the feedback required to stabilize gondolas inertially to a high degree of precision (sub-arcsecond), with noise specifications on the order of 0.001 deg/rt-hr angle random walk and <0.0001 deg/hr bias stability. Given thermal considerations and potential fluctuations in the balloon-borne environment, it is worth noting that this level of precision in feedback is frequently only achieved in a closed loop, with external “absolute” sensors that actively correct for temperature-dependent biases and nonlinear effects [11], [12], [13].

2.2.3. Sun Sensors & Magnetometers

Sun sensors and magnetometers are common devices used on balloon-borne gondolas to obtain absolute orientation information in a way that is reasonably easy to implement and has low design impact. When implemented appropriately, both these device types have the ability to provide full 3-axis pointing information, limited only by the fidelity of the external reference models used.

For sun sensors, the unit information provided is the relative angle of the sensor with respect to the Sun. When used in conjunction with accurate GNSS positioning and model-based estimates for the local Sun pointing vector, sun sensors can also provide absolute orientation and pointing feedback. A common approach is to use a pinhole and photo-sensor as a pinhole sun sensor (PSS) device, which maps the spot position of the Sun to offset pointing relative to it. Multiple PSS devices have been shown to be effective as PSS arrays, offering additional benefits through redundant measurements and sensitivity to roll about any given PSS field-of-view center. Although, of course, limited to purely daytime operations, typical performance for these PSS devices has been shown at sub-degree accuracy and precision, and judicious calibration has shown arcminute-level performance for balloon-borne applications. Furthermore, the requirements for a sun sensor to have an unobstructed view of the Sun often necessitate mounting it on the external structure towards the top of the gondola. The best results are achieved when it is mounted on extended structures, such as an antenna boom or co-mounted with gondola solar arrays. In any case, sun sensors for use in pointing solar arrays or providing daytime feedback for anti-Sun pointing have been shown to be effective when implemented on modern balloon-borne gondolas.

Magnetometers are devices canonically utilized for balloon-borne and space-based applications, as the Earth’s magnetic field provides reasonable infrastructure-independent orientation information, either as a primary or secondary source of feedback. The simplest implementation applied to balloon-borne gondolas involves utilizing knowledge of the local magnetic declination to provide north-pointing information with an accuracy of approximately 1 degree, effectively utilizing the magnetometer as a higher-accuracy compass. When combined with other sensors, such as accelerometers or sun sensors, full three-dimensional pointing information (roll, pitch, and yaw) can be obtained with similar accuracy or better. Magnetometer accuracy may be improved by the use of magnetic models, such as those provided by the International Geomagnetic Reference Field (IGRF), which allows for the computation of full pointing information with a degeneracy about the magnetic pointing vector. In any implementation case, magnetometers are understandably sensitive to ferrous materials as well as electrical currents; therefore, the best balloon-borne implementations provide magnetometer mounting on extended structures or booms that allow for physical separation from magnetic

interference. Given these effects, it should be noted that magnetometers nearly always require in-flight calibration to achieve high accuracy since the balloon-borne environment is devoid of surrounding structures and ground support equipment, which have been shown to confound ground-based calibration.

With all these factors considered, sun sensors and magnetometers can be considered a fairly robust solution for providing gondola pointing information during balloon-borne flights. However, for applications requiring higher fidelity feedback, these types of devices are often considered backup or secondary sources, but are nonetheless necessary to complete a balloon-borne system [14], [15], [16].

2.2.4. Star Cameras

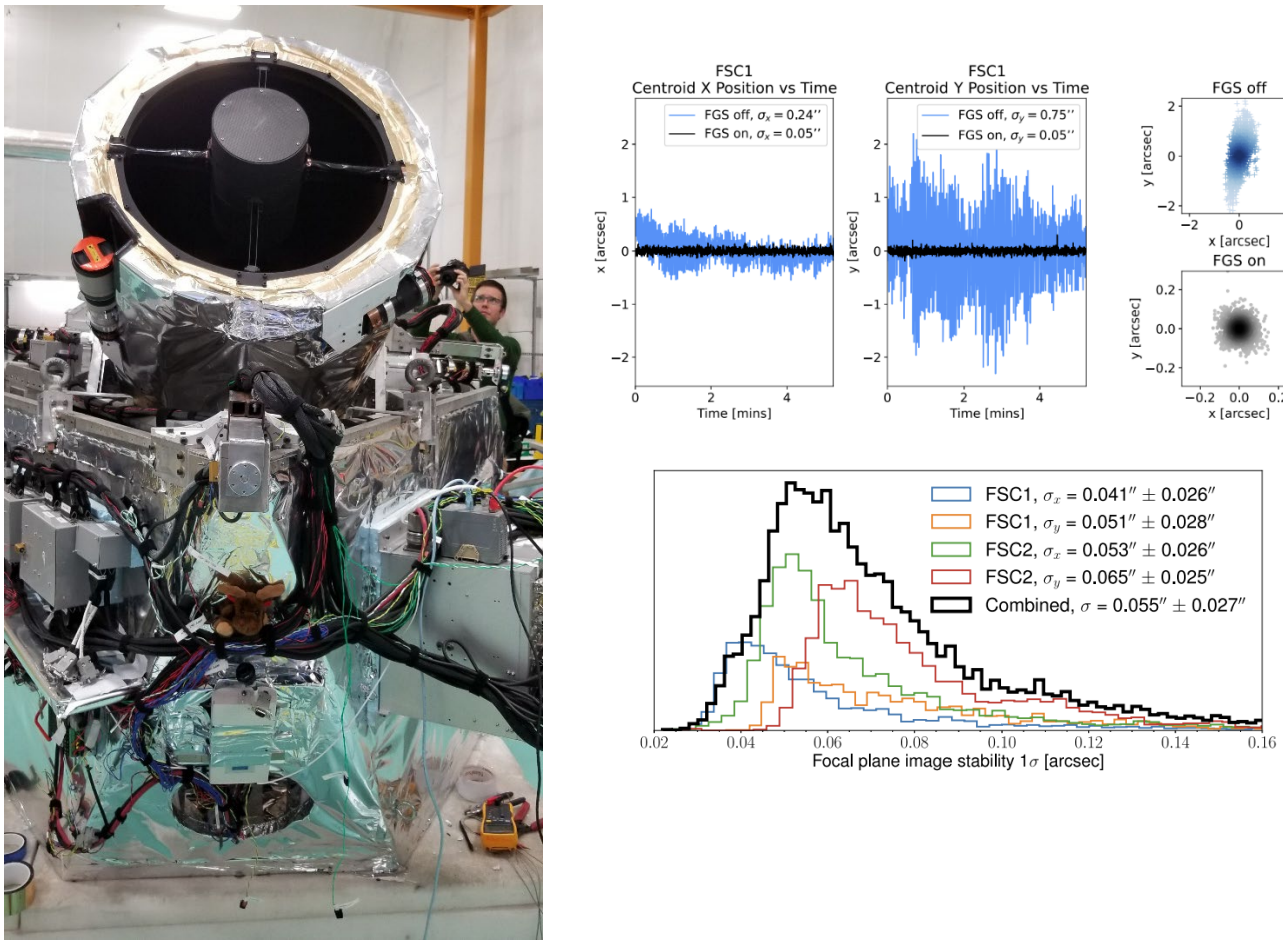


Figure 13-2: Example pictures of SuperBIT star camera data (right top, displays centroid behavior, and right bottom, a histogram of the standard deviation of the multi-axis star camera centroids)and the physical device on the left [17].

The need for high-accuracy pointing feedback for gondola instrumentation has become increasingly important for various balloon-borne

applications, including astronomy imaging and Earth observation, as well as high-speed, narrow-band, and optically based communications. Star cameras (or star trackers) provide a solution for high-accuracy feedback in balloon-borne and satellite applications, offering arcsecond and sub-arcsecond precision and accuracy onboard, both in real-time and for post-flight reconstruction. Star cameras have also benefited from the commercial demand for smaller form factor sensors, which boast low noise and high sensitivity, reduce power and mass, and offer compact, high-performance lenses. Both factors enable the implementation of robust off-the-shelf star cameras and their constituent components for balloon-borne applications.

The specifications for a given star camera can vary depending on the application, whether balloon-borne or otherwise. While detailed star camera specifications and design are indeed a deep subject closely tied to given mission requirements, the goal of this section is to provide some general remarks and guidelines for star camera selection in the context of modern balloon-borne applications.

2.2.4.1. Modes of Operation

Star camera attitude determination and general pointing feedback are achieved by using star sources as references, where a canonical method is to compare the angular positions of observed stellar sources with an onboard catalog to reconstruct pointing (i.e., so-called lost-in-space). When the angular scale on the sky (i.e., plate scale) is unknown, star camera pointing reconstruction algorithms (i.e., so-called lost-in-space) require a minimum of 4 stars within any given observed star camera region to solve, the accuracy for which is driven by the star camera plate scale, the performance of the star camera search and centroid algorithm, and the fidelity of the onboard catalog. Given that lost-in-space is typically computationally intensive, commercial star camera systems implemented for balloon-borne applications have been demonstrated to provide full pointing feedback at a maximum rate of 1–3 Hz (the NASA systems from Wallops Flight Facility operate at 10 Hz).

While much of the discussion of star cameras centers on full pointing feedback from so-called lost-in-space applications, high-performance applications often require high-fidelity pointing feedback at a higher readout rate than lost-in-space algorithms can provide. As such, many star camera systems may include differential pointing modes, in which subframes around target stars are read out at a high rate, providing high-rate, real-time pointing information due to the motion from which they are derived. When combined with knowledge of the given target star as well as prior lost-in-space solutions and inertial sensor feedback, this technique can provide full three-axis pointing feedback at a high rate (10–100 Hz), as is often needed for high-performance balloon-borne

systems that require this level of feedback for equally high fidelity pointing control.

2.2.4.2. Trade-offs

Specifications for performance are centered on achieving the necessary sensitivity (i.e., signal-to-noise ratio) on sufficient sources to reconstruct pointing. With reasonable simplification, star camera specifications always involve a trade-off between field of view (FOV) and sensitivity regarding stellar sources. The former is driven by the focal length (i.e., f-number and aperture diameter) as well as the physical size of the focal plane for a given lens system, while the latter is a function of sensor performance (i.e., quantum efficiency, read noise, dark current), aperture area, and optics throughput. The trade-off between field of view and sensitivity manifests in the balance between having sufficient stellar sources in any given field of view that are above the star camera's sensitivity, with the ability to reconstruct pointing at the required accuracy.

For example, a star camera system with a wide FOV would have access to a larger number of stars that are above its sensitivity threshold but would, in general, be less precise since the pixel size projected on the sky (i.e., pixel scale, typically in arcseconds per pixel) would be large. This may be mitigated by using smaller physical pixel sizes; however, at the time of this writing, commercial camera sensors typically do not have pixels smaller than 2 µm. In contrast, reducing the FOV to obtain higher precision and accuracy through a smaller pixel scale reduces the total number of stars available per field, which would impose higher sensitivity requirements. This would be mitigated with larger aperture optics, improved throughput, or higher sensor quantum efficiency, all of which have constraints related to available payload volume, cost, and complexity. For newly developed star camera systems, it is crucial to make this trade-off: conducting full-sky cataloged surveys of star availability for a given application allows for a comprehensive understanding of the relationship between sensitivity and field of view in relation to a specific star camera requirement. That said, provided here for reference, sufficient access to stars for lost-in-space is achieved at a (circular) FOV of 1.35 degrees with sensitivity to a limiting magnitude of 11.5 (AB) over 99.9% of the sky versus a FOV of 3.30 degrees with a sensitivity to a limiting magnitude of 8.5 (AB) over 99.9% of the sky.

2.2.4.3. Operational Considerations

One of the major factors in selecting and designing a star camera is its mode of operation, specifically whether it is intended for daytime operations from a balloon-borne environment. Even at the highest altitudes, balloon-borne systems still observe significant sky

backgrounds during the day due to residual atmospheric effects at a level sufficient to effectively reduce the relative star camera sensitivity to stellar sources. To mitigate this, daytime filters can be selected to cut off the majority of the sky background at shorter wavelengths while maintaining sensitivity at higher wavelengths by using an appropriate sensor. Figure 13-3 shows the typical sky background relative intensities from the balloon-borne environment at 30 km altitude, which suggests filtering above 600–650 nm and using star camera sensors that are preferentially sensitive to longer wavelengths in the red and near-infrared (IR) regions. This type of mitigation has been demonstrated to be effective for daytime star camera use in several recent balloon-borne missions.

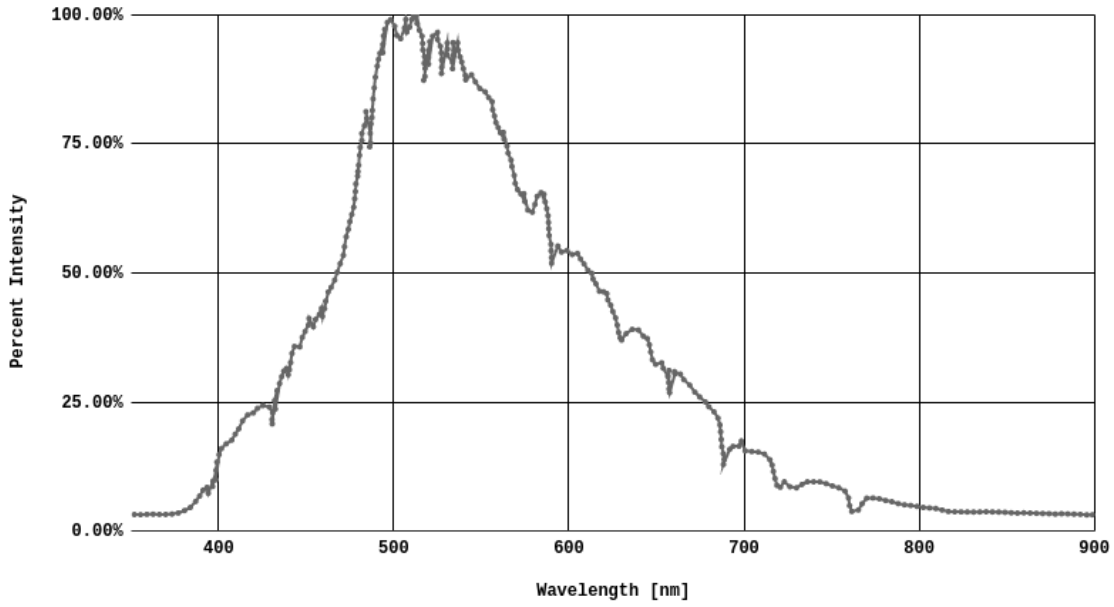


Figure 13-3: Sky background relative intensity within the visible spectrum

Additionally, the balloon-borne environment affects star camera performance both in instantaneous operation and over extended use. While ambient pressure has been discussed in previous sections as a relatively minimal concern for modern star camera optics, the balloon-borne thermal and ambient radiation environments have been shown to affect the performance of star cameras operating in the stratosphere. For thermal purposes, temperature differentials have been shown to affect the relative positioning of optical assemblies in a way that primarily shifts the optical focus. While not strictly detrimental to a star camera system, improper focus does reduce star camera sensitivity through the dispersion of stellar source signals across a larger number of pixels (i.e., lower signal-to-noise). This can be mitigated through the implementation of active and commanded focus for star camera systems, which is particularly useful for optical systems with lower f-number optics that are more sensitive to optomechanical defocus. For ambient

radiation, star camera sensors are sensitive to cosmic rays, which manifest on short timescales as intermittent “hot pixels,” which can degrade to permanent pixel damage over time. Thus, software mitigation for hot pixel rejection, both per image and integrated over time, is essential for robust star camera performance. For reference, certain modern star camera systems operating in balloon-borne environments have been shown to exhibit a permanent hot pixel rate accumulation of about 1–10 pixels per day.

3. Gondola Pointing & Stabilization Control

Balloon-borne gondolas are designed for a variety of applications in Earth sciences, astronomy, surveillance, communications, and general technology development, and these applications continually drive the scope and breadth of instrumentation capabilities. While many balloon-borne applications across this spectrum are intended for uncontrolled or passive flight, gondolas are increasingly required to provide levels of in-flight control, ranging from simple azimuthal pointing of solar arrays to sub-arcsecond accuracy and stabilization. This section discusses varying degrees of gondola control in this respect for balloon-borne applications, with reference to recent missions and instruments that have demonstrated successful implementation.

3.1. Coarse Control & Pendulation Dampening

For the purposes of this work, so-called coarse gondola control refers to the control or stabilization of gondola dynamics about the primary azimuth axis, which is perhaps the naturally controlled degree of freedom for a balloon-borne payload at the sub-degree precision. Such control is relevant for applications that involve pointing solar arrays or general application-driven pointing, requiring control fidelity of no better than 1–10 arcminutes. A description of typical approaches to coarse control and their impact on gondola multi-axis stabilization is provided here.

The canonical implementation of azimuth control involves actuating the connection between the balloon-borne gondola and the flight train that attaches to the balloon. This connection point, or “pivot,” is the primary mechanical connection between the gondola and the balloon and is, therefore, central in qualifying a balloon-borne system for flight amid a number of loading regimes. While a description of mechanical considerations and qualifications for the pivot connection points is not discussed here, it is essential to note that general engineering standards and best practices for mechanical certification are well established for balloon flight and are available through the respective launch providers.

3.1.1. Rotators & Pivots

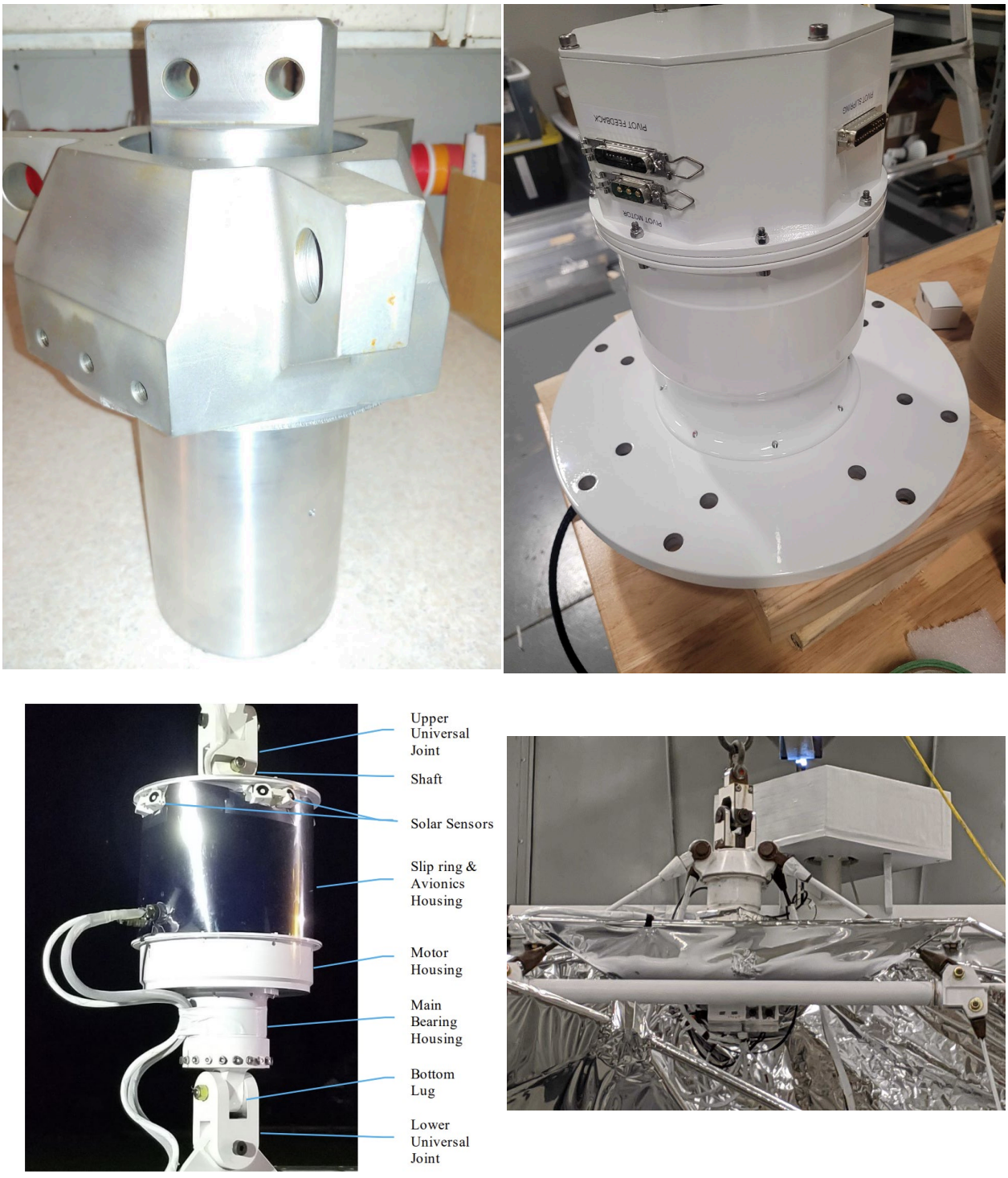


Figure 13-4: Pictures of example rotators; NASA 5.5k bottom left[18], BLAST bottom right, EXCITE top left, TAURUS top right

When actuated to provide a controlled degree of freedom in azimuth, the pivot connection, or now referred to as the "rotator," offers the ability

to use torques imposed through the flight train to servo the gondola both in speed and position. Rotators have been implemented on balloon-borne systems, both in a purely speed-controlled regime (e.g., stepper motor) and with a torque-controlled servo motor (e.g., brushless 3-phase motor). The trade-off between these two regimes depends on the application and the degree of control desired. Speed-controlled rotators offer more precise control for slow speeds or zero-speed stability due to high output speed fidelity, but they lack the torque needed for high-acceleration slew maneuvers. On the other hand, torque-controlled rotators, in general, have been demonstrated to be effective in high-torque applications, such as those requiring slew maneuvers at high speeds, as their principal mode of operation. Implementing a servo motor with both torque and speed control has been demonstrated to be effective in gondola azimuth control, meeting overlapping application requirements.

The kinematics and dynamics of a rotator-controlled system may be modeled as 1) a high inertia balloon with 2) a rotational spring (i.e., flight train) connected to 3) an inertial mass (i.e., gondola) through 4) a control input degree of freedom (i.e., rotator), the interactions between which produce a notable phase delay in any actuator output as seen by the gondola. That is, the ratio of gondola inertia to flight train spring constant for large payloads is usually such that the motion of the gondola has a significant lag, an effect that is exacerbated for smaller balloons, where balloon inertia and atmospheric drag also come into play. A suitable control scheme for a rotator-only controlled gondola involves servoing pivot output with feedback on gondola azimuth speed (and/or position) as well as gondola azimuth acceleration in a PID-style controller [19], [20], [21], [22], [23], [24].

3.1.2. Reaction Wheels

Reaction wheels (or “flywheels”) provide balloon-borne instrumentation, a means by which orientation may be controlled and/or stabilized through angular momentum transfer and storage in a way similar to satellites in orbit. Unlike satellites, the gravity-driven pendulation dynamics of a balloon-borne system only allow, in general, for full reaction wheel-based control about the azimuth axis, while the other “pendulation axes” are more limited. Furthermore, reaction wheels provide a mechanism for storing angular momentum, which can provide gyroscopic stiffness to a balloon-borne gondola. This can be especially effective for pendulation stability when implemented correctly. Balloon-borne implementations of gimballed reaction wheel devices (i.e., control moment gyroscopes) have been shown to be effective in active pendulation stabilization for applications requiring highly stabilized gondolas.

For azimuth control and stabilization, balloon-borne implementations of reaction wheels have demonstrated high fidelity and highly responsive



Figure 13-5: SuperBIT as-flown reaction wheel

control authority, capable of precision at sub-arcsecond levels. Several implementation factors are typically considered that directly affect reaction wheel performance, both in general and specifically for balloon-borne applications. First, reaction wheel balance is a primary consideration for balloon-borne systems, as any imbalance will invariably drive gondola pendulations to a level beyond what is tolerable for a given application. The level to which reaction wheel imbalance can be tolerated is highly application-dependent and, in fact, often determined empirically through judicious ground-based testing (i.e., hang tests) of the as-integrated balloon-borne system. That said, a general rule of thumb is to require that reaction wheel imbalance does not exceed 70 g-mm per kg of gondola mass in order to ensure that fundamental balloon-borne pendulations (at roughly 0.1 Hz and 1 Hz) are not driven beyond the natural 1–2 arcminutes disturbance level. For example, a 100 kg gondola mass requires a 200 mm diameter reaction wheel to be calibrated so that any imbalance is no more than 70 g at the wheel edge to not drive pendulations [10], [25].

Secondly, the nominal operating points of a reaction wheel used for azimuth control should be considered in the context of the azimuth slew requirements for a balloon-borne application, as with any reaction wheel-driven system. It is generally beneficial to offset reaction wheel speed at some speed ω_{nom} in a way that prevents direction reversal (i.e., "biasing" a reaction wheel), so for a gondola that requires a maximum azimuth slew speed of ω_{slew}:

$$\omega_{nom} \geq M_{slew} * \eta_{inertia} * \omega_{slew} \quad (13\text{-}1)$$

where $\eta_{inertia}$ (generally greater than 1) is the ratio of gondola inertia I_{gond} to reaction wheel inertia I_{rw}, and $M_{slew} > 1$ is the design-imposed slew margin (10–30% margin is typically good practice). As such, the angular momentum storage L_{rw} required for a reaction wheel system is given by:

$$L_{rw} \geq 2 * M_{store} * \omega_{nom} * I_{gond} / \eta_{inertia} \quad (13\text{-}2)$$

where $M_{store} > 1$ is the margin on angular momentum storage, with implementationally practical values at the 4–8x level. For example, a gondola reaction wheel system with $\eta_{inertia} = 50$ and a slew requirement of 10 deg/s for a 100 kg·m² inertia gondola would typically have a bias design speed of 108 rpm and a designed angular momentum storage of roughly Lrw = 360 N·m·s.

Lastly, the torque requirements for reaction wheels implemented for azimuth control directly affect control performance, as this torque provides the necessary control authority to servo and/or stabilize a balloon-borne system. To first order, reaction wheel torque sets the responsivity of the system to changes in azimuthal speed, which simply amounts to a torque τ_{rw} given by:

$$\tau_{rw} \geq N_{torque} * I_{gond} * \alpha_{gond} \quad (13\text{-}3)$$

where α_{gond} is the desired angular acceleration, and $N_{slew} > 1$ is the torque margin (typically at the 1.5–2x level). Here, the desired angular acceleration can be set by simple slew requirements, but may also be driven by system responsiveness to precision control effort at a higher control bandwidth. In any case, second-order torque effects, including bearing nonlinearities and torque ripple, play a key role in balloon-borne control applications. These effects have been empirically demonstrated to be relevant for highly stabilized systems, such as sub-arcsecond stabilizers. While less constrained systems may, for example, tolerate torque ripple at the 10% level, these highly stabilized systems have been shown to be sensitive to torque nonlinearities at the 0.1–1% level, which significantly influences motor selection and commutation feedback criteria.

3.1.3. Principle of Pendulation Dampening

In the discussion of gondola azimuth control, there is a uniquely balloon-borne result that relates co-actuation between a gondola rotator and a reaction wheel in a way that provides pendulation stabilization properties. This has been rigorously proven in the literature using Lyapunov stability criteria techniques and has been demonstrated successfully on several balloon-borne systems that employ a co-actuated rotator-reaction wheel system. In broad strokes, the rotator provides a

mechanism by which angular momentum build-up on the reaction wheel can be transferred from the gondola up the flight train to the balloon, providing an effective "momentum dump" for excess momentum built up during balloon-borne operations. In parallel, the biased reaction wheel design speed provides a level of gyroscopic stiffness that couples pendulation motion in one given direction to pendulation in the orthogonal direction, as well as to motion in the azimuth direction. The result is that balloon-borne pendulations may be effectively damped via this rotator-reaction-wheel scheme in a way that is otherwise passive in the pendulation degrees of freedom, altogether offering a unique approach to overall gondola stabilization.

More specifically, this pendulation-damping effect may be achieved if the following criteria are met:

1. The reaction wheel is acting as the primary azimuth control, actively controlling the gondola azimuth to a given speed;
2. The rotator is acting solely as a means to mitigate reaction wheel speed deviations from nominal reaction wheel design speed, effectively providing momentum dumping for the gondola and
3. The balloon-borne gondola is inertially asymmetric about the pendulation directions.

The first point ensures that the reaction wheel explicitly facilitates the primary control of gondola azimuth, while the second point provides a means by which energy can be dissipated away from the balloon-borne system. The third point couples the dynamics from the separate pendulation directions with the azimuth degree of freedom, effectively transferring kinetic and potential energy from pendulations into azimuthal motion. Altogether, this implementation allows for disturbance-driven pendulations to be damped and effectively stabilized through pure azimuth control.

In implementation, it is worth noting that the timescale over which this scheme provides pendulation damping is significantly longer than the typical azimuth control timescale (e.g., typically on the order of minutes, compared to azimuth control timescales of seconds). As such, this approach should be considered a means to enhance the robustness of balloon-borne platform stability against external or self-induced pendulation disturbances, providing pendulation stability at a level of no better than sub-arcminutes. For applications requiring gondola pendulation stability (e.g., in pitch and roll) on timescales and at levels beyond the capabilities of this passive method, active pendulation stability has been demonstrated to be effective using control moment gyroscopes, which reduce gondola pendulations to a level sufficient for high-precision applications. For applications requiring high fidelity and high-performance pointing control in general, additional methods may

be employed to meet the application-driven criteria within the balloon-borne environment, as discussed in the following subsection.

3.2. Fine Control & Stabilization

For applications requiring a high degree of pointing accuracy, precision, and/or stabilization, several recent missions have successfully demonstrated the capabilities of balloon-borne instrumentation utilizing high control fidelity approaches to achieve three-axis control stabilization. This section discusses these approaches within the context of missions that have demonstrated successful implementations.

3.2.1. Gimbal Systems

As discussed with regard to coarse pointing systems, there are limitations in the degree of stabilization and control of a balloon-borne gondola in the pitch and yaw directions simply because a balloon-borne system is subject to gravity. Though pendulations can be damped to a level sufficient for many applications, gimbal-type systems are still required to achieve the control authority required to point instrumentation within the full range of pitch and/or roll with sufficient accuracy. This may take the form of single-axis "elevation drives" as employed on missions like BOOMERaNG, BLAST, and PILOT, as well as multi-axis systems such as SuperBIT, FIREBALL, and PICTURE-C (utilizing the Wallops ArcSecond Pointer, aka WASP, system). In all cases, implementation factors include considerations for gimbal balance as well as nonlinear effects such as static friction and control decoupling. A brief description of three successful and flight-demonstrated approaches to gimbal-based balloon-borne control is given here.

3.2.1.1. Wallops Arcsecond Pointer (WASP)

The WASP system consists of a rotator-controlled gondola for azimuth control, a primary elevation axis, and a cross-elevation axis to provide three-axis control of a given instrument, such as PICTURE-C. Note that the three-axis system is not orthogonal; the WASP system does not control centerbody roll. For feedback, the WASP system utilizes extremely high-fidelity rate gyroscopes (Northrop Grumman, ITAR-restricted) as well as a high-precision star camera to provide stabilization and accurate target acquisition. To solve the static friction problem, WASP employs a unique continuously rotating bearing solution, ensuring that bearings are always in a more linear dynamic friction regime, thereby removing the nonlinearities that break static friction at low speeds. By using a multiplicative extended Kalman filter (MEKF) to combine noisier star tracker data with gyroscopic data, WASP has successfully demonstrated absolute pointing at the sub-arcsecond level. In addition to PICTURE-C, the WASP system promotes modularity and multi-mission compatibility by

providing WASP as a generic pointed platform that meets pointing and stabilization requirements for a broader variety of missions, including successful flights of the X-Calibur and XL-Calibur X-ray science applications [26], [27], [28].



Figure 13-6: PICTURE-C (with the WASP system) pre-flight prior to the successful 2019 test flight out of Ft. Sumner, New Mexico.

providing WASP as a generic pointed platform that meets pointing and stabilization requirements for a broader variety of missions, including successful flights of the X-Calibur and XL-Calibur X-ray science applications [26], [27], [28].

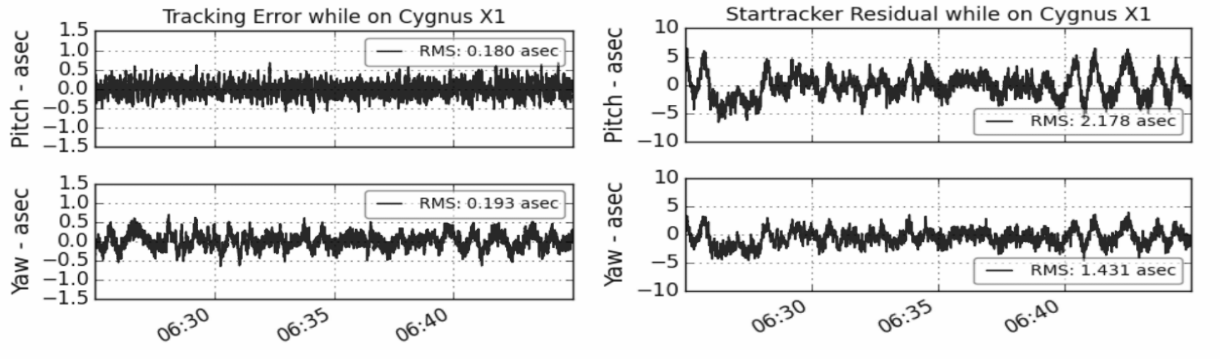


Figure 13-7: Typical in-flight performance from the WASP system showing (left) tracking error from rate gyroscopes and (right) star tracker residuals from on-sky pointing at a given target

3.2.1.2. The FIREBall Pointing & Guidance System

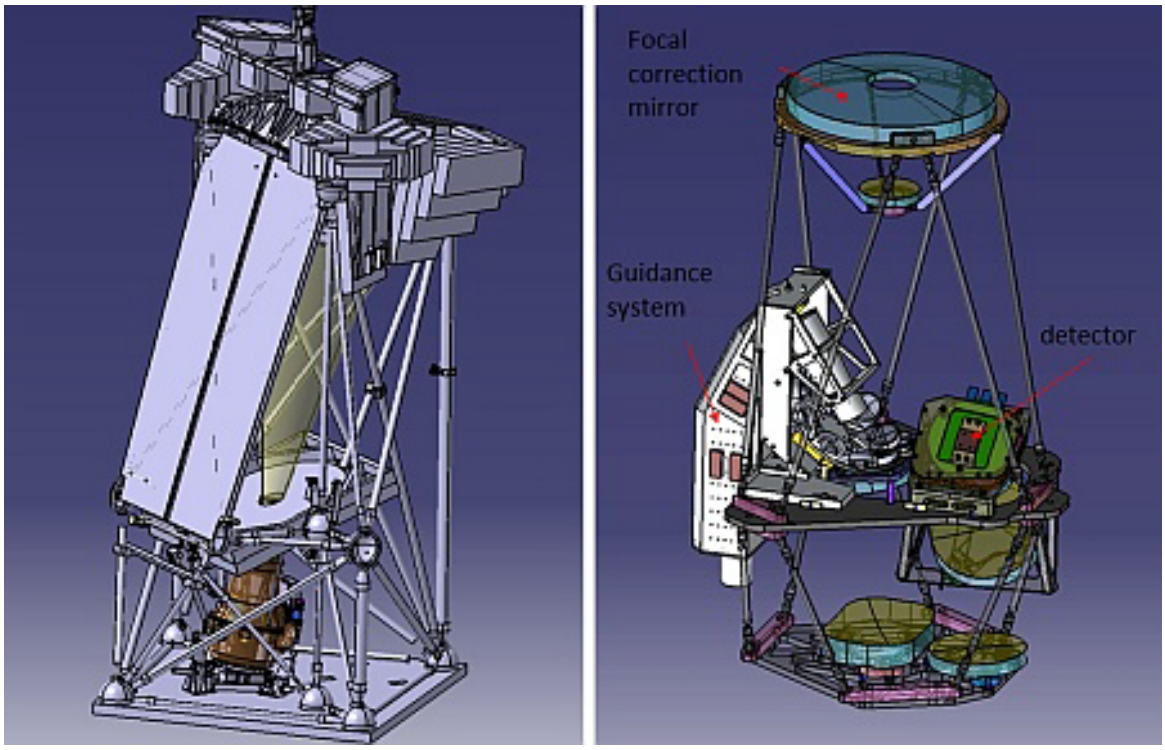


Figure 13-8: Schematic of FIREBALL-2

The Faint Intergalactic Red-shifted Emission Balloon (FIREBall) is a balloon-borne science mission that has successfully implemented and demonstrated high-performance pointing at a sub-arcsecond level as required by highly precise measurements in astronomy. The FIREBall pointing and guidance system utilizes a rotator-only azimuth control with active damping of pendulations via high-performance control moment gyroscopes. As a result of stabilizing the main gondola structure, the FIREBall telescope instrument uses a siderostat to point its primary optics at a given region of interest and to correct for residual disturbances. With this scheme, the FIREBall pointing and guidance system has successfully demonstrated pointing and stabilization performance at the 0.5 arcseconds (RMS) level and better for periods up to 1 hour of continuous observation, which highlights the robustness of the system over long timescales (Figure 13-9). At the time of this writing, the FIREBall system has been demonstrated on two successful balloon flights (FIREBall and FIREBall-2) [29], [30], [31].

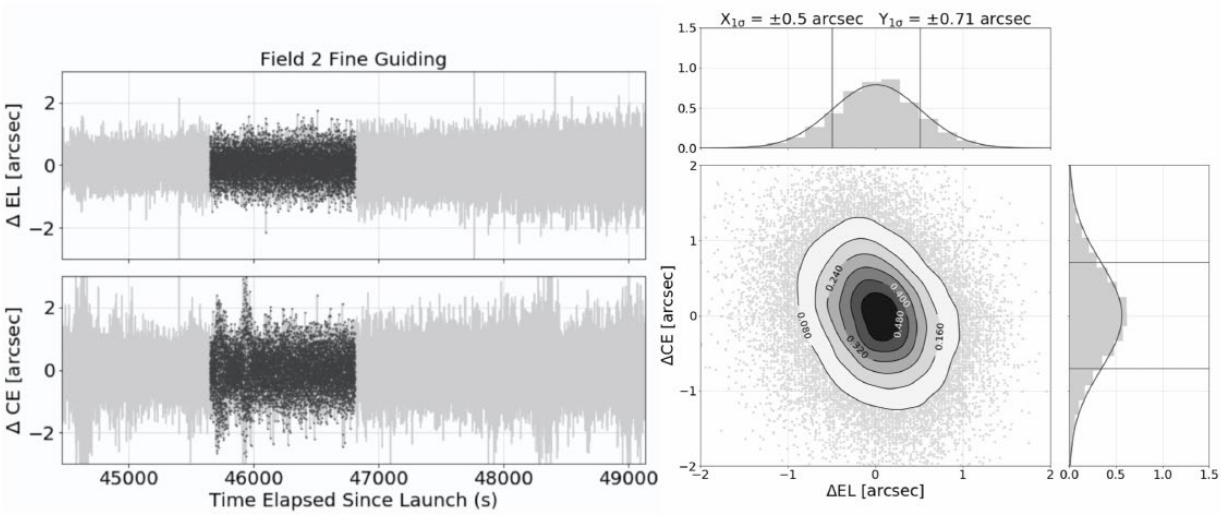


Figure 13-9: In-flight performance from the FIREBall pointing and guidance system showing (left) the time history of fine guiding and (right) a summary of elevation and cross-elevation residual errors during a 1-hour observation

3.2.1.3. The SuperBIT Pointing System

The Super-pressure Balloon-borne Image Telescope (SuperBIT) is a wide-field, multi-band, diffraction-limited optical-to-near-ultraviolet imaging system, which requires pointing performance at the sub-arcsecond level. The SuperBIT pointing system makes use of a rotator-reaction-wheel co-actuated azimuth system that maintains passive damping of the primary gondola structure at the arcminute level. To remove residual pendulation disturbances, a two-stage gimbal system is employed, consisting of a roll-actuated middle frame that contains a pitch-actuated inner frame and telescope. This configuration enables the removal of pendulations in a near-decoupled regime. Each frame solves the static friction problem by utilizing linear flexure bearings that trade off limited motion range for a smooth torque profile over that range. Extended elevation control is achieved through the dual-actuation of the inner frame and telescope, featuring a coarse stage for large motions and a fine flexure bearing stage for stabilization and precision pointing. Over four successful flights, SuperBIT consistently demonstrated platform and telescope stability at a 0.5 arcsecond (RMS) level or better over 30- to 90-minute timescales (Figure 12-11), with the final super pressure flight achieving nearly 500 hours of high-precision pointing performance over 45 days of science-capable flight time. The SuperBIT platform and its derived technologies are currently being leveraged for several high-performance applications with similar pointing requirements in the fields of astronomy and Earth observation [32], [33], [34].



Figure 13-10: SuperBIT in Wanaka, New Zealand, in pre-flight prior to its highly successful 45-day science observational campaign; this flight was facilitated by NASA's Columbia Scientific Balloon Facility (CSBF) utilizing the Super-Pressure Balloon (SPB) capabilities that enable mid-latitude flights.

3.2.2. Image & Component Stabilization

While many flight-proven techniques have demonstrated effective pointing and stabilization of primary gondola structures at 0.5 to 1 arcsecond (RMS), many extreme-precision applications require even higher precision for specific balloon-borne components and imagers. Several approaches have been successfully implemented on board balloon-borne gondolas, all of which involve very specific high-bandwidth control and stabilization of highly designed components mounted to the primary gondola structure. In this way, sub-arcsecond stabilization of the gondola can be used as a "first stage" to provide a stable environment in which these component-level stabilization techniques may operate.

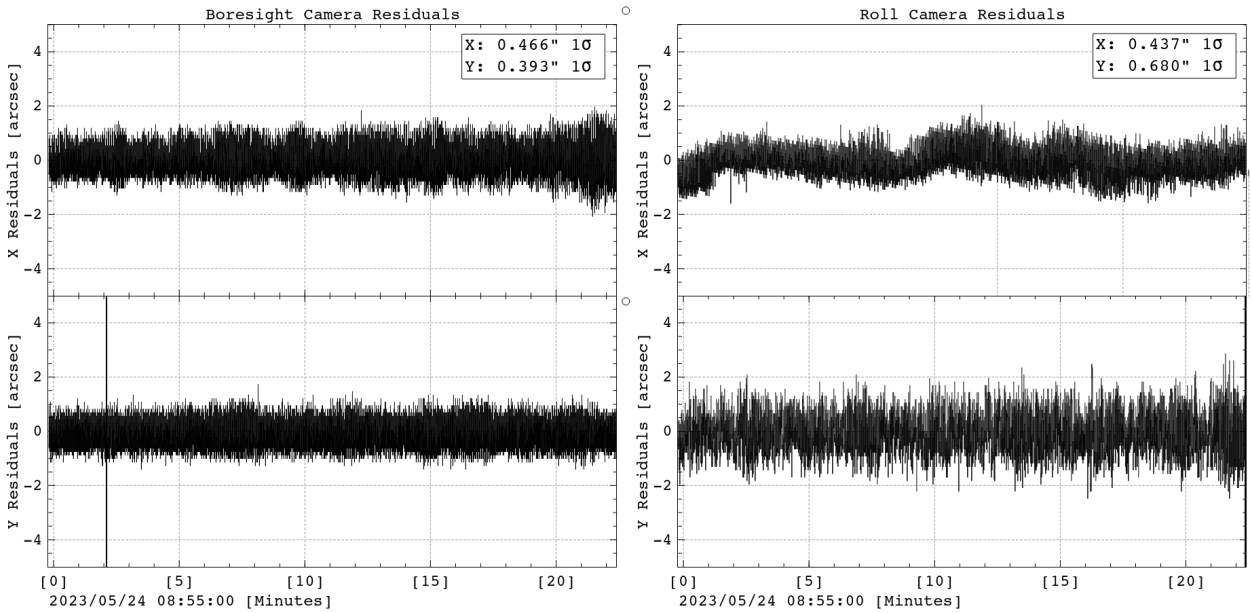


Figure 13-11: In-flight performance from the SuperBIT pointing system during the 45-day super pressure flight; (left) boresight star camera residual tracking errors and (right) roll star camera residual tracking errors over 30 minutes of tracking on a single target

3.2.2.1. Flight Demonstrations

Current approaches that have demonstrated success through in-flight testing include the SuperBIT Fine Guidance System (FGS), which leverages the pointing control and stabilization capabilities of the SuperBIT pointing system to achieve 0.5 arcseconds of pointing accuracy and improves image stabilization at the primary science imaging plane by an order of magnitude (i.e., 0.05 arcseconds). The approach involves using a high-bandwidth, low-range piezoelectric tip-tilt actuator to correct for residual disturbances from the gondola pointing system, with feedback from optically co-located rate gyroscopes, as well as guide stars selected from the science imaging plane. This approach enables image stabilization over a wide field of view (0.5 degrees), with the necessary stabilization performance to demonstrate diffraction-limited imaging of SuperBIT's half-meter telescope, allowing for observation periods of up to 90 minutes per target. During SuperBIT's highly successful 45-day super pressure flight, the SuperBIT FGS demonstrated consistent 0.05 arcsecond (RMS) pointing stability and control at the science focal plane over nearly 500 hours of science observation time from the stratosphere.

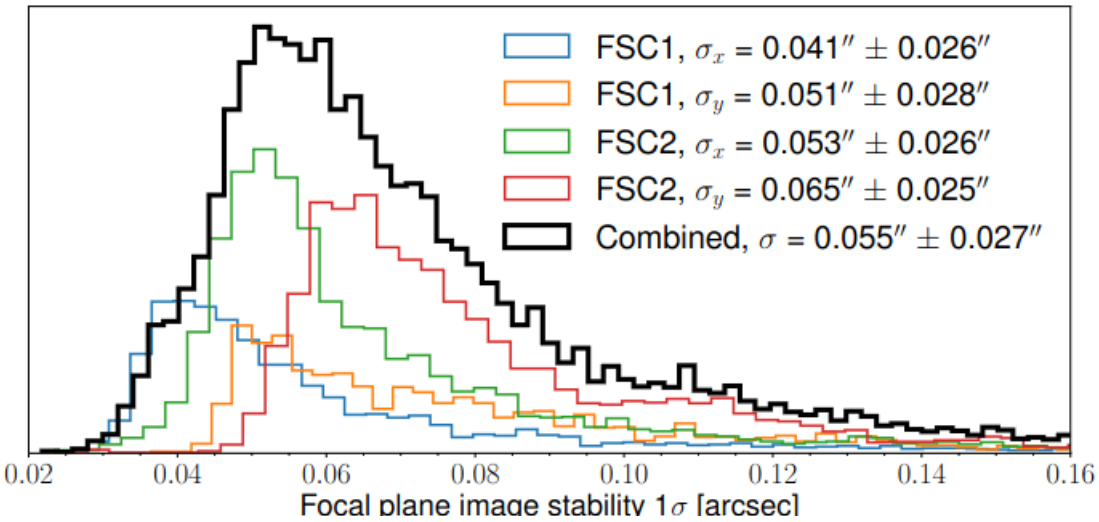


Figure 13-12: In-flight performance from the SuperBIT FGS during the 45-day super pressure flight; image stabilization runs over nearly 500 hours of science observation time, and is collated to show performance throughout the flight

3.2.2.2. Prospective Applications

The approaches to extreme precision stabilization of balloon-borne components are being leveraged for the design and development of new and highly capable platforms, including the soon-to-be-flown EXoplanet Infrared Climate TElescope (EXCITE), the in-progress Gigapixel-class Balloon-borne Imaging Telescope (GigaBIT), and the proposed PICTURE-D mission. In addition to these prospects, significant interest has been generated in applying the concept of extreme precision to balloon-borne instrumentation for applications beyond imaging. In particular, the concept of optical communications has spurred the need for further development in providing sufficiently pointed and stabilized optical terminals onboard balloon-borne instrumentation, where communication quality and bandwidth are directly linked and, in the case of balloons, limited by pointing performance. Using techniques as mentioned in this work for gondola and component-level pointing would not only enable balloon-borne payload operations with high bandwidth communications but could also potentially provide a baseline for balloon-borne networking and data relaying as a supplement or alternative to currently in-development space-based communications systems. Research and development in this area is currently underway in the private sector.

4. Conclusions

Continuous monitoring of gondola health and operational state allows engineers and mission controllers to detect anomalies early, adapt to changing environmental conditions, and extend mission lifetimes. By integrating data streams from sensors that measure pressure,

temperature, structural loads, and energy systems, modern health assessment approaches provide real-time insights that were previously impossible in earlier decades. These advances in monitoring contribute directly to the reliability and safety of balloon missions, especially as they move toward increasingly autonomous operations in remote or planetary environments.

Equally important is the role of predictive modeling in anticipating failure modes before they occur. By simulating thermal stresses, material fatigue, and atmospheric interactions, engineers can refine balloon designs and operational protocols, reducing risks for both science objectives and mission infrastructure. These models, combined with ground-test validation, help ensure that mission health metrics remain robust even in the face of unexpected environmental challenges.

Looking ahead, the fusion of artificial intelligence, advanced materials, and miniaturized instrumentation promises a new era in balloon health management. Future systems may self-correct minor anomalies, reconfigure power usage autonomously, or even deploy backup communication nodes to maintain mission continuity. As balloon missions expand into more extreme environments—from the upper reaches of Earth's atmosphere to the cloud layers of Venus or the skies of Titan—health and state monitoring will remain a cornerstone for safe, efficient, and scientifically productive exploration.

References

[1] K. S. Lay, L. Li, and M. Okutsu, "High altitude balloon testing of Arduino and environmental sensors for CubeSat prototype," *HardwareX*, vol. 12, p. e00329, Oct. 2022, doi: 10.1016/j.ohx.2022.e00329.

[2] F. Kreith, "Thermal Design of High-Altitude Balloons and Instrument Packages," *J. Heat Transf.*, vol. 92, no. 3, pp. 307–332, Aug. 1970, doi: 10.1115/1.3449667.

[3] W. Zhu, Y. Xu, H. Du, and J. Li, "Thermal performance of high-altitude solar powered scientific balloon," *Renew. Energy*, vol. 135, pp. 1078–1096, May 2019, doi: 10.1016/j.renene.2018.12.083.

[4] H. Rokujo *et al.*, "Development of a balloon-style pressure vessel gondola for balloon-borne emulsion gamma-ray telescopes," *J. Instrum.*, vol. 14, no. 09, p. P09009, Sept. 2019, doi: 10.1088/1748-0221/14/09/P09009.

[5] N. P. Lourie *et al.*, "Design and characterization of a balloon-borne diffraction-limited submillimeter telescope platform for BLAST-TNG," in *Ground-based and Airborne Telescopes VII*, SPIE, July 2018, pp. 631–649. doi: 10.1117/12.2314380.

[6] "In-Flight Performance of the BLAST-TNG Balloon-Borne Far-Infrared Telescope and Development of a Reconfigurable Readout on the RFSoC Platform for Frequency Multiplexed Superconducting Detector Arrays - ProQuest." Accessed: Aug. 21, 2025. [Online]. Available: https://www.proquest.com/openview/6b929b6bb073fc26b27a49eed9620a7b/1?pq-origsite=gscholar&cbl=18750&diss=y

[7] Z. Wang, M. Huang, L. Qian, B. Zhao, and G. Wang, "High-Altitude Balloon-Based Sensor System Design and Implementation," *Sensors*, vol. 20, no. 7, p. 2080, Jan. 2020, doi: 10.3390/s20072080.

[8] L. Parayitam, S. Sirikonda, S. Palleboina, and N. Chari, "Navigation—A General Overview," in *Biophysics of Insect Flight*, N. Chari, P. Mukkavilli, and L. Parayitam, Eds., Singapore: Springer Nature, 2021, pp. 167–186. doi: 10.1007/978-981-16-5184-7_13.

[9] G. Zhang and L.-T. Hsu, "Intelligent GNSS/INS integrated navigation system for a commercial UAV flight control system," *Aerosp. Sci. Technol.*, vol. 80, pp. 368–380, Sept. 2018, doi: 10.1016/j.ast.2018.07.026.

[10] M. Safonova *et al.*, "Measurements of gondola motion on a stratospheric balloon flight," July 21, 2016, *arXiv*: arXiv:1607.06397. doi: 10.48550/arXiv.1607.06397.

[11] M. Gemignani and S. Marcuccio, “Dynamic Characterization of a High-Altitude Balloon during a Flight Campaign for the Detection of ISM Radio Background in the Stratosphere,” *Aerospace*, vol. 8, no. 1, p. 21, Jan. 2021, doi: 10.3390/aerospace8010021.

[12] R. Lawler *et al.*, “Active Guidance for High Altitude Balloon Payloads,” in *2025 Regional Student Conferences*, American Institute of Aeronautics and Astronautics. doi: 10.2514/6.2025-98678.

[13] T. J. Schneeberger and K. W. Barker, “High-altitude balloon experiment: a testbed for acquisition, tracking, and pointing technologies,” in *Acquisition, Tracking, and Pointing VII*, SPIE, Oct. 1993, pp. 2–15. doi: 10.1117/12.156595.

[14] M. J. Devlin *et al.*, “The Balloon-borne Large Aperture Submillimeter Telescope (BLAST),” in *Millimeter and Submillimeter Detectors for Astronomy II*, SPIE, Oct. 2004, pp. 42–54. doi: 10.1117/12.555258.

[15] B. E. Catanzaro, T. Pham, L. Olmi, K. E. Martinson, and M. Devlin, “Design and fabrication of a lightweight 2-m telescope for the balloon-borne large-aperture sub-millimeter telescope: BLAST,” in *Infrared Spaceborne Remote Sensing X*, SPIE, Dec. 2002, pp. 71–78. doi: 10.1117/12.453708.

[16] M. Somov and S. Venuganti, “Solar Panel Efficiency and Visible Light Detection On High Altitude Balloons,” *Acad. High Alt. Conf.*, vol. 2024, no. 2, June 2024, doi: 10.31274/ahac.17926.

[17] A. S. Gill *et al.*, “SuperBIT Superpressure Flight Instrument Overview and Performance: Near diffraction-limited Astronomical Imaging from the Stratosphere,” *Astron. J.*, vol. 168, no. 2, p. 85, Aug. 2024, doi: 10.3847/1538-3881/ad5840.

[18] C. Burth, “NASA’s 5.5K Rotator.” [Online]. Available: https://ntrs.nasa.gov/api/citations/20220010843/downloads/PSB.1-0029-22_BURTH.pdf

[19] E. Barbazán García, “Design and Implementation of an Attitude Control System for High-Altitude Platforms,” 2020, Accessed: Aug. 21, 2025. [Online]. Available: https://hdl.handle.net/10016/36793

[20] J. Ashenberg, “Conceptual Study of Gondola Stabilization in a Balloon System,” *J. Aircr.*, vol. 45, no. 2, pp. 486–492, 2008, doi: 10.2514/1.29710.

[21] L. Wasilenko, “High altitude balloon with stabilized camera system.” Accessed: Aug. 21, 2025. [Online]. Available: https://open.library.ubc.ca/soa/cIRcle/collections/undergraduateresearch/52966/items/1.0074456

[22] K. L. Dietz, B. D. Ramsey, C. D. Alexander, J. A. Apple, K. Ghosh, and W. R. Swift, "Daytime aspect camera for balloon altitudes," *Opt. Eng.*, vol. 41, no. 10, pp. 2641–2651, Oct. 2002, doi: 10.1117/1.1501566.

[23] M. Safonova *et al.*, "Measurements of gondola motion on a stratospheric balloon flight," July 21, 2016, *arXiv*: arXiv:1607.06397. doi: 10.48550/arXiv.1607.06397.

[24] A. Lecinski, G. Card, M. Knölker, and B. Hardy, "The Design and Performance of the Gondola Pointing System for the Sunrise II Balloon-Borne Stratospheric Solar Observatory," *J. Astron. Instrum.*, May 2017, doi: 10.1142/S2251171717400074.

[25] M. Henderson, "Design and Optimization of a 1.5m Telescope Balloon Borne Gondola".

[26] K. Hewawasam *et al.*, "The low-order wavefront control system for the PICTURE-C mission: high-speed image acquisition and processing," in *Techniques and Instrumentation for Detection of Exoplanets VIII*, SPIE, Sept. 2017, pp. 564–572. doi: 10.1117/12.2274125.

[27] E. Kassarian, F. Sanfedino, D. Alazard, J. Montel, and C.-A. Chevrier, "Robust line-of-sight pointing control on-board a stratospheric balloon-borne platform," Dec. 20, 2021, *arXiv*: arXiv:2112.10458. doi: 10.48550/arXiv.2112.10458.

[28] C. B. Mendillo, K. Hewawasam, G. A. Howe, J. Martel, T. A. Cook, and S. Chakrabarti, "The PICTURE-C exoplanetary direct imaging balloon mission: first flight preparation," in *Techniques and Instrumentation for Detection of Exoplanets IX*, SPIE, Sept. 2019, pp. 101–111. doi: 10.1117/12.2529710.

[29] I. Cevallos-Aleman *et al.*, "FIREBall-2 2023: fine guidance system performance for UV balloon telescope flight," in *Space Telescopes and Instrumentation 2024: Ultraviolet to Gamma Ray*, SPIE, Aug. 2024, pp. 917–923. doi: 10.1117/12.3020671.

[30] M. Matuszewski *et al.*, "FIREBALL: instrument pointing and aspect reconstruction," in *Space Telescopes and Instrumentation 2010: Ultraviolet to Gamma Ray*, SPIE, July 2010, pp. 742–750. doi: 10.1117/12.857869.

[31] J. Montel *et al.*, "Design and improvements of the Attitude Control System of the FIREBall balloon experiment," in *Space Telescopes and Instrumentation 2016: Ultraviolet to Gamma Ray*, SPIE, July 2016, pp. 1117–1135. doi: 10.1117/12.2236224.

[32] L. J. Romualdez *et al.*, "Overview, design, and flight results from SuperBIT: a high-resolution, wide-field, visible-to-near-UV balloon-borne astronomical telescope," in *Ground-based and*

Airborne Instrumentation for Astronomy VII, SPIE, July 2018, pp. 222–236. doi: 10.1117/12.2307754.

[33] "Modeling and Control for Fine Pointing and Jitter Management in Balloon-Borne Telescopes - ProQuest." Accessed: Aug. 21, 2025. [Online]. Available: https://www.proquest.com/openview/6cfebee7d550decab78d10d50d99daaf/1?pq-origsite=gscholar&cbl=18750&diss=y

[34] P. Voyer *et al.*, "From SuperBIT to GigaBIT: informing next-generation balloon-borne telescope design with fine guidance system flight data," in *Ground-based and Airborne Telescopes X*, SPIE, Sept. 2024, pp. 1946–1958. doi: 10.1117/12.3017869.

Chapter 14
Decelerators & Deployables

Alvin Morris
Revised by Tim Lachenmeier[1] and Javier Romualdez[2]

[1] Aerostar International LLC, Sioux Falls, SD
[2] StarSpec Technologies Inc., Toronto, Canada

Table of Contents

1. Introduction 5

2. Decelerators 5

2.1. Description of a Parachute System 5

2.2. Parachute Descent 8

2.2.1. A Simplified Descent Model 11

2.2.2. Phase 1 13

2.2.3. Phase 2 14

2.2.4. Phase 3 20

2.2.5. Phase 4 21

2.3. Considerations in Selecting a Parachute 22

2.3.1. Parachute Size 23

2.3.2. Multiple Parachutes 26

2.3.3. Time of Descent 28

3. Deployables and Extension Mechanisms 29

3.1. Extension Mechanisms 29

3.2. High-Altitude Deployables 30

4. Conclusions 31

References 33

Table of Figures

Figure 14-1: Parachute nomenclature..... 6

Figure 14-2: The prismoidal multipoint suspension system..... 7

Figure 14-3: Acceleration versus time for a parachute system for which terminal velocity is constant. Acceleration is in effect plotted as multiples of the acceleration of gravity and time as multiples of $-vT$/g. 16

Figure 14-4: Acceleration traces of quick-opening and delayed-opening parachutes..... 18

Figure 14-5: Descent velocity vs time for a parachute system for which terminal velocity is constant. Velocity is plotted as a multiple of vT and time as a multiple of $-vT/g$..... 19

Figure 14-6: Loss of altitude vs time for a parachute system for which the terminal velocity is constant. Height difference is in effect plotted in multiples of $vT2/g$ and time in multiples of $-vT/g$. 20

Figure 14-7: Sea level terminal velocity of a parachute as a function of parachute system mass and the product of parachute area and drag coefficient. Numbers on the abscissa and ordinate may be multiplied concurrently by any factor 10n to cover all non-zero values..... 24

Figure 14-8: Nominal diameter of a parachute as a function of area and drag coefficient. Numbers on the ordinate may be multiplied by 10n if numbers on the abscissa are concurrently multiplied by 10^2n to cover all non-zero values..... 25

Figure 14-9: Terminal velocity and time of descent, terminal velocity and altitude in the U.S. Standard Atmosphere, 1962..... 27

Figure 14-10: SuperBIT Data Recovery System (red circles) during pre-flight of the 2019 test flight campaign from Timmins, Ontario, in northern Canada..... 31

Table of Symbols

Symbol	Definition / Description	Dimensions
A	Cross-sectional area, effective area of inflated canopy	L^2
A'	Nominal area, area of material in the canopy	L^2
B	Subscript identifying association with balloon system	—
C	Constant of integration	—
C_D	Drag coefficient (dimensionless)	—
$C_{D'}$	Pseudo drag coefficient, using an area other than the effective area	—
D	Diameter of canopy	L
D'	Nominal diameter of a canopy (area = A′)	L
d	Differential operator (e.g., d/dt)	—
g	Acceleration due to gravity	$L\ T^{-2}$
H	Height above sea level	L
m	Mass of parachute system	M
m_{vv}	Virtual mass of the accelerating parachute system	M
N	Number of parachutes in cluster	—
n	Exponent of 10 used to expand scales in Figs. 6–7	—
o	Subscript for base or zero level	—
Re	Reynolds number (dimensionless)	—
T	Subscript used with v to denote terminal or equilibrium velocity	—
t	Time	T
v	Vertical velocity; (+) upward, (−) downward	$L\ T^{-1}$
v_T	Terminal/equilibrium velocity	$L\ T^{-1}$
v_W	Horizontal speed of surface wind	$L\ T^{-1}$
ρ	Air density	$M\ L^{-3}$

1. Introduction

Decelerators and deployable mechanisms are critical components of balloon-borne systems, ensuring both the safe recovery of scientific payloads and the operational success of flight missions. Parachutes, extension mechanisms, and deployable systems must be carefully engineered to balance safety, reliability, and mission requirements. This chapter presents an overview of the fundamental theory, practical considerations, and demonstrated applications of decelerators and deployables in the context of high-altitude scientific ballooning. By examining both traditional parachute systems and modern innovations in deployable recovery and extension mechanisms, the discussion highlights how these technologies contribute to mission assurance, payload protection, and the advancement of balloon-borne science[3].

2. Decelerators

Parachutes are used on most scientific balloon flights to return the scientific instruments aboard the gondola to the ground in a reusable state. This section presents a simplified theory of parachute behavior during descent and outlines procedures for selecting a suitable parachute. For a more complete discussion of parachute theory and practice, the reader is referred to two invaluable resources, 1. Theo Knacke's *Parachute Recovery Systems Design Manual* [1] and 2. the U.S. Air Force *Recovery Systems Design Guide* [2].

2.1. Description of a Parachute System

A parachute consists of a woven textile or plastic canopy attached to the load by means of suspension lines, commonly referred to as shroud lines. The canopy may take various forms, but is usually axially symmetric about the vertical axis, and can be made with or without holes. For some special purposes, the canopy is made of ribbons.

Figure 14-1 illustrates a schematic of a descending parachute with an attached load. Most features of parachutes used in scientific ballooning are illustrated, although variations may be observed. A parachute, along with its payload and ancillary equipment, will be referred to as a parachute system.

The suspension lines attach to the canopy at its outer perimeter, or skirt. They are normally fastened to the skirt at the seams between gores, and they may or may not continue upward over the canopy to the vent on the top. Not all parachutes have vents, but, although the theory

[3] Both the introduction and conclusion of this chapter were written by ChatGSFC.

of parachute behavior is far from complete, it is generally believed that parachutes with an axially symmetric canopy benefit from the vent [3], [4].

The porosity of the canopy material affects the performance of a parachute in several important ways. A highly porous canopy fills more slowly, is more stable, and has a lower drag coefficient than a less porous canopy. The effective porosity of a cloth is defined as the ratio of the average speed of air through the porous sheet to the speed of the free stream. A canopy can be made more porous than the cloth from which it is made by leaving open areas in it. Geometric porosity is defined as the ratio of the open area of a canopy's drag-producing surface to the total area of the drag-producing surface. [5].

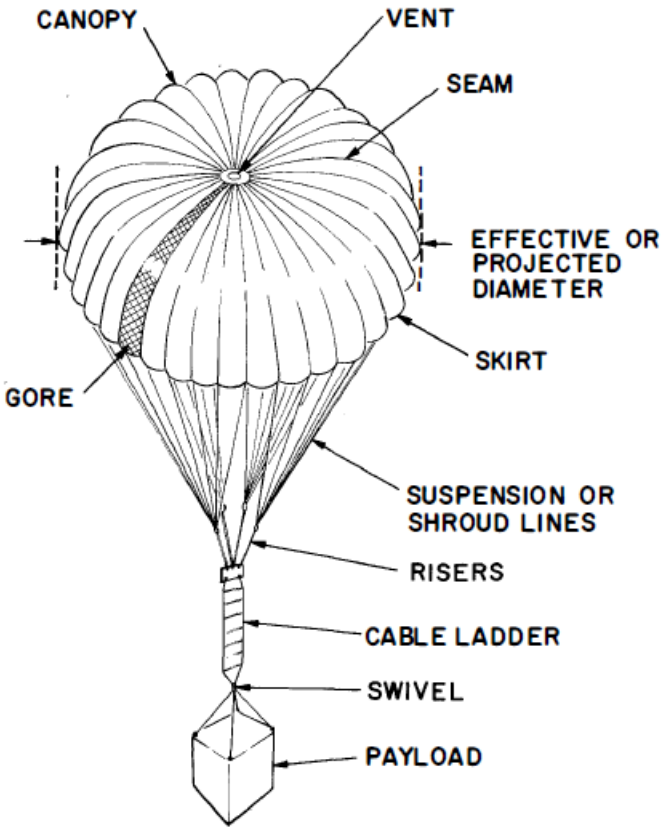


Figure 14-1: Parachute nomenclature.

The payload may be fastened directly to the lower end of the risers; however, if there are reasons to suspend it lower (i.e., increasing the field of view, reducing the launch stress index, or preventing entanglement of the shroud lines with the launch vehicle used in a dynamic launch), a cable ladder may be used. Operationally, the cable ladder is key to laying out the system over the launch vehicle and is used with all NASA launch configurations. A prismoidal, multipoint suspension system, Figure 14-2, consisting of two or more cables, is

commonly used to help provide torsional stability between the payload and the balloon. If it is desirable for the payload to be free to turn independently of the parachute, a swivel may be placed in the suspension system at any point below the risers. For payloads that require pointing, a rotator fitting is used in place of the swivel.

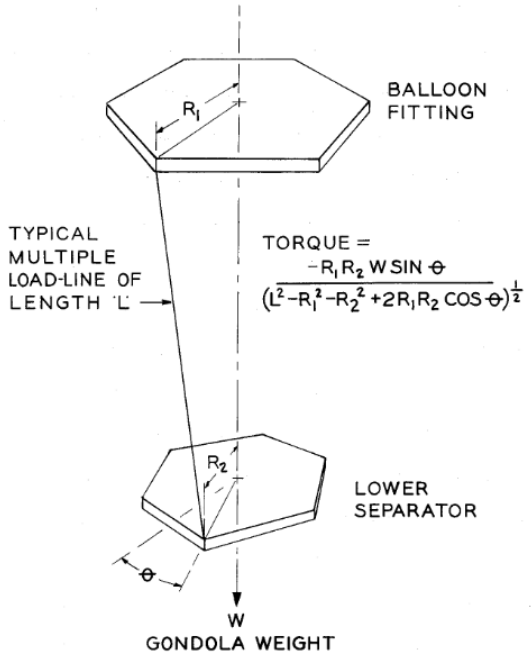


Figure 14-2: The prismoidal multipoint suspension system.

Parachutes are usually described by their nominal diameter, the diameter of a circle whose area is equal to the area of the drag-producing surface of the canopy. Thus, the nominal diameter of a flat circular canopy is the diameter of the parachute in its flat form, whereas the effective diameter is the projected diameter of the inflated parachute, as shown in Figure 14-1. The latter is a function of the parachute's design and the load it is carrying.

Packed parachutes are used less frequently in scientific ballooning. The primary reasons for using a packed chute are to shorten the overall flight train length and reduce the parachute opening shock. The reductions in length can be significant (i.e., one and a half times the nominal parachute diameter), and a factor of 3 or more can reduce the opening shock. Instead, most large scientific balloon systems are flown with the parachute pre-deployed (extended), and inflation can start immediately upon separation from the balloon. [6], [7]. In this configuration, the parachute serves as a link in the suspension system between the balloon and payload. This is particularly attractive in cases where the gondola instrument cannot sense through the balloon and requires a greater distance for a larger field of view.

2.2. Parachute Descent

Existing theory cannot describe the complete behavior of a parachute system in flight; however, it provides some insight into the behavior and serves as the foundation for selecting parachutes for specific applications.

The equation of motion of a body through a still fluid subject to the forces of gravity and fluid drag may be written:

$$\frac{d(m_v v)}{dt} = -\frac{1}{2} C_D \rho A |v| v - mg \qquad (14\text{-}1)$$

Where m_v is the virtual mass of the moving body, v is its vertical velocity, C_D is a dimensionless drag coefficient, ρ is the density of the fluid, A is the cross-sectional area of the body normal to its direction of motion, m is the mass of the body, and g is the acceleration due to gravity.

Virtual mass is discussed in Chapter 4. The virtual mass of a parachute system, when the canopy is fully inflated, is approximately equal to the mass of the system plus an added mass that is equivalent to 0.7 times the mass of a spherical volume of air with the density of the ambient air and a radius equal to the effective radius of the parachute canopy. The mass, m, of a descending parachute system is equal to the mass of the payload, the parachute, the suspension system, and all other attached objects. At the high altitudes (low densities) at which parachutes dropped from balloons are normally inflated, the added mass is small compared to the mass of the parachute system; therefore, the approximation $m = mv$ will be used henceforth.

The coordinates and units discussed in Chapter 4 will be used in this section. Thus, during descent, the vertical velocity causes a positive, or upward, acceleration, and the weight of the system (mg) causes it to accelerate negatively, or downward. Since the direction of the velocity vector is determined by its algebraic sign, vector notation is not used.

For a parachute, C_D is a function primarily of the shape and porosity of the canopy. It is weakly dependent on Reynolds number.

If the fluid is compressible and the motion causes appreciable compression, C_D is a function of Mach number also. However, unless a parachute system's descent velocity exceeds half the speed of sound, compressibility may be ignored. In practice, the drag coefficient is normally considered constant for a given parachute system throughout descent.

Air density is a function of altitude in the atmosphere. This functional relationship is discussed in detail in Chapter 7. It is necessary to consider the variation of ρ with time in a descending parachute system, but some phases of the descent are of such short duration that during those phases, ρ can be considered constant.

For typical scientific high altitude balloon recovery parachutes, the cross-sectional area of the parachute system during descent is essentially the effective cross-sectional area of the parachute canopy, as the payload contributes a negligible area by comparison. The canopy's area is dependent on the design and size of the parachute, as well as the load it bears. Prior to the start of inflation, A is negligible; after the canopy is inflated and a steady state descent is reached, A can be calculated from known conditions. While inflation is occurring, A may momentarily have any value from nearly zero to the area of the flat canopy.

The vertical velocity of a parachute system is considered here, as a still or motionless fluid has been specified. Equation (14-1) is valid in a moving fluid if v is defined as the relative velocity vector of the body through the fluid, but the magnitude of vertical motion of the atmosphere is small enough compared to the magnitude of the descent velocity of a parachute system that vertical atmospheric motions are neglected. If parachute descents were made in convective cells such as thunderstorms, the theory developed here would differ markedly from practice. An equation similar to Equation (14-1) may also be used to calculate the horizontal motion of a parachute system in a moving atmosphere, but it is usually assumed that the parachute system moves horizontally at the speed of the wind system in which it is embedded. Since the time it takes for the parachute and payload to be horizontally accelerated to the wind speed is usually short compared to their time in the wind system, this is generally a good approximation.

For convenience of discussion, a parachute descent may be divided into four phases: 1) the initiation of descent and deployment of the parachute, 2) inflation of the canopy and acceleration to terminal velocity, 3) steady state descent at terminal velocity, and 4) landing.

A parachute descent is initiated when the parachute system is separated from the balloon. A parachute is deployed when it is fully extended just before or even during inflation. Packed parachutes typically deploy before they start to inflate. Parachutes, which serve as a link in the suspension system (see Figure 14-3, Section 2), usually contract like a stretched spring upon separation from the balloon and then deploy again as inflation begins. This can cause undesirable opening shock forces on the payload, and a rip-stitch decelerator is often used to attenuate these forces [8], [9]. This is just one of many unique design factors for a high-altitude decelerator system [10], [11], [12]. Packed

parachutes do not have any pretension in the canopy and shroud lines and begin creating drag during the initial opening phase, and continue to slow the payload down as the canopy fully inflates. This results in considerably lower opening shocks (i.e., <2g for packed versus 6-10g for fully extended).

During inflation, air rams into the open lower side of the canopy and fills it under slightly greater pressure than ambient air pressure. The adjustment of the canopy to the incoming air is rapid, as revealed by cameras on the payload; however, the canopy undergoes several oscillations about its equilibrium shape before settling into it. Drag force develops rapidly as the canopy inflates. Parachutes are often referred to as decelerators, implying that they decrease the speed of the parachute system. In scientific ballooning use, a system frequently continues to gain speed after the parachute is inflated.

Terminal velocity (also called equilibrium velocity) is the velocity that a parachute system would have if it were descending without acceleration, i.e., if $dv/dt = 0$ or $v = const$. Under conditions of terminal velocity and constant virtual mass, Equation (14-1) becomes

$$\frac{1}{2} C_D \rho A |v_T| v_T = -mg \tag{14-2}$$

$$v_T = -\sqrt{\frac{2mg}{C_D \rho A}} = const. \tag{14-3}$$

Now, for a parachute system in phase 3, descending in the atmosphere, m, C_D, and A may all be expected to remain constant, and g varies quite slowly. Air density, however, increases from near 4 X 10 $^{-3}$kg/m^3 at 40km to near 1.2kg/m^3 at sea level. Therefore, v_T at 40km cannot be the same as v_T at sea level. If not, a parachute system must accelerate as it descends, and thus, the condition for terminal velocity is not fulfilled. Although a descending parachute system may never achieve terminal velocity, the concept remains useful if its limitations are kept in mind.

For example, the descent velocity of a parachute system may be quite adequately computed by Equation (14-3) for a thin stratum in the atmosphere, using for ρ the mean density of the stratum. Also, by using many thin strata, the time of descent from any given level to any lower level may be satisfactorily calculated. Ultimately, the concept of terminal velocity streamlines the theoretical analysis of parachute descent.

As a parachute system nears the surface, motions other than the vertical motion may become important. The most critical of these are drift and oscillation. An ideal landing is one in which the parachute system

descends at a known rate in a perfectly vertical position, without horizontal motion, onto a readily accessible, unoccupied, and firm surface. Human parachute systems have been developed to the point where this sort of landing can be made with relative ease. The user must, of course, plan ahead, making his descent only at times and in places where the parachute system controls are used within their limitations. To a lesser extent, a parachute system can be controlled remotely. Although some experimental remote-controlled descents have been made, such systems are neither common nor well-developed. Anyone planning a parachute drop from a balloon must anticipate that the landing site cannot be selected precisely, that the system will be drifting horizontally at the time of impact, and that an oscillation of the system probably will cause the payload to be tilted at touchdown. There are options for guided recovery if the required mass and power can be dedicated to that system [11], [13].

Proper planning and execution can make parachute descents safe and effective, even in challenging conditions. Carefully designed buffer systems, such as a framework that yields progressively or honeycomb crush pads, can be used to absorb the kinetic energy that the system has at the moment of impact [14]. Various wind models (GFS, ECMWF, HRR) and sounding data can be used to help prevent flights from being undertaken when low-level winds at the landing site are likely to be excessive. They can also provide descent drift vectors in the flight termination area. A drift vector is based on the winds anticipated at all levels through which the parachute system must descend. This allows an estimate of the landing site to be calculated from the known position of the balloon system at the time-of-flight termination. Stable parachutes, i.e., cross or ribbon parachutes that have reduced oscillation during descent, can also be used to increase the probability that the payload will land upright, allowing the landing buffer system to function properly. Unfortunately, choosing a stable parachute may lead to other compromises, such as slow opening or less certain opening. The typical flat circular recovery chute can oscillate 45 degrees or more during the initial stages of descent, compared to a cross chute that typically oscillates closer to 15 degrees. Both types of chutes have their oscillations essentially damped out prior to reaching the ground, unless they encounter low-level wind shear, so the primary tipping force is due to the surface wind velocity.

2.2.1. A Simplified Descent Model

Equation (14-1) and the concept of terminal velocity provide a starting point for a simplified theoretical model of a parachute system descending in the atmosphere, simulating many features of a real descent. For a given parachute system at a level in the atmosphere where ρ and g are known, a value of v_T can be calculated using Equation (14-3). Unless the parachute system has reached the steady state phase of its descent, the

terminal velocity will not constitute a good approximation to the actual velocity. It may, however, be viewed as a value toward which the actual velocity tends, and it is a convenient single variable that may be substituted for a combination of others.

Substituting from Equation (14-2) into Equation (14-1) and rearranging gives

$$\frac{dv}{dt} = \frac{g}{v_T^2}(v^2 - v_T^2) \tag{14-4}$$

if it is assumed that $mv = m = const$. Equation (14-4) may also be written

$$\frac{dv}{v^2 - v_T^2} = \frac{g}{v_T^2}dt \tag{14-5}$$

Now although both g and v_T are functions of time during descent, they both change slowly. Let it be assumed that over a short time interval, they may be treated as constants.

In phase 1 of the descent, the canopy is not inflated. Consequently, the cross-sectional area of the system is quite small. Air density will also be small, and although the drag coefficient may be relatively large, the magnitude of v_T will be large during phase 1. Assume further that the change from phase 1 to phase 2 is instantaneous--that is, the canopy snaps instantly from its deployed but uninflated state to a state of full inflation. This is not entirely in keeping with the actual behavior of a parachute, but as will be shown later, it leads to conservative results from a design and planning perspective.

Throughout phases 2 and 3, the parachute remains essentially unchanged; therefore, A may be considered constant. The drag coefficient is a function of Reynolds number, Re, and therefore of the actual speed and dimensions of the parachute system, the air density, and air viscosity. For Reynolds numbers associated with a parachute system in phases 2 and 3, however, the dependence of C_D on Re is weak, and the assumption of constant C_D is realistic.

Density is then essentially the only variable in v_T; therefore, any time interval in which ρ does not change significantly, will be short enough to justify the assumption that v_T is constant.

Integrating Equation (14-5) once yields

$$-\frac{1}{v_T}\tanh^{-1}\left(\frac{v}{v_T}\right) = \frac{gt}{v_T^2} + C \qquad \text{for } \frac{v}{v_T} < 1 \tag{14-6}$$

$$-\frac{1}{v_T}\coth^{-1}\left(\frac{v}{v_T}\right)=\frac{gt}{v_T^2}+C \qquad \text{for } \frac{v}{v_T^2}>1 \qquad (14\text{-}7)$$

$$v=const=v_T \qquad \text{for } \frac{v}{v_T}=1 \qquad (14\text{-}8)$$

2.2.2. Phase 1

Let $t=0$ be the time at which the parachute is separated from the balloon. At that time $v=v_B$ (velocity of the balloon); consequently, the constant of integration, C, in Equation (14-6) is $-\tanh^{-1}(v_B/v_T)/v_T$. Because v_B is frequently zero and is always small compared to v_T, the integration constant may be ignored in most descents. It will be considered negligible here in further discussions of phase 1. In phase 1, $v/v_T<1$; therefore, Equations (14-7) and (14-8) are not applicable.

Equation (14-6) may now be written:

$$v=v_T\tanh\left(-\frac{gt}{v_T}\right) \qquad (14\text{-}9)$$

Note that in the coordinate system in use here, $v_T<0$. Thus, the argument of the hyperbolic tangent is positive and grows linearly with time. As time increases, $\tanh(-gt/v_T)$ also increases, approaching but never reaching one. Similarly, v will approach but never reach v_T. This tendency of v to approach v_T as a limiting value is characteristic of the descent model used here. For practical purposes, $v=v_T$ and Equation (14-6) degenerates into Equation (14-8) when $-gt/v_T$ grows larger than three.

Substituting dH/dt for v in Equation (14-9) and integrating yields

$$H=-\frac{v_T^2}{g}\ln\left(\cosh\left(-\frac{gt}{v_T}\right)\right)+C \qquad (14\text{-}10)$$

Where H is the height and C is the constant of integration. When $t=t_0$, $H=H_0$; therefore $C=H_0$ and:

$$H=H_0-\frac{v_T^2}{g}\ln\left(\cosh\left(-\frac{gt}{v_T}\right)\right) \qquad (14\text{-}11)$$

Differentiating Equation (14-9) yields acceleration in terms of t as follows:

$$\frac{dv}{dt} = g\left[\tanh^2\left(-\frac{gt}{v_T}\right) - 1\right] \qquad (14\text{-}12)$$

Examination of Equation (14-12) shows the acceleration to be made up of two parts, one of which is downward (negative) and one upward, and the upward acceleration grows with time.

The growth term can never quite reach one, although for practical purposes, it will have done so when $-gt/v_T$ has reached 3.0. At that time, acceleration will have ceased, and the descending system will have reached terminal velocity.

Equations (14-9), (14-11), and (14-12) contain a description of the motion of a parachute system starting from rest and descending without change of shape in a homogeneous atmosphere. If interest is restricted to a short time interval so that the stratum through which the system falls in that interval is thin, the restriction on homogeneity may be relaxed.

2.2.3. Phase 2

Equations (14-7) and (14-8), as well as Equation (14-6), must be considered in a discussion of phase 2 because the magnitude of the downward velocity may be less than, equal to, or greater than the magnitude of v_T. The initial velocity in phase 2 in the descent model being used is equal to the final velocity in phase 1. This allows for the evaluation of the constants of integration in Equations (14-6) and (14-7). Thus, for $t = t_1$ (the time of inflation of the canopy and the initiation of phase 2) $v = v_1$, and from Equations (14-6) and (14-7) respectively.

$$C = -\frac{1}{v_T}\tanh^{-1}\left(\frac{v_1}{v_T}\right) - \frac{gt}{v_T^2}$$

$$C = -\frac{1}{v_T}\coth^{-1}\left(\frac{v_1}{v_T}\right) - \frac{gt}{v_T^2}$$

Substituting these in Equations (14-6) and (14-7) and solving for v yields

$$v = v_T \tanh\left[\tanh^{-1}\left(\frac{v_1}{v_T}\right) - \frac{g(t - t_1)}{v_T}\right] \qquad \text{for } \frac{v_1}{v_T} < 1 \qquad (14\text{-}13)$$

$$v = v_T \tanh\left[\coth^{-1}\left(\frac{v_1}{v_T}\right) - \frac{g(t - t_1)}{v_T}\right] \qquad \text{for } \frac{v_1}{v_T} > 1 \qquad (14\text{-}14)$$

Integrating Equations (14-13) and (14-14) gives

$$H = H_1 + \frac{v_T^2}{g}\left\{\ln\left[\cosh\left(\tanh^{-1}\left(\frac{v_1}{v_T}\right)\right)\right] - \ln\left[\cosh\left(\tanh^{-1}\left(\frac{v_1}{v_T}\right) - \frac{g(t-t_1)}{v_T}\right)\right]\right\} \quad \text{for } \frac{v_1}{v_T} < 1 \qquad (14\text{-}15)$$

$$H = H_1 + \frac{v_T^2}{g}\left\{\ln\left[\sinh\left(\coth^{-1}\left(\frac{v_1}{v_T}\right)\right)\right] - \ln\left[\sinh\left(\coth^{-1}\left(\frac{v_1}{v_T}\right) - \frac{g(t-t_1)}{v_T}\right)\right]\right\} \quad \text{for } \frac{v_1}{v_T} < 1 \qquad (14\text{-}16)$$

Similarly, Equation (14-8) may be integrated to give:

$$H = H_1 - v_T(t - t_1) \quad \text{for } \frac{v_1}{v_T} = 1 \qquad (14\text{-}17)$$

Differentiating Equations (14-13) and (14-14) provides the following expressions for acceleration as functions of t:

$$C = -\frac{1}{v_T}\tanh^{-1}\left(\frac{v_1}{v_T}\right) - \frac{gt}{v_T^2}$$

$$\frac{dv}{dt} = g\left\{\tanh^2\left[\tanh^{-1}\left(\frac{v_1}{v_T}\right) - \frac{g(t-t_1)}{v_T}\right] - 1\right\} \quad \text{for } \frac{v_1}{v_T} < 1 \qquad (14\text{-}18)$$

$$\frac{dv}{dt} = g\left\{\coth^2\left[\coth^{-1}\left(\frac{v_1}{v_T}\right) - \frac{g(t-t_1)}{v_T}\right] - 1\right\} \quad \text{for } \frac{v_1}{v_T} > 1 \qquad (14\text{-}19)$$

Also, from the definition of v_T:

$$\frac{dv}{dt} = 0 \quad \text{for } \frac{v_1}{v_T} = 1 \qquad (14\text{-}20)$$

Equations (14-18) through (14-20) are plotted in dimensionless form in Figure 14-3. Two distinctive features of the descent model are immediately obvious. First, the acceleration at time $t = t_1$ is very sensitive to the value of the ratio v_1/v_T. Thus, for low acceleration, the parachute should inflate when this ratio is small. In fact, if inflation occurs before the velocity of the system has reached the inflated terminal velocity, downward acceleration will continue until

$v = v_T$. If inflation should occur just as the inflated terminal velocity is reached, acceleration will cease.

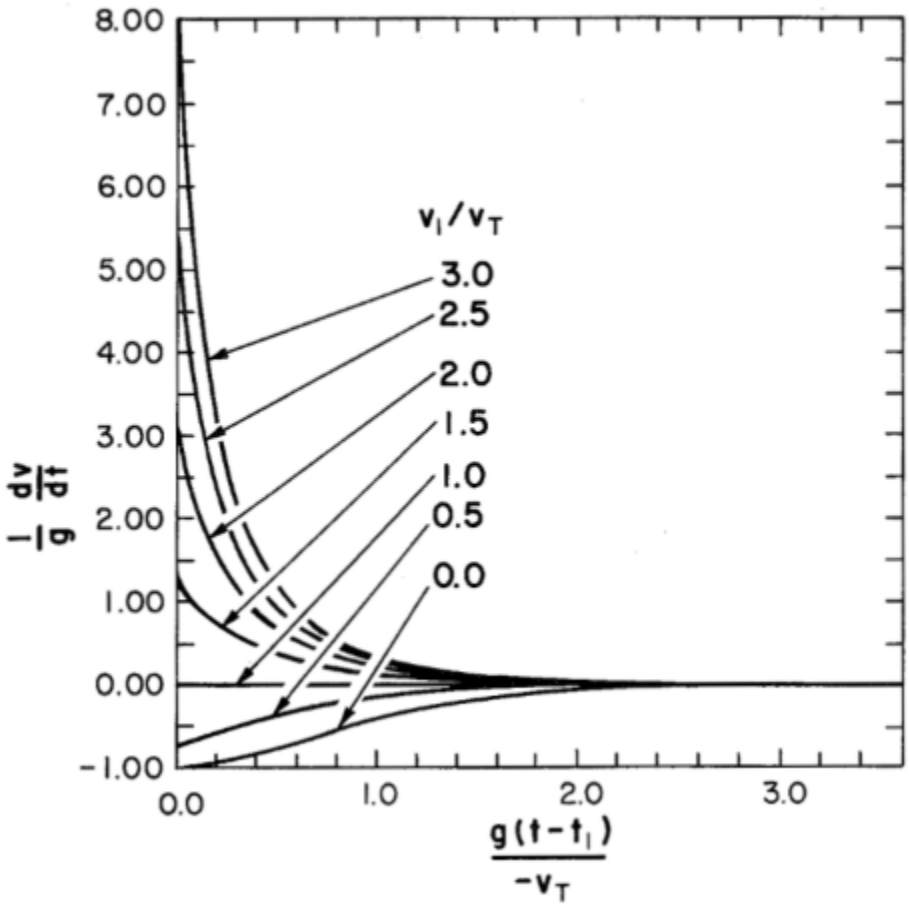


Figure 14-3: Acceleration versus time for a parachute system for which terminal velocity is constant. Acceleration is in effect plotted as multiples of the acceleration of gravity and time as multiples of $-v_T/g$.

If, on the other hand, inflation does not occur until the system velocity has exceeded the terminal velocity of the inflated system, an upward acceleration will immediately start to slow the descent. The magnitude of that acceleration is most easily determined from Equation (14-4) written as follows:

$$\left(\frac{dv}{dt}\right)_1 = g\left[\left(\frac{v_1}{v_T}\right)^2 - 1\right]$$

The subscript 1 is used to denote that the events are occurring at the instant of inflation, i.e., at $t = t_1$. If this equation is multiplied through by the mass of the system, it may be written:

$$m\left(\frac{dv}{dt}\right)_1 = mg\left(\frac{v_1}{v_T}\right)^2 - mg$$

Thus, the forces acting on the system are the upward drag and the downward weight. Since the drag is exerted almost wholly on the canopy of the parachute, the suspension system must be strong enough to withstand at least the force $mg(v_1/v_T)^2$. This force is called the opening shock. In this model, it is proportional to the square of the velocity at the time of inflation [15]. There are additional considerations for opening shock when the canopy is under tension that have not been fully studied.

Equation (14-9) shows that the system velocity increases in phase 1 as a function of time up to its uninflated terminal velocity, and since the uninflated terminal velocity can be several times as great as the inflated terminal velocity, early inflation will assure low opening shocks, while delayed inflation will cause large opening shocks. This is contrary to the experience of parachutists jumping from high-speed aircraft. Their initial speed through the air is generally greater than the magnitude of their terminal velocity without a parachute. Therefore, their speed starts to decrease immediately, and they realize a lower opening shock by waiting until they have reached their own terminal velocity to "pop the chute."

The second distinctive feature of Figure 14-3 is that regardless of the magnitude of the acceleration at the time of inflation, it has, for practical purposes, been reduced to zero after an elapsed time $(t - t_1) = -3v_T/g$. Figure 14-4 The diagram shows time vs. acceleration traces for two parachute systems descending according to this model. Since time is shown in a dimensionless form, which involves v_T, the time scale changes at $t = t_1$. The symbols $v_{T,1}$ and $v_{T,2}$ are used for the terminal velocities in phases 1 and 2, respectively.

The curve for a system that does not open until $v = v_1 = 2v_{T,2}$. This is the curve labeled 1,2,3,4,5,6. At point 1, the parachute is separated from the balloon.

A downward acceleration of 1g occurs immediately, as shown by point 2. The magnitude of that acceleration is then decreased slowly by the drag of the system with a deployed but uninflated parachute. At point 3, opening occurs instantaneously, and the acceleration changes to an upward acceleration of 3g (point 4). This decays rapidly, reaching zero at point 6. More realistically, the parachute does not open instantaneously, and the transition from downward to upward acceleration occurs over a small time increment along a path, similar to what is shown from point 3 to point 5. This decreases the maximum acceleration the system will experience; therefore, the model used here is conservative from a design perspective. A more realistic model is discussed by Heinrich and Noreen

[16], who have studied the forces on a parachute during its opening period.

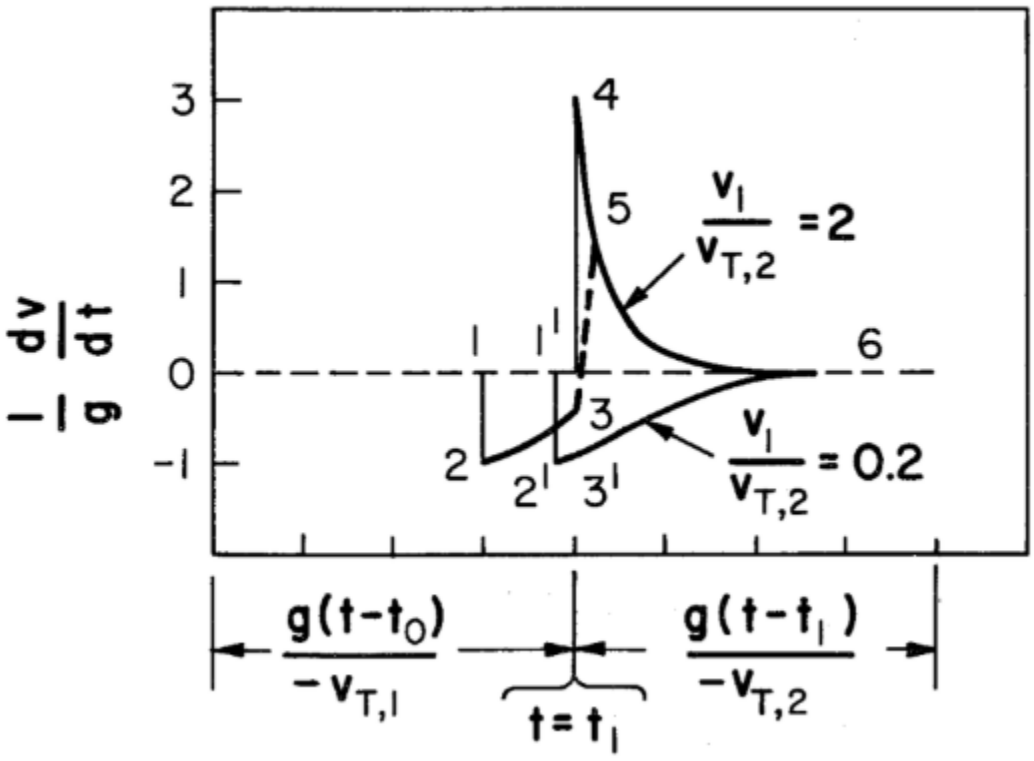


Figure 14-4: Acceleration traces of quick-opening and delayed-opening parachutes.

The curve labeled 1',2',3',6 is representative of a parachute system whose parachute opens well before the system velocity has reached $v_{T,2}$. Its general characteristics have already been explained.

Opening accelerations as great as 16g have been reported in parachute drops from balloons by Niccum and Aube [7], but 70% of the accelerations they reported were under 4g. The accelerometers used were mounted in such a way that they may have sensed large accelerations that were internal to the suspension system. Unfortunately, neither the time of opening nor the downward speed at that moment could be determined reliably from the data; therefore, attempts to verify these data against other observations and theory yielded inconclusive results. These data indicate the possibility of high opening accelerations, but the known uncertainties in the measurements suggest that the values are too high, making them generally conservative for design purposes.

The graphs of Equations (14-8), (14-13), and (14-14) are shown in Figure 14-5, also in dimensionless form. The curves of $v_1/v_T = const.$ on this graph resembles the curves in Figure 14-3. The most significant feature is that, regardless of the velocity at the time of inflation, within an elapsed time given by $(t - t_1) = -3v_T/g$, the descent velocity will have become very nearly equal to the terminal velocity.

Equations (14-15) through (14-17) are plotted in dimensionless form in Figure 14-6. The curves clearly show that a parachute system will descend further in a given time if it has a high downward velocity at the time of inflation than if its velocity is low. After $-g(t - t_1)/v_T$ exceeds 3.0; however, the separation remains virtually constant.

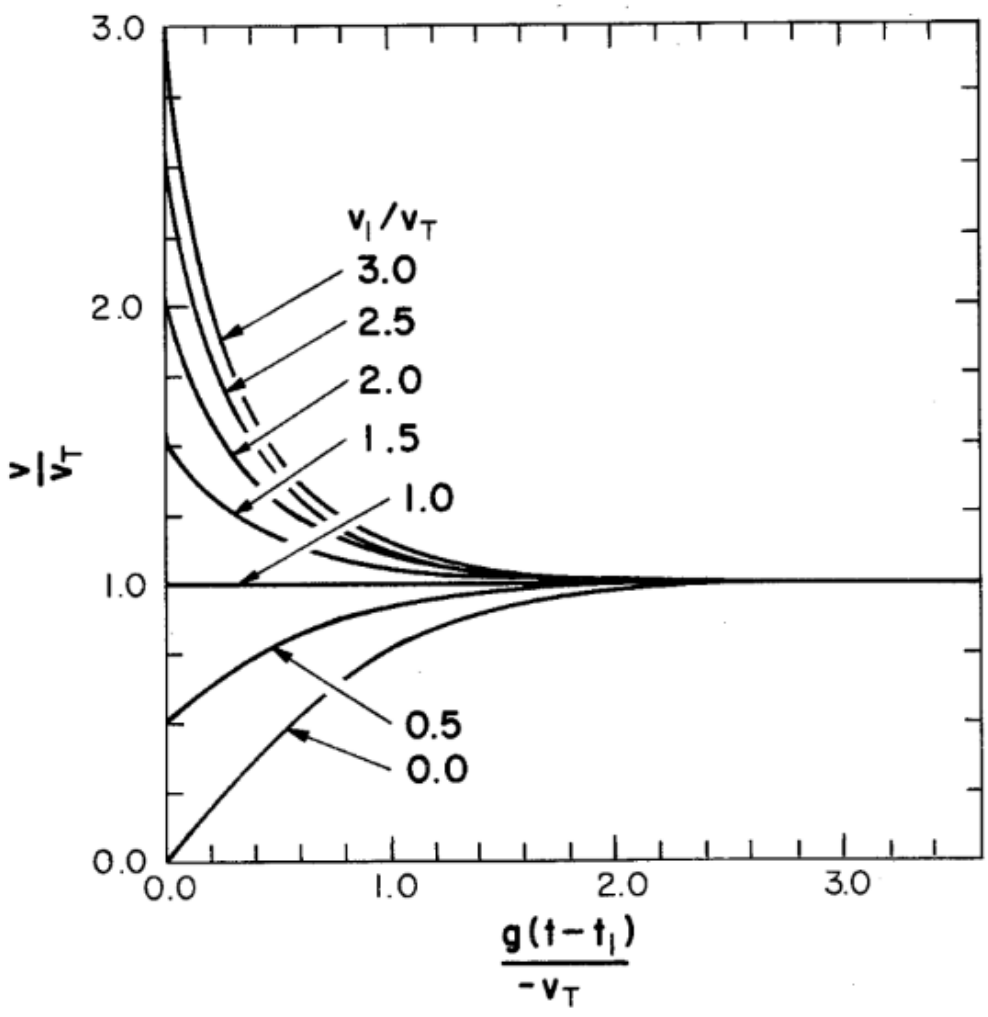


Figure 14-5: Descent velocity vs time for a parachute system for which terminal velocity is constant. Velocity is plotted as a multiple of v_T and time as a multiple of $-v_T/g$.

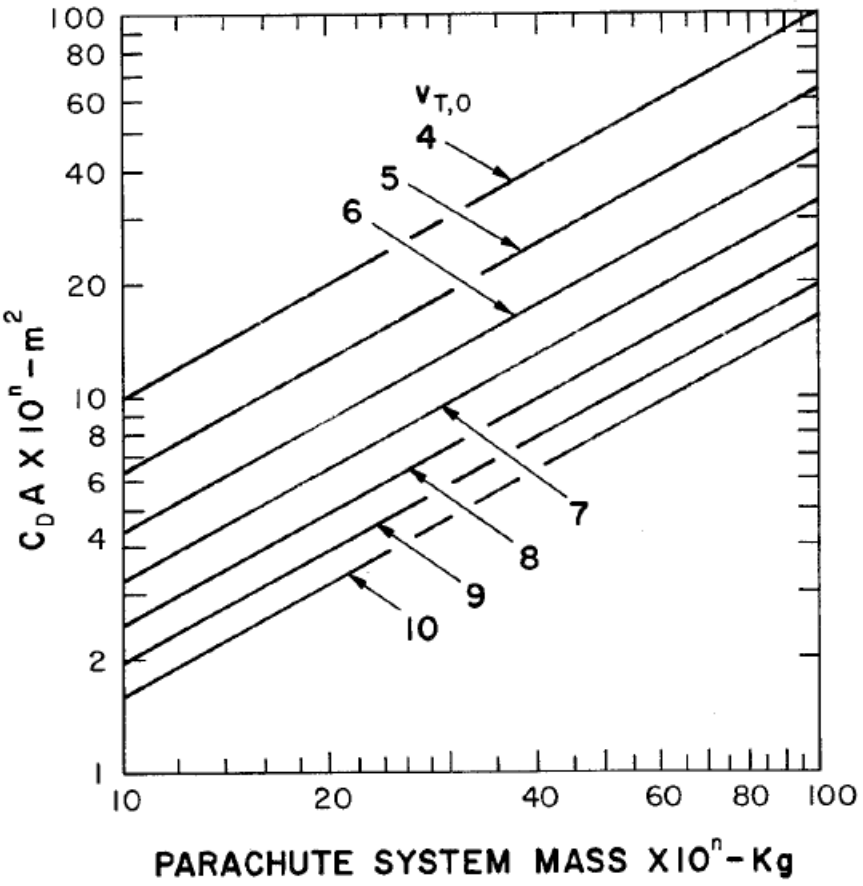


Figure 14-6: Loss of altitude vs time for a parachute system for which the terminal velocity is constant. Height difference is in effect plotted in multiples of v_T^2/g and time in multiples of $-v_T/g$.

The time period given by $(t_2 - t_1) = -3v_T/g$ is the period required for a descending parachute system to accelerate from its opening velocity, v_1, to its terminal velocity, v_T. Time, t_2, is then the time at which phase 2 ends and phase 3 begins. The change of v_T during phase 2, because of the change in air density, is large enough, in descents from altitudes in excess of 30km, that holding it constant may produce errors of up to 10% in the calculated distance traveled during phase 2. Such errors are rarely important, but they can be overcome by slicing the atmosphere into thin strata and using the mean value of the terminal velocity within each stratum to calculate descent data.

2.2.4. Phase 3

As soon as an inflated parachute system has reached terminal velocity, i.e., when $(t - t_1) = -3v_T/g$, it will enter phase 3. Equations (14-13) through (14-20) and Equation (14-8) are valid for this phase of descent; however, the smaller set, consisting of Equations (14-8), (14-17), and

(14-20) provide an adequate description of the descent in phase 3 for this model.

Because v_T is not constant throughout the deep atmospheric stratum through which a parachute system descends in phase 3, the equations must be applied through a number of thin strata with v_T calculated from Equation (14-3) for each stratum.

2.2.5. Phase 4

The few seconds immediately preceding and following the actual landing of a parachute system are the most critical in the descent. Descent velocity is given adequately by Equation (14-8) and hence by Equation (14-3) if the system has passed through phase 2 before reaching the surface.

Any significant acceleration of the payload immediately prior to landing will be due to an oscillation of the system about the vertical axis. Such accelerations are internal to the parachute system; their principal consequence is to decrease the probability that the payload will land on its base. However, the motion of the payload due to them may cause the payload to have a velocity significantly different from the motion of the system as a whole.

Horizontal motion is quite important, and an appropriate balance between the horizontal and vertical velocity components is a consideration in selecting a parachute for a given job. From Equation (14-3) it appears that large parachutes can be selected to produce a low vertical velocity and assure a relatively soft landing.

If winds exist near the surface, lower vertical velocities increase the likelihood that the system will encounter obstacles, such as power lines or trees, during the final seconds of descent. This, in turn, raises the risk of damage to people, property, and the payload. A large parachute also increases the likelihood that the wind will drag the payload after landing. The drag force is given approximately by Equation (14-2), written as:

$$F = \frac{1}{2} C_D \rho A v_W^2$$

where v_W is the speed of the surface wind.

Separation of the parachute and payload upon landing eliminates the danger of dragging, unless the separation mechanism is unreliable. Several balloon launch providers, including NASA currently employ this method.

2.3. Considerations in Selecting a Parachute

For scientific ballooning to be satisfactory, a parachute must be highly reliable and prevent accelerations, including landing accelerations that can be destructive to the payload. Choosing a parachute involves making compromises between conflicting demands. Due to incomplete knowledge of parachute behavior at high altitudes, selecting one type of parachute over another is often a matter of personal preference.

This discussion is therefore limited to a brief summary of the questions typically considered when selecting a parachute and to aids that are general enough to be used with several types of parachutes. The most important factors in selecting a parachute are those directly related to safety. At the very least, a parachute must open reliably and be strong enough to withstand any opening shocks and carry the weight of the payload in all conceivable situations; it must also be capable of slowing the entire system to an acceptable vertical velocity at landing. Other features may also be desirable, such as ensuring the parachute does not swing or spin during descent; however, unless these can be provided without sacrificing essential safety features, they should not be considered.

Two types of parachutes have been used enough for scientific ballooning flights to be considered proven. One has a flat circular canopy with a vent in the center, while the other has a cross-shaped canopy with no vent. The flat circular canopy is known to open reliably and rapidly, even at the high altitudes where it is used in scientific ballooning. It is commercially available in multiple sizes, and two or more can be used together.

Its terminal velocity can be predicted accurately when the object is used within proper load limits. Its chief drawback is its tendency to oscillate more than is desirable during descent.

Parachutes with cross-shaped canopies have been used in scientific ballooning less frequently, with initial use by the Naval Research [17]. They have performed well in all respects and are much less subject to oscillation than flat canopy parachutes and have a lower tendency to spin. The majority of balloon experience had been with payloads less than 365 kg (800 lbs), though NASA uses them to recover 1200lb Black Brant Sounding Rocket payloads. NASA’s Balloon Program has almost exclusively relied on flat circular in-line chutes for all of their large scientific balloon flights. Conversely, many small balloon programs have used cross chutes extensively with high reliability and better performance.

2.3.1. Parachute Size

To determine the parachute size required for a particular job, the mass of the payload and the permissible vertical velocity at impact must be known. The mass of the payload can usually be determined by simply weighing it, but the permissible vertical velocity at impact must normally be based on a value judgment.

If a payload is particularly sensitive to shock on landing, a large parachute can be used. An oversized parachute is not likely to provide greater protection than a smaller one unless it is used when surface winds are lower, which will cause the opening shock to be greater. Therefore, using a larger parachute than is considered optimum for general safety will increase the descent time and increase the exposure to ground winds. Added to those performance costs is the cost of purchasing and maintaining the larger parachute. Since most of the reasons underlying the determination of an acceptable vertical landing speed can only be stated qualitatively, a general guide is that Vertical speeds of 7 to 8 m/s (~22-25 ft/s) at ground impact have been found to yield results that are acceptable for most payloads.

A solution of Equation (14-3) in SI units, using sea level values of g and ρ from the U.S. Standard Atmosphere, 1962, is shown in graphical form in Figure 14-7. On the first pass through this graph, the user typically does not know the parachute mass and must approximate it. The mass of the payload multiplied by 1.05 is an adequate first approximation of the total system mass. With values for the system mass and the sea level terminal velocity, one may use the graph to determine the product of C_D*A.

Note that the numbers on the abscissa may be multiplied by a factor 10n, where *n* may take any value, provided only that the numbers on the ordinate are also multiplied by the same factor. Thus, the graph can be used for any non-zero mass.

Having obtained a first approximation for C_D*A from Figure 14-7, one may enter that value in Figure 14-8 to obtain the diameter of a parachute if the value of C_D is known. Figure 14-8 is a graphical representation of the equation $C_D*A = C_D\pi(D/2)^2$; therefore, if the C_D for an inflated circular parachute is used, the value of D obtained from Figure 14-8 will be the effective or projected diameter of the parachute (see Figure 14-1). This value of D is not often of direct interest, however, because the nominal diameter of the canopy describes parachutes. To obtain the nominal diameter from Figure 14-8, a pseudo drag coefficient must be used. Although the pseudo drag coefficient is usually determined experimentally, its significance can be readily explained.

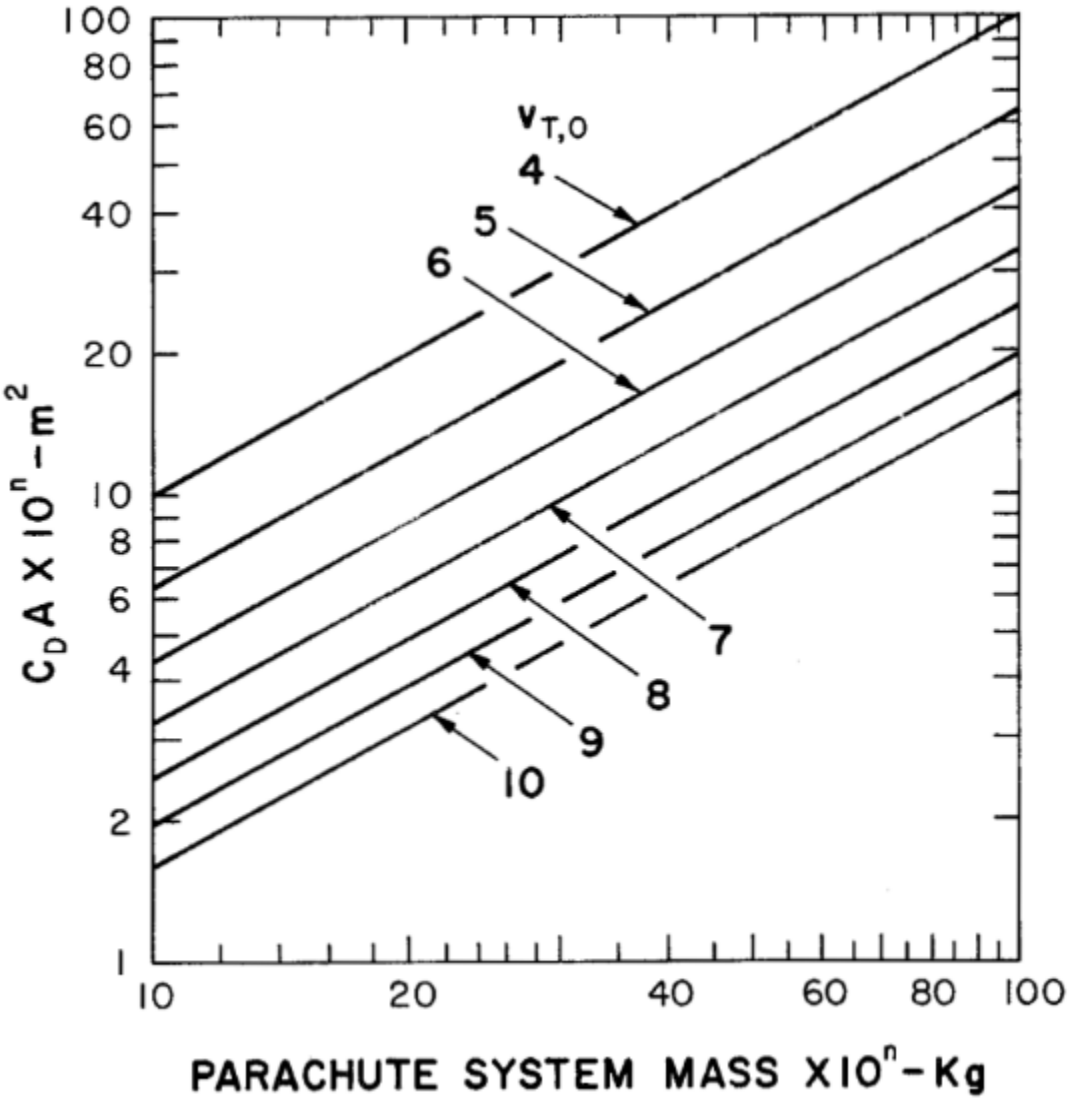


Figure 14-7: Sea level terminal velocity of a parachute as a function of parachute system mass and the product of parachute area and drag coefficient. Numbers on the abscissa and ordinate may be multiplied concurrently by any factor 10n to cover all non-zero values.

Let C_D and A' be the pseudo drag coefficient and the nominal area, respectively, of a parachute having an effective drag coefficient CD and effective area A so that C_D'*A' = C_D*A.

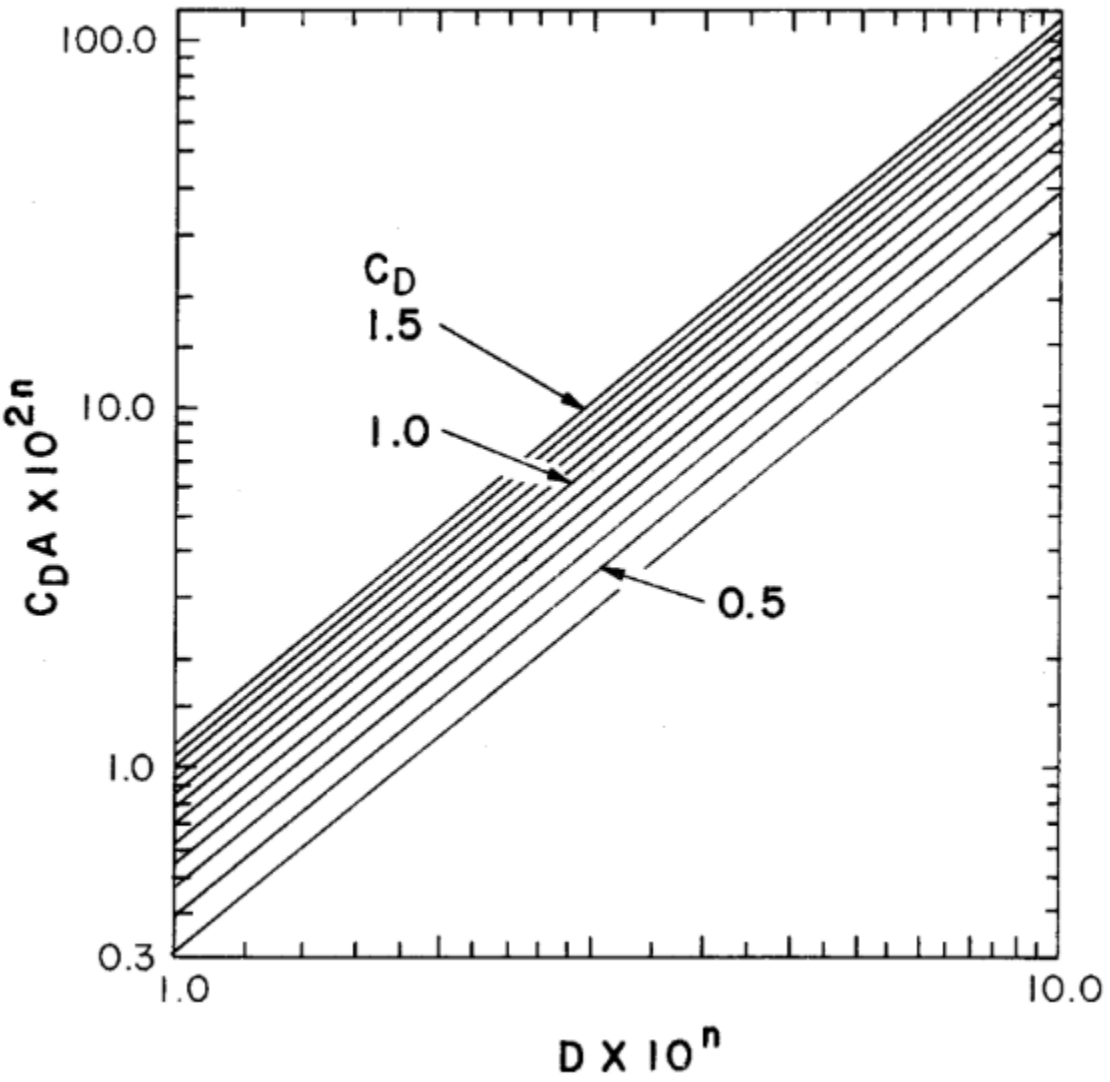


Figure 14-8: Nominal diameter of a parachute as a function of area and drag coefficient. Numbers on the ordinate may be multiplied by 10n if numbers on the abscissa are concurrently multiplied by 10²n to cover all non-zero values.

Also, let the nominal area be defined as the area of a circle of nominal diameter D'. Then, if $C^{D'}$ is defined so that $C_DA = C_{D'}\pi(D'/2)^2$ and its value is known, D' can be determined from Figure 14-8. An excellent example of the concept of pseudo drag coefficient is the cross-shaped canopy. Rarely is its effective area or its drag coefficient known, but for one such parachute design, the product of the two is known to be given with acceptable accuracy by multiplying the area of a circle whose diameter is equal to the length of one of the cross members of the canopy by 0.55. Thus, $C_{D'}$ is 0.55 and D' is the length of the cross member for this particular parachute design.

Although parachutes can be manufactured in any size, it is more practical to manufacture them in certain discrete sizes. It is rare that the size indicated by the selection process described thus far will precisely match one of the commonly manufactured sizes. Typically, a scientific ballooning group will have parachutes of various sizes on hand, allowing a size to be selected that has a nominal diameter close to the initial estimate of the required value. The known mass and the C_D'A' of that parachute can then be used in conjunction with Figure 14-7 to obtain the sea level terminal velocity of the parachute system.

If the velocity is too low or too high to be satisfactory, the data of the next smaller or larger parachute may be checked. It is possible that the altitude of the anticipated landing site will be so far above sea level that the terminal velocity there will be significantly different from that at sea level. The curve in Figure 14-9, labeled v_T, provides a simple way to approximate the terminal velocity at any level up to 52 km if the sea-level terminal velocity is known. If v_T is the sea level terminal velocity and v_T is the terminal velocity at any other level, then from Equation (14-3)

$$\frac{v_T}{v_{T_0}} = \sqrt{\frac{\rho_0}{\rho}} \qquad (14\text{-}21)$$

assuming that m, g, C_D, and A do not change with height. From Equation (14-21) v_T/v_{To} may readily be plotted as a function of ρ, and since ρ is a function of height in the atmosphere, v_T/v_{To} may also be plotted as a function of height. That has been done in Figure 14-9, using the relationship between ρ and H given in the U.S. Standard Atmosphere, 1962. Thus, it is only an approximation of the real atmosphere.

It is apparent that the change of v_T/v_{To}, in the lowest 3 km, is not great enough to be resolved satisfactorily in Figure 14-9. Yet it is that stratum in which almost all landings will occur. In it, the linear relations $v_T/v_{To} = 1 + 5\times10^{-5}H$, where H is in meters above sea level, and $v_T/v_{To} = 1 + 1.52\times10^{-5}H$, where H is in feet, yield good approximations. Thus, at 1 km (~3000 ft), v_T is 5% larger than at sea level, a difference which is nearly equal to the difference (error) which must be anticipated between the calculated and observed sea level terminal velocities. Nonetheless, the difference will occasionally justify using a larger parachute for a landing at a higher altitude than at sea level.

2.3.2. Multiple Parachutes

It is sometimes convenient or necessary to use two or more parachutes to lower a load. Many low-level parachute drops have been made; a few have been successful from balloon float altitudes. Thus, it is known that drops using a cluster of parachutes are feasible; however, the

number of multiple-parachute flights on balloons to date has been too limited to warrant the degree of confidence established for parachutes used singly.

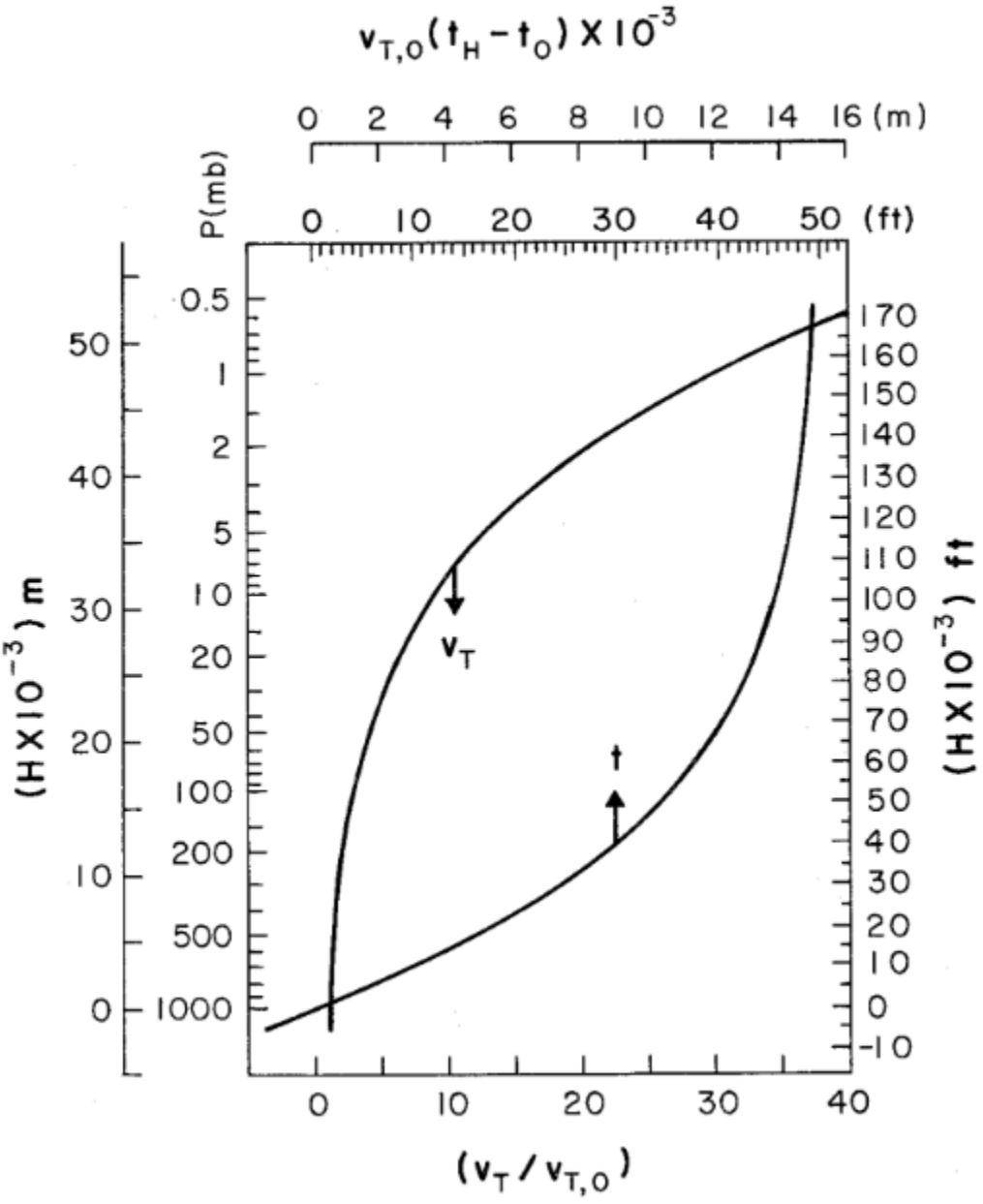


Figure 14-9: Terminal velocity and time of descent, terminal velocity and altitude in the U.S. Standard Atmosphere, 1962.

The number and size of parachutes required to lower a load when more than one is needed may be determined by the procedure discussed above if 1) all parachutes used together are alike and the same size, 2) the drag coefficient of the cluster can be determined from the drag coefficient of one parachute used alone, and 3) the nominal area of a

cluster of N parachutes is equal to the nominal area of a single one times N. Then one may enter Figure 14-7 with 1.05 times the mass of the payload and the desired landing velocity (suitably corrected to sea level terminal velocity) to obtain C_DA. Dividing C_DA by N and entering Figure 14-8 with the quotient and $C_{D'}$ for the cluster, yields D' for one of the parachutes of the cluster. If there are N parachutes of nominal diameter D' available, the solution should be checked using the mass and C_D data of the actual parachutes. If there are not N parachutes of diameter D' available, another value of N may be tried. When a satisfactory check is achieved using the available parachute data, the problem is solved.

The value of CD' for a cluster of identical flat, circular, solid cloth D canopy parachutes may be approximated by the equation CD'(cluster) = CD' (individual) X (0.95 - 0.3N) for $2 \leq N \leq 6$.

Incidentally, a cluster of flat canopy parachutes is more stable than a single one. The value of CD' for a cluster of identical parachutes whose canopies have large geometric porosity (e.g., ribbon, ring slot, or cross-shaped parachutes) is nearly identical to the value of CD' for one of the individual parachutes.

2.3.3. Time of Descent

Recalling that $v_T = (dH/dt)T$, Equation (14-21) may be written

$$\frac{dH}{dT} = v_{T,0}\sqrt{\frac{\rho_0}{\rho}} \tag{14-22}$$

Where one of the T subscripts has been omitted for convenience. This may be integrated as follows:

$$v_{T,0}(t_H - t_0) = \rho_0^{1/2}\int_0^H \rho^{1/2}\, dH \tag{14-23}$$

The integration indicated on the right side of Equation (14-23) can be performed if ρ is a known function of H; integration in the Standard Atmosphere yields the curve labeled t in Figure 14-9. A value of $v_{To}(t_H - t_o)$ may be determined from the curve if the altitude of a parachute system is known. That value divided by the sea level terminal velocity of the system is the time required for the system to descend to sea level. The time of descent between any two levels may also be determined; it is the difference between the two $v_{To}(t_H - t_o)$ values divided by v_{To}.

If the two levels are close together, however, a more accurate result may be obtained by dividing the thickness of the stratum by the mean velocity within the stratum as determined from the v_T curve.

Several auxiliary scales have been added to Figure 14-9 to enhance its versatility. The terminal velocity, v_T, obtained from the figure will be in the units in which $v_{T,o}$ is expressed. Since $v_{T,o}(t_H-t_o)$ is a length, scales are given in both meters and feet; the scale to be used must be compatible with the units in which v is expressed. The resulting time units are easily determined: for example, if $v_{T,o}(t_H-t_o)$ is read in feet and $v_{T,o}$ is expressed in feet per minute, time will be determined in minutes.

3. Deployables and Extension Mechanisms

Apart from the active primary gondola pointing mechanisms employed on many modern missions, this section discusses the active components of a balloon-borne gondola, which include deployable, extendable, or detachable elements specified to meet mission requirements. With all classes of mechanisms, safety and operational assurance are paramount, given that deployable or detachable elements introduce risk to both balloon-borne mission success and to elements external to the gondola (i.e., people, infrastructure, property, etc., along the path of the balloon trajectory). This section provides descriptions of a few specific and successfully implemented balloon-borne mechanisms of this class within the context of modern balloon-borne instruments.

3.1. Extension Mechanisms

For the purposes of this discussion, extension mechanisms include any component, device, or structure that involves some aspect of differential movement while remaining attached to the primary gondola structure. Many subclasses of these types of mechanisms, including star camera shutters, frame locks, let-down reels, and extendable booms, are not only used once but are often mission-critical for their continued operation. For each of these, care must be taken to ensure a robust design, as deployment failure would result in mission failure (i.e., a permanently shuttered camera or locked stabilization frame would prevent the mission from operating).

For star camera shutters (or shutters in general), commercial off-the-shelf lens-integrated solutions have been implemented on missions such as BLAST, with the potential intent of preventing light from the Sun or other sources from damaging the camera sensors, particularly during uncontrolled ascent [18]. Similarly, the FIREBall and FIREBall-2 instruments employed and flight-demonstrated a large, deployed window (aka a “large shutter”) over the entire FIREBall aperture for this purpose. Of course, any deployed mission-critical mechanisms must trade off the risk of damage to equipment due to lack of shuttering with the risk of mission failure due to improper operation of a given shuttering mechanism [19], [20], [21]. Empirically, it has been the practice of modern balloon missions that balloon-borne components at the sensitivity

of a star camera or other tracking device tend towards a no-shutter solution to de-risk deployment failure, where mitigations for ascent use launch configurations that limit Sun exposure (e.g., launching at high instrument elevation when it is known that a launch would take place in the morning). Conversely, science instrumentation (such as the BLAST cryostat shutter and the FIREBall deployment window) is often highly sensitive to incident light and therefore mitigations tend towards using a robust shutter solution that is rigorously designed and tested for failure modes during pre-flight integration and testing to mitigate the risk of mission failure

In-flight deployed extension mechanisms can also include those that operate outside of the main gondola structure. For instance, a let-down reel can be used to extend instrumentation below the main gondola structure after launch. Examples of this approach include the flight-demonstrated CNES Wind Fisher and the NASA ANITA systems, which utilized drop-down reels to extend science instrumentation after the balloon reaches float altitude. In these cases, a let-down reel approach was considered when the launch geometry or application requirements are too constrained within the normal payload envelope. Further, while trade-offs are necessary to justify the need for a let-down reel solution, this type of extension mechanism also requires additional design and testing scrutiny due to the increased risk of mechanical failure causing damage or harm to external elements.

3.2. High-Altitude Deployables

Beyond extendable or deployed mechanisms that remain attached to a balloon-borne gondola is the high-altitude deployment of components for the purpose of mid-flight recovery of items such as data storage devices. As can be expected, this type of deployment is not only subject to mission assurance and reliability considerations, similar to those that remain attached, but also to regulatory considerations that vary by region, payload type, and mass class.

One successful balloon-borne implementation is the SuperBIT Data Recovery System (Figure 14-10), which comprises in-flight data disks equipped with a parachute and GPS transponder to enable safe deployment, descent, and recovery during or after the completion of the balloon flight. This “download by parachute” system has been successfully demonstrated during SuperBIT’s 2019 flight from Timmins, Ontario, as well as at the end of the SuperBIT 2023 science flight from Wanaka, New Zealand. Both of which not only showed proof of concept in the specific deployable recovery system designs, but also utilized predictive software to determine landing locations of the data payloads to within 200 meters [22]. Current and similar implementations include various designs created as part of NASA’s FLOATing DRAGON (Formulate, Lift, Observe, And Testing; Data Recovery and Guided On-board Node)

competition, which shares similar objectives regarding data recovery through "physical telemetry". While these designs have yet to be demonstrated from a balloon-borne system, at the time of this writing, similar programs have been expanded for test operations in remote regions, such as Antarctica (e.g., the IceDRAGON competition), with the continued intention of reducing the load on balloon-borne telemetry downlink systems.

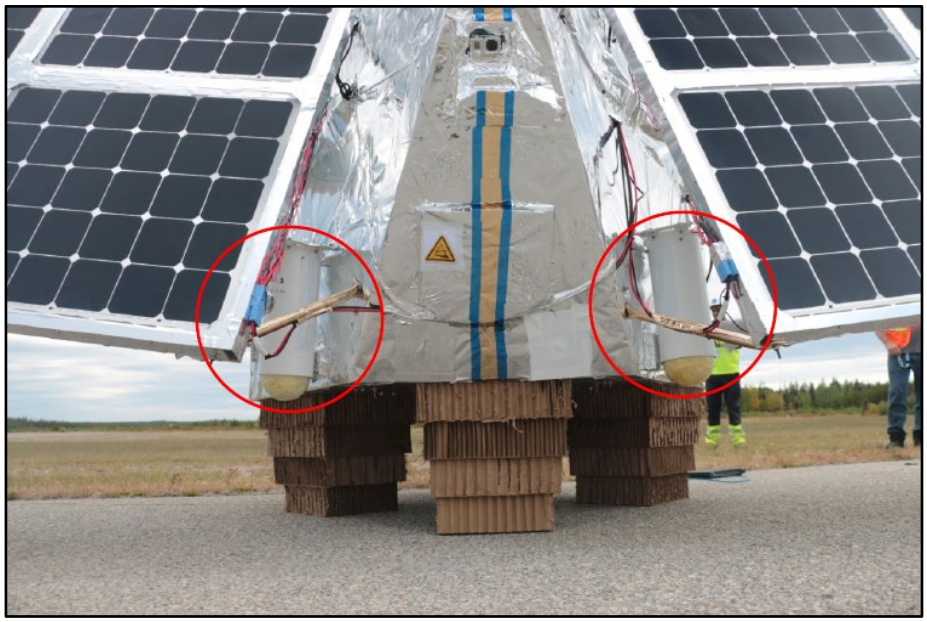


Figure 14-10: SuperBIT Data Recovery System (red circles) during pre-flight of the 2019 test flight campaign from Timmins, Ontario, in northern Canada.

4. Conclusions

Decelerators such as parachutes remain the most proven and widely used systems for the recovery of scientific balloon payloads. Their design reflects a balance between fundamental physics, practical engineering, and the constraints of high-altitude operations. Whether deployed in pre-extended or packed configurations, parachutes must reliably manage opening shock, terminal velocity, and landing stability to safeguard mission-critical instruments. The nuanced interplay of canopy geometry, porosity, and cluster configurations underscores the importance of careful selection and testing for each flight profile.

At the same time, deployables and extension mechanisms have expanded the capability of balloon-borne platforms beyond recovery. Mechanisms such as shutters, let-down reels, and extendable booms enable new mission profiles by protecting sensitive optics, extending instruments into advantageous geometries, or increasing the field of view. Likewise, mid-

flight deployable recovery systems, exemplified by the SuperBIT Data Recovery System, demonstrate how physical telemetry can complement or even reduce reliance on bandwidth-limited communication systems. These innovations, though inherently riskier, have proven their value when engineered with rigorous attention to redundancy, safety, and failure mitigation.

Looking forward, the continued integration of decelerators and deployables into balloon-borne science will hinge on balancing operational reliability with scientific ambition. As payloads grow in complexity and sensitivity, so too must the systems designed to protect and extend them. Advances in predictive modeling, guided recovery, and robust deployable architectures will play a decisive role in enabling safer landings, higher mission success rates, and expanded scientific reach. Ultimately, these technologies not only ensure the safe return of instruments but also extend the scientific frontier accessible to high-altitude ballooning.

References

[1] T. W. Knacke, *Parachute recovery systems : design manual*. Santa Barbara, CA : Para Pub., 1992. Accessed: Aug. 23, 2025. [Online]. Available: http://archive.org/details/parachuterecover0000knac

[2] United States: Defense Department: Air Force Department *et al.*, *Recovery Systems Design Guide*. in AFFDL-TR ; AFFDL-TR-78-151. Defense Department, 1978. Accessed: Aug. 23, 2025. [Online]. Available: https://purl.fdlp.gov/GPO/LPS103309

[3] V. Alieksieiev, P. Kazan, O. Korolova, and I. Dronyuk, "Promising Modern Steerable Parachute for Unmanned Aircraft Systems," in *Advances in Artificial Systems for Logistics Engineering*, Z. Hu, Q. Zhang, S. Petoukhov, and M. He, Eds., Cham: Springer International Publishing, 2022, pp. 431–439. doi: 10.1007/978-3-031-04809-8_38.

[4] J. A. Lyon, "The Effect of Parachute Canopy Shape and Apex Venting on Parachute Performance".

[5] H. G. Heinrich and E. L. Haak, "Stability and Drag of Parachutes with Varying Effective Porosity," Art. no. AFFDLTR7158, Feb. 1971, Accessed: Aug. 23, 2025. [Online]. Available: https://apps.dtic.mil/sti/html/tr/AD0729858/

[6] J. F. Dwyer, *The Problem: Instantaneously Effecting Controlled Balloon-system Descent from High Altitude*. Air Force Geophysics Laboratory, Air Force Systems Command, United States Air Force, 1980.

[7] A. AUBE and R. NICCUM, "Heavy load recovery from high altitude balloon borne platforms," in *2nd Aerodynamic Deceleration Systems Conference*, American Institute of Aeronautics and Astronautics. doi: 10.2514/6.1968-965.

[8] W. Machalick, M. Kandis, A. Witkowski, and E. Klein, "Energy Modulators for Recovery of High Altitude Balloon Payloads," in *AIAA Balloon Systems Conference*, American Institute of Aeronautics and Astronautics. doi: 10.2514/6.2009-2821.

[9] J. Bruggemann, "Advances in Balloon Flight Train Shock Mitigation," in *AIAA Balloon Systems Conference*, American Institute of Aeronautics and Astronautics. doi: 10.2514/6.2007-2610.

[10] M. SILBERT, A. MOLTEDO, and G. GILBERTSON, "High altitude decelerator systems," in *10th Aerodynamic Decelerator Conference*, American Institute of Aeronautics and Astronautics. doi: 10.2514/6.1989-882.

[11] M. Cowan, T. Provence, C. Biney, C. Coronado, I. Lucic, and D. E. Bering, "Design of the Guided Parachute Recovery System for Small High Altitude Balloon Payloads," in *2025 Regional Student Conferences*, American Institute of Aeronautics and Astronautics. doi: 10.2514/6.2025-98605.

[12] M. CHAURASIA and R. KUMAR, "High altitude parachute and its military applications," in *10th Aerodynamic Decelerator Conference*, American Institute of Aeronautics and Astronautics. doi: 10.2514/6.1989-893.

[13] R. Scott and T. Bohaboj, "An Inexpensive Guided Recovery System for Stratospheric Balloons," in *AIAA Balloon Systems Conference*, American Institute of Aeronautics and Astronautics. doi: 10.2514/6.2007-2629.

[14] F. Haider, *Development and Evaluation of a New Configuration of a Landing Impact Protection System for Stratospheric Balloon Gondolas*. 2018. Accessed: Aug. 23, 2025. [Online]. Available: https://urn.kb.se/resolve?urn=urn:nbn:se:kth:diva-230751

[15] D. Bulikhov, "Stratospheric sky-diving: parachute opening shock and impact forces analysis".

[16] H. G. HEINRICH and R. A. NOREEN, "Analysis of parachute opening dynamics with supporting wind-tunnel experiments," *J. Aircr.*, vol. 7, no. 4, pp. 341–347, 1970, doi: 10.2514/3.44175.

[17] W. Cross CDR USN, "Personal Communication," Feb. 22, 1972.

[18] E. Pascale *et al.*, "The Balloon-borne Large Aperture Submillimeter Telescope: BLAST," *Astrophys. J.*, vol. 681, no. 1, p. 400, July 2008, doi: 10.1086/588541.

[19] B. Milliard *et al.*, "FIREBALL: the Faint Intergalactic medium Redshifted Emission Balloon: overview and first science flight results," in *Space Telescopes and Instrumentation 2010: Ultraviolet to Gamma Ray*, SPIE, July 2010, pp. 25–37. doi: 10.1117/12.857850.

[20] J. S. Li *et al.*, "FIREBall-2 UV balloon telescope in-flight calibration system," *J. Astron. Telesc. Instrum. Syst.*, vol. 10, no. 3, p. 035002, Aug. 2024, doi: 10.1117/1.JATIS.10.3.035002.

[21] V. Picouet *et al.*, "End-to-end ground calibration and in-flight performance of the FIREBall-2 instrument," *J. Astron. Telesc. Instrum. Syst.*, vol. 6, no. 4, p. 044004, Nov. 2020, doi: 10.1117/1.JATIS.6.4.044004.

[22] "Download by parachute: retrieval of assets from high altitude balloons - IOPscience." Accessed: Aug. 23, 2025. [Online].

Available: https://iopscience.iop.org/article/10.1088/1748-0221/15/05/P05014/meta

Chapter 15
Solar Balloons

Zachary Yap[1], Taylor D. Swaim[2], Emalee E. Hough[3], Tristan K. Schuler[4], Daniel C. Bowman[5], Jamey D. Jacob[6], and Brian R. Elbing[7]

[1] Oklahoma State University, R&D Engineer, OAIRE
[2] Pennsylvania State University, Engineer, Applied Research Laboratory
[3] Oklahoma State University, R&D Engineer, OAIRE
[4] U.S. Naval Research Laboratory, Research Scientist, NCARAI
[5] Pacific Northwest National Laboratory, Geophysicist, Signals Detection & Analysis
[6] Oklahoma State University, Professor and OAIRE Director, Mechanical and Aerospace Engineering
[7] Oklahoma State University, Professor, Mechanical and Aerospace Engineering

Acknowledgments

Thank you to Professor Eric Benton at Oklahoma State University for sharing details of his current work examining cosmic ionizing radiation and his plans to utilize heliotropes for future measurements.

Data from the BASS 2021 Flight Campaign are available on the JPL Dataverse (dataverse.jpl.nasa.gov) at the public DOI: 10.48577/jpl.C933HF.

Contributions from Brian. R. Elbing were supported by the Gordon and Betty Moore Foundation (grant DOI: 10.37807/gbmf11559).

Thank you to the dedicated staff at the Federal Aviation Administration for their work in keeping the skies safe for solar balloons and everyone else. The sky is not your limit.

Table of Contents

1. Introduction 10

2. Solar Balloon Physics-Based Model 10

2.1. Dynamic Equations..... 11

3. Balloon Design Considerations 12

3.1. Balloon Materials and Construction..... 12

3.2. Alternative Designs..... 16

3.2.1. Tetrahedral Balloon, “Tetroons” 16

3.2.2. Zebra Balloon 18

4. Flight Operation Considerations 18

4.1. Launch Site Location and Setup..... 18

4.2. Flight Safety and Notifications..... 21

4.3. Launch Methods..... 22

4.3.1. Ground Wind Effects on a Solar Balloon Envelope 22

4.3.2. Ground Launch (traditional) 23

4.3.3. Helium-Augmented Launch 24

4.3.4. Helium-Assisted (grand slam) Launch 25

5. Balloon Flight Characteristics 28

5.1. Flight Stages..... 28

5.1.1. Launch and Ascent 31

5.1.2. Float 33

5.1.3. Descent and Landing 36

5.2. Altitude Control..... 38

5.3. Flight Tracking and Communications..... 40

6. Conclusion 42

References..... 43

Table of Figures

Figure 15-1: Picture of a heliotrope shortly after launch with the envelope, cut-down system, parachute, and three scientific payloads identified..... 11

Figure 15-2: Illustration showing the folding and cutting sequence for making the gores of a 6-m heliotrope. Point A marks the same position on the plastic sheet for each step. The figure was adapted from Bowman et al. [2]..... 14

Figure 15-3: Front and bottom views illustrate the recommended procedure for reinforcing the balloon vent/mouth. The figure was adapted from Jacob et al. [16]..... 15

Figure 15-4: Sample of solar balloons with various sizes and shapes, and the nominal maximum free lift mFL. 16

Figure 15-5: Illustration showing how to prepare gores for a 10-m tetroon. (a) Coordinates to cut the initial strip with coordinates in meters. (b) The method involves taping segments together to form a triangle. (c) Tape triangles together to form a larger triangle..... 17

Figure 15-6: Picture of a partially inflated 10-m tetrahedral balloon (i.e., tetroon) shortly after launch..... 17

Figure 15-7: (a, b) Pictures of the 6-m zebra balloon (a) pre-flight indoor fill test and (b) after launch. (c) Altitude versus time elapsed and (d) flight path of the zebra balloon..... 19

Figure 15-8: Launch site from the BASS 2021 flight campaign [Swaim et al.], which is a representative setup for a recommended launch site. 20

Figure 15-9: (top row) Illustration and (bottom row) representative pictures of balloon inflations showing (left) the start of inflation, (middle) partial inflation with the balloon being buffeted by wind, and (right) nearing full inflation..... 23

Figure 15-10: A sequence of images from a nominal heliotrope launch (25 Aug 2022) showing (a) initial fill, (b) stopping fan, (c) running mouth under the balloon, (d) excess charcoal dumping out, (e) balloon mouth being released, (f) payloads being walked with the balloon, (g) first payload in the air and (h) moment when second payload left the team member's hand..... 24

Figure 15-11: Picture at the end of filling showing (a) an underfilled balloon, (b) a nominally filled balloon, and (c) an overfilled balloon that just burst at the top..... 25

Figure 15-12: Sketch of the (left) top view and (right) side view of the rigging for a helium-assisted (grand slam) launch..... 26

Figure 15-13: Pictures from a helium-assisted (grand slam) launch showing (a) a typical flight line, (b) prior to releasing the helium balloon, (c) immediately after releasing the helium balloon, (d) when the heliotrope envelope lifts off the ground, and (e) when the first payload lifts off..... 28

Figure 15-14: A figure adapted from Schuler et al. [5] shows an example of a helium-assisted heliotrope launch. The top row shows (A) the uninflated heliotrope envelope being towed by the weather balloon, (B) the burst of the weather balloon, (C) the heliotrope rapidly inflating, and (D) the heliotrope reaching its neutral buoyancy level. These reference points are also marked on the altitude readings from a GPS-based altimeter during two different flights..... 29

Figure 15-15: Typical flight (flight 4.2 from Swaim et al. [7]) illustrating the various flight stages. The data from the upper IMU and APRS tracker are included, along with reference lines for the start and end stages, as well as sunrise/sunset times. This figure is adapted from Swaim et al. [7]..... 30

Figure 15-16: Pictures of (a,c) traditional ground and (b,d) helium-assisted launches (a,b) just prior to launch and (c,d) after the envelope was airborne..... 31

Figure 15-17: Launch sequence for (a) ground, (b) helium-augmented, (c) helium-assisted type-1, and (d) helium-assisted type-2. The time was measured from the time of launch for all flights. This figure is adapted from Swaim et al. [7]..... 33

Figure 15-18: Vertical Velocity vs Elevation scaled by the float elevation during ascent for (a) ground, (b) helium augmented, (c) helium-assisted type-1, and (d) helium-assisted type-2. The blue dashed line marks two-thirds of the float elevation. A positive vertical velocity indicates the heliotrope ascending, while a negative vertical velocity indicates the heliotrope descending. This figure is adapted from Swaim et al. [7]..... 34

Figure 15-19: Examples of float behaviors observed during the BASS 2021 flight campaign with (a) Flight 4.2 experiencing a steady float altitude and (b) Flight 9.2 displaying both upward excursions and a gradual decrease in altitude during the float period. This figure is adapted from Swaim et al. [7]..... 35

Figure 15-20: IMU data (top) time trace and (bottom) spectrogram of the vertical deviation from the average float altitude Δz from the upper payload during the float period (Flight 16.1 of Swaim et al. [7]). The time is measured relative to the start of the float period. The color indicates the amplitude of altitude fluctuation at the corresponding period..... 36

Figure 15-21: The civil twilight at the heliotrope location and altitude during the BASS 2021 flight campaign, and the onset of the descent stage as a function of the day of the year. Lines are the linear best-fit curves with slopes of -1.6 and -1.5 min/day for the sunset and descent onset, respectively. This figure is adapted from Swaim et al. [7]... 37

Figure 15-22: Vertical velocity as a function of elevation normalized by the float altitude during the descent stage for (a) nominal and (b) hard landings. Hard landings were descents that had the envelope separate from the flight line. This figure is adapted from Swaim et al. [7].. 37

Figure 15-23: Mechanical Vent attached to a heliotrope on August 22, 2025 (Schuler et al. [50] before launch in Belen, New Mexico..... 39

Figure 15-24: Map of four SHAB-V flights launched back-to-back 15 minutes apart. SHAB12-V is red, SHAB13-V is magenta, SHAB14-V is green (and did not vent), SHAB15-V is blue in Albuquerque, New Mexico in August 2022 [50]..... 40

Figure 15-25: Altitude profile of SHAB12-V using P-D control to maneuver to 6 altitude set points during a flight campaign in Albuquerque, New Mexico, in August 2022 [50]. Some lower altitude setpoints were unobtainable, most likely due to thunderstorms in the area..... 40

Table of Tables

Table 15-1: Ascent stage characteristics of the BASS 2021 flight campaign [7]. Only flights that weighed 7.05 kg are included..... 32

Table 15-2: Average descent rate, time to landing, and speed impact for nominal descents and hard landings. The hard landings were caused by envelope separation from the flight line..... 39

Table of Symbols

Symbol	Definition	Dimension
A_{proj}	The projected area of the balloon	L^2
A_{surf}	Balloon surface area	L^2
C_d	Balloon drag coefficient	-
C_p	Specific heat	$L^2T^{-2}\theta^{-1}$
c	Circumference in gore curve equation	L
c_v	Specific heat capacity	$L^2T^{-2}\theta^{-1}$
C_{virt}	Virtual mass coefficient	-
CF	Cloud cover percentage	-
e	Orbital eccentricity	-
d	Balloon diameter	L
f	True anomaly	-
F_b	Buoyancy force	MLT^{-2}
F_d	Drag force	MLT^{-2}
F_g	Gravitational force	MLT^{-2}
F_s	Solar constant	MT^{-3}
g	Gravitational acceleration	LT^{-2}
h	Heat transfer coefficient	$MT^{-3}\theta^{-1}$
h_{int}	Heat transfer coefficient, internal	$MT^{-3}\theta^{-1}$
h_n	Heat transfer coefficient, natural	$MT^{-3}\theta^{-1}$
I_0	Total solar radiation at the top of the atmosphere	MT^{-3}
I_{sun}	Solar irradiance flux	MT^{-3}
$I_{sun,reflected}$	Reflected radiation from the surface	MT^{-3}
$I_{sun,sky}$	Diffuse radiation from the sky	MT^{-3}
k	Thermal conductivity of the fluid	$MLT^{-3}\theta^{-1}$
l	Length along curve cut in gore curve equation	L
m_a	Air mass ratio between the balloon and the sun	-
$m_{envelope}$	Mass of the envelope	M
m_{gas}	Mass of the gas in the balloon	M
$m_{payload}$	Mass of the payload	M
Nu	Nusselt number	-
$Nu_{ext,f}$	Nu, forced external convection	-
$Nu_{ext,n}$	Nu, natural buoyancy-driven external convection	-
Nu_{int}	Nu, internal convection	-
n	Total number of gores used gore curve equation	-
P_0	Pressure at sea level	$ML^{-1}T^{-2}$

Symbol	Definition	Dimension
$P(z)$	Pressure at a given elevation Z	$ML^{-1}T^{-2}$
Pr	Prandtl number	-
Q_{albedo}	Radiative heat load from the albedo	ML^2T^{-3}
Q_{conv}	Convective heat transfer per unit of time	ML^2T^{-3}
$Q_{IR,emit}$	Radiative heat load emitted by the balloon	ML^2T^{-3}
$Q_{IR,sky}$	Radiative heat load from IR sky	ML^2T^{-3}
$Q_{IR,surface}$	Radiative heat load from IR surface	ML^2T^{-3}
Q_{rad}	Heat load due to radiation	ML^2T^{-3}
Q_{Sun}	Radiative heat load from sunlight	ML^2T^{-3}
$q_{IR,0}$	IR radiation at the ground level	$M\ T^{-3}$
$q_{IR,g}$	Ground diffuse radiation at a specific altitude	MT^{-3}
$q_{IR,sky}$	IR radiation from the sky	MT^{-3}
R_{AU}	Mean orbital radius in astronomical units	-
R_{planet}	Planet radius	L
Ra	Rayleigh number	-
Re	Reynolds number	-
T_{atm}	Atmospheric temperature	θ
T_g	Absolute ground temperature	θ
T_{int}	Balloon internal temperature	θ
T_s	Balloon surface temperature	θ
U	Balloon ascent rate	LT^{-1}
V_{bal}	Balloon volume	L^3
VF	View factor	-
w	Wide for the gore curve	L
z	Balloon altitude	L
$\ddot{z}$	Vertical balloon acceleration	LT^{-2}
α	Thermal diffusivity	L^2T^{-1}
α_{alb}	Albedo	-
$\alpha_{alb,c}$	Cloud albedo	-
$\alpha_{alb,g}$	Ground albedo	-
β	Thermal expansion coefficient	θ^{-1}
γ	Added resistance coefficient	-
ϵ_g	Ground emissivity	-
ζ	Solar zenith angle	-
μ_{air}	Dynamic viscosity of air	$ML^{-1}T^{-1}$
ν	Kinematic viscosity	L^2T^{-1}
ρ_{atm}	Density of the atmosphere	ML^{-3}

Symbol	Definition	Dimension
ρ_{int}	Density inside of the balloon	ML^{-3}
σ	Stefan-Boltzmann constant	$MT^{-3}\theta^{-4}$
τ_{atm}	Atmospheric transmittance	-
$\tau_{atm,IR}$	IR atmospheric transmittance	-
ϕ_{hc}	Cone half angle	-

1. Introduction

The cost and complexity of traditional zero- and super-pressure balloons, combined with recent helium shortages [1], motivated the exploration of lighter-than-air flight systems that do not depend on lift gas. This led to the development of a passive solar-powered hot-air balloon called the heliotrope[8] [2] adapted from hobbyist designs fielded in the early 2010s. The heliotrope can deliver payloads ranging from grams to kilograms to the upper troposphere and lower stratosphere (Figure 15-1). These solar balloons can maintain nearly level multi-hour float times, only landing via means of cut down or sunset. They are easily fabricated using inexpensive, readily available materials and require no lifting gas. They are an effective vehicle for research programs aiming for multi-hour flights of kilogram-scale payloads in the lower stratosphere, especially when cost or lack of facilities prevent other approaches.

Given the rapid growth in their use, this chapter aims to guide best practices established for solar hot air balloon design, fabrication, and deployment. First, the governing equations related to a physics-based model of heliotrope flights are presented in Section 2.1, which closely follows the work of Schuler and his colleagues [5,9]. The design characteristics for traditional spherical heliotropes and a few non-traditional designs are discussed in Section 3. Section 4 describes established best practices for flight operations [10]. Then, Section 5 describes the typical flight characteristics of a heliotrope. This section focuses primarily on the 2021 Balloon-based Acoustic Seismology Study (BASS) flight campaign [7] due to it being one of the few instances where a relatively large sample of heliotropes were flown with similar configurations.

2. Solar Balloon Physics-Based Model

The equations and empirical relationships that estimate solar and infrared radiation in Earth's atmosphere as a function of data, coordinates, and altitude have been covered in the Energy Balance Chapter (Chapter 5). Please refer to that chapter for a detailed discussion of the relevant equations and derivation of the heat transfer model for balloon buoyancy. Given that solar balloons utilize no lift gas other than heated air due to solar heating, these equations are critical to understand for a solar balloon user [11].

[8] The name 'heliotrope' originates from a variety of chalcedony believed to cause eclipses, as described by Dante Alighieri in Inferno, Canto 24. 'Heliostat' would have been a better name, but unfortunately that word refers to another mechanical device. -DCB

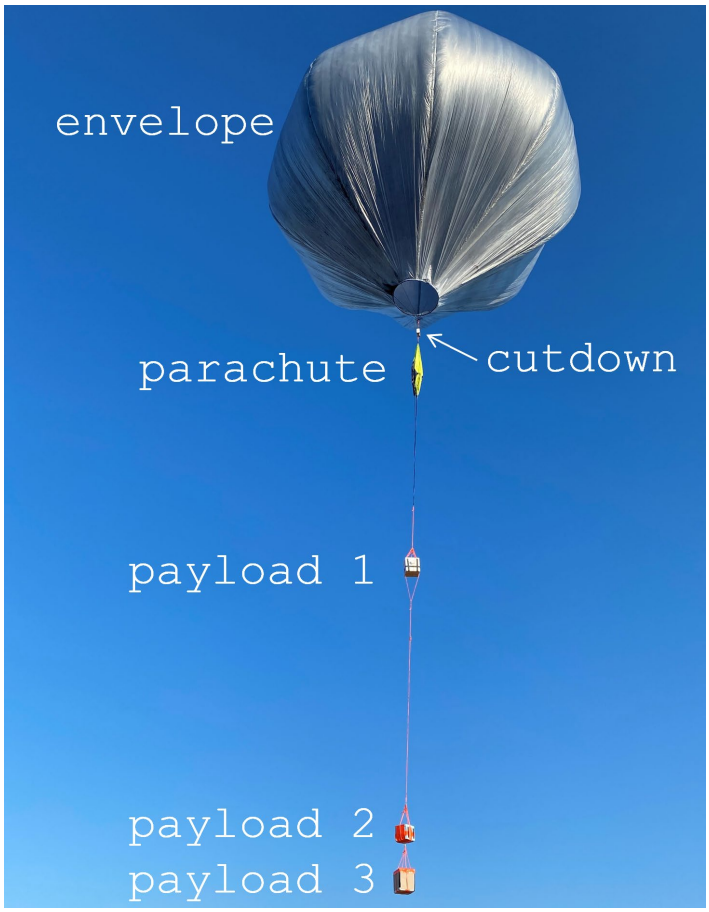


Figure 15-1: Picture of a heliotrope shortly after launch with the envelope, cut-down system, parachute, and three scientific payloads identified.

2.1. Dynamic Equations

A series of differential equations can be formed from thermal balance and heat transfer relationships developed in Chapter 5 to predict the vertical dynamic response of the solar balloon. The change in the surface temperature of the balloon envelope is given in Equation (15-1), where the dot over the variables indicates a temporal derivative. Similarly, a differential equation can be formed for the internal air temperature, which is given in Equation (15-2). Finally, the conservation of momentum on the balloon can be used to form an equation for the vertical acceleration of the balloon ($\ddot{z}$) as given in Equation (15-3). The total mass is the sum of the payload, envelope, and virtual mass of the air as given in Equation (15-4), where the virtual mass coefficient (C_{virt}) is assumed to be 0.5 for a balloon envelope approximated as spherical.

$$\dot{T}_s = \frac{\dot{Q}_{rad} + \dot{Q}_{conv,ext} - \dot{Q}_{conv,int}}{c_{v,env} \cdot m_{envelope}} \tag{15-1}$$

$$\dot{T}_i = \frac{\dot{Q}_{conv,int} - \dot{Q}_{vent}}{c_{v,CO_2} \cdot m_{gas}} \tag{15-2}$$

$$\ddot{z} = \frac{F_b - F_g - F_d}{m_{total}} \tag{15-3}$$

$$m_{total} = m_{payload} + m_{envelope} + C_{virt} \cdot \rho_{atm} \cdot V_{bal} \tag{15-4}$$

The buoyancy force, gravitational force, and drag force are given in Equations (15-5), (15-6), and (15-7), respectively. Here, the drag coefficient (F_d) is assumed to be 0.5 for a spherical envelope [15]. An added resistance coefficient (Υ) is included and empirically derived from solar balloon experiments to match the ascent speeds. For a 6-m diameter spherical solar balloon, Υ of approximately 2.0 produces ascent speeds that closely match observations. Without this added resistance, the simulated trajectory would ascend too quickly compared to an actual solar balloon altitude profile. This variation is conjectured to be due to the spherical envelope compressing as it ascends, resulting in both a shape change and a loss of lift gas through the bottom vent.

$$F_b = (\rho_{atm} - \rho_{int}) \cdot V_{bal} \cdot g \tag{15-5}$$

$$F_g = \left(m_{payload} + m_{envelope}\right) \cdot g \tag{15-6}$$

$$F_d = \frac{1}{2} \cdot C_d \cdot \rho_{atm} \cdot U^2 \cdot A_{proj} \cdot \Upsilon \tag{15-7}$$

3. Balloon Design Considerations

3.1. Balloon Materials and Construction

Constructing a solar balloon is a low-cost and easy process, and most of the required materials are readily available at typical hardware stores and online. The low barrier to entry makes these balloons ideal for university and other student programs looking to develop flight programs. While there are variations in design and construction (some of which will be briefly discussed later), the focus in this chapter is on the heliotrope envelope used in the majority of science missions [2, 3, 7, 10, 16]. Materials include a 122 m (400 ft) by 3.66 m (12 ft) roll of 7.87 µm (0.31 mil) thick high-density polyethylene plastic (commonly sold as '*light-duty paint drop cloth*'), several rolls of clear packing tape, stiff plastic tubing or hula hoops (preferred for creating a secure

bottom vent used for filling the balloon) and charcoal dust (available through online pyrotechnics supply stores as “air float charcoal”; extra fine artist’s charcoal may also be used in a pinch). Note that not all packing tapes are effective at low temperatures. Most heliotropes have successfully used a specific type (Scotch brand Heavy Duty Clear Packing Tape). Still, recent in-flight failures have indicated that even this brand might lose adhesion to the plastic under some conditions. The tools needed for the construction include scissors, permanent markers, and a tape measure. All necessary safety precautions should be followed.

The specific construction details for a 6m-diameter heliotrope, as described in Bowman et al. [2], are provided here for illustration purposes. The required balloon size for a given application depends on the total mass that needs to be lifted, emphasizing the importance of closely monitoring the weight of every component in the system. Larger or smaller balloons can be constructed by varying the number and length of the gores per Equation (15-8).

1. Cut five 9.14 m (30 ft) long strips of plastic from the roll of plastic.
2. Unfold and fully lay out the 3.66 m (12 ft) by 9.14 m (30 ft) plastic rectangle (see Figure 15-2a).
3. Fold across the long axis once (Figure 15-2a) and then across the short axis (Figure 15-2b) to create a 1.82 m (6 ft) by 4.57 m (15 ft) plastic rectangle (see Figure 15-2c).
4. Repeat for all five plastic strips and set them on top of each other, all with the same orientation. Ensure that each sheet in the stack has the same orientation and that all edges are aligned.
5. Draw the gore shape as illustrated in Figure 15-2c on the topmost sheet (See Eq. (15-8)).
6. Cut along the curve slowly, creating five blunted diamond shapes that will be the individual gores.
7. Tape two of the gores together. Starting at the top, overlay the two gores and lay tape along the overlapped plastic. The overlap of the plastic prevents the tape from sticking to the remaining plastic of the gores. See Bowman [17] for more guidance on taping the gores together.
8. Repeat the taping of seams until all gores are connected.
9. From the extra plastic, cut a circular piece to serve as a *cap* for the top of the balloon.
10. Cut a hole with a diameter of approximately 0.97 m (38 in) to 1.07 m (42 in) for the bottom vent (or mouth).
11. Cut a hole with a diameter of approximately 0.97 m (38 in) to 1.07 m (42 in) for the bottom vent (or mouth).

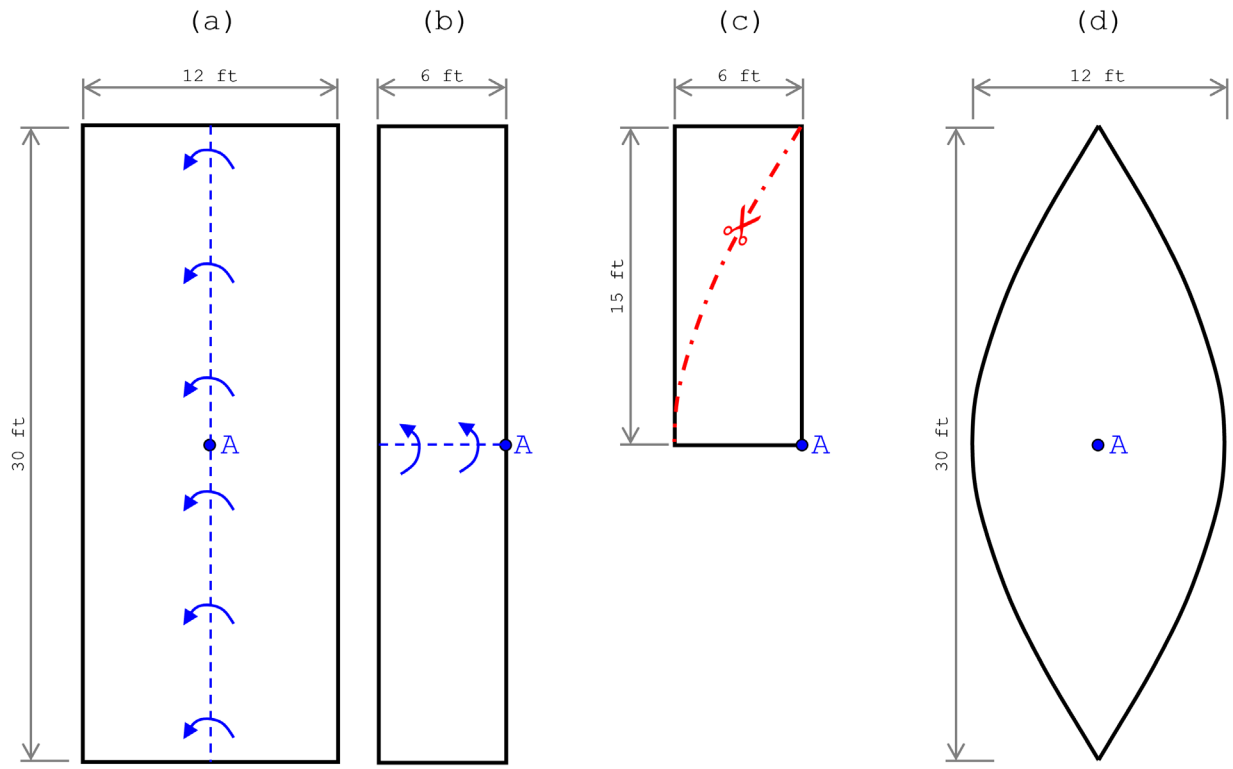


Figure 15-2: Illustration showing the folding and cutting sequence for making the gores of a 6-m heliotrope. Point A marks the same position on the plastic sheet for each step. The figure was adapted from Bowman et al. [2].

12. Reinforce the vent/mouth as described in the following procedures and illustrated in Figure 15-3. Note that these instructions are modified from those recommended in Bowman [17], which was done due to some recurring balloon failures at the balloon vent/mouth.
    a. Place a layer of tape circumferentially around the inside and outside of the mouth.
    b. Equally, place 10 to 15 (quantity dependent on balloon size) squares of Dyneema composite fabric adhesive around the mouth circumference.
    c. Cut a small opening in the center of each Dyneema square that also goes through the tape and plastic layers.
    d. Thread about 0.15 m (6 in) of fishing line through each opening and use it to secure a hoop of stiff plastic tubing (a hula hoop is a convenient method for creating the hoop).
    e. Use a paracord line to attach the plastic hoop to the flight line, as shown in Figure 15-3.
13. Darken the inside of the envelope by coating it with charcoal dust. The charcoal should be filled inside and moved around to coat all the interior surfaces, and then the excess should be removed to minimize weight during the launch.

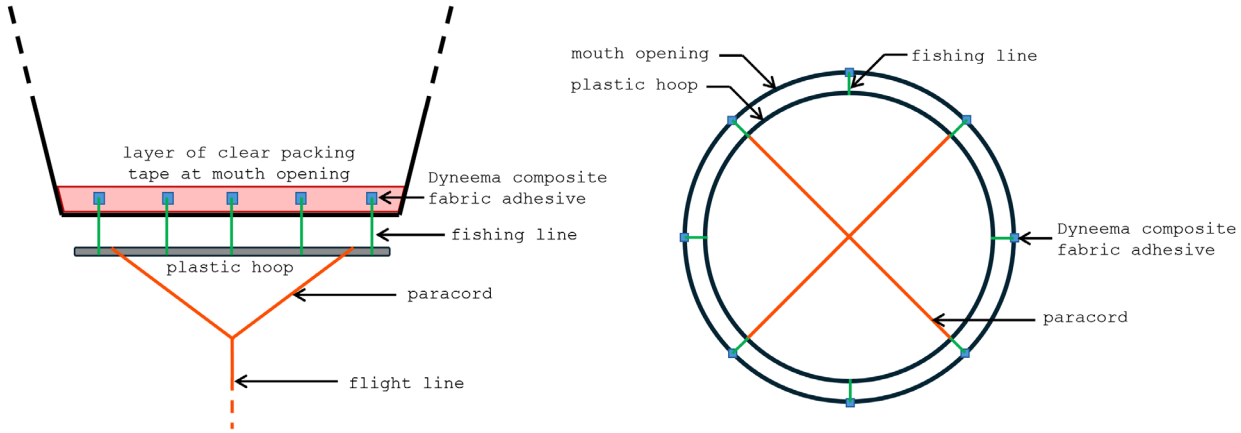


Figure 15-3: Front and bottom views illustrate the recommended procedure for reinforcing the balloon vent/mouth. The figure was adapted from Jacob et al. [16].

While using tape to seal the gores together, as described above, is the most common method, heat sealing has also been done. Heat sealing can be accomplished using an industrial heat sealer or a standard clothes iron. Like the taping procedure, the edges of the two gores are overlapped, and the heat sealer is run along the overlap to seal them together.

The gore curve is defined by Equation (15-8), where w is the width of the gore, c is the desired circumference of the balloon, n is the number of gores, and l varies along the curve from 0 to $\frac{c}{4}$. Larger or smaller balloons can readily be produced by varying the input parameters in Equation (15-8). This equation has been used to make balloons of different sizes, including 3-m, 6-m, 7-m, and 10-m diameter balloons.

$$w = \frac{c}{2n} cos\left(2\pi \frac{l}{c}\right) \tag{15-8}$$

Balloons larger than about 8 m in diameter tend to rupture during ascent due to stresses on the envelope. This can be ameliorated by reinforcing the gores with paracord up to about 10 m diameter, beyond which even this method fails. A larger solar hot air balloon envelope requires more sophisticated designs and/or materials; designing one is a worthy subject for future engineering teams.

Figure 15-4 shows a selection of standard (i.e., designed using Equation (15-8)) and non-standard designs that Oklahoma State University has explored. The figure includes the number of gores used to make the balloon and the nominal maximum free lift (m_{fl}). Alternative designs are currently needed to lift larger payloads. Thus, a brief overview of the two non-standard balloons in Figure 15-4 is provided in the next section.

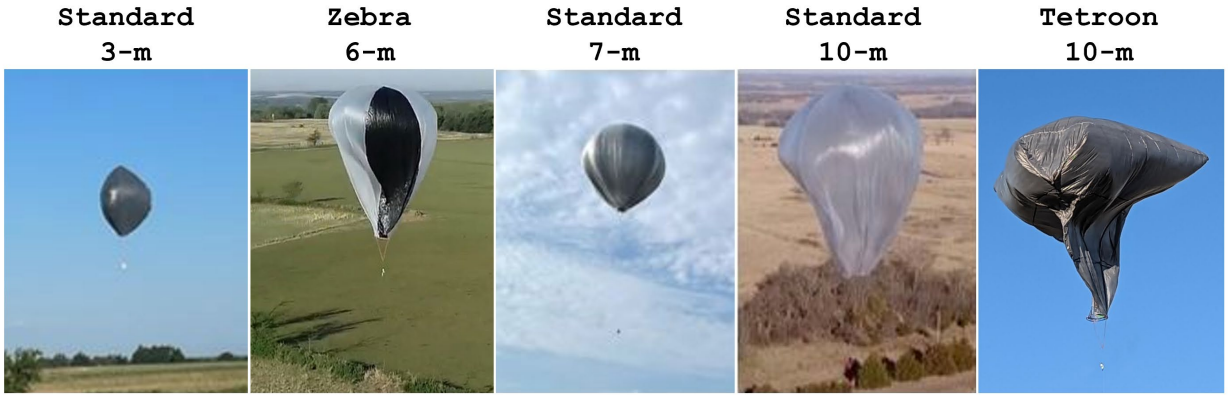


Figure 15-4: Sample of solar balloons with various sizes and shapes, and the nominal maximum free lift (m_{FL}).

3.2. Alternative Designs

3.2.1. Tetrahedral Balloon, "Tetroons"

The vast majority of heliotropes flown to date have been spherical, using the guidelines listed in the previous section. An alternative balloon shape is a tetrahedral-shaped balloon, known as a "tetroon," which was the preferred solar hot air balloon design in the first two decades of the 21st century. This design continues to interest the ballooning community due to its ease of construction. Here, the construction of a 10-m tetroon balloon (e.g., [16]) is provided in detail, allowing for adjustment to other sizes. The materials required are the same: a 122 m (400 ft) by 2.7 m (9 ft) roll of 7.87 μm (0.31 mil) high-density polyethylene plastic, tape (clear packing tape and Dyneema composite fabric adhesive), rigid plastic hoop, fishing line, paracord, and air-float charcoal. The recommended steps to construct a 10-m tetroon are:

1. Cut four strips of plastic from the polyethylene plastic roll, each 17.2 m (56.5ft) by 2.7 m (9 ft).
2. Cut each of the four plastic strips into three smaller pieces, as shown in Figure 15-5a. The coordinates in Figure 15-5a are in meters to make a 10-m tetroon.

3. Tape the three pieces cut from one plastic strip into one triangle, as shown in Figure 15-5b. Repeat for each of the strips to produce four gores.
4. Tape the four large triangles together, as shown in Figure 15-5c, to create one larger triangle.
5. Each flange of the large triangle is then taped to the corresponding edges to create a tetrahedral pyramid shape, as shown in Figure 15-6. Leave one corner open to serve as the balloon's vent/mouth.

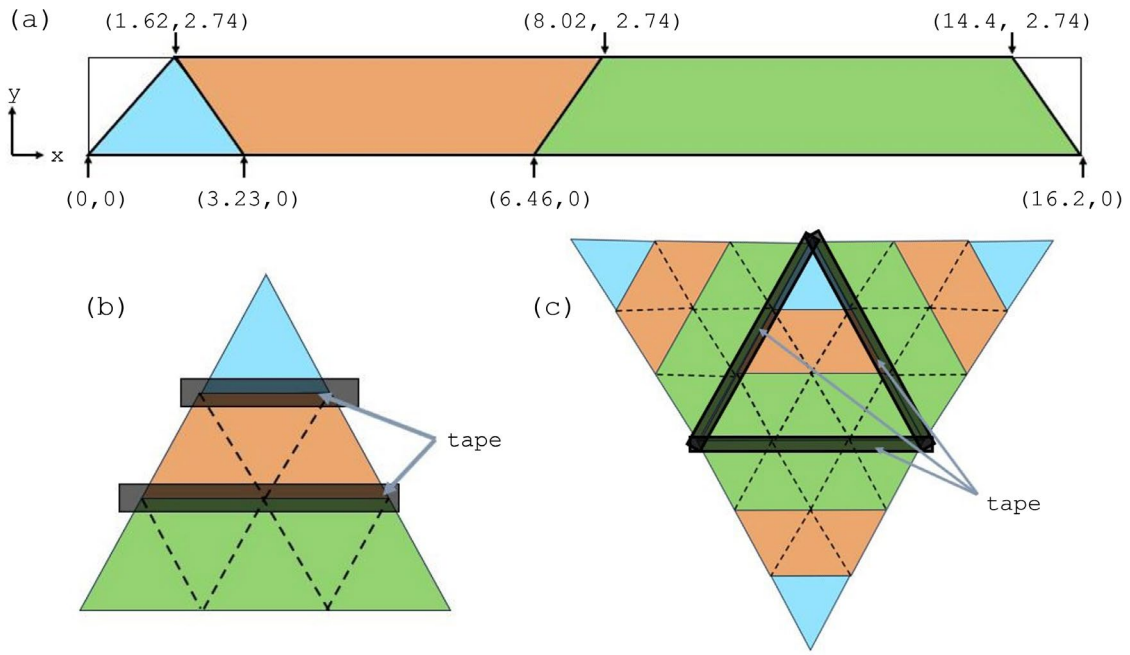


Figure 15-5: Illustration showing how to prepare gores for a 10-m tetroon. (a) Coordinates to cut the initial strip with coordinates in meters. (b) The method involves taping segments together to form a triangle. (c) Tape triangles together to form a larger triangle.



Figure 15-6: Picture of a partially inflated 10-m tetrahedral balloon (i.e., tetroon) shortly after launch.

6. Reinforce the balloon vent/mouth as described for the traditional spherical balloon.
7. Darken the inside of the envelope by coating it with air-float charcoal. The charcoal should be filled inside and moved around to coat all the interior surfaces, and then the excess should be removed to minimize weight during the launch.

3.2.2. Zebra Balloon

A natural solution to the darkening problem is to simply use black plastic. However, black plastic melts under the intense solar radiation of the lower stratosphere, causing anomalously low float levels and/or flight termination [47]. One attempted solution is to balance the solar absorptivity by varying between transparent and black plastic gores. During the spring of 2022, a team of students at Oklahoma State University [16] tested this concept by making a spherical 6-m heliotrope using alternating clear and black plastic gores (i.e., 50% clear and 50% black), which was termed a zebra balloon. Pictures of the 6-m zebra balloon are provided in Figure 15-7. In addition, Figure 15-7 shows the flight trajectory for the first 5.7 hours, which shows that it was able to achieve float after just over 3 hours and then maintained a relatively constant altitude. This behavior is consistent with traditional spherical heliotropes, in which 7-m spherical balloons with a ground launch achieve float in 3.7±0.3 hours [7]. However, the presence or absence of melt holes on the black plastic portion was not conclusively determined.

4. Flight Operation Considerations

4.1. Launch Site Location and Setup

Before the launch day, a potential launch site should be scouted to identify potential fill locations and obstructions in each direction. The ideal launch location will have a relatively large area, minimal hazards and obstacles, and level ground. Hazards and obstacles to consider are those that could cause a team member to trip or the balloon to get snagged, such as uneven terrain, shrubbery, trees, fences, power lines, buildings, and ponds [16]. A large open area in the direction of the ground wind is preferred for walking/running the balloon after the initial air filling, while it is being heated and gaining buoyancy to lift the payload(s). The required space depends on the launch method, flight line (length and weight), and ground conditions. These considerations are discussed further in the next section, but the ground launch method requires the maximum area. Regardless of the method, it is recommended to maintain a minimum of 10 balloon diameters between the fill location and any obstruction in case the winds shift during the fill.

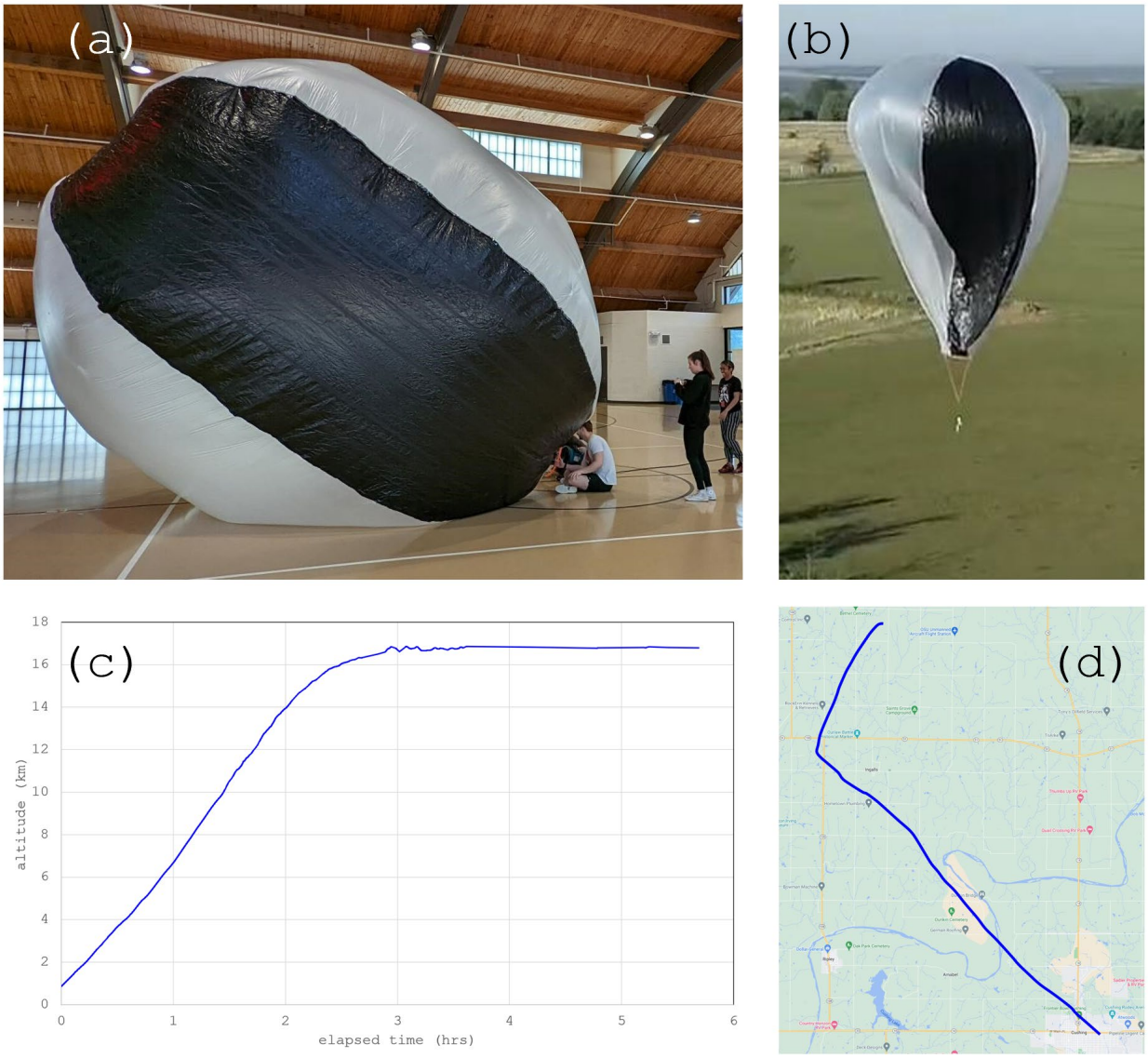


Figure 15-7: (a, b) Pictures of the 6-m zebra balloon (a) pre-flight indoor fill test and (b) after launch. (c) Altitude versus time elapsed and (d) flight path of the zebra balloon.

A typical launch site setup is shown in Figure 15-8, which was used during the BASS 2021 flight campaign [7]. For this campaign, a specific spot was selected each day to fill the envelope, maximizing the unobstructed field in the direction of the wind while maintaining the recommended minimum unobstructed distance in all directions. A tarp secured with sandbags was spread out at the site to prevent tearing the envelope while it was in contact with the ground. A large industrial fan and the helium tank (for assistance with takeoff, see following sections) were positioned at the farthest upwind edge of the tarp. The envelope

and flight line should be laid in the direction of the wind (i.e., in Figure 15-8, the wind would be from the right to the left). Weather and flight telemetry stations were also set up. The telemetry station was used to confirm the proper operation of all tracking devices and instrumentation before launch. It is recommended that an Automated Packet Reporting System (APRS) relay station be included in the telemetry station, as it is common for a remote launch site to be unable to confirm APRS operation without an on-site station. The weather station (e.g., a Lufft WS600-UMB Smart Weather Sensor) measures current ground conditions, including wind speed and direction, solar irradiance, and temperature. As solar irradiance increases, it is common for local wind conditions to also increase, resulting in a narrow window for ideal launch conditions. During the BASS 2021 flight campaign, launches would be performed once the solar irradiance exceeded ~190 W/m². Power was provided by either a generator or an extension cord (if possible). It is recommended that helium tanks always be on hand if a conventional (i.e., no helium) launch is impossible. The individual mass of each component should be measured, though this is typically done the day before in preparation for the launch. It is also recommended that checklists be used for each launch, with separate checklists for each launch method. See Hough [10] for examples of checklists.

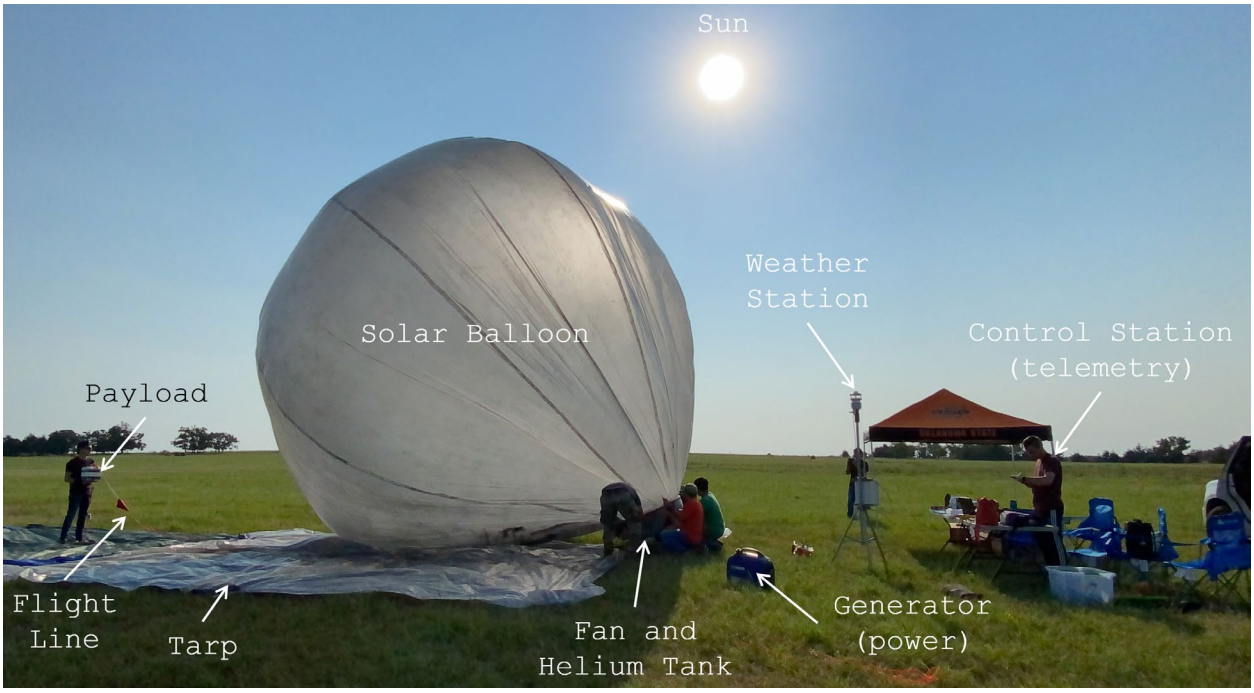


Figure 15-8: Launch site from the BASS 2021 flight campaign [Swaim et al.], which is a representative setup for a recommended launch site.

4.2. Flight Safety and Notifications

The deployment of uncrewed scientific balloons, solar or otherwise, poses safety considerations to people and property not associated with the operation. In the United States, the operation of uncrewed free balloons is outlined in 14 CFR Part 101 Subpart D. This set of regulations stipulates an exemption for balloons falling beneath certain weight limits, among other criteria. The majority of the flights described in this chapter are covered by this exemption. Heliotrope operators should consult the latest version of the uncrewed free balloon regulations to ensure they are compliant, as the rules may change over time.

In the United States, it is best practice to coordinate with the Federal Aviation Administration even when operating an exempt balloon. A Notice to Airmen (NOTAM) should be filed for the launch operation so that aircraft in the area are aware that low-altitude balloons may be present. Air Route Traffic Control Centers (ARTCCs) that may be traversed by the balloon(s) should be notified of the planned operation. It is especially important to remain in communication with the appropriate ARTCC when the balloon is below 60,000 ft (either ascending or descending) so aircraft can be routed around the area. Notifying the ARTCC several weeks in advance is advised, especially if this is the first time they have hosted solar balloon flights. Certain airspace areas may require additional permissions to overfly. These include Restricted Airspace (RA) and Military Operations Areas (MOAs).

Falling payloads and balloon envelopes pose hazards to the ground. All payloads should be equipped with a parachute to provide a landing speed of 5 m/s (12 mph) or less. This is necessary even when the solar hot air balloon envelope will remain attached, because failure of the envelope upon descent will result in a very rapid impact speed.

If the flight is terminated by a cut-down system, an attempt should be made to recover both the balloon envelope and the payload. This can be accomplished by ‘flipping’ the balloon upside down by means of a termination line running from the payload to the top of the envelope. When the termination is commanded, the payload suspension line from the bottom of the balloon is cut, causing the balloon to become top-heavy. This method works well for balloons smaller than about 6m across but has proven difficult to execute successfully for larger ones.

Balloon launch points and termination zones should be selected to ensure landing zones minimize the risk of injury and property loss. In particular, urban areas should be strictly avoided. Landing in protected areas, such as national parks and wildlife refuges, is discouraged. Mountainous, wet, densely forested, or other difficult to access areas may result in payload loss and the inability to recover envelope debris.

Once payloads have landed, they must be retrieved from the field. In the United States, owner information can be obtained using apps such as OnX. In rural areas, contacting the clerk at the local post office is usually successful – this person is familiar with all the property owners in the area and is often happy to help. If the payload falls on a road, in a busy area, or anywhere else where it might cause damage or public alarm, the best course of action is to call the local sheriff's office. They appreciate knowing beforehand (rather than having to try and track the operators down) and will often help recover the payload at no cost. If the payload falls on a military base, national park, or other restricted-use land, contact the relevant authorities. However, it is highly encouraged to avoid these areas if at all possible. In almost all cases, private landowners and public officials are willing to work with the operators to recover the envelope and payload.

4.3. Launch Methods

4.3.1. Ground Wind Effects on a Solar Balloon Envelope

Ground wind conditions significantly impact the launch method, and a traditional (i.e., no helium) ground launch is preferred. However, to perform such a launch, the ground wind must be very low (e.g. walking pace) to reduce stress and tension at points around the balloon vent/mouth. Under ideal conditions, a 6m diameter heliotrope can be inflated and launched in about 5 minutes. However, even with low wind speeds, the envelope gets buffeted around, as illustrated in Figure 15-9, which leads to stress concentrations around the balloon mouth. Once the balloon is partially inflated and the air inside begins to warm, it becomes more susceptible to being pushed by the wind, causing the envelope to act like a sail. This motion is problematic because, with the envelope not fully inflated and insufficient heated air to ascend, the balloon will take much longer to gain lift and will be dragged along the ground. This scenario must be avoided; therefore, holding the balloon mouth at the fan is critical until it is fully inflated. It will become increasingly difficult for team members to hold the balloon, and the tension at the mouth will increase, making it more susceptible to holes forming in the plastic. For this reason, it is important to rapidly fill the balloon to minimize time spent in this phase, which is why the pioneer of heliotropes says:

"*Do not fight the wind, the wind fights you*!" – Danny Bowman, 2021.

Once the balloon has nearly sufficient air, the wind will push it vertically and horizontally. The specifics of how this fill and launch process is performed depend on the launch method, which is based on the ground wind speeds.

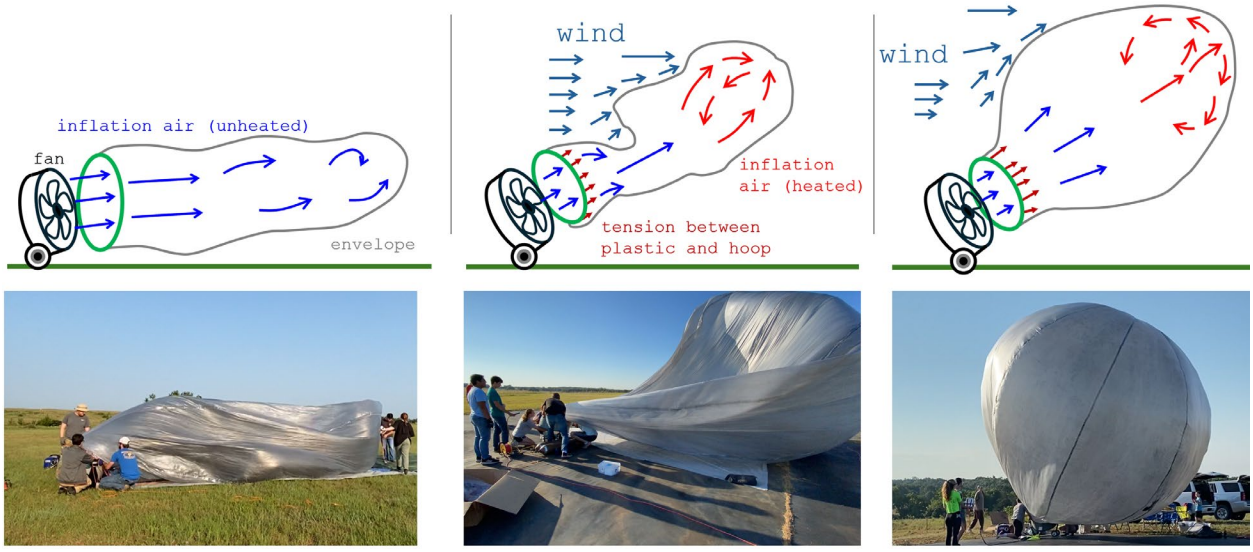


Figure 15-9: (top row) Illustration and (bottom row) representative pictures of balloon inflations showing (left) the start of inflation, (middle) partial inflation with the balloon being buffeted by wind, and (right) nearing full inflation.

4.3.2. Ground Launch (traditional)

The target conditions for a traditional ground launch are low winds (<~2.2 m/s), sunny (solar irradiance level above 170 W/m^2), and minimal cloud coverage. However, variations for these requisite conditions occur based on the launch site terrain, the length of the unobstructed path in the direction of the wind, and the flight line length. With the launch site setup described in the previous section, the solar balloon mouth is positioned near the fan with the rest of the envelope laid downwind along with the flight line. The flight line should be stretched out downwind so that team members holding the payloads are ahead of the rising balloon when it starts to ascend. Being in front of the balloon as it ascends is important to prevent additional drag on the balloon as it tries to lift each payload. Filling the envelope can begin once the solar irradiance reaches ~190 W/m^2. In addition to a team member holding each payload, one team member should control the fan while up to 3 other team members hold the balloon mouth during the fill. Any additional team members should be stationed along the expected flight path to help if there is significant walking/running due to a relatively slow lifting period. For example, if there is a fence downwind, a team member should be positioned on the opposite side of the fence, if possible, to take over guiding the balloon through ascent. Once all members are in position, the balloon is filled with air using the fan. A sequence of images from a nominal ground launch is shown in Figure 15-10.

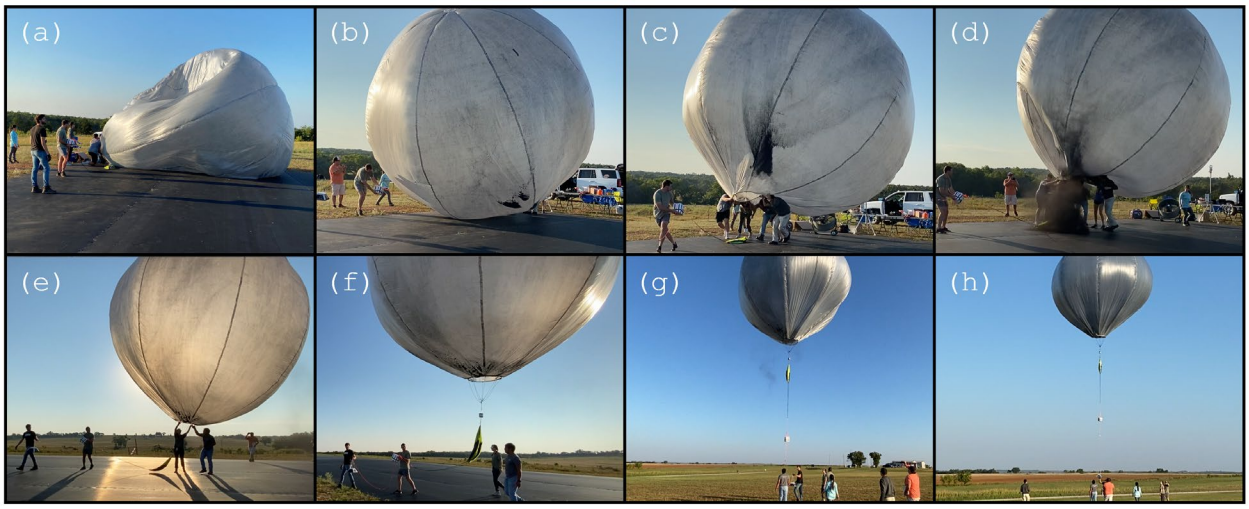


Figure 15-10: A sequence of images from a nominal heliotrope launch (25 Aug 2022) showing (a) initial fill, (b) stopping fan, (c) running mouth under the balloon, (d) excess charcoal dumping out, (e) balloon mouth being released, (f) payloads being walked with the balloon, (g) first payload in the air and (h) moment when second payload left the team member's hand.

As the balloon inflates, the team lead should stand approximately one balloon diameter away to assess when the balloon is sufficiently filled, while still being able to communicate with the fill team members. Overfilling can potentially burst the balloon, but underfilling will require longer before the balloon gains sufficient lift. Example images of balloons at various fill amounts are shown in Figure 15-11. Once the fan is turned off, the inflation team needs to briefly run forward while holding the vent/mouth parallel to the ground until the mouth is directly below the envelope. This method is done to keep the warm air inside the balloon from escaping. The inflation team will continue to move forward until the balloon is buoyant and rises. With the balloon envelope airborne, the team members holding the payloads must run/walk to stay in front of the balloon while leaving slack in the line until their payload lifts out of their hands. It is common for the payload to slightly descend after it is lifted out of their hand, especially in low irradiance situations and/or with heavy system mass, due to insufficient lift to hold the full payload weight. Therefore, the team members should assist the payload until it rises steadily without further assistance.

4.3.3. Helium-Augmented Launch

The helium-augmented launch method was developed during the BASS 2021 flight campaign [7]. Helium-augmented launches are typically used when there is heavy cloud coverage over the launch area, limiting solar radiation and/or winds slightly above the target wind for a traditional launch. This involves filling the envelope with air from a fan; however, prior to walking the heliotrope, helium is also pumped directly into the heliotrope envelope. This pre-fill gives the heliotrope some

instantaneous lift, significantly reducing the inflation period near the ground, where most failures occur due to wind and low solar heating. This method uses significantly less helium than the helium-assisted launches (discussed below). More details about the launching of heliotropes are provided in Hough et al. [16].

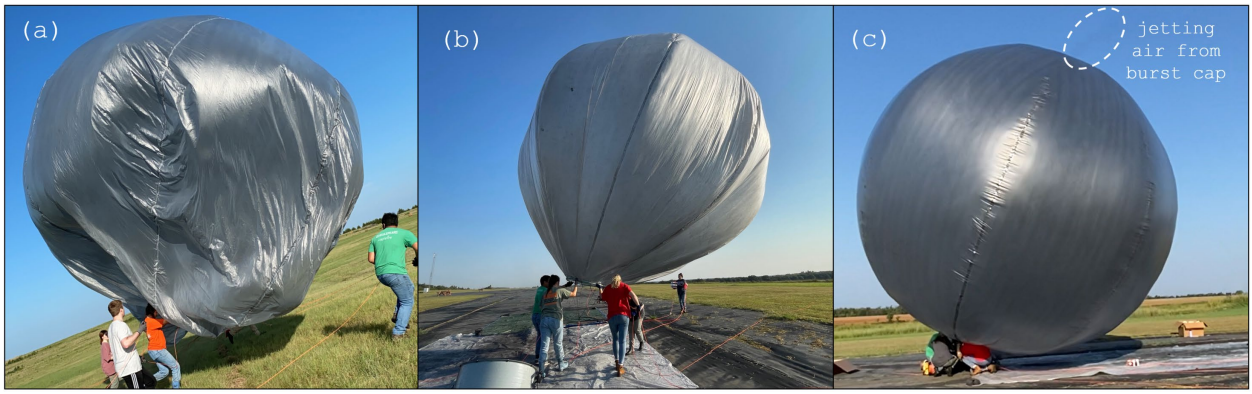


Figure 15-11: Picture at the end of filling showing (a) an underfilled balloon, (b) a nominally filled balloon, and (c) an overfilled balloon that just burst at the top.

This technique is nearly identical to a traditional ground launch, with the only difference in setup being that a helium tank is positioned next to the fan, and a dedicated team member operates the tank. Towards the end of the fan inflation, the helium tank nozzle should be placed inside the balloon mouth, and helium should be released directly into the balloon envelope. Once the balloon is full of air, the fan is turned off, and (if possible) additional helium is pumped into the envelope. Then, the remainder of the launch sequence follows the description of the traditional launch. Analysis of the ascent rates shows that the helium vents out of the envelope prior to reaching float. However, it significantly increases the takeoff speed (i.e., vertical velocity immediately after launch). Swaim et al. [7] show that the average takeoff speed was increased from 0.54 m/s for a traditional launch to 1.22 m/s for a helium-augmented launch. This method uses significantly less helium than the helium-assisted (i.e., grand slam) method, which will be discussed next.

4.3.4. Helium-Assisted (grand slam) Launch

The helium-assisted launch method is utilized when launch conditions are unfavorable due to high winds and/or significant cloud coverage. It has also been used when a predawn launch was required to meet mission needs. In this method, termed the “grand slam”, a helium balloon is attached to the top of an uninflated heliotrope envelope, rapidly lifting the heliotrope away from the ground. Depending on the quality of the helium

balloon and the amount of helium, the balloon bursts at an altitude between 12 and 23 km, releasing the heliotrope. The heliotrope envelope then ram-inflates as it descends. The sun heats the air, which is then contained within the envelope, and the heliotrope ascends or descends to its stable float altitude.

Additional rigging is required for a helium-assisted launch to secure the uninflated heliotrope for a safe tow to altitude. The same materials used to reinforce the mouth are used for the additional rigging.

1. Cut a segment of paracord that is 0.9 m (3 ft) to 1.2 m (4 ft) long.
2. Tie this paracord segment into a circle.
3. Lay the top of the balloon out as flat as possible.
4. Tape the paracord circle using duct tape every 0.15 m (6 in) around the circle circumference, which should take about 8 pieces of tape. See Figure 15-12 for a sketch of how this is performed.

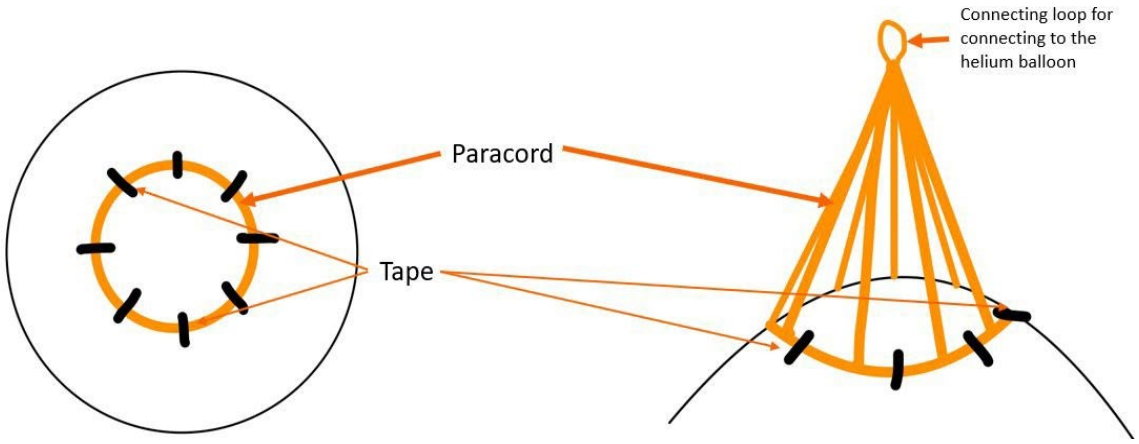


Figure 15-12: Sketch of the (left) top view and (right) side view of the rigging for a helium-assisted (grand slam) launch.

5. Cut eight 1.5-m (5 ft) long segments of paracord.
6. One end of these 1.5-m segments should be tied to the paracord circle between tape segments.
7. The other end of these segments should be gathered and formed into a loop.
8. A carabiner is used to attach the paracord loop to the helium balloon to tow the uninflated balloon.
9. Typically, a ~3 m (10 ft) long segment of paracord is used to separate the towed heliotrope from the helium balloon.

For most helium-assisted launches, a 600-gram latex weather balloon filled with helium served as the helium balloon that towed the uninflated envelope to altitude. The required amount of helium must be calculated to ensure sufficient lift to twice the full weight of the system (helium balloon, heliotrope envelope, and flight line). These calculations are

relatively straightforward, given the mass of the envelope and flight line components. However, common online tools are available for these calculations (e.g. [18]). Then, the tow (weather) balloon is filled with helium, and the required free lift should be confirmed using a handheld digital scale or other such method. While the tow balloon is being filled, the other team members should have the flight line laid out downwind of the balloon envelope, like the other launch methods.

Prior to removing the helium regulator from the tow balloon, tightly tie off the helium balloon's mouth. It is common to do this with zip-ties, but it is important that the excess of the zip-tie be cut off and wrapped with duct tape to prevent the sharp end from poking the balloon. A 3m (10 ft) length of paracord should be used to separate the tow balloon from the heliotrope envelope. This attachment is done by tying a loop on each end of the 3 m segment. One loop is clipped to the carabiner attached to the loop at the top of the new rigging, and the other threads over the tow balloon mouth. With the loop around the helium balloon's mouth, the mouth should be folded upwards and tied together, typically using zip ties and duct tape. Once the tow balloon is filled, it should be carried to the heliotrope envelope and attached to the tow rigging via the carabiner.

With the full flight line attached and ready for launch, final confirmation of all tracking devices and payloads should be performed. One team member is recommended to hold the helium balloon, while another holds the heliotrope mouth perpendicular to the ground. Each payload has one team member holding it. The team lead will verbally confirm that all team members are ready for launch, perform a countdown, and then release the helium balloon. Figure 15-13 shows a typical flight line as well as a sequence of images from a helium-assisted launch during the BASS 2021 flight campaign (flight 8.1 from Swaim et al. [7]). This process will be significantly faster than the other launch methods, which typically require the payload holders to move quickly for a short period. For this reason, the flight line should be laid out in the downwind direction, but with more slack in case the balloon quickly moves in an unexpected direction. Note that a unique checklist for a helium-assisted launch should be used; example checklists are provided in Hough [10].

Depending on the helium balloon quality and the amount of helium, the helium balloon bursts either above or below the final float altitude. An example of a helium-assisted launch with the helium balloon burst from Schuler et al. [5] is provided in Figure 15-14. In this example, an upward-facing camera and GPS-based altimeter were used to document the release of the heliotrope envelope. The camera is positioned so that both the helium balloon and the heliotrope (uninflated or inflated) are in view. After the helium balloon bursts, the heliotrope envelope ram-inflates as it initially descends. The sun heats the air within the

envelope, and the heliotrope either ascends or descends to its stable float altitude.

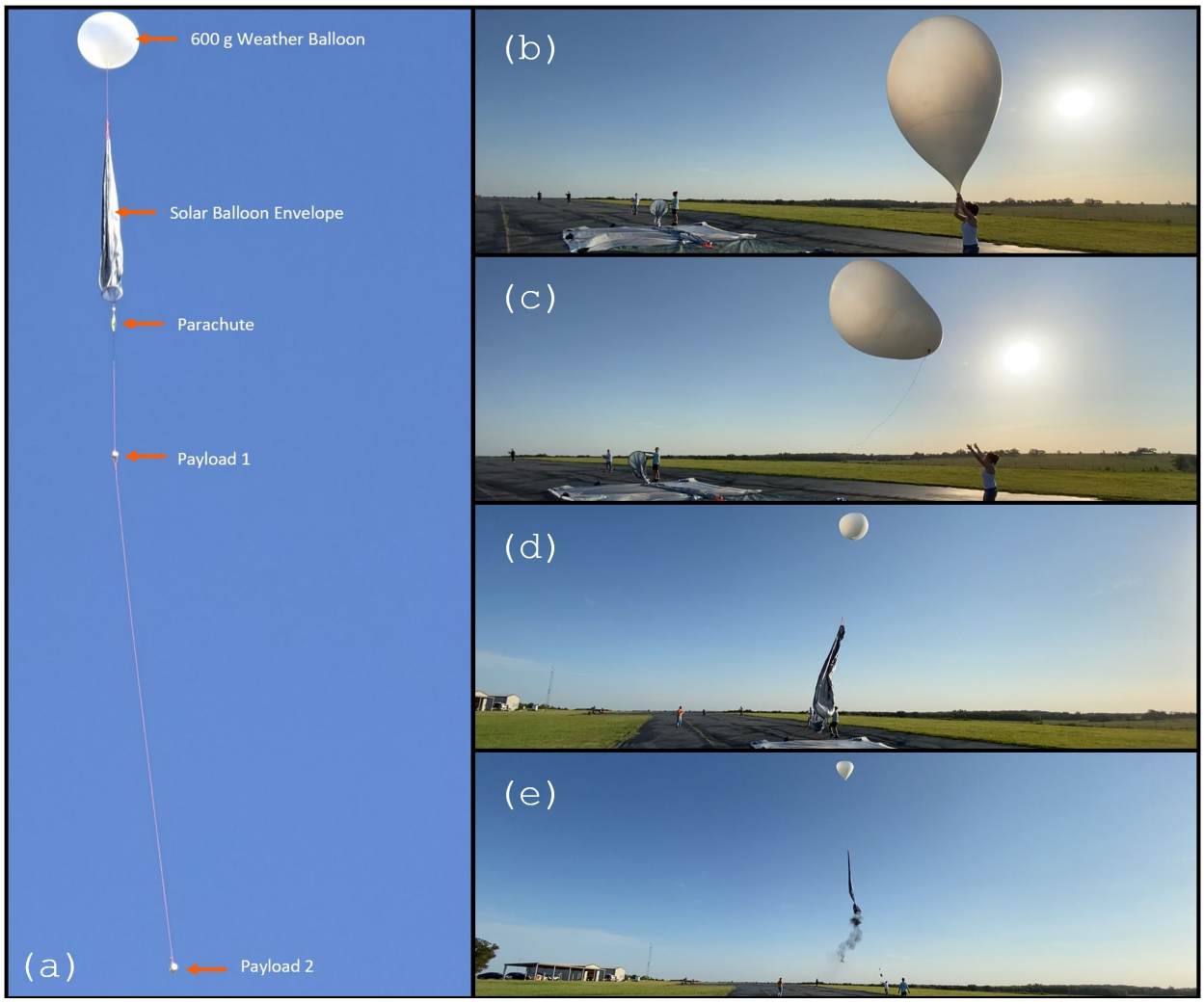


Figure 15-13: Pictures from a helium-assisted (grand slam) launch showing (a) a typical flight line, (b) prior to releasing the helium balloon, (c) immediately after releasing the helium balloon, (d) when the heliotrope envelope lifts off the ground, and (e) when the first payload lifts off.

5. Balloon Flight Characteristics

5.1. Flight Stages

This section primarily focuses on the flight characteristics observed during the BASS 2021 flight campaign [7]. While there are numerous other designs and, consequently, flight characteristics, the BASS 2021 flight campaign was unusual in that it launched a relatively large number of solar balloons with nearly identical flight lines and balloon sizes. This large dataset enables the quantification of both typical flight

performance and the range of variation, even when launching from the same location and time of year. Rather than being a definitive characterization of flight performance, this should serve as a reference for planning and assessing flight performance under different conditions.

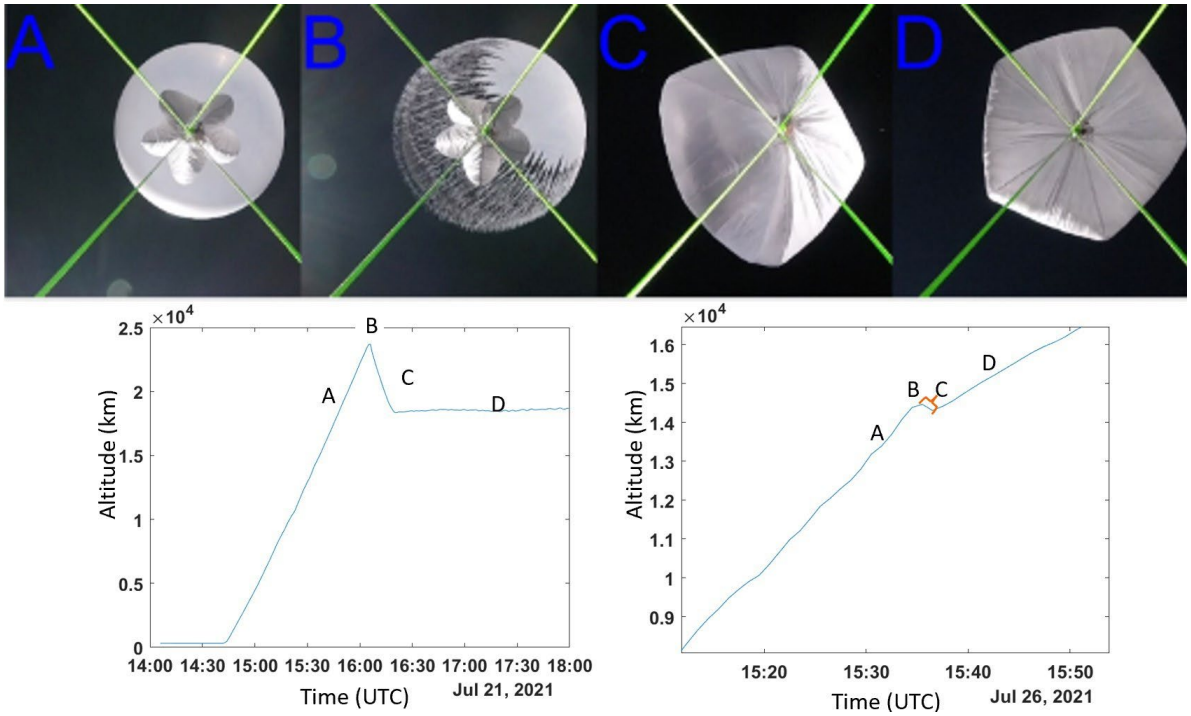


Figure 15-14: A figure adapted from Schuler et al. [5] shows an example of a helium-assisted heliotrope launch. The top row shows (A) the uninflated heliotrope envelope being towed by the weather balloon, (B) the burst of the weather balloon, (C) the heliotrope rapidly inflating, and (D) the heliotrope reaching its neutral buoyancy level. These reference points are also marked on the altitude readings from a GPS-based altimeter during two different flights.

Following the convention defined in Bowman et al. [2], a heliotrope balloon flight is generally divided into three distinct flight stages: ascent, float or neutral buoyancy, and descent (see Figure 15-15).

For ground and helium-augmented launches, the end of the ascent stage was defined as the point at which the vertical velocity of the heliotrope drops below 1.2 m/s. For a helium-assisted launch, the ascent occurs at the moment the helium balloon bursts. Several factors influence when this occurs: the force on the helium balloon wall due to the pressure differential with the surrounding air, UV damage, which deteriorates balloon material, and balloon quality (e.g., material uniformity). Consequently, the BASS 2021 campaign exhibited significant variation in burst altitude, resulting in bursts occurring either above (type 1) or below (type 2) the final float elevation.

The float or neutral buoyancy stage, similar to conventional ballooning, is characterized by maintaining a relatively constant altitude, with the average vertical velocity dropping to nearly zero. A transitional stage exists between the ascent, float, and descent stages. Notably for the data examined here, the power ran out on the high-frequency IMU measurements prior to descent (see Figure 15-15), which required the end of float to be defined using only the lower-resolution APRS tracker.

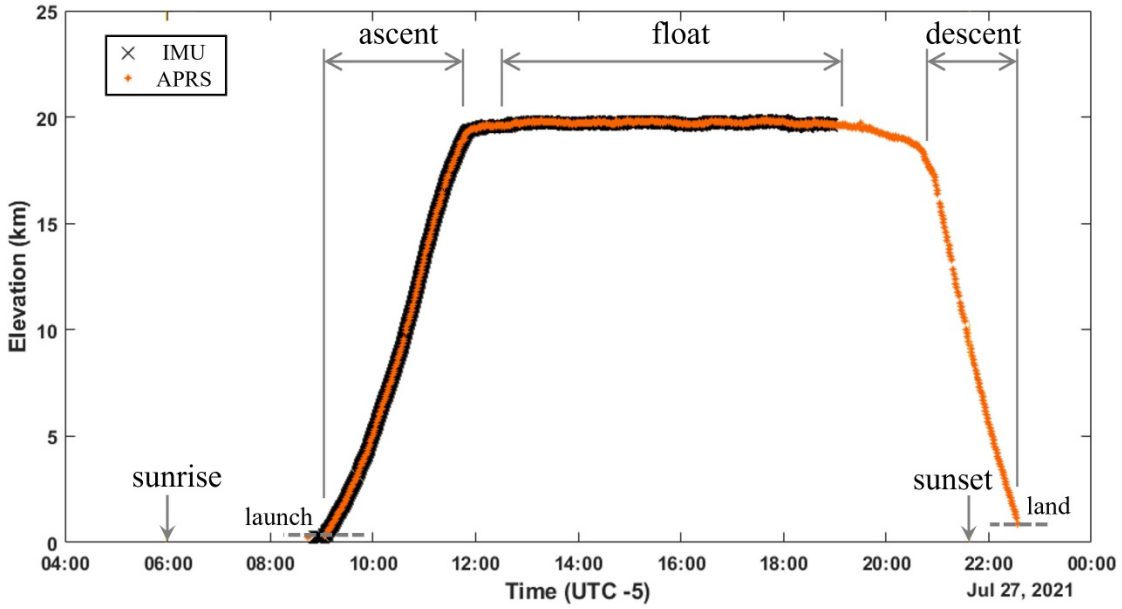


Figure 15-15: Typical flight (flight 4.2 from Swaim et al. [7]) illustrating the various flight stages. The data from the upper IMU and APRS tracker are included, along with reference lines for the start and end stages, as well as sunrise/sunset times. This figure is adapted from Swaim et al. [7].

Here, the descent stage is determined to begin once the vertical velocity decreases below -2 m/s. The solar irradiance level decreases as sunset approaches due to increased path length within the atmosphere (i.e., increased scattered light), resulting in the heliotrope beginning to slowly descend prior to the start of what would be definitively characterized as the descent stage. The heliotrope continues to descend until the conclusion of the flight, when the payloads land on the ground. During the BASS campaign, the APRS tracker typically lost signal a couple of hundred meters above the ground elevation. The SPOT TRACE GPS tracker attached to each payload provided the final landing elevation and location (latitude and longitude), which sent the coordinates 5 minutes after movement stopped. The APRS data were linearly extrapolated to the landing elevation provided by SPOT to determine the approximate time that descent was complete.

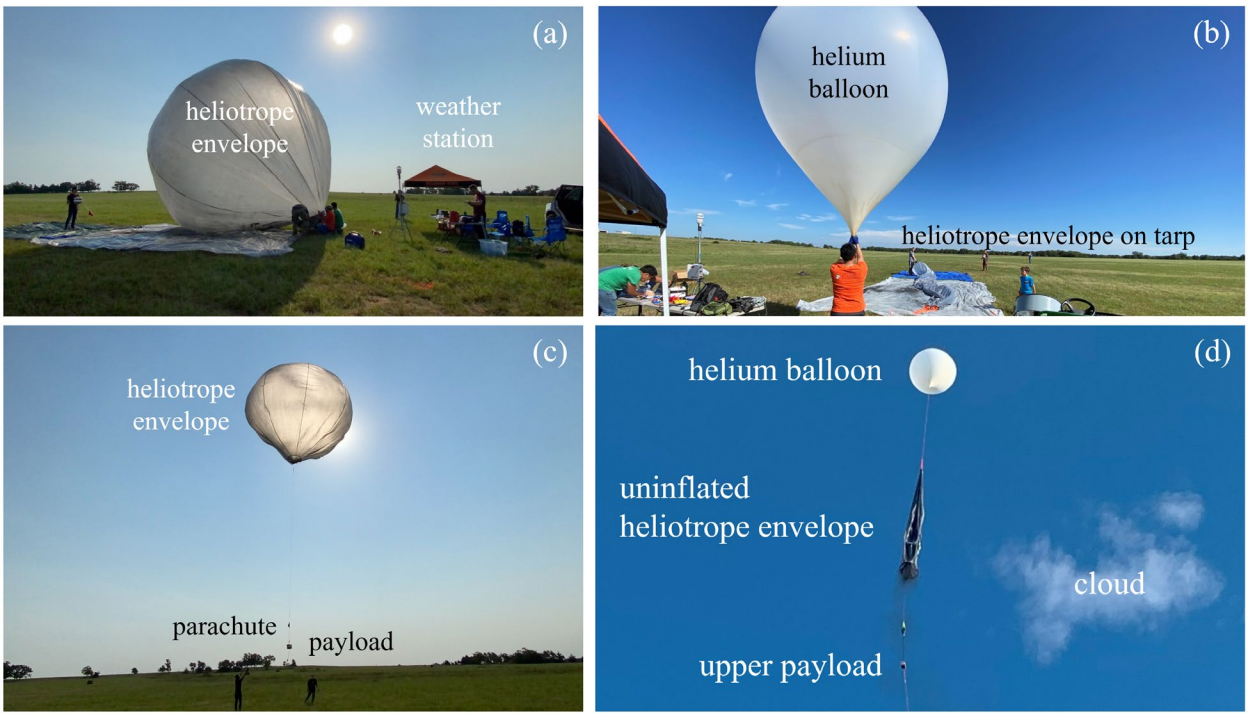


Figure 15-16: Pictures of (a,c) traditional ground and (b,d) helium-assisted launches (a,b) just prior to launch and (c,d) after the envelope was airborne.

5.1.1. Launch and Ascent

The 2021 BASS flight campaign had ten (10) ground, eight (8) helium-augmented, five (5) helium-assisted (type-1), and six (6) helium-assisted (type-2) launches that successfully reached float with data. Table 15-1 summarizes the various launch methods' takeoff velocities, ascent rates, and total ascent times. The average takeoff velocity is defined here as the ascent rate from launch until the balloon reaches 50 m above the ground. A comparison of the ground and helium-augmented launches reveals that the helium added an additional 0.25 m/s to the initial takeoff velocity, accompanied by reduced variability (i.e., standard deviation). This resulted in a 34% increase in takeoff velocity, accompanied by a 25% decrease in duration when the flight line was at the height of nearby obstacles (i.e., trees, power lines, etc.). Consequently, there were no failed helium-augmented launches due to flight line damage from these objects.

Table 15-1: Ascent stage characteristics of the BASS 2021 flight campaign [7]. Only flights that weighed 7.05 kg are included.

		Ground	Helium Augmented	Helium-Assisted	
				Type-1 (above)	Type-2 (below)
Takeoff Velocity ($m*s^{-1}$)	Avg	0.54	1.22	4.2	4.5
	Std	0.17	0.30	0.89	0.74
Ascent Rate ($m*s^{-1}$)	Avg	1.80	2.1	5.4	3.9
	Std	0.14	0.17	1.3	0.83
Time to Float (min)	Avg	223	196	104	118
	Std	19.0	10.2	29	22

The helium-assisted launches had different takeoff velocities, with type-2 (burst below float) being, on average, 0.3 m/s faster than type-1 (burst above float). This difference was primarily due to type-1 launches having less helium in the weather balloon and, thus, less net lift force. The type-2 ascents caused the weather balloon to become over-pressurized at a lower altitude, resulting in the balloon bursting prior to reaching the float elevation. The average burst elevation of helium-assisted type-1 and type-2 was 22,500 ± 1,760 m and 14,300 ± 5,780 m, respectively, with the uncertainty equal to two standard deviations.

In contrast, type-1 ascents traveled at a steady velocity to an elevation above float elevation before the helium balloon burst. The drop in altitude after the helium balloon bursts is less for type-2 as it still has lift and has not reached the neutral buoyancy point, whereas type-1 launches did not have enough lift to sustain float at the burst altitude and dropped elevation, as shown in Figure 15-17.

Bowman et al. [2] observed that the heliotropes reach maximum rise rate when they reach approximately two-thirds of their float elevation, and the rise rate oscillates with an amplitude of up to 1 m/s. These trends were consistent with those observed in the BASS 2021 flight campaign, as shown in Figure 15-18. Bowman et al. [2] previously noted differing ascent rates and hypothesized that this could depend on balloon configuration, which is likely most affected by the variability in the use of carbon to darken the balloon envelope. The BASS 2021 campaign used the same configuration for each launch, with the only exception being the lower total weight for four launches (see Table 1 of Swaim et al. [7]) due to the lower payload being cut during the launch and an inconsistency with the level of envelope darkness for the first half of the campaign, which was resolved starting on 3 Aug 2022 by having balloons re-darkened with higher quality air-float charcoal prior to launch.

5.1.2. Float

For the BASS 2021 flight campaign, the average float elevation of all flights was 19.3 km ± 2.0 km, where the variation is twice the standard deviation of the flight averages. The minimum and maximum average float elevations were 17.4 km and 22.2 km, respectively. While the standard deviation of average float elevations was relatively large, the fluctuations during an individual flight were much lower. Dividing the flights based on the total weight shows that the flights weighing 5.43 kg and 7.05 kg had average float altitudes of 20.7 km and 19.1 km, respectively. There also did not appear to be any significant impact on the launch method, with the average float elevation for ground, helium-augmented, and helium-assisted launches being 19.5 km, 19.4 km, and 19.0 km, respectively. Table A2 of Swaim et al. [7] provides a summary of the float's average and standard deviation for each balloon.

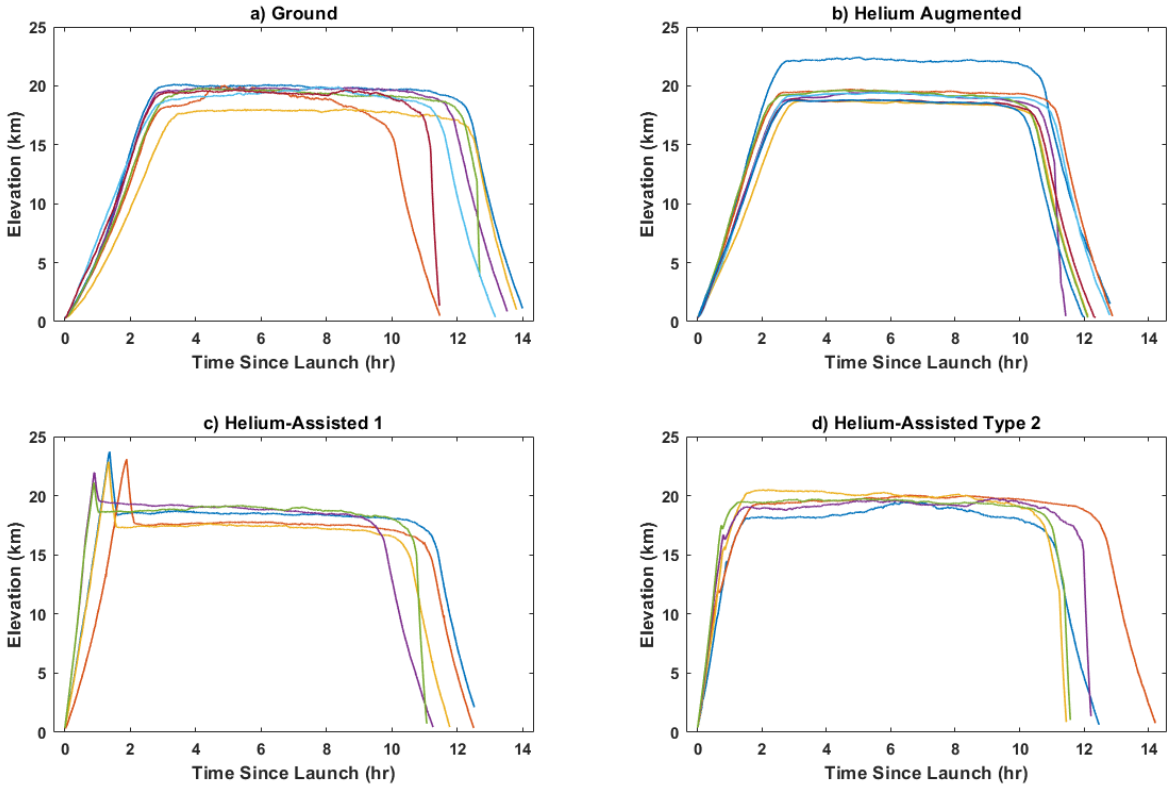


Figure 15-17: Launch sequence for (a) ground, (b) helium-augmented, (c) helium-assisted type-1, and (d) helium-assisted type-2. The time was measured from the time of launch for all flights. This figure is adapted from Swaim et al. [7].

Bowman et al. [2] identified some of the different behaviors that a heliotrope experiences during the float period: (i) steady altitude, (ii) gradual decrease through the flight, and (iii) upward excursions on the scale of an hour. Bowman et al. [2] also noted that any combination of these behaviors could be observed even with similar balloons launched at close to the same time. These three behaviors, either individually or in combination, were observed in the current study, and a few examples are shown in Figure 15-19. The gradual decrease behavior is apparent from examining the average elevation slope during the float periods. Most flights have an average slope of approximately -30 m/hr, but a few flights experience slopes of over -100 m/hr. For reference, flight 9.2, shown in Figure 15-19, had a slope of -129 m/hr during the float period.

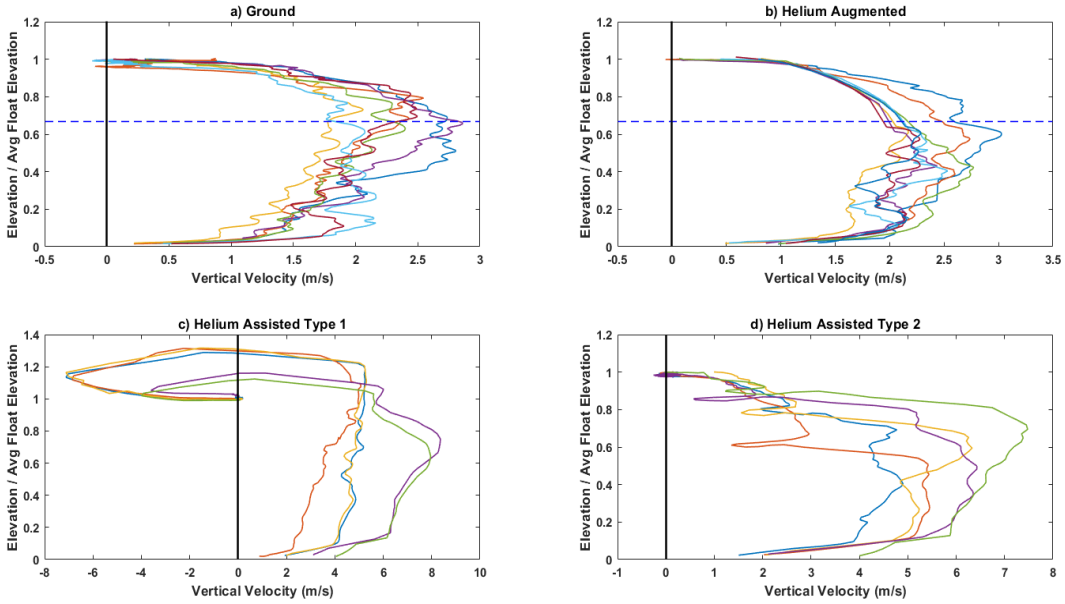


Figure 15-18: Vertical Velocity vs Elevation scaled by the float elevation during ascent for (a) ground, (b) helium augmented, (c) helium-assisted type-1, and (d) helium-assisted type-2. The blue dashed line marks two-thirds of the float elevation. A positive vertical velocity indicates the heliotrope ascending, while a negative vertical velocity indicates the heliotrope descending. This figure is adapted from Swaim et al. [7].

Higher-order statistics can provide a quantitative assessment of these qualitative descriptions. The skewness of the float altitude was negative for nearly every flight, indicating a long tail towards lower elevations. This is also apparent in Figure 15-19 for the steady elevation flight (flight 4.2), where most points are at higher elevations, with the lower elevation points having larger deviations from the mean. These deviations are due, in part, to the fact that the elevation consistently begins to decline gradually towards the end of the float period as sunset approaches. Kurtosis is another higher-order statistic that measures the tails of the distribution. The average kurtosis of all the flights was

4.3, indicating a kurtosis of three, which corresponds to a normal distribution. This result indicates that the tails of the distribution are, on average, slightly heavier than a normal distribution. There were three flights (4.2, 11.1, 11.2) that had significantly larger kurtosis (> 8) than the other flights, which is likely the result of the definitions for the onset and end of the float stage. This is evident in Figure 15-19, where a slight 4.2 is observed, indicating that the elevation was still increasing rapidly at the start of the float stage.

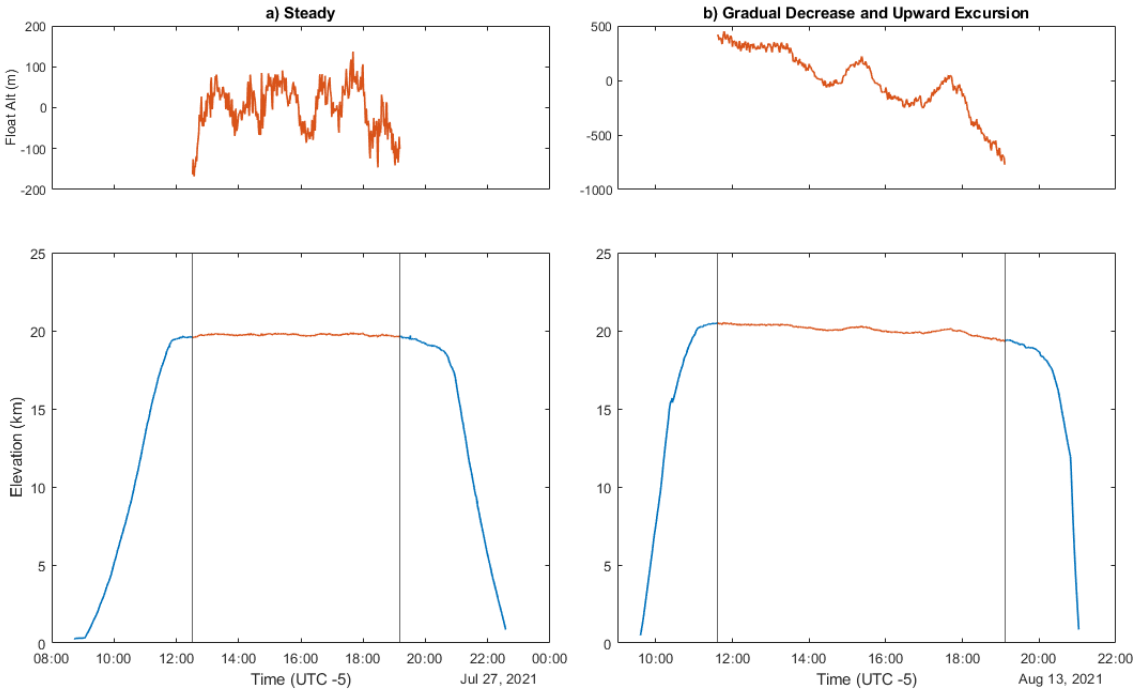


Figure 15-19: Examples of float behaviors observed during the BASS 2021 flight campaign with (a) Flight 4.2 experiencing a steady float altitude and (b) Flight 9.2 displaying both upward excursions and a gradual decrease in altitude during the float period. This figure is adapted from Swaim et al. [7].

Spectrograms of the altitude during the float stage show minimal frequency content with periods shorter than ~150 seconds. Spectral content was observed in every flight, with periods longer than ~150 seconds. Most flights showed elevated spectral content between 100 and 200 seconds. An example with consistent spectral content within this band and relatively weak spectral content outside of it is shown in Figure 15-20. Most flights exhibited larger spectral content with periods longer than 200 seconds, and the vertical oscillations appeared to be nonlinear at these longer periods. Bowman et al. [2] reported significantly non-linear oscillations with a period centered around 300 seconds. Bowman et al. [2] note that atmospheric gravity waves may induce vertical oscillations in heliotropes, leading to the heliotrope

ingesting or exhausting air during the oscillation cycle, contributing to the observed non-linear behavior at larger periods.

5.1.3. Descent and Landing

As the sun begins to set below the horizon, the heliotrope begins to descend. Solar irradiance levels begin to decline before civil sunset, causing the heliotrope to lose lift gradually and, consequently, descend in altitude. The descent began on average 36 ± 6 min before civil sunset. This is illustrated in Figure 15-21, which plots the sunset time (based on balloon location and altitude) and the start of the descent stage as a function of the day of the year. Comparing the slopes of the curve fits for the subset and descent stage onset reveals that the descent onset had a 6% shallower slope than the sunset, indicating a weak seasonal dependence. Note that the gradual decrease in sunset time indicates the seasonal variation of the sunset during the BASS 2021 flight campaign.

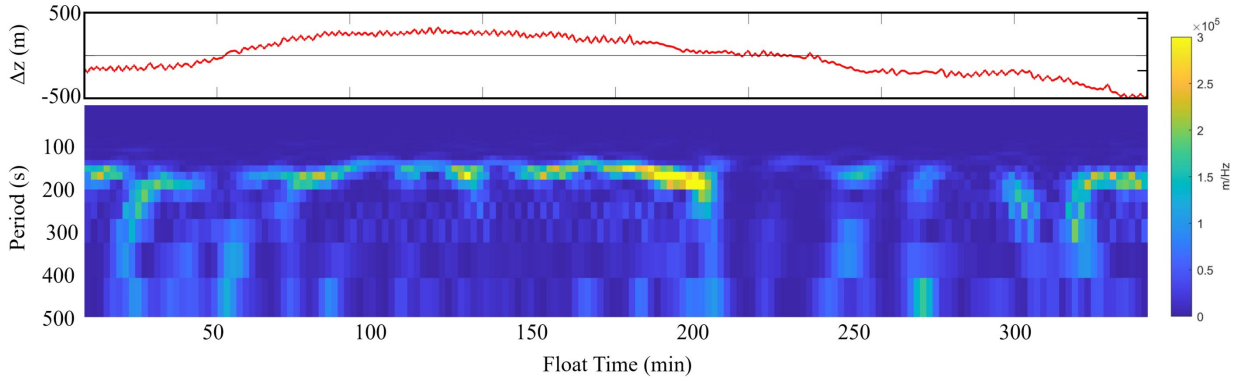


Figure 15-20: IMU data (top) time trace and (bottom) spectrogram of the vertical deviation from the average float altitude (Δz) *from the upper payload during the float period (Flight 16.1 of Swaim et al. [7]). The time is measured relative to the start of the float period. The color indicates the amplitude of altitude fluctuation at the corresponding period.*

During descent, the balloon envelope functioned as a drag skirt to slow the rate of descent and the impact speed. However, for a subset of flights (8 total), the envelope detached from the shroud ring during descent, resulting in higher descent rates and impact speeds, which have been classified as "hard landings." Table 15-2 summarizes the average descent rate, time to landing, and the average impact speed for nominal and hard landings, in which the hard landings are grouped based on the additional parachute(s) used. For the 20 nominal descents, the average descent rate was 2.8 ± 0.3 $m*s^{-1}$ with an average impact speed of 2.2 ± 0.26 $m*s^{-1}$. For the hard landings, the descent and impact speeds depended on the configuration of the redundant parachutes added to the flight line. The vertical variation during the descent for the nominal and hard landing cases is shown in Figure 15-22.

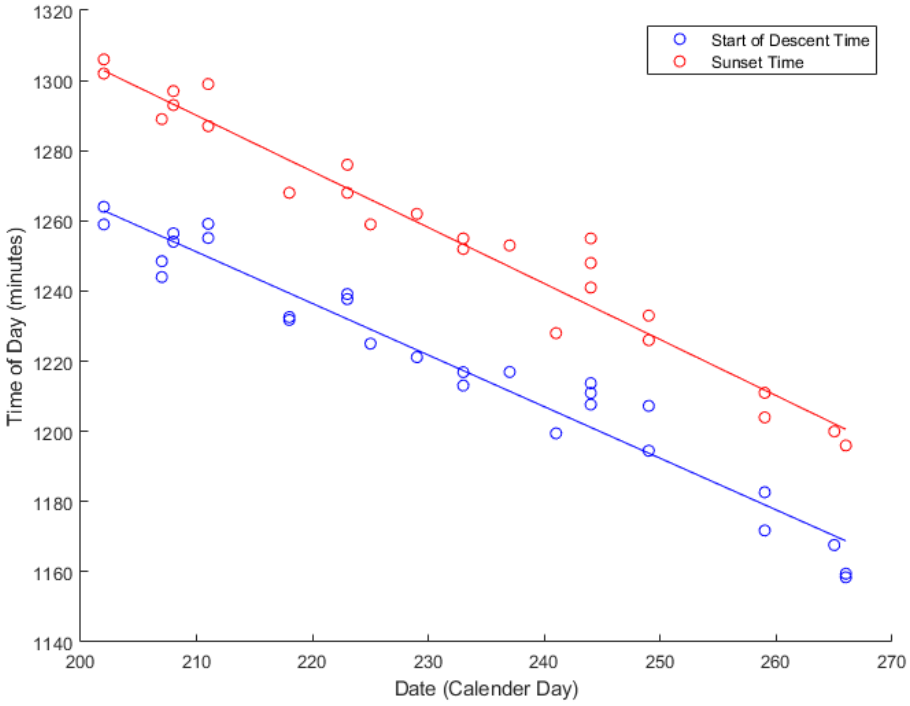


Figure 15-21: The civil twilight at the heliotrope location and altitude during the BASS 2021 flight campaign, and the onset of the descent stage as a function of the day of the year. Lines are the linear best-fit curves with slopes of -1.6 and -1.5 min/day for the sunset and descent onset, respectively. This figure is adapted from Swaim et al. [7].

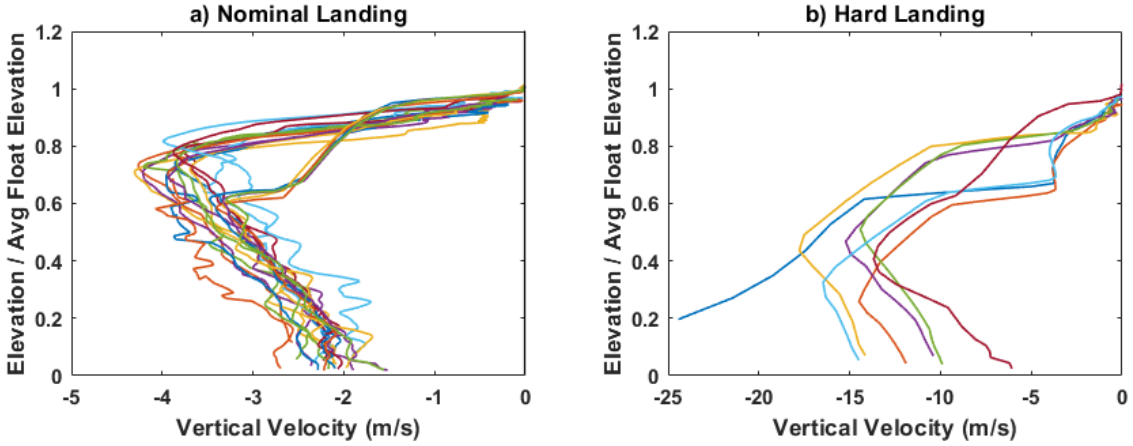


Figure 15-22: Vertical velocity as a function of elevation normalized by the float altitude during the descent stage for (a) nominal and (b) hard landings. Hard landings were descents that had the envelope separate from the flight line. This figure is adapted from Swaim et al. [7].

The landing outcome is dependent on the local terrain and ground wind speed. The envelope can drag the payloads some distance, but the envelope usually gets torn apart by the terrain. Landed balloons have occasionally launched themselves back into the air the following day if the envelope survives the night [7]. Every payload was successfully recovered, though some were more challenging than others. Some payloads were stuck in tall trees, and an arborist was required to recover them.

5.2. Altitude Control

Researchers at the University of Arizona developed and patented [48] a mechanical vent that mounts to the top of a heliotrope envelope. Further development by researchers at the U.S. Naval Research Laboratory enabled control over the outgassing of hot air [49,50], as shown in Figure 15-23. The vent is inspired by a flapping butterfly valve; the flaps are actuated downward into the balloon to prevent them from being exposed to external forces, such as wind and turbulence. The frame of the vent can be constructed from multiple inexpensive, lightweight materials, such as expanding polystyrene, low-density wood, and other composites. Additional weight savings can be achieved by using the balloon envelope material itself or other lightweight films for the bulk area of the vent. To mount a vent to the top of a heliotrope envelope, a hole matching the circumference of the vent was cut from the top of a standard 6m envelope, and then it was attached to the envelope using adhesive (such as glue, tape, or epoxy). Actuating the vent is accomplished with one or two high-torque servos mounted to the vent frame, and control rods connect the servo(s) to the flaps. Two methods have been demonstrated for powering and sending commands to the vent 1) A cable harness was run along the outside or through the center of the envelope, down the flight line, down to the gondola for power and control 2) A secondary independent power supply and short-range radio were mounted directly to the vent and contained within a Styrofoam housing for thermal regulation.

Schuler et al. demonstrated altitude control with four vented solar balloons (SHAB-Vs), “riding” varying wind flows and forming a square-like trajectory around Albuquerque in August 2022, as shown in Figure 15-24. These initial vented solar high-altitude balloon flights (SHAB-Vs) used simple PID control to maneuver to and maintain altitudes, as shown by SHAB12-V’s altitude and venting profile in Figure 15-25. The four balloons had six timed altitude set points throughout the flight, evenly spaced 1.5 hours apart. Due most likely to thunderstorms and increased albedo from the cloud top layer (along with possible updrafts and downdrafts), SHAB12-V was unable to reach full descent velocity under 17.5 km, unlike previous flight campaigns. The zoomed-in portion of Figure 15-25 shows that, on average, SHAB12-V oscillated between ±75m at the various altitude set points. These oscillations at altitude are similar in performance to the natural oscillations of unvented solar balloons at float altitude, as previously discussed.

Table 15-2: Average descent rate, time to landing, and speed impact for nominal descents and hard landings. The hard landings were caused by envelope separation from the flight line.

	Descent Rate (m/s)		Time to Land (min)		Impact Speed (m/s)	
	Avg	Std	Avg	Std	Avg	Std
Nominal	2.8	0.3	91	19	2.2	0.26
Hard Landing (drag skirt)	3.7	--	30	--	27.0	--
Hard Landing (drag skirt and small parachutes)	3.8	0.3	29	1.3	12.0	2.2
Hard Landing (drag skirt and large parachute)	3.2	--	41	--	6.2	--



Figure 15-23: Mechanical Vent attached to a heliotrope on August 22, 2025 (Schuler et al. [50] before launch in Belen, New Mexico.

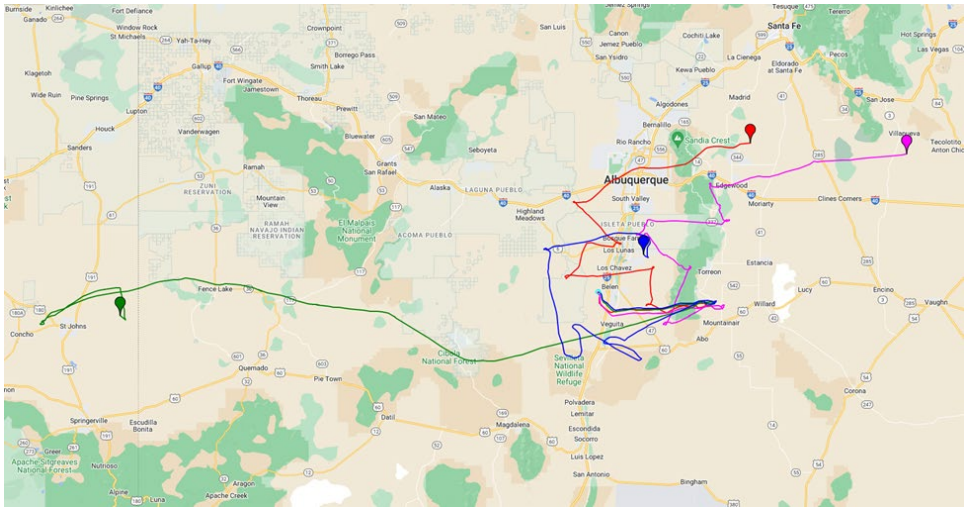


Figure 15-24: Map of four SHAB-V flights launched back-to-back 15 minutes apart. SHAB12-V is red, SHAB13-V is magenta, SHAB14-V is green (and did not vent), SHAB15-V is blue in Albuquerque, New Mexico in August 2022 [50].

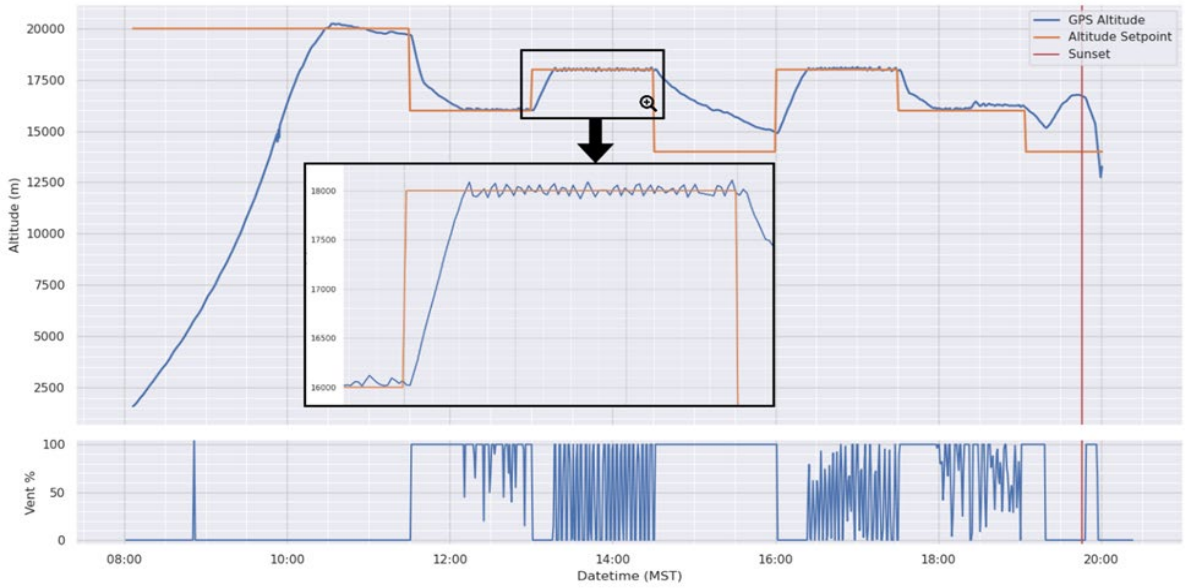


Figure 15-25: Altitude profile of SHAB12-V using P-D control to maneuver to 6 altitude set points during a flight campaign in Albuquerque, New Mexico, in August 2022 [50]. Some lower altitude setpoints were unobtainable, most likely due to thunderstorms in the area.

5.3. Flight Tracking and Communications

Flight tracking is rarely a primary measurement, but it is routine and can provide valuable information during processing. Most instrumented heliotrope flights have some form of GPS tracking (e.g., [6, 19-21, 43, 44]). A relatively standard configuration includes a method for real-

time tracking, as well as a more precise means of identifying the final landing location. Real-time balloon location and altitude monitoring are typically performed using the Automatic Packet Reporting System (APRS), an amateur radio community (HAM) protocol that enables real-time GPS tracking. Using the APRS system requires that at least one team member hold a ham radio technician license, as mandated by U.S. law. In the United States, APRS enables real-time GPS tracking on the 144.39 MHz band. It is common to embed additional measurements, such as sensor temperature and pressure, within these signals. The APRS tracking data can be viewed in real time via a web-based interface (https://aprs.fi/). APRS trackers, such as the High-Altitude Science StratoTrack and the QRP Labs Light APRS tracker, are routinely used on heliotropes (e.g., [7, 10, 22, 25, 43, 44]).

However, APRS trackers are line-of-sight measurements, typically losing the signal once it is a few kilometers above the ground. The altitude at which the APRS tracking will be lost depends on the configuration of the receiver network within the vicinity of the landing location. Hence, it is standard practice (e.g., [4, 6, 7, 10, 20, 22, 25, 43]) to include a satellite tracker (e.g. SPOT TRACE) that can provide a precise position of the final landing location. The ballooning team at Oklahoma State University typically uses the satellite tracker configuration to ping automatically at a specified time every day, as recommended by colleagues at Sandia National Laboratories, and ping whenever movement has stopped for at least five minutes. Thus, GPS coordinates would be sent nominally five minutes after landing, and if anything moves the payload due to atmospheric, animal, or human causes.

Both the APRS and satellite trackers would be a form of external communication (i.e., communication from the heliotrope to an external receiver). Ongoing work is improving the transmission and reception of external communications [43-45]. While these developing communications transmit real-time data (like the APRS signals), they also enable the control of heliotrope movement. Schuler et al. [43, 44] utilized a satellite Iridium module to communicate with a ground station, which was used to control a vent (e.g., [46]) located at the top of the heliotrope. Another method of internal communication between the gondola and the vent was achieved using an XBee 2.6 GHz radio, allowing for external altitude control. Yap [45] provides preliminary work using long-range (LoRa) radio communications as a means of communication between heliotropes, which, when combined with Schuler et al. [43, 44] altitude control, would enable control of the separation distance between balloons.

6. Conclusion

Solar balloons, or heliotropes, have rapidly evolved from simple hobbyist designs to scientifically robust tools for atmospheric exploration. Through physics-based modeling, standardized construction techniques, and refined operational protocols, these platforms now offer reliable access to the lower stratosphere for multi-hour, kilogram-scale payload missions at minimal cost.

Field campaigns, particularly BASS 2021, have demonstrated the scalability and repeatability of heliotrope flights, enabling detailed characterization of ascent profiles, float dynamics, and descent behaviors across diverse environmental conditions and launch methods. The development of helium-augmented and helium-assisted launch strategies has further expanded operational flexibility, while emerging technologies for active altitude control promise new capabilities for targeted measurements and adaptive mission profiles.

With growing applications in infrasound detection, atmospheric sensing, radiation monitoring, and solar research, heliotropes represent a democratization of high-altitude ballooning—accessible to universities, small research teams, and citizen scientists alike. Future advancements in materials, flight control, and sensor integration will likely enhance performance, reliability, and scientific return, ensuring that solar balloons remain a key asset in Earth and atmospheric sciences.

References

[1] D. Kramer, "Helium users are at the mercy of suppliers," *Physics Today*, vol. 72, no. 4, pp. 26-29, 2019, doi: 10.1063/PT.3.4181.

[2] D. C. Bowman et al., "Multihour stratospheric flights with the heliotrope solar hot-air balloon," *Journal of Atmospheric and Oceanic Technology*, vol. 37, no. 6, pp. 1051–1066, 2020, doi: 10.1175/JTECH-D-19-0175.1.

[3] Q. Brissaud et al., "The first detection of an earthquake from a balloon using its acoustic signature," *Geophysical Research Letters*, vol. 48, no. 12, e2021GL093013, 2021, doi: 10.1029/2021gl093013.

[4] D. C. Bowman and S. Krishnamoorthy, "Infrasound from a buried chemical explosion recorded on a balloon in the lower stratosphere," *Geophysical Research Letters*, vol. 48, no. 21, e2021GL094861, 2021, doi: 10.1029/2021GL094861.

[5] T. K. Schuler, D. C. Bowman, J. S. Izraelevitz, D. Sofge, and J. Thangavelautham, "Long duration flights in Venus' atmosphere using passive solar hot air balloons," *Acta Astronautica*, vol. 191, pp. 160-168, 2022, doi: 10.1016/j.actaastro.2021.10.030.

[6] E. A. Silber, D. C. Bowman, and M. Ronac Giannone, "Detection of the large surface explosion coupling experiment by a sparse network of balloon-borne infrasound sensors," *Remote Sensing*, vol. 15, no. 2, 542, 2023, doi: 10.3390/rs15020542.

[7] T. D. Swaim et al., "Performance characterization of heliotrope solar hot-air balloons during multihour stratospheric flights," *Journal of Atmospheric and Oceanic Technology*, vol. 41, no. 4, pp. 357-373, 2024, doi: 10.1175/JTECH-D-23-0091.1.

[8] E. A. Silber, D. C. Bowman, C. G. Carr, D. P. Eisenberg, B. R. Elbing, et al., "Geophysical observations of the 24 September 2023 OSIRIS-REx sample return capsule reentry," *Planetary Science Journal*, vol. 5, no. 9, 213, 2024, doi: 10.3847/PSJ/ad5b5e.

[9] T. Schuler, "Solar balloons – an aerial platform for planetary exploration," M.S. Thesis, Aerospace and Mechanical Engineering, University of Arizona, Tucson, AZ, 2020.

[10] E. Hough, "Design and operations of multihour stratospheric solar hot air balloons," M.S. Thesis, Mechanical and Aerospace Engineering, Oklahoma State University, Stillwater, OK, 2023.

[11] R. Farley, "BalloonAscent: 3-D simulation tool for the ascent and float of high-altitude balloons," in *AIAA Aviation*, AIAA2005-7412, Arlington, VA, Sep. 26-28, 2005, doi: 10.2514/6.2005-7412.

[12] F. Kreith and J. F. Kreider, "Numerical prediction, of the performance of high altitude balloons," NCAR Technical Note, NCAR-TN/STR-65, 1974, doi: 10.5065/D64X55SR.

[13] J.-J. Wu and J. Jone, "Performance model for reversible fluid balloons," in *11th Lighter-than-Air Systems Technology Conference*, AIAA-95-1608-CP, p. 1608, 1995, doi: 10.2514/6.1995-1608.

[14] Q. Dai, X. Fang, X. Li, and L. Tian, "Performance simulation of high altitude scientific balloons," *Advances in Space Research*, vol. 49, no. 6, pp. 1045-1052, 2012, doi: 10.1016/j.asr.2011.12.026.

[15] L. Carlson and W. Horn, "A new thermal and trajectory model for high altitude balloons," *Journal of Aircraft*, vol. 20, no. 6, pp. 500-507, 1983, doi: 10.2514/6.1981-1926.

[16] E. Hough et al., "Solar balloon development for high altitude observations," in *AIAA Aviation*, AIAA2022-4113, Chicago, IL, Jun. 27–Jul. 1, 2022, doi: 10.2514/6.2022-4113.

[17] D. C. Bowman, "How to build a heliotrope solar hot air balloon," Sandia Technical Report, SAND2020-3763R, 2020, doi: 10.2172/1608516.

[18] A. Greig, "CUSF landing predictor 2.5," Cambridge University Space Flight, Cambridge University, Mar. 2010. [Online]. [Accessed: Aug. 11, 2024].

[19] E. F. Young et al., "Explosion-generated infrasound recorded on ground and airborne microbarometers at regional distances," *Seismological Research Letters*, vol. 89, no. 4, pp. 1497–1506, 2018, doi: 10.1785/0220180038.

[20] D. C. Bowman and S. A. Albert, "Acoustic event location and background noise characterization on a free flying infrasound sensor network in the stratosphere," *Geophysical Journal International*, vol. 213, no. 3, pp. 1524–1535, 2018, doi: 10.1093/gji/ggy069.

[21] S. A. Albert, D. C. Bowman, E. A. Silber, and F. K. Dannemann Dugick, "The AtmoSOFAR channel: First direct observations of an elevated acoustic duct," *Earth and Space Science*, vol. 10, no. 10, e2023EA003149, 2023, doi: 10.1029/2023EA003149.

[22] T. Swaim, K. Spillman, E. Hough, Z. Yap, J. Jacob, and B. R. Elbing, "Development and evaluation of windscreen designs for high altitude balloons," *Proceedings of Meetings on Acoustics*, vol. 51, no. 1, 040002, 2023, doi: 10.1121/2.0001785.

[23] D. C. Bowman, S. Krishnamoorthy, E. A. Silber, S. K. Popenhagen, and M. A. Garces, "Airborne acoustic observations of the OSIRIS-REx reentry," in *Seismological Society of America Annual Meeting*, Anchorage, AK, Apr. 29-May 3, 2024.

[24] L. B. Wheeler et al., "LDRD project end report: Releasing, detecting, and modeling trace aerosols and gases in the earth's stratosphere," Sandia Technical Report, SAND2022-14965, 2022.

[25] M. Fathepure, N. Wang, J. Clemmons, and J. D. Jacob, "Evaluating high altitude impacts of solar cell performance with high altitude balloons," in *AIAA SCITECH 2024 Forum*, AIAA2024-0728, Orlando, FL, Jan. 8-12, 2024, doi: 10.2514/6.2024-0728.

[26] E. Hough, Z. Yap, K. B. Spillman, B. R. Elbing, and J. D. Jacob, "Solar balloon observations of the 2024 North American eclipse," in *AIAA Aviation Forum*, AIAA2024-3895, Las Vegas, NV, Jul. 29-Aug. 2, 2024, doi: 10.2514/6.2024-3895.

[27] O. D. Lamb, J. M. Lees, and D. C. Bowman, "Detecting lightning infrasound using a high-altitude balloon," *Geophysical Research Letters*, vol. 45, no. 14, pp. 7176-7183, 2018, doi: 10.1029/2018GL078401.

[28] D. C. Bowman and J. M. Lees, "Infrasound in the middle stratosphere measured with a free-flying acoustic array," *Geophysical Research Letters*, vol. 42, no. 22, pp. 10,010-10,017, 2015, doi: 10.1002/2015GL066570.

[29] D. C. Bowman and J. M. Lees, "Direct measurement of the acoustic wave field in the stratosphere," in *2016 IEEE Aerospace Conference*, Big Sky, MT, 2016, pp. 1-7, doi: 10.1109/AERO.2016.7500701.

[30] D. C. Bowman and J. M. Lees, "A comparison of the ocean microbarom recorded on the ground and in the stratosphere," *Journal of Geophysical Research: Atmospheres*, vol. 122, no. 18, pp. 9773-9782, 2017, doi: 10.1002/2017JD026474.

[31] D. C. Bowman, "Airborne infrasound makes a splash," *Geophysical Research Letters*, vol. 48, no. 23, e2021GL096326, 2021, doi: 10.1029/2021GL094555.

[32] J. F. Anderson, J. B. Johnson, D. C. Bowman, and T. J. Ronan, "The Gem infrasound logger and custom-built instrumentation," *Seismological Research Letters*, vol. 89, no. 1, pp. 153-164, 2017, doi: 10.1785/0220170067.

[33] J. F. Anderson, K. S. Anderson, and T. Beschorner, "gemlog: Data conversion for the open-source gem infrasound logger," *Journal of Open Source Software*, vol. 8, no. 86, 5256, 2023, doi: 10.21105/joss.05256.

[34] B. B. Rosenblatt, J. B. Johnson, J. F. Anderson, K. Kim, and S. J. Gauvain, "Controls on the frequency content of near-source infrasound at open-vent volcanoes: A case study from Volcán Villarrica, Chile," *Bulletin of Volcanology*, vol. 84, no. 12, 103, 2022, doi: 10.1007/s00445-022-01607-y.

[35] G. Averbuch, M. Ronac-Giannone, S. Arrowsmith, and J. F. Anderson, "Evidence for short temporal atmospheric variations observed by infrasonic signals: 1. The troposphere," *Earth and Space Science*, vol. 9, no. 3, e2021EA002036, 2022, doi: 10.1029/2021ea002036.

[36] L. T. Scamfer and J. F. Anderson, "Exploring background noise with a large-N infrasound array: waterfalls, thunderstorms, and earthquakes," *Geophysical Research Letters*, vol. 50, no. 24, e2023GL104635, 2023, doi: 10.1029/2023GL104635.

[37] J. M. Larotonda and M. J. Townsend, "Data Release Report for the Source Physics Experiment Phase II: Dry Alluvium Geology Experiments (DAG-1 through DAG-4), Nevada National Security Site," Technical Report, DOE/NV/03624—1220, 2021.

[38] S. Krishnamoorthy et al., "Detection of artificially generated seismic signals using balloon-borne infrasound sensors," *Geophysical Research Letters*, vol. 45, no. 8, pp. 3393–3403, 2018, doi: 10.1002/2018GL077481.

[39] S. Krishnamoorthy et al., "Aerial seismology using balloon-based barometers," *IEEE Transactions on Geoscience and Remote Sensing*, vol. 57, no. 12, pp. 10191–10201, 2019, doi: 10.1109/TGRS.2019.2931831.

[40] S. Krishnamoorthy, D. C. Bowman, A. Komjathy, M. T. Pauken, and J. A. Cutts, "Origin and mitigation of wind noise on balloon-borne infrasound microbarometers," *Journal of the Acoustical Society of America*, vol. 148, no. 4, pp. 2361–2370, 2020, doi: 10.1121/10.0002356.

[41] J. D. Carmichael et al., "Persistent, 'mysterious' seismoacoustic signals reported in Oklahoma state during 2019," *Bulletin of the Seismological Society of America*, vol. 112, no. 1, pp. 553-574, 2022, doi: 10.1785/0120210145.

[42] T. C. Wilson, C. E. Petrin, and B. R. Elbing, "Infrasound and low-audible acoustic detections from a long-term microphone array deployment in Oklahoma," *Remote Sensing*, vol. 15, no. 5, 1455, 2023, doi: 10.3390/rs15051455.

[43] T. K. Schuler et al., "Solar high altitude balloons as a long duration controllable aerial platform," in *AIAA SCITECH 2022 Forum*, AIAA2022-0282, San Diego, CA, 2022, doi: 10.2514/6.2022-0282.

[44] T. Schuler, M. Debbins, M. Cobar, J. Thangavelautham, and D. Sofge, "Altitude control with vented solar high altitude balloons (SHAB-Vs)," in *2023 IEEE Aerospace Conference*, Big Sky, MT, 2023, pp. 1-11, doi: 10.1109/AERO55745.2023.10116024.

[45] Z. Yap, "Solar balloon communication and flight augmentation systems," M.S. Thesis, Mechanical and Aerospace Engineering, Oklahoma State University, Stillwater, OK, 2023.

[46] M. Debbins, T. Schuler, J. C. Goolsby, and J. Thangavelautham, "Solar hot air balloon vent," U.S. Patent 2025/0066008 A1, Feb. 27, 2025.

[47] D. C. Bowman et al., "Final report for 'Earth monitoring platforms in perpetual flight through solar/infrared ballooning technology'," Report No. SAND2204-11013, Sandia National Laboratories, 2024.

[48] M. Debbins, T. Schuler, D. Goolsby, J. Crest, and J. Thangavelautham, "Solar hot air balloon vent," U.S. Patent Application US20250066008A1, Jan. 5, 2023.

[49] T. K. Schuler et al., "Solar high altitude balloons as a long duration controllable aerial platform," in *AIAA SCITECH 2022 Forum*, AIAA2022-0282, San Diego, CA, 2022.

[50] T. Schuler, M. Debbins, M. Cobar, J. Thangavelautham, and D. Sofge, "Altitude control with vented solar high altitude balloons (SHAB-Vs)," in *2023 IEEE Aerospace Conference*, Big Sky, MT, 2023, pp. 1-11.

Chapter 16
Planetary Balloons

Jeffery L. Hall[1], Jacob S. Izraelevitz[1], James A. Cutts[1] and Michael T. Pauken[1]

[1] Jet Propulsion Laboratory, California Institute of Technology
This work was carried out at the Jet Propulsion Laboratory, California Institute of Technology, under a contract with the National Aeronautics and Space Administration (80NM0018D0004).

Table of Contents

1. Introduction 6

2. Planetary Environments 7

2.1. Atmosphere Modeling and Comparisons 9

2.2. Solar and IR Flux Data 13

2.2.1. Venus 13

2.2.2. Mars 18

2.2.3. Titan 19

3. General Design and Operational Drivers 20

4. Balloon Technology Details for Venus, Mars, and Titan 26

4.1. Venus 26

4.1.1. Super-pressure Helium Balloons 27

4.1.2. Variable-Altitude Phase-Change Fluid Balloon 29

4.1.3. Controllable, Variable-Altitude Helium Balloons 30

4.1.3.1. Balloon-in-a-Balloon Altitude Control 31

4.1.3.2. Mechanical Compression Balloons 34

4.1.4. Solar Montgolfière 35

4.2. Mars 35

4.3. Titan 39

4.3.1. Hot-air (Montgolfière) Type Balloons 39

4.3.2. Super-pressure Balloons 41

4.3.3. Blimp Aerobot Systems 41

4.3.4. Variable-Altitude Balloon Systems 43

4.4. Scientific Instrumentation 43

5. Conclusions 44

References..... 45

Table of Figures

Figure 16-1: VeGa Prototype Balloon..... 7

Figure 16-2: Atmospheric temperature and density profiles Venus, Earth, Mars, and Titan..... 12

Figure 16-3: Vertical structure of the Venus clouds as derived by the Venera and Pioneer Venus descent probes. The color lines show mean temperature profiles at low (red), middle (blue), and high (green) latitudes, with a single black line representing the temperature structure below 30 km. The typical vertical profile of aerosol extinction [20] is shown on the left. The static stability profile from the VIRA model [21] is shown in the middle. Reproduced from Figure 1 of Titov et al. [22]..... 14

Figure 16-4: Direct solar flux in the Venus atmosphere from 60 to 100 km for solar zenith up to 85°..... 16

Figure 16-5: Downward diffuse solar flux as a function of solar zenith angle and altitude..... 16

Figure 16-6: Upward diffuse solar flux as a function of zenith angle and altitude..... 17

Figure 16-7: IR Thermal flux as a function of altitude in the Venus atmosphere..... 17

Figure 16-8: Martian diurnal surface solar flux of the direct (B, blue line), diffuse (D, green line), and total (T, red line) at four different values of τ at the equator at Ls = 270° during the Northern Hemisphere winter solstice. The flux at the TOA (E) is represented by the black line..... 18

Figure 16-9: Titan thermal fluxes from Robinson's variable n Titan model [26]. Upwelling (F^+) and downwelling (F^-) fluxes (short dashed) are labeled, and their difference is the net thermal flux (long dashed). Also shown is the net thermal flux from a Titan radiative transfer model by Tomasko [27]..... 19

Figure 16-10: VeGa lander and balloon inflation tanks inside spherical aeroshell..... 21

Figure 16-11: VeGa lander and balloon atmospheric entry sequence [28] 22

Figure 16-12: The first 5.5 m prototype Venus balloon based on Vectran fabric and metalized Teflon film..... 28

Figure 16-13: Snapshots of parachute-assisted deployment and inflation of a Venus super-pressure balloon prototype. Top left – balloon after deployment. Bottom left – balloon nearly fully inflated. Right – balloon, tanks, and parachute approaching ground..... 29

Figure 16-14: Passive altitude cycling flight trajectory from an ALICE prototype..... 31

Figure 16-15: Balloon-in-balloon altitude control architecture for Venus, as described in the 2020 Venus Flagship Mission Study..... 33

Figure 16-16: Prototype variable altitude aerobot in at launch (left) and in flight (right) over Black Rock Desert, Nevada..... 33

Figure 16-17: Mechanical compression balloon, with tendon cable pole-to-pole for volume control. Prototype shown in top right..... 34

Figure 16-18: Mars “snake” balloon being tested in the California desert in 1990..... 36

Figure 16-19: Mars spherical helium super-pressure balloon top-down view during aerial deployment and inflation test in the Earth’s stratosphere [65]..... 38

Figure 16-20: Single wall Montgolfière cryogenic Titan balloon..... 40

Figure 16-21: Temperature profiles and stream functions inside a single-walled balloon on the left and a double-walled balloon on the right from the CFD-thermal model [70]..... 40

Figure 16-22: A 16-gore, 1.5-m diameter Titan (at 1kPa super-pressure) balloon prototype made using a 6-layer polyester film..... 42

Figure 16-23: Titan blimp aerobot under cryogenic flight test with insulated electric propeller motors..... 43

Table of Tables

Table 16-1: Parameters for Planetary Atmospheric Pressure and Density Calculations..... 11

Table of Symbols

Symbol	Definition	Dimension
A	Area (e.g., balloon surface)	L^2
C_p	Specific heat capacity (constant pressure)	$L^2T^{-2}\theta^{-1}$
E	Energy	ML^2T^{-2}
F	Force	MLT^{-2}
g	Gravitational acceleration	LT^{-2}
h	Altitude/height	L
k	Thermal conductivity	$MLT^{-3}\theta^{-1}$
M	Molar mass	M
m	Mass	M
P	Pressure	$ML^{-1}T^{-2}$
Q	Heat	ML^2T^{-2}
R	Specific gas constant	$L^2T^{-2}\theta^{-1}$
T	Temperature	θ
t	Time	T
V	Volume	L^3
v	Velocity	LT^{-1}
α	Absorptivity	–
ε	Emissivity	–
ρ	Density	ML^{-3}
σ	Stefan–Boltzmann constant	$MT^{-3}\theta^{-4}$

1. Introduction

In June 1985, the Soviet Union successfully flew two balloons in the atmosphere of Venus - one each as part of the VeGa-1 and VeGa-2 missions, as illustrated in Figure 16-1. They were identical 3.5 m diameter helium-filled super-pressure balloons that flew for approximately 46 hours each at an altitude between 50 and 53 kilometers in the clouds of Venus. The balloons arrived in darkness near the equator and traveled almost a third of the way around the planet, moved by the prevailing high-speed equatorial winds at that altitude. The balloons carried a 7 kg gondola that featured miniaturized instruments to measure pressure, temperature, vertical wind, solar illumination, and cloud particle backscatter. Data was radioed back to Earth at a rate of 1 to 4 bits per second, resulting in a small but valuable data return. Balloon longitude was determined by Doppler tracking of the radio signal from Earth's ground-based radio antennas. Both balloons crossed the night-to-day terminator at approximately 35 hours elapsed time and continued flying to the 46-hour mark. At that point, electrical power became exhausted, and radio contact was lost. Details on this highly successful pair of balloon missions can be found in a series of reports published in the journal Science in 1986 [1], [2], [3], [4] [5], [6], [7]. To date, these are the only balloons to have flown on another planet.

Concepts for balloons to fly on other planets date back to the early days of space exploration. Jacques Blamont first presented the idea of exploring Venus with a balloon in 1967 as a possible collaboration between France and the Soviet Union [1], [8]. Work by the two countries on Venus balloon concepts continued for many years, culminating in the VeGa missions in 1985. The Voyager-1 spacecraft's flyby of Saturn’s moon Titan in 1980 revealed that it had a thick nitrogen atmosphere, which prompted an early study of using a balloon to explore that world [9]. Concepts for flying a balloon in the thin atmosphere of Mars date back at least to the mid-1980s, when France and the Soviet Union collaborated on a space mission that would have launched in 1994 [10]. The motivation for flying a balloon in mission concepts is to conduct a scientific investigation of the atmosphere and/or surface during a long-range traverse while consuming minimal or zero power to generate lift. Using buoyancy to fly is particularly appealing for space missions, given the general scarcity of available power at other planetary destinations and the high energy demands of powered flight.

Every type of balloon developed and flown on Earth can, in principle, be adapted and used to fly on another planet. This includes the standard workhorses of zero-pressure, super-pressure, and hot-air balloons. The published literature over the past few decades is filled with examples of this planetary balloon diversity.

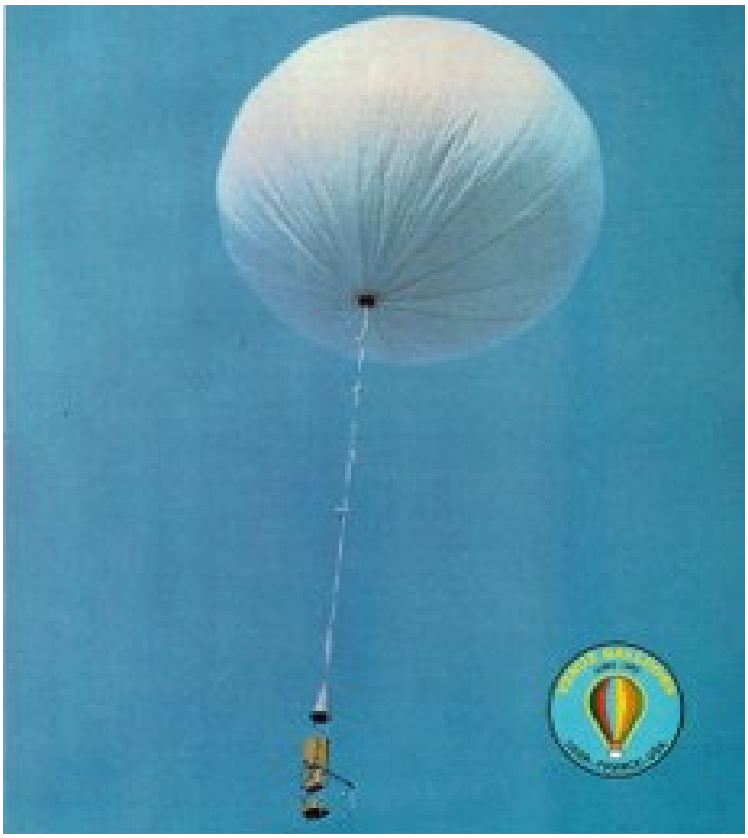


Figure 16-1: VeGa Prototype Balloon

A central theme of planetary balloons is that the atmosphere of each extraterrestrial body is different, thus driving specific design choices and adaptations. The next section will describe different planetary environments, followed by a section that explains how these environments influence balloon design choices in conjunction with other significant space mission constraints. The chapter then closes with a survey of historical planetary balloon prototypes and associated technical advances, grouped by target planet, to provide the reader with an overview of the field.

2. Planetary Environments

The atmospheric properties of temperature, pressure, density, and gas composition have a significant impact on the design of balloons. These properties are different for the worlds beyond Earth. Venus, Mars, and Titan are the most viable extraterrestrial places for balloon exploration because they feature high molecular weight atmospheric gases that produce significant buoyancy with helium or hydrogen-filled balloons.

Venus has a thick atmosphere composed primarily of carbon dioxide (96.5%), with nitrogen (~3%) and trace amounts of other gases, including sulfur dioxide (SO_2) and water vapor. The carbon dioxide creates a

significant greenhouse effect, trapping heat and resulting in surface temperatures up to 460°C, making it the hottest planet in the solar system, hot enough to melt lead. At its surface, the Venusian atmosphere has a pressure of approximately 92 bars and a density of roughly 65 kg/m³. At approximately 52 km, the Venusian atmosphere attains an Earth-like density of 1.2 kg/m³. Venus's atmosphere contains thick layers of clouds composed of sulfuric acid aerosols over an altitude range of 47 to 70 kilometers. These clouds completely cover the planet and reflect a significant portion of the sunlight that reaches Venus, contributing to its high albedo (reflectivity). Despite Venus's slow retrograde rotation (it takes longer for Venus to complete one rotation on its axis than it does to orbit the Sun), its atmosphere experiences super rotation, characterized by extremely high-speed ground-relative winds in the mid-latitudes of this cloud region, reaching speeds of up to 360 km/h. Balloons swept around the planet in these high-altitude winds provide opportunities to investigate not only atmospheric chemistry and meteorology, but also geophysics and geology, taking advantage of the comparatively benign temperature conditions that permit the use of state-of-the-art instrumentation.

Like Venus, Mars has an atmosphere that is comprised mainly of carbon dioxide (95%), with a smaller amount of nitrogen (2.6%), and an added component of Argon (1.9%), rather than sulfur compounds and trace gases. Unlike Venus, Mars has wide fluctuations in temperature from -153°C at the poles at night to +20°C near the equator during the day, which is due to the fragile atmosphere (surface pressure of 6.1 mbar and surface density of 0.013 kg/m^3), thus not creating sufficient conditions to produce a greenhouse effect. As a result, temperature variations are influenced by factors such as elevation, season, and local geography. Mars experiences frequent - and sometimes massive - dust storms driven by strong winds that can cover large portions of the planet and last on the order of days or even months. These dust storms have significant effects on the Martian climate, temperature, and surface reflectivity. The challenges of heavier-than-air flight that result from this tenuous atmosphere have already been proven surmountable by the Ingenuity rotorcraft (with its 4-foot rotors and tissue box-sized fuselage), which made 72 flights but was constrained by the high power required for flight, resulting in flight no longer than a minute each. Future balloon flights on Mars would enable much longer flights over regional or global distances.

Titan, the largest moon of Saturn, has a dense atmosphere composed primarily of nitrogen (95%) and methane (5%), with trace amounts of other hydrocarbons and gases. Methane exists in both gaseous and liquid form on Titan, with methane clouds and lakes observed on its surface. Methane plays a crucial role in Titan's atmospheric chemistry, participating in complex photochemical reactions that produce a variety of organic molecules. Other hydrocarbons, such as ethane and propane, are formed

through the photolysis of methane. These hydrocarbons contribute to the haze layers in Titan's atmosphere and are thought to rain down onto the surface. The atmospheric temperature on Titan averages around -180°C at the surface. The surface pressure is 1.5 bars, and the surface density is 5.4 kg/m^3.

Exploring Titan offers a valuable opportunity to advance our understanding of planetary science and astrobiology. Titan is the only body in the solar system besides Earth known to have stable liquid on its surface [11]. Investigating the composition and behavior of these hydrocarbon lakes and seas can enhance our understanding of planetary geology and the potential for forms of life [12]. Titan's conditions could harbor exotic forms of life adapted to its cold, hydrocarbon-rich environment [13]. The Dragonfly rotorcraft, which is scheduled to arrive at Titan in the mid-2030s, will be limited, like its Martian predecessor, Ingenuity, to short and low-altitude flights. It is primarily focused on science obtained on the surface. Future lighter-than-air vehicles on Titan will not be as restricted in duration or altitude, enabling regional and global investigations.

2.1. Atmosphere Modeling and Comparisons

The US Standard Atmosphere is typically used as a reference for designing Earth balloons. Standard reference atmospheric profiles for Venus, Mars, and Titan balloon systems can be developed using scientific literature resources, and planetary mesoscale atmospheric models can be employed to create an initial design for the balloon system. Balloon performance during in-situ atmospheric missions would depend heavily upon diurnal, seasonal, and local temperature and pressure changes. Refer to Chapter 7 for information on the Earth's atmosphere.

It is convenient to model planetary atmospheric properties using temperature profiles, the barometric formula for calculating pressure, and the ideal gas law to determine the atmospheric density as a function of altitude in a planetary atmosphere. One can divide the atmosphere into vertical segments where the temperature changes linearly with altitude at a constant lapse rate. The lapse rate is the negative of the rate of temperature change with altitude. The relationship describing the hydrostatic pressure of a column of gas can be used to derive the following equation to compute the pressure of the atmosphere as a function of altitude for a non-zero lapse rate [14]:

$$P = P_b \left[1 - \frac{L_b}{T_b}(Z - Z_b)\right]^{\chi} \quad (16\text{-}1)$$

where the exponent term is: $\chi = \frac{g_0 \cdot M}{R \cdot L_b}$

P_b = reference pressure (Pa)
T_b = reference temperature (K)
L_b = temperature lapse rate (°C/m)
Z = altitude (m)
Z_b = reference altitude b (m)
R = universal gas constant: 8.314 J/(mol*K)
g_0 = gravitational acceleration (m/s^2)
M = molar mass of planetary atmospheric gas mixture (kg/mol)

There are certain regions in the atmosphere where the temperature changes very little with altitude. In these regions, the lapse rate is essentially zero, and the barometric equation simplifies to the hydrostatic pressure equation as follows:

$$P = P_b exp\left[\frac{-g_0 \cdot M(Z - Z_b)}{R \cdot T_b}\right] \quad (16\text{-}2)$$

The local atmospheric gas mixture density, ρ, is determined by the ideal gas law using absolute temperature units:

$$\rho = \frac{P \cdot M}{R \cdot T} \quad (16\text{-}3)$$

Numerous detailed data sources exist for planetary atmospheres, with some variation between them. The Venus atmospheric properties can be found in the "Venus International Reference Atmosphere (VIRA)" [15] up to an altitude of 100 km. This standard profile is based on data collected by Soviet Venera Landers and the U.S. Pioneer Venus probes. Earth's atmospheric data is based on the International Standard Atmosphere, a common reference for temperature, pressure, and density profiles published by ISO 2533:1975. Data for the Mars atmosphere is based on Reference [16], which used models of the Mars atmosphere to design the entry, descent, and landing of the Mars 2020 mission. The models were compared to post-flight data analysis and contain tabulated data on pressure, temperature, and density. The Titan atmospheric data is based on analysis of measurements made by the Huygens probe [17].

The following table provides data for approximately calculating atmospheric pressure and density as a function of altitude using a multilayer model for Venus, Earth, Mars, and Titan, based on Equations (16-1)-(16-3).

Table 16-1: Parameters for Planetary Atmospheric Pressure and Density Calculations

Quantity	Base altitude	Base Temp	Lapse Rate	Base Pressure	Base density	Barometric Exponent value	Molar Mass	Gravity
Variable	Z_b	T_b	L_b	P_b	ρ	χ	M	g
Units	m	K	°C/m	Pa	kg/m^3		kg/mol	m/s^2
Planet Layer								
Venus 1	0	737	0.00773	9210000	65.3	5.9965	0.04345	8.87
Venus 2	50000	350	0.00877	107000	1.59	5.2854		
Venus 3	60000	262	0.00311	23600	0.46	14.9046		
Venus 4	90000	169	-0.00188	37	0.001	-24.6559		
Earth 1	0	288	0.0065	101325	1.22	5.2575	0.02896	9.81
Earth 2	11000	216	0	22632	0.364	0		
Earth 3	20000	216	-0.001	5475	0.088	-34.174		
Earth 4	32000	228	-0.0028	868	0.0132	-12.205		
Mars 1	0	223	0.00419	586	0.0137	4.615	0.04334	3.71
Mars 2	1500	218	0.000897	513	0.0123	21.56		
Mars 3	5000	215	0.002205	375	0.00912	8.770		
Mars 4	10000	204	0.002205	236	0.00605	8.770		
Titan 1	0	93	0.000929	149000	5.40	4.9105	0.028	1.354
Titan 2	14000	80	0.000385	71200	3.00	11.8554		
Titan 3	40000	70	-0.00025	15500	0.75	-18.2391		
Titan 4	60000	75	-0.00255	4710	0.21	-1.7881		
Titan 5	80000	126	-0.00088	1980	0.053	-5.1677		

The data in Table 16-1 was used to produce the plots of atmospheric temperature and density in Figure 16-2 for altitudes most likely to be of interest to balloon system designs for Venus, Earth, Mars, and Titan, for side-by-side comparisons. Density is plotted on a log scale to account for the exponential decrease in pressure with varying altitudes, whereas the temperature profile is on a linear scale. Key points of comparison and contrast for this atmospheric data include:

- The extraordinarily high temperature (460°C) and pressure (92 atm) found at the surface of Venus.
- The very low pressure (586 Pa) found at the surface of Mars.
- The cryogenically cold temperature (93 K) found at the surface of Titan.
- The gradual decrease in pressure and density with altitude (scale height) at Titan, compared to the other planets, primarily resulting from lower gravity.
- The much more extended atmospheres for Venus and Titan have the same ~0.1 kg/m^3 density at 70 km altitude, which occurs at only 20 km at Earth.

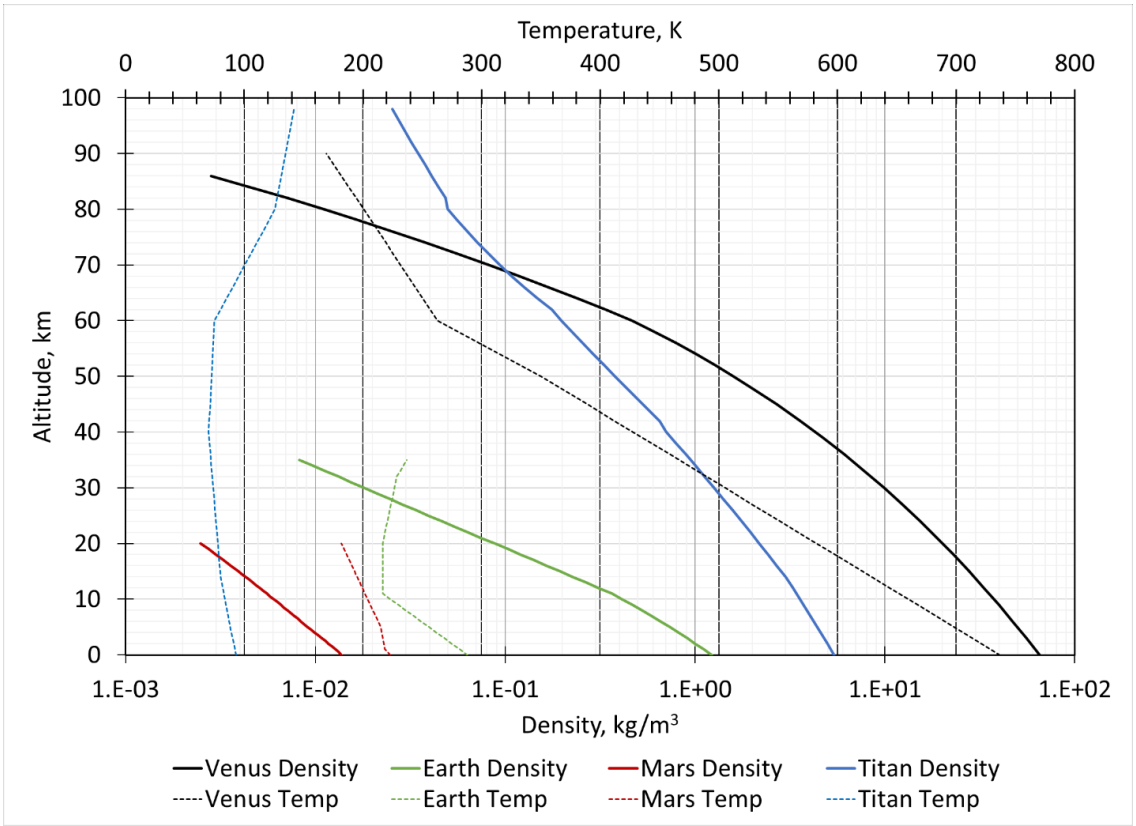


Figure 16-2: Atmospheric temperature and density profiles Venus, Earth, Mars, and Titan.

2.2. Solar and IR Flux Data

The heat balance on balloons is often driven by radiative heat transfer, changing the temperature and, therefore, the buoyancy of the internal lifting gas at different times of day or transmission conditions. Accordingly, the inclusion of solar and IR fluxes can be of equal importance in balloon design as the pressure and temperature. Solar radiation is also a good option for an extended power source for planetary balloons designed to operate for more than a few days. Refer to Chapter 5 for more information on thermal balance for terrestrial ballooning.

The solar environments of the three planetary targets of interest are quite divergent, with Venus experiencing approximately 200%, Mars about 50%, and Titan just 1% of the solar insolation of the Earth. Seasonal effects are also quite divergent, with Venus's axial tilt only 2.7 degrees relative to the Earth's 23.4 degrees, meaning that it effectively has no seasons. Mars has an axial tilt of 25 degrees and a year length of 687 Earth days. Titan, tidally locked to Saturn, experiences identical seasons with an axial tilt of 27 degrees and a year length of 29 Earth years. Further details for each of these three worlds are provided below.

2.2.1. Venus

The optical properties of the Venusian atmosphere have been characterized by both in-situ and remote sensing missions. The upper cloud layer appears to be very stable, with little variation in time and location, but other parts of the cloud and haze layers have shown considerable variation. A diagram depicting the Venus cloud layers appears in Figure 16-3.

For Venus, a treatment of thermal flux profiles using radiative transfer modeling techniques was published by Crisp in 1989 [18]. The most recent atmospheric radiation modeling effort utilizes a linearized flux evolution technique to determine flux values from a full-physics radiative transfer model. This approach has been applied to numerous planetary atmospheres, as developed in Reference [19]. In this technique, the atmosphere is divided into multiple constant-pressure layers, which reflect and transmit light in the upward and downward directions. *Ragent et al.* [20] provide detailed model predictions for solar and IR flux, emphasizing the particulate matter in the Venusian atmosphere. Results for these models are shown in Figure 16-4 through Figure 16-7.

In the upper atmosphere, the total solar load includes direct solar and diffuse solar components (downwelling and upwelling). The summation of the direct and diffuse downward solar flux exceeds the incoming solar flux at the TOA (Top of the Atmosphere). The abundance of upward and

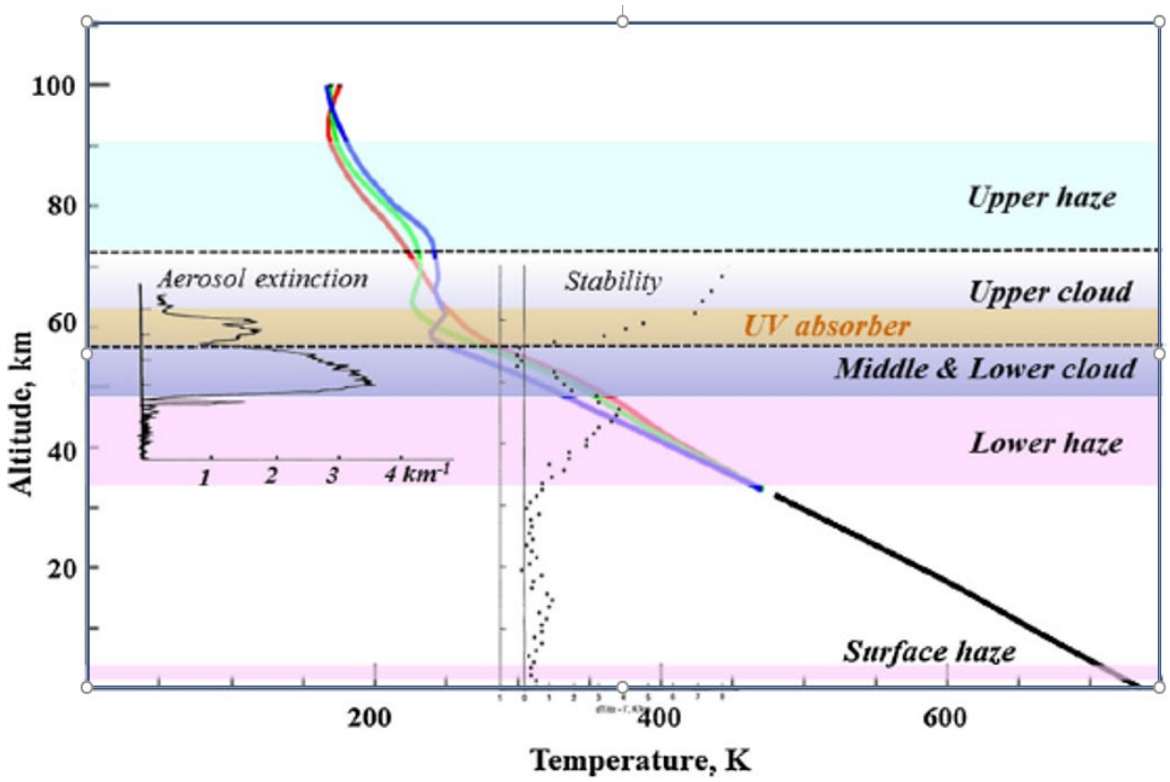


Figure 16-3: Vertical structure of the Venus clouds as derived by the Venera and Pioneer Venus descent probes. The color lines show mean temperature profiles at low (red), middle (blue), and high (green) latitudes, with a single black line representing the temperature structure below 30 km. The typical vertical profile of aerosol extinction [20] is shown on the left. The static stability profile from the VIRA model [21] is shown in the middle. Reproduced from Figure 1 of Titov et al. [22].

downward solar flux is due to the multiple reflections that occur between the upward and downward diffuse flux components. Below an altitude of 65 km (i.e., the middle cloud layer), the direct solar flux contribution is negligible and thus may be approximated as zero. Above 65 km, the direct solar flux, ϕ, as shown in Figure 16-4, may be calculated for a solar zenith angle (θ) and pressure (P) at a given altitude (Z) using the following equation. This relation is applicable over an altitude range of 65 to 100 km and solar zenith angles up to 85°.

$$\Phi_{Dir}(\theta, P) = \Phi(TOA) * \cos(\theta) * exp^{\frac{-\tau(0,P)}{\cos(\theta)}} \qquad (16\text{-}4)$$

In this equation, the variable τ is the column-integrated extinction optical depth between TOA (i.e., P = 0) and a non-zero pressure level (P) at a given altitude. The extinction optical depth of the Venus clouds can be found in Figures 3-4(b) in Ref. [20]. From these data, the optical depth as a function of pressure P (in Bar) for the Venus atmosphere is expressed using an exponential fit of the form shown in Equation as:

$$\tau(0,P) = 47.46 * P^{[1.052]} \quad (16\text{-}5)$$

Cloud layers in the atmosphere create significant diffuse components of downward and upward solar flux. Figure 16-5 and Figure 16-6 show diffuse downward and upward solar flux (respectively) as a function of the altitude and solar zenith angle.

The change in solar flux shown in Figure 16-4 through Figure 16-6 The various altitudes correspond to different cloud particle densities. At the base of the cloud layer, ~47 km above the surface, there is an inflection point in the solar flux curves as the cloud disappears. Below this point, the downward flux decreases more slowly with depth, primarily due to Rayleigh scattering. The flux increases more rapidly with depth as the atmospheric density increases. The difference between the downward flux and the reflected upward flux at a given altitude and solar zenith angle is equal to the sum of the solar flux absorbed by the atmosphere below that location and by the surface of the planet.

The thermal flux profile in the IR spectrum is shown in Figure 16-7. Above the cloud tops at approximately 70 km, the upward IR flux is constant due to the lack of attenuation by Rayleigh scattering. The temperature of the sky, which is a function of the integrated optical depth to the top of the atmosphere, governs the downward IR flux until the cloud layer is reached. Below the cloud layer, the intense heat from the surface results in high IR flux values as the surface is approached. On the night side of the planet, the solar flux values are effectively zero. However, the IR thermal flux values shown in Figure 16-7 remain as environmental thermal loads.

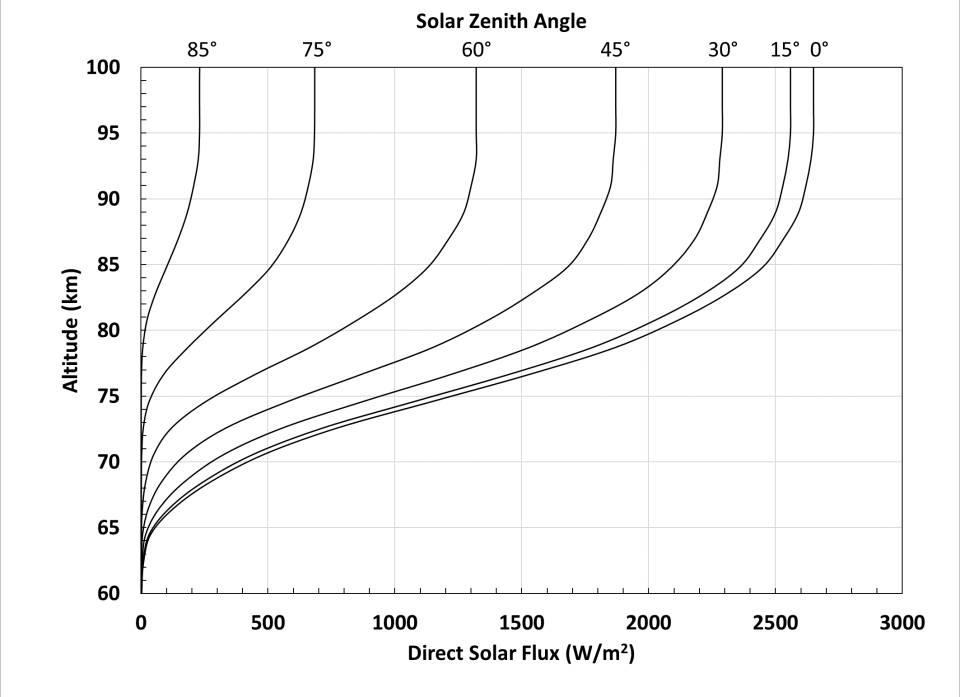


Figure 16-4: Direct solar flux in the Venus atmosphere from 60 to 100 km for solar zenith up to 85°.

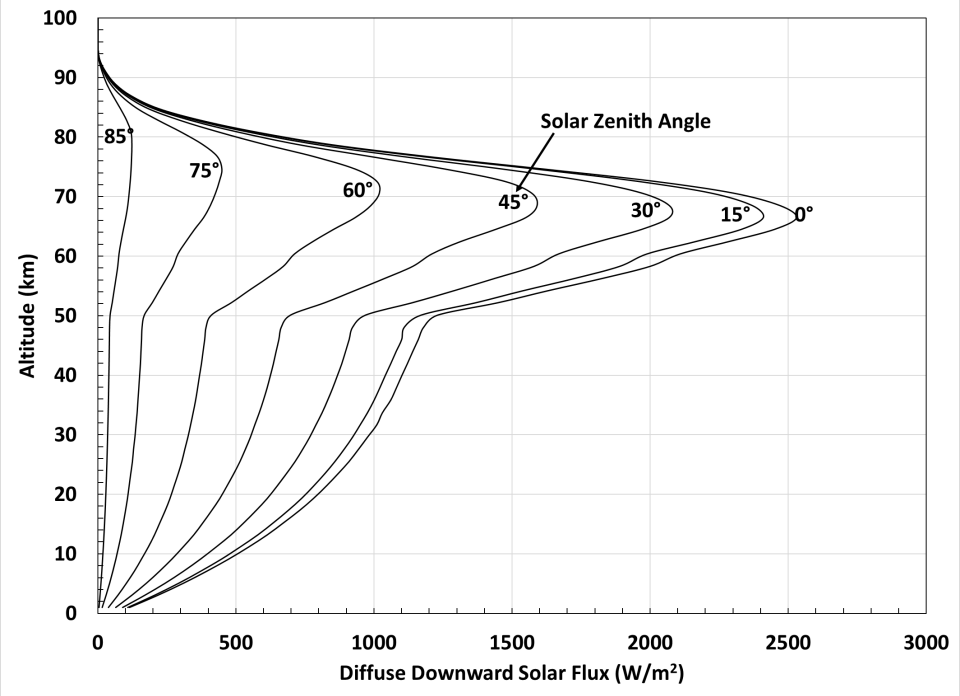


Figure 16-5: Downward diffuse solar flux as a function of solar zenith angle and altitude.

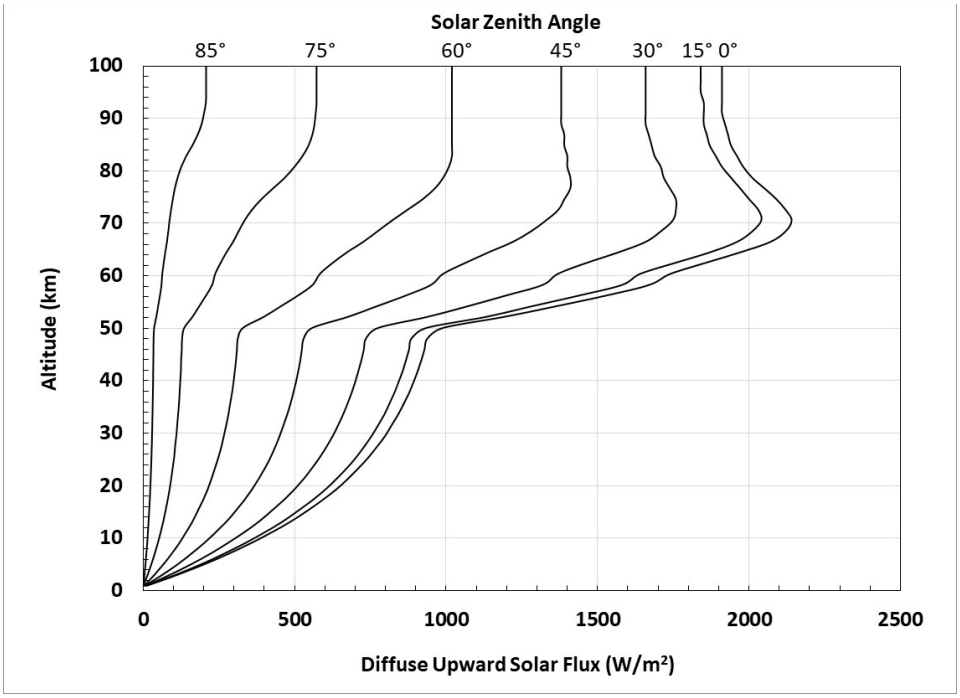


Figure 16-6: Upward diffuse solar flux as a function of zenith angle and altitude.

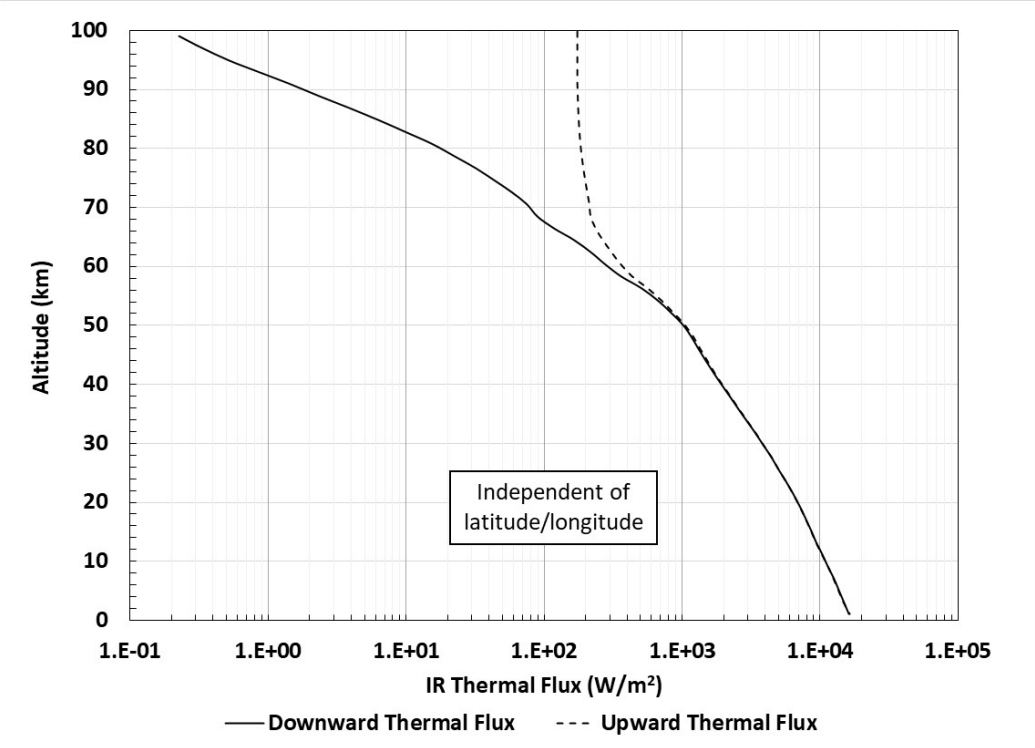


Figure 16-7: IR Thermal flux as a function of altitude in the Venus atmosphere.

2.2.2. Mars

For Mars, solar irradiance and IR flux vary with location on a diurnal and seasonal cycle similar to that of Earth. A useful model of the solar flux within the Mars atmosphere is described in Reference [23]. The dust within the Mars atmosphere contributes to significant variations between direct and diffuse solar loads, as shown in Figure 16-8 for an equatorial location on the Northern winter solstice. The extinction optical depth is shown for a totally clear atmosphere, $\tau = 0$, a typical clear day, $\tau = 0.3$, a high dust day $\tau = 1.0$, and lastly, a severe dust storm where $\tau = 4.6$. In contrast to Venus, where aerosols scatter most of the energy that falls on them, on Mars, the dust particles absorb energy, which is then deposited throughout the atmosphere. The IR flux within the Mars atmosphere is a representation of the effective ground and sky temperatures surrounding a balloon. Several models exist ([24], [25]) to determine the radiative effect of the dusty atmosphere.

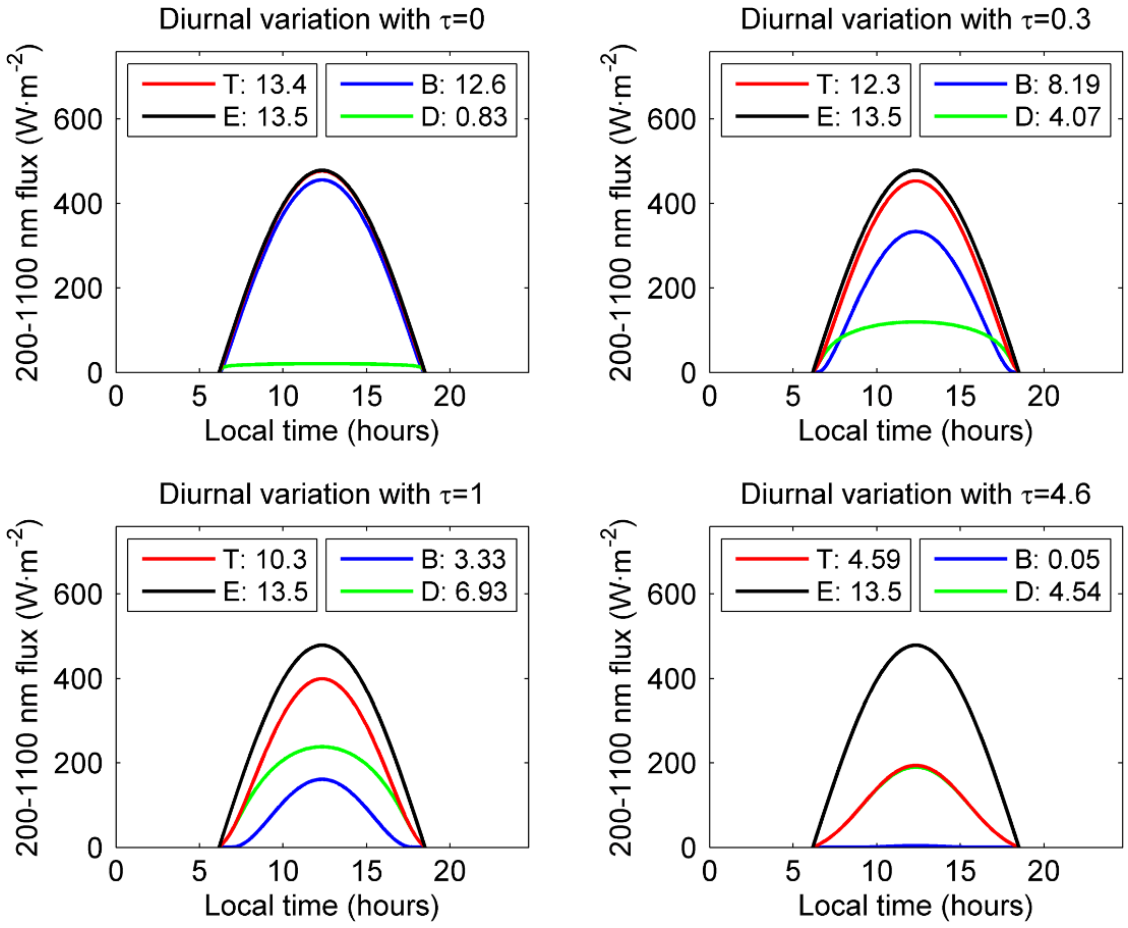


Figure 16-8: Martian diurnal surface solar flux of the direct (B, blue line), diffuse (D, green line), and total (T, red line) at four different values of τ at the equator at Ls = 270° during the Northern Hemisphere winter solstice. The flux at the TOA (E) is represented by the black line.

2.2.3. Titan

For Titan, the solar irradiance is about 14 W/m^2 at the top of the atmosphere. With a bond albedo of approximately 0.27, the net solar flux into the atmosphere is approximately 10 W/m^2; further atmospheric absorption reduces the insolation at the surface to approximately 3.6 W/m^2. The cloud layers below 60 km altitude in the atmosphere are cold relative to the surface temperature. Thus, the upward IR flux from the surface exceeds the downward IR flux from the cloud layers, as shown in Figure 16-9. Overall, the magnitude of solar and IR flux values within the Titan atmosphere is low enough to be neglected to the first order in balloon energy balance analyses.

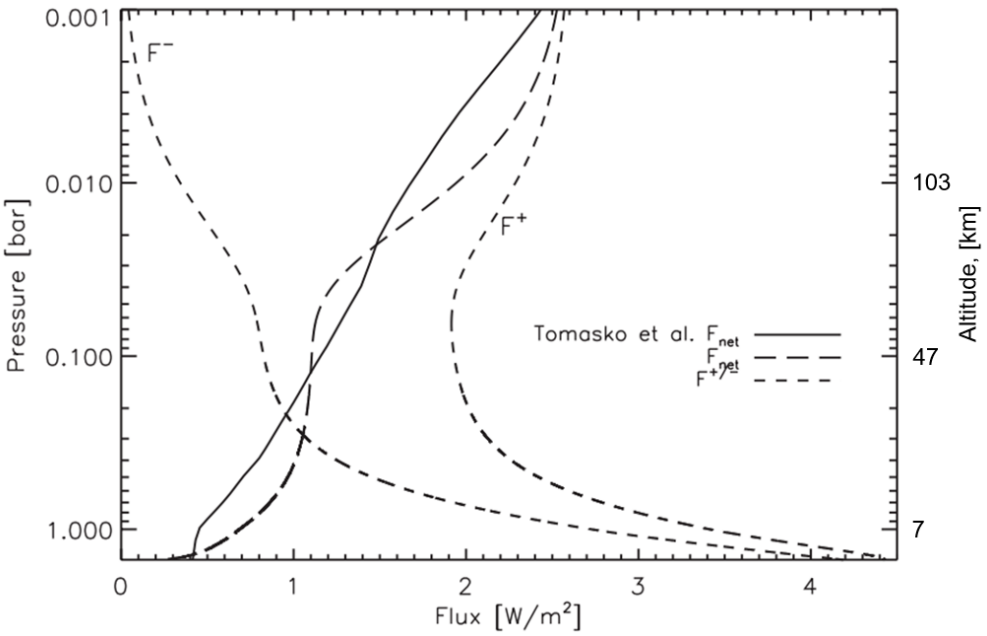


Figure 16-9: Titan thermal fluxes from Robinson's variable n Titan model [26]. Upwelling (F^+) and downwelling (F^-) fluxes (short dashed) are labeled, and their difference is the net thermal flux (long dashed). Also shown is the net thermal flux from a Titan radiative transfer model by Tomasko [27].

3. General Design and Operational Drivers

The planetary atmospheres described in the previous section are the primary drivers of balloon design outside of the Earth. The fundamental design equations for buoyancy, heating, and dynamics are the same as those for terrestrial balloons, albeit with different values for atmospheric properties, gravity, and solar and infrared fluxes. These differences are particularly strong drivers in the choice of balloon materials when the temperature exposure exceeds terrestrial norms, on either the hot or cold side, or when there is exposure to corrosive elements such as the sulfuric acid clouds at Venus. These details will be further described in the later sections of this chapter, where specific examples are presented on a planet-by-planet basis.

There is a set of additional design drivers that result from the need to send the balloon vehicle to another planetary atmosphere on a rocket and then decelerate it to a survivable speed upon arrival. Interplanetary trajectories dictate that the arrival features a multi-kilometer-per-second approach speed, and all that relative speed must be removed. By far the most mass-efficient means of doing so is to use atmospheric drag to slow down the vehicle rather than consuming large amounts of propellant in a rocket-executed deceleration. However, when starting at kilometer-per-second speeds or higher, that friction will generate a significant amount of heat from the dissipation of kinetic energy and create temperatures that can damage or destroy most spacecraft components. The solution to this problem is to place the entire entering spacecraft inside a protective structure known as an aeroshell and then to jettison the aeroshell when it is no longer needed.

This aeroshell packaging approach is illustrated in Figure 16-10, which shows the VeGa lander and part of the balloon inflation system that went to Venus in 1985. In this case, both a lander and a balloon were contained within the same spherical aeroshell and then separated from each other once an altitude of 63 km was reached in the atmosphere. Six small spherical helium tanks are mounted above the lander’s drag plate, three of which are seen in the picture. The balloon and its toroidal container are not shown in this image but were also located above the drag plate, wrapped around the antenna, and slightly inboard of the tanks.

The VeGa mid-air deployment and inflation sequence is schematically illustrated in Figure 16-11. After most of the vehicle’s kinetic energy had been dissipated by atmospheric drag at very high altitudes, a parachute was deployed at a 64 km altitude to further slow the vehicle in preparation for the automated separation and deployment sequence. The top part of the aeroshell (labeled as “capsule” in Figure 16-11) was mechanically disconnected at 63 km, after which parachute drag caused it to pull away from the rest of the aeroshell containing the lander.

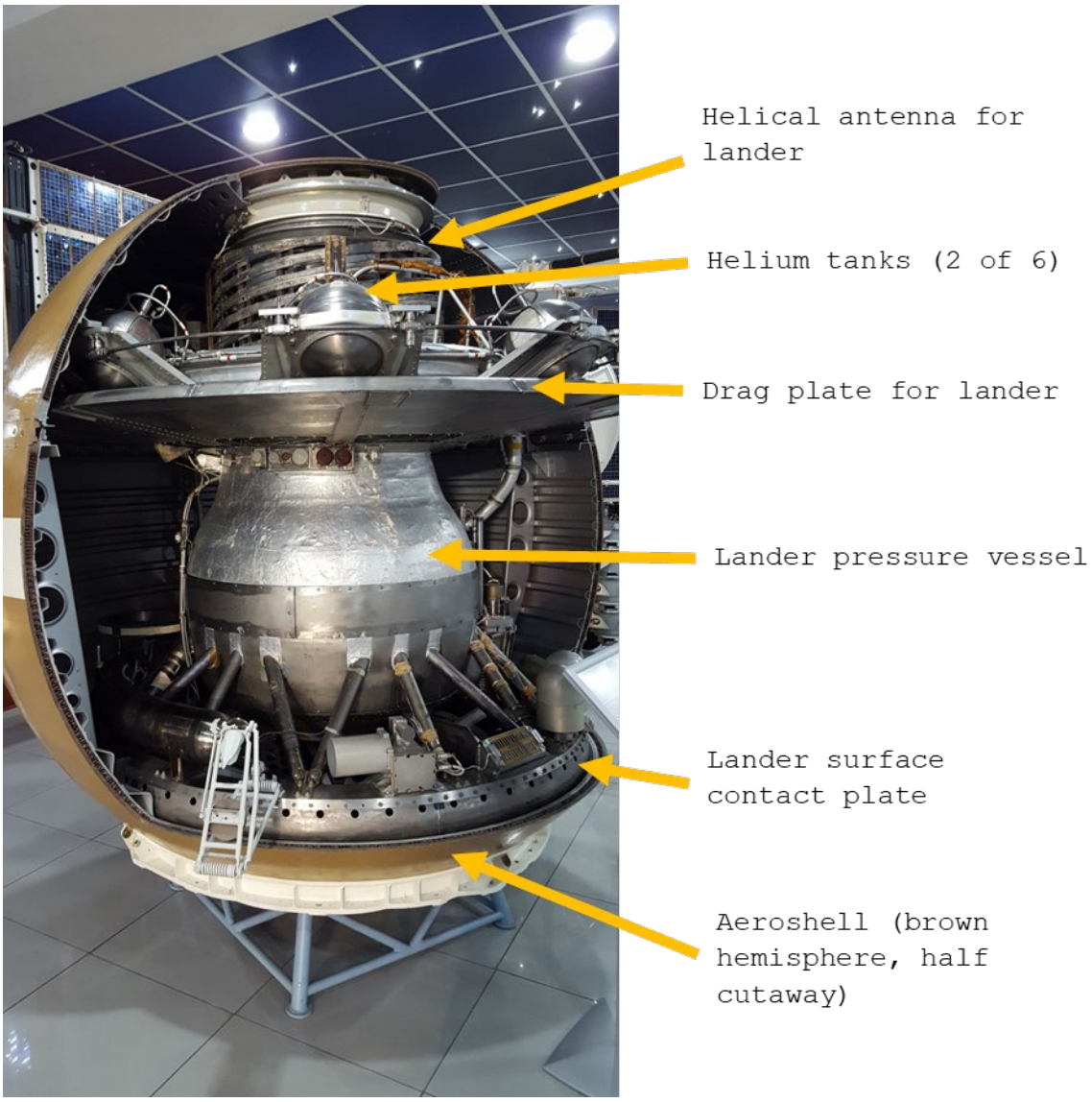


Figure 16-10: VeGa lander and balloon inflation tanks inside spherical aeroshell.

Image credit: Jeffery L. Hall, model in the Lavochkin museum, Moscow

The balloon system was mechanically attached to the top aeroshell section, causing it to also pull away from the rest of the aeroshell. Afterward, the now-separated balloon and lander continued their separate trajectories. For the balloon, a second, larger parachute was deployed at an altitude of 55 km to further slow the vehicle in preparation for mid-air deployment and inflation. Inflation with helium gas began at an altitude of 54 km after extraction from its container and continued for almost 4 minutes, finishing at an altitude of 53 km. Another separation event then occurred with the mechanical disconnection of the parachute and helium tanks from the balloon which continued to descend due to the presence of extra ballast mass in the form of the bottom part of the

toroidal balloon container [28]. The balloon and ballast combination continued to free-fall faster than the parachute and tanks for another 3 km, at which time the ballast was released, and the now positively buoyant balloon, along with its payload, began to ascend to the equilibrium float altitude of ~54 km. The different horizontal wind speeds across those 3 km caused horizontal separation between the balloon and parachute, so that there would be no recontact of the ascending balloon and descending helium tanks under the parachute.

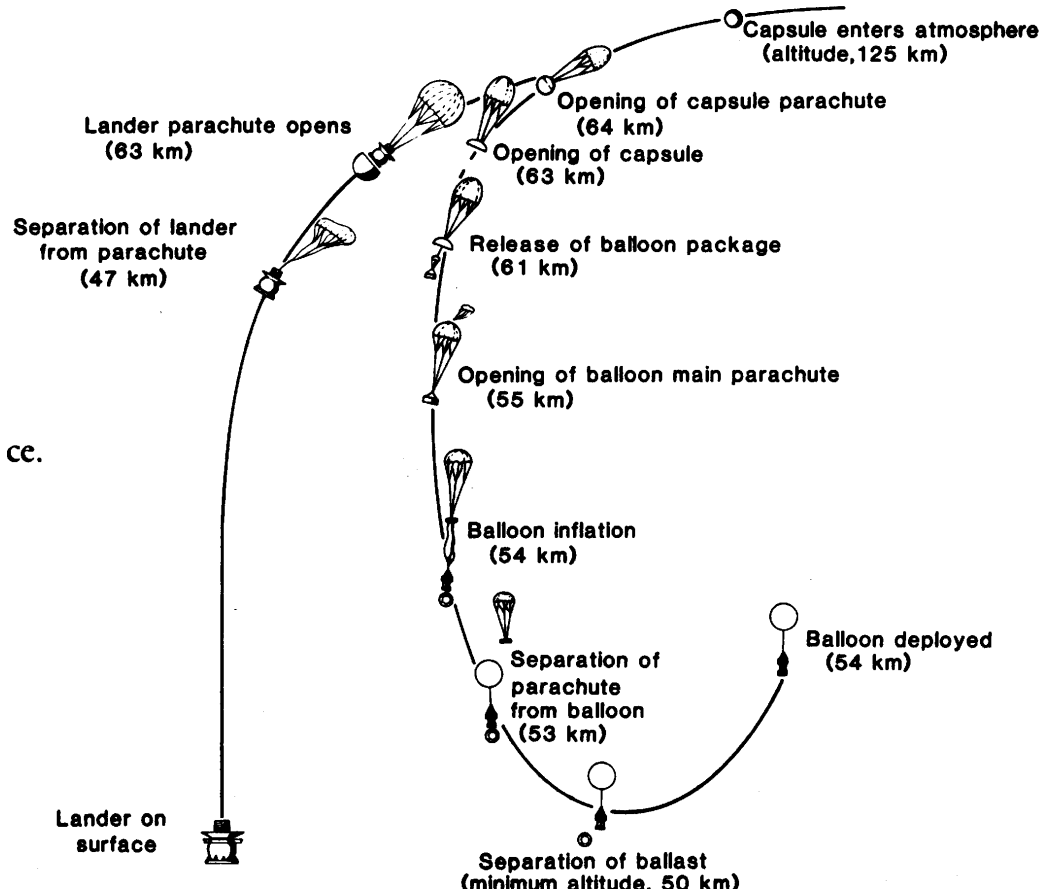


Figure 16-11: VeGa lander and balloon atmospheric entry sequence [28]

Any future mission that uses mid-air deployment for the balloon will likely employ a variant of the VeGa system described above. It is a complex sequence of events involving parachute deployments, mechanical separations, and the flow of buoyancy gas from tank to balloon. The entire sequence subjects the balloon to aerodynamic and mechanical loads that differ from and often exceed what it will experience during the nominal floating mission. Although the balloon itself can be designed with enhanced strength to meet this challenge, two key mitigation features are typically incorporated into the overall sequence to minimize those extra loads:

1. As shown with VeGa, a parachute is used to slow the descent of the vehicle during mid-air deployment and inflation. This limits the dynamic pressure of the atmosphere on the balloon to a small value (~ 30 Pa for VeGa [28]) and typically suppresses any damaging aeroelastic phenomenon, such as rapid oscillation of balloon material flapping in the wind like a flag.
2. The transition from folded to deployed balloon can potentially cause dangerous shock loading if not moderated. Specifically, a balloon is typically many meters in size, and the bottom of the balloon, with its payload, can free-fall that distance after being released from the balloon storage container. Since the top of the balloon is attached to the parachute, the balloon will quickly reach its full length. At this point, the balloon's bottom and attached payload will jerk to a stop, converting all that kinetic energy into strain energy in the balloon material. Such a shock load can readily break the balloon. A typical mitigation for this problem is to use one or more auxiliary load lines parallel to the balloon. These load lines not only take some of the mechanical loads but can also be connected to a descent rate limiter device that prevents rapid free fall in the first place by paying out the load line at whatever slow speed is required.

The VeGa balloons used parachutes to mitigate the aerodynamic loading on the balloon but did not use load lines to help reduce the shock loads during deployment. In the case of VeGa, the balloon size and payload mass were small, which limited the deployment shock loads to the point that somewhat enhanced balloon material strength sufficed.

Another key design choice is whether to put the buoyancy gas tanks above or below the balloon. If the tanks are located below the balloon, they are easy to drop once emptied; however, the additional weight adds to the load on the balloon and exacerbates the deployment shock loading problem. These problems vanish if the tanks are above the balloon, like VeGa, but then the issue becomes dropping the tanks when they are emptied and not having them fall on the balloon hung below. VeGa kept those tanks under the parachute once detached and had to accept 3 km of balloon-free fall after inflation to achieve enough wind shear-induced lateral spacing to prevent re-contact.

Although nominally analogous to the shipment by aircraft of terrestrial balloons to launch sites around the world, rocket launches feature much more severe mechanical loads that require special design considerations. While each rocket and spacecraft combination is different, it is typical to experience axial accelerations during launch of up to 6 gees (6 times Earth's gravity), lateral accelerations of up to 2 gees, and sine vibration amplitudes of up to 1 gee across the frequency range of 5 to 100 Hz [29]. Additional loads are imposed by random vibration, shock acceleration from separation events, and loud acoustics from the rocket engines and vibrating structure. Protection of the balloon from this environment requires a combination of careful folding of the balloon

plus external structural support. This external support is achieved by placing the balloon inside a protective container that isolates the balloon from the rest of the spacecraft and exerts enough compression force on the packaged balloon to greatly reduce relative motion and fold-to-fold rubbing. A proper folding pattern also helps minimize the packed balloon's volume and limit the number of corner folds that can facilitate pinhole formation when loaded.

Parachute packaging on a spacecraft shares these constraints with balloons. However, parachutes do not have to be gas-tight structures and, therefore, are not nearly as sensitive to the creation of localized pinhole defects. This lack of sensitivity generally allows parachutes to be compressed into a smaller volume than balloons during the packing process. Another important transient load shared by both packaged balloons and parachutes is the high deceleration experienced during the atmospheric entry process. These are not shock loads, but the peak deceleration pulse tends to be of short duration in the range of tens of seconds. Peak deceleration is typically 10 to 20g’s at Mars and 50 to 100g’s or more at Venus.

The fact that a balloon is a gas-tight structure does pose a packaging challenge not shared by parachutes. It is never possible to completely remove all gas from inside the balloon prior to launch, and it is unwise to attempt it, as the outside air pressure will push the material together, creating sharp folds that are prone to pinhole formation. However, once the vehicle is launched, the spacecraft experiences the vacuum of space, and therefore any residual gas inside the balloon will expand. Therefore, the balloon must be constrained by the storage container in such a way that no damaging expansion of the balloon occurs. The danger is both frictional rubbing of balloon material against itself or the container walls and being pushed out of the container and into nearby spacecraft components with sharp edges or points that could cut the material. This constraining function is complicated by the necessity of having penetrations through the balloon container, such as the buoyancy gas fill pipe, a tether to connect the top of the balloon to the parachute, and a tether to connect the bottom of the balloon to the payload (gondola).

The last special design consideration of note for this discussion is the challenge of communicating with planetary balloons and the resulting design drivers. Specifically, there are three related problems to deal with:

1. There is a very long transmission distance from balloon to Earth, ranging from approximately 40 million kilometers to Venus at closest approach, to 1.2 billion kilometers to Saturn’s moon Titan. Therefore, the energy cost per bit of data transmitted is

significantly higher compared to terrestrial balloons, which communicate over a range of at most hundreds of kilometers.
2. These long transmission ranges have round-trip light times that range from approximately 4 minutes to Venus to 2.2 hours with Titan. This time lag precludes real-time control from operators on Earth and, therefore, motivates highly autonomous operation of the vehicle.
3. The combination of orbital mechanics, planetary winds, and no local communications infrastructure (e.g., relay satellites) means that there can be no communications possible for perhaps days at a time while the balloon is on the other side of the planet from Earth. This reinforces the need for highly autonomous vehicle operation.

These three challenges primarily affect the design of the command, data handling, power, and radio systems on the vehicle. The effect on balloon design is indirect and primarily involves sizing the balloon correctly to accommodate the other systems.

Even more so than their terrestrial counterparts, space missions to other planets tend to be prohibitively expensive to design, build, and launch, providing a strong motivation to maximize the longevity of the balloon flight as much as possible. This motivation generally aligns with science objectives that benefit from observations over long periods of time. Such long-duration missions generally cannot be performed with only energy stored onboard in batteries, which was the design approach used by the short-duration VeGa balloons. Therefore, as with terrestrial missions, long-duration missions to Venus and Mars would likely require solar panels to provide the necessary energy. In contrast, missions to Titan would likely require nuclear (radioisotope) power, given the very low level of sunlight available. Onboard rechargeable batteries would augment these power systems for at least the Venus and Mars mission concepts to provide power during nighttime. This is of particular importance at Venus because the periods of darkness can be as long as 3 or 4 Earth days in duration, which increases the battery mass and, consequently, the size of the balloon needed to carry it.

All planetary balloon missions will collect far more data than can be transmitted to Earth due to the bottleneck created by the limited onboard energy and the very long distance of the radio transmission. The VeGa balloons themselves had to collect and transmit data only a small fraction of the time to conserve electrical energy. This data transmission bottleneck is a strong driver for on-board processing of the raw data and an automated assessment that selects only the most important data for transmission. This requires significant onboard computing resources and a thorough verification and validation process on the flight hardware and software prior to use on a future space mission.

4. Balloon Technology Details for Venus, Mars, and Titan

In this section, we provide technical details for different balloons that have been designed, tested, and/or proposed for missions to Venus, Mars, and Titan. The intention is to give the reader a general introduction to the specific balloon design issues and progress for each of these planets. A list of references for further reading is also provided.

4.1. Venus

The success of the VeGa balloons in the cloud layer of Venus inspired many further technological developments for follow-on missions. No balloon has flown on Venus since VeGa in 1985, but several missions have been proposed to NASA and ESA (although none have been selected yet), and component technologies, subsystems, and instruments have also been pursued. Many types of Venus balloons have been investigated, even one metallic balloon designed to operate near the surface where there exists temperatures up to 460°C and a dense atmosphere of 65 kg/m^3 [30] [31]. The lack of scientific instrumentation and engineering subsystems that can currently operate at such elevated temperatures means that balloon missions for that region are far in the future. Therefore, the remainder of this section will focus on balloon concepts for exploring the cloud layer.

As noted in Section 2.2.1 above, a unique attribute of the Venus cloud layer environment near 53 km altitude (the nominal VeGa flight altitude is that it matches the average 1.2 kg/m^3 atmospheric density at the Earth's surface. Accordingly, a balloon made for the Venus cloud layer can be readily flown on Earth during the technology development process, allowing for the testing of the balloon's lift capacity and aerodynamics. However, the materials used for a Venus balloon must be resistant to the sulfuric acid aerosols of Venus. In addition to density, similar pressure and temperatures to those on Earth can also be found in the Venus cloud layer. However, the primarily carbon dioxide atmosphere, rather than nitrogen, means that slightly higher temperatures and lower pressures are required to achieve the same buoyancy conditions. For example, at a 53 km altitude on Venus, the average pressure is 0.71 bar and the temperature is 50°C, resulting in an atmospheric density of 1.2 kg/m^3, compared to 1 bar and 25°C on Earth. Altitudes near 53 km on Venus have therefore become a region of interest, as they are well within the capabilities of existing instruments, power components, and avionics, with limited or no adaptation needed from their Earth analogs. Altitudes between 52 to 62 km (60°C to -20°C) are generally acknowledged as currently feasible [32]. Outside of this range, new thermal technologies are required.

4.1.1. Super-pressure Helium Balloons

The VeGa mission used super-pressure balloons to fly at an approximately fixed altitude, mitigating both vertical winds and thermally induced buoyancy changes due to diurnal cycling [4]. Super-pressure balloons are nominally constant-volume structures that are inherently stable in altitude (see Chapter 10). They gain buoyancy if displaced downwards into denser air and lose buoyancy if displaced upwards, both of which return the balloon to its equilibrium altitude after the displacement. The balloon is kept at a fixed volume by maintaining an internal pressure above the ambient, acting in a sense as an extremely lightweight pressure vessel.

Venus super-pressure balloon developments following VeGa were primarily conducted by JPL and its partners, with the goal of creating a larger balloon with significantly more payload capacity than VeGa, capable of flying for weeks or months instead of just two days. Many of the desirable scientific instruments for planetary study can only be accommodated on such larger balloons, most notably a mass spectrometer for measuring gas and aerosol composition. Helium was used as the buoyancy gas in these efforts, just like VeGa. Much of this development work focused on the super-pressure balloon envelope with the following key design features:

- **An outer fluorocarbon coating to tolerate sulfuric acid aerosols.** The aerosols on Venus can have concentrations exceeding 90% sulfuric acid, and higher temperatures in the lower clouds further amplify their reactivity.
- **A high-strength component to allow the balloon to be pressurized to maintain altitude.** This can be fabric or fiber-reinforced envelopes or tendon-reinforced "pumpkin" constructions.
- **An outer surface with high emissivity and low absorptivity.** Even in the clouds of Venus, radiative fluxes can greatly increase the temperature and, hence, pressurize super-pressure balloons. Minimizing the absorptivity-to-emissivity ratio helps keep the buoyancy gas cooler in sunlight.
- **A pinhole-resistant gas barrier to contain the lift gas.** This barrier must stay gas-tight during launch, deployment, and in flight.
- **A foil or metalized film as a gas diffusion barrier.** Even a pinhole-free plastic barrier will allow helium to slowly diffuse out. This effect is mitigated on scientific balloons on Earth, as they generally fly in the freezing stratosphere; however, helium diffusion is non-negligible at the target Venus altitudes.

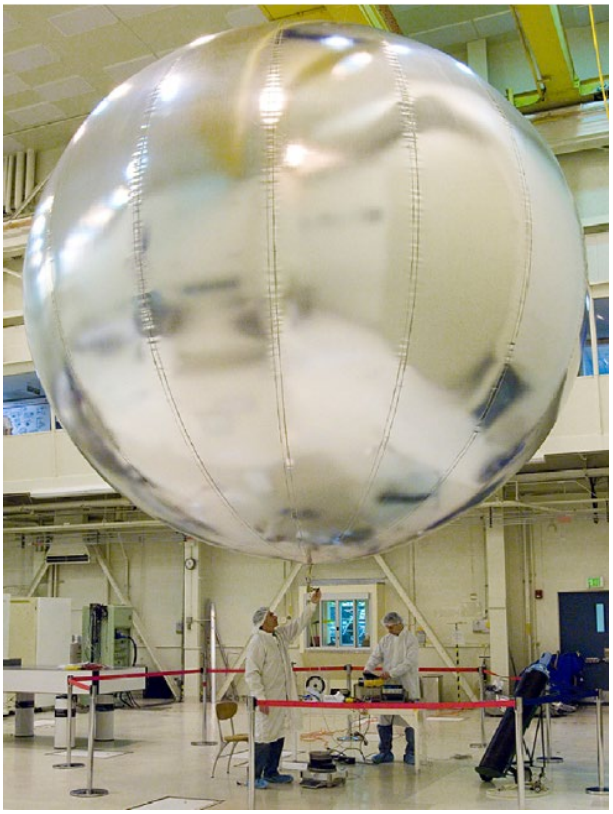


Figure 16-12: The first 5.5 m prototype Venus balloon based on Vectran fabric and metalized Teflon film.

Image from Reference [33].

Multiple Venus super-pressure balloon prototypes were fabricated under JPL leadership between 2005 and 2014. Unlike the VeGa balloons of heavy fluorocarbon-impregnated cloth [34], these prototypes used Vectran fabric as the strength-bearing element in a laminate with a Mylar gas barrier and a fluoropolymer (Teflon) film as the acid-resistant barrier [33]. Figure 16-12 shows the first of two 5.5-meter-diameter Venus prototypes built at ILC Dover in partnership with JPL and NASA Wallops. The metallic appearance is due to the vapor-deposited aluminum layer underneath the transparent fluoropolymer film. This metallization serves the dual purposes of reflecting sunlight and acting as a helium diffusion barrier. Later prototypes investigated new seam designs for both acid protection and heat rejection [35], thicker aluminum foil as an improved diffusion barrier [36], alternative fluoropolymers to Teflon (such as Aclar [36] and PFA [37]), and the effect of pinholes on the sulfuric acid tolerance of the envelope material [37].

Flight tests were not conducted during the JPL-led Venus super-pressure balloon program; however, a successful mid-air deployment and inflation test was accomplished [78], which involved a helicopter drop of a prototype balloon and its deployment system, as illustrated in Figure

16-13. In contrast to the VeGa approach described in Section 3, this mid-air deployment and inflation test inflated the balloon from the bottom and utilized an external load line unreeled at a constant speed to limit the shock forces generated when the balloon completed deployment. The load line was cut after deployment, and inflation started. Unlike a real planetary deployment, this test did not separate the heavy helium tanks after inflation; the system, post-inflation, fell to the ground and was recovered without a float phase.

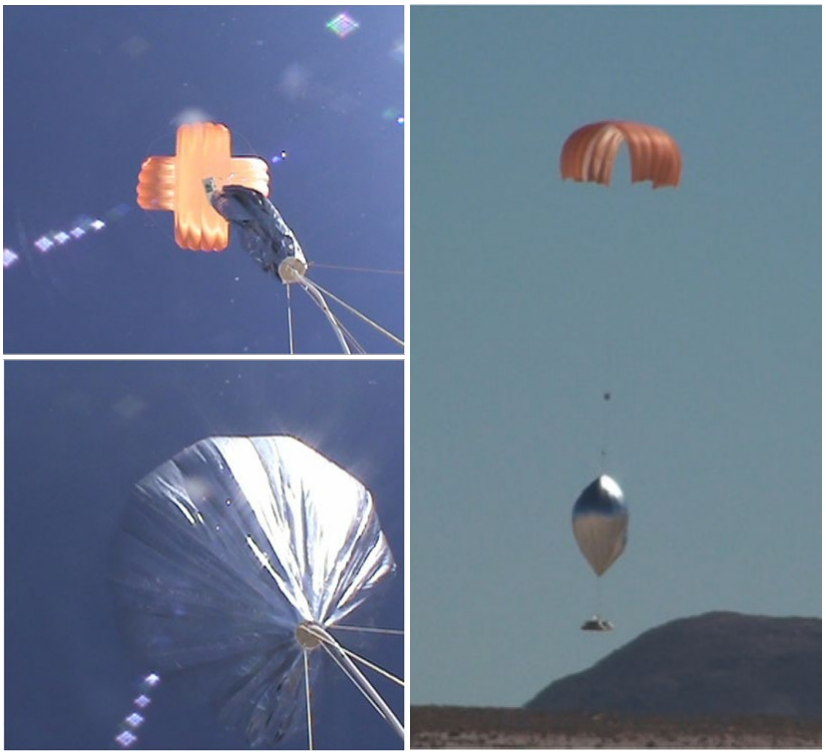


Figure 16-13: Snapshots of parachute-assisted deployment and inflation of a Venus super-pressure balloon prototype. Top left – balloon after deployment. Bottom left – balloon nearly fully inflated. Right – balloon, tanks, and parachute approaching ground.

Images from Reference [32]

This Venus super-pressure balloon technology was proposed to NASA for implementation under the moniker of the "VALOR" mission concept, but it was not selected. A brief description can be found in Reference [38]. Other mission studies in support of NASA guidance documents have been completed that rely on lessons in the design of the Venus super-pressure balloon [39].

4.1.2. Variable-Altitude Phase-Change Fluid Balloon

Significant development occurred in the 1990s on a very different type of balloon for Venus. This was a zero-pressure balloon that intentionally

cycled over an altitude range by using a condensable lift gas. The basic principle is that the fluid condenses at the colder, higher altitudes, losing buoyancy and causing the balloon to descend. As the balloon descends, it warms and evaporates the buoyancy fluid, generating more buoyancy, which causes the balloon to arrest its descent and start to rise again. An appropriate choice of buoyancy fluid and sufficient heat exchange between the fluid and the environment will create continuous cycling at altitude. Exploring over an altitude range is clearly of scientific value, as it allows for a more comprehensive exploration of atmospheric properties and determines their altitude dependence.

A key advantage of the mostly carbon dioxide atmosphere at Venus (molar mass of ~44 g/mol) is that more lifting gases are feasible than on Earth (molar mass of ~29 g/mol). Water vapor and ammonia, in particular, can provide significant buoyancy and will condense and evaporate at useful altitudes at Venus. Studies have shown that helium-water and ammonia-water mixtures work best for achieving large altitude ranges at Venus [32]. On Earth, however, these fluids don't work for the altitude cycling concept; instead, prototype flights employed a helium and Freon (R114) mixture [40]. Figure 16-14 presents results from one test flight that shows the altitude cycling behavior and good agreement with predictive models. Further information about the theory and prototype results from these altitude-cycling balloon developments can be found in References [41] and [42].

Despite significant work done on phase-change lift gas balloons for Venus, the technology remains only partly developed. A particular challenge is the verification and validation of Venus balloon designs, as the buoyancy fluids that work on Venus do not work on Earth, posing a substantial challenge for validating the coupled thermal and buoyancy models. While Earth's troposphere is an excellent density analog for most balloon architectures, the phase-change buoyancy-fluid concept explicitly relies on a key difference between Earth and Venus for a new type of balloon, which adds considerable challenges for validation testing. High-temperature heat condensers and thermal payload protection for the concept also remain incompletely developed.

4.1.3. Controllable, Variable-Altitude Helium Balloons

A 2018 NASA trade study examining planet exploration options for Venus recommended a controllable variable-altitude helium balloon for its potentially large science return on a modest investment. Underlying this recommendation were the results of the Google Loon project, which had recently demonstrated altitude control on Earth for flight durations approaching a year [43]. The Loon design was a two-compartment super-pressure balloon with one compartment filled with helium gas and the other with air pumped in from the atmosphere. Changing the amount of air inside the balloon changed the mass, causing the balloon to move upwards

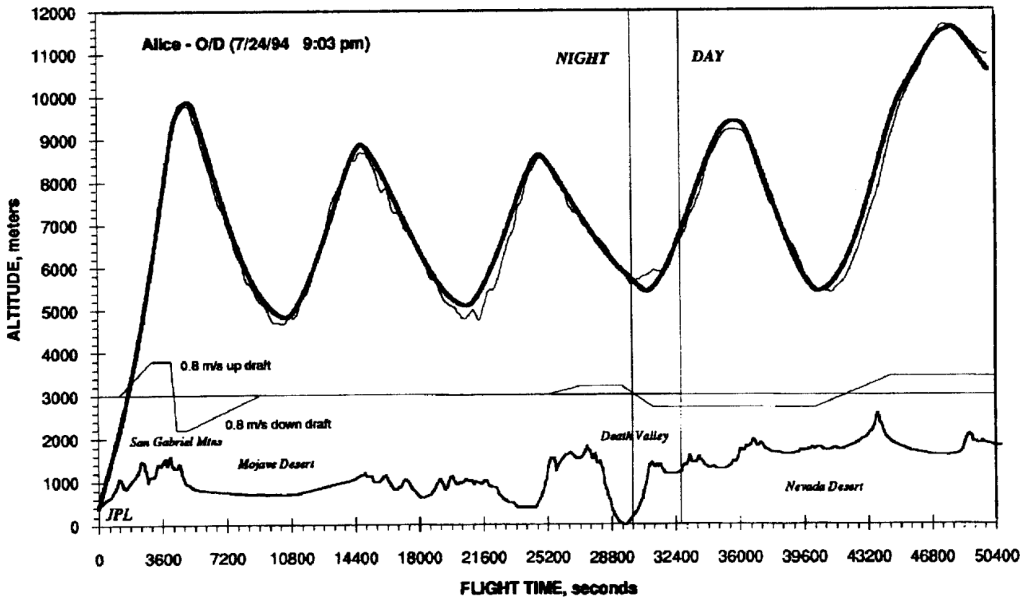


Figure 16-14: Passive altitude cycling flight trajectory from an ALICE prototype.

Image from [40]

or downwards. This altitude control methodology was combined with wind knowledge to demonstrate the loitering flight behavior of the balloon by using different wind directions at different altitudes to keep the balloon over a specific area on the ground.

While the Loon architecture is suitable for Earth, a variation is necessary for Venus to mitigate the challenge posed by sulfuric acid cloud aerosols. Specifically, moving air into the balloon will also bring acid aerosols that pose a significant challenge to the survival of the envelope and the air pump. Furthermore, station keeping is not possible on Venus, given the dominant high-speed zonal wind flow; however, altitude variation is crucial for meeting scientific objectives. At the time of this writing, two approaches have been prototyped so far to meet this challenge:

1. A balloon-in-a-balloon design in which helium alone is pumped between compartments in a two-compartment balloon.
2. A mechanical compression balloon, in which the entire balloon is volumetrically compressed or expanded to change buoyancy.

4.1.3.1. Balloon-in-a-Balloon Altitude Control

The balloon-in-a-balloon architecture was chosen by a JPL-led team after the completion of a trade study that concluded it was the most mass and power-efficient approach [44]. This type of balloon was pioneered by Prof. Voss at Smith College, who made dozens of small prototypes and

used them for meteorological research on Earth [45] [46]. In this concept, a super-pressure balloon is placed inside a zero-pressure balloon. Both balloons are filled with helium, but the pressurized helium in the super-pressure balloon provides less buoyancy due to its slightly higher density. Therefore, compressing and moving helium into the super-pressure balloon reduces buoyancy, while venting that helium back into the zero-pressure balloon increases buoyancy. This provides repeatable buoyancy modulation and, hence, altitude control is limited only by the availability of pumping power and the pressure and volume limits of the compartments/balloons. Note that the system is closed with a constant amount of helium in the absence of leakage or diffusion.

A key advantage of the balloon-in-a-balloon design for Venus is the separation of the functions of the two envelopes: the zero-pressure balloon is exposed to sunlight and sulfuric aerosols but not required to withstand pressurization loads, while the inner pressurized balloon is isolated from environmental effects but designed to withstand pressurization loads. This architecture is also highly resistant to helium loss: helium that leaks out of the super-pressure balloon simply enters the zero-pressure balloon, as little driving pressure exists to push the helium out of the zero-pressure balloon, where it would be lost. Figure 16-15 illustrates the construction and altitude control scheme of the platform [47].

Multiple balloon-in-balloon Venus prototypes, ranging in diameter from 4 to 6.5 m, have been fabricated and tested by JPL and Aerostar LLC [48]. This testing includes indoor flights in the Tillamook airship hangar [49] and outdoor flights over the Black Rock dry lakebed in Nevada (Figure 16-16) [50]. A high-fidelity simulation model has also been created, and the flight test results have been used to validate and improve the model [49] [50]. The balloon envelope materials are derived from earlier super-pressure balloons, featuring a metalized Teflon-Kapton laminate for the outer zero-pressure envelope and a Vectran fabric with a urethane bladder as the inner super-pressure envelope. Additional work has been done on the deployment and inflation system for these kinds of balloons, including laboratory testing of small prototypes inflated from hanging configurations [51].

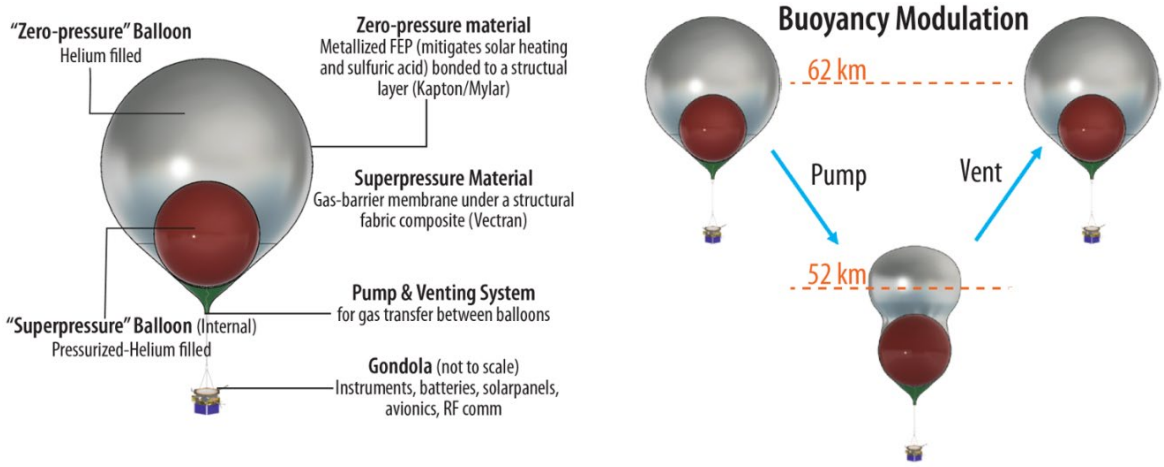


Figure 16-15: Balloon-in-balloon altitude control architecture for Venus, as described in the 2020 Venus Flagship Mission Study.

Image from Reference [47]



Figure 16-16: Prototype variable altitude aerobot in at launch (left) and in flight (right) over Black Rock Desert, Nevada.

Images from Reference [50]

4.1.3.2. Mechanical Compression Balloons

The mechanical compression balloon, developed by Thin Red Line Aerospace and illustrated in Figure 16-17, consists of a vertical stack of smaller tendon-reinforced balloons that are internally connected to share helium gas [52]. A central tension cable runs from the top to the bottom of the stack and is extended or retracted to adjust the total length and volume of the stack, and thus the balloon's internal pressure. As the stack shortens, buoyancy reduces, and when the stack grows, it increases, thereby affecting altitude control. The Zylon® tendon reinforcement in each balloon segment provides the material strength necessary to withstand induced forces resulting from length modulation. All gas barriers are fabricated as flat sheets, making the assembly naturally flat-packed with fewer folds than standard gore constructions. For Venus applications, an external fluoropolymer sulfuric acid barrier film protects the balloon from the sulfuric acid aerosols [52]. Laboratory experiments show that large and repeatable volumetric changes are possible.

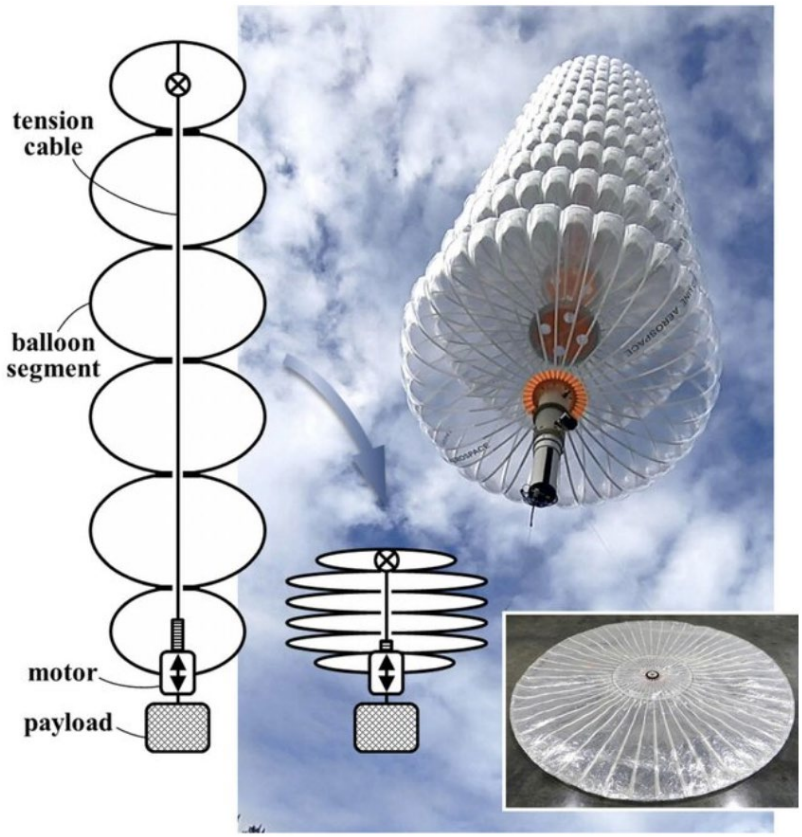


Figure 16-17: Mechanical compression balloon, with tendon cable pole-to-pole for volume control. Prototype shown in top right.

Image from Reference [52]

4.1.4. Solar Montgolfière

Solar-heated Montgolfière balloons obtain buoyancy by using the sun's energy to heat the air inside the balloon and make it less dense than the surrounding atmosphere. This type of balloon at Venus would result in a smaller overall system mass than helium (or other light gas) balloons because they do not require storage tanks and plumbing systems. Instead, they are ram air-inflated upon arrival at Venus. Solar-heated balloons on Venus are likely restricted to daylight hours, although the possibility exists to generate some buoyancy at night from the surface IR flux, similar to how the Infrared Montgolfière balloon works on Earth [53].

Detailed envelope material optimization and testing in Venus' acidic aerosol conditions have not been carried out for this type of balloon, but the inherent short lifetime for a solar Montgolfière balloon suggests that less acid-resistant materials could be pursued, possibly even polyethylene or other non-fluorinated polymers. Pinholes and punctures do not seriously affect the performance of a solar Montgolfier, as the internal gas is the same as the external atmosphere. Solar heating on Venus and candidate materials would permit flights far above the Venus cloud layer (even to 75 km) [54], an altitude regime that cannot be easily measured by entry vehicles, which move at hypersonic speeds at those altitudes.

Construction of solar Montgolfière polyethylene and Zylon film balloons has been attempted [55], with carbon-black dusted "Heliotrope" polyethylene, significantly pursued by Sandia National Laboratory [56]. Heliotropes have demonstrated ram-air inflations (see Chapter 15, Figure 15-14) and sufficient aerodynamic noise suppression for seismic infrasound detection [57]. Solar balloons are explained further in Chapter 15.

4.2. Mars

The Martian atmosphere is just barely dense enough to allow for practical flying vehicles. This was notably demonstrated for heavier-than-air vehicles with the Ingenuity Mars helicopter that performed 72 short-range flights from 2021 to 2024 [58]. No balloon flight on Mars has yet been attempted, but several concepts have been proposed, and some prototypes have been constructed and tested in Earth's atmosphere.

The French space agency CNES was the early pioneer in developing concepts for Mars balloons in the late 1980s and early 1990s, following the success of the VeGa balloons at Venus. The difficulty of floating in the low-density atmosphere prompted an initial focus on balloons that would only fly during the daylight hours and then land at night [59]. These were, in essence, helium-filled zero-pressure balloons that absorbed

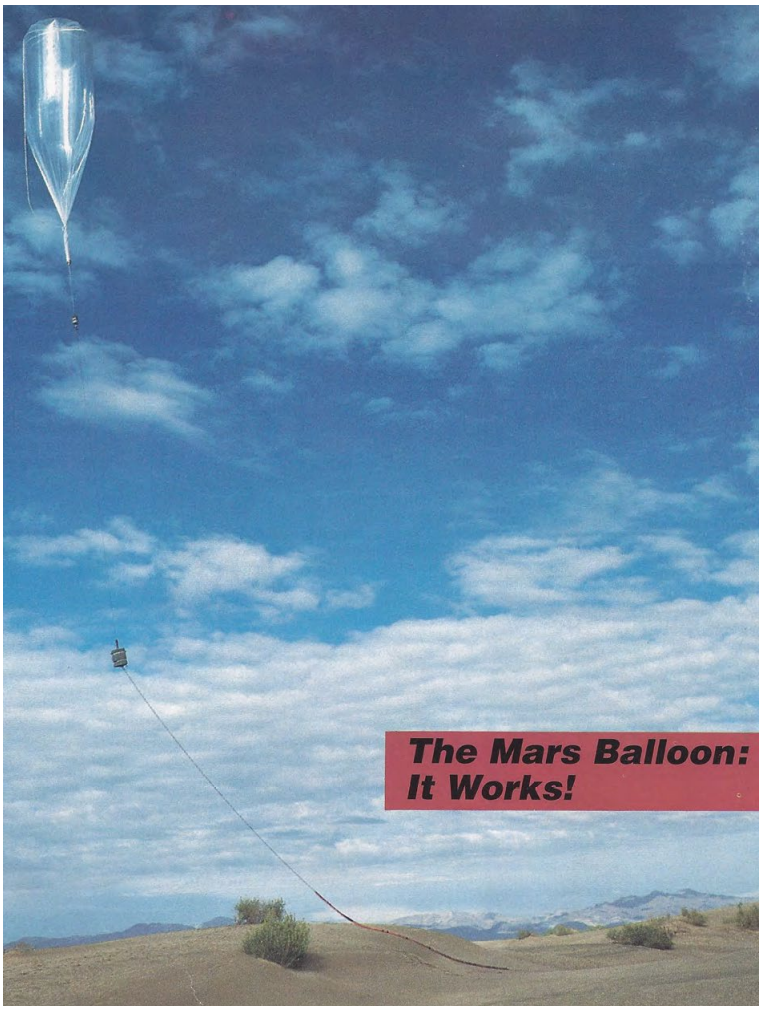


Figure 16-18: Mars "snake" balloon being tested in the California desert in 1990.

Image from the cover page of The Planetary Report, Vol. XI, No.1, 1991 [60]

sunlight during the day and became sufficiently buoyant to fly until the sun went back down. The payload was separated into two parts: a traditional box-like gondola and a lower guide rope or "snake," which was the only part that would touch the ground. The guide rope was ruggedized to withstand the dragging motion of the vehicle across the surface caused by lateral winds. Prototype experiments on this guide rope concept were conducted by CNES in cooperation with the U.S.-based Planetary Society (Figure 16-18) [60]. The results showed some successful flights but lingering challenges with the durability of the snake and occasional jamming of the snake on ground obstacles. Although originally intended to fly on the Soviet Mars 1994 and then the 1996 missions but was cancelled in 1995.

Many organizations became interested in Mars balloons in the 1990s and 2000s, but with a switch from the development of zero-pressure to helium-

filled super-pressure balloons (Refs. [61], [62], [63], [64], [65], [66], [67]) and solar infrared Montgolfière aerobots [68] [69]. However, while multiple prototypes were designed, fabricated, and tested in the Earth's atmosphere, no fully spaceflight-ready balloon was ever produced or launched to Mars. The technology development of Mars balloons has stalled significantly after ~2010, with no notable progress in prototyping or flight testing since then.

The very low-density Martian atmosphere remains the key technical driver. The nominal Martian atmospheric density at the surface is approximately 0.014 kg/m^3 and is composed of 95% CO_2, 3% N_2, and 2% Ar (See Section 2.1). Helium buoyancy gas under these conditions has a density of approximately 0.00127 kg/m^3, which, when used in a zero-pressure balloon, results in a gross buoyancy per unit volume of 0.0127 kg/m^3, a factor approximately 80 times less than the buoyancy per unit volume on the surface of the Earth. As an example, to illustrate the magnitude of the challenge this poses, carrying the small 7 kg payload of the VeGa balloon at the Martian surface would require a large 515 m^3 balloon (9.9 m diameter), even if the balloon itself were massless. Significantly larger volumes are required for non-zero balloon mass and to fly over Martian topography just a few kilometers above the zero-altitude planetary datum. Note that the size of a solar-heated Mars Montgolfière balloon without helium can be even larger, given the generally lower buoyancy per unit volume provided. All this motivates the development and use of miniaturized payloads suitable for future Mars aerial missions, utilizing large-volume balloons made of lightweight balloon envelope materials.

The conclusion from this analysis is that Mars balloons must be of large volume for even small payload masses and require very lightweight balloon envelope materials. There is ample precedent for flying very large and lightweight balloons on Earth, but the complicating factor for Mars is the requirement to deploy and inflate the balloon without careful human handling. Most approaches for Mars have focused on autonomous aerial deployment and inflation, following the example of VeGa. However, experiments conducted in the Earth's stratosphere, where the atmospheric density matches that of Mars, have demonstrated the severe challenge of large, lightweight balloons surviving the transient structural loads during this process.

The published literature documents many deployment and inflation flight test experiments conducted in the Earth's stratosphere, with the results showing a mixture of success and failure for both helium super-pressure balloons [63], [64], [65] and solar Montgolfière balloons [68]. All development work was terminated before the failures were fully understood and corrected.

In principle, a Mars balloon could be deployed, inflated, and launched from the surface of Mars using automated approaches developed for smaller balloons in terrestrial applications. However, the large balloon size required for even the smallest of payloads (10+ m diameter) poses a severe challenge for such automated techniques. The lightweight material and the growing gas bubble inside have a density similar to that of the atmosphere, so the balloon can easily be pushed into the ground and damaged by lateral winds, even in the thin atmosphere of Mars. In addition, the need to safely land first on Mars is itself a major challenge, requiring a significant landed mass for the lander, balloon, balloon container, deployment mechanisms, and helium tanks.

Many different types of materials have been considered for Mars balloons. For Mars super-pressure balloons, these include simple thin-film Mylar (Figure 16-19) [64] [65], laminates of Mylar film reinforced with Kevlar-scrim (fabric) [67] [62], and pumpkin balloons using polyethylene film and PBO tendons [65]. Mylar combines high strength with low weight but has poor tear strength. Fabric-reinforced material is much stronger but heavier. Pumpkin balloons have the advantage of superior strength in the pole-to-pole direction due to the tendons, which help with transient deployment loads but not with flagging loads. For solar-heated Montgolfière balloons, materials are commonly a thin film polyethylene with a black carbon additive to maximize solar energy absorption [68] [69].

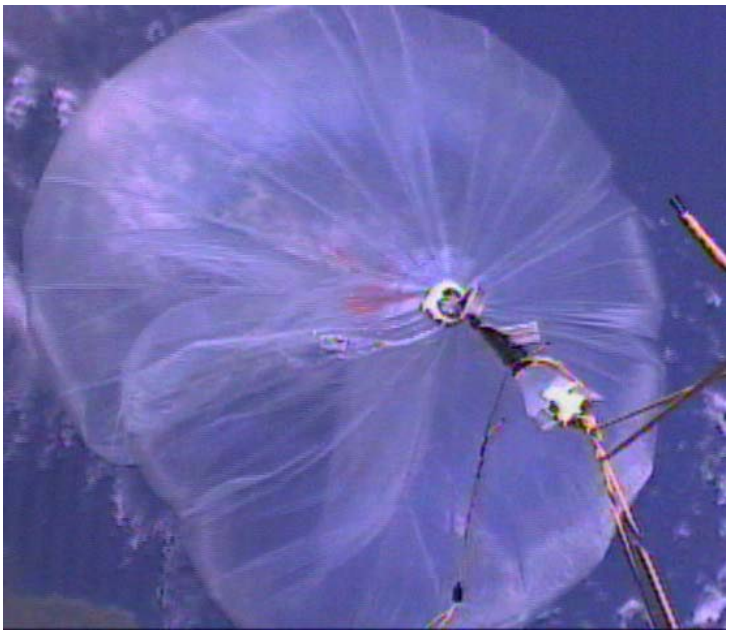


Figure 16-19: Mars spherical helium super-pressure balloon top-down view during aerial deployment and inflation test in the Earth's stratosphere [65]

4.3. Titan

The relatively high atmospheric density at Titan allows for a variety of balloon vehicle concepts. The following sections describe the main concepts that have been developed so far.

4.3.1. Hot-air (Montgolfière) Type Balloons

The long distance of Titan from the sun and the thick cloud cover generally precludes the use of solar power technology for in-situ exploration. Therefore, the baseline power system for all vehicle concepts would be nuclear power, typically in the form of a radioisotope thermoelectric generator (RTG). The Multi-Mission RTG used for space vehicles, such as NASA's Perseverance Mars rover, produces approximately 2 kW of thermal energy and 100 W of electric power on a continuous basis. In principle, this type of heat source can produce buoyancy in a Titan hot air balloon filled with atmospheric gas in addition to powering the platform. Work done to date on that concept includes detailed computational fluid dynamics simulations and cryogenic experiments on small-scale balloon prototypes [70] [71]. Two sphere-on-cone balloon designs were considered: a single-wall balloon and a double-wall balloon. The rationale for the double-wall balloon was to investigate whether the added mass of the second layer was sufficiently advantageous for reducing heat loss.

A photo of the 16-gore, 1 m scale single-wall balloon constructed from aluminized Mylar film with nylon scrim is shown in Figure 16-20. In the double-wall design, the inner and outer walls were connected at the gore seams with interconnecting ribs constructed from aluminized mylar film.

The numerical modeling results are shown in Figure 16-21, where it is clear that the double-wall balloon has a higher internal temperature than the single-wall balloon. Convective heat loss dominates radiation heat loss from the balloon skin as the temperature is very low, and the outer layer has a low emissivity. The double-wall balloon provided about 25% more net buoyancy than the single-wall balloon in both the experimental measurements made in a cryogenic chamber and through numerical analysis.

The mass of a double-wall balloon envelope is about twice the mass of a single-wall design. For an 8-m diameter single-wall balloon at Titan, the balloon envelope mass would be about 20 kg, assuming the areal density is 0.1 kg/m^2. The payload mass is expected to be about 80 kg, floating at an 8 km altitude with a 2 kW RTG heat source and a 2x design margin against environmental and operations uncertainties [72].

A Titan Montgolfière balloon with a comprehensive scientific payload was a critical element of the mission architecture proposed to NASA and ESA

in 2009 for consideration as a joint flagship mission called the Titan Saturn System Mission (TSSM) [73] [74]. This proposal was not selected for implementation, and no significant further work has been performed since.



Figure 16-20: Single wall Montgolfière cryogenic Titan balloon.

Photo credit: M. Pauken

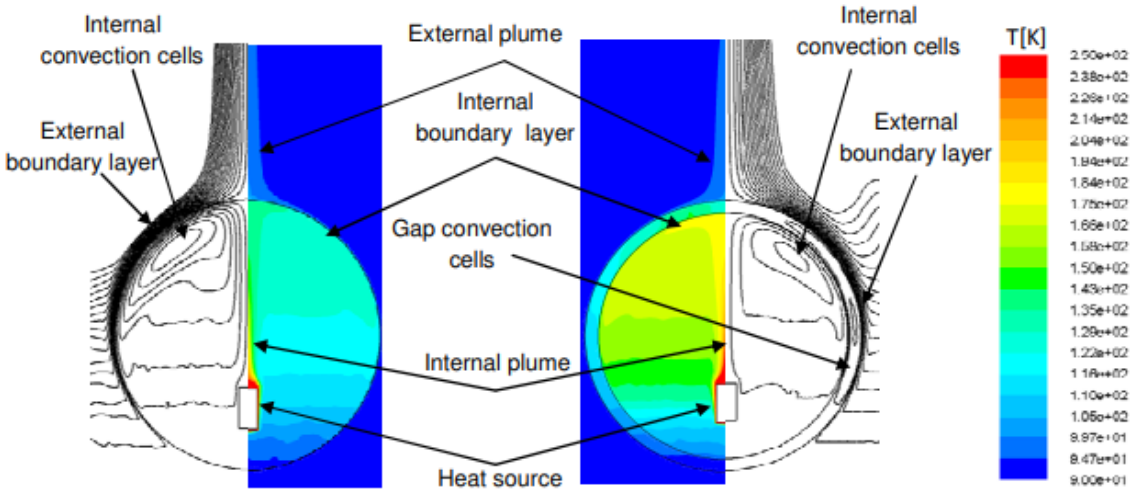


Figure 16-21: Temperature profiles and stream functions inside a single-walled balloon on the left and a double-walled balloon on the right from the CFD-thermal model [70].

4.3.2. Super-pressure Balloons

Light-gas super-pressure balloons are also an attractive option for Titan. The Titan atmosphere is very dense near the surface, allowing small balloons to carry large payloads. For example, a helium super-pressure balloon floating at 8 km would be only 4.6 m in diameter but would be able to carry a payload of 170 kg. The helium mass would be 28 kg, and the balloon mass would be 9 kg with a super-pressure of 1 kPa [30]. Hall et al. [75] developed cryogenic materials for super-pressure balloon and blimp envelopes constructed of a 6-layer Mylar film laminate bonded to a polyester fabric with an aerial density of 94 g/m^2. A 1.5-meter-diameter super-pressure balloon prototype constructed of this material is shown in Figure 16-22. Testing this balloon at cryogenic temperatures for 70 hours demonstrated that helium leakage through the balloon by diffusion drops to essentially zero at 93 K, as expected by the theory of gas diffusion through a membrane [76].

Super-pressure balloons at Titan have three main advantages compared to RTG-heated hot air balloons:

- Inherent altitude stability as per all super-pressure balloons as described in Chapter 10.
- Almost no uncertainty in predicting buoyancy performance, unlike the Montgolfière option, which has significant uncertainties due to the complex heat transfer behavior and its sensitivity to balloon motion.
- Much greater flexibility in positioning the RTG on the vehicle since it does not need to provide heat to the balloon itself, as is required for the Montgolfière option.

The primary disadvantage of super-pressure balloons is the additional mass required for high-pressure storage tanks to transport the helium or hydrogen to Titan.

4.3.3. Blimp Aerobot Systems

The presumed low winds on Titan are conducive to using a self-propelled blimp vehicle to conduct a directed global exploration instead of only being moved by the winds. Such a vehicle could also control altitude over some range through the use of a standard ballonet. Following early concept studies [118], a 4.6 m long blimp prototype, depicted in Figure 29, was fabricated from the same 6-layer polyester laminate film used for the super-pressure Titan balloon prototype shown in Figure 28. The blimp was approximately 1/3 of the scale required for a Titan aerobot mission and included a small gondola with twin insulated electric motors [75]. The prototype was operated in a large cryogenic chamber at 93K for several hours, demonstrating the feasibility of running electric motors in a cryogenic environment.



Figure 16-22: A 16-gore, 1.5-m diameter Titan (at 1kPa super-pressure) balloon prototype made using a 6-layer polyester film.

Photo credit: M. Pauken

The design of the blimp aerobot places the RTG power source directly under the airship hull. Concerns over the waste heat from the RTG on the temperature and pressure state of the blimp were addressed by computational fluid dynamics (CFD) modeling and laboratory experiments. Analysis showed that most of the waste heat went into the wake of the airship as it moved through the atmosphere. However, under conditions where the airship was not propelled and floated with the atmosphere, the waste heat would largely enter the blimp, causing a rise in temperature and pressure. The additional lift and pressure in this situation would be controlled by using ballonets that are filled with ambient gas. Additional technical developments for the Titan blimp have included a demonstration of aerial deployment and inflation under a parachute descent, and a floating gimbal steerable antenna operation [75].



Figure 16-23: Titan blimp aerobot under cryogenic flight test with insulated electric propeller motors.

4.3.4. Variable-Altitude Balloon Systems

The variable altitude balloon concepts described for use at Venus in Section 4.1 above can be adapted for use at Titan. Background theory and a Titan trade study of competing approaches can be found in Reference [44]. The Titan balloon has lower super-pressure requirements than a Venus balloon system due to the lack of solar heating. The helium mass for Titan balloons is greater than that of Venus because light gas balloons produce less buoyancy per unit mass in a nitrogen atmosphere than in a carbon dioxide atmosphere because of the molecular weight difference. However, the energy required to reduce altitude on Titan is an order of magnitude less than that required on Venus [44]. No specific prototyping work has been conducted on any of these variable-altitude aerobot concepts for Titan.

4.4. Scientific Instrumentation

Many of the scientific questions about planetary atmospheres can be addressed with the same types of measurements used in terrestrial investigations from balloons or aircraft. A key difference for a planetary aerobot is that instruments generally must be much smaller and consume less power. The total scientific payload may be no more than a few tens of kg in the largest aerobots contemplated today and possibly much less. Necessarily, this excludes some instruments that might be flown on terrestrial balloons or aircraft, but it also provides a significant impetus for miniaturization. Further discussion of scientific instrumentation can be found in Chapter 17.

5. Conclusions

Planetary balloons represent a unique synthesis of scientific ambition and engineering ingenuity. By harnessing buoyancy in alien atmospheres, they provide a platform that bridges the gap between orbiters, landers, and rovers. Unlike orbiters that view planets from afar or landers constrained to a single location, balloons offer mobility, persistence, and regional context at scales that would otherwise be inaccessible. This middle ground is crucial for understanding planetary processes in their full complexity, from atmospheric circulation to surface–atmosphere interactions.

The history of balloon exploration has shown both the challenges and the promise of this approach. Early missions demonstrated the feasibility of aerial platforms on other worlds, while more recent studies and design efforts continue to push the boundaries of endurance, data return, and control. Advances in materials, miniaturized sensors, and autonomous navigation now allow balloons to survive longer and probe more deeply into hostile atmospheres such as those of Venus or the gas giants. These technological improvements not only enhance the return on science but also broaden the range of possible mission architectures.

From a scientific perspective, planetary balloons are especially well-suited for studying atmospheric chemistry, cloud dynamics, and weather systems. They provide in-situ measurements over extended timescales, enabling researchers to resolve variability and capture transient phenomena. Balloons can also serve as relays or scouts for other assets, extending the reach of planetary exploration networks. In this way, balloon missions complement both traditional spacecraft and future human exploration, ensuring that planetary environments are characterized with the detail and resilience required for long-term planning.

Looking ahead, international collaboration will likely play a decisive role in realizing the next generation of planetary balloon missions. Agencies such as NASA, ESA, CNES, and ISRO bring complementary expertise in ballooning, planetary science, and mission operations. By combining resources and knowledge, these organizations can accelerate progress and reduce risks, ensuring that balloons become a mainstay of planetary exploration rather than a rare experiment. Ultimately, planetary balloons embody the spirit of exploration itself: creative, adaptive, and daring in their pursuit of knowledge across new frontiers.

References

[1] R. Z. Sagdeev, V. M. Linken, J. E. Blamont and R. A. Preston, "The VEGA Venus Balloon Experiment," *Science,* vol. 231, pp. 1407-1408, 1986.

[2] J. E. Blamont, R. E. Young, A. Seiff and e. al., "Implications of the VEGA Balloon Results for Venus Atmospheric Dynamics," *Science,* vol. 231, pp. 1422-1425, 1986.

[3] V. M. Linkin, V. V. Kerzhanovich, A. N. Lipitov and e. al., "Thermal Structure of the Venus Atmosphere in the Middle Cloud Layer," *Science,* vol. 231, pp. 1420-1422, 1986.

[4] V. M. Linkin, V. V. Kerzhanovich, A. N. Lipatov and e. al., "VEGA Balloon Dynamics and Vertical Winds in the Venus Middle Cloud Region," *Science,* vol. 231, pp. 1416-1420, 1986.

[5] R. A. Preston, C. E. Hilderbrand, J. G. H. Purcell, J. Ellis and e. al., "Determination of Venus Winds by Ground-Based Radio Tracking of the VEGA Balloons," *Science,* vol. 231, pp. 1414-1416, 1986.

[6] R. Z. Sagdeev, V. M. Linkin, V. V. Kerzhanovich, A. N. Lipatov and e. al., "Overview of VEGA Venus Balloon in Situ Meteorological Measurements," *Science,* vol. 231, pp. 1411-1414, 1986.

[7] R. S. Kremnev, V. M. Linkin, A. N. Lipatov, K. M. Pichkadze and e. al., "VEGA Balloon System and Instrumentation," *Science,* vol. 231, pp. 1408-1411, 1986.

[8] J. Blamont, "Balloons on Other Planets," *Advances in Space Research,* vol. 1, pp. 63-69, 1981.

[9] A. L. Friedlander, "Titan Buoyant Station," *Journal of the British Interplanetary Society,* vol. 37, pp. 381-387, 1984.

[10] C. Tarrieu and C. Sirmain, "Mars balloon: A French contribution to the Mars 94 Soviet Mission," in *IAF-88-396*, 1988.

[11] E. Stofan and e. al, "Dragonfly: In Situ Exploration of Titan's Prebiotic Organic Chemistry and Habitability," in *Proc. IEEE Aerospace Conference*, Big Sky, 2013.

[12] F. Raulin, C. McKay, J. Lunine and T. Owen, "Titan Astrobiology," in *Titan from Cassini-Huygens*, Springer, 2010, pp. 215-234.

[13] C. Neish and e. al, "Organic Input to Titan's Subsurface Ocean Through Impact Cratering," *Astrobiology,* vol. 24, no. 2, 2024.

[14] G. Lente and K. Osz, "Barometric formulas: various derivation and comparisons to environmentally relevant observations," *Chem Texts,* vol. 6, no. 13, 2020.

[15] A. Kliore, V. Moroz and G. Keating, "The Venus International Reference Atmosphere," *Advances in Space Research,* vol. 5, pp. 1-304, 1985.

[16] S. Dutta, C. Karlgaard, D. Kass, M. Mischna and G. and Villar III, "Postflight Analysis of Atmospheric Properties from Mars 2020 Entry, Descent and Landing," *Journal of Spacecraft and Rockets,* vol. 60, no. 3, pp. 1022-1033, 2023.

[17] M. Fulchignoni, F. Ferri, F. Angrilli and e. al., "In situ measurements of the physical characteristics of Titan's Environment," *Nature,* vol. 438, pp. 785-791, 2005.

[18] D. Crisp, "Radiative forcing of the Venus mesosphere: II. Thermal fluxes, cooling rates, and radiative equilibrium temperatures," *Icarus,* vol. 77, pp. 391-413, 2018.

[19] T. D. Robinson and D. Crisp, "Linearized Flux Evolution (LiFE): A technique for rapidly adapting fluxes from full-physics radiative transfer models," *Journal of Quantitative Spectroscopy and Radiative Transfer,* vol. 211, pp. 78-95, 2018.

[20] B. Ragent, L. Esposito, M. G. Tomasko, M. Marov, V. Shari and V. Lebede, "Particular Matter in the Venus Atmosphere," *Advances in Space Research,* vol. 5, no. 11, pp. 85-115, 1985.

[21] A. Sieff, J. T. Schofield, A. J. Kliore and e. al, "Models of the structure of atmosphere of Venus from the surface to 100 kilometers altitude," *Adv. Space Research,* vol. 5, no. 11, pp. 3-58, 1985.

[22] D. Titov, N. I. Ignatiev, K. McGouldrick, V. Wilquet and C. F. Wilson, "Clouds and Hazes of Venus," *Space Science Reviews,* vol. 214, no. 126, 2018.

[23] Á. Vicente-Retortillo, F. Valero, L. Vázquez and G. Martínez, "A model to calculate solar radiation fluxes on the Martian surface," *J. Space Weather Space Climate,* vol. 5, 2015.

[24] S. Lewis, "Modelling the Martian atmosphere," *Astronomy & Geophysics,* vol. 44, pp. 4.6-4.14, 2003.

[25] H. H. Kieffer, "Thermal model for analysis of Mars infrared mapping," *JGR Planets,* vol. 118, no. 3, pp. 451-470, 2013.

[26] T. Robinson and D. Catling, "AN ANALYTIC RADIATIVE-CONVECTIVE MODEL FOR PLANETARY ATMOSPHERES," *The Astrophysical Journal,* vol. 757, pp. 1-13, 2012.

[27] M. G. Tomasko, L. Doose, S. Engel and e. al, "A model of Titan's aerosols based on measurements made inside the atmosphere," *Planetary and Space Science,* vol. 56, no. 5, pp. 669-707, 2008.

[28] ESKOS, "Venera/Vega Projects: An Analysis Of The Operational Experience Obtained In The Study Of the Atmosphere And Surface Of Venus," ESKOS, Saint-Ouen, 1994.

[29] SpaceX, "SpaceX Falcon User's Guide," 2021.

[30] V. Kerzhanovich, J. Hall, A. Yavrouian and J. Cutts, "Two Balloon System to Lift Payloads for the Surface of Venus," in *AIAA 5th ATIO and 16th Lighter-Than-Air Sys Tech. and Balloon Systems Conferences*, Arlington, 2005.

[31] M. Adams, L. Glaze, M. Amato and C. and Baker, "Venus Mobile Explorer Final Report," 2009.

[32] Venus Aerial Platforms Study Team, "Aerial Platforms for the Scientific Exploration of Venus," JPL D-102569, Pasadena, 2018.

[33] J. L. Hall, D. Fairbrother, T. Frederickson, V. V. Kerzhanovich, M. Said, C. Sandy, C. Willey and A. H. Yavrouian, "Prototype design and testing of a Venus long duration, high altitude balloon," *Advances in Space Research,* vol. 42, pp. 1648-1655, 2008.

[34] M. Y. Marov and W. T. Huntress, Soviet Robots in the Solar System: Mission technologies and discoveries, Chichester: Springer-Praxis, 2011.

[35] J. L. Hall, V. V. Kerzhanovich, A. H. Yavrouian, G. A. Plett, M. Said, D. Fairbrother, C. Sandy, T. Frederickson, G. Sharpe and S. Day, "Second generation prototype design and testing for a high altitude Venus balloon," *Advances in Space Research,* vol. 44, pp. 93-105, 2008.

[36] J. L. Hall, A. H. Yavrouian, V. V. Kerzhanovich, T. Fredrickson, C. Sandy, M. T. Pauken, E. A. Kulczycki, G. J. Walsh, M. Said and S. Day, "Technology Development for a Long duration, Mid-Cloud Level Venus Balloon," *Advances in Space Research,* vol. 48, pp. 1238-1247, 2011.

[37] J. L. Hall and A. H. Yavrouian, "Pinhole Effects on Venus Superpressure Balloon Lifetime," in *AIAA-2013-1292*, Daytona Beach, 2013.

[38] K. Baines, S. K. Atreya, D. Crisp, J. L. Hall, V. V. Kerzhanovich, S. S. Limaye and K. Zahnle, "IN-SITU EXPLORATION OF VENUS BY BALLOON - SCIENCE OBJECTIVES AND MISSION ARCHITECTURE," in *40th Lunar and Planetary Sciences Conference*, 2009.

[39] Venus Science and Technology Definition Team, "Venus Flagship Mission Study," JPL, 2009.

[40] K. T. Nock, K. M. Aaron, J. A. Jones, D. P. McGee, G. E. Powell, A. H. Yavrouian and J. J. Wu, "BALLOON ALTITUDE CONTROL EXPERIMENT (ALICE) PROJECT," in *11th Lighter Than Air Systems Technology Conference*, Clearwater Beach, 1995.

[41] J. Jones, "Reversible Fluid Balloon Altitude Control Concepts, AIAA Paper 95-1621," in *11th Lighter-than-Air Systems Technology Conference*, Clearwater Beach, 1995.

[42] J.-J. Wu and J. A. Jones, "PERFORMANCE MODEL FOR REVERSIBLE FLUID BALLOONS, AIAA Paper AIAA 95-1608," in *11th Lighter-than-Air Systems Technology Conference*, Clearwater Beach, 1995.

[43] A. Alexander, M. Alvidrez, W. Beg, Z. Benezet-Parsons, L. Bouygues, S. Coriell, J. Dempsey, U. Dogruer, B. Freedman, J. Grazer, D. Herbert, B. Ho, R. Lange, M. Lelièvre, D. Nguyen, J. Nutzmann and e. al., "Loon Library: Lessons from Building Loon's Stratospheric Communications Service," Loon LLC, 2021.

[44] J. L. Hall, J. M. Cameron, M. T. Pauken, J. S. Izraelevitz, M. W. Dominguez and K. T. Wehage, "Altitude-Controlled Balloon Concepts for Venus and Titan," in *AIAA Paper 2019-3194*, Dallas, 2019.

[45] P. B. Voss, "Advances in Controlled Meteorological (CMET) Balloon Systems," in *AIAA Paper 2009-2810*, Seattle, 2009.

[46] P. B. Voss, L. R. Hole, E. F. Helbling and T. J. Roberts, "Continuous In-Situ Soundings in the Arctic Boundary Layer: A New Atmospheric Measurement Technique Using Controlled Meteorological Balloons," *Journal of Intelligent & Robotic Systems,* vol. 70, pp. 609-617, 2012.

[47] Venus Flagship MIssion Study Team, "2020 Venus Flagship Mission Study," A Planetary Mission Concept Study Report Presented to the Planetary and Astrobiology Decadal Survey, 2020.

[48] J. L. Hall, M. T. Pauken, A. Schutte, S. Krishnamoorthy, C. Aiazzi, J. S. Izraelevitz, T. Lachenmeier and C. Turner, "Prototype Development of a Variable Altitude Aerobot," in *AIAA Aviation Forum, AIAA Paper 2021-2696*, 2021.

[49] J. Izraelevitz, M. Pauken, S. Krishnamoorthy, A. Goel, C. Aiazzi, L. Dorsky, J. Cutts, H. J. L., C. Turner and T. Lachenmeier, "Subscale Prototype and Hangar Test Flight of a Venus Variable-Altitude Aerobot," in *IEEE Aerospace Conference*, Big Sky, 2022.

[50] J. S. Izraelevitz, S. Krishnamoorthy, A. Goel, C. Aiazzi, M. Pauken, G. Walsh, C. Leake, C. Lim, A. Jain, L. Dorsky, K. Baines, J. Cutts and J. L. Hall, "Flight Demonstration of a Prototype Variable-Altitude Venus Aerobot," *AIAA Journal of Aircraft,* vol. TBD, p. UNDER REVIEW, TBD.

[51] V. L. Gatto, J. S. Izraelevitz, M. T. Pauken, A. Goel, R. Lam and J. L. Hall, "Inflation sequence tradeoffs and laboratory demonstration of a prototype variable-altitude Venus aerobot," *Acta Astronautica,* vol. 214, pp. 757-773, 2024.

[52] W. P. Buchanan, M. d. Jong, R. Agrawal, J. J. Petkowski, A. Arora, S. J. Saikia, S. Seager and J. Longuski, "Aerial Platform Design Options for a Life-Finding Mission at Venus," *Aerospace,* vol. 9, no. 363, 2022.

[53] P. Malaterre, "Long duration balloon flights in the middle stratosphere," *Advances in Space Research,* vol. 13, no. 2, pp. 107-114, 1993.

[54] T. K. Schuler, D. C. Bowman, J. S. Izraelevitz, D. Sofge and J. Thangavelautham, "Long duration flights in Venus' atmosphere using passive solar hot air balloons," *Acta Astronautica,* vol. 191, pp. 160-168, 2022.

[55] J. A. J. a. M. K. Heun, "Montgolfiere balloon aerobots for planetary atmospheres," in *AIAA Paper 1997-1445*, 1997.

[56] D. C. Bowman and e. al., "Multihour stratospheric flights with the heliotrope solar hot-air balloon," *Journal of Atmospheric and Oceanic Technology,* vol. 37, no. 6, pp. 1051-1066, 2020.

[57] Q. Brissaud and e. al., "The first detection of an earthquake from a balloon using its acoustic signature," *Geophysical Research Letters,* vol. 48, 2021.

[58] T. Tzanetos and e. al., "Ingenuity Mars Helicopter: From Technology Demonstration to Extraterrestrial Scout," in *IEEE Aerospace Conference, pp 1-19*, Big Sky, 2022.

[59] J. Blamont, "Balloons for the Exploration of Mars," *Advances in Space Research,* vol. 13, no. 2, pp. 137-144, 1993.

[60] C. M. Anderson, "Wind, Sand and Mars: the 1990 Tests of the Mars Balloon and Snake," *The Planetary Report,* vol. 11, no. 1, pp. 12-15, 1991.

[61] T. Gamber, K. T. Nock, J. Balaram, M. K. Heun and I. S. Smith, "Mars 2001 Aerobot/Balloon System Overview," in *AIAA Paper 97-1447*, 1997.

[62] I. S. Smith, J. M. Simpson, S. M. Raque, M. A. Said and H. M. Cathey, "The Mars 2001 Balloon Design," in *AIAA Paper 97-1442*, 1997.

[63] A. Vargas, J. Evrard and P. Mauroy, "Mars 96 Aerostat – An Overview of Technology Developments and Testing," in *AIAA Paper 97-1449*, 1997.

[64] V. V. Kerzhanovich, J. A. Cutts, H. W. Cooper, J. L. Hall, B. A. McDonald, M. T. Pauken, C. V. White, A. H. Yavrouian, A. Castano, H. M. Cathey, D. A. Fairbrother, I. S. Smith, C. M. Shreves, T. Lachenmeier, E. Rainwater and M. Smith, "Breakthrough in Mars Balloon Technology," *Advances in Space Research,* vol. 33, pp. 1836-1841, 2004.

[65] J. L. Hall, M. T. Pauken, V. V. Kerzhanovich, G. J. Walsh, D. Fairbrother, C. Shreves and T. Lachenmeier, "Flight Test Results for Aerially Deployed Mars Balloons," in *AIAA Paper 2007-2626*, Williamsburg, 2007.

[66] H. S. Griebel, B. Hausler, H. Rapp and C. Mundt, "Project Archimedes: A Novel Approach to Balloon Deployment on Mars," in *55th International Astronautical Congress*, Vancouver, 2004.

[67] K. T. Nock, J. Balaram, M. K. Heun, I. S. SMith and T. Gamber, "Mars 2001 Aerobot/Balloon System Overview," in *AIAA Paper 97-1447*, San Francisco, 1997.

[68] J. A. Jones and J. J. Wu, "Solar Montgolfiere Balloons for Mars," in *AIAA Paper 99-3852*, 1999.

[69] J. A. Jones, D. Fairbrother, A. Lemieux, T. Lachenmeier and R. Zubrin, "Wind-Driven Montgolfeire Balloons for Mars," in *AIAA Paper 2005-844*, 2005.

[70] Y. Feldman, T. Colonius, M. Pauken, J. L. Hall and J. A. Jones, "Numerical and Experimental Modeling of Natural Convection for a Cryogenic Prototype of a Titan Mongolfiere," in *AIAA Paper 2011-6869*, Virginia Beach, 2011.

[71] J. Nott and J. Rand, "The Titan Sky Simulator Test Facility," in *AIAA Paper 2007-2625*, 2007.

[72] R. Lorenz, "A Review of Balloon Concepts for Titan," *Journal of the British Interplanetary Society,* vol. 61, pp. 2-13, 2008.

[73] J.-P. Lebreton, C. Erd, J. Romstedt and P. Falkner, "TSSM In Situ Elements: ESA Contribution to Titan Saturn System Mission," ESA-SRE(2008)4, 2009.

[74] Team, Joint Titan Saturn System Mission Science Definition, "TSSM NASA/ESA Joint Summary Report," NASA/ESA, 2009.

[75] J. Hall, J. Jones, V. Kerzhanovich, T. Lachenmeier, P. Mahr, J. Mennella, M. Pauken, G. Plett, M. Smith, M. Van Luvender and A. Yavrouian, "Experimental results for Titan aerobot thermo-mechanical subsystem development," *Advances in Space Research,* vol. 42, pp. 1641-1647, 2008.

[76] M. T. Pauken and J. L. Hall, "Development and Testing of a Titan Superpressure Balloon Prototype," in *11th Interplanetary Probe Workshop*, Pasadena, 2014.

[77] A. L. Friedlander and H. Feingold, "Balloon-Assisted Ascent to Venus Orbit," in *AIAA/AAS Astrodynamics Conference paper 78-1438*, Palo Alto, 1978.

[78] V. Kerzhanovich, J. Hall, A. Yavrouian and J. Cutts, "Two Balloon System to Lift Payloads for the Surface of Venus," in *AIAA Paper 2005-7322*, Arlington, 2005.

[79] V. Scott, "Venus In Situ Transfer and Analysis (VISTA) Mission," DOI: 10.26206/78tbr-5ta74, 2023.

[80] National Academies of Science, Engineering and Medicine, "Origins, Worlds, and Life: A Decadal Strategy for Planetary Science and Astrobiology 2023-2032," The National Academies Press, 2023.

[81] J. B. Garvin, S. A. Getty, G. N. Arney and e. al., "Revealing the Mysteries of Venus: The DA VINCI Mission," *The Planetary Science Journal,* vol. 3, no. 5, pp. 1-17, 2022.

[82] C. R. Webster, A. E. Hofmann, P. R. Mahaffy, S. K. Atreya, C. H. House, A. A. Simon and J. B. Garvin, "Tunable Laser Spectrometers for Planetary Science," *Space Science Reviews Vol 2019,* 2023.

[83] K. Baines, D. Nikolic, J. Cutts, J.-B. Renard, S. M. Madzunkov, L. Barge, O. Mousis and S. Limaye, "Investigation of Venus Cloud Aerosol and Gas Composition Including Potential Biogenic Materials

via an Aerosol-Sampling Instrument Package," *Astrobiology,* vol. 21, no. 10, 2021.

[84] R. G. Knollenberg and D. M. Hunten, "The Microphysics of the Clouds of Venus: Results of the Pioneer Venus Particle Size Spectrometer Experiment," *JOURNAL OF GEOPHYSICAL RESEARCH,* Vols. VOL. 85, , no. NO. AI3, pp. 8039-8058, 1980.

[85] J.-B. Renard, F. Dulac, G. Berthet et al., T. Lurton, D. Vignelles and F. Jegon, "LOAC: A small aerosol optical counter/sizer for ground-based and balloon measurements of the size distribution and nature of atmospheric particles - Part 2: First results from balloon and unmanned aerial vehicle flights.," *Atmos. Meas. Tech.,* vol. 9, pp. 3673-3686., 2016b.

[86] G. Israel, C. Szopa, F. Raulin, H. B. Niemann, S. K. Atreya and S. J. Bauer, "Complex Organic Matter In Titan's atsmospheric aerosols from in siut pyrolyis an danalysis," *Nature VOl 438/B,* pp. 796-799, 2005.

[87] Aerodyne_Research, "Aerosol Mass Spectrometer," 29 04 2024. [Online]. Available: https://aerodyne.com/particle-instruments/ams-acsm/#htof-ams-anchor.

[88] M. L. Delitsky and K. H. Baines, "Cloud chemistry on Venus: Sulfuric acid reactions and supercooling in Venus liquid cloud droplets," *Planetary and Space Science,* p. https://doi.org/10.1016/j.pss.2023.105750 , 2023.

[89] S. Seager, "Venus Mission Concept Study," MIT , https://venuscloudlife.com/venus-life-finder-mission-study/, 2021.

[90] K. M. Cheung, "Single-Satellite Real-Time Positioning of Balloon and Helicopter for Aerial Exploration in Extraterrestrial Atmosphere," in *Mobile Satellte Communications*, 2019.

[91] S. Ploen, J. Aldrich, D. Bayard, L. Dorske, A. Katake, E. Konefat, C. C. Liebe and J. Shields, "Bias Compensated Inertial Navigation for Venus Balloon Missions," in *IEEE Aerospace Conference*, 2022.

[92] D. Banfield, D. W. Schindel and R. W. Dissly, "A Martian acoustic anemometer," *Journal Acoustic Society of America 140 (2),* pp. 1420-1428, 2016.

[93] C. Raymond, "PICCARD: A Balloon Magnetometer Mission to Mars," in *Lunar and Planetary Science Conference*, 1999.

[94] A. Coustenis, J. Lunine, K. Reh, J.-P. Lebreton, C. Erd, P. Beauchamp, C. Sotin and D. Matson, "Titan Saturn System Mission Instrumentation," in *Internatonal Workshop on Instrumentation for Planetary Missions*, 2012.

[95] J. G. O'Rourke, J. Buz, R. Fu and R. Lillis, "Detectability of Remanent Magnetism in the Crust of Venus," *Geophys. Res. Lett.,* vol. 46, no. 11, p. 5768–5777, 2019.

[96] F. Simoes, R. Grard, M. Hamelin, J. J. Lopes-Moreno, K. Schwingenschuh, C. Beghin, F. Ferri and Molina-Cuberos, "Investgiation of Titan electric environment and the Titan Electric Environment Packaage for the TandEM Mission," in *European Planetary Science Congress* , 2010.

[97] M. Hamelin, C. Beghin, V. J. G. Brown, P. Falkner and R. Grard, "Titan's Atmospheric Electricity from the Measurements of the PWA-HAIS instrument on board the Huygens probe," in *EUROPLANET*, Berlin, 2006.

[98] R. E. Grimm, "Aerial electromagnetic sounding of the lithosphere of Venus," *Icarus,* vol. 217, no. 2, p. 462–473, 2012.

[99] R. Grimm, Interviewee, *Sounding the Venus Lithosphere.* [Interview]. 7 Jan 2020.

[100] S. Goosens, T. J. Sabaka, Wieczorek, G. A. Neumann, F. G. Mazarico, J. B. Nicholas, D. E. Smith and M. T. Zuber, "High Resolution Gravity Field Models from GRAIL Data and Implications for Models of the Density Structure of the Moon's Curst," *JGR Planets,* pp. 1-31, 2019.

[101] B. Bills, S. Krishnamoorthy and A. Komjathy, "Balloon Borne Gravity Survey of Venus," Jet Propulsion Laboratory - Internal Report, 2020.

[102] R. Ghail and T. Voirin, "EnVision Understanding why Earth's closest neighbour is so different; Assessment Study Report," European Space Agency, 2021.

[103] S. Krishnamoothy et. al. , "Detection of Artificially Generated Seismic Signals Using Balloon-Borne Infrasound Sensors," *Geophys. Res. Lett.,* vol. 45, no. 8, p. 3393–3403, 2018.

[104] S. Krishnamoorthy et. al. , "Aerial seismology using balloon-based barometers," *IEEE Trans. Geosci. Remote Sens.,* vol. 57, no. 12, p. 10191–10201, 2019.

[105] Q. Brissaud et. al., "The first detection of an earthquake from a balloon using its acoustic signature," *Geophys. Res. Lett.,* vol. doi.org/10.1029/2021GL093013, 2021.

[106] A. D. Jolly et. al., "Capturing the Acoustic Radiation Pattern of Strombolian Eruptions using Infrasound Sensors Aboard a Tethered Aerostat, Yasur Volcano, Vanuatu," *Geophys. Res. Lett.,* vol. 44, no. 19, pp. 9672-9680, 2017.

[107] R. Garcia, P. Lognonné and X. Bonnin, "Detecting atmospheric perturbations produced by {Venus} quakes," *Geophys. Res. Lett.,* vol. 32, no. 16, 2005.

[108] R. F. Garcia, A. Klotz, A. Herzog, R. MArtin, S. Gerier, E. Kassarian, J. Bordereau, S. Venel and D. Mimoun, "Infrasound rof LArge Earthquakes Recorded on a Network of Balloons in the Stratosphere," *Geophysical Research Letters,* p. 10.1029/2022GL098844, 2022.

[109] ESA_Science&Exploration, "View from ten kilometers high on Titan," 17 01 2005. [Online]. Available: https://www.esa.int/Science_Exploration/Space_Science/Cassini-Huygens/View_from_ten_kilometres_high.

[110] J. Cutts, "Exploring the Clouds of Venus: Science Driven Aerobot Missions to our Sister Planet," in *IEEE Aerospace Conference*, Big Sky, MO, 2022.

[111] S. A. Cohn, T. Hock, P. Cocquerez, J. Wang and F. Rabier, "Driftsondes: Providing In Situ Long Duration Dropsond Observations over Remote Regions," *American Meteorological Society,* pp. 1661-1674, 2013.

[112] A. B. Davis, K. H. Baines, B. M. Sutin, J. A. Cutts, L. I. Dorsky and P. K. Byrne, "Feasibility of high-spatial-resolution nighttime near-IR imaging of Venus' surface from a platform just below the clouds: A radiative transfer study accounting for the potential of haze," *Planetary and Space Science,* vol. 242, 2024.

[113] K. Klaasen and R. Greeley, "VEVA Discovery Mission: Exploration of Volcanoes and Atmosphere," *Acta Astronautica 53 (2-6),* 2003.

[114] J. Izraelevitz and J. Hall, "Minimum Mass limits for streamlined Venus Atmospheric probes," *AIAA Journal of Spacecraft and Rocket,* 2020.

[115] D. Bowman, P. E. Norman, M. T. Pauken, S. A. Albert, D. Dexheimer, X. Yang, S. Krishnamorrthy, A. Komjathy and J. A. Cutts, "Multihour Stratospheric Flights with the Heliotrope Solar Hot-Air Balloon,"

Journal of American Meteorology, pp. DOI: 10.1175/JTECH-D-19-0175.1, 2020.

[116] H. Laplace, C. Tarrieu, J. Cantrell and B. Schurmier, "The Guiderope for the Soviet-French Mars 96 balloon Mission," in *43rd International Astronautical COngress*, Washington, D. C., 1992.

[117] M. Badescu, S. Sherrit, J. Jones and J. Hall, "Self-Contained Harpoon and Sample Handling Device for a Remote Platform," in *Sensors and Smart Structures Technologies for Aerospace System*, 2009.

[118] P. McGarey, B. Hockman, B. Sutin, J. Izraelevitz, A. Davis, J. Cutts, L. Dorsky and K. Baines, "A Tethered Towbody Payload for In- and Sub-Cloud Sensing on Venus," in *International Planetary Probe Workshop-Virtual*, 2021.

[119] Bachelder, Aaron; Nock, Kerry; Heun, Matthew; Balaram, J.; Hall, J.; Jones, J.; Kerzhanovich, V.; McGee, D.; Stofan, E.; , J. Wu; Yavrouian, A., "Venus Geoscience Aerobot Study (VEGAS)," in *AIAA International Balloon Technology Conference*, Norfolk, 1999.

[120] Venus Aerial Platforms Study Team, "Aerial Platforms for the Scientific Exploration of Venus," JPL D-102569, Pasadena, 2018.

[121] J. L. Hall, J. Lunine, C. Sotin, K. Reh, A. Vargas and P. Couzin, "Titan Aerial Explorer (TAE): Exploring Titan by Balloon," in *Interplanetary Probe Workshop 8*, Portsmouth, 2011.

[122] J. L. Hall, V. V. Kerzhanovich, A. H. Yavrouian, J. A. Jones, C. White, B. A. Dudik, G. A. Plett, J. Mennella and A. Elfes, "An Aerobot For Global In Situ Exploration of Titan," *Advances in Space Research*, vol. 37, pp. 2108-2119, 2006.

[123] B. M. Andreiechikoc, I. K. Akhmetshin, B. N. Korchuganov, L. M. Mukhin and B. I. Ogorodnikov, "X-Ray Radiometric Analysis of Vensu Cloud Aerosol by Vega 1 and 2 automated interplanetary probes," *British Library UDC 523.042:523.42: Kosmicheskie Issledovaniia (ISSN 0023-4206), vol. 25, Sept.-Oct. 1987, p. 721-736. In Russian,* pp. 554-567, 1986.

[124] A. Coustenis, S. K. Atreya, T. Balint, R. H. Brown, M. K. Dougherty and F. Ferri, "TandEM: Titanand Enceladus mission," *Experimental Astronomy Vol 23*, pp. 893-946, 2009.

[125] D. Sampietro, A. H. Mansi and M. Capponi, "A New Tool for Airborne Gravimetry Survey Simulation," *Geosciences 10`8*, p. 292, 2018.

Chapter 17
Instrumentation

(in alphabetical order)

Daniel C. Bowman[1], James A. Cutts[9], Brian R. Elbing[2], Jeffery L. Hall[3], Emalee E. Hough[3], Jacob S. Izraelevitz[9], Jamey D. Jacob[4], Michael T. Pauken[9], Tristan K. Schuler[5], Taylor D. Swaim[6], Zachary Yap[7], Christopher D. Yoder[8]

[1] Pacific Northwest National Laboratory, Geophysicist, Signals Detection & Analysis

[2] Oklahoma State University, Professor, Mechanical and Aerospace Engineering

[3] Jet Propulsion Laboratory, California Institute of Technology
This work was carried out at the Jet Propulsion Laboratory, California Institute of Technology, under a contract with the National Aeronautics and Space Administration (80NM0018D0004).
[4] Oklahoma State University, Professor and OAIRE Director, Mechanical and Aerospace Engineering

[5] U.S. Naval Research Laboratory, Research Scientist, NCARAI

[6] Pennsylvania State University, Engineer, Applied Research Laboratory

[7] Oklahoma State University, R&D Engineer, OAIRE

[8] NASA Wallops Flight Facility, Aerospace Engineer, Balloon Program Office

Table of Contents

1. Introduction 4

2. Terrestrial balloon health and status 4

2.1. Zero-pressure vehicles..... 4

2.2. Super-pressure vehicles..... 5

2.3. Environmental instrumentation..... 7

3. Scientific Payload Instrumentation 7

3.1. Infrasound (microbarometers)..... 7

3.2. Other Scientific Payloads..... 8

3.3. Flight Tracking and Communications..... 8

4. Extra-terrestrial Instrumentation 9

4.1. Atmospheric Chemistry and Astrobiology..... 10

4.2. Atmospheric Dynamics..... 12

4.3. Geophysical Profiling..... 13

4.4. Infrasound Seismology..... 15

4.5. Surface Imaging and Imaging Spectroscopy..... 16

4.6. Dropsondes and Risesondes..... 17

4.7. Tether Deployment of Payloads..... 18

5. Summary 18

References..... 19

Table of Figures

Figure 17-1: Image of the NASA 18.8mcf SPB during the Wanaka 2025 campaign during daytime (top) and nighttime (bottom)..... 6

Figure 17-2: Sequence of still images taken from a heliotrope on 8 April 2024 during the total solar eclipse [29]..... 8

Figure 17-3: A tunable laser spectrometer (Left) has been used on the Mars Curiosity mission and is being developed for flight on a Venus probe to measure targeted trace gas species. The Light Optical Aerosol Counter (LOAC) has been demonstrated on several terrestrial aerobot flights, confirming its ability to discriminate aerosol particles from various sources..... 11

Figure 17-4: Miniaturized aerosol separator (left) for the Gas and Aerosol Mass Spectrometer (right). Advanced inkjet technology has been applied to reduce the mass and power requirements for this instrument by more than a factor of ten below the currently used terrestrial instrument..... 12

Figure 17-5: The radiometer developed for the Mars 2020 mission includes sensors with different pass bands measuring radiation from different azimuths and elevation angles (left). The instrument also features a wide field-of-view visible camera that views vertically. The configuration on the right has the radiometer viewing away from the zenith and nadir to avoid radiation from the aerobot above and the magnetometer and infrasound sensors deployed below..... 13

Figure 17-6: The magnetometer head was deployed to the surface of Mars by the InSight mission (left). For application at Venus, the sensor would be deployed away from the gondola to escape stray magnetic fields. Measurements taken between 52 and 62 km in altitude, within the Venus atmosphere, using this instrument, would enable the detection of a much thinner magnetized crust than is possible from orbit..... 14

Figure 17-7: Infrasound measurements involve the deployment of precision barometers (center) beneath the aerobot with separations sufficient to discriminate the arrival times of acoustic waves (left). The first-ever detection of a terrestrial quake from aerobot infrasound (right) was a 4.2-magnitude aftershock of the Ridgecrest, California, earthquake in July 2019..... 16

1. Introduction

This handbook has underscored the importance of scientific balloons for a wide range of research, technology development, and educational programs. However, what has not been offered are the instruments used to implement these programs. This chapter provides an overview of the instrumentation on the balloon itself for balloon health and status monitoring, science instrumentation onboard the gondola for solar and planetary applications, and any other supporting instrumentation of note.

2. Terrestrial balloon health and status

2.1. Zero-pressure vehicles

Balloon operators must monitor the vehicle system's performance during flight to assess its health. For a zero-pressure balloon vehicle, altitude is the most common method for assessing vehicle performance. GPS units can be packaged in small form factors and provide decent altitude estimates when the sky is clear. It is important to note that often COCOM limits (Coordinating Committee for Multilateral Export Controls), which are set at 18 km (59000 kft), must be removed prior to flight, as they can prevent the GPS from reporting above that altitude. Accuracies vary from a few meters to sub-meter resolution [1]. Further, GPS units provide other useful information, such as latitude, longitude, speed, direction, and, if equipped with a GPS compass, heading.

Along with GPS altitude, pressure altitude is another common assessment for determining vehicle health and performance. Instruments to obtain this information usually include the use of pressure transducers that measure the ambient atmospheric pressure. Conversion to an altitude relative to atmospheric pressure at sea level is done according to standard practices. Evaluating the surrounding atmospheric pressure relative to a sounding measurement (or forecast) from the same day also provides insight into weather modeling. However, pressure altitude is often more difficult to assess than GPS altitude because of the need for multiple calibrated pressure transducers for the ~1000x reduction in pressure from the surface to 160,000 ft. altitude [2].

Assuming the balloon system is carrying a payload (or gondola) to altitude, an up-looking camera can be vital for observations of the vehicle. There are events (such as when the shell is damaged) that are difficult to measure with sensors that benefit from simple images. Any camera for viewing the balloon should be capable of capturing the desired field of view, robust to temperature and vacuum conditions, and various lighting scenarios (i.e., daytime, nighttime, and cases where the Sun is in frame). If there are small features of interest, a pan-tilt-zoom camera may be desired. If fast updates are required, video streaming is

possible but will require significant battery and communication resources.

Instrumentation can also be applied to measuring the design of balloon envelopes. Past characterization has been performed where small strain gauges have been applied to the film of balloon envelopes to directly measure the deformation and stresses that occur during the normal oscillations of flight [3]. Thin film strain transducers are applied to the film in a non-interference manner that prevents potential damage to the vehicle. Measurements have captured multi-directional strain resulting from the stresses on the film, including thermal contraction and expansion over time. Care must be taken to ensure the desired accuracy is achieved in the presence of the temperature changes seen during a balloon flight.

2.2. Super-pressure vehicles

Super-pressure balloon vehicles require the same basic instrumentation as zero-pressure balloons, with additional parameters that should be measured. Differential pressure, the difference in pressure between the internal lifting gas and the external atmosphere, is a key parameter for NASA's Ultra Long-duration Balloon (ULDB) program [4–6]. In the event of a leak, the differential pressure (measured at the apex of NASA's balloons) will have a downward trend that leads to the GPS altitude loss by approximately 1-3 days. For super-pressure balloons in general, if the differential pressure is measured at the base of the balloon, the head height of the balloon is not measured, and vacuum conditions in the rope section of the balloon may be directly measured early in flight. For balloons with air ballonet systems, additional pressure sensors in the ballonet may be useful for preventing overpressure scenarios and monitoring for potential leaks.

Gas mass is a valuable parameter to understand during a super-pressure balloon flight. If a hole is present and the vehicle leaks gas, the performance of the vehicle is greatly diminished. However, gas mass cannot be measured directly in a balloon system and must be estimated. If on the ground, pressure/temperature tables and flowmeters can be used (i.e., during inflation, see Chapter 6: Lift Gases) to estimate the total gas mass in the vehicle to some nominal accuracy. In flight, gas mass is often estimated by the ideal gas law and measurements of gas pressure, gas volume, and gas temperature. This process helps understand the system's observed behavior, but is prone to noise from assumptions (e.g., fully inflated vs strained volume, gas temperature measurement accuracy, etc.). A robust methodology for filtering noise and refining estimates is critical.

Balloon shape is another tricky value to measure directly. Shape is of concern when validating a new balloon design, as was the case during the clefting issues for NASA's 18.8mcf super-pressure balloon in the early

2000s [7–9]. One method is to use a structural analysis of the balloon to determine a volume change due to material strain as a function of differential pressure. More challenging methods include measuring the height and diameter of the vehicle in flight. These measurements are difficult due to undulations of the balloon, resulting in motion of the apex fitting relative to the base fitting (complicating range finding instrumentation). One method with mild success in the NASA ULDB program is to use a camera from the gondola to observe the diameter and compensate for the length of the flight train (see Figure 17-1 for an example). This technique was used in Wanaka 2025 for SN11 and SN12.

Balloon structure is an area of interest, especially when validating a new balloon design. Depending on the design paradigm, film strain may be a concern for the structural engineer. Sensors to measure film strain were investigated by the NASA ULDB project [10,11]. And flown on several flights with mixed results. Other groups have used cameras to directly observe wrinkling in film with success, albeit without a quantifiable metric of strain [12]. For balloon systems with tendons in the structure, load cells or load pins can be used to directly measure tendon tension. This method has been implemented with greater success, both in ground tests and flight [8,10].

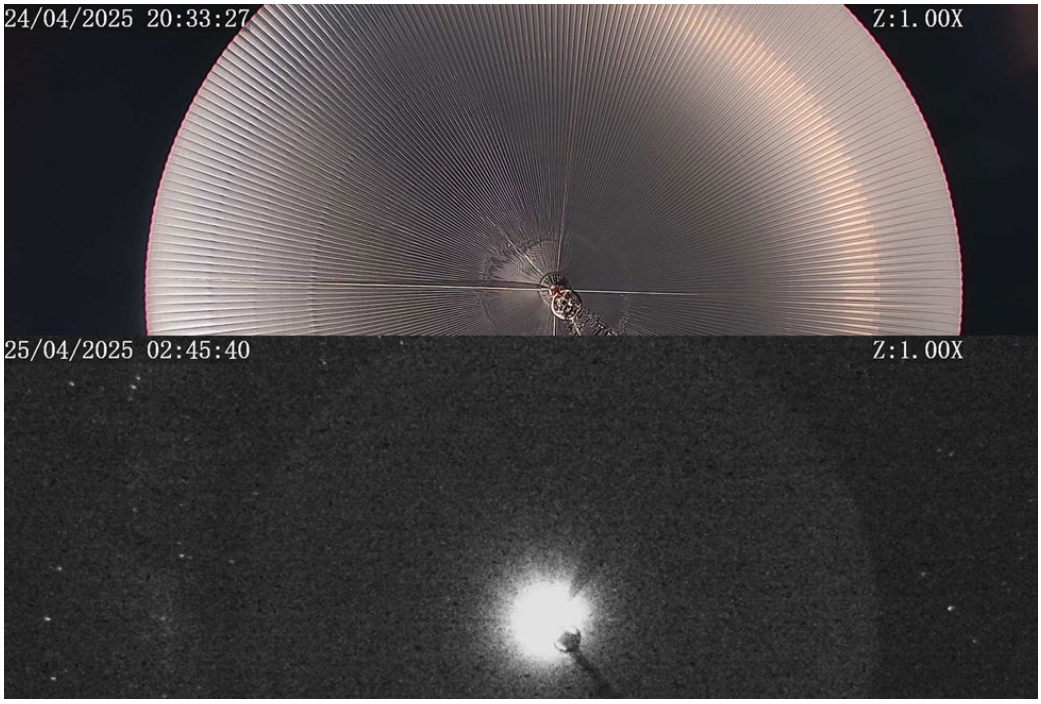


Figure 17-1: Image of the NASA 18.8mcf SPB during the Wanaka 2025 campaign during daytime (top) and nighttime (bottom).

Finally, ballast mass (mass carried for controlled drops to preserve altitude) is important to estimate during the flight. A simple method of timed ballast mass valve openings can be used for robust, proven flight systems. For systems that require greater accuracy, load cells can be used to measure the ballast dropped. Finally, the valve itself can be instrumented (e.g., encoders, voltage monitor, current monitor, etc.) to confirm open and closed states.

2.3. Environmental instrumentation

One of the most common sensors used to understand the ambient balloon environment not mentioned above is solar sensors, which measure the solar flux on the gondola. Solar sensors mounted on the solar panels can measure the incident radiation and provide an assessment of incoming power.

The radiation from the Earth is a second value which, when used in tandem with solar radiation, can provide a nearly complete understanding of the radiation environment. Down-looking radiometers can provide a measure of changes in up-welling radiation, such as that due to cold cloud tops or changes in ground terrain. While useful, radiometers have a field-of-view (FOV) and must be sized to match the FOV of the balloon vehicle to get a full vehicle estimation.

Finally, several groups have attempted to measure the relative wind seen by balloon vehicles [13–17]. Such information is useful to some science groups who require fine pointing, as well as thermal engineers modeling convection over large gondola structures. Further, there is a history of using balloon vehicles as wind traces to improve the forecasts for high-altitude winds [18]. Such technology may have alternate uses for airships and other aerial vehicles.

3. Scientific Payload Instrumentation

3.1. Infrasound (microbarometers)

A common form of instrumentation, especially for small balloons, such as heliotropes (solar balloons), has included microbarometers. Microbarometers are highly sensitive pressure sensors that can detect minute changes in atmospheric pressure. Microbarometer sensors come in two forms: absolute and differential pressure measurement. The absolute microbarometer can record during the ascent and descent stages when differential microbarometers are saturated due to the rapidly changing pressure associated with altitude changes. However, to isolate the acoustic signal with absolute microbarometers, the impact of altitude changes must be removed. Measurements of small pressure changes are ideal for detecting infrasound, which is the measure of sound at frequencies below the range of human hearing. These sensors have evolved to be

portable, easy to use, low-power, and low-cost, making them ideal for low-size, weight, and power (SWAP) vehicles. These sensors are widely used for volcano monitoring [19], atmospheric monitoring [20], earthquake monitoring [21], and with high-altitude balloons [22–25], such as heliotropes.

Recent examples include flying infrasound sensors on heliotrope systems recording chemical explosions. Infrasound from a 1-ton TNT-equivalent chemical ground explosion was detected 300 km away at an altitude of 16 km. Subsequently, several reports have been made of using infrasound sensors to record ground explosions from heliotropes. Low-frequency sound loggers on heliotropes have also recorded a variety of sources, including an earthquake in 2019 [26], a rocket launch in 2021 [27], airplanes [28], and the OSIRIS-REx Sample Recovery Capsule (SRC) reentry in 2023 [23,26].

3.2. Other Scientific Payloads

Often, scientific payloads are equipped with supplemental instrumentation to collect data that can later be used for validation and analysis. Inertial measurement units (IMUs) provide not only GPS but, depending on the component's sophistication, three-axis velocity, acceleration, and orientation. This data is useful for correlating flight events with observations from the scientific instrument. Meteorological sensors that can record temperature, pressure, and/or humidity also assist in interpreting results from flights. Though more qualitative, cameras are an effective measurement method, particularly for assessing flight performance. However, cameras can offer valuable scientific data for certain operational objectives. Hough et al. [29] recently utilized multiple GoPro cameras on two heliotropes to capture the total solar eclipse on April 8, 2024. The heliotrope was inflated and captured the eclipse, as shown in a sequence of still images from the videos in Figure 17-2.

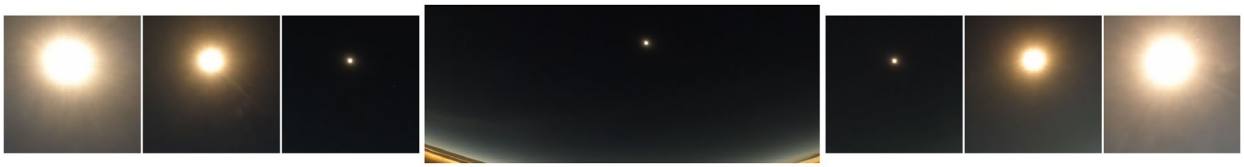


Figure 17-2: Sequence of still images taken from a heliotrope on 8 April 2024 during the total solar eclipse [29]

3.3. Flight Tracking and Communications

For small balloons and amateur systems, real-time balloon location and altitude can be monitored using the Automatic Packet Reporting System (APRS), an amateur radio (HAM) protocol that enables GPS tracking. Using

the APRS system requires that at least one team member hold a ham radio technician license, as mandated by U.S. law. In the United States, APRS enables real-time GPS tracking on the 144.39 MHz band. It is common to embed additional measurements, such as sensor temperature and pressure, within these signals. The APRS tracking data can be viewed in real time via a web-based interface (https://aprs.fi/). APRS trackers, such as the High Altitude Science StratoTrack and the QRP Labs Light APRS tracker, are routinely used on heliotropes (e.g., [28,30–34]).

However, APRS trackers are line-of-sight measurements, typically losing the signal once it is a few kilometers above the ground. The altitude at which the APRS tracking will be lost depends on the configuration of the receiver network within the vicinity of the landing location. Hence, it is standard practice (e.g., [25,28,30–32,34–36]) to include a satellite tracker (e.g. SPOT TRACE) that can provide a precise position of the final landing location. Further information on communications can be found in Chapter 12.

4. Extra-terrestrial Instrumentation

This section covers the various scientific motivations for using buoyant vehicles to explore other worlds, as well as the types of measurements and the required instrument technologies that are under development to achieve this goal. The scope of this discussion encompasses the planets Venus and Mars, as well as Saturn's moon Titan. They are all solar system bodies with atmospheres and defined surfaces – solid in the case of Mars and Venus, and partially liquid in the case of Titan with its methane lakes. The term aerobot used here encompasses:

- the envelope containing buoyancy gas,
- the power, avionics, and communications systems to safely carry out their task, and
- the experimental payload.

Aerobots may feature altitude control as well as technologies for tolerating the extreme environments in which they operate.

Many of the scientific questions about planetary atmospheres can be addressed with the same types of measurements used in terrestrial investigations from balloons or aircraft. A key difference for a planetary aerobot is that instruments generally must be much smaller and consume less power. The total scientific payload may be no more than a few tens of kg in the largest aerobots contemplated today and possibly much less. Necessarily, this excludes some instruments that might be flown on terrestrial balloons or aircraft, but it also provides a significant impetus for miniaturization. In describing possible instruments for aerobot exploration, information is drawn from proposals made for aerobot missions to Mars, Venus, and Titan over the last several

decades, but which have never flown. In addition, descriptions of instruments for atmospheric probes, landers, and rovers relevant to aerobot missions and deployed on these three target worlds on other platforms are provided. Some of these instruments have measured various parameters, leveraging common data systems. Here, our focus is on the measurement types with a particular emphasis on the impact of miniaturization, which is so vital in planetary science.

4.1. Atmospheric Chemistry and Astrobiology

Investigations of planetary atmospheres can be divided into two categories: those that focus on the constituents of the gas phase and those that examine the aerosol or cloud particles embedded within the gas. For aerobot missions, prime instrument candidates are those that have already been landed on Mars to study the composition of the atmosphere, and those that are under development for a Venus descent probe to fly as part of the DaVinci mission [39].

Gas Chemistry: Mass spectrometers are used to determine the abundances of noble or inert gases, such as helium, neon, argon, krypton, and xenon, as well as their isotopes. Additionally, they are used to detect chemically active species, including sulfur dioxide and carbon monoxide. The Venus Mass Spectrometer (VMS), which is projected to be flown on the DAVINCI mission in 2030 [39], is an example of such an instrument. A more advanced mass spectrometer with greater mass resolution should enable gases of astrobiological significance, such as phosphine, methane, or hydrogen sulfide, to be detected if present at the parts per billion level or higher [40]. Another instrument, the Tunable Laser Spectrometer (TLS) [41], provides complementary information on gas chemistry for trace species that cannot be easily detected with the mass spectrometer (Figure 17-3, left). Aerobot deployment of these instruments could extend the observation time by roughly four orders of magnitude compared to a probe, enabling lower detection limits and greater measurement accuracy. In addition, variations in time of day and latitude can be observed, providing a more complete picture of the processes influencing atmospheric chemistry.

Aerosol Physics and Chemistry: Investigating solid or liquid particles embedded in the gas phase is a critical aspect of understanding processes in a planetary atmosphere. Characterizing the presence of such particles can be accomplished with a very small and compact instrument. The VeGa aerobot missions included a tiny instrument that measured the backscattering of light from cloud particles throughout each flight [42], but did not provide specific information on their sizes or numbers. NASA's Pioneer Venus probe mission accomplished this for a single descent profile [43]. A modernized and compact version called the Light Optical

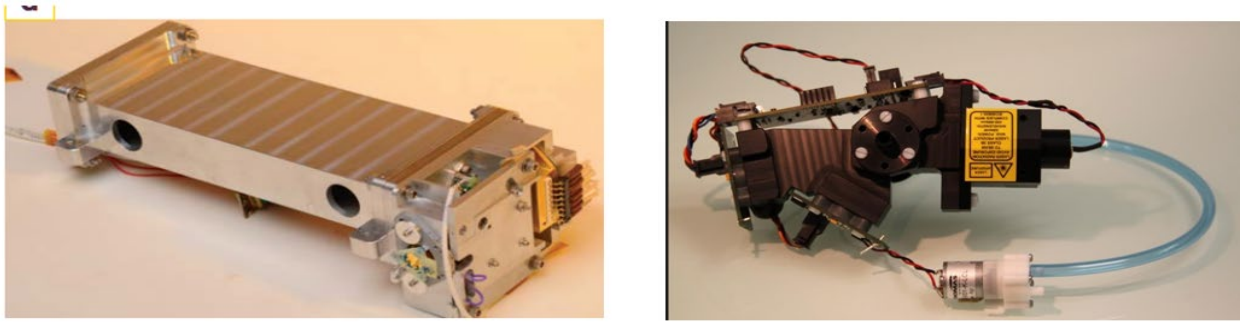


Figure 17-3: A tunable laser spectrometer (Left) has been used on the Mars Curiosity mission and is being developed for flight on a Venus probe to measure targeted trace gas species. The Light Optical Aerosol Counter (LOAC) has been demonstrated on several terrestrial aerobot flights, confirming its ability to discriminate aerosol particles from various sources

Aerosol Counter (Figure 17-3, right) has been extensively tested in terrestrial aerobot flights [44] and it is being modified to tolerate measurements of acidic aerosols at Venus.

Measuring the chemical composition of aerosol particles on Mars, Venus, or Titan is a more formidable challenge. Attempts to measure aerosol chemistry with instruments using mechanical filters were deployed on the VeGa 1 and 2 lander missions to Venus [45] and on the ESA Huygens probe to Titan [46], but were very constrained in sampling by the aerosol collection method [40].

The development of aerodynamic methods of separating aerosols from gas using an efficient aerodynamic particle lens has enabled a class of instruments to be developed with real-time particle chemical analyses [47]. Commercial versions of these instruments currently weigh 150 kg and consume 600 Watts. To accommodate the mass limitations of aerobots, JPL and its industrial partners, Integrated Deposition Solutions Inc. and Creare LLC, have been working on miniaturizing an aerosol separator that would be used with the same mass spectrometer employed for gas analysis. The resulting Gas and Aerosol Mass Spectrometer (GAMS) has a target mass of less than 15 kg and is shown in Figure 17-4 [40].

The possibility that primitive life forms might exist in the Venus cloud layer has been stimulated by a controversial observation of phosphine in the cloud layer. Measurements with GAMS could demonstrate whether phosphine is indeed present in the gas phase or, more likely, that phosphorus, a key element in all terrestrial life forms, is contained in aerosols [48]. A broad range of potential aerobot-borne experiments has been conceived by an MIT-led team with an emphasis on habitability characterization of the Venusian clouds, including a miniature nephelometer that detects fluorescence in addition to other particle properties [49].

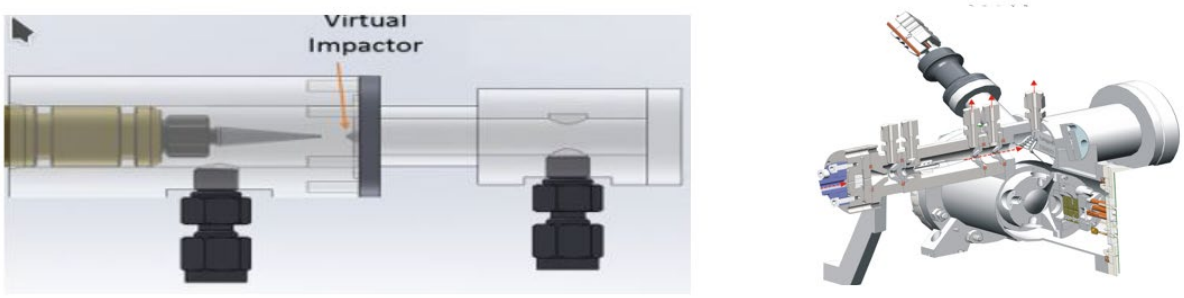


Figure 17-4: Miniaturized aerosol separator (left) for the Gas and Aerosol Mass Spectrometer (right). Advanced inkjet technology has been applied to reduce the mass and power requirements for this instrument by more than a factor of ten below the currently used terrestrial instrument.

4.2. Atmospheric Dynamics

Investigations of atmospheric dynamics require measuring the magnitude and direction of the prevailing winds, the time-variable convective and turbulent atmospheric motions, and the radiation fluxes within the atmosphere that are important in driving atmospheric motions.

Prevailing winds: Tracking the motion of the aerobot with radiometric measurements from a spacecraft in orbit or from tracking stations on Earth can be used to determine wind velocity, given the good assumption that the aerobot moves at the same speed as the wind [50]. For periods when there is no radio tracking, inertial measurements can be used to interpolate the vehicle motion. The drift in inertial sensors generally limits these periods to an hour or less [51].

Wind Variability: Wind variability is expressed in the movement of the atmosphere relative to the aerobot, as well as inertial measurements of the response of the aerobot to those time variable disturbances. The VeGa Venus balloons had a vertical wind sensor implemented as a mechanical rotor [52]. Today, the preferred wind sensing technology is ultrasonic time-of-flight anemometry, which requires no moving parts and works well at the ambient pressures of 10^3 to 10^5 Pa at which the aerobot will be operating. Extending the wind measurement to three dimensions and employing an inertial measurement unit (IMU) on the aerobot would greatly increase the turbulence measurement capability.

Atmospheric Temperature: Ultrasound can also be used to measure atmospheric temperature more accurately and with a faster response time than a thermistor, which may take tens of seconds to equilibrate with the atmosphere. Ultrasound instruments must be tailored for effective coupling with the atmosphere, which depends on atmospheric density [14].

Radiation Fluxes: The measurement of radiative fluxes in a planetary atmosphere plays a vital role in understanding where radiant energy is deposited and determining the driving forces for atmospheric dynamics and the planet's heat balance. Measurement of both up- and down-welling radiative fluxes in multiple spectral bandpass channels is needed for this. The spectral channels would be tailored to the atmospheric characteristics. The Radiation and Dust Sensor for Mars Environmental Dynamic Analyze (MEDA) carried on the deck of the Mars Rover Perseverance is an upward-viewing sensor and exemplifies what is possible with current technology (Figure 17-5). Adaptation to an aerobot platform would provide upward and downward viewing, adapted for partial occultation by the balloon and the carried payload.

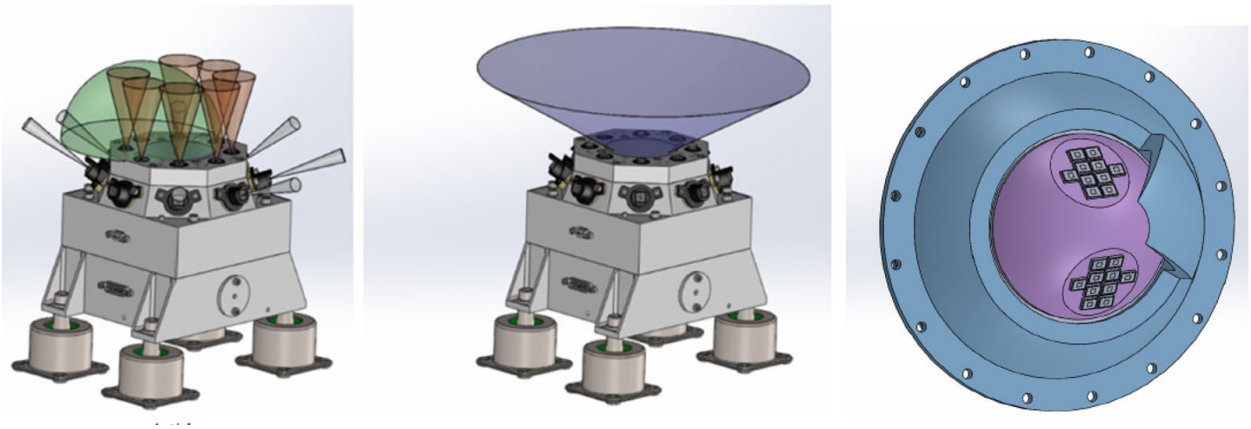


Figure 17-5: The radiometer developed for the Mars 2020 mission includes sensors with different pass bands measuring radiation from different azimuths and elevation angles (left). The instrument also features a wide field-of-view visible camera that views vertically. The configuration on the right has the radiometer viewing away from the zenith and nadir to avoid radiation from the aerobot above and the magnetometer and infrasound sensors deployed below.

4.3. Geophysical Profiling

Use of instruments to measure geophysical profiles on a balloon improves spatial resolution, which is generally controlled by the height of the platform above the surface, and the sensitivity, which may depend even more sharply on altitude compared to orbiters. An additional advantage is conferred by physical contact with the atmosphere, enabling direct detection of acoustic waves as discussed in the next section.

Magnetic Fields: Magnetic field measurements are used to detect and characterize a permanent magnetic field, remanent magnetism from an ancient field, and interactions between interplanetary fields and the target object. Balloon-borne magnetic measurements have been proposed for Mars [53], Titan [54] and Venus [55]. None of these targets is known to have a permanent magnetic field, but Mars has a remanent magnetic field that has been detected from orbit. An aerobot magnetic field

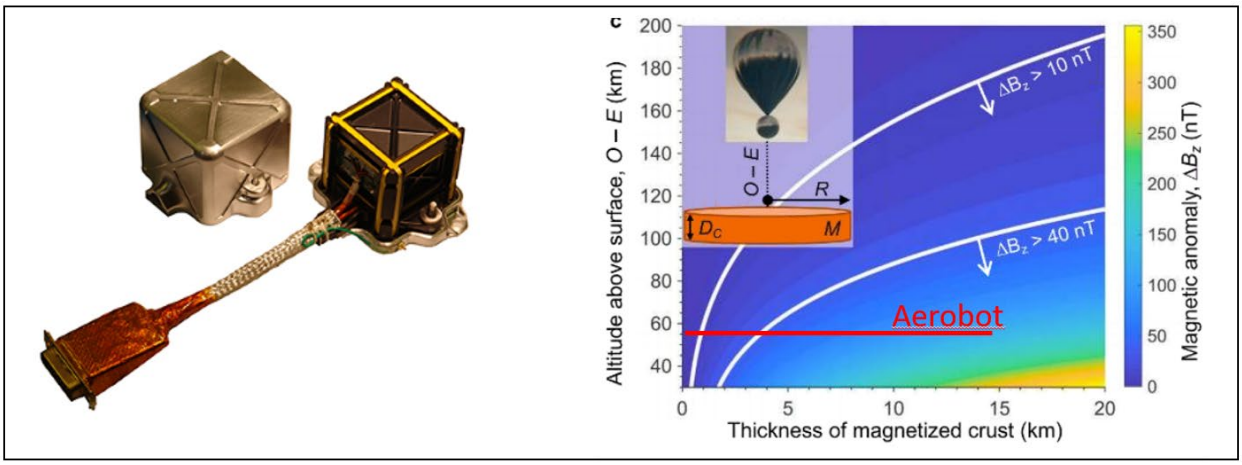


Figure 17-6: The magnetometer head was deployed to the surface of Mars by the InSight mission (left). For application at Venus, the sensor would be deployed away from the gondola to escape stray magnetic fields. Measurements taken between 52 and 62 km in altitude, within the Venus atmosphere, using this instrument, would enable the detection of a much thinner magnetized crust than is possible from orbit.

investigation could be conducted at any of these worlds with a sensor mass less than 1 kg and power less than 1W (Figure 17-6, left panel).

Electric Fields: Electric field measurements are used to investigate the electrical conductivity of the ionosphere, atmospheric layers, and the planetary crust and interior. An example of this is the Permittivity Wave and Altimetry (PWA) experiment conducted on the ESA's Huygens probe at Titan [56]. It identified a conductive layer peaking at 60 to 70 km and an extremely low frequency (ELF) signature resembling a Schumann resonance, although the interpretation of this is controversial [57]. A Titan Electric Environment Package (TEEP) was proposed for the Titan Montgolfière balloon component of the TandEM mission concept [58] with the goal of resolving the ambiguities and uncertainties left by the Huygens probe mission [56]. Balloon Transverse Electromagnetic sounding of the upper mantle of Venus using electrical field measurements has also been proposed for a Venus balloon mission [59]; however, it now appears that magnetic detection may be more practical [60].

Gravity Fields: Gravity field measurements are used on the Earth to map the distribution of rocks of different densities and, hence, composition. They are carried out routinely in exploration geophysics with aircraft deployment, but require a stabilized platform whose position is determined by a Global Navigation Satellite System (GNSS) [61]. In planetary science, gravity and gravity gradient measurements are conducted using spacecraft tracking, in some cases by ranging between pairs of spacecraft for enhanced sensitivity [62]. Measurements from a balloon platform, which operates much closer to the planet's surface than is possible for an orbiter, offer the potential for greatly improved

spatial resolution along the ground track [63]. However, for a platform drifting with the wind, discriminating the rate of change of the gravity signal from other disturbances and instrument drift remains a formidable challenge.

Active electromagnetic (EM) sounding: Probing the subsurface with low-frequency EM waves enables the mapping of structures with different EM properties and the potential for resolving structures at different depths, which is not practical with passive methods. An electromagnetic-sounding instrument was proposed for the Titan Aerial Explorer (TAE) mission concept [54] that would have probed the subsurface at wavelengths between 150 MHz and 300 MHz, with a penetration depth greater than 350 m and a vertical resolution of 6 m. This would be a vast improvement over the performance of a Titan orbiter whose minimum altitude is greater than 1000 km because of the very large thickness (large-scale height) of the Titan atmosphere.

For Venus, the Subsurface Radar Sounder (SRS), which will be deployed on the ESA Envision Orbiter, will operate at 9 MHz [64]. It will operate at an altitude ranging between 220 and 540 km and will penetrate to a few hundred meters depth in silicate materials at Venus' surface temperatures. An aerobot-carried sounder, like that proposed for Titan, could achieve improved performance because of its relative proximity to the surface of Venus.

4.4. Infrasound Seismology

Ground motion caused by seismic activity also moves the adjacent atmosphere and creates low-frequency acoustic waves known as infrasound. These infrasound waves can travel large distances and be detected by surface or aerial pressure sensors. This is, in principle, a powerful diagnostic for detecting seismic activity from aerobots on other planets, particularly on Venus, where the extremely high surface temperature precludes the use of traditional surface-mounted seismometers.

The technology discussed above on terrestrial balloons can be applied to extraplanetary balloons as well. The coupling between the solid planet and the atmosphere is approximately 60 times better on Venus than on Earth, owing to the higher atmospheric density [65] and several times better on Titan compared to that generated by a similar event on Earth. Possible non-seismic or volcanic infrasound sources include bolides, wind–mountain interactions, atmospheric turbulence, convective storms, vortices, and electrostatic discharges. Data collected for infrasound investigation would, therefore, also address these related atmospheric science questions. The development of techniques for infrasound detection is an active area of research. While the initial deployment of infrasound in a planetary mission is likely to be on a single aerobot,

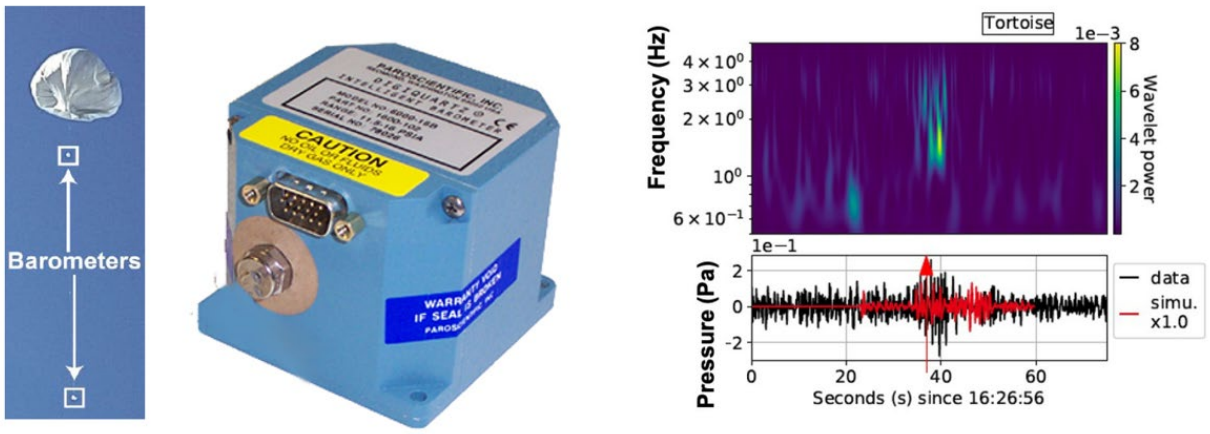


Figure 17-7: Infrasound measurements involve the deployment of precision barometers (center) beneath the aerobot with separations sufficient to discriminate the arrival times of acoustic waves (left). The first-ever detection of a terrestrial quake from aerobot infrasound (right) was a 4.2-magnitude aftershock of the Ridgecrest, California, earthquake in July 2019.

the advantages of a network have been demonstrated by measurements from the French Strateole balloons on Earth [66].

4.5. Surface Imaging and Imaging Spectroscopy

The proximity of an aerobot to the surface has long been recognized as a significant advantage, as the closeness to the surface and reduced haze background provide major benefits over observations from orbit. For Mars, advances in orbital imaging technology (e.g., the HiRISE camera on the Mars Reconnaissance Orbiter) and the comparative clarity of the atmosphere, except during global dust storms, have removed the advantage that aerobots once had. For Titan and Venus, however, the dense global clouds mean that those advantages remain.

For Titan, where the haze is permanent and extends over a very deep atmosphere, the advantage of imaging from within the atmosphere was well demonstrated by descent images from the Huygens probe. A composite of 30 descent images acquired between 8 and 13 km above the surface revealed surface features not visible from orbit [67]. The Dragonfly rotorcraft, which is planned to arrive at Titan in 2034, will use imaging for navigation and make a series of short hops of a few kilometers in a 200 km total traverse. In contrast, lighter-than-air aerobot vehicles can, in principle, provide much longer traverses on a global scale. For example, the TandEM aerobot mission concept promised sustained flight for many months while acquiring visual images from its VISTA-B instrument at 1 m resolution over a 12,000 km ground track in a 2-year mission [54]. The Balloon Imaging Spectrometer, operating from 1 to 5.6 μm on the same platform, would acquire imaging at a 2.5 m resolution.

On Venus, clouds and haze are denser than on Titan, and Rayleigh scattering by the clear atmosphere beneath the clouds also hinders imaging. Concepts for deploying a camera just below the clouds would enable imaging of the surface in emission during nighttime [68]. To avoid overheating the camera at the elevated temperature below the cloud, either the aerobot itself descends for a period of several hours from a cooler region of the atmosphere or deploys a camera on a tether. A surface resolution of 10 m over a 20 km wide swath appears feasible.

4.6. Dropsondes and Risesondes

An aerobot can be used to deploy secondary payloads for supplemental investigations. For example, payloads known as dropsondes that fall by gravity to the surface have been used in remote regions of the Earth to obtain in situ measurements that are not accessible with any other means [69]. In addition to dropsondes, aerobot missions can also enable the deployment of "risesondes," which are balloons themselves that can ascend and access regions higher in the atmosphere than the parent vehicle itself can achieve.

Dropsondes and risesondes have been mostly examined in the context of Venus missions. Early Venus aerobot concepts, such as the Venus Exploration of Volcanoes and Atmosphere (VEVA) mission [70] proposed deploying dropsondes that could rapidly descend to the surface and send image data at a high rate to the aerobot, where it would be stored for later relay to Earth. These dropsondes need to be at least several kilograms in size to have enough insulation and thermal inertia to ensure that the interior temperature does not rise to insupportable levels before arrival at the surface [71]. They could be guided to optimize data return.

Nighttime imaging of emitted radiation, which can be accomplished from just below the cloud layer at an altitude of 47 km, will be feasible with smaller dropsondes that do not need to survive to the surface. Nighttime imaging of active lava flows, where exposure times can be so short that stabilization is not required, may be feasible with dropsondes weighing less than a kilogram, which are now being miniaturized with communications relays [72]. These dropsondes could also serve as ballast to offset the leakage of helium, thereby extending mission duration and acquiring meteorological data from different parts of the cloud, as well as imaging various surface sites.

The possibility of probing upward towards and above the cloud tops at 71 km has also been examined. The current design for a Venus variable altitude aerobot has a ceiling of 62 km [73]. Entry probes are generally traveling too fast during descent to make measurements at the cloud tops. Solar balloons or heliotropes [74]. Deployed from the aerobot and ram inflated before they heat in the sun, this is a potential approach to a

“risesonde” implementation that could reach and characterize the cloud tops near 72 km and 2.5 X 10^-2 bars.

4.7. Tether Deployment of Payloads

One of the earliest planetary balloon concepts, the Mars Balloon mission planned as a joint French-Soviet mission, envisioned a payload deployed from a tether or “guide-rope” [75] that would come into contact with the ground at night, thereby stabilizing the balloon's altitude. Early concepts for sampling the surface from Titan aerobots envisioned probes deployed from a tether to sample the surface [76]. More recently, attention has focused on tethered payloads from a Venus balloon, which would be used to access regions beneath the clouds [77].

5. Summary

In general, the instrumentation used during balloon flights all serve similar objectives: altitude, pressure, and environmental sensing. Terrestrial and solar ballooning benefits from low-cost, COTS systems encased in ruggedized housings and using temperature compensation. For extraterrestrial systems, the same instrumentation must be designed specifically for the environment, radiation-hardened, and optimized for weight and space savings. The science benefit for all three cases is similar: aerial observation of the atmosphere and surface features. Further refinements in navigation, observation, and scientific measurements on Earth should be encouraged, as they directly benefit balloon flight systems.

References

[1] "GPS Accuracy | GPS.Gov," GPS Accuracy. [Online]. Available: https://www.gps.gov/gps-accuracy-0. [Accessed: Oct. 28, 2025].

[2] J. Warren, J. Smalley, and A. Morris, "Aerostatic Lift of Helium and Hydrogen in the Atmosphere," UCAR/NCAR, 1971, p. 4088 KB, doi: 10.5065/D6057CWH.

[3] J. Rand, "Balloon Film Strain Measurement," *Advances in Space Research*, vol. 3, no. 6, pp. 45–48, 1983, doi: 10.1016/0273-1177(83)90075-3.

[4] H. M. Cathey, D. A. Fairbrother, and M. A. Said, "Performance Highlights of NASA Super Pressure Balloon Mid-Latitude Flights," presented at the AIAA Balloon Systems Conference, Denver, Colorado, 2017, doi: 10.2514/6.2017-3091.

[5] H. M. Cathey, "Development of the NASA Long Duration Balloon Vehicle," *Advances in Space Research*, vol. 26, no. 9, pp. 1345–1348, 2000, doi: 10.1016/S0273-1177(00)00058-2.

[6] H. M. Cathey, "Test Flights of the NASA Ultra-Long Duration Balloon," *Advances in Space Research*, vol. 33, no. 10, pp. 1633–1641, 2004, doi: 10.1016/j.asr.2003.07.036.

[7] X. Deng and S. Pellegrino, "Dimensional Analysis of Clefting of Constant-Stress (CS) Design Super-Pressure Balloons."

[8] H. Cathey and D. Pierce, "Duration Flight of the NASA Super Pressure Balloon," presented at the AIAA Balloon Systems Conference, Seattle, Washington, 2009, doi: 10.2514/6.2009-2808.

[9] F. E. Baginski, K. A. Brakke, and W. W. Schur, "Cleft Formation in Pumpkin Balloons," *Advances in Space Research*, vol. 37, no. 11, pp. 2070–2081, 2006, doi: 10.1016/j.asr.2005.04.104.

[10] L. G. Young and C. D. Yoder, "NASA Super Pressure Balloon Laboratory Test Program."

[11] K. Yang, R. Natherson, C. D. Yoder, and S. Roth, "Two Non-Contact Strain Measurement Techniques for Scientific Ballooning," presented at the AIAA AVIATION 2021 FORUM, VIRTUAL EVENT, 2021, doi: 10.2514/6.2021-2697.

[12] A. Alexander, "Loon Library: Lessons from Building Loon's Stratospheric Communications Service."

[13] T. J. Cheng, C. Yoder, T. Curran, F. Steve, D. Banfield, and R. D. White, "Test Flight of a Stratospheric Sonic Anemometer Prototype," 2024, doi: 10.1175/JTECH-D-24-0010.1.

[14] D. Banfield, D. W. Schindel, S. Tarr, and R. W. Dissly, "A Martian Acoustic Anemometer," *The Journal of the Acoustical*

Society of America, vol. 140, no. 2, pp. 1420–1428, 2016, doi: 10.1121/1.4960737.

[15] R. D. White and D. Banfield, "Sonic Anemometry on a High Altitude Balloon," *The Journal of the Acoustical Society of America*, vol. 151, no. 4_Supplement, pp. A185–A185, 2022, doi: 10.1121/10.0011044.

[16] E. I. F. de Bruijn, F. C. Bosveld, S. de Haan, and B. G. Heusinkveld, "Measuring Low-Altitude Winds with a Hot-Air Balloon and Their Validation with Cabauw Tower Observations," *Journal of Atmospheric and Oceanic Technology*, vol. 37, no. 2, pp. 263–277, 2020, doi: 10.1175/JTECH-D-19-00431.

[17] M. D. Yamanaka, Y. Matsuzaka, J. Nishimura, T. Yamagami, and H. Tanaka, "Stratospheric Balloon-Borne 'Adapted Gill-Type' Propeller Anemometer," *Journal of Atmospheric and Oceanic Technology*, vol. 2, no. 4, pp. 472–481, 1985, doi: 10.1175/1520-0426(1985)002%253C0472:SBBGTP%253E2.0.CO;2.

[18] L. Coy, M. R. Schoeberl, S. Pawson, S. Candido, and R. W. Carver, "Global Assimilation of Loon Stratospheric Balloon Observations," *Journal of Geophysical Research: Atmospheres*, vol. 124, no. 6, pp. 3005–3019, 2019, doi: 10.1029/2018JD029673.

[19] B. B. Rosenblatt, J. B. Johnson, J. F. Anderson, K. Kim, and S. J. Gauvain, "Controls on the Frequency Content of Near-Source Infrasound at Open-Vent Volcanoes: A Case Study from Volcán Villarrica, Chile," *Bulletin of Volcanology*, vol. 84, no. 12, p. 103, 2022, doi: 10.1007/s00445-022-01607-y.

[20] G. Averbuch, M. Ronac-Giannone, S. Arrowsmith, and J. F. Anderson, "Evidence for Short Temporal Atmospheric Variations Observed by Infrasonic Signals: 1. The Troposphere," *Earth and Space Science*, vol. 9, no. 3, p. e2021EA002036, 2022, doi: 10.1029/2021EA002036.

[21] L. T. Scamfer and J. F. Anderson, "Exploring Background Noise With a Large-N Infrasound Array: Waterfalls, Thunderstorms, and Earthquakes," *Geophysical Research Letters*, vol. 50, no. 24, p. e2023GL104635, 2023, doi: 10.1029/2023GL104635.

[22] Q. Brissaud et al., "The First Detection of an Earthquake From a Balloon Using Its Acoustic Signature," *Geophysical Research Letters*, vol. 48, no. 12, p. e2021GL093013, 2021, doi: 10.1029/2021GL093013.

[23] E. A. Silber et al., "Geophysical Observations of the 2023 September 24 OSIRIS-REx Sample Return Capsule Reentry," *The Planetary Science Journal*, vol. 5, no. 9, p. 213, 2024, doi: 10.3847/PSJ/ad5b5e.

[24] E. F. Young, D. C. Bowman, J. M. Lees, V. Klein, S. J. Arrowsmith, and C. Ballard, "Explosion-Generated Infrasound Recorded on Ground and Airborne Microbarometers at Regional Distances," *Seismological Research Letters*, vol. 89, no. 4, pp. 1497–1506, 2018, doi: 10.1785/0220180038.

[25] D. C. Bowman and S. A. Albert, "Acoustic Event Location and Background Noise Characterization on a Free Flying Infrasound Sensor Network in the Stratosphere," *Geophysical Journal International*, vol. 213, no. 3, pp. 1524–1535, 2018, doi: 10.1093/gji/ggy069.

[26] D. C. Bowman, "Airborne Infrasound Makes a Splash," *Geophysical Research Letters*, vol. 48, no. 23, p. e2021GL096326, 2021, doi: 10.1029/2021GL096326.

[27] S. A. Albert, D. C. Bowman, E. A. Silber, and F. K. Dannemann Dugick, "The AtmoSOFAR Channel: First Direct Observations of an Elevated Acoustic Duct," *Earth and Space Science*, vol. 10, no. 10, p. e2023EA003149, 2023, doi: 10.1029/2023EA003149.

[28] T. Swaim, K. Spillman, E. Hough, Z. Yap, J. Jacob, and B. Elbing, "Development and Evaluation of Windscreen Designs for High Altitude Balloons," presented at the 184th Meeting of the Acoustical Society of America, Chicago, Illinois, 2023, doi: 10.1121/2.0001785.

[29] E. Hough, Z. Yap, K. Spillman, B. Elbing, and J. D. Jacob, "Solar Balloon Observations of the 2024 North American Eclipse," presented at the AIAA AVIATION FORUM AND ASCEND 2024, Las Vegas, Nevada, 2024, doi: 10.2514/6.2024-3895.

[30] T. D. Swaim et al., "Performance Characterization of Heliotrope Solar Hot-Air Balloons during Multihour Stratospheric Flights," *Journal of Atmospheric and Oceanic Technology*, vol. 41, no. 4, pp. 357–373, 2024, doi: 10.1175/JTECH-D-23-0091.1.

[31] E. Hough, "Design and Operations of Multi-Hour Stratospheric Solar Hot-Air Balloons - ProQuest." [Online]. Available: https://www.proquest.com/openview/03eebea1d84fff70e1665b7d696dddf8/1?pq-origsite=gscholar&cbl=18750&diss=y. [Accessed: Oct. 22, 2025].

[32] T. Schuler et al., "Solar High Altitude Balloons as a Long Duration Controllable Aerial Platform," presented at the AIAA SCITECH 2022 Forum, San Diego, CA & Virtual, 2022, doi: 10.2514/6.2022-0282.

[33] T. Schuler, M. Debbins, M. Cobar, J. Thangavelautham, and D. Sofge, "Altitude Control with Vented Solar High Altitude Balloons

(SHAB-Vs)," presented at the 2023 IEEE Aerospace Conference, Big Sky, MT, USA, 2023, doi: 10.1109/AERO55745.2023.10116024.

[34] M. Fathepure, J. Clemmons, N. Wang, and J. D. Jacob, "Evaluating High Altitude Impacts of Solar Cell Performance with High Altitude Balloons," presented at the AIAA SCITECH 2024 Forum, Orlando, FL, 2024, doi: 10.2514/6.2024-0728.

[35] D. C. Bowman and S. Krishnamoorthy, "Infrasound From a Buried Chemical Explosion Recorded on a Balloon in the Lower Stratosphere," *Geophysical Research Letters*, vol. 48, no. 21, p. e2021GL094861, 2021, doi: 10.1029/2021GL094861.

[36] E. A. Silber, D. C. Bowman, and M. Ronac Giannone, "Detection of the Large Surface Explosion Coupling Experiment by a Sparse Network of Balloon-Borne Infrasound Sensors," *Remote Sensing*, vol. 15, no. 2, p. 542, 2023, doi: 10.3390/rs15020542.

[37] B. Stilwell and M. Siemon, "A New TDRSS Compatible Transceiver for Long Duration HIgh Altitude Scientific Balloon Missions," in *34th COSPAR Scientific Assembly*, vol. 34, 2002, pp. 1470.

[38] S. Miller, "Starlink as an Interface on NASA CSBF Balloon Missions," presented at the 2025 Scientific Ballooning Technologies Workshop, Minneapolis, MN, 2025.

[39] J. B. Garvin et al., "Revealing the Mysteries of Venus: The DAVINCI Mission," *The Planetary Science Journal*, vol. 3, no. 5, p. 117, 2022, doi: 10.3847/PSJ/ac63c2.

[40] K. H. Baines et al., "Investigation of Venus Cloud Aerosol and Gas Composition Including Potential Biogenic Materials via an Aerosol-Sampling Instrument Package," *Astrobiology*, vol. 21, no. 10, pp. 1316–1323, 2021, doi: 10.1089/ast.2021.0001.

[41] C. R. Webster, A. E. Hofmann, P. R. Mahaffy, S. K. Atreya, C. H. House, A. A. Simon, and J. B. Garvin, "Tunable Laser Spectrometers for Planetary Science," *Space Science Reviews*, vol. 219, no. 8, p. 78, 2023, doi: 10.1007/s11214-023-01023-4.

[42] R. Z. Sagdeev et al., "Overview of VEGA Venus Balloon in Situ Meteorological Measurements," *Science*, vol. 231, no. 4744, pp. 1411–1414, 1986, doi: 10.1126/science.231.4744.1411.

[43] R. G. Knollenberg and D. M. Hunten, "The Microphysics of the Clouds of Venus: Results of the Pioneer Venus Particle Size Spectrometer Experiment," *Journal of Geophysical Research: Space Physics*, vol. 85, no. A13, pp. 8039–8058, 1980, doi: 10.1029/JA085iA13p08039.

[44] J.-B. Renard et al., "LOAC: A Small Aerosol Optical Counter/Sizer for Ground-Based and Balloon Measurements of the Size

Distribution and Nature of Atmospheric Particles – Part 2: First Results from Balloon and Unmanned Aerial Vehicle Flights," doi: 10.5194/amtd-8-10057-2015.

[45] B. M. Andreiechikoc, I. K. Akhmetshin, B. N. Korchuganov, L. M. Mukhin, and B. I. Ogorodnikov, "X-ray radiometric analysis of Venus cloud aerosols by Vega-1 and-2 automated interplanetary probes," *British Library UDC 523.042:523.42: Kosmicheskie Issledovaniia*, vol. 25, pp. 721–736, 1987.

[46] G. Israël et al., "Complex Organic Matter in Titan's Atmospheric Aerosols from in Situ Pyrolysis and Analysis," *Nature*, vol. 438, no. 7069, pp. 796–799, 2005, doi: 10.1038/nature04349.

[47] Aerodyne Research, "Aerosol Mass Spectrometer - Aerodyne," Aerosol Mass Spectrometer, Jan. 04, 2023. [Online]. Available: https://aerodyne.com/particle-instruments/ams-acsm/. [Accessed: Oct. 23, 2025].

[48] M. L. Delitsky and K. H. Baines, "Cloud Chemistry on Venus: Sulfuric Acid Reactions and Supercooling in Venus Liquid Cloud Droplets," *Planetary and Space Science*, vol. 237, p. 105750, 2023, doi: 10.1016/j.pss.2023.105750.

[49] S. Seager et al., "Venus Life Finder Mission Study," doi: 10.48550/arXiv.2112.05153.

[50] K.-M. Cheung, W. Jun, C. Lee, and G. Lightsey, "Single-Satellite Real-Time Positioning of Balloon and Helicopter for Aerial Exploration in Extra-Terrestrial Atmosphere," presented at the 70th International Astronautical Congress, Washington, DC, 2019.

[51] S. Ploen et al., "Bias Compensated Inertial Navigation for Venus Balloon Missions," presented at the 2023 IEEE Aerospace Conference, Big Sky, MT, USA, 2023, doi: 10.1109/AERO55745.2023.10115888.

[52] R. S. Kremnev et al., "VEGA Balloon System and Instrumentation," *Science*, vol. 231, no. 4744, pp. 1408–1411, 1986, doi: 10.1126/science.231.4744.1408.

[53] C. Raymond, "PICCARD: A Balloon Magnetometer Mission to Mars," presented at the Lunar and Planetary Science Conference, 1999.

[54] A. Coustenis, J. Lunine, K. Reh, J. P. Lebreton, C. Erd, P. Beauchamp, C. Sotin, and D. Matson, "Titan Saturn System Mission Instrumentation," presented at the International Workshop on Instrumentation for Planetary Missions, 2012.

[55] J. G. O'Rourke, J. Buz, R. R. Fu, and R. J. Lillis, "Detectability of Remanent Magnetism in the Crust of Venus,"

Geophysical Research Letters, vol. 46, no. 11, pp. 5768–5777, 2019, doi: 10.1029/2019GL082725.

[56] F. Simões, R. Grard, M. Hamelin, J. J. Lopez Moreno, K. Schwingenschuh, C. Béghin, F. Ferri, and G. Molina-Cuberos, "Investigations of Titan Electric Environment and the Titan Electric Environment Package for the TandEM Mission," vol. 5, Rome, Italy, 2010, pp. EPSC2010-905.

[57] M. Hamelin, C. Beghin, V. Brown, P. Falkner, and R. Grard, "Titan's Atmospheric Electricity from the Measurements of the PWA-HAIS Instrument on Board the Huygens Probe," Berlin, Germany, 2006.

[58] A. Coustenis et al., "TandEM: Titan and Enceladus Mission," *Experimental Astronomy*, vol. 23, no. 3, pp. 893–946, 2009, doi: 10.1007/s10686-008-9103-z.

[59] R. E. Grimm, A. C. Barr, K. P. Harrison, D. E. Stillman, K. L. Neal, M. A. Vincent, and G. T. Delory, "Aerial Electromagnetic Sounding of the Lithosphere of Venus," *Icarus*, vol. 217, no. 2, pp. 462–473, 2012, doi: 10.1016/j.icarus.2011.07.021.

[60] R. Grimm, "Sounding the Venus Lithosphere," Jan. 07, 2020.

[61] D. Sampietro, A. H. Mansi, and M. Capponi, "A New Tool for Airborne Gravimetry Survey Simulation," *Geosciences*, vol. 8, no. 8, p. 292, 2018, doi: 10.3390/geosciences8080292.

[62] S. Goossens et al., "High-Resolution Gravity Field Models from GRAIL Data and Implications for Models of the Density Structure of the Moon's Crust," *Journal of Geophysical Research: Planets*, vol. 125, no. 2, p. e2019JE006086, 2020, doi: 10.1029/2019JE006086.

[63] B. Bills, S. Krishnamoorthy, and A. Komjathy, "Balloon Borne Gravity Survey of Venus," Internal Report, Jet Propulsion Laboratory, 2020.

[64] T. Widemann et al., "EnVision: Undestanding Why Earth's Closest Neighbour is so Different."

[65] R. Garcia, P. Lognonné, and X. Bonnin, "Detecting Atmospheric Perturbations Produced by Venus Quakes," *Geophysical Research Letters*, vol. 32, no. 16, 2005, doi: 10.1029/2005GL023558.

[66] R. F. Garcia et al., "Infrasound From Large Earthquakes Recorded on a Network of Balloons in the Stratosphere," *Geophysical Research Letters*, vol. 49, no. 15, p. e2022GL098844, 2022, doi: 10.1029/2022GL098844.

[67] "View from Ten Kilometres High." [Online]. Available: https://www.esa.int/Science_Exploration/Space_Science/Cassini-Huygens/View_from_ten_kilometres_high. [Accessed: Oct. 23, 2025].

[68] J. Cutts et al., "Exploring the Clouds of Venus: Science Driven Aerobot Missions to Our Sister Planet," presented at the 2022 IEEE Aerospace Conference (AERO), Big Sky, MT, USA, 2022, doi: 10.1109/AERO53065.2022.9843740.

[69] S. A. Cohn et al., "Driftsondes: Providing In Situ Long-Duration Dropsonde Observations over Remote Regions," *Bulletin of the American Meteorological Society*, vol. 94, no. 11, pp. 1661–1674, 2013, doi: 10.1175/BAMS-D-12-00075.1.

[70] K. P. Klaasen and R. Greeley, "VEVA Discovery Mission to Venus: Exploration of Volcanoes and Atmosphere," *Acta Astronautica*, vol. 52, nos. 2–6, pp. 151–158, 2003, doi: 10.1016/S0094-5765(02)00151-0.

[71] J. S. Izraelevitz and J. L. Hall, "Minimum-Mass Limits for Streamlined Venus Atmospheric Probes," *Journal of Spacecraft and Rockets*, vol. 57, no. 4, pp. 683–691, 2020, doi: 10.2514/1.A34437.

[72] A. B. Davis, K. H. Baines, B. M. Sutin, J. A. Cutts, L. I. Dorsky, and P. K. Byrne, "Feasibility of High-Spatial-Resolution Nighttime near-IR Imaging of Venus' Surface from a Platform Just below the Clouds: A Radiative Transfer Study Accounting for the Potential of Haze," *Planetary and Space Science*, vol. 242, p. 105853, 2024, doi: 10.1016/j.pss.2024.105853.

[73] J. L. Hall et al., "Prototype Development of a Variable Altitude Venus Aerobot," presented at the AIAA AVIATION 2021 FORUM, VIRTUAL EVENT, 2021, doi: 10.2514/6.2021-2696.

[74] D. C. Bowman et al., "Multihour Stratospheric Flights with the Heliotrope Solar Hot-Air Balloon," *Journal of Atmospheric and Oceanic Technology*, vol. 37, no. 6, pp. 1051–1066, 2020, doi: 10.1175/JTECH-D-19-0175.1.

[75] H. Laplace, C. Tarrieu, J. Cantrell, and B. Shurmier, "The Guiderope for the Soviet-French Mars 96 Balloon Mission," presented at the 43rd International Astronautical Congress, Washington, DC, 1992.

[76] M. Badescu, S. Sherrit, J. Jones, and J. Hall, "Self-Contained Harpoon and Sample Handling Device for a Remote Platform," presented at the SPIE Smart Structures and Materials + Nondestructive Evaluation and Health Monitoring, San Diego, California, USA, 2009, doi: 10.1117/12.815394.

[77] K. Baines, L. Dorsky, J. Cutts, A. Davis, J. Izraelvitz, B. Sutin, B. Hockman, and P. McGarey, "A Tethered Towbody Payload for In- and Sub-Cloud Sensing on Venus," presented at the International Planetary Probe Workshop-Virtual, 2021.

Reference Material

Christopher D. Yoder[1]

[1] NASA Wallops Flight Facility, Aerospace Engineer, Balloon Program Office

Acknowledgements

Most of this content is taken from the original handbook and reproduced here for readability. It is largely assumed that standard properties and values of physical constants have not changed significantly in 50 years. For original references and context, please consult the original handbook. AI tools were used in the reproduction of table values (for text extraction), and some errors may be present due to the poor quality of the original book scans. Any errors in the table are solely due to transcription and are not intended by the author.

Table of Contents

1. Overview 6

2. Balloon Cross-Sectional Area 10

3. Balloon Azimuthal Rotation 11

4. Useful Gas Coefficients 12

4.1. Specific Gas Constant..... 12

4.2. Thermal Conductivity..... 12

4.3. Dynamic Viscosity..... 14

4.4. Prandtl Number..... 16

4.5. Miscellaneous Parameters..... 16

5. Gases in Cylinders 19

6. Sunrise and Sunset 24

7. Aerostatic Values within the Atmosphere 26

8. Mini-Profiles of Key Contributors to the Field (1925-2025) ... 33

8.1. Foundational & Mid-Century (1925–1965)..... 33

8.2. NASA/Modern Era & Industry (1960–2025)..... 35

References..... 41

Comprehensive Acronym List..... 46

Table of Figures

Figure AA-1: (left) Area of a sphere-on-cone figure projected on a plane normal to relative wind, vr. (right) Sailed balloon diagram. 10

Figure AA-2: Frequency of observation of rotation, and corresponding speeds of rotation, for large balloon systems..... 11

Figure AA-3: Relationship between cutoff/final pressure ratio and final/initial pressure ratio..... 19

Figure AA-4: Equation of time (ET) in minutes plotted vs day of the year. Blue (above the curve) means a watch will be fast, while red (below the curve) means a watch will be slow..... 25

Table of Tables

Table AA-1: Common parameters..... 6

Table AA-2: High level comparison of balloon types..... 7

Table AA-3: Launch sites and durations..... 8

Table AA-4: Classes of payloads and typical parameters..... 9

Table AA-5: Specific gas constant in various units. Note: in this table, calories are gram calories..... 12

Table AA-6: Parameter 'n' for common gases..... 12

Table AA-7: Values of thermal conductivity, k0, at 273.15K..... 13

Table AA-8: Values of k/k0 across temperatures of interest in ballooning. 13

Table AA-9: Coefficient S..... 14

Table AA-10: Reference values for dynamic viscosity..... 14

Table AA-11: $\mu/\mu 0$ for various temperatures. 15

Table AA-12: Prandtl numbers for various gases..... 16

Table AA-13: Common properties of common ballooning gases..... 17

Table AA-14: Lift (kg/m3) of Helium gas contained in steel cylinders 20

Table AA-15: Lift (kg/m3) of Hydrogen gas contained in steel cylinders 22

Table AA-16: Abbreviated version of 1962 Standard Atmosphere table.. 27

1. Overview

The following are useful tables for general balloon and scientific knowledge.

Table AA-1: Common parameters

Quantity	**Symbol**	**Value (SI)**	**Value (Imperial)**
Standard Gravity	g	9.80665 m/s^2	32.174 ft/s^2
Gas Constant for Dry Air	R	287.05 J/kg K	53.35 ft lbf/lbm °R
Boltzmann Constant	k	1.380649×10^{-23} J/K	1.380649×10^{-16} erg/K
Stefan-Boltzmann Constant	σ	$5.670374419 \times 10^{-8}$ $W/m^2 K^4$	1.714×10^{-9} $Btu/ft^2 h °R^4$
Earth Radius (mean)	R_e	6.371×10^6 m	20.9×10^6 ft
Avogadro's Number	N_a	$6.02214076 \times 10^{23}$ mol^{-1}	
Universal Gas Constant	R_u	8.314462618 J/mol K	1.9859 Btu/lb-mol °R

Table AA-2: High level comparison of balloon types

Parameter	Zero-Pressure Balloon (ZPB)	Super-Pressure Balloon (SPB)	Solar Balloon	Planetary Balloon
Lift Gas	He or H_2	He or H_2	Heated air + He	CO_2, H_2, He (varies by planet)
Typical Volume	10^5 – 10^6 m^3	10^4 – 10^5 m^3	10^3 – 10^4 m^3	10^3 – 10^5 m^3
Envelope Material	Polyethylene	Polyethylene + strength film	Mylar or Kapton	Vectran / Kapton hybrid
Flight Duration	8 – 40 h	30 – 100+ days	1 – 8 h	Hours to months (dep. on planet)
Altitude Range	30–42 km	32–38 km	15–25 km	50–60 km (Venus) / 10–30 km (Titan)
Main Advantages	Simplicity & lift capacity	Constant altitude & long duration	Low cost, rapid launch	Planetary science capability
Limitations	Diurnal venting loss	Complex fabric stress design	Weather-limited	Harsh environment, telemetry

Table AA-3: Launch sites and durations

Site / Operator	Latitude	Typical Float Altitude	Wind Regime	Season of Operation	Key Notes
Fort Sumner, NM (USA)	34.5° N	33–37 km	Low shear	May–Oct	Primary North Hemisphere campaign site
McMurdo Station (Antarctica)	77.8° S	36–38 km	Circumpolar	Dec–Feb	Ultra-long-duration SPB missions
Wānaka, New Zealand	44.7° S	33–37 km	Stable westerlies	Mar–Jun	Southern Hemisphere SPB launch site
Palestine, TX (USA)	31.8° N	Test up to 40 km	Variable	Year-round	CSBF test site / training
Esrange, Kiruna (Sweden)	67.9° N	35–38 km	Polar easterlies	Jun–Aug	European summer campaigns
Hyderabad (India)	17.4° N	35 km	Tropical	Jan–Mar	TIFR / ISRO science missions
Alice Springs (Australia)	23.7° S	35 km	Subtropical jet low	Apr–Aug	CNES and CSIRO joint operations

Table AA-4: Classes of payloads and typical parameters

Instrument Class	Example Payloads	Mass Range (kg)	Power Demand (W)	Data Rate (Mbps)	Notes
Optical Imager	SPIDER, BICEP, SuperBIT	500–1500	300–1000	5–50	Cryogenic detectors, high pointing accuracy
IR / Sub-mm Telescopes	BOOMERANG, BLAST	1000–2000	500–1500	10–50	Heavy cryostat requirements
Particle / Cosmic-Ray	CREAM, ATIC	500–1500	300–700	1–10	High-altitude shielding needed
Atmospheric Sensing	LASE, DIAL, ozonesondes	50–400	50–300	< 1	Often multi-instrument gondolas
Remote Sensing	Hyperspectral, EOIR	25-250	50-500	0.5-15	Earth observation
Student Payloads (HASP)	HASP, Cube in Space	< 20	< 50	< 1	Multiplexed on common bus

2. Balloon Cross-Sectional Area

A balloon in flight can be modeled as a "sphere-on-cone" shape. The cross-sectional area, A_D, is given by Equation (*AA*-1) (approximation by Equation (*AA*-2)) and plotted in Figure AA-1.

$$A_D/r = \left[\sin\left(\cos^{-1}\left(\frac{\sin\theta}{\cos b}\right)\right)\right]\left\{\left(\cot^2\theta - 1 + \frac{\sin^2\theta}{\sin^2 b}\right)^{\frac{1}{2}} \sin\left(b - \tan^{-1}\left(\frac{\tan^2\theta}{\tan b}\right)\right)\right\} + \pi + \frac{\sin\theta}{\sin b} \tag{AA-1}$$

$$A_D/r \approx \pi + \left(\theta - \frac{\pi}{2} + \cot\theta\right)\sin b \tag{AA-2}$$

For a balloon that has formed a sail-shape, the cross-sectional area reduces to a function of the fully inflated balloon volume, V:

$$A_D = 1.21\left(\frac{1 + \sin b}{2}\right)V^{\frac{2}{3}} \tag{AA-3}$$

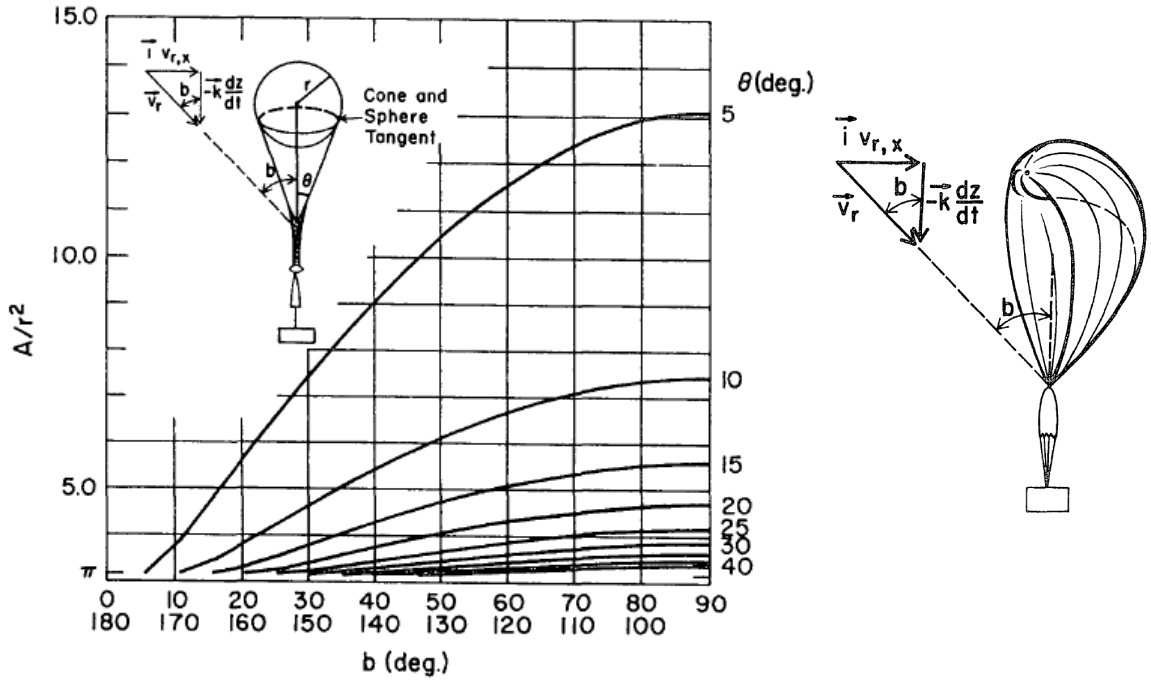


Figure AA-1: (left) Area of a sphere-on-cone figure projected on a plane normal to relative wind,$\vec{v}_r$. (right) Sailed balloon diagram.

3. Balloon Azimuthal Rotation

During flight, a balloon will experience rotation in azimuth. The rate of rotation varies with the phase of flight. Unless mitigated with an azimuthal pointing system, the gondola will rotate with the balloon. From flight data, the balloon was found to rotate equal to or less than the curve in Figure AA-2. For example, large balloons were observed to rotate at 30 deg/min (or slower) in 50% of flights during ascent and approximately 95% of flights at float.

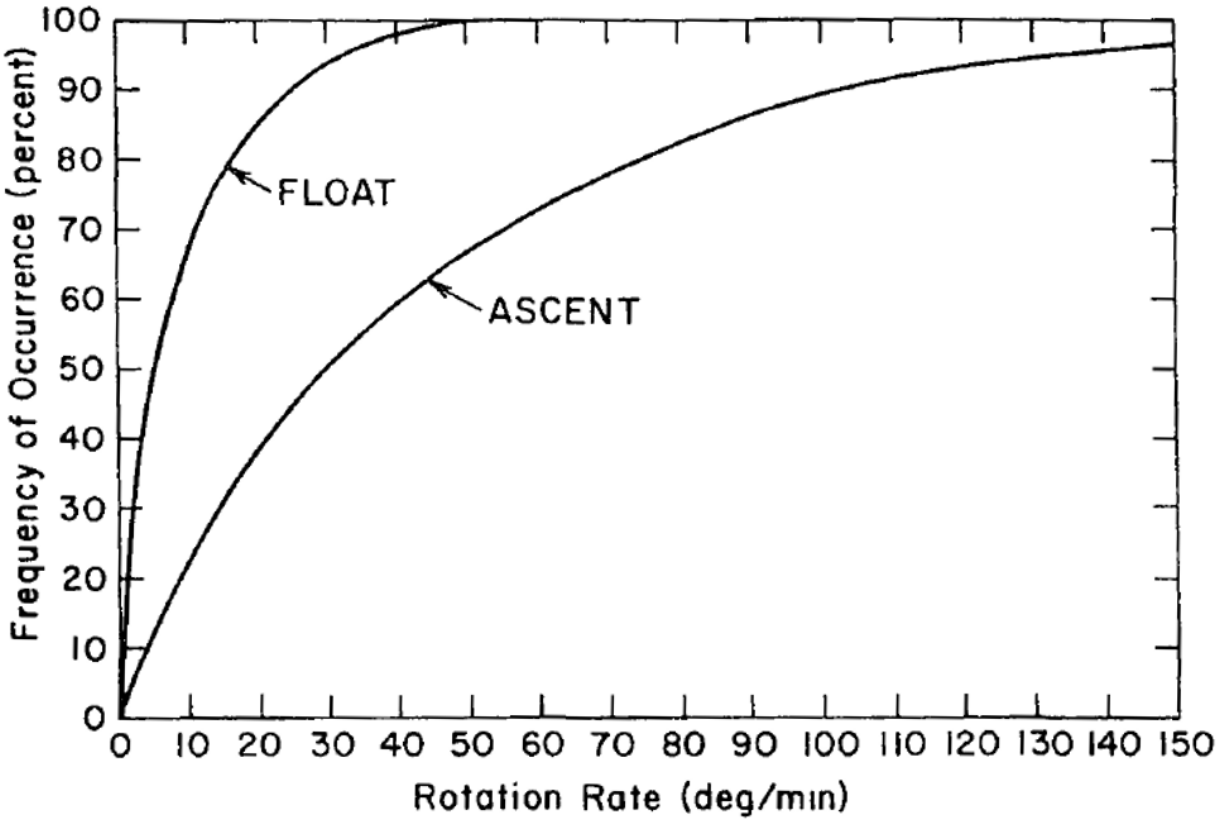


Figure AA-2: Frequency of observation of rotation, and corresponding speeds of rotation, for large balloon systems.

The curves in Figure AA-2 for float (Equation (*AA*-4)) and ascent (Equation (*AA*-5)) are:

$$y = 100\left(\tanh\frac{x}{22}\right)^{1/2} \qquad \text{(AA-4)}$$

$$y = 100\left(\tanh\frac{x^2}{94 + (x+8)}\right)^{1/2} \qquad \text{(AA-5)}$$

4. Useful Gas Coefficients

4.1. Specific Gas Constant

Values for the specific gas constants for different gases are found below.

Table AA-5: Specific gas constant in various units.
Note: in this table, calories are gram calories.

Units	Air	Helium	Hydrogen	Nitrogen	Ammonia	Mixture 3H2+N2	Methane
J/(kg-Mol) K	8314.3	8314.3	8314.3	8314.3	8314.3	8314.3	8314.3
J/kg K	287.06	2077.2	4124.4	296.8	488.19	976.43	518.25
*Cal/(g-Mol) K	1.9872	1.9872	1.9872	1.9872	1.9872	1.9872	1.9872
cal/g K	0.06861	0.49615	0.98526	0.07094	0.11668	0.22338	0.12387
BTU/(lb-Mol) R	1.9859	1.9859	1.9859	1.9859	1.9859	1.9859	1.9859
BTU/lb R	0.06856	0.49615	0.98512	0.0709	0.11661	0.22322	0.12379

4.2. Thermal Conductivity

For pressures of interest to ballooning, the thermal conductivity of gases at other temperatures can be approximated by:

$$\frac{k}{k_0} = \left(\frac{T}{T_0}\right)^n \qquad \text{(AA-6)}$$

where k_0 is a known thermal conductivity at absolute temperature T_0, T is the desired absolute temperature, and n is specific to the gas. Morris found that the curve fit for temperatures ranging from 150K to 775K with less than 5% error.

Table AA-6: Parameter 'n' for common gases.

Parameter	Air	Helium	Hydrogen	Nitrogen	Ammonia	Mixture 3H2+N2	Methane
n	0.9	0.7	0.85	0.8	1.53	0.84	1.33

Some common reference values for thermal conductivity are:

Table AA-7: Values of thermal conductivity, k_0, at 273.15K.

Units	Air	Helium	Hydrogen	Nitrogen	Ammonia	Mixture 3H2+N2	Methane
Watts/m°K (x10²)	2.41	14.4	16.82	2.42	2.1	9.8	3.07
Cal/cm sec°K (x10^5)	5.77	34.4	40.18	5.78	5.03	23.4	7.33
k Cal/m hr°K (x10²)	2.08	12.38	14.46	2.08	1.81	8.4	2.64
BTU/ft hr°R (x10²)	1.4	8.32	9.72	1.4	1.22	5.7	1.77

The ratio of k/k_0 for the same gases across temperatures is found below in Table 4.

Table AA-8: Values of k/k_0 across temperatures of interest in ballooning.

Temp (K)	Air	Helium	Hydrogen	Nitrogen	Ammonia	Mixture 3H2+N2	Methane	Temp (˚R)
150	0.612	0.657	0.601	0.619	--	0.604	0.451	270
160	0.645	0.688	0.635	0.652	--	0.638	0.491	288
170	0.678	0.718	0.668	0.684	--	0.671	0.532	306
180	0.710	0.747	0.702	0.716	--	0.704	0.574	324
190	0.743	0.776	0.735	0.748	--	0.737	0.617	342
200	0.774	0.804	0.767	0.779	--	0.770	0.661	360
210	0.806	0.832	0.800	0.810	--	0.802	0.705	378
220	0.837	0.859	0.832	0.841	--	0.834	0.750	396
230	0.868	0.887	0.864	0.871	--	0.866	0.796	414
240	0.899	0.913	0.896	0.902	--	0.897	0.842	432
250	0.930	0.940	0.927	0.932	0.873	0.928	0.889	450
260	0.960	0.966	0.959	0.961	0.927	0.959	0.936	468
270	0.991	0.992	0.990	0.991	0.987	0.990	0.985	486
280	1.021	1.017	1.021	1.020	1.039	1.021	1.033	504
290	1.050	1.043	1.052	1.049	1.096	1.052	1.083	522
300	1.080	1.068	1.083	1.078	1.154	1.082	1.133	540
310	1.109	1.093	1.114	1.107	1.214	1.112	1.183	558
320	1.139	1.117	1.144	1.135	1.274	1.142	1.234	576
330	1.168	1.142	1.174	1.163	1.335	1.172	1.286	594
340	1.197	1.166	1.205	1.191	1.398	1.202	1.338	612
350	1.225	1.190	1.235	1.219	1.461	1.232	1.391	630

4.3. Dynamic Viscosity

The dynamic viscosity of various gases for less than two atmospheres of pressure can be approximated using Sutherlands approximation. Given that dynamic viscosity is of the form:

$$\frac{\mu}{\mu_0} = \left(\frac{T}{T_0}\right)^{1.5} \frac{S + T_0}{S + T} \qquad \text{(AA-7)}$$

where μ_0 is a reference viscosity at T_0, T_0 is a reference absolute temperature (273.15K), and S is a constant found in Table AA-9.

Table AA-9: Coefficient S

Property	Air	Helium	Hydrogen	Nitrogen	Ammonia	Mixture 3H2+H2	Methane
S	110.4	--	--	100.1	670	98.9	93.5

Reference values for dynamic viscosity at 273.15K are found in Table AA-10.

Table AA-10: Reference values for dynamic viscosity.

Units	Air	Helium	Hydrogen	Nitrogen	Ammonia	Mixture 3H2+H2	Methane
kg/m sec ($x10^6$)	1.716	1.895	0.841	1.652	0.9	1.43	1.089
*poise ($x10^6$)	1.716	1.895	0.841	1.652	0.9	1.43	1.089
lbm/ft sec ($x10^5$)	1.153	1.273	0.565	1.11	0.605	0.96	0.732
lbm/ft hr ($x10^2$)	4.152	4.586	2.035	3.998	2.178	3.46	2.635
lbf sec/ft² ($x10^7$)	3.586	3.961	1.758	3.453	1.881	2.99	2.276
slug/ft hr ($x10^4$)	12.9	14.25	6.324	12.42	6.768	10.75	8.189

Finally, the values of μ/μ_0 are found in Table AA-11.

Table AA-11: Values for μ/μ_0 at various temperatures.

Temp (K)	Air	Helium	Hydrogen	Nitrogen	Ammonia	Mixture 3H2+N2	Methane	Temp (˚R)
150	0.599	0.679	0.666	0.631	--	0.642	0.613	270
160	0.635	0.707	0.696	0.666	--	0.676	0.648	288
170	0.671	0.736	0.726	0.699	--	0.709	0.683	306
180	0.706	0.764	0.755	0.732	--	0.740	0.717	324
190	0.740	0.791	0.783	0.763	--	0.771	0.750	342
200	0.773	0.817	0.811	0.794	--	0.801	0.783	360
210	0.806	0.844	0.838	0.824	--	0.830	0.814	378
220	0.838	0.869	0.865	0.854	--	0.859	0.845	396
230	0.870	0.895	0.892	0.882	--	0.886	0.876	414
240	0.901	0.920	0.918	0.911	--	0.914	0.905	432
250	0.931	0.944	0.943	0.938	0.898	0.940	0.934	450
260	0.961	0.969	0.969	0.965	0.942	0.966	0.963	468
270	0.990	0.993	0.994	0.992	0.986	0.992	0.991	486
280	1.019	1.016	1.018	1.018	1.030	1.017	1.019	504
290	1.047	1.039	1.043	1.043	1.075	1.042	1.046	522
300	1.075	1.063	1.067	1.068	1.119	1.066	1.072	540
310	1.102	1.085	1.091	1.093	1.163	1.089	1.098	558
320	1.129	1.108	1.114	1.117	1.208	1.113	1.124	576
330	1.155	1.130	1.137	1.141	1.252	1.136	1.150	594
340	1.181	1.152	1.161	1.164	1.297	1.158	1.174	612
350	1.207	1.174	1.183	1.187	1.341	1.180	1.199	630

4.4. Prandtl Number

The Prandtl number is expressed as:

$$Pr = \frac{C_p \mu}{k} \qquad \text{(AA-8)}$$

where C_p must be expressed in terms of energy per unit mass per degree. Morris performed various curve fits of empirical data in order to estimate Prandtl number for various gases as a function of temperature, found in Table AA-12.

Table AA-12: Prandtl numbers for various gases.

Temp (K)	Air	Helium	Hydrogen	Nitrogen	Ammonia	Mixture 3H2+N2	Methane	Temp (˚R)
150	0.755	0.705	0.725	0.766	--	0.493	0.793	270
160	0.752	0.703	0.724	0.763	--	0.493	0.791	288
170	0.749	0.702	0.723	0.759	--	0.492	0.788	306
180	0.745	0.700	0.721	0.755	--	0.491	0.785	324
190	0.742	0.699	0.72	0.752	--	0.491	0.782	342
200	0.739	0.697	0.719	0.748	--	0.49	0.779	360
210	0.736	0.695	0.718	0.745	--	0.49	0.776	378
220	0.732	0.694	0.716	0.741	--	0.489	0.773	396
230	0.729	0.692	0.715	0.737	--	0.489	0.77	414
240	0.726	0.691	0.714	0.734	--	0.488	0.767	432
250	0.723	0.689	0.713	0.73	0.871	0.488	0.764	450
260	0.719	0.687	0.711	0.726	0.871	0.487	0.762	468
270	0.716	0.686	0.71	0.723	0.87	0.487	0.759	486
280	0.713	0.684	0.709	0.719	0.869	0.486	0.756	504
290	0.710	0.683	0.708	0.715	0.868	0.486	0.753	522
300	0.706	0.681	0.706	0.712	0.868	0.485	0.75	540
310	0.703	0.679	0.705	0.708	0.867	0.485	0.747	558
320	0.700	0.678	0.704	0.705	0.866	0.484	0.744	576
330	0.697	0.676	0.703	0.701	0.866	0.484	0.741	594
340	0.693	0.675	0.701	0.697	0.865	0.483	0.738	612
350	0.690	0.673	0.7	0.694	0.864	0.482	0.735	630

4.5. Miscellaneous Parameters

Finally, a variety of useful parameters are listed in Table AA-13.

Table AA-13: Common properties of common ballooning gases.

Property	Units	Dry Air	Helium	Hydrogen	Nitrogen	Ammonia	Decomp. Ammonia	Methane	Oxygen
Chemical Formula	--	--	He	H2	N2	NH3	3H2+N2	CH4	O2
Molecular Wt (M)	kg/kg-Mol	28.964	4.0026	2.0159	28.01	17.031	8.915	16.043	32
Molecular Wt (M)	lb/lb-Mol	28.964	4.0026	2.0159	28.01	17.031	8.915	16.043	32
Gas Constant (R/M)	J/kg-Mol K	287.060	2077.2	4124.4	296.8	488.19	976.43	518.25	259.82
Gas Constant (R/M)	ft lb/lb-Mol R	53.360	386.1	766.6	55.17	90.74	181.5	96.33	48.3
Density (273.15K 101325 N/m2)	kg/m3	1.292	0.1786	0.0899	1.25	0.76	0.38	0.716	1.428
Density (491.67R 14.696 lbf/in2)	lbm/ft3 (x10^-1)	8.070	1.11	0.561	7.8	4.74	2.37	4.47	8.91
Density (288.15K 101325 N/m2)	kg/m3	1.225	0.1693	0.0853	1.185	0.72	0.36	0.679	1.353
Density (518.67R 14.696 lbf/in2)	lbm/ft3 (x10^-1)	7.650	1.057	0.532	7.4	4.49	2.25	4.24	8.45
Density of Liquid at Normal Boiling Point	kg/m3	--	128	71.5	811	682	--	426	1090
Density of Liquid at Normal Boiling Point	lbm/ft3	--	7.99	4.46	50.6	42.6	--	26.6	68
Normal Boiling Point (101325 N/m2)	K	78.800	4.21	20.4	87.4	239.6	--	111.6	90.2

Normal Boiling Point (14.696 lbf/in2)	R	141.800	7.58	36.7	157.3	431.3	--	200.9	162.4
Latent Heat of Vaporiz-ation at BP	J/kg(x10^3)	--	20.7	448	199	1370	--	510	213
Latent Heat of Vaporiz-ation at BP	Btu/lbm	--	8.73	193	85.6	589	--	219	91.6
Flammable limits in air	% by volume	--	--	4-75	--	15-28	7-73	5.3-14	--
Critical Temp	K	132.500	5.25	33.3	126.2	405.4	--	190.6	154.8
Critical Temp	R	238.500	9.45	59.9	227.2	729.7	--	343.1	278.6
Critical Pressure	N/m2 (x10^6)	3.770	0.229	1.297	3.39	11.3	--	4.62	5.08
Critical Pressure	lbf/in2 (x10^2)	5.470	0.332	1.88	4.92	16.4	--	6.7	7.37
Critical Density	kg/m3	312.000	69.3	31	311	235	--	162	410
Critical Density	lbm/ft3	19.500	4.33	1.94	19.4	14.7	--	10.1	25.6
Critical Volume	m3/kg-Mol	0.090	0.058	0.065	0.09	0.072	--	0.099	0.078
Critical Volume	ft3/lb-Mol	1.440	0.93	1.04	1.44	1.15	--	1.59	1.25
Critical Compress-ibility	--	0.318	0.307	0.304	0.291	0.243	--	0.288	0.308

5. Gases in Cylinders

The water volume method is outlined in Chapter 6 in detail. The pieces below are critical when using the water volume method to calculate a precise amount of gas. First, the relationship between the ratio of cutoff to final pressure and the ratio of final to initial pressure is seen in Figure AA-3. The second is a reproduction of the lift per unit volume of Helium (Table AA-14) and Hydrogen (Table AA-15) in steel cylinders in SI units. A reference of Engineering Units can be found in the original handbook. Note that there may be transcription errors in the tables below due to the poor quality of reproduction of the original handbook.

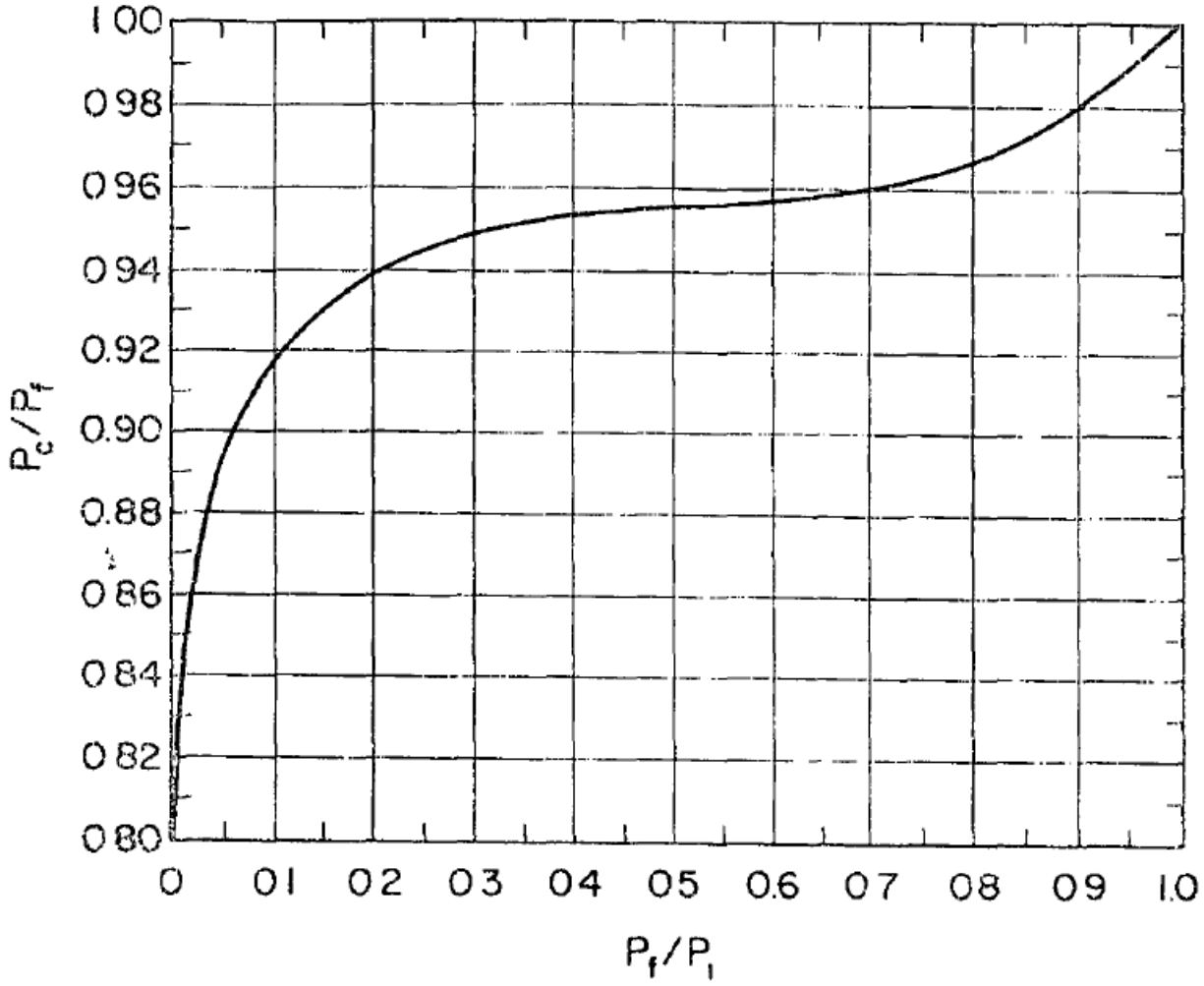


Figure AA-3: Relationship between cutoff/final pressure ratio and final/initial pressure ratio.

Table AA-14: Lift (kg/m3) of Helium gas contained in steel cylinders

G Press. (x10^6) (N/m²)	Gas Temperature ˚C							
	-25	-20	-15	-10	-5	0	5	10
0	1.224	1.200	1.177	1.154	1.134	1.113	1.093	1.074
5	7.241	7.099	6.965	6.833	6.707	6.586	6.469	6.356
10	13.224	12.965	12.719	12.481	12.252	12.031	11.818	11.612
15	19.174	18.802	18.446	18.099	17.768	17.448	17.140	16.842
20	25.094	24.605	24.138	23.688	23.256	22.839	22.437	22.048
25	30.974	30.376	29.802	29.248	28.715	28.202	27.707	27.229
30	36.825	36.117	35.435	34.779	34.147	33.538	32.951	32.386
35	42.645	41.827	41.039	40.282	39.552	38.848	38.170	37.515
40	48.433	47.505	46.615	45.756	44.929	44.132	43.365	42.621
45	54.189	53.154	52.159	51.202	50.279	49.390	48.531	47.703
50	59.914	58.773	57.676	56.620	55.602	54.621	53.675	52.751
55	65.608	64.362	63.166	62.010	60.899	59.827	58.793	57.795
60	71.271	69.922	68.623	67.373	66.169	65.008	63.890	62.806
65	76.904	75.452	74.055	72.710	71.413	70.163	68.957	67.793
70	82.507	80.953	79.458	78.019	76.632	75.294	74.003	72.756
75	88.080	86.476	84.834	83.302	81.824	80.400	79.029	77.597
80	93.624	91.970	90.183	88.558	86.992	85.481	84.023	82.615
85	99.138	97.286	95.504	93.784	92.134	90.540	89.001	87.517
90	104.620	102.670	100.800	98.992	97.251	95.571	93.950	92.403
95	110.080	108.040	106.070	104.170	102.340	100.580	98.878	97.246
100	115.510	113.370	111.310	109.320	107.410	105.570	103.780	102.060
105	120.910	118.680	116.520	114.450	112.450	110.530	108.670	106.870
110	126.200	123.950	121.710	119.560	117.470	115.470	113.530	111.650
115	131.630	129.210	126.860	124.630	122.470	120.380	118.370	116.420
120	136.940	134.430	132.030	129.690	127.440	125.280	123.180	121.160
125	142.230	139.630	137.110	134.720	132.390	130.150	127.980	125.880
130	147.500	144.810	142.220	139.720	137.320	134.990	132.750	130.580
135	152.740	149.960	147.280	144.700	142.220	139.820	137.510	135.260
140	157.950	155.090	152.320	149.660	147.100	144.620	142.230	139.920
145	163.130	160.180	157.340	154.600	151.950	149.400	146.940	144.560
150	168.290	165.250	162.170	159.510	156.790	154.160	151.630	149.180
155	173.420	170.310	167.250	164.400	161.600	158.900	156.290	153.770
160	178.530	175.320	172.240	169.240	166.390	163.620	160.940	158.350
165	183.610	180.320	177.160	174.100	171.160	168.310	165.570	162.910
170	188.670	185.330	182.050	178.920	175.880	172.990	170.170	167.450
175	193.700	190.260	186.970	183.720	180.630	177.640	174.760	171.970
180	198.710	195.180	191.780	188.500	185.330	182.200	179.320	176.470
185	203.690	200.080	196.600	193.250	190.010	186.890	183.870	180.960
190	208.650	204.950	201.410	197.970	194.680	191.480	188.380	185.420
195	213.590	209.820	206.190	202.650	199.320	196.050	192.900	189.850
200	218.500	214.560	210.940	207.380	203.940	200.610	197.390	194.280
205	223.390	219.470	215.660	212.050	208.540	205.140	201.860	198.680
210	228.250	224.250	220.410	216.700	213.110	209.650	206.310	203.070
215	233.100	229.030	225.110	221.320	217.670	214.150	210.740	207.440
220	237.920	233.770	229.780	225.930	222.210	218.620	215.150	211.790
225	242.710	238.500	234.430	230.510	226.730	223.080	219.560	216.120
230	247.490	243.200	239.070	235.080	231.230	227.510	223.920	220.460
235	252.240	247.880	243.680	239.620	235.710	231.930	228.270	224.740
240	256.970	252.540	248.270	244.150	240.170	236.330	232.610	229.720
245	261.680	257.180	252.840	248.650	244.610	240.710	236.930	233.290

Table AA-14 (cont): Lift (kg/m3) of Helium gas contained in steel cylinders

G Press. (x10^6) (N/m²)	Gas Temperature ˚C							
	15	20	25	30	35	40	45	50
0	1.055	1.037	1.020	1.004	0.987	0.972	0.957	0.942
5	6.247	6.142	6.040	5.942	5.847	5.755	5.665	5.579
10	11.414	11.222	11.037	10.858	10.684	10.516	10.353	10.196
15	16.556	16.279	16.011	15.751	15.500	15.257	15.022	14.794
20	21.674	21.312	20.962	20.623	20.295	19.978	19.671	19.372
25	26.767	26.321	25.890	25.473	25.069	24.678	24.299	23.932
30	31.837	31.308	30.796	30.301	29.822	29.358	28.908	28.472
35	36.882	36.271	35.680	35.108	34.554	34.017	33.498	32.994
40	41.904	41.212	40.542	39.893	39.266	38.658	38.071	37.502
45	46.903	46.130	45.382	44.658	43.957	43.278	42.619	41.981
50	51.878	51.025	50.200	49.401	48.628	47.878	47.152	46.447
55	56.831	55.898	54.997	54.124	53.278	52.455	51.657	50.881
60	61.760	60.750	59.772	58.826	57.909	57.021	56.160	55.325
65	66.667	65.579	64.527	63.507	62.520	61.564	60.635	59.736
70	71.552	70.387	69.260	68.169	67.112	66.088	65.094	64.130
75	76.414	75.173	73.973	72.810	71.684	70.593	69.534	68.507
80	81.254	79.938	78.665	77.432	76.237	75.079	73.956	72.866
85	86.073	84.682	83.336	82.033	80.771	79.547	78.359	77.207
90	90.869	89.405	87.988	86.615	85.285	83.996	82.745	81.531
95	95.645	94.107	92.619	91.178	89.781	88.427	87.114	85.838
100	100.400	98.789	97.231	95.721	94.259	92.840	91.464	90.129
105	105.130	103.450	101.820	100.250	98.717	97.236	95.798	94.402
110	109.840	108.090	106.390	104.750	103.160	101.610	100.110	98.658
115	114.530	112.710	110.950	109.240	107.590	105.980	104.430	102.940
120	119.200	117.310	115.480	113.710	111.980	110.320	108.700	107.120
125	123.850	121.890	119.990	118.150	116.370	114.640	112.960	111.330
130	128.480	126.450	124.490	122.590	120.740	118.950	117.210	115.530
135	133.080	131.000	128.970	127.000	125.090	123.240	121.440	119.700
140	137.680	135.520	133.420	131.390	129.420	127.510	125.660	123.860
145	142.250	140.020	137.860	135.770	133.740	131.770	129.860	128.000
150	146.800	144.510	142.280	140.130	138.040	136.010	134.040	132.130
155	151.330	148.970	146.690	144.470	142.320	140.230	138.210	136.240
160	155.850	153.420	151.070	148.790	146.580	144.440	142.360	140.330
165	160.340	157.850	155.440	153.100	150.830	148.630	146.490	144.410
170	164.810	162.260	159.790	157.390	155.060	152.810	150.610	148.480
175	169.270	166.650	164.120	161.660	159.280	156.960	154.720	152.530
180	173.700	171.030	168.430	165.920	163.480	161.110	158.800	156.570
185	178.120	175.380	172.730	170.160	167.660	165.230	162.860	160.590
190	182.520	179.720	177.010	174.380	171.820	169.340	166.940	164.590
195	186.900	184.040	181.270	178.580	175.970	173.440	170.980	168.590
200	191.260	188.340	185.510	182.770	180.110	177.520	175.010	172.560
205	195.610	192.630	189.740	186.940	184.230	181.590	179.040	176.530
210	199.940	196.900	193.960	191.100	188.330	185.640	183.020	180.470
215	204.260	201.150	198.150	195.240	192.410	189.670	187.000	184.410
220	208.540	205.380	202.330	199.360	196.490	193.690	190.970	188.330
225	212.810	209.600	206.490	203.470	200.540	197.690	194.940	192.230
230	217.070	213.800	210.640	207.570	204.580	201.680	198.870	196.130
235	221.310	217.990	214.770	211.640	208.610	205.660	202.790	200.000
240	225.530	222.160	218.880	215.700	212.620	209.620	206.700	203.870
245	229.740	226.310	222.980	219.750	216.610	213.570	210.600	207.720

Table AA-15: Lift (kg/m3) of Hydrogen gas contained in steel cylinders

G Press. (x10^6) (N/m²)	Gas Temperature ˚C							
	-25	-20	-15	-10	-5	0	5	10
0	1.322	1.296	1.271	1.246	1.223	1.202	1.180	1.160
5	7.918	7.766	7.519	7.377	7.241	7.110	6.984	6.862
10	14.274	13.996	13.729	13.470	13.222	12.983	12.752	12.530
15	20.689	20.286	19.898	19.525	19.165	18.820	18.487	18.165
20	27.064	26.537	26.030	25.543	25.074	24.622	24.187	23.766
25	33.397	32.747	32.123	31.523	30.945	30.389	29.852	29.335
30	39.689	38.919	38.175	37.460	36.781	36.120	35.484	34.865
35	45.941	45.050	44.195	43.372	42.580	41.816	41.081	40.371
40	52.151	51.142	50.171	49.240	48.343	47.478	46.644	45.842
45	58.321	57.195	56.113	55.072	54.070	53.104	52.174	51.276
50	64.450	63.208	62.014	60.866	59.761	58.696	57.669	56.679
55	70.539	69.182	67.878	66.624	65.415	64.253	63.131	62.049
60	76.587	75.117	73.704	72.344	71.036	69.775	68.560	67.387
65	82.595	81.013	79.492	78.023	76.620	75.260	73.955	72.693
70	88.563	86.869	85.242	83.677	82.169	80.717	79.317	77.966
75	94.490	92.687	90.955	89.288	87.683	86.137	84.646	83.208
80	100.377	98.467	96.630	94.863	93.162	91.523	89.943	88.418
85	106.225	104.208	102.269	100.403	98.606	96.875	95.206	93.596
90	112.034	109.911	107.870	105.905	104.015	102.194	100.437	98.744
95	117.802	115.575	113.434	111.374	109.391	107.479	105.636	103.857
100	123.532	121.202	118.962	116.807	114.732	112.731	110.803	108.941
105	129.222	126.791	124.454	122.204	120.038	117.951	115.937	113.994
110	134.874	132.343	129.909	127.565	125.311	123.137	121.044	119.016
115	140.487	137.857	135.326	132.894	130.550	128.291	126.114	124.068
120	146.062	143.334	140.711	138.187	135.756	133.412	131.151	128.969
125	151.598	148.775	146.059	143.445	140.928	138.501	136.160	133.903
130	157.097	154.170	151.371	148.670	146.067	143.558	141.137	138.800
135	162.556	159.546	156.649	153.860	151.173	148.483	146.084	143.671
140	167.981	164.877	161.891	159.016	156.247	153.577	151.000	148.513
145	173.367	170.172	167.099	164.139	161.288	158.539	155.886	153.324
150	178.716	175.432	172.272	169.223	166.297	163.470	160.742	158.107
155	184.029	180.656	177.411	174.286	171.274	168.370	165.567	162.861
160	189.305	185.845	182.515	179.309	176.220	173.239	170.363	167.585
165	194.545	190.999	187.587	184.301	181.133	178.078	175.129	172.281
170	199.749	196.118	192.624	189.259	186.016	182.887	179.866	176.949
175	204.917	201.203	197.629	194.186	190.867	187.665	184.574	181.589
180	210.050	206.254	202.600	199.081	195.687	192.414	189.253	186.203
185	215.148	211.271	207.535	203.944	200.477	197.133	193.903	190.783
190	220.211	216.254	212.445	208.775	205.237	201.822	198.525	195.339
195	225.239	221.204	217.319	213.576	209.966	206.480	203.118	199.867
200	230.234	226.121	222.161	218.345	214.665	211.114	207.684	204.363
205	235.194	231.006	226.971	223.086	219.335	215.716	212.221	208.841
210	240.120	235.856	231.750	227.793	223.975	220.290	216.731	213.291
215	245.014	240.676	236.498	232.471	228.589	224.836	221.213	217.711
220	249.873	245.463	241.214	237.113	233.168	229.354	225.668	222.106
225	254.706	250.218	245.900	241.737	237.721	233.843	230.097	226.474
230	259.495	254.942	250.556	246.327	242.246	238.306	234.498	230.817
235	264.257	259.634	255.181	250.886	246.742	242.740	238.873	235.133
240	268.987	264.296	259.776	255.417	251.211	247.148	243.221	239.424
245	273.685	268.927	264.342	259.913	255.651	251.528	247.544	243.690

Table AA-15 (cont): Lift (kg/m3) of Hydrogen gas contained in steel cylinders

G Press. (x10^6) (N/m²)	Gas Temperature ˚C							
	15	20	25	30	35	40	45	50
0	1.140	1.121	1.102	1.084	1.067	1.050	1.033	1.018
5	6.744	6.630	6.520	6.414	6.311	6.212	6.116	6.022
10	12.316	12.100	11.910	11.714	11.527	11.346	11.170	11.000
15	17.854	17.555	17.266	16.984	16.713	16.451	16.196	15.950
20	23.361	22.969	22.591	22.225	21.870	21.527	21.195	20.873
25	28.835	28.352	27.886	27.435	26.998	26.576	26.167	25.770
30	34.277	33.704	33.151	32.615	32.096	31.596	31.111	30.640
35	39.686	39.024	38.384	37.766	37.168	36.588	36.027	35.483
40	45.064	44.314	43.589	42.888	42.210	41.555	40.917	40.300
45	50.409	49.572	48.763	47.980	47.223	46.490	45.779	45.091
50	55.723	54.799	53.906	53.043	52.208	51.399	50.615	49.855
55	61.005	59.996	59.020	58.077	57.164	56.280	55.424	54.594
60	66.255	65.162	64.105	63.082	62.093	61.134	60.206	59.306
65	71.474	70.297	69.159	68.058	66.993	65.962	64.962	63.993
70	76.662	75.402	74.184	73.006	71.866	70.762	69.692	68.655
75	81.819	80.477	79.180	77.925	76.711	75.535	74.395	73.290
80	86.945	85.522	84.147	82.815	81.528	80.281	79.072	77.901
85	92.040	90.538	89.085	87.679	86.319	85.001	83.724	82.486
90	97.105	95.523	93.994	92.514	91.082	89.694	88.350	87.047
95	102.139	100.479	98.874	97.321	95.818	94.362	92.951	91.582
100	107.143	105.406	103.726	102.100	100.527	99.003	97.529	96.093
105	112.117	110.303	108.549	106.852	105.209	103.618	102.075	100.579
110	117.061	115.172	113.345	111.577	109.865	108.207	106.600	105.041
115	121.976	120.012	118.112	116.274	114.495	112.771	111.100	109.479
120	126.861	124.823	122.852	120.945	119.098	117.309	115.575	113.893
125	131.716	129.606	127.564	125.589	123.676	121.822	120.025	118.282
130	136.543	134.360	132.248	130.206	128.227	126.310	124.451	122.647
135	141.340	139.087	136.907	134.796	132.753	130.773	128.853	126.991
140	146.109	143.785	141.537	139.361	137.254	135.211	133.231	131.310
145	150.849	148.456	146.146	143.899	141.720	139.604	137.554	135.565
150	155.561	153.099	150.717	148.411	146.178	144.013	141.914	139.878
155	160.245	157.715	155.268	152.898	150.603	148.378	146.220	144.127
160	164.900	162.304	159.792	157.359	155.003	152.716	150.503	148.354
165	169.528	166.866	164.290	161.795	159.379	157.035	154.762	152.558
170	174.129	171.401	168.761	166.205	163.729	161.328	158.999	156.739
175	178.702	175.910	173.208	170.591	168.055	165.597	163.212	160.899
180	183.248	180.392	177.628	174.951	172.357	169.842	167.403	165.035
185	187.768	184.848	182.023	179.287	176.632	174.065	171.571	169.150
190	192.259	189.278	186.393	183.598	180.890	178.264	175.716	173.243
195	196.724	193.683	190.738	187.886	185.121	182.440	179.839	177.314
200	201.163	198.061	195.058	192.149	189.328	186.593	183.940	181.364
205	205.576	202.415	199.353	196.386	193.513	190.724	188.019	185.392
210	209.963	206.743	203.624	200.603	197.674	194.833	192.076	189.399
215	214.324	211.046	207.871	204.794	201.812	198.919	196.111	193.385
220	218.660	215.324	212.093	208.963	205.927	202.983	200.125	197.350
225	222.970	219.578	216.292	213.107	210.020	207.025	204.117	201.294
230	227.255	223.807	220.467	217.229	214.090	211.045	208.088	205.217
235	231.515	228.012	224.616	221.328	218.138	215.043	212.038	209.120
240	235.750	232.193	228.746	225.405	222.164	219.020	215.968	213.003
245	239.961	236.349	232.850	229.458	226.168	222.976	219.876	216.865

6. Sunrise and Sunset

The local hour angle of sunrise or sunset on the surface of the Earth can be approximated as:

$$(LHA)_A = \cos^{-1}\left[\frac{-0.01 - \sin(\lambda_1)\sin(\delta_S)}{\cos(\lambda_1)\cos(\delta_S)}\right] \quad \text{(AA-9)}$$

where λ_1 is the latitude of the observer and δ_S is the solar declination angle, given as:

$$\delta_S = -23.45\cos\left(\frac{360}{365}\right)(n + 10) \quad \text{(AA-10)}$$

where n is the number of the day in the year (n=1 for January 1st). The $(LHA)_A$ result is expressed in radians. To calculate sunrise or sunset:

$$t_S = t_{noon} \pm (LHA)_A\left(\frac{180}{15\pi}\right) \quad \text{(AA-11)}$$

where t_S is the time, in hours, of sunrise (sunset) when subtracting (adding) to the time of solar noon, t_{noon}. The value of solar noon, t_{noon}, is measured using instrumentation or found from a reference manual. If neither is available, then approximating solar time as apparent time (local time in the time zone of the observer) could be used with an error within $\pm$15 minutes. This approximation implies that $ET = 0$.

A better approximation was outlined previously by Farley (Farley, 2020), starting with the general form of Solar Time, t_{solar}, as:

$$t_{solar} = t_{GMT} + ET + \frac{86400}{2\pi}\lambda \quad \text{(AA-12)}$$

where t_{GMT} is the Greenwich Mean Time (in seconds), λ is the longitude in radians, and ET is the equation of time in seconds given by:

$$ET = \frac{86400}{2\pi}[0.000075 + 0.001868\cos\beta - 0.032077\sin\beta - 0.014615\cos(2\beta) - 0.04089\sin(2\beta)] \quad \text{(AA-13)}$$

Where:

$$\beta = 2\pi\left(\frac{n}{86400} - 1\right)/365.25 \quad \text{(AA-14)}$$

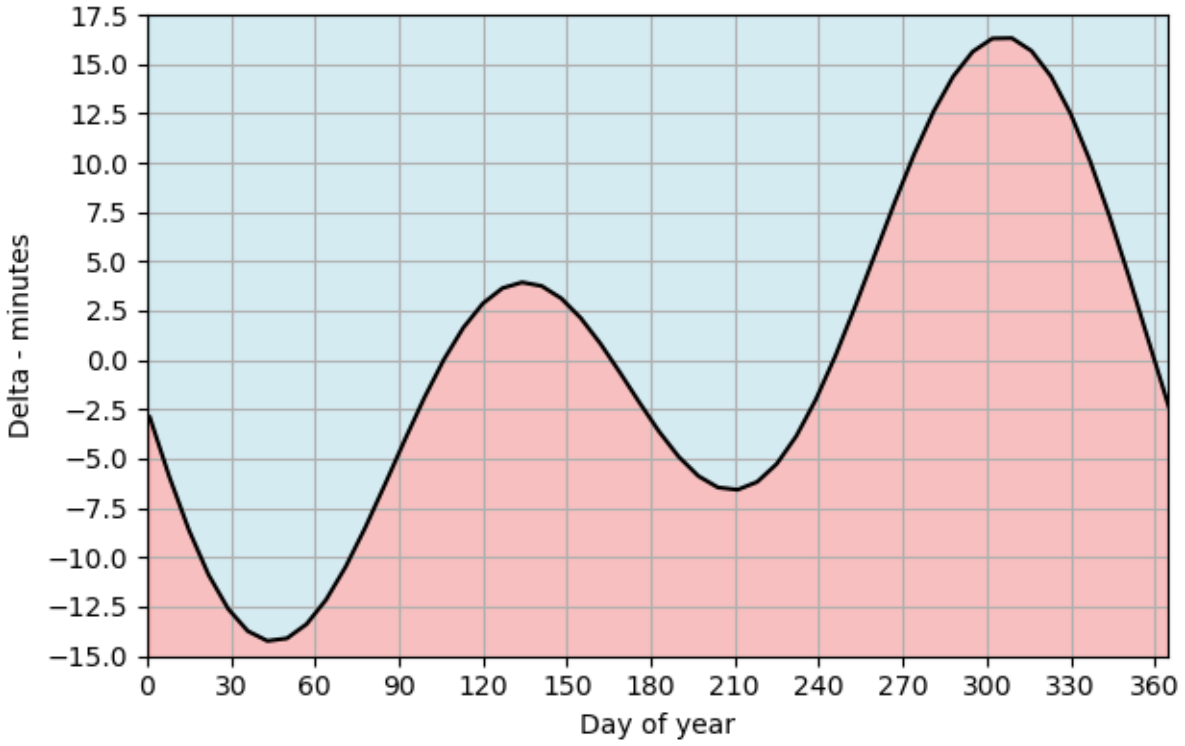


Figure AA-4: Equation of time (ET) in minutes plotted vs day of the year. Blue (above the curve) means a watch will be fast, while red (below the curve) means a watch will be slow.

Generalizing Equation (AA-9) for the altitude of the balloon yields:

$$(LHA)_B = \cos^{-1}\left[\frac{-\sqrt{2H/r} - 0.016 - \sin(\lambda_1)\sin(\delta_S)}{\cos(\lambda_1)\cos(\delta_S)}\right] \qquad \text{(AA-15)}$$

where the height of the balloon above the surface is H and the radius of the Earth is r, both expressed in the same units.

The length of a day on the surface of the Earth at a point is:

$$\Delta t_{daylight} = 2(LHA)_A\left(\frac{180}{15\pi}\right) \qquad \text{(AA-16)}$$

Note that Equation (AA-10) can be re-purposed to find the length of sunlight on a balloon using $(LHA)_B$, but the Eastward/Westward motion of the balloon is neglected, which could shorten or lengthen the day.

7. Aerostatic Values within the Atmosphere

The 1962 Standard Atmosphere has been used for many years during the design and operations of balloons at all scales. Warren et al provided a seminal work entitled “Aerostatic Lift of Helium and Hydrogen in the Atmosphere” (NCAR-TN/IA-69). An abbreviated version is reproduced below.

Table AA-16: Abbreviated version of 1962 Standard Atmosphere table.

Pressure (mb)	Int. air mass (kg/m2)	Geopot. Alt. (m)	Geopot. Alt. (ft)	Temp. (˚C)	Density (kg/m3)	Gas exp. -	Lift of H2 (kg/m3)	Lift of He (kg/m3)	Lift of He (lb/ft3)
1050	1.073E+04	-302	-989	16.96	1.2609E+00	0.972	1.1731E+00	1.0866E+00	6.7832E-02
1040	1.062E+04	-220	-723	16.43	1.2511E+00	0.979	1.1640E+00	1.0782E+00	6.7308E-02
1030	1.052E+04	-139	-454	15.9	1.2414E+00	0.987	1.1550E+00	1.0698E+00	6.6784E-02
1020	1.042E+04	-56	-184	15.36	1.2316E+00	0.995	1.1459E+00	1.0614E+00	6.6258E-02
1010	1.032E+04	27	89	14.82	1.2218E+00	1.003	1.1368E+00	1.0529E+00	6.5732E-02
1000	1.022E+04	111	364	14.28	1.2120E+00	1.011	1.1277E+00	1.0445E+00	6.5204E-02
990	1.012E+04	195	641	13.73	1.2022E+00	1.019	1.1185E+00	1.0360E+00	6.4676E-02
980	1.001E+04	281	920	13.18	1.1923E+00	1.027	1.1094E+00	1.0275E+00	6.4146E-02
970	9.911E+03	366	1202	12.62	1.1825E+00	1.036	1.1002E+00	1.0190E+00	6.3615E-02
960	9.805E+03	453	1486	12.06	1.1726E+00	1.045	1.0910E+00	1.0105E+00	6.3084E-02
950	9.707E+03	540	1773	11.49	1.1627E+00	1.054	1.0818E+00	1.0020E+00	6.2551E-02
940	9.605E+03	628	2062	10.92	1.1528E+00	1.063	1.0725E+00	9.9343E-01	6.2018E-02
930	9.503E+03	717	2353	10.34	1.1428E+00	1.072	1.0633E+00	9.8486E-01	6.1483E-02
920	9.401E+03	807	2647	9.75	1.1329E+00	1.081	1.0540E+00	9.7628E-01	6.0947E-02
910	9.299E+03	897	2944	9.17	1.1229E+00	1.091	1.0447E+00	9.6768E-01	6.0410E-02
900	9.197E+03	989	3243	8.57	1.1129E+00	1.101	1.0354E+00	9.5906E-01	5.9872E-02
890	9.096E+03	1081	3545	7.98	1.1029E+00	1.111	1.0261E+00	9.5042E-01	5.9333E-02
880	8.994E+03	1173	3850	7.37	1.0928E+00	1.121	1.0168E+00	9.4176E-01	5.8792E-02
870	8.892E+03	1267	4157	6.76	1.0828E+00	1.131	1.0074E+00	9.3309E-01	5.8251E-02
860	8.790E+03	1362	4468	6.15	1.0727E+00	1.142	9.9802E-01	9.2439E-01	5.7708E-02
850	8.688E+03	1457	4781	5.53	1.0626E+00	1.153	9.8861E-01	9.1568E-01	5.7164E-02
840	8.586E+03	1554	5098	4.9	1.0524E+00	1.164	9.7918E-01	9.0695E-01	5.6619E-02
830	8.484E+03	1651	5417	4.27	1.0423E+00	1.175	9.6973E-01	8.9820E-01	5.6073E-02
820	8.382E+03	1749	5740	3.63	1.0321E+00	1.187	9.6026E-01	8.8942E-01	5.5525E-02
810	8.280E+03	1849	6065	2.98	1.0219E+00	1.199	9.5077E-01	8.8063E-01	5.4976E-02
800	8.178E+03	1949	6394	2.33	1.0117E+00	1.211	9.4125E-01	8.7182E-01	5.4426E-02
790	8.076E+03	2050	6727	1.67	1.0014E+00	1.223	9.3171E-01	8.6298E-01	5.3874E-02
780	7.974E+03	2153	7063	1.01	9.9113E-01	1.236	9.2215E-01	8.5413E-01	5.3321E-02
770	7.872E+03	2256	7402	0.34	9.8083E-01	1.249	9.1256E-01	8.4525E-01	5.2767E-02
760	7.770E+03	2361	7745	-0.34	9.7050E-01	1.262	9.0296E-01	8.3635E-01	5.2211E-02

Table AA-16 (cont): Abbreviated version of 1962 Standard Atmosphere table.

Pressure (mb)	Int. air mass (kg/m2)	Geopot. Alt. (m)	Geopot. Alt. (ft)	Temp. (˚C)	Density (kg/m3)	Gas exp. -	Lift of H2 (kg/m3)	Lift of He (kg/m3)	Lift of He (lb/ft3)
750	7.668E+03	2466	8091	-1.03	9.6015E-01	1.276	8.9332E-01	8.2743E-01	5.1654E-02
740	7.566E+03	2573	8442	-1.72	9.4977E-01	1.290	8.8367E-01	8.1848E-01	5.1096E-02
730	7.464E+03	2681	8796	-2.43	9.3936E-01	1.304	8.7398E-01	8.0951E-01	5.0536E-02
720	7.362E+03	2790	9154	-3.14	9.2893E-01	1.319	8.6428E-01	8.0052E-01	4.9975E-02
710	7.260E+03	2901	9516	-3.85	9.1847E-01	1.334	8.5454E-01	7.9151E-01	4.9412E-02
700	7.158E+03	3012	9882	-4.58	9.0798E-01	1.349	8.4479E-01	7.8247E-01	4.8848E-02
690	7.056E+03	3125	10253	-5.31	8.9746E-01	1.365	8.3500E-01	7.7340E-01	4.8282E-02
680	6.954E+03	3239	10628	-6.06	8.8692E-01	1.381	8.2519E-01	7.6432E-01	4.7715E-02
670	6.852E+03	3355	11008	-6.81	8.7634E-01	1.398	8.1535E-01	7.5520E-01	4.7146E-02
660	6.749E+03	3472	11392	-7.57	8.6573E-01	1.415	8.0548E-01	7.4606E-01	4.6575E-02
650	6.647E+03	3591	11780	-8.34	8.5510E-01	1.433	7.9558E-01	7.3689E-01	4.6003E-02
640	6.545E+03	3711	12174	-9.12	8.4443E-01	1.451	7.8566E-01	7.2770E-01	4.5429E-02
630	6.443E+03	3832	12573	-9.91	8.3373E-01	1.469	7.7570E-01	7.1848E-01	4.4853E-02
620	6.341E+03	3955	12977	-10.71	8.2300E-01	1.488	7.6572E-01	7.0923E-01	4.4276E-02
610	6.239E+03	4080	13386	-11.52	8.1223E-01	1.508	7.5570E-01	6.9996E-01	4.3697E-02
600	6.137E+03	4206	13801	-12.34	8.0143E-01	1.529	7.4565E-01	6.9065E-01	4.3116E-02
590	6.035E+03	4335	14221	-13.17	7.9060E-01	1.549	7.3557E-01	6.8131E-01	4.2533E-02
580	5.933E+03	4464	14647	-14.02	7.7973E-01	1.571	7.2546E-01	6.7195E-01	4.1948E-02
570	5.831E+03	4596	15079	-14.87	7.6883E-01	1.593	7.1532E-01	6.6255E-01	4.1362E-02
560	5.729E+03	4730	15517	-15.74	7.5789E-01	1.616	7.0514E-01	6.5312E-01	4.0773E-02
550	5.627E+03	4865	15962	-16.62	7.4691E-01	1.640	6.9493E-01	6.4366E-01	4.0183E-02
540	5.525E+03	5003	16413	-17.52	7.3590E-01	1.665	6.8468E-01	6.3417E-01	3.9590E-02
530	5.423E+03	5142	16871	-18.43	7.2484E-01	1.690	6.7439E-01	6.2464E-01	3.8995E-02
520	5.321E+03	5284	17336	-19.35	7.1375E-01	1.715	6.6407E-01	6.1508E-01	3.8398E-02
510	5.219E+03	5428	17809	-20.28	7.0261E-01	1.743	6.5371E-01	6.0549E-01	3.7799E-02
500	5.116E+03	5574	18289	-21.23	6.9144E-01	1.772	6.4331E-01	5.9586E-01	3.7198E-02
490	5.014E+03	5723	18777	-22.19	6.8022E-01	1.801	6.3287E-01	5.8619E-01	3.6595E-02
480	4.912E+03	5874	19273	-23.18	6.6895E-01	1.831	6.2239E-01	5.7648E-01	3.5989E-02
470	4.810E+03	6028	19777	-24.18	6.5765E-01	1.863	6.1187E-01	5.6674E-01	3.5380E-02
460	4.708E+03	6184	20290	-25.2	6.4629E-01	1.895	6.0131E-01	5.5695E-01	3.4769E-02

Table AA-16 (cont): Abbreviated version of 1962 Standard Atmosphere table.

Pressure (mb)	Int. air mass (kg/m2)	Geopot. Alt. (m)	Geopot. Alt. (ft)	Temp. (˚C)	Density (kg/m3)	Gas exp. -	Lift of H2 (kg/m3)	Lift of He (kg/m3)	Lift of He (lb/ft3)
450	4.606E+03	6344	20812	-26.23	6.3489E-01	1.929	5.9070E-01	5.4713E-01	3.4156E-02
440	4.504E+03	6506	21344	-27.29	6.2344E-01	1.965	5.8005E-01	5.3726E-01	3.3540E-02
430	4.402E+03	6671	21886	-28.36	6.1195E-01	2.002	5.6935E-01	5.2735E-01	3.2922E-02
420	4.299E+03	6839	22438	-29.45	6.0040E-01	2.040	5.5861E-01	5.1740E-01	3.2300E-02
410	4.197E+03	7011	23000	-30.57	5.8879E-01	2.081	5.4781E-01	5.0740E-01	3.1676E-02
400	4.095E+03	7185	23574	-31.71	5.7714E-01	2.123	5.3697E-01	4.9736E-01	3.1049E-02
390	3.993E+03	7364	24160	-32.87	5.6543E-01	2.167	5.2607E-01	4.8727E-01	3.0419E-02
380	3.891E+03	7546	24758	-34.05	5.5366E-01	2.213	5.1512E-01	4.7712E-01	2.9786E-02
370	3.789E+03	7732	25369	-35.26	5.4183E-01	2.261	5.0412E-01	4.6693E-01	2.9150E-02
360	3.687E+03	7923	25993	-36.5	5.2994E-01	2.312	4.9306E-01	4.5669E-01	2.8510E-02
350	3.584E+03	8117	26631	-37.76	5.1799E-01	2.365	4.8194E-01	4.4639E-01	2.7867E-02
340	3.482E+03	8316	27285	-39.06	5.0597E-01	2.421	4.7076E-01	4.3603E-01	2.7221E-02
330	3.380E+03	8520	27954	-40.38	4.9389E-01	2.480	4.5951E-01	4.2562E-01	2.6570E-02
320	3.278E+03	8729	28640	-41.74	4.8174E-01	2.543	4.4821E-01	4.1514E-01	2.5917E-02
310	3.176E+03	8944	29343	-43.14	4.6951E-01	2.609	4.3683E-01	4.0461E-01	2.5259E-02
300	3.073E+03	9164	30065	-44.57	4.5721E-01	2.679	4.2538E-01	3.9401E-01	2.4597E-02
290	2.971E+03	9390	30807	-46.04	4.4483E-01	2.754	4.1387E-01	3.8334E-01	2.3931E-02
280	2.869E+03	9623	31570	-47.55	4.3236E-01	2.833	4.0227E-01	3.7260E-01	2.3261E-02
270	2.767E+03	9862	32355	-49.1	4.1982E-01	2.918	3.9060E-01	3.6179E-01	2.2586E-02
260	2.664E+03	10109	33164	-50.71	4.0718E-01	3.008	3.7884E-01	3.5090E-01	2.1906E-02
250	2.562E+03	10363	33999	-52.36	3.9445E-01	3.106	3.6700E-01	3.3993E-01	2.1221E-02
240	2.460E+03	10626	34861	-54.07	3.8163E-01	3.210	3.5507E-01	3.2887E-01	2.0531E-02
230	2.358E+03	10898	35753	-55.83	3.6870E-01	3.322	3.4304E-01	3.1773E-01	1.9836E-02
220	2.255E+03	11180	36679	-56.5	3.5375E-01	3.463	3.2913E-01	3.0485E-01	1.9031E-02
210	2.153E+03	11475	37646	-56.5	3.3767E-01	3.623	3.1417E-01	2.9100E-01	1.8166E-02
200	2.051E+03	11784	38662	-56.5	3.2159E-01	3.809	2.9921E-01	2.7714E-01	1.7301E-02
190	1.948E+03	12109	39729	-56.5	3.0552E-01	4.010	2.8425E-01	2.6328E-01	1.6436E-02
180	1.846E+03	12452	40854	-56.5	2.8944E-01	4.232	2.6929E-01	2.4943E-01	1.5571E-02
170	1.744E+03	12815	42043	-56.5	2.7336E-01	4.481	2.5433E-01	2.3557E-01	1.4706E-02
160	1.641E+03	13199	43304	-56.5	2.5728E-01	4.761	2.3937E-01	2.2171E-01	1.3841E-02

Table AA-16 (cont): Abbreviated version of 1962 Standard Atmosphere table.

Pressure (mb)	Int. air mass (kg/m2)	Geopot. Alt. (m)	Geopot. Alt. (ft)	Temp. (˚C)	Density (kg/m3)	Gas exp. -	Lift of H2 (kg/m3)	Lift of He (kg/m3)	Lift of He (lb/ft3)
150	1.539E+03	13608	44647	-56.5	2.4120E-01	5.079	2.2441E-01	2.0785E-01	1.2976E-02
140	1.437E+03	14046	46082	-56.5	2.2512E-01	5.442	2.0945E-01	1.9400E-01	1.2111E-02
130	1.334E+03	14516	47624	-56.5	2.0904E-01	5.860	1.9449E-01	1.8014E-01	1.1246E-02
120	1.232E+03	15024	49290	-56.5	1.9296E-01	6.349	1.7953E-01	1.6628E-01	1.0381E-02
110	1.129E+03	15575	51100	-56.5	1.7688E-01	6.926	1.6457E-01	1.5243E-01	9.5157E-03
100	1.027E+03	16180	53083	-56.5	1.6080E-01	7.618	1.4961E-01	1.3857E-01	8.6506E-03
95	9.757E+02	16505	54150	-56.5	1.5276E-01	8.019	1.4213E-01	1.3164E-01	8.2181E-03
90	9.245E+02	16848	55275	-56.5	1.4472E-01	8.465	1.3465E-01	1.2471E-01	7.7856E-03
85	8.732E+02	17210	56464	-56.5	1.3668E-01	8.963	1.2716E-01	1.1778E-01	7.3530E-03
80	8.220E+02	17595	57726	-56.5	1.2864E-01	9.523	1.1968E-01	1.1086E-01	6.9205E-03
75	7.707E+02	18004	59069	-56.5	1.2060E-01	10.158	1.1220E-01	1.0393E-01	6.4880E-03
70	7.195E+02	18442	60504	-56.5	1.1256E-01	10.883	1.0472E-01	9.6999E-02	6.0554E-03
65	6.682E+02	18912	62046	-56.5	1.0452E-01	11.720	9.7244E-02	9.0070E-02	5.6229E-03
60	6.169E+02	19419	63711	-56.5	9.6478E-02	12.697	8.9763E-02	8.3142E-02	5.1904E-03
55	5.656E+02	19971	65522	-56.5	8.8439E-02	13.851	8.2283E-02	7.6213E-02	4.7578E-03
50	5.143E+02	20576	67507	-55.92	8.0185E-02	15.277	7.4805E-02	6.9101E-02	4.3138E-03
45	4.630E+02	21247	69708	-55.25	7.1945E-02	17.027	6.6937E-02	6.2000E-02	3.8705E-03
40	4.116E+02	22000	72177	-54.5	6.3731E-02	19.261	5.9295E-02	5.4921E-02	3.4288E-03
35	3.603E+02	22856	74987	-53.64	5.5547E-02	22.053	5.1681E-02	4.7868E-02	2.9883E-03
30	3.089E+02	23849	78244	-52.65	4.7397E-02	25.845	4.4098E-02	4.0845E-02	2.5499E-03
29	2.986E+02	24068	78962	-52.43	4.5772E-02	26.763	4.2586E-02	3.9445E-02	2.4625E-03
28	2.884E+02	24294	79706	-52.21	4.4148E-02	27.747	4.1075E-02	3.8045E-02	2.3751E-03
27	2.781E+02	24530	80478	-51.97	4.2526E-02	28.806	3.9566E-02	3.6648E-02	2.2878E-03
26	2.679E+02	24774	81280	-51.73	4.0906E-02	29.947	3.8059E-02	3.5251E-02	2.2007E-03
25	2.575E+02	25029	82115	-51.47	3.9287E-02	31.180	3.6553E-02	3.3857E-02	2.1136E-03
24	2.473E+02	25294	82984	-51.21	3.7671E-02	32.518	3.5049E-02	3.2464E-02	2.0266E-03
23	2.370E+02	25570	83892	-50.93	3.6056E-02	33.975	3.3547E-02	3.1072E-02	1.9398E-03
22	2.267E+02	25860	84841	-50.64	3.4444E-02	35.565	3.2047E-02	2.9683E-02	1.8530E-03
21	2.164E+02	26163	85836	-50.34	3.2835E-02	37.309	3.0548E-02	2.8295E-02	1.7664E-03
20	2.061E+02	26481	86881	-50.02	3.1225E-02	39.231	2.9052E-02	2.6909E-02	1.6799E-03

Table AA-16 (cont): Abbreviated version of 1962 Standard Atmosphere table.

Pressure (mb)	Int. air mass (kg/m2)	Geopot. Alt. (m)	Geopot. Alt. (ft)	Temp. (˚C)	Density (kg/m3)	Gas exp. -	Lift of H2 (kg/m3)	Lift of He (kg/m3)	Lift of He (lb/ft3)
19	1.958E+02	26816	87981	-49.68	2.9620E-02	41.358	2.7558E-02	2.5525E-02	1.5935E-03
18	1.856E+02	27170	89142	-49.33	2.8016E-02	43.725	2.6066E-02	2.4144E-02	1.5072E-03
17	1.753E+02	27545	90371	-48.95	2.6416E-02	46.374	2.4577E-02	2.2764E-02	1.4211E-03
16	1.650E+02	27943	91678	-48.56	2.4818E-02	49.360	2.3090E-02	2.1387E-02	1.3351E-03
15	1.547E+02	28368	93071	-48.13	2.3223E-02	52.750	2.1606E-02	2.0012E-02	1.2493E-03
14	1.444E+02	28823	94564	-47.68	2.1631E-02	56.632	2.0125E-02	1.8641E-02	1.1637E-03
13	1.341E+02	29313	96170	-47.19	2.0042E-02	61.121	1.8647E-02	1.7272E-02	1.0782E-03
12	1.238E+02	29843	97909	-46.66	1.8457E-02	66.370	1.7173E-02	1.5906E-02	9.9296E-04
11	1.135E+02	30420	99804	-46.08	1.6876E-02	72.588	1.5701E-02	1.4543E-02	9.0790E-04
10	1.032E+02	31055	101985	-45.45	1.5299E-02	80.070	1.4234E-02	1.3184E-02	8.2307E-04
9.5	9.807E+01	31397	103008	-45.1	1.4512E-02	84.410	1.3502E-02	1.2506E-02	7.8074E-04
9	9.292E+01	31758	104193	-44.74	1.3727E-02	89.240	1.2771E-02	1.1829E-02	7.3848E-04
8.5	8.777E+01	32141	105448	-44.11	1.2928E-02	94.750	1.2028E-02	1.1141E-02	6.9552E-04
8	8.262E+01	32548	106785	-42.97	1.2107E-02	101.180	1.1265E-02	1.0434E-02	6.5136E-04
7.5	7.747E+01	32984	108215	-41.74	1.1291E-02	108.500	1.0505E-02	9.7301E-03	6.0743E-04
7	7.231E+01	33453	109755	-40.43	1.0479E-02	116.900	9.7494E-03	9.0302E-03	5.6374E-04
6.5	6.716E+01	33959	111414	-39.01	9.6715E-03	126.660	8.9982E-03	8.3344E-03	5.2030E-04
6	6.200E+01	34509	113220	-37.47	8.8690E-03	138.120	8.2517E-03	7.6430E-03	4.7714E-04
5.5	5.685E+01	35112	115196	-35.79	8.0721E-03	151.760	7.5103E-03	6.9563E-03	4.3427E-04
5	5.169E+01	35777	117377	-33.93	7.2812E-03	168.200	6.7744E-03	6.2747E-03	3.9172E-04
4.8	4.963E+01	36063	118317	-33.12	6.9666E-03	175.800	6.4817E-03	6.0036E-03	3.7479E-04
4.6	4.756E+01	36362	119299	-32.29	6.6531E-03	184.100	6.1900E-03	5.7334E-03	3.5792E-04
4.4	4.550E+01	36676	120329	-31.41	6.3407E-03	193.200	5.8994E-03	5.4641E-03	3.4112E-04
4.2	4.344E+01	37006	121411	-30.48	6.0294E-03	203.200	5.6098E-03	5.1960E-03	3.2437E-04
4	4.137E+01	37353	122551	-29.51	5.7194E-03	214.200	5.3213E-03	4.9288E-03	3.0769E-04
3.8	3.931E+01	37720	123753	-28.48	5.4106E-03	226.400	5.0340E-03	4.6627E-03	2.9108E-04
3.6	3.724E+01	38108	125027	-27.4	5.1032E-03	240.000	4.7480E-03	4.3978E-03	2.7454E-04
3.4	3.518E+01	38520	126379	-26.24	4.7972E-03	255.400	4.4633E-03	4.1340E-03	2.5808E-04
3.2	3.312E+01	38959	127828	-25.01	4.4926E-03	272.700	4.1799E-03	3.8716E-03	2.4169E-04
3	3.105E+01	39429	129362	-23.7	4.1896E-03	292.400	3.8980E-03	3.6104E-03	2.2539E-04

Table AA-16 (cont): Abbreviated version of 1962 Standard Atmosphere table.

Pressure (mb)	Int. air mass (kg/m2)	Geopot. Alt. (m)	Geopot. Alt. (ft)	Temp. (˚C)	Density (kg/m3)	Gas exp. -	Lift of H2 (kg/m3)	Lift of He (kg/m3)	Lift of He (lb/ft3)
2.8	2.898E+01	39935	131019	-22.28	3.8882E-03	315.100	3.6176E-03	3.3507E-03	2.0918E-04
2.6	2.692E+01	40481	132810	-20.75	3.5886E-03	341.400	3.3389E-03	3.0926E-03	1.9306E-04
2.4	2.485E+01	41074	134757	-19.09	3.2909E-03	372.200	3.0619E-03	2.8360E-03	1.7705E-04
2.2	2.279E+01	41723	136887	-17.28	2.9952E-03	409.000	2.7868E-03	2.5812E-03	1.6114E-04
2	2.072E+01	42440	139238	-15.27	2.7018E-03	453.400	2.5137E-03	2.3283E-03	1.4535E-04
1.8	1.865E+01	43239	141859	-13.03	2.4107E-03	508.200	2.2429E-03	2.0774E-03	1.2969E-04
1.6	1.658E+01	44140	144815	-10.51	2.1222E-03	577.200	1.9745E-03	1.8289E-03	1.1417E-04
1.4	1.451E+01	45172	148202	-7.62	1.8367E-03	666.900	1.7089E-03	1.5828E-03	9.8814E-05
1.2	1.245E+01	46378	152158	-4.24	1.5546E-03	788.000	1.4464E-03	1.3397E-03	8.3634E-05
1	1.038E+01	47820	156890	-2.5	1.2872E-03	951.700	1.1976E-03	1.1092E-03	6.9247E-05
0.9	9.340E+00	48655	159059	-2.5	1.1584E-03	1057.500	1.0778E-03	9.9830E-04	6.2322E-05
0.8	8.304E+00	49588	162690	-2.5	1.0297E-03	1189.600	9.5805E-04	8.8738E-04	5.5397E-05
0.7	7.268E+00	50646	166161	-2.5	9.0101E-04	1359.600	8.3830E-04	7.7646E-04	4.8473E-05
0.6	6.232E+00	51867	170167	-2.5	7.7229E-04	1586.200	7.1854E-04	6.6553E-04	4.1548E-05
0.5	5.195E+00	53305	174895	-5.11	6.4384E-04	1885.100	6.0461E-04	5.6001E-04	3.4960E-05
0.4	4.158E+00	55044	180592	-8.59	5.2674E-04	2325.800	4.9005E-04	4.5390E-04	2.8336E-05
0.3	3.121E+00	57254	187840	-13.01	4.0174E-04	3049.200	3.7378E-04	3.4621E-04	2.1613E-05
0.2	2.082E+00	60305	197850	-19.11	2.7426E-04	4486.500	2.5517E-04	2.3635E-04	1.4755E-05
0.1	1.043E+00	65281	214176	-37.62	1.4791E-04	8282.100	1.3762E-04	1.2746E-04	7.9573E-06

8. Mini-Profiles of Key Contributors to the Field (1925-2025)

This appendix commemorates individuals whose work shaped the field of scientific ballooning over the last five decades. Each profile includes key contributions, roles, and publications where available. This section was generated by AI, based on data from Chapter 1 and the AIAA Otto Winzen Award recipients.

8.1. Foundational & Mid-Century (1925–1965)

Orvil A. Anderson (1895–1965)

- Role/Organization: USAAC officer/balloonist.
- Contributions: Commanded/crewed Explorer II record flight (1935).
- Awards/Notables: Harmon Trophy; later USAF leadership.
- Reference: [8]

Victor F. Hess (1883–1964)

- Role/Organization: Physicist; University of Innsbruck; Fordham.
- Contributions: Discovery of cosmic rays via balloon flights.
- Awards/Notables: 1936 Nobel Prize in Physics.
- Reference: [10]

Edward P. Ney (1920–1996)

- Role/Organization: Physicist, Univ. of Minnesota.
- Contributions: Balloon-borne cosmic-ray & infrared astronomy; pioneered university scientific ballooning.
- Awards/Notables: NAS member; mentor to generations of balloon scientists.
- Reference: [13]

Auguste Piccard (1884–1962)

- Role/Organization: Physicist & aeronaut; ETH Zürich; University of Brussels.
- Contributions: First stratospheric manned balloon ascent (FNRS-1, 1931), pioneering use of pressurized gondolas for scientific observation.
- Awards/Notables: FAI Gold Air Medal; popularized high-altitude science flight.
- References: [1], [2]

Jean Piccard (1884–1963)

- Role/Organization: Chemist/aeronaut; General Mills Aeronautical Research (consultant).
- Contributions: Advanced plastic balloon concepts and skyhook ideas; mentor to Winzen and early U.S. plastic balloon efforts.
- Awards/Notables: FAI records; with Jeannette, advanced U.S. stratospheric flights.
- References: [3], [4]

Jeannette Piccard (1895–1981)

- Role/Organization: Aeronaut, educator; later NASA consultant.
- Contributions: Stratospheric flight (1934) with sealed gondola operations; STEM outreach and later NASA public engagement.
- Awards/Notables: 1934 Harmon Trophy; later honors and Hall of Fame recognitions.
- Reference: [5]

Erich Regener (1881–1955)

- Role/Organization: Physicist; Stuttgart.
- Contributions: Early cosmic-ray/ozone balloon soundings; high-altitude instrumentation.
- Awards/Notables: Influenced pre-war balloon-borne atmospheric physics.
- Reference: [6]

Thomas "Tex" Settle (1895–1980)

- Role/Organization: U.S. Navy balloonist.
- Contributions: Early high-altitude manned flights; race and record attempts that refined operations.
- Awards/Notables: 1933 Gordon Bennett Balloon Race winner.
- Reference: [9]

Vera Simons (1920–2012)

- Role/Organization: Co-founder, Winzen Research (VP); artist/engineer.
- Contributions: Patented construction/envelope innovations; built and led teams ("balloon girls") for giant plastics; later record/art flights.
- Awards/Notables: "Pre-Astronauts" cohort; major women's pioneer.
- Reference: [18]

Project Skyhook / General Mills team (late 1940s–1950s)

- Role/Organization: ONR/General Mills Aeronautical Research.
- Contributions: First large-scale plastic (polyethylene) balloon program; enabled routine cosmic-ray & upper-air research.

- Awards/Notables: Operational template for later national balloon programs.
- Reference: [14]

Albert W. Stevens (1886–1949)

- Role/Organization: US Army Air Corps balloonist/photographer.
- Contributions: Explorer II stratosphere flights (1935) pioneering high-altitude aerophotography.
- Awards/Notables: Set altitude records with Orvil A. Anderson.
- Reference: [7]

Ralph Hazlett Upson (1888–1968)

- Role/Organization: Goodyear engineer; academic.
- Contributions: Balloon design/airship engineering and training; racing advances.
- Awards/Notables: Early U.S. ballooning champion, educator.
- Reference: [12]

Ward Van Orman (1894–1978)

- Role/Organization: Goodyear Aeronautics balloonist.
- Contributions: National/FAI records; transition toward plastics and long-range ops.
- Awards/Notables: Multi-time Gordon Bennett winner.
- Reference: [11]

Otto C. Winzen (1917–1979)

- Role/Organization: Co-founder, Winzen Research, Inc.
- Contributions: Industrialization of ultra-thin polyethylene balloons; supplied Skyhook, Manhigh, Strato-Lab.
- Awards/Notables: Namesake of AIAA Otto C. Winzen Lifetime Achievement Award.
- References: [15], [16], [17]

8.2. NASA/Modern Era & Industry (1960–2025)

Danny R. Ball (living)

- Role/Organization: Site Manager, Columbia Scientific Balloon Facility (CSBF).
- Contributions: Expanded global launch ops; ops/equipment modernization (Antarctica LDB campaigns).
- Awards/Notables: AIAA Winzen Award (2013).
- References: [37], [48], [49], [50]

Tracy L. Barnes (1939–2019)

- Role/Organization: The Balloon Works (co-founder); Blimp Works; Firefly lineage.

- Contributions: Invented/standardized parachute-top vent; triangular basket; altitude record flights.
- Awards/Notables: FAI CIA Hall of Fame (2017); National Balloon Museum Hall of Fame.
- References: [27], [28], [29], [30]

Felix Baumgartner (1969-2025)

- Role/Organization: Red Bull Stratos.
- Contributions: 2012 supersonic freefall from ~39 km; advanced capsule/pressure suit & balloon ops public demo.
- Awards/Notables: Multiple FAI records; major public engagement for stratospheric ballooning.
- Reference: [66]

Henry M. Cathey (living)

- Role/Organization: NMSU/PSL (Aerospace Div.); longtime NASA balloon R&D partner.
- Contributions: ULDB evolution leadership; program/industry coordination; awards for NASA support.
- Awards/Notables: Agency and community recognitions.
- References: [57], [58]

Alan Eustace (living)

- Role/Organization: StratEx (Paragon Space Dev. lead team).
- Contributions: 2014 altitude jump record (~41.4 km) using balloon-lifted pressure suit system.
- Awards/Notables: FAI absolute records; engineering-first suit-suspended architecture.
- Reference: [67]

Debora Fairbrother (living)

- Role/Organization: Chief, NASA Balloon Program Office (BPO).
- Contributions: Program leadership through SPB tests, workforce & university engagement.
- Awards/Notables: Featured among NASA science leaders.
- Reference: [56]

Rodger E. Farley (1957–2024)

- Role/Organization: NASA engineer (GSFC/WFF).
- Contributions: SPB design & simulations; program technical leadership.
- Awards/Notables: AIAA Winzen Award (2021).
- Reference: [37], [54]

Michael L. Fortenberry (living)

- Role/Organization: NASA/CSBF engineer.

- Contributions: Launch systems (padded spool vehicle); reliability/ops improvements papers.
- Awards/Notables: AIAA conference contributions (1990s).
- References: [60], [63]

Arthur A. Giannetti (1935–2022)

- Role/Organization: Program manager at AFCRL (from 1959); ATA Engineering.
- Contributions: Long career in high-altitude balloon design/operations across DoD/NASA programs, advised on Felix Baumgartner balloon jump
- Awards/Notables: AIAA Winzen Award (2007).
- References: [37], [42]

Gregory T. Guzik (1952–2025)

- Role/Organization: LSU Physics; Director, LaSPACE; HASP PI.
- Contributions: High Altitude Student Platform founder; decades of cosmic-ray/space-physics ballooning.
- Awards/Notables: State/national STEM leadership; numerous student mission cohorts.
- References: [51], [52]

W. Vernon Jones (1939–2020)

- Role/Organization: NASA HQ Program Scientist; cosmology balloon advocate.
- Contributions: Visionary for LDB/SPB cosmology payloads (e.g., BESS); program support/leadership.
- Awards/Notables: AIAA Winzen Award (2011).
- References: [37], [44], [48]

Erich Klein (living)

- Role/Organization: CSBF engineer.
- Contributions: Launch support systems—padded spool vehicle, LDSD tower, Antarctic launch vehicle.
- Awards/Notables: AIAA Winzen Award (2017).
- Reference: [37], [53]

Tim Lachenmeier (living)

- Role/Organization: Founder/leader, Near Space Corporation; Aerostar collaborator.
- Contributions: High-altitude testing & commercial stratospheric services; industry partnerships.
- Awards/Notables: Long-time HAPS/stratospheric test pioneer.
- References: [64], [65]

Vincent E. Lally (1922–2005)

- Role/Organization: Director, NSBF (1961–65); NCAR program lead (GHOST/SPB).
- Contributions: Global superpressure (GHOST) concept; long-duration frameworks and operations.
- Awards/Notables: AIAA Winzen Award (2003); AMS Cleveland Abbe Award.
- Reference: [37], [36]

Charles B. Moore (1920–2010)

- Role/Organization: Physicist; NYU/AF Mogul; NMT Langmuir Lab chair.
- Contributions: Project Mogul balloon engineering; Strato-Lab science; atmospheric electricity research.
- Awards/Notables: AIAA Lifetime Achievement (1997); prominent role in clarifying Roswell via Mogul work.
- References: [31], [32], [33], [34]

David L. Pierce (living)

- Role/Organization: NASA Wallops Director; former Chief, Balloon Program Office (2004–2011).
- Contributions: Led NASA BPO safety/ops; later SMD suborbital and WFF leadership.
- Awards/Notables: NASA Exceptional Service/Achievement Medals.
- Reference: [55]

Don Piccard (1926–2020)

- Role/Organization: Balloon pioneer; Raven collaborator; founder, Piccard Balloons; BFA founder.
- Contributions: Early post-war sport ballooning; 1963 Channel crossing with Yost; commercial sport designs.
- Awards/Notables: U.S. ballooning popularizer; industry builder.
- References: [25], [26], [27]

James L. Rand (1935–2022)

- Role/Organization: Texas A&M; SwRI; CEO Winzen International; founder Winzen Engineering.
- Contributions: Balloon shape/stress modeling; manufacturing methods; film strain-gauge innovations; numerous patents.
- Awards/Notables: AIAA Winzen Award (2004); AIAA/ASME Fellow.
- References: [37], [39], [40]

Raven Industries & Aerostar (founded 1956; Aerostar 1986)

- Role/Organization: U.S. balloon/aerostat manufacturer (Sioux Falls).

- Contributions: High-altitude research balloons for Navy/ONR; later Aerostar SPB/stratospheric platforms.
- Awards/Notables: Longstanding NASA/DoD provider; HAPS applications.
- References: [22], [23], [24]

James J. Rotter (living)

- Role/Organization: NSBF engineer/author.
- Contributions: Led/author of the NSBF "Heavy Load Program Final Report" (1980) referenced in NASA balloon design literature.
- Awards/Notables: Cited in NASA design/criteria papers.
- References: [61], [62]

Loren G. Seely (1943–2022)

- Role/Organization: Materials/tape/film innovator for scientific balloons.
- Contributions: SSA-10/SSA-20 tape; Stratofilm 372—raised ZP reliability and life.
- Awards/Notables: AIAA Winzen Award (2009).
- References: [37], [43]

Alfred E. Shipley (1922–2017)

- Role/Organization: Early plastics balloon engineer (industry/defense).
- Contributions: Early ZP/SPB manufacturing practice; community mentorship.
- Awards/Notables: AIAA Winzen Award (1994).
- Reference: [37], [45]

Justin H. Smalley (1924-2017)

- Role/Organization: NCAR balloon systems engineer.
- Contributions: Advanced free-flight balloon systems; operations engineering (ret. 1989).
- Awards/Notables: AIAA Winzen Award (1996).
- References: [37], [38]

I. Steve Smith (living)

- Role/Organization: NASA Balloon Program/SwRI collaborator; ULDB co-author.
- Contributions: Balloon flight systems; ULDB analyses; Stress indices and design standardization; program management roles.
- Awards/Notables: Author of NASA balloon strategy papers.
- References: [60], [61]

Sigvard J. "Sig" Stenlund (1932–2019)

- Role/Organization: GT Sheldahl (SPB film); NCAR engineer.
- Contributions: Early superpressure balloon film/tapes; parachute/atmospheric systems at NCAR.
- Awards/Notables: AIAA Winzen Award (2005).
- References: [37], [41]

David Stuchlik (living)

- Role/Organization: NASA WFF engineer/PI.
- Contributions: Arc-Second Pointer (WASP) development/flight demos improving sub-arcsecond pointing.
- Awards/Notables: Successful WASP engineering flight demos under NASA BPO.
- Reference: [59]

James A. Winker (1928–2017)

- Role/Organization: Engineer/historian; Raven; curator of balloon technology knowledge.
- Contributions: Broad engineering leadership (1951→); NASA Balloon Tech Database preservation.
- Awards/Notables: AIAA Winzen Award (1999); NBM Hall of Fame.
- References: [37], [46], [47]

Ed (Paul E.) Yost (1919–2007)

- Role/Organization: Founder, Raven Industries; "Father of modern hot-air balloon."
- Contributions: Propane-burner hot-air systems; 1960 free flight; 1963 English Channel crossing with Don Piccard; seeded sport & scientific use.
- Awards/Notables: Multiple FAI records; BFA founder.
- References: [19], [20], [21]

References

[1] Wikipedia Contributors, “Auguste Piccard,” *Wikipedia*, Sep. 2, 2025.

[2] “Auguste Piccard | Swiss-Belgian physicist | Britannica,” *www.britannica.com*. https://www.britannica.com/biography/Auguste-Piccard-Swiss-Belgian-physicist.

[3] Wikipedia Contributors, “Jean Piccard,” *Wikipedia*, Sep. 2, 2025.

[4] “Project Skyhook,” Wikipedia (context on Piccard/General Mills), accessed Sep. 2, 2025.

[5] Wikipedia Contributors, “Jeannette Piccard,” *Wikipedia*, Sep. 2, 2025.

[6] Wikipedia Contributors, “Erich Regener,” *Wikipedia*, Sep. 2, 2025.

[7] Wikipedia Contributors, “Albert William Stevens,” *Wikipedia*, Sep. 2, 2025.

[8] Wikipedia Contributors, “Orvil A. Anderson,” *Wikipedia*, Sep. 2, 2025.

[9] Wikipedia Contributors, “Thomas G. ‘Tex’ Settle,” *Wikipedia*, Sep. 2, 2025.

[10] Wikipedia Contributors, “Victor Francis Hess,” *Wikipedia*, Sep. 2, 2025.

[11] Wikipedia Contributors, “Ward Van Orman,” *Wikipedia*, Sep. 2, 2025.

[12] Wikipedia Contributors, “Ralph Hazlett Upson,” *Wikipedia*, Sep. 2, 2025.

[13] Wikipedia Contributors, “Edward P. Ney,” *Wikipedia*, Sep. 2, 2025.

[14] Wikipedia Contributors, “Project Skyhook (ONR/General Mills),” *Wikipedia*, Sep. 2, 2025.

[15] Wikipedia Contributors, “Otto C. Winzen,” *Wikipedia*, Sep. 2, 2025.

[16] Wikipedia Contributors, “Winzen Research,” *Wikipedia*, Sep. 2, 2025.

[17] Wikipedia Contributors, “Otto C. Winzen – bio & award,” *Wikipedia*, Sep. 2, 2025.

[18] Wikipedia Contributors, “Vera Simons (Vera Winzen),” *Wikipedia*, Sep. 2, 2025.

[19] Wikipedia Contributors, "Ed Yost," *Wikipedia*, Sep. 2, 2025.

[20] Wikipedia Contributors, "Raven Industries—history," *Wikipedia*, Sep. 2, 2025.

[21] D. L. Piccard, "Balloon flight | History, Examples, Hot-Air Balloon, & Facts," *Encyclopedia Britannica*, Apr. 17, 2008. https://www.britannica.com/technology/balloon-flight/Balloons-reach-the-stratosphere.

[22] Wikipedia Contributors, "Raven Industries," *Wikipedia*, Sep. 2, 2025.

[23] Aerostar, "History," *Aerostar*, May 29, 2024. https://aerostar.com/about/history, (accessed Sep. 2, 2025).

[24] "Home - Aerostar," *Aerostar*, Oct. 21, 2025. https://manufacturing.aerostar.com/ (accessed Sep. 2, 2025).

[25] Wikipedia Contributors, "Don Piccard," *Wikipedia*, Sep. 2, 2025.

[26] "Gondola, Balloon, Don Piccard | National Air and Space Museum," *Si.edu*, 2025. https://airandspace.si.edu/collection-objects/gondola-balloon-don-piccard/nasm_A19750124000 (accessed Sep. 02, 2025).

[27] B. Gevik, "The Birth of the Modern Hot Air Balloon," *SDPB*, Sep. 28, 2017. https://www.sdpb.org/rural-life-and-history/the-birth-of-the-modern-hot-air-balloon (accessed Sep. 02, 2025).

[28] J. H. Barnes, "A message from John H. Barnes, President of AAU," *Aircraft Engineering and Aerospace Technology*, vol. 80, no. 2, Mar. 2008, doi: 10.1108/aeat.2008.12780bab.036.

[29] D. L. Piccard, "Balloon flight | History, Examples, Hot-Air Balloon, & Facts," *Encyclopedia Britannica*, Apr. 17, 2008. https://www.britannica.com/technology/balloon-flight/Balloons-reach-the-stratosphere.

[30] "Tracy Barnes' Altitude Record Setting Flight | National Balloon Museum," *Nationalballoonmuseum.com*, 2025. https://www.nationalballoonmuseum.com/tracy-barnes-altitude-record-setting-flight/ (accessed Sep. 02, 2025).

[31] Wikipedia Contributors, "Charles B. Moore," *Wikipedia*, Sep. 2, 2025.

[32] "New Mexico Tech Notes Passing of Noted Atmospheric Researcher: New Mexico Tech," *Nmt.edu*, 2025. https://www.nmt.edu/news/2010/charles-moore.php (accessed Sep. 02, 2025).

[33] USAF "Roswell Report," 1997/2010 re-release.

[34] Wikipedia Contributors, "Roswell Incident," *Wikipedia*, Sep. 2, 2025.

[35] "Balloon Museum, Home of the Hall of Fame, Welcomes Two New Inductees," *City of Albuquerque*, 2021. https://www.cabq.gov/artsculture/news/balloon-museum-home-of-the-hall-of-fame-welcomes-two-new-inductees (accessed Sep. 02, 2025).

[36] Wikipedia Contributors, "Vincent E. Lally," *Wikipedia*, Sep. 2, 2025.

[37] "Otto C. Winzen Lifetime Achievement Award - AIAA - Shaping the future of aerospace," *AIAA – Shaping the future of aerospace*, Aug. 04, 2025. https://aiaa.org/awards/otto-c-winzen-lifetime-achievement-award/ (accessed Sep. 02, 2025).

[38] Legacy, "Justin Smalley Obituary (2017) - Boulder, CO - The Daily Camera," *Legacy.com*, Jul. 2017. https://www.legacy.com/us/obituaries/dailycamera/name/justin-smalley-obituary?id=14061292 (accessed Sep. 02, 2025).

[39] Legacy, "James Rand Obituary (2022) - San Antonio, TX - San Antonio Express-News," *Legacy.com*, Sep. 03, 2022. https://www.legacy.com/us/obituaries/sanantonio/name/james-rand-obituary?id=36377097 (accessed Dec. 09, 2025).

[40] "November 2022 AIAA Bulletin," *Aerospace America*, Nov. 2022. https://aerospaceamerica.aiaa.org/bulletin/november-2022-aiaa-bulletin/ (accessed Sep. 02, 2025).

[41] "Sig J. Stenlund," *Dignity Memorial*, 2019. https://www.dignitymemorial.com/obituaries/boulder-co/sig-stenlund-8726063 (accessed Sep. 02, 2025).

[42] Arthur Armando Giannetti," *Tributearchive.com*, 2022. https://www.tributearchive.com/obituaries/24005011/arthur-armando-giannetti (accessed Dec. 09, 2025).

[43] "Obituary for Loren G. Seely | West Oaks Funeral Home," *Obituary for Loren G. Seely | West Oaks Funeral Home*, Aug. 09, 2022. https://www.westoaksfuneralhome.com/obituary/Loren-Seely (accessed Dec. 09, 2025).

[44] W. V. Jones, "Evolution of scientific ballooning and its impact on astrophysics research," *Advances in Space Research*, vol. 53, no. 10, pp. 1405-1414, doi: 10.1016/j.asr.2013.12.028.

[45] "Alfred Shipley Obituary | 1922 - 2025 | Palestine Herald-Press," *Palestineherald.com*, 2025. https://obituaries.palestineherald.com/obituary/alfred-shipley-862196052 (accessed Dec. 09, 2025)

[46] Legacy, "James WINKER Obituary (1928 - 2017) - Burnsville, MN - Pioneer Press," *Legacy.com*, Apr. 09, 2017.

https://www.legacy.com/us/obituaries/twincities/name/james-winker-obituary?id=10723383 (accessed Dec. 09, 2025)

[47] "Endowment Campaign," *Augustana University*, 2017. https://www.augie.edu/campus-community/center-western-studies/support-cws/endowment-campaign (accessed Dec. 09, 2025)

[48] "Volume XX-08 Number 01 Inside Wallops," 2008. Accessed: Dec. 09, 2025. [Online]. Available: https://ufdcimages.uflib.ufl.edu/AA/00/05/48/79/00464/01-07-2008.pdf.

[49] T. M. Randolph, R. Mullenax, C. Schwantes, S. W. Sell and D. R. Ball, "The first balloon flight of the Low Density Supersonic Decelerator technology demonstration mission," *2015 IEEE Aerospace Conference*, Big Sky, MT, USA, 2015, pp. 1-12, doi: 10.1109/AERO.2015.7119212.

[50] S. Gordon, "Missing Space Telescope Found Near Dallas," *NBC 5 Dallas-Fort Worth*, May 30, 2012. https://www.nbcdfw.com/news/local/nasa-balloon-telescope-goes-missing-near-dallas/1918679/ (accessed Dec. 09, 2025).

[51] L. State, "T. Gregory Guzik," *Lsu.edu*, 2023. https://www.lsu.edu/physics/people/faculty/guzik.php (accessed Sep. 02, 2025).

[52] "T. Gregory Guzik," *Dignity Memorial*, 2025. https://www.dignitymemorial.com/obituaries/baton-rouge-la/t-guzik-12491307 (accessed Sep. 02, 2025).

[53] G. Muellner, Award Letter, Erick Klein, AIAA Houston, https://www.aiaahouston.org/documents/2017_WInzen_WInner.pdf (accessed Dec. 09, 2025).

[54] "Rodger Farley - NESC Academy Biography - NASA," *NASA*, Apr. 22, 2015. https://www.nasa.gov/people/rodger-farley-nesc-academy-biography/ (accessed Dec. 09, 2025).

[55] "David L. Pierce - NASA," *NASA*, Jan. 27, 2023. https://www.nasa.gov/people/david-l-pierce/ (accessed Sep. 02, 2025).

[56] NASA Goddard, "NASA | Debora Fairbrother Women@NASA 2014," *YouTube*, Dec. 02, 2014. https://www.youtube.com/watch?v=1iAPaD-CqpA (accessed Dec. 09, 2025).

[57] "Aerospace & UAS Test Flight Site Director | New Mexico State University | BE BOLD. Shape the Future.," *Nmsu.edu*, 2015. https://psl.nmsu.edu/about/leadership-pages/director-aerospace.html (accessed Dec. 09, 2025).

[58] H. Cathey, "Evolution of the NASA Ultra Long Duration Balloon," *AIAA Balloon Systems Conference*, 2007, doi: 10.2514/6.2007-2615

[59] D. Stuchlik and R. J. Lanzi, "The NASA Wallops Arc-Second Pointer (WASP) System for Precision Pointing of Scientific Balloon Instruments and Telescopes," AIAA SciTech 2017, doi: 10.2514/6.2017-3609.

[60] I. Smith, M. Lee, M. Fortenberry, R. Judy, "HiSentinel80: Flight of a High-Altitude Airship" *11th AIAA Aviation, Technology, Integration, and Operations (ATIO) Conference*, 2011. Doi: 10.2514/6.2011-6973.

[61] I. S. Smith Jr., "NASA balloon design & flight: philosophy and criteria," *Advances in Space Research*, vol. 13, no. 2, Feb. 1993, pp. 59-62, doi: 10.1016/0273-1177(93)90276-H.

[62] J. Rotter, M. Marquez, G. D. Orr, "Zero-Pressure Balloon Reliability Factors," *AIAA Balloon Systems Conference*, 2007, doi: 10.2514/6.2007-2614.

[63] M. Fortenberry, "Balloon flight simulator – Running SINBAD in real-time," *AIAA 34th Aerospace Sciences Meeting*, 1996, doi: 10.2514/6.1996-358.

[64] T. Banse, "Robotic balloons to explore Venus? An Oregon company is working on it," *Northwest News Network*, Apr. 09, 2021. https://www.nwnewsnetwork.org/science-and-technology/2021-04-09/robotic-balloons-to-explore-venus-an-oregon-company-is-working-on-it (accessed Dec. 09, 2025).

[65] T. Lachenmeier@nsc and Aero, 2013. Accessed: Dec. 09, 2025. [Online]. Available: https://www.kiss.caltech.edu/workshops/airships/presentations/lachenmeier.pdf.

[66] Wikipedia Contributors, "Felix Baumgartner," *Wikipedia* (Red Bull Stratos), Sep. 2, 2025.

[67] Wikipedia Contributors, "Alan Eustace," *Wikipedia* (StratEx), Sep. 2, 2025.

Comprehensive Acronym List

Acronym	Definition
AAAS	American Association for the Advancement of Science
ADC	Analog-to-Digital Converter
ADCS	Attitude Determination and Control System
AWS	Automated Weather Station
BEXUS	Balloon EXperiments for University Students
BICEP	Background Imaging of Cosmic Extragalactic Polarization
BLASTPol	Balloon-borne Large Aperture Submillimeter Telescope for Polarimetry
BOOMERANG	Balloon Observations Of Millimetric Extragalactic Radiation and Geophysics
BPO	Balloon Program Office
C3	Command, Control, and Communications
C4ISR	Command, Control, Communications, Computers, Intelligence, Surveillance, and Reconnaissance
CAD	Computer-Aided Design
CBO	Community-Based Organization
CCD	Charge-Coupled Device
CDF	Cumulative Distribution Function
CFD	Computational Fluid Dynamics
CFD-DEM	Computational Fluid Dynamics–Discrete Element Method
CFRP	Carbon-Fiber-Reinforced Polymer
CNES	Centre National d'Études Spatiales (French space agency)
CPU	Central Processing Unit
CRS	Cosmic Ray Science
CSBF	Columbia Scientific Balloon Facility (renamed from NSBF)
DAQ	Data Acquisition System
DEIA	Diversity, Equity, Inclusion, Accessibility
EDL	Entry, Descent, and Landing
ELL	English Language Learner
ESA	European Space Agency
ESL	English as a Second Language
FAA	Federal Aviation Administration
FEA	Finite Element Analysis
FOV	Field of View
FTS	Flight Termination System
FWHM	Full Width at Half Maximum
GEO	Geostationary Orbit
GFS	Global Forecast System (NOAA weather model)
GigaBIT	(successor to SuperBIT, larger platform)
GNC	Guidance, Navigation, and Control

Acronym	Definition
GPS	Global Positioning System
GUI	Graphical User Interface
HALO	High Altitude Lensing Observatory
HAPS	High Altitude Platform Systems
HASP	High Altitude Student Platform
HBCU	Historically Black Colleges and Universities
IDEA	Individuals with Disabilities Education Act
IEP	Individualized Education Program
IR	Infrared
IRWASP	Wallops Arc-Second PointerInfrared
ISRO	Indian Space Research Organisation
JPL	Jet Propulsion Laboratory
K-12	Kindergarten through 12th grade (U.S. school system)
LDB	Long Duration Balloon
LDSD	Low Density Supersonic Decelerator
LEO	Low Earth Orbit
LMS	Learning Management System
LOS	Line-of-Sight
LTA	Lighter-Than-Air (aircraft)
MCF / mcm	Million cubic feet / million cubic meters (balloon volume units)
MOOC	Massive Open Online Course
MSI	Minority Serving Institutions
NASA	National Aeronautics and Space Administration
NCAR	National Center for Atmospheric Research
NESC	NASA Engineering and Safety Center
NGSS	Next Generation Science Standards
NSBF	National Scientific Balloon Facility
NSF	National Science Foundation
PBL	Project-Based Learning
PBO	Polar Balloon Observatory
PD	Professional Development
PID	Proportional-Integral-Derivative (controller)
PMC-Turbo	Polar Mesospheric Cloud Turbulence mission
PMT	Photomultiplier Tube
PSF	Point Spread Function
REXUS	Rocket EXperiments for University Students
RF	Radio Frequency
RFZMC-2	Zeppelin Metal Clad 2 (metal-clad airship)Radio Frequency
SATCOM	Satellite Communications
SEEC	Space Exploration Educators Conference

Acronym	Definition
SIP	Support Instrumentation Package
SNR	Signal-to-Noise Ratio
SPARCS	Small Payload Advanced Research and Communications System
SPB	Super-Pressure Balloon
SPIDER	Suborbital Polarimeter for Inflation, Dust and the Epoch of Reionization
SRB	Solid Rocket Booster
STEAM	Science, Technology, Engineering, Arts, and Mathematics
STEM	Science, Technology, Engineering, and Mathematics
SuperBIT	Super Pressure Long Duration Balloon-borne Imaging Telescope
TRL	Technology Readiness Level
UAV	Unmanned Aerial Vehicle
ULDB	Ultra Long Duration Balloon
UMinn	University of Minnesota
UV	Ultraviolet
UVIT	Ultraviolet Imaging Telescope
WASP	Wallops Arc-Second Pointer
WFF	Wallops Flight Facility
ZPB	Zero-Pressure Balloon